



**HAL**  
open science

# Epigenetic control of the ovarian transcriptome in *Drosophila melanogaster*

Daniela Torres Campana

► **To cite this version:**

Daniela Torres Campana. Epigenetic control of the ovarian transcriptome in *Drosophila melanogaster*. Genetics. Université de Lyon, 2021. English. NNT : 2021LYSE1176 . tel-03793803

**HAL Id: tel-03793803**

**<https://theses.hal.science/tel-03793803>**

Submitted on 2 Oct 2022

**HAL** is a multi-disciplinary open access archive for the deposit and dissemination of scientific research documents, whether they are published or not. The documents may come from teaching and research institutions in France or abroad, or from public or private research centers.

L'archive ouverte pluridisciplinaire **HAL**, est destinée au dépôt et à la diffusion de documents scientifiques de niveau recherche, publiés ou non, émanant des établissements d'enseignement et de recherche français ou étrangers, des laboratoires publics ou privés.



N°d'ordre NNT :2021LYSE1176

**THESE de DOCTORAT DE L'UNIVERSITE DE LYON**  
opérée au sein de  
**l'Université Claude Bernard Lyon 1**

**Ecole Doctorale N° 340**  
**Biologie Moléculaire, Intégrative et Cellulaire**

**Spécialité de doctorat** : Biologie moléculaire et cellulaire  
**Discipline** : Épигénétique

Soutenue publiquement le 28/09/2021, par :  
**Daniela TORRES CAMPANA**

---

**Contrôle épigénétique du transcriptome ovarien chez *Drosophila melanogaster***

---

Devant le jury composé de :

<b>VIEIRA-HEDDI</b> , Cristina Professeure des Universités, Université Lyon 1, Lyon	Présidente
<b>DI STEFANO</b> , Luisa, Chargée de recherche CNRS, Centre de Biologie Intégrative, Toulouse	Rapporteuse
<b>MARTINEZ</b> , Anne-Marie, Professeure des Universités, Université de Montpellier, Montpellier	Rapporteuse
<b>DOSTATNI</b> , Nathalie, Professeure des Universités, Sorbonne Université, Paris	Examinatrice
<b>LOPPIN Benjamin</b> , Directeur de Recherche CNRS, Laboratoire de Biologie et Modélisation de la Cellule, Lyon	Directeur de thèse
<b>ORSI Guillermo</b> , Chargé de recherche, INSERM Laboratoire de Biologie et Modélisation de la Cellule, Lyon	Co-directeur de thèse

## **Université Claude Bernard – LYON 1**

Président de l'Université	M. Frédéric FLEURY
Président du Conseil Académique	M. Hamda BEN HADID
Vice-Président du Conseil d'Administration	M. Didier REVEL
Vice-Président du Conseil des Etudes et de la Vie Universitaire	M. Philippe CHEVALLIER
Vice-Président de la Commission de Recherche	M. Petru MIRONESCU
Directeur Général des Services	M. Pierre ROLLAND

### **COMPOSANTES SANTE**

Département de Formation et Centre de Recherche en Biologie Humaine	Directrice : Mme Anne-Marie SCHOTT
Faculté d'Odontologie	Doyenne : Mme Dominique SEUX
Faculté de Médecine et Maïeutique Lyon Sud - Charles Mérieux	Doyenne : Mme Carole BURILLON
Faculté de Médecine Lyon-Est	Doyen : M. Gilles RODE
Institut des Sciences et Techniques de la Réadaptation (ISTR)	Directeur : M. Xavier PERROT
Institut des Sciences Pharmaceutiques et Biologiques (ISBP)	Directrice : Mme Christine VINCIGUERRA

### **COMPOSANTES & DEPARTEMENTS DE SCIENCES & TECHNOLOGIE**

Département Génie Electrique et des Procédés (GEP)	Directrice : Mme Rosaria FERRIGNO
Département Informatique	Directeur : M. Behzad SHARIAT
Département Mécanique	Directeur M. Marc BUFFAT
Ecole Supérieure de Chimie, Physique, Electronique (CPE Lyon)	Directeur : Gérard PIGNAULT
Institut de Science Financière et d'Assurances (ISFA)	Directeur : M. Nicolas LEBOISNE
Institut National du Professorat et de l'Education	Administrateur Provisoire : M. Pierre CHAREYRON
Institut Universitaire de Technologie de Lyon 1	Directeur : M. Christophe VITON
Observatoire de Lyon	Directrice : Mme Isabelle DANIEL
Polytechnique Lyon	Directeur : Emmanuel PERRIN
UFR Biosciences	Administratrice provisoire : Mme Kathrin GIESELER
UFR des Sciences et Techniques des Activités Physiques et Sportives (STAPS)	Directeur : M. Yannick VANPOULLE
UFR Faculté des Sciences	Directeur : M. Bruno ANDRIOLETTI



# Remerciements

Après une explosion, un déménagement et une pandémie, elle est là cette thèse et je tiens à remercier les personnes qui ont fait ça possible.

Tout d'abord je veux remercier mon directeur, Benjamin Loppin, de m'avoir ouvert les portes de l'équipe Épigénétique et Formation du Zygote pour la réalisation de ma thèse. Je le remercie de m'avoir proposé un projet si intéressant qui m'a passionné du début à la fin.

Ensuite, je tiens à remercier mon co-directeur, Guille. (El gracias se queda corto para todo lo que hiciste por mí durante estos años). Merci pour ton encadrement de qualité, ton soutien, ta patience, ta pédagogie et ta bonne humeur. Ce fût une expérience très enrichissante d'avoir travaillé à tes côtés. Je te souhaite le meilleur pour le #OrsiLab.

Je veux également remercier Béa qui, pour l'anecdote, fût la première personne à m'avoir parlé d'épigénétique quand j'étais une jeune étudiante en première année de licence. Merci pour ton accompagnement, tes conseils et ton aide au cours de ces années. Merci également à Raphaëlle d'avoir pris le temps de répondre à mes questions, d'avoir passé mes commandes etc. Enfin, merci à vous deux de m'avoir intégré dans cette belle équipe.

Je remercie également les anciens membres de l'équipe. Plus particulièrement Daniel qui est arrivé au bon moment pour m'aider à démarrer cette aventure qu'est la thèse et qui s'est converti en un grand ami. Merci aussi à Fabiola, qui a rajouté une dose de bonne humeur aux journées au labo. J'ai mangé des bons burgers avec cette Latino Team mais j'ai surtout vécu des moments inoubliables avec vous.

Mes chers collègues du M4 RdC, merci d'avoir créé une super ambiance au labo. Je parle, en partie, des gens qui sont venus envahir mon bureau, Marion, Jérôme, Agnès, mais avec qui, malgré la pandémie, j'ai partagé de très bons moments. Merci Jérôme pour avoir égayé les longues journées au labo et pour les nombreuses conversations pouvant aller du fruit préféré jusqu'aux questions les plus philosophiques. Merci Marion, déjà, pour avoir été notre guide LBMC et surtout pour lâcher des phrases mythiques que je ne retranscrirais pas. Merci Victor pour ton soutien et ta patience surtout pendant la rédaction de ce manuscrit.

Quiero por supuesto agradecer a mi familia y amigos quienes, de cerca o de lejos, siempre me han brindado su apoyo.

Agradezco a mis padres por su incondicional apoyo, por enseñarme a perseguir mis sueños y por no dejar que un océano les impida estar siempre a mi lado.

Finalmente, quiero agradecer a la persona que ha estado siempre a mi lado apoyándome, aguantándome, consolándome, ayudándome y un sinnúmero mas de cosas: mi hermana. Gracias por ser mi hogar durante todos estos años y por demostrarme lo que es la valentía.

La thèse, comme la transcription, est un processus complexe, nécessitant de plusieurs étapes et acteurs et rencontrant souvent des obstacles à contourner. Néanmoins ça reste une période riche en créations et en rencontres. Pour moi, la thèse, fût non seulement une période d'intense apprentissage scientifique mais également de croissance personnelle qui m'a laissé beaucoup de leçons. C'est une période qui nous met à l'épreuve et qui n'est pas simple mais qu'avec les bonnes personnes (mentionnées ci-dessus) peut devenir une expérience épanouissante comme elle le fût pour moi.

*¡ Gracias totales!*

*To my sister,  
It got better.*

*« La curiosité est nécessaire à la nature humaine, sans elle, on croupirait dans l'ignorance » -Le Taureau Blanc, Voltaire*

## Résumé :

La régulation dynamique de l'épigénome est à la base de la plasticité cellulaire et permet aux cellules de répondre aux programmes développementaux et de différenciation. Les effecteurs épigénomiques entraînent des changements tels que la modification des queues des histones, le positionnement des histones ou l'incorporation de variants d'histones, ce qui impacte la structure de la chromatine et donc l'expression génique. Cependant, les mécanismes moléculaires sous-jacents restent, en grande partie, inconnus. Un défi majeur du domaine est l'établissement de liens fonctionnels directs entre modificateurs épigénétiques, qui ont tendance à avoir un effet global sur le génome, et expression de gènes effecteurs.

Mon projet de thèse s'est justement basé sur la découverte d'une connexion fonctionnelle entre une série d'effecteurs épigénomiques et un effecteur de la formation du zygote chez *Drosophila melanogaster* : la thiorédoxine maternelle Deadhead (Dhd). Dhd est cruciale pour le remodelage de la chromatine paternelle à la fécondation et donc pour la formation du zygote.

Tout d'abord, un crible génétique basé sur l'expression de shRNAs dans la lignée germinale femelle m'a permis d'identifier : (i) l'histone demethylase Lid/dKDM5 (ii) les membres du complexe déacétylase Sin3A et Rpd3 (iii) la sous-unité Snr1 du remodeleur de la chromatine Swi/Snf et (iv) le facteur chromatinien Mod(mdg4), comme étant essentiels pour l'expression de *dhd*. Pour la suite des analyses je me suis focalisée sur Lid, Sin3A, Snr1 et Mod(mdg4). Des analyses transcriptomiques ont montré que *dhd* est parmi les gènes les plus exprimés dans les ovaires et que cette expression est abolie lors du *knockdown* dans la lignée germinale femelle de *lid*, *sin3a*, *snr1* ou *mod(mdg4)*. De façon remarquable la quantité de gènes dérégulés dans les ovaires *knockdown* est limitée. Ceci suggère que ces complexes ubiquitaires et conservés sont dédiés à la régulation de *dhd* dans ce tissu. Ce cas paradigmatique m'a donc offert une opportunité pour disséquer les mécanismes moléculaires agissant sur le contrôle épigénomique de l'établissement de programmes transcriptionnels spécifiques, comme c'est le cas lors de l'ovogénèse.

Ensuite, en utilisant la méthode de profilage de la chromatine Cut&Run et une stratégie d'analyse de données dédiée, j'ai trouvé que *dhd* est intégré dans un mini-domaine enrichi en marques hétérochromatiques H3K27me3/H3K9me3 et délimité par des éléments régulateurs.

De plus, l'élément régulateur à proximité du promoteur de *dhd* s'est avéré essentiel pour son expression. De façon surprenante, Lid, Sin3A, Snr1 et Mod(mdg4) ont des effets différents sur H3K27me3 et sur ces éléments régulateurs. Néanmoins, j'ai mis en évidence que ces effecteurs activent *dhd* de façon indépendante de H3K27me3/H3K9me3. De plus, j'ai trouvé que ces marques ne sont pas nécessaires pour réprimer *dhd* dans les tissus adultes.

Mes travaux de thèse ont donc révélé plusieurs caractéristiques inhabituelles, au niveau génomique et épigénomique, au locus *dhd*. Cependant je n'ai pas établi un trait unique qui conduise à l'hyperactivation de *dhd* dans la lignée germinale femelle. La régulation de *dhd* dépendrait non pas d'une seule caractéristique mais plutôt d'une combinaison de traits particuliers.

À travers l'exemple de *dhd*, mes travaux démontrent la complexité des processus qu'implique l'activation d'un gène au bon endroit, au bon moment et en bonne quantité. Ils illustrent également la difficulté d'établir des règles générales sur les mécanismes de régulation transcriptionnelle médiés par la chromatine, qui sont très souvent contexte-spécifique.

Mots clés: épigénétique, épigénomique, régulation transcriptionnelle, ovogénèse, *Drosophila melanogaster*, Deadhead, transition ovocyte-zygote

## Summary:

Dynamic regulation of the epigenome underlies cellular plasticity and allows cells to respond to developmental and differentiation programs. Epigenomic effectors can mediate changes such as modification of histone tails, nucleosome positioning or the incorporation of specific histone variants, altering chromatin structure and thus gene expression. Yet, the molecular mechanisms underpinning these processes remain largely unknown. A major challenge in the field is to establish direct functional connections between upstream chromatin factors, which generally have broad impact on chromatin, and the controlled expression of specific cellular effectors.

My PhD project was precisely based on the discovery of a specific functional link between a series of epigenomic effectors and the highly regulated terminal effector of zygote formation in *Drosophila melanogaster*: the maternal thioredoxin Deadhead (Dhd). Dhd is critical to ensure paternal chromatin remodeling at fertilization, and thus zygote formation.

First, an shRNA-based genetic screen in the female germline led me to identify (i) the H3K4me3 demethylase Lid, (ii) the members of the deacetylase complex Sin3A and Rpd3, (iii) the Snr1 subunit of the chromatin remodeler Swi/Snf and (iv) the chromatin factor Mod(mdg4), as essential for the expression of *dhd*. For further analyses I focused on Lid, Sin3A, Snr1 and Mod(mdg4). Transcriptomic analyses showed that *dhd* is among the most highly expressed genes in ovaries and this expression is completely abolished when I deplete Lid, Sin3A, Snr1 or Mod(mdg4) specifically in the female germline. Remarkably, there is a paucity of misregulated genes in *knockdown* ovaries. This suggested that these broadly conserved, ubiquitous complexes are mostly dedicated to regulation of *dhd* in this tissue. This paradigmatic case presented the opportunity to dissect the mechanisms at play in the epigenomic control of the establishment of specific transcriptional programs, as is the one set during oogenesis.

Next, using Cut&Run chromatin profiling with a dedicated data analysis strategy, I found that *dhd* is embedded in a heterochromatic H3K27me3/H3K9me3-enriched mini-domain flanked by DNA regulatory elements, including a *dhd* promoter-proximal element essential for its expression. Surprisingly, Lid, Sin3A, Snr1 and Mod(mdg4) impact H3K27me3 and this regulatory element in distinct manners. However, I showed that these effectors activate *dhd*

independently of H3K27me3/H3K9me3 and that these marks are not required to repress *dhd* in adult tissues.

Altogether, my work uncovered multiple unusual genomic and epigenomic characteristics at the *dhd* locus, but did not identify a single feature that was truly defining ovarian hyperactivation. The dramatic regulation of *dhd* may rely not on an individual trait but rather on a unique combination of such rare features.

Through the example of *dhd*, my work demonstrates the puzzling process that is gene activation in the right place, at the right time and in the right amount. It also illustrates the difficulty to establish general rules on chromatin-based regulatory systems, which are very often context-dependent.

Keywords: epigenetics, epigenomics, transcriptional regulation, oogenesis, *Drosophila melanogaster*, Deadhead, oocyte-to-zygote transition

## Table of Contents

### INTRODUCTION

<b>I. PART I: MECHANISMS OF EUKARYOTIC TRANSCRIPTION</b> .....	<b>16</b>
1. THE PROCESS OF EUKARYOTIC TRANSCRIPTION .....	16
2. PROMOTER-ENHANCER INTERACTIONS REGULATE TRANSCRIPTION .....	19
3. REGULATION OF GENE EXPRESSION BY UNTRANSLATED REGIONS.....	24
<b>II. PART II: SHAPING OF THE CHROMATIN REGULATES GENE TRANSCRIPTION</b> .....	<b>26</b>
1. THE NUCLEOSOME: THE BASIC UNIT OF CHROMATIN .....	26
2. DIVERSITY OF EPIGENOMIC EFFECTORS .....	28
3. NUCLEOSOME DYNAMICS IMPACT TRANSCRIPTION .....	32
4. THE HETEROCHROMATIC H3K9ME3/HP1 PATHWAY.....	37
5. POLYCOMB EFFECTORS MEDIATE GENE SILENCING...AND MORE? .....	42
6. COUNTERACTING REPRESSION TO PROMOTE ACTIVATION.....	47
7. HISTONE PTMS IN ACTIVE TRANSCRIPTION .....	49
A. <i>Histone PTMs during transcription elongation</i> .....	50
B. <i>Is H3K4me3 instructive for transcription activation?</i> .....	51
8. BIVALENT PROMOTERS .....	53
9. GENOME FOLDING AND TRANSCRIPTION.....	55
<b>III. PART III EPIGENOMIC REGULATION DURING D. MELANOGASTER OOGENESIS</b> .....	<b>60</b>
1. MAIN STEPS OF DROSOPHILA OOGENESIS .....	61
2. TRANSCRIPTIONAL PROGRAMS OF NURSE AND FOLLICLE CELLS ARE ESSENTIAL FOR OOCYTE NUTRITION AND MATURATION .	64
3. MECHANISMS OF EPIGENOMIC REGULATION IN THE FEMALE GERMLINE .....	65
A. <i>Silencing of bulk chromatin by the piRNA system</i> .....	65
B. <i>The importance of fine transcriptional regulation during oogenesis</i> .....	67
<b>IV. PART IV THE PECULIAR CASE OF DHD REGULATION</b> .....	<b>70</b>
1. THE ESSENTIAL ROLE OF DEADHEAD AT FERTILIZATION.....	71
2. DHD, A THIOREDOXIN NOT LIKE THE OTHERS.....	73
3. THE INTRICATE DHD LOCUS .....	74
4. STATE-OF-THE ART OF DHD REGULATORS IN TRANSCRIPTION REGULATION.....	77
A. <i>The histone demethylase Lid/dKDM5</i> .....	77
B. <i>The Sin3-HDAC complex</i> .....	79
C. <i>The nucleosome remodeler subunit Snr1</i> .....	80
D. <i>The multifaceted protein Mod(mdg4)</i> .....	81

### RESULTS &DISCUSSION

<b>I. AN SHRNA SCREEN IDENTIFIES MATERNAL CHROMATIN FACTORS REQUIRED FOR THE OOCYTE-TO-ZYGOTE TRANSITION</b> .....	ERREUR ! SIGNET NON DEFINI.
1. ARTICLE PRESENTATION .....	ERREUR ! SIGNET NON DEFINI.

<b>II. THE CONCERTED ACTIVITY OF EPIGENOMIC EFFECTORS IS ESSENTIAL TO ESTABLISH TRANSCRIPTIONAL PROGRAMS DURING OOGENESIS.....</b>	<b>ERREUR ! SIGNET NON DEFINI.</b>
1. ARTICLE PRESENTATION .....	<b>ERREUR ! SIGNET NON DEFINI.</b>
<b>III. ADDITIONAL RESULTS AND DISCUSSION .....</b>	<b>ERREUR ! SIGNET NON DEFINI.</b>
1. IS THERE AN "OVARIAN HYPERACTIVATION CODE"?	<b>ERREUR ! SIGNET NON DEFINI.</b>
2. AN UNUSUAL HETEROCHROMATIC DOMAIN.....	<b>ERREUR ! SIGNET NON DEFINI.</b>
3. DIFFERENT ROLES FOR EPIGENOMIC REGULATORS.....	<b>ERREUR ! SIGNET NON DEFINI.</b>
4. AN APPROACH TO PROFILE REGULATORY ARCHITECTURE OF CHROMATIN DOMAINS. ....	<b>ERREUR ! SIGNET NON DEFINI.</b>
<b>GENERAL CONCLUSION .....</b>	<b>211</b>
<b>REFERENCES.....</b>	<b>212</b>

# Abbreviations

CDS: CoDing sequence

ESCs: Embryonic Stem Cells

GSC: Germ Stem Cell

GTF: General Transcription Factors

HAT: Histone Acetyltransferase

HDAC: Histone DeAcetylase

HDMT: Histone DeMethylase

HMT: Histone Methyltransferase

HP1: Heterochromatin Protein 1

IBP: Insulator Binding Protein

NDR: Nucleosome Depleted Region

PcG: Polycomb Group

piRNA: piwi-RNA

PRC: Polycomb Repressive Complex

PRE: Polycomb Response Element

PTM: PostTranslational Modification

RNA Pol: RNA Polymerase

shRNA: short hairpin RNA

siRNA: small interference RNA

SNBPs: Sperm Nuclear Basic Proteins

TAD: Topologically Associated Domain

TE: Transposable Element

TF: Transcription Factor

TrxG: Trithorax Group

TSS: Transcription Start Site

# INTRODUCTION

<b>I. PART I: MECHANISMS OF EUKARYOTIC TRANSCRIPTION.....</b>	<b>16</b>
1. THE PROCESS OF EUKARYOTIC TRANSCRIPTION.....	16
2. PROMOTER-ENHANCER INTERACTIONS REGULATE TRANSCRIPTION.....	19
3. REGULATION OF GENE EXPRESSION BY UNTRANSLATED REGIONS.....	24
<b>II. PART II: SHAPING OF THE CHROMATIN REGULATES GENE TRANSCRIPTION.....</b>	<b>26</b>
1. THE NUCLEOSOME: THE BASIC UNIT OF CHROMATIN.....	26
2. DIVERSITY OF EPIGENOMIC EFFECTORS.....	28
3. NUCLEOSOME DYNAMICS IMPACT TRANSCRIPTION.....	32
4. THE HETEROCHROMATIC H3K9ME3/HP1 PATHWAY.....	37
5. POLYCOMB EFFECTORS MEDIATE GENE SILENCING...AND MORE?.....	42
6. COUNTERACTING REPRESSION TO PROMOTE ACTIVATION.....	47
7. HISTONE PTMS IN ACTIVE TRANSCRIPTION.....	49
A. <i>Histone PTMs during transcription elongation.....</i>	<i>50</i>
B. <i>Is H3K4me3 instructive for transcription activation?.....</i>	<i>51</i>
8. BIVALENT PROMOTERS.....	53
9. GENOME FOLDING AND TRANSCRIPTION.....	55
<b>III. PART III EPIGENOMIC REGULATION DURING <i>D. MELANOGASTER</i> OOGENESIS.....</b>	<b>60</b>
1. MAIN STEPS OF DROSOPHILA OOGENESIS.....	61
2. TRANSCRIPTIONAL PROGRAMS OF NURSE AND FOLLICLE CELLS ARE ESSENTIAL FOR OOCYTE NUTRITION AND MATURATION.....	64
3. MECHANISMS OF EPIGENOMIC REGULATION IN THE FEMALE GERMLINE.....	65
A. <i>Silencing of bulk chromatin by the piRNA system.....</i>	<i>65</i>
B. <i>The importance of fine transcriptional regulation during oogenesis.....</i>	<i>67</i>
<b>IV. PART IV THE PECULIAR CASE OF <i>DHD</i> REGULATION.....</b>	<b>70</b>
1. THE ESSENTIAL ROLE OF DEADHEAD AT FERTILIZATION.....	71
2. DHD, A THIOREDOXIN NOT LIKE THE OTHERS.....	73
3. THE INTRICATE <i>DHD</i> LOCUS.....	74
4. STATE-OF-THE ART OF DHD REGULATORS IN TRANSCRIPTION REGULATION.....	77
A. <i>The histone demethylase Lid/dKDM5.....</i>	<i>77</i>
B. <i>The Sin3-HDAC complex.....</i>	<i>79</i>
C. <i>The nucleosome remodeler subunit Snr1.....</i>	<i>80</i>
D. <i>The multifaceted protein Mod(mdg4).....</i>	<i>81</i>

Germ cells retain the potential to reproduce an entire organism upon fertilization. Gametogenesis represents thus an extreme cellular differentiation process where complex transcriptional programs must be tightly regulated. Chromatin-based regulation of gene expression and thus epigenomic effectors are crucial in the establishment of specific transcriptional programs in the female germline. Yet, the molecular mechanisms underpinning this regulation remain largely unknown. A major challenge in the field is to establish direct functional connections between upstream chromatin factors, which generally have a broad impact on chromatin, and the controlled expression of highly specialized terminal effectors. My PhD project was precisely based on the discovery of a specific functional connection between a series of epigenomic effectors and the highly regulated terminal effector of zygote formation in *Drosophila melanogaster*: the maternal thioredoxin Deadhead (Dhd). In this introduction I will first describe the mechanisms of eukaryotic transcription followed by the presentation of chromatin-based regulatory mechanisms of gene expression. Next, I will focus on the importance of transcriptional regulation during oogenesis. I will finish by the presentation of the maternal thioredoxin Deadhead and its epigenomic regulators.

## **I. PART I: Mechanisms of eukaryotic transcription**

The DNA molecule carries the genetic information necessary for an organism's development and functioning. Yet, in multicellular organisms, each cell has specific features that define its identity and function. Therefore, information stored in the DNA molecule needs to be used at the right place at the right time. Indeed, gene expression is temporarily, spatially and quantitatively regulated. Various factors affect gene expression and regulation can be exerted at transcriptional, post transcriptional and post translational levels. My case study, the *dhd* gene, is a hyperactivated gene, it is thus important to put it in perspective the mechanisms of transcription, which is the focus of these paragraphs.

### **1. The process of eukaryotic transcription**

Globally, the process of transcription can be divided into three main steps: initiation, elongation and termination. During initiation, the RNA polymerase (RNA Pol) complex is formed on the gene's promoter with the help of general transcription factors (GTFs), resulting in the assembly of the Pre-initiation complex (PIC), which begins transcription and can go into pause. Next, throughout the elongation step, the RNA Pol moves along the template strand, synthesizing the RNA molecule. The polymerase continues transcribing until it reaches the terminator sequence. Finally, the nascent mRNA and the RNA Pol II are released constituting the termination step (Fig1). Transcription is thus a multistep process and all these steps can undergo regulatory control that depends on the gene, the cell type, as well as internal and external signaling.

In eukaryotes not all genes are transcribed by the same polymerase. Three RNA polymerases (RNA Pol I-III) have been identified, differing in their subunit composition and targeting different classes of genes (Sentenac, 1985) RNA Pol I transcribes ribosomal RNAs, RNA Pol II transcribes protein coding genes and some non-coding RNAs and finally, RNA Pol III transcribes small ribosomal 5S RNA, tRNAs and other small non-coding RNAs. On the contrary, prokaryotes use the same RNA Pol to transcribe all their genes. This reflects the increased complexity that is regulation of gene expression in eukaryote systems. Why develop different enzymes? Differences in the structure and composition of the three RNA Pol are linked to the genes they transcribe. For example, to abundantly synthesize tRNAs, RNA Pol III must efficiently terminate and re-initiate transcription on the short genes it targets. Structural analysis of this enzyme revealed that specific subunits permit a loose binding of the RNA:DNA hybrid thereby allowing a fast termination of transcription (Arimbasseri and Maraia, 2016; Hoffmann et al., 2015). Also, two RNA Pol I-specific subunits are needed for the high polymerase loading rate and enhancement of the rRNA gene transcription cycle (Albert et al., 2011). At last, RNA Pol II targets a large set of differently regulated genes, including protein-encoding genes, which is why it has been of particular interest for the study of the regulation of gene expression and will be the main focus of the next paragraph.

RNA Pol II is composed of 12 subunits Rpb1-12 (RNA polymerase B) and is conserved from yeast to human. The largest subunit Rpb1 has a C-terminal domain (CTD) containing a repeat sequence of 7 amino acids (Tyr1-Ser2-Pro3-Thr4-Ser5-Pro6-Ser7) necessary for the proper functioning of RNA Pol II (Hsin and Manley, 2012). Specific residues in the CTD repeats can be phosphorylated and these post-translational modifications (PTM) play an important

role in the regulation of RNA Pol II activity during the transcription cycle (Fig1) (Buratowski, 2009; Hsin and Manley, 2012). Deletion of the RNA Pol II's CTD, negatively affects mRNA processing, including capping, cleavage/polyadenylation and splicing (S. McCracken et al., 1997; Susan McCracken et al., 1997), indicating thus a crucial role in mRNA processing. First, phosphorylation of serine 5 (Ser5P) is found concomitant with transcription initiation and it has been shown that this modification recruits and stimulates capping machinery at the nascent pre-mRNA. This mark is also important for initial RNA Pol II progression through DNA by the unbinding of the specific proteins that recruited it. During elongation Ser5P undergoes progressive dephosphorylation coincident with the release of 5' processing factors. Next, phosphorylation of Ser2 marks the elongation phase of transcription and is increasingly enriched towards the ends of genes. It has been observed that Ser2P is required for the recruitment of polyadenylation factors to the 3' end of genes in vivo (Ahn et al., 2004). Additionally, genome-wide ChIP experiments showed that peaks of 3' processing factors followed Ser2P peaks, consistent with the view that CTD Ser2P contributes to the recruitment of the polyadenylation complex (Mayer et al., 2012, 2010). Also, Ser7 phosphorylation is found early in transcription initiation and retained until transcription termination in all RNA Pol II-dependent genes. However, this mark has been found to be particularly required for expression of a sub-class of genes encoding small nuclear (sn)RNAs, where it facilitates recruitment of the gene-specific Integrator complex (Egloff et al., 2012, 2007). Finally, hypophosphorylation of the CTD is a prerequisite for RNA pol II to enter the preinitiation complex therefore at the end of the transcription cycle, the regeneration of the hypophosphorylated state of the CTD is critical for RNA Pol II recycling. In conclusion, the CTD "code" allows the coupling of transcription with co-transcriptional RNA processing through the timely recruitment of the appropriate factors at the right point of the transcription cycle. Transcription dynamics, efficiency and rate can thus be regulated, in part, by modifying the enzyme that synthesizes the RNA molecule.

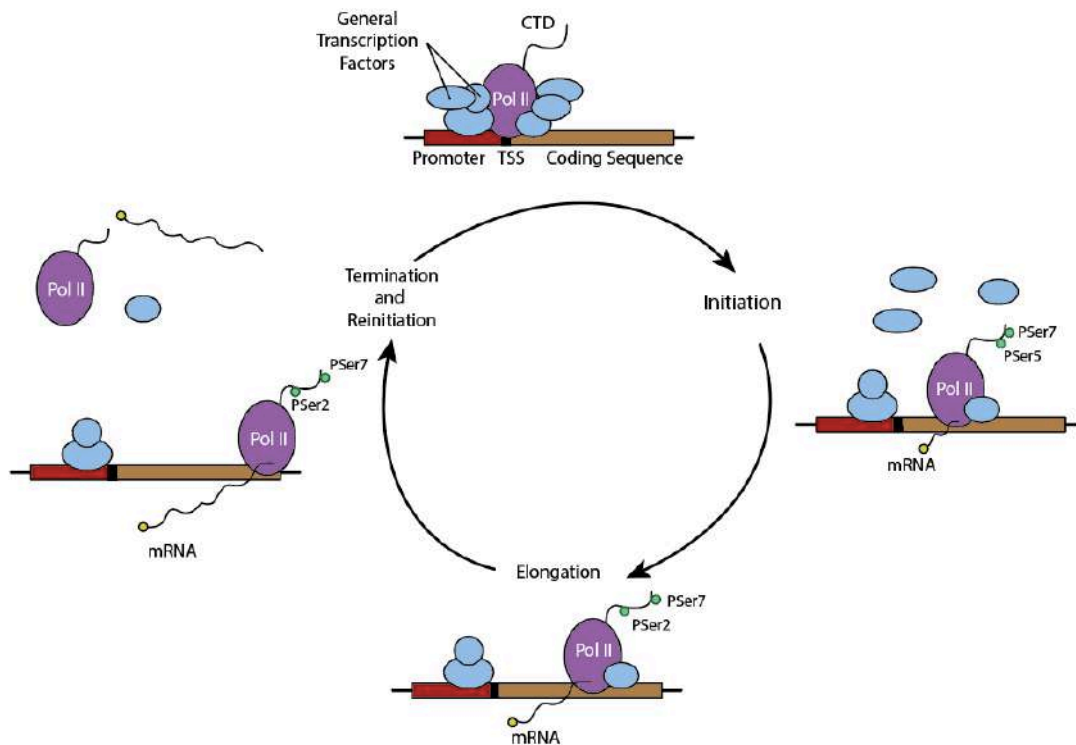


**Fig1-Schematic representation of the main steps of the RNA Pol II transcription cycle.**

The main steps of the transcription cycle: initiation elongation and termination. Phosphorylations of Serines 2, 5 and 7 on the RNA Pol II C-terminal domain (CTD) are shown. RNA Pol II binds the gene promoter assisted by general transcription factors (GTFs). The polymerase is released and begins active RNA synthesis throughout the elongation phase. Finally, polymerase is dephosphorylated and released along with the mRNA and can be recruited for a new cycle (inspired from Chang Hongh, 2016).

## 2. Promoter-Enhancer interactions regulate transcription

Promoters are DNA sequences that define where transcription of a gene by the RNA Pol begins. Indeed, transcription initiates at a defined positioned, the transcription start site (TSS) located at the 5' end of a gene. The TSS is embedded within a core promoter which is the minimal stretch of contiguous DNA sequence sufficient to direct transcription initiation. The core promoter serves as a binding platform for the assembly of the transcription machinery. Indeed, general transcription factors (GTFs) bind DNA sequences at the core promoter elements and subsequently recruit the RNA Pol II to form the preinitiation complex (Matsui et al., 1980; Orphanides et al., 1996). However, core promoters generally have low basal activity that can be activated by enhancers (Banerji et al., 1981; Shlyueva et al., 2014). Enhancers are segments of DNA that enable transcriptional regulation in a spatio-temporal

manner. Central to the communication between enhancer and promoters are transcription factors (TFs) and cofactors (Haberle and Stark, 2018). TFs are DNA binding proteins, recognizing specific sequence motifs on promoters and enhancers which in turn recruit cofactors having a variety of biochemical functions. These are thus central effectors of transcriptional regulation. Therefore, to better understand transcriptional regulation it is important to gain insight on all these regulatory elements and their interactions.

Computational analyses of core promoters in fly (Ohler et al., 2002) and human (FitzGerald et al., 2006) have revealed a series of over-represented sequence motifs in these regions. For example, the TATA-box is a core promoter element recognized by one of the GTFs that mediates RNA Pol II recruitment. It has a well-defined position and might thereby determine the choice of TSS at a fixed downstream position. Although it is a well conserved element from yeast to human it is found only at a minority of core promoters, in flies they correspond to ~5% of core promoters (FitzGerald et al., 2006; Ohler et al., 2002). A more widely used element is the initiator (Inr) motif. Although its consensus sequence differs between flies and humans, this element, as the TATA-box, has a well-defined position, that in this case, overlaps with the TSS (FitzGerald et al., 2006). In promoters that lack a TATA-box, the Inr motif is often accompanied by another motif, the downstream promoter element (DPE), which is positioned downstream of the TSS (Burke and Kadonaga, 1996) and functions cooperatively with the Inr for GTFs binding. Increasing or decreasing of one nucleotide the spacing between the Inr and DPE results in reduced binding of GTFs and decrease in transcriptional activity (Kutach and Kadonaga, 2000), indicating thus the importance of a strict Inr–DPE spacing. In addition to these three most abundant core promoter motifs, other motifs either with defined positions relative to the TSS or not, have been identified showing the variety of core promoters.

Interestingly, TATA-box and DPE rarely co-occur in flies, they were thus suggested to be associated with functionally distinct groups of genes (FitzGerald et al., 2006; Ohler et al., 2002). This raised thus the question of the association of core promoters and gene function. Integrating data of sequence composition and motifs with other properties including transcription initiation pattern (focused or dispersed), chromatin configuration and gene function revealed three main types of core promoter in metazoa (Fig2) (Haberle and Stark, 2018; Vo ngoc et al., 2017). First, promoters found at adult tissue-specific genes and differentiated cell-specific genes, characterized by TATA-box and Inr motifs, sharp initiation

patterns and imprecisely positioned nucleosomes (see section II-3). Second, promoters of broadly expressed housekeeping genes, in flies were enriched for the motifs DRE (DNA replication-related element) and ohler 1/6 and in mammals they overlapped with CpG islands. They were also associated with dispersed transcription initiation and a well-defined nucleosome-depleted region. Third, core promoters of developmental TFs, in mammals they resemble to housekeeping gene core promoters. In flies, they tend to contain a DPE motif and focused initiation of transcription. There is thus a correlation between features of core promoters and gene function. Notably, a bias between gene function and specificity of promoter-enhancer interaction has also been observed. Zabidi and colleagues studied this specificity on a genome-wide scale, by high-throughput genome-wide screening of enhancer activity in housekeeping and developmental core promoters (Arnold et al., 2013; Zabidi et al., 2015). Their study revealed different motif enrichment in both core promoters and enhancers between housekeeping and developmental genes (summarized in Table1). Developmental and housekeeping core promoter enhancer elements also show proximity bias. Enhancer sequences activating developmental core promoters appeared to be gene promoter-distal while enhancers activating housekeeping core promoters were generally found proximal to the gene promoter (Arnold et al., 2013). This suggests that some transcriptional enhancers exhibit preferences for certain core promoter elements. Overall, these data show that specific features of cis regulatory elements are linked to gene function. However, the mechanisms of how these features can influence a specific transcription pattern are yet to be elucidated.

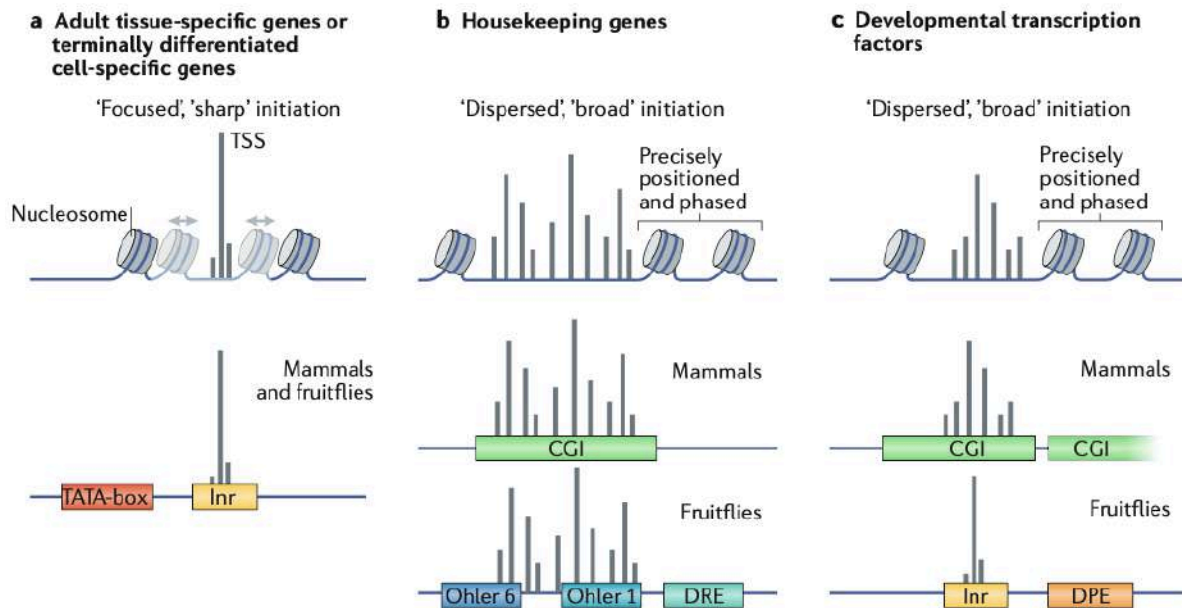


**Fig2-Three types of core promoters in metazoa**

Main categories of core promoters in *Drosophila* and mammals based on different properties, including initiation pattern (focused or dispersed), sequence composition motifs and gene function (Haberle and Stark, 2018).

	dCP enhancers	hkCP enhancers
Target gene function	Signaling, patterning, morphogenesis	House-keeping
Enhancer location	Distal or intronic	Promoter-proximal
Target gene promoter motifs	TATA, Inr, MTE, DPE	DRE, TCT, others
Enhancer motifs	GAGA (GAGAG)	DRE (TATCGATA)
Transcription factors	Trithorax-like (Trl) / GAF	DRE binding factor (Dref)

**Table 1: Summary of differences between developmental and housekeeping core promoters and their enhancers.**

(From Lorberbaum and Barolo 2015 based on the result by Zabidi et al., 2015).

Enhancers can be located near the promoter of their cognate gene or be distally positioned. Distances can vary from a few kb to several megabases. Active promoters however, are often in spatial proximity to their enhancer and the establishment of these contacts are tightly linked to 3D organization of DNA in the nucleus (mechanisms to achieve genome folding will be detailed in section II-9).

The regulatory input that core promoters receive from enhancers is mediated by TF binding both of these elements and by transcriptional cofactors, which are recruited by TFs through protein–protein interactions (Fig3). Importantly, cofactors often have enzymatic activities and can post-translationally modify components of the transcription machinery and the surrounding nucleosomes. It has been observed that the Mediator complex, a cofactor, recruited to enhancers and interacting with core promoters can increase RNA Pol II recruitment and PIC assembly (Eychenne et al., 2016), thereby increasing transcription rate. Mediator in yeast can stimulate phosphorylation of Ser5 at the CTD of RNA Pol II (Esnault et al., 2008), which is important for mRNA processing and RNA Pol II progression through the transcription cycle. The interaction between bound TFs and recruited cofactors can thus lead to transcription activation.

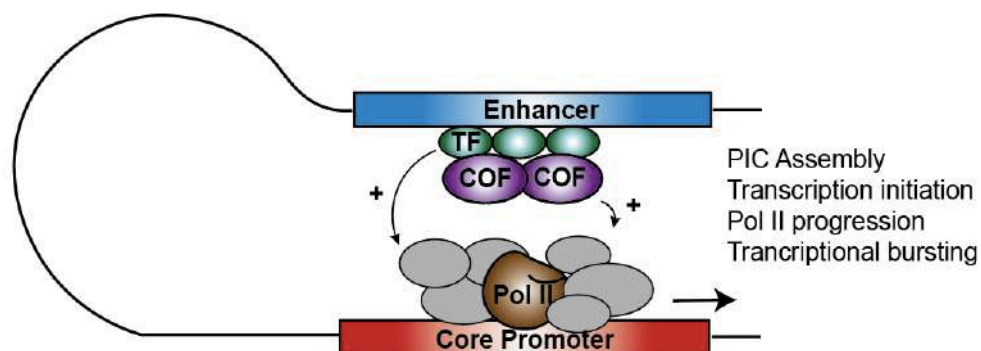


**Fig 3-Enhancers communicate with promoters through transcription factors and cofactors.** Enhancers and promoters can bind transcriptional factors (TF) which in turn bind cofactors (COF) thereby mediating enhancer-promoter communication. This communication results in stimulation of transcription via different mechanisms such as PIC assembly, transcription initiation, stimulation of RNA Pol II progression or modulation of transcriptional bursts.

Another mechanism through which enhancers can regulate promoter activation is by modulating transcription bursts. Transcription is episodic consisting on short but intense

“bursts”, which comprise initiation events separated by periods of inactivity (Chubb et al., 2006; Raj et al., 2006). Patterns of these bursts can have important roles in development. For example, when visualizing transcription in living fly embryos, it was observed that lengthening of transcriptional activity periods is important for the establishment of boundaries during embryo patterning (Lucas et al., 2013). It is therefore important to understand how these “bursts” are regulated. Another study in living *Drosophila* embryos revealed that the levels of gene activity depend on the frequency of transcriptional bursts and that this frequency can be regulated by enhancers (Fukaya et al., 2016). The authors evaluated the effect of different developmental enhancers on transcriptional bursting of a reporter gene, and observed that enhancers produced transcriptional bursts with similar amplitudes and duration but generated different bursting frequencies, with strong enhancers producing more bursts than weak enhancers. This result suggests thus that regulation of bursting frequencies by enhancers can be a parameter of gene control. Moreover, it was observed that mutations in the TATA-box led to a decrease in burst size, that is the number of transcribing RNA Pol II molecules per burst (Hornung et al., 2012), suggesting that burst size is a promoter-specific property. These data show that several factors can influence transcription bursts, either in frequency or in amplitude and thereby regulate the transcriptional output. Further research will be needed to fully understand the mechanisms regulating transcriptional bursts.

### 3. Regulation of gene expression by untranslated regions

Additional sequences within the gene can also provide a regulatory point for transcription. Majority of eukaryotic genes contain introns. The process of removing introns is energy and time-consuming, however, these elements have been evolutionary conserved which is indicative of a biological functional role. The most obvious advantage they confer is increasing the repertoire of proteins through alternative splicing, meaning that a single gene can produce multiple isoforms of a protein depending on cell type and environment (Nilsen and Graveley, 2010). Additional research in the field has associated introns to a variety of functions such as protection against environmental stress, or as the source of non-coding RNAs (Dwyer et al., 2021). A third role for introns, well established in the literature, is their function in regulating gene expression. It has been observed in yeast that in a physiological

context, genes require promoter proximal introns for full transcriptional output (Furger et al., 2002). Additionally, a quantitative analysis of constructs containing a human intron in the open reading frame of a reporter gene, revealed that its presence increased not only the accumulation of mature mRNA but also the efficiency of their translation (Nott, 2003). The capacity of introns to increase gene expression has been observed in many eukaryotes including mammals, plants, yeast, and insects (Shaul, 2017), however the underlying mechanisms are not fully elucidated. Studies in budding yeast have started to provide hints for the mechanisms at play. It was observed that the presence of an intron within a gene results in formation of a multi-looped gene architecture. When looping is defective, these interactions are abolished and there is no enhancement of transcription despite normal splicing (Agarwal and Ansari, 2016). Introns are thus important players in the regulation of gene expression.

Furthermore, the 5' and 3' untranslated regions (UTR) located at the extremities of a given gene have also been involved in the regulation of expression. A study investigated the role of alternative 5'UTRs of the same gene on mRNA translation efficiency with an *in vivo* reporter assay (McClelland et al., 2009). They observed that among the 5'UTRs tested, three enhanced translation while two had repressive effects. Modeling of the mRNA secondary structure in the 5'UTR revealed the presence of compact structures around the start codon in the repressive 5'UTRs. Translational efficiency was also found inversely correlated to 5'UTR length. Additionally, genome-wide studies in human revealed differences in structure and nucleotide content of 5'UTRs of housekeeping and developmental genes (Ganapathi et al., 2005). *In silico* comparisons of genes with low and high levels of protein output showed that 5'UTRs that enable efficient translation are short, have low GC content, are relatively unstructured, and do not contain upstream AUG codons (Kochetov et al., 1999). Although mechanisms describing how 5'UTR sequence can influence transcription are not well understood, these data suggest a correlation between this gene element and regulation of transcription. The 3'UTR, situated downstream of the protein coding sequence, has also been involved in the regulation of gene expression. Indeed, the poly(A) tail at the 3' end mRNAs provide a binding platform for poly(A) binding proteins (PABP) that have roles in mRNA export, stability, decay and translation (Gorgoni, 2004; Mangus et al., 2003). For example, PABP mRNAs can bind poly(A) tracts in their own 5'UTRs, resulting in translational repression. Moreover, in human, it was observed that the generation of alternative 3' UTR isoforms is a characteristic of ubiquitously transcribed genes that are involved in diverse gene

regulatory processes and are distinct from the classical housekeeping genes that generate single UTRs (Lianoglou et al., 2013). These ubiquitously transcribed multi-UTR genes use different 3' UTR isoforms to achieve tissue- and context-dependent expression. Changes in the 3'UTR isoform expression represents thus a component of gene expression programs. Altogether, these data shows that untranslated regions can have an important role in transcriptional regulation but mechanisms are yet to be elucidated.

To conclude, transcription is a complex process that can be modulated by regulatory elements encoded within the DNA molecule and by the binding of specific proteins. However, DNA is not naked in the nucleus but wrapped around histone proteins. This structure represents thus a major point of transcriptional regulation.

## **II. Part II: Shaping of the chromatin regulates gene transcription**

### **1. The Nucleosome: the basic unit of chromatin**

The basic unit of organization of chromatin is the nucleosome, formed of 146 bp of DNA that wrap around an octamer of histones. This octamer is composed of two copies of the four “core histones”: H2A, H2B, H3 and H4. Additionally, linker DNA between two nucleosome cores is bound by the linker histone H1 (Fig4). Histones have positively charged surfaces formed by basic amino acid side chains which allow them to interact with the negatively charged DNA backbone forming thus a highly tight bound.

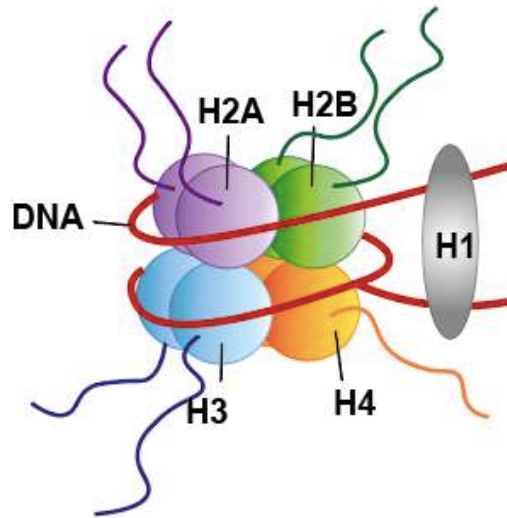


**Fig4-Schematic representation of the nucleosome.**

The nucleosome core is composed of 146 bp of DNA wrapped around a histone octamer containing two H2A-H2B dimers and two H3-H4 dimers. Linker DNA between two nucleosome cores is bound by the linker histone H1.

The amino acid sequences of the core histones (H2A, H2B, H3 and H4) are extremely well conserved in evolution. Histones are small proteins (10-15 kDa) that share a globular domain with a  $\alpha$ -helical arrangement called histone fold, implicated in histone dimerization (Arents et al., 1991; Luger et al., 1997). Importantly, core histones possess flexible N-terminal regions, called histone tails, that associate more loosely with the nucleosome and remain accessible for posttranslational modifications. The most well-studied histone modifications include acetylation, phosphorylation, methylation, and ubiquitylation, although many other modifications have been reported. These modifications play a central role in the regulation of gene expression as well as many other DNA processes such as repair, replication and recombination (Bannister and Kouzarides, 2011). Notably, these histone modifications are reversible by specific enzymes giving the possibility of a dynamic and fine regulation of transcription.

Nucleosome composition can be altered by the insertion of histone variants (Martire and Banaszynski, 2020; Talbert and Henikoff, 2017). These are encoded by a different set of genes and show slight variations in the amino acid sequence. Different variants of histones can be incorporated. Variations of histone H3 and histone H2A are common while histones H2B and H4 appear to be predominantly canonical.

To date, the H2A family contains the greatest sequence diversity of identified variants. The variant H2A.Z, H2Av in *Drosophila*, is present in almost all organisms and has been associated to diverse transcriptional states. Indeed, several studies have shown that H2A.Z nucleosome occupancy at promoters is inversely correlated with transcription (Guillemette et al., 2005; Zhang et al., 2005). However, it has also been observed that H2A.Z is required for activation of heat shock genes during heat shock responses (Zhang et al., 2005) and that it can promote the recruitment of the RNA Pol II (Adam et al., 2001). Additionally, in *Drosophila*, the presence of H2Av, the homolog of H2A.Z (van Daal et al., 1988), correlates with paused RNA Pol II (Mavrich et al., 2008). It was later observed that H2Av occupies the promoter in absence of gene expression but it decreases upon gene induction (Kusch et al., 2014). Together, these results suggest that the role of H2A.Z may be to recruit Pol II and poise genes for activation.

Histone H3 possesses two universal variants. First, CENP-A, who is found at chromosome centromeres and is important for cohesin recruitment at these regions (Santaguida and Musacchio, 2009). Second, H3.3 enriched at gene bodies and regulatory elements such as promoters and enhancers (Ahmad and Henikoff, 2002; Mito et al., 2007), suggesting an association with active transcription. Although, absence of H3.3 in *Drosophila* led to transcriptional defects, the latter could be compensated by increased expression of variant H3.1 (Sakai et al., 2009). This suggests that transcription was affected by lack of histone replacement rather than by the variant of H3. Additionally, H3.3 has also been found at transcriptionally silent regions such as telomeres and centromeres (Goldberg et al., 2010; Szenker et al., 2012). These data suggests thus that the link of H3.3 with transcription is more complex than initially thought. Overall, even though the mechanisms are not fully elucidated, histone variants can influence transcription and have thus functional roles in the genome.

Dynamic histone PTMs and variants contribute to the complexity of epigenetic regulation of the genome. Chromatin dynamics is mediated by epigenomic effectors it is thus crucial to understand how these factors work.

## 2. Diversity of epigenomic effectors

The chromatin is highly dynamic and can be shaped to respond to the needs of the cells through a wide variety of mechanisms that will be detailed throughout this manuscript. Accordingly, the molecular actors behind chromatin shaping are also very varied. They can essentially be classified in three main categories: histone modifiers, nucleosome remodelers and histone chaperones. During my PhD I also focused on insulator binding proteins, that even though they do not interact with histones, they are also important for the organization of the chromatin landscape. I will thus also describe this category.

**Histone modifiers**: Histone PTMs play vital roles in regulating both gene activation and repression. These modifications are reversible which helps fine-regulate gene transcription according to specific cues. Over the years a plethora of histone modifiers i.e., enzymes catalyzing changes in histone PTMs have been identified. These epigenetic players have been categorized as writers: that introduce various chemical modifications on histones, readers: the specialized domain containing proteins that identify and interpret those modifications and erasers: the dedicated group of enzymes proficient in removing these chemical tags. Writers and erasers are divided into classes on the basis of the specific PTM they effect (Fig5) (Bannister and Kouzarides, 2011; Biswas and Rao, 2018). The corresponding enzymatic activities are referred to as histone acetyltransferases (HATs), histone methylases (HMTs), histone kinases and histone ubiquitin-transferases. Analogously, erasers comprise histone deacetylases (HDACs) histone demethylases (HDMs, or KDMs for lysine demethylases) phosphatases and deubiquitinating enzymes. In general, HDACs have relatively low substrate specificity by themselves, a single enzyme being capable of deacetylating multiple sites within histones. HKMTs and HKDMs on the contrary possess a high level of substrate specificity with respect to their target lysine.

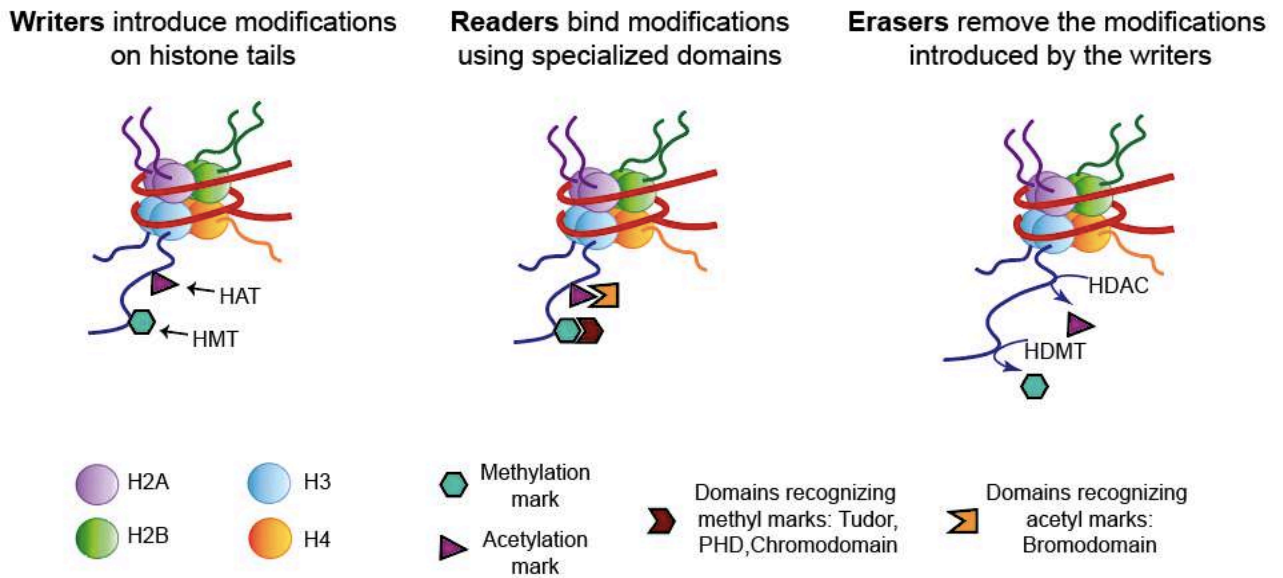


**Fig 5-Actions of epigenetic writers, readers and erasers.**

Enzymes and proteins capable of adding, binding or removing posttranslational modifications on histone tails are known as writers, readers and erasers respectively. Examples for methylation and acetylation are represented. HAT: histone acetyltransferase, HMT: histone methyltransferase, HDAC: histone deacetylase, HDMT: histone demethylase (modified from Biswas and Rao, 2018).

**Nucleosome remodelers** are a category of enzymes capable of altering DNA-histone interactions at target nucleosomes, thereby locally and differentially regulating access to DNA. Remodelers can (i) mediate nucleosome sliding i.e., the translational movement of a nucleosome in either direction to expose a region that was previously occluded, (ii) exchange a core histone for a variant histone and (iii) induce eviction of a nucleosome to expose the associated DNA (Fig6). A conserved feature among remodelers is the use of the energy from ATP hydrolysis to achieve these reconfigurations (Becker and Workman, 2013; Clapier and Cairns, 2009).

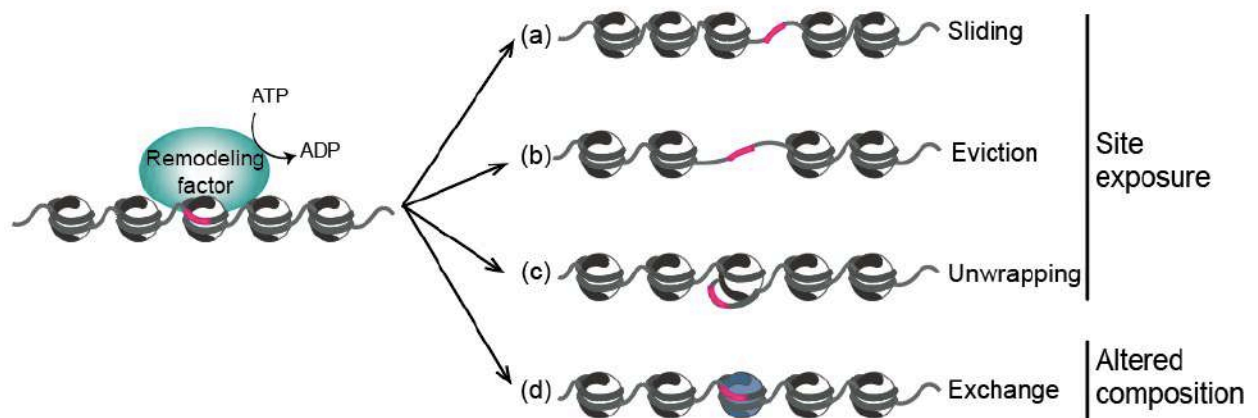


**Fig6-Outcomes of nucleosome remodeling**

Models for nucleosome remodeling. Remodelers (green) alter nucleosome-DNA interactions in an ATP-dependent manner. They mediate: (a) nucleosome sliding, the translational movement of a nucleosome, (b) nucleosome eviction, (c) localized unwrapping or (d) nucleosome exchange. Processes (a) to (c) lead to DNA site exposure while (d) results in altered composition of the nucleosome (modified from Clapier and Cairns, 2009).

**Histone chaperones** are proteins that handle non-nucleosomal histones *in vivo*. They accompany and safeguard histones throughout their cellular life. Histone chaperones escort histones, preventing them from aggregating or from spurious interactions with DNA (Hammond, 2017). Importantly, histone chaperones are necessary for deposition of canonical histones as well as of histone variants into particular places in the genome thereby participating in the regulation of chromatin processes. Interestingly, the conserved histone chaperone CAF-1 complex involved in the assembly of H3-H4 histone dimers on newly synthesized DNA, has also been found to participate in the maintenance of heterochromatin through interaction with heterochromatin effectors in fly (Roelens et al., 2017). Overall, this shows the importance of chromatin dynamics regulation by histone chaperones.

**Insulators** are conserved DNA elements that help organize eukaryotic genomes into physically and functionally regions through diverse mechanisms. They are thought to act by recruiting specific Insulator Binding Proteins (IBPs). The first IBP to be discovered was the CCCTC-binding factor (CTCF). To date, CTCF remains the major protein implicated in insulation in vertebrates (Lobanenkov et al., 1990). On the contrary, in flies, various insulator sequences have been identified and classified according to the proteins they bind. Experiments in *Drosophila* have identified a dozen or more IBPs binding specific DNA

sequences (Melnikova et al., 2020; Özdemir and Gambetta, 2019). They were identified based on their ability to bind to characterized insulators and mediate their function or in genetic screens as being required for the function of a specific insulator. Interestingly, most of these proteins are also classified as transcription factors, such as the conserved dCTCF/CTCF or the GAGA factor (GAF). While most IBPs exhibit direct DNA binding, additional proteins were identified as necessary for insulator activity. This is particularly the case for the cofactors CP190 and Mod(mdg4) which are required along with the DNA-binding protein Su(Hw) at the gypsy transposon for proper insulator function (Georgiev and Gerasimova, 1989; Gerasimova et al., 1995; Pai et al., 2004). Subsequently, studies have shown that CP190 is common to almost all insulators (Ahanger et al., 2013). At least one of the roles of these co-factors is to mediate homotypic and heterotypic protein-protein interactions bridging thus contacts between distant genomic regions. Initially, insulators were defined as having either an enhancer blocker role or a barrier role between euchromatin and heterochromatin. However, extensive research has now associated insulators to broader functions in nuclear biology, such as nuclear organization.

Chromatin dynamics enables the cell to tightly regulate fundamental activities of the genome. It is thus the concerted activity of epigenomic effectors (modifiers, remodelers, chaperones) along with nuclear organizing proteins (insulators), that achieve fine gene regulation. Malfunctioning of these machineries is tightly linked to diseases such as cancer or intellectual disability. It is thus crucial to understand the molecular mechanisms mediated by epigenomic effectors to modulate transcription.

### 3. Nucleosome dynamics impact transcription

An unavoidable side effect of the structural organization of chromatin is the occlusion of DNA sequences and thus of its regulatory elements and binding sites. Nucleosomes represent a barrier for RNA Pol II progression, therefore, the coordination of histones sliding, leaving, recycling, depositing and positioning together with RNA Pol II passage is crucial in defining transcriptional activity (Fig7).

Nucleosome positioning and composition are regulated processes that can reflect DNA-related activities such as transcription. Genome-wide analyses of nucleosome landscapes have revealed a general feature of eukaryotic promoters. Two well-positioned nucleosomes, designated “+1” and “-1”, separated by a nucleosome-depleted region (NDR) of variable length, demarcate the site of transcription initiation (Jiang and Pugh, 2009). In yeast, a nucleosome is part of the TSS [Albert et al., 2007] while in higher metazoans the TSS does not overlap with a nucleosome, but there is one just downstream (Mavrich et al., 2008).

What determines nucleosome positioning? Some DNA sequences like poly(dA:dT) stretches are unfavorable to DNA wrapping around histones *in vitro* and AT-rich sequences are good predictors of nucleosome-depleted regions *in vivo* (Segal and Widom, 2009). Additionally, DNA-binding activator proteins can recruit nucleosome remodelers and generate nucleosome-depleted regions (Schwabish and Struhl, 2007). Importantly, elongation by RNA Pol II needs cycles of disassembly/reassembly of nucleosomes in coding regions. This complex process implies nucleosome disruption, mobilization and reassembly after the RNA Pol II passage. As a result, a decrease on nucleosomal density can be observed at highly transcribed genes (Lee et al., 2004; Schwabish and Struhl, 2004). Additionally, high rates of histone turnover have been observed at active genes while repressed regions showed low histone turnover in ESCs and *Drosophila* cells (Deal et al., 2010; Deaton et al., 2016). A recent study has shown that transcription is the major cause of old histones eviction, with a more pronounced effect on the variant H3.3 than on the canonical H3.1 (Torné et al., 2020). The authors also described a mechanism ensuring histone recycling and new deposition dependent on the histone chaperone HIRA during transcription. Overall, these data show the complex processes around nucleosome dynamics which are crucial for transcriptional activity.

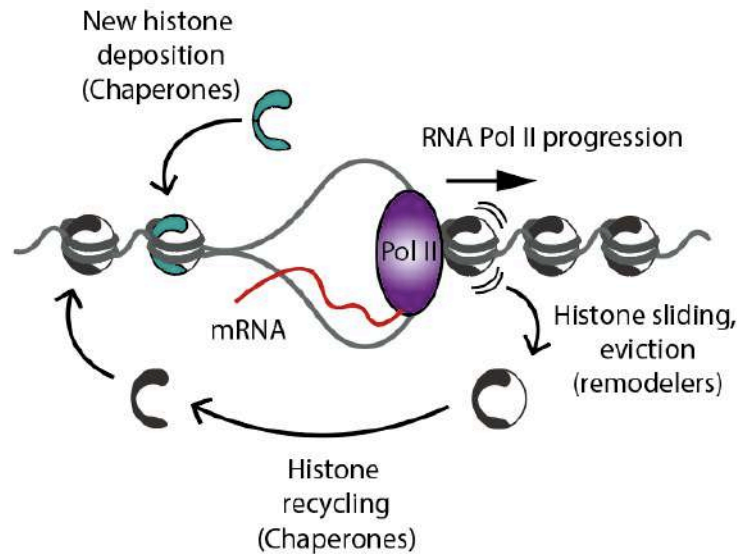


**Fig7-Nucleosome dynamics during transcription.**

Examples of nucleosomes dynamics during transcription. To allow RNA Pol II progression and reassemble chromatin after, histones are evicted and can then be recycled or a *de novo* histone deposition can take place. These processes are mediated by epigenomic effectors (inspired from Torné et al., 2020).

Despite showing a stereotypical nucleosomal landscape around TSS, not all genes have the same nucleosome stability. At these regions the occupancy of nucleosomes containing the histone variants H3.3/H2A.Z was observed in *Drosophila* and yeast (Henikoff et al., 2008; Xi et al., 2011) and it was shown that these are highly unstable nucleosomes. Although why these nucleosomes are unstable remains unclear, this could provide a mean to achieve NDR regions and promote transcription. Additionally, genome-wide characterization of *in vivo* promoter nucleosome landscapes in yeast revealed two types of promoters. One type is characterized by the presence of dynamic, unstable nucleosomes and is found at highly expressed genes. The other type, contains well-known stable nucleosomes and is found at less frequently expressed genes. Current hypothesis is that the presence of dynamic nucleosomes at highly expressed genes helps to rapidly unwind DNA and as often as necessary, resulting in an increased access of transcriptional machinery to the promoter (Kubik et al., 2015). Accordingly, TSSs of many constitutively expressed housekeeping promoters are usually depleted of nucleosomes and so depend less on nucleosome remodeling (Cairns, 2009; Ganapathi et al., 2005; Rach et al., 2011). In contrast, tightly regulated genes, depend more on remodeling factors to clear their promoters. These data highlight the importance of nucleosome positioning in transcription activity.

To achieve nucleosome depleted regions necessary for transcription, a specific interplay between different categories of epigenomic effectors can take place. Nucleosome remodelers play a crucial role in generating NDRs but they are not the only actors in this process. Indeed, acetylation of histone tails can eliminate positive charges on this residue, decreasing thus their interaction with the negative charged DNA and result in chromatin decompaction (Bannister and Kouzarides, 2011). Many chromatin remodeling enzymes contain protein motifs that recognize modified histones, opening thus the possibility of an interaction between these epigenomic effectors. Interestingly, two *in vitro* studies using budding yeast enzymes showed such interaction. First, Carey and colleagues observed that histone acetylation is sufficient to recruit the remodeler Rsc to nucleosomes (Carey et al., 2006). In turn, Rsc facilitated the passage of RNA Pol II in an ATP-hydrolysis dependent manner, resulting in stimulation of transcription elongation. Second, a study using several yeast nucleosome remodelers showed that specific patterns of histone acetylation resulted in increased rate of nucleosome repositioning or eviction (Ferreira et al., 2007). Notably, a single histone mark combined with different remodelers had different outcomes. This was observed for histone H4 tetra-acetylation, which increased nucleosome transfer by the Rsc complex but reduced the activity of two other remodelers, Chd1 and Isw2. These data show how histone PTMs can recruit remodelers and/or alter their activity impacting thus nucleosome dynamics. In budding yeast, the cooperation between the remodeler complex Swi/Snf and the histone deacetylase complex Saga was found necessary for induction of the stress response transcriptional program (Sanz et al., 2016). Upon cell wall stress, the TF Rlm1 is activated by phosphorylation and interacts with the Swi/Snf complex. It was then observed that Saga subunits are recruited to the promoter of cell wall stress-responsive genes, in a Rlm1 and Swi/Snf-dependent manner, where it acetylates histone H3 at promoters. Interestingly, both Swi/Snf and Saga complexes were necessary for H3 eviction, Rlm1 recruitment and subsequent gene expression. This data suggests thus a cooperation between epigenomic effectors in order to create a favorable chromatin environment for transcriptional activity. Nonetheless, further *in vivo* studies are required to investigate if this is a more general mechanism for the establishment of basal transcriptional programs, to identify the actors at play and assess the impact on transcription

A relationship between nucleosome density and transcription level was also observed in mouse ESCs (Fig8). The comparison of nucleosome density profiles for genes with

varying levels of transcriptional activity showed that patterns emerge from a featureless profile as transcription level elevates. Interestingly, the qualitative trends observed in mouse ESCs are conserved across multi-cellular organisms (Jiang and Zhang, 2021). A correlation between nucleosome positioning and transcription has been observed for a while but how positioning is determined has not been entirely elucidated. Recently, a “tug-of-war” model was proposed based on stochastic simulations. On one hand, enzymes that regulate and reduce inter-nucleosome spacing tend to drive the nucleosome array away from the transcription start site (TSS). On the other hand, positioning enzymes help to align nucleosomes towards the TSS. Competition between these enzymes results in two types of density profiles with well- and ill- positioned +1 nucleosome that qualitatively reproduce in vivo results from both yeast and mouse ESC (Jiang and Zhang, 2021). This results show how the coordinated activity of enzymes could potentially achieve a specific nucleosome positioning.

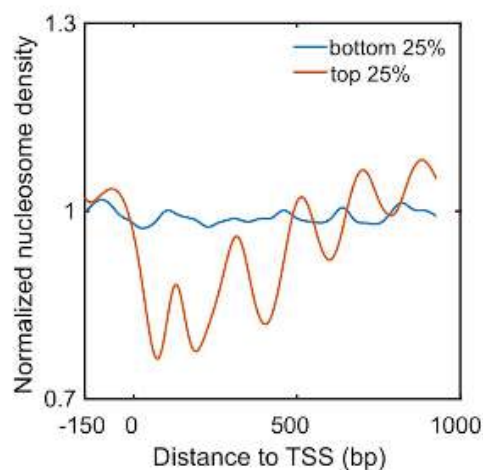


**Fig8-Nucleosome density is correlated to transcription level.**

Normalized nucleosome density profile in mouse embryonic stem cells near the transcription start site (TSS). Genes were separated depending on levels of transcription activity. Bottom 25% corresponds to the quartile of most inactive genes and top 25% corresponds to the quartile of most active genes (from Jiang & Zhang, 2021).

Overall, these data show the tight link between nucleosome dynamics and the process of transcription. Complex mechanisms and numerous actors determine nucleosome positioning, composition and movements. Further research will be thus necessary to continue to elucidate these mechanisms and their impact on transcription.

#### 4. The heterochromatic H3K9me3/HP1 pathway

Heterochromatin is an architectural feature of eukaryotic chromosomes. It corresponds to tightly packed chromatin and refers to molecular subtypes of transcriptionally repressed domains. One type of heterochromatin has been named “constitutive heterochromatin” since it’s found at structural chromosomal elements such as telomeres and pericentromeres, as well as transposable elements (TEs) and virus-derived sequences (Allshire and Madhani, 2018). This chromatin is distinguished by the formation of heterochromatin blocks characterized by histone hypoacetylation, methylation of histone H3 at lysine 9 (H3K9me) and the presence of the protein HP1 (Heterochromatin Protein 1).

Loss of H3K9me3 following depletion of silencing guides or effectors is associated with transcriptional upregulation of normally silenced regions decorated with this mark (Karimi et al., 2011; Matsui et al., 2010; Smolko et al., 2018). Additionally, artificial recruitment of H3K9 histone methyltransferases or other silencing factors such as HP1 to euchromatin regions result in transcriptional silencing of reporter genes (Ayyanathan, 2003; Ivanov et al., 2007). These data suggest thus, that repressive mechanisms use H3K9me3 and HP1 to achieve this transcriptional state.

Chromatin-based silencing can be achieved by a denser chromatin structuring process that results in efficient exclusion of RNA polymerases or other nuclear enzymes. To create this structure, di- and tri-methylation of H3K9 act as molecular anchors to recruit proteins that either directly modify chromatin or recruit others that do so (see below). Additionally, HP1 proteins can also serve as platforms to establish a repressive chromatin structure. For example, the two HP1 proteins in *S. pombe*, Swi6 and Chp2 are associated with histone deacetylases (HDACs) (Fischer et al., 2009; Yamada et al., 2005). Swi6, Chp2 and their associated HDACs were found to limit RNA Pol II occupancy at centromeric repeats. Furthermore studies *in vitro* and *in vivo* showed that the Swi6 protein can promote repression by capturing transcripts and direct them to the RNA degradation machinery (Keller et al., 2012). Finally, recent work has indicated roles of human and *Drosophila* HP1 in regulating higher-order chromatin structure through the formation of liquid-liquid phase-separated compartments (Larson et al., 2017; Strom et al., 2017). These studies suggest that heterochromatin-mediated gene silencing occurs in part, through sequestration of compacted

chromatin in specific nuclear compartments. These compartments can isolate repressed chromatin from transcription factors and machinery while maintaining a high concentration of factors required for heterochromatin formation, such as HP1 and H3K9 methyltransferases.

How is H3K9me3 chromatin targeted to specific genomic territories? Two main mechanisms have been described relying: (i) on an RNA-based recognition system to appropriately localize histone modification enzymes and HP1 proteins and initiate the heterochromatin formation cascade or (ii) on protein recognition of specific DNA sequences (Fig9).

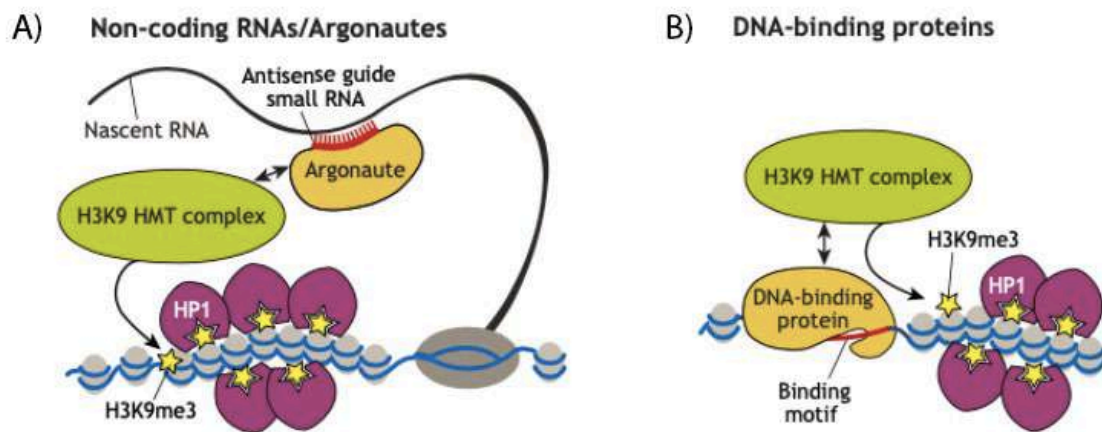


**Fig 9-Recruitment of the H3K9me3 machinery**

H3K9 methyltransferases can be recruited to specific genomic targets by (A) small non coding RNAs associated with Argonaute proteins or (B) by sequence specific DNA-binding proteins. (Adapted from Ninova et al., 2019)

Studies mainly in *S. pombe* helped elucidate the mechanisms of heterochromatin nucleation. It was observed that the deletion of *argonaute* (*ago*), *dicer* (*dcr*) and *RNA-dependent RNA polymerase* gene homologs resulted in loss of H3K9 methylation and derepression of transgenes at centromeres (Volpe, 2002). The depleted genes belong to the RNA interference (RNAi) machinery hinting thus on a mechanism involving this pathway. Additionally, induced double-stranded RNA (dsRNA) in fission yeast was sufficient to generate synthetic small interfering RNAs (siRNAs) and direct H3K9me-heterochromatin formation at the locus producing the dsRNAs [Simmer et al., 2010]. Verdel and colleagues purified indeed a nuclear Ago complex, the RITS (RNA-induced initiation of transcriptional gene silencing) complex,

which uses Dcr-generated siRNAs to localize to heterochromatic domains (Verdel, 2004). Indeed, when cells lack Dcr, the loss of siRNAs is accompanied by delocalization of RITS from centromeric regions. Further research revealed that the RITS complex can associate with the Clr4 complex, which contains the Clr4 enzyme, the sole H3K9 methyltransferase in fission yeast (Zhang et al., 2008). This interaction promotes thus nucleation of heterochromatin at determined regions. The RITS complex associates also with the RNA-dependent RNA polymerase complex (RDRC). RDRC uses primary transcripts as templates for synthesis of dsRNA, which is subsequently processed into siRNAs, thereby increasing siRNA production and amplifying the system of heterochromatin formation (Allshire and Madhani, 2018). The established model proposes thus that RNA Pol II transcribes RNAs from heterochromatin repeats which are then processed into siRNAs. These siRNAs are next bound by the Ago1 protein and are used to target homologous nascent repeat transcripts, resulting in the recruitment of silencing factors such as H3K9 methyltransferases. In metazoans, RNAi-based targeting and silencing mechanism involve another class of small non coding RNAs, piwi-interacting RNAs (piRNAs). This system of silencing is used for transposable elements in most Metazoa, particularly in the female germline and will be detailed in section III-3-A.

RNA independent mechanisms to target heterochromatin nucleation involve DNA binding proteins. In mammalian systems, the KRAB-containing zinc finger proteins (KRAB-ZFPs) have been found to induce H3K9me3-dependent silencing at endogenous retrovirus targets (Wolf et al., 2015) and TEs (Ecco et al., 2016; Imbeault et al., 2017), presumably by recruitment of H3K9 methyltransferases. Additionally, a high concordance between heterochromatic repeat regions and some transcription factor-binding sites in mouse has been observed. For example, paired box 3 (Pax3) and Pax9 have binding sites in pericentric heterochromatin and depletion of these factors results in derepression of satellite transcripts and impairment of heterochromatic marks (Bulut-Karslioglu et al., 2012). The data points to a model where specific DNA-binding proteins could attract silencing effectors to their DNA-bound region. Interestingly, in some cases, binding of specific transcription factors to euchromatic sites appears to trigger the formation of small blocks of heterochromatin to achieve silencing. In *Drosophila*, phosphorylated Hers (Histone gene-specific Epigenetic Repressor in late S phase) binds to histone gene regulatory regions and anchors HP1a and the H3K9 methyltransferase Su(var)3-9 to induce silencing of this repeated gene cluster (Ito et al., 2012). Similarly, the corepressor TIF1b/KAP1 (Transcription Intermediary Factor 1-

beta/KRAB-associated protein 1) targets HP1 to specific loci in the euchromatic arms to silence those genes (Cammass, 2004; Schultz, 2002). Importantly, in contrast to pericentric heterochromatin, there is little spreading (see below) of the silencing marks in these cases, suggesting a silencing state that differs in some key characteristics from classic heterochromatin formation. Unfortunately, there has been little study of this process to date.

Once established, histone methylation serves as a molecular anchor. In *Drosophila*, di- or tri-methylation of H3K9 by the HMT Su(var)3-9 provides binding sites for HP1a resulting in a stable interaction (Eskeland et al., 2007; Jacobs et al., 2001). Chromatin-bound HP1 in turn mediates the recruitment of more HMTs Su(var)3-9, either directly or through the bifunctional binding partner, Su(var)3-7 (Delattre et al., 2000). Su(var)3-9 is the main producer of H3K9 methylation and as long as it carries out this reaction on an adjacent histone, the heterochromatin assembly process continues. By recognizing both the histone modification and the enzyme responsible for that modification, HP1a provides a mechanism for heterochromatin spreading and maintenance (Fig10). Similarly, in fission yeast, nucleated heterochromatin repeat elements can spread in a Swi6/HP1-dependent manner (Hall, 2002). A key feature of heterochromatin is thus its ability to propagate, thereby influencing gene expression in a region-specific, sequence-independent manner.

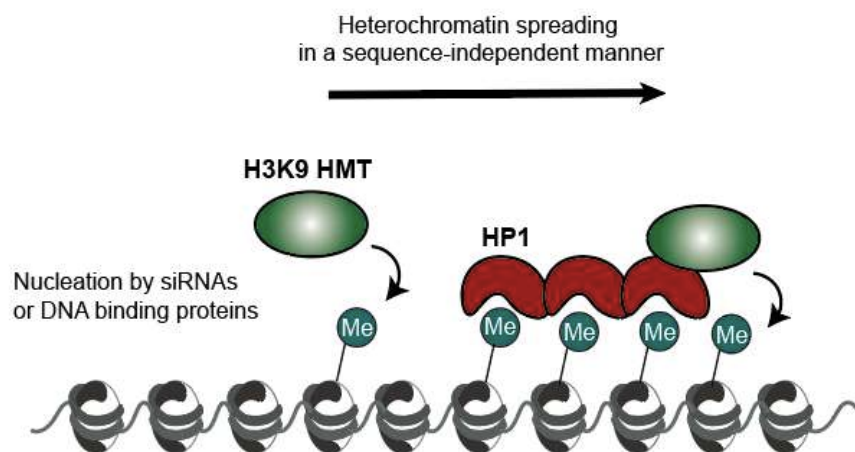


**Fig 10-H3K9me3/HP1 heterochromatin spreading**

Once nucleated, di-and tri-methylated H3K9 provide a binding platform for HP1 proteins. In turn HP1 can recruit H3K9 methyltransferases and the process is repeated, thereby spreading heterochromatin structure in a region-specific manner. Abbreviations: HMT= histone methyltransferase, Me= methyl mark.

Because heterochromatin can spread, mechanisms to restrict its expansion are necessary to avoid erroneous and potentially deleterious gene silencing. tRNA genes are a class of heterochromatin-spreading barrier conserved from yeast to human (Raab et al., 2012; Scott et al., 2006). Binding sites for transcription factors associated to the RNA Pol III can function as heterochromatin barriers independent of tRNA genes, revealing their role in barrier function. Another mechanism to restrain heterochromatin spreading is the generation of nucleosome depleted regions. This is observed at the silent mating type region in fission yeast which contains large nucleosome free regions that form a ‘gap’ in chromatin over which some reader–writer machineries cannot cross (Garcia et al., 2010). The existence of multiple mechanisms to limit heterochromatin spreading highlights the importance of proper chromatin organization in maintaining genome homeostasis.

Interestingly, HP1a can also have a role in transcription of genes residing in heterochromatin. In *Drosophila*, two genes, *light* and *rolled*, found within a heterochromatin domain show a loss of expression upon depletion of HP1a (Lu et al., 2000; Wakimoto and Hearn, 1990). There is a loss of silencing marks at the TSS of active genes in these domains although the usual heterochromatic marks, including H3K9me<sub>2/3</sub>, are still present upstream and across the gene body. The TSSs are occupied by RNA Pol II and are flanked downstream by nucleosomes with euchromatic marks. This data shows that the presence of H3K9 methylation on the gene body, but not on the TSS, is compatible with transcription. Further work will be required to determine if the specific localization of these marks has a role on active transcription.

Furthermore, a non-repressive role for H3K9me<sub>3</sub> was described in a recent study by the Torres-Padilla laboratory. Immediately after fertilization, the paternal pronucleus of mammalian embryos acquires *de novo* H3K9me<sub>3</sub> via catalysis by the methyltransferase SUV39H2 which in turn is negatively regulated by satellite RNAs transcribed from the paternal pericentromere. *De novo* H3K9me<sub>3</sub> is initially non-repressive for gene expression, but instead bookmarks promoters for compaction later during development, suggesting that the mark is not repressive per se (Burton et al., 2020). This study provides an illustration of the complex role of heterochromatin and demonstrates that heterochromatin function can vary depending on the cellular and developmental context.

In conclusion, H3K9/HP1 heterochromatin is a potent silencing mechanism. However, the actors involved in this pathway seem to have a more complex role in transcriptional regulation than just promote transcriptional repression.

## 5. Polycomb effectors mediate gene silencing...and more?

The Polycomb group (PcG) genes were first discovered in *Drosophila* as crucial epigenetic repressors of homeotic (*Hox*) genes. They have since then been discovered to control hundreds of genes in insects, mammals and many other branches. Indeed, PcG genes and targets are conserved in evolution and their study has allowed unveiling regulation of a plethora of cellular processes.

The PcG machinery is mainly composed of two biochemical complexes: Polycomb Repressive Complex 1 (PRC1) and PRC2. PRC1 contains the E3 ligase activity for monoubiquitylation of H2A at Lys 118 in *Drosophila* and Lys 119 in mammals (Wang et al., 2004). PRC2 contains histone methyltransferase activity specifically targeting H3K27 (Cao et al., 2002; Czermin et al., 2002; Kassis et al., 2017; Kuzmichev, 2002; Müller et al., 2002; Schuettengruber et al., 2017). H3K27me<sub>3</sub> is found on many silenced regions in a cell-specific manner (Beuchle et al., 2001; Plath, 2003; Ringrose and Paro, 2004). This mark is deposited by the histone methyltransferase E(z)/EZH2, a subunit of the PRC2 complex and its catalytic activity is required for *Hox* gene repression (Czermin et al., 2002; Müller et al., 2002). Additionally, it was observed that flies carrying a point mutation in lysine 27 of H3 fail to repress PRC2-target genes demonstrating thus the need of this mark for PcG-mediated repression (Pengelly et al., 2013). Contrariwise, it was observed that the mark catalyzed by the PRC1 complex is dispensable for repression of canonical PcG targets during *Drosophila* embryogenesis (Kahn et al., 2016; Pengelly et al., 2015). H2AK118ub is carried out by the PRC1 subunit Sce in *Drosophila*. Flies with catalytically inactive Sce or with pointmutated H2A were generated and it was observed that H2Aub-deficient animals fully maintain repression of PRC1 target genes. These data suggest thus that catalytic activity of PRC2, *i.e.*, H3K27 methylation, is necessary for repression however PRC1 represses canonical targets independently of its catalytic activity.

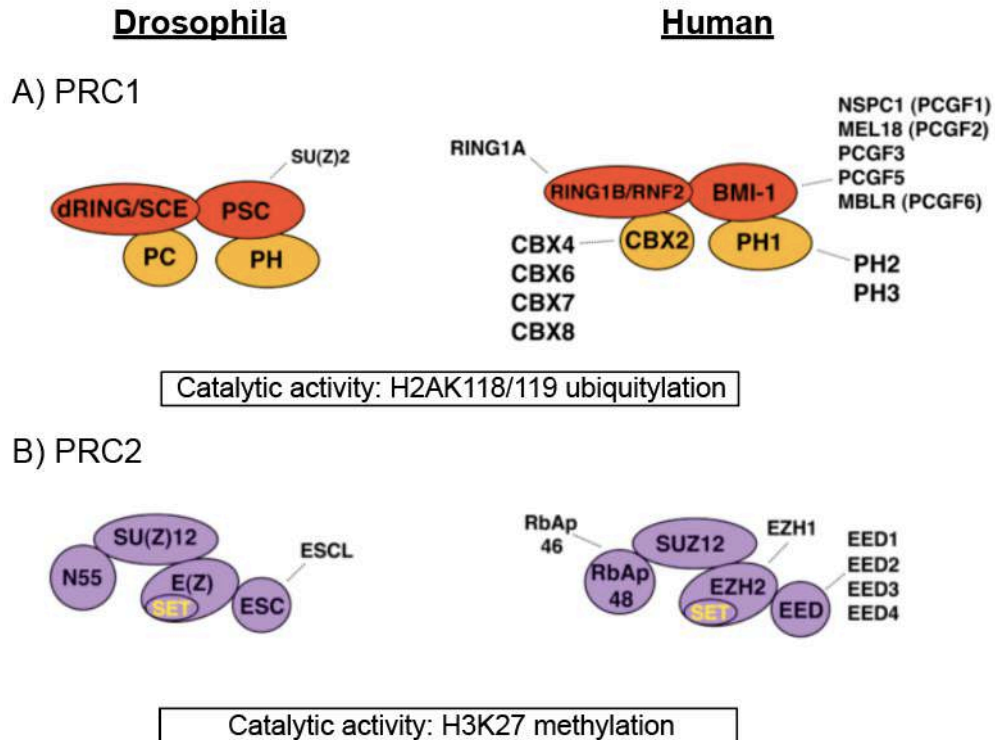


**Fig 11-Composition of Polycomb Repressive Complexes (PRC) in *Drosophila* and Human.**

(A) PRC1 complex contains four core subunits. Its catalytic activity is ubiquitylation of H2AK118 in *Drosophila* and H2AK119 in mammals, conferred by the dRING/RING subunit. (B) PRC2 complex contains four core subunits. Its catalytic activity is methylation of H3K27 conferred by the subunit E(z)/EZH2. Dashed lines indicate alternative subunits (Simon and Kingston, 2013).

What is then the role of H3K27me3? It has been suggested that H3K27me3 stabilizes interactions between DNA-bound PcG complexes and the surrounding chromatin. It was observed that abolishing H3K27me3 within a promoter or transcriptional unit of a target gene impairs the interactions of DNA-anchored PcG complexes with these gene elements (Kahn et al., 2016). By promoting interaction stability with these gene regions, H3K27me3 would deliver PcG complexes that can interfere with transcription. Stable loops could also contribute to spreading and maintenance of H3K27me3 from its anchor points, thereby reinforcing the system. Additionally, a bulk tri-methylation of H3K27 may contribute to the repression directly by competing with acetylation of H3K27, a mark involved in gene activation. Furthermore, PRC1 subunit Pc/CBX can inhibit the acetyltransferase activity of dCBP/CBP (Tie et al., 2016, 2009). Even if the importance of H3K27me3 for polycomb-

mediated silencing has been shown, the precise mechanism by which it allows gene repression is not fully understood.

Initially, it was observed that PcG proteins and H3K27me3 marked histones accumulate in discrete nuclear foci: “Polycomb bodies” (Buchenau et al., 1998; Messmer et al., 1992), indicating that nuclear compartmentalization could play a functional role in Polycomb-mediated repression. Interestingly, interactions with elements of the nuclear periphery seem to be important for the formation of these compartments and for gene repression. Indeed, the knock-down of lamin A/C causes the dispersion of Polycomb bodies and leads to impaired PcG-mediated transcriptional silencing in both mammalian and *Drosophila* cell lines (Cesarini et al., 2015; Marullo et al., 2016). Nuclear compartmentalization could thus play an important role in PcG-mediated silencing.

Although targets and PcG proteins are well conserved, the mechanisms to recruit them at target sequences vary between species. The *Drosophila* genome is equipped with, Polycomb Response Elements (PREs), these are discrete DNA elements to which PRC1 and PRC2 are targeted. These elements contain binding sites for many different DNA-binding proteins such as Pho, GAF/Psq, Dsp1, Spps, Zeste, Grh, Adf1, Cg and many others (Blastyák et al., 2006; Brown and Kassis, 2010; Déjardin et al., 2005; Orsi et al., 2014; Ray et al., 2016). These TFs play an important role in PcG recruitment however none of them is sufficient to recruit PcG complexes on their own. Initially, a hierarchical recruitment model was proposed in which TFs recruit PRC2, which subsequently recruits PRC1 via the interaction of the Pc subunit with the PRC2-deposited mark, H3K27me3. Accumulating evidence has challenged this model (Dorafshan et al., 2017). For instance, it has been observed that PRC1 can bind PREs in the absence of PRC2 but at many PREs, PRC2 requires PRC1 to be targeted (Kahn et al., 2016). Additionally, PRC1-bound regions devoid of H3K27me3 exist in both *Drosophila* and human cultured cells (Loubiere et al., 2016; Schwartz et al., 2006). Moreover, none of the histone marks deposited by PRCs complexes are required for their targeting at PREs, suggesting that PREs work upstream to histone mark deposition (Kahn et al., 2016). The relationship among TFs, PRC1, and PRC2 seems thus cooperative rather than hierarchical. Whilst PRE characterization in flies is well advanced, their mammalian counterpart has not been clearly identified. In mammals it has been shown that CpG islands can recruit PcG proteins (Lynch et al., 2012; Mendenhall et al., 2010; Reddington et al., 2013), a genomic feature (CpG islands) that has not been found in flies. Nonetheless, similarly to *Drosophila*, *de novo* PRC2 recruitment is independent of

H3K27me3 and H2AK118ub in ESCs (Lavarone et al., 2019). Some mammalian PREs have binding sites for TF important at *Drosophila* PREs (Kassis and Brown, 2013). For example, a homolog of the *Drosophila* protein Polycomb-like, can bind DNA and recruit PRC2 in mouse ESCs. It selectively binds regions with high density of unmethylated CpGs which discriminate target from non-target CpG islands (Li et al., 2017; Perino et al., 2018). The quest for mammalian PREs is still a field of active ongoing research that will shed light into the specific targeting PcG proteins in mammals.

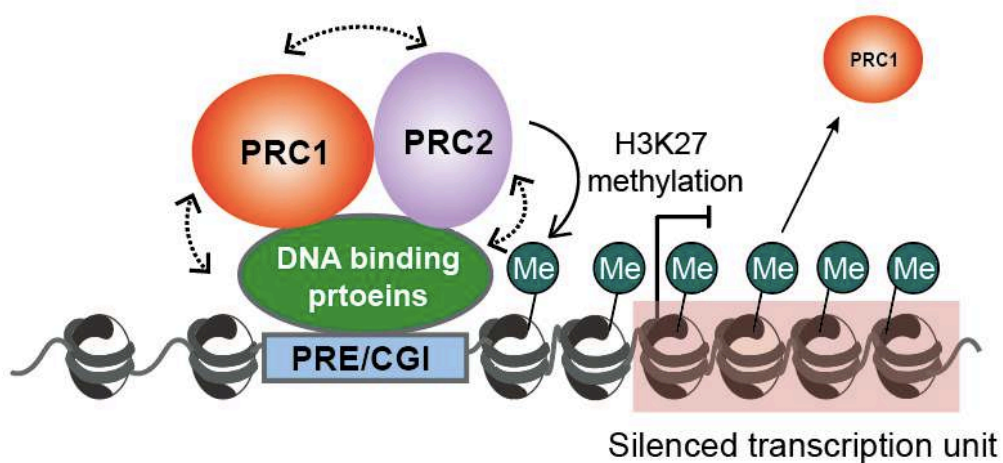


**Fig 12-Polycomb Repressive Complex recruitment**

PcG proteins are recruited to specific DNA sequences, in flies these are Polycomb Response Element (PREs). In mammals CpG islands have been found capable of recruiting PcG proteins. PREs contain binding sites for numerous DNA binding proteins important for Polycomb Repressive complexes (PRC) recruitment. Dashed arrows represent a cooperative relationship between DNA binding proteins and PRCs to target them at PREs/CGIs. PRC2 catalyzes H3K27me3 necessary for transcriptional silencing and PRC1 is capable of binding this modification thereby stabilizing their recruitment to chromatin.

Although many elements required for targeting and establishment of PcG-mediated repression are known, more and more evidence are revealing other roles for the actors involved. Firstly, fragments of DNA that contain PREs have been shown to mediate gene activation in transgenes under certain conditions and at some chromosomal insertion sites (Kassis and Brown, 2013), suggesting that these regulatory elements can have dual regulatory functions. Indeed, during *Drosophila* embryogenesis, some classic PREs can recruit tissue-

specific TFs and function as developmental enhancers *in vivo*, activating spatio-temporal expression of a reporter gene (Erceg et al., 2017). Conversely, a subset of developmental enhancers binds the PcG complex, Pho-RC, resulting in polycomb-dependent transcriptional silencing. This dual activity of *cis*-regulatory elements may help fine-tune gene expression and ensure the timely maintenance of cell identities. The same *cis*-regulatory element can thus have opposite outcomes on gene transcription in a context-dependent manner. Furthermore, the characterization of the *in vivo* role of the two PREs near the *vestigial* (*vg*) gene, reported a promoter that requires a PRE for expression during development (Ahmad and Spens, 2019). On one hand, the PRE near the *vg* promoter is required for its activation and not for repression. On the other hand, the distal PRE, located in the middle of the chromatin domain, is required for high-level of H3K27me3 in the domain. Surprisingly, removal of both PREs does not completely eliminate H3K27me3 across the *vg* domain and this residual methylation is similar to that in cells where the *vg* gene is active. These data confirms that PREs can also have a role in gene activation and the definition of their roles might depend on the factors they bind.

Interestingly, the binding of factors implicated in PcG silencing are not incompatible with transcription. PRC1 components were found to bind actively transcribed genes in *Drosophila* larval imaginal discs and human cultured cells (Loubiere et al., 2016). Strikingly, despite the proven need of H3K27me3 for polycomb-mediated repression, its presence was not incompatible with transcription of the *vg* gene (Ahmad and Spens, 2019). Normal transcription of the *vg* gene occurs concomitantly with a basal enrichment of H3K27me3 at the endogenous locus. This shows the complexity of the roles of the PcG proteins.

We also mentioned that PRC1 can be recruited independently of H3K27me3, suggesting that it might have functions independently of PRC2. It was observed in *Drosophila* that PRC1 components are targeted to a distinct set of genes that lack H3K27me3 during larval development (Loubiere et al., 2016). The redeployment of PRC1 was also observed in human differentiated cells when compared to embryonic stem cells. In both species PRC1-only gene targets were involved in regulation of cell proliferation, polarity and signaling. Mutations in PRC1, but not PRC2 resulted in the upregulation of a majority of these new target genes, suggesting that PRC1 has a role dampening a specific subset of genes independently of PRC2. Moreover, RNAi depletion of PRC1 subunits in *Drosophila* cell culture alters phosphorylation of RNA Pol II at most active genes and enhancers (Pherson et al., 2017). These effects coincide with changes in nascent RNA density indicating altered transcriptional

elongation and RNA processing. Although the mechanisms by which PRC1 can alter gene transcription are not fully elucidated, these findings describe a role for PRC1 components beyond epigenetic silencing.

Overall, these data reveal the complexity of the Polycomb system showing that factors and DNA regulatory elements involved can play different roles in a context-dependent manner, hence the inability to establish absolute rules for its role in transcriptional regulation.

## 6. Counteracting repression to promote activation

Gene repression can be accomplished by creating a chromatin configuration that blocks access to the large number of proteins required for transcription. A way to promote gene activation is thus to counteract silencing mechanisms.

There is a regulatory interplay between epigenomic effectors that supposes a balance between their activities in order to ensure the proper transcriptional outcome. One of the most well-studied epigenetic regulatory systems is the Polycomb group (PcG) and Trithorax group (TrxG) genes. These two groups of genes were discovered in *Drosophila* by their opposing effects on homeotic gene (*Hox*) expression. PcG proteins exert a negative effect on transcription while TrxG are positive regulators. Given the complexity of factors required for gene expression, the biochemical nature of TrxG proteins is a very heterogeneous group that includes remodelers and histone modifiers, acting at different levels of gene transcription (Kassis et al., 2017; Kingston and Tamkun, 2014; Schuettengruber et al., 2017).

How can regulators of these groups achieve antagonistic effects at their targets? One proposed mechanism by which TrxG can promote activation is by counteracting Polycomb-mediated repression. This was proposed for the TrxG histone methyltransferases Trx and Ash1. Indeed, genetic studies in *Drosophila* showed that the removal of PcG complexes reactivates genes even in the absence of Trx and Ash1, suggesting that these proteins function as PcG antirepressors rather than direct activators (Klymenko and Müller, 2004). Trx and Ash1 methyltransferases target H3K4 and H3K36 respectively, both of which are considered active marks (see section II-7). In agreement with genetic studies, *in vitro* assays using

engineered methylated histones showed that H3K4me3 or H3K36me2/3 can inhibit H3K27 methylation on the same histone by fly or human PRC2 complex (Schmitges et al., 2011). Therefore, these data suggest mechanistic antagonism between these two groups could be mediated by histone PTMs.

As mentioned, the TrxG encompasses a great diversity of biochemical activities indicating that mechanisms involving other type of epigenomic effectors could also be at play. Several subunits of the nucleosome remodeler SWI/SNF complex, including the catalytic subunit, have been classified as TrxG proteins. The opposition between PRCs and the SWI/SNF complex has been the focus of extensive research especially because of its implication in development and disease such as cancer (Kadoch and Crabtree, 2015). Recent studies have unveiled the mechanisms for the interaction between these two groups of regulators. It was observed in cultured cells, that recruitment of the mammalian SWI/SNF complex leads to a rapid, ATP-dependent eviction of both PRC1 and PRC2 (Kadoch et al., 2017). The reversal of this process results in reassembly of Polycomb-mediated heterochromatin. This study proposes thus a mechanism in which a TrxG remodeler opposes Polycomb complexes by their active removal, resulting in chromatin accessibility (Fig13). Interestingly, a recent study reported that degradation of the SWI/SNF ATPase subunit in mouse ESCs resulted in derepression of genes highly occupied by Polycomb, such as *Hox* genes, suggesting also a role for SWI/SNF in promoting PcG-based repression (Weber et al., 2021). Upon rapid depletion of the catalytic SWI/SNF subunit, PRC1 and PRC2 are redistributed away from sites where they usually accumulate, like *Hox* clusters. Collectively, these findings reveal the complexity of the regulatory interplay of the Polycomb-Trithorax axis to achieve proper gene expression.

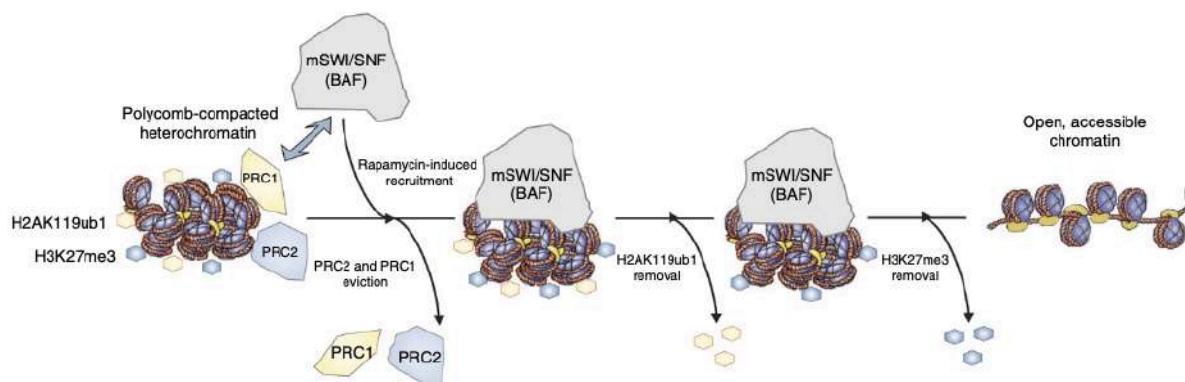


### **Fig 13-Model for opposition between mSWI/SNF and Polycomb**

Recruitment of the mSWI/SNF complex to Polycomb-repressed regions leads to an ATP-dependent eviction of PRC1 and PRC2 complexes, followed by H2AK119 and H3K27me3 removal resulting in an increase of DNA accessibility (modified from Kadoch et al., 2017)

Another mechanism used to counteract repression is to create a boundary between regions of different transcriptional activities. In fly embryos, insulators and their insulator binding proteins (IBPs) can be found at borders between different chromatin landscapes and block the spreading of histone modifications at *Hox* genes (Bowman et al., 2014; Fujioka et al., 2013; Kahn et al., 2006). Additionally, the IBPs, Beaf-32, CP190, dCTCF and Mod(mdg4) can be found enriched at promoter pairs of differentially expressed genes (Nègre et al., 2010) suggesting that insulators and their binding proteins can indeed separate different transcriptional states. However, in *Drosophila* cultured cells, knock-downs of the mentioned IBPs led to changes of the repressive mark H3K27me3 within the chromatin domain rather than spreading outside of it (Van Bortle et al., 2012). IBPs can indeed be found enriched at borders of H3K27me3 domains but only a fraction of these sites can actually restrict the mark's spreading (Schwartz et al., 2012). One possibility is that additional co-factors are necessary to inhibit the repressive mark spreading. Such example was described in *Drosophila* embryonic cells, where the IBP Beaf-32 is capable of recruiting the H3K36 histone methyltransferase dMes-4 to promote transcription of flanking genes by antagonizing the spread of H3K27 methylation from nearby regions (Lhoumaud et al., 2014). More work is needed to identify this type of co-factors and their role at heterochromatin/euchromatin borders. Nonetheless, these data suggest a cooperation between epigenomic effectors to maintain appropriate transcriptional states.

Altogether, this suggests that repression counteracting is the result of an interplay between epigenomic effectors. Although this can contribute to promote gene expression, activation of a gene requires numerous steps and actors and thus many other mechanisms involved.

## **7. Histone PTMs in active transcription**

As for a silenced state of transcription, histone modifications can also be associated to an active state of transcription. For example, genome-wide studies have found H3K27ac and

H3K4me1 at active enhancers, H3K4me3 and H3/H4 acetylation are found at promoters of active genes, H2Bub1 at promoters and gene bodies and finally high levels of H3K79me3 and increasing H3K36me3 towards the 3' end are found at actively transcribing genes (Fig14) (Gates et al., 2017). While these correlations have been widely described, determining which modifications are causal drivers and by which mechanisms they promote transcription is not completely understood. Nonetheless, roles for histone marks, particularly during the elongation step, have been described.

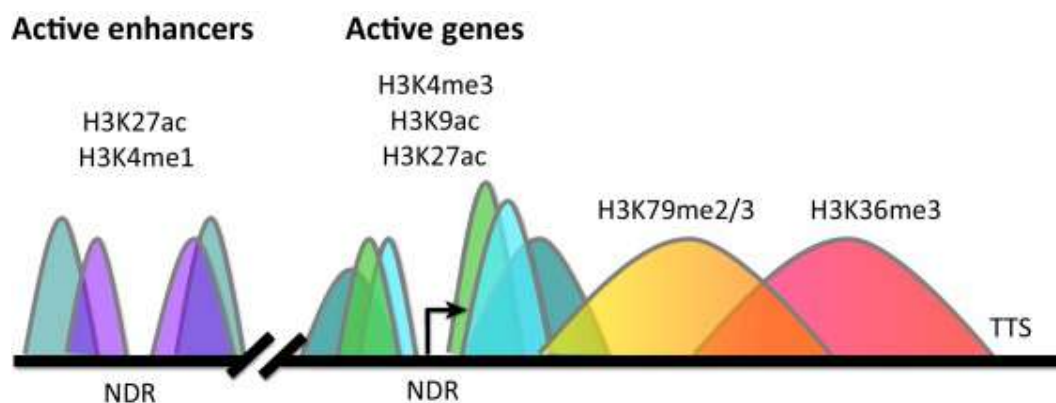


**Fig 14-Histone marks at active genes.**

Non-exhaustive illustration of the distribution of histone modifications at active genes and enhancers. Regions in color represent ChIP-signal at eukaryotic genes. H3K4me3 and H3K9ac are associated with transcriptionally active gene promoter regions while H3K36me3 and H3K79me3 are localized at gene bodies. H3K27ac localizes to both active gene promoters and enhancer regions, and H3K4me1 is predominantly enriched at enhancers. Abbreviations: NDR= nucleosome depleted region, TTS = transcription termination site, the transcription start site is shown by an arrow (adapted from Gates et al., 2017).

### A. Histone PTMs during transcription elongation

Trimethylation of H3K36me3 during elongation has been found important for maintaining transcription fidelity. Studies in budding yeast have indeed investigated the function of H3K36 methylation during transcription. Successive transcription may cause histone hyperacetylation in gene bodies leading to cryptic transcription initiation. The RNA Pol II phosphorylated on the Serine 2 *i.e.*, the elongating Pol II, recruits the histone methyltransferase Set2 to deposit H3K36me3 which serves as a docking site for the Rpd3S

histone deacetylase complex to actively transcribed genes. In turn, Rpd3S catalytic activity, ensures that coding regions remain hypoacetylated, which is important to suppress cryptic transcription initiation (Carrozza et al., 2005; Drouin et al., 2010). Additionally, it was later observed that longer genes and genes transcribed at lower frequency had a stronger dependency on the Set2-Rpd3S pathway to suppress spurious transcription (Li et al., 2007). Transcription elongation-coupled SETD2 recruitment and H3K36me3 deposition are conserved in mammals, as well as the role of H3K36me3 to prevent aberrant transcription initiation [Huang and Zhu, 2018]. However, in mouse embryonic cells it was observed that this depended on the recruitment of DNA methyltransferases to the gene body by H3K36me3 (Neri et al., 2017). Although mechanisms to prevent spurious transcription may be different, these data highlight the importance of H3K36me3 in maintaining transcription fidelity.

Another mark associated with transcription elongation is the monoubiquitination on histone H2B (H2Bub1). This mark has been found enriched at promoters and open reading frames of actively transcribed genes (Kao, 2004; Minsky et al., 2008), suggesting thus a role in gene activation. *In vitro* experiments showed that H2B monoubiquitination by the ubiquitin ligase RNF20/40 jointly with the ubiquitin-conjugating enzyme UbcH6 facilitates displacement of the H2A/H2B dimer from the core nucleosome, facilitating RNA Pol II passage and enhancing transcript elongation rates on chromatin templates (Pavri et al., 2006). This effect was observed while H2ub1 remained in the chromatin but *in vivo* observations in yeast showed that both ubiquitination and deubiquitination are important for full transcription activation at the *Gall* promoter (Henry, 2003). Further research is needed to understand the full extent of this histone mark on transcription initiation and elongation.

These data show the implication of histone PTMs in elongation and reflects how the epigenome can regulate gene expression at different points of the transcription process.

## B. Is H3K4me3 instructive for transcription activation?

A connection between H3K4 methylation and transcriptional activity was first evoked when this mark was observed to decorate the transcriptionally active macronucleus but not the transcriptionally inert micronucleus in the single-celled eukaryote *Tetrahymena*. (Strahl et al., 1999). When mapped in genome-wide experiments, the histone mark H3K4me3 was

found at TSSs of transcriptionally active genes in various organisms and the levels of this mark were strongly correlated to nascent transcripts (Bernstein et al., 2005; Guenther et al., 2007; Heintzman et al., 2007; Howe et al., 2017; Nojima et al., 2015). This led to the classification of H3K4me3 as a hallmark of active promoters resulting in the use of it as a marker of active transcription. Supporting this view, studies in human cultured cells showed that H3K4me3 interacts with TAF3, a subunit of the general transcription factor TFIID, facilitating thereby the formation of the transcriptional pre-initiation complex (Lauberth et al., 2013). This resulted in the enhancement of specific p53-dependent transcription in response to genotoxic stress. A more recent study, again in human cells, employed epigenome editing to investigate the role of H3K4me3 in transcriptional activation (Cano-Rodriguez et al., 2016). They used the methyltransferase PRDM9 to locally induce H3K4me3 and observed re-expression of silenced targets. However, maintenance of this re-expression was dependent on chromatin environment, particularly on hypomethylated DNA and H3K79me. Indeed, when H3K4me was targeted to a hypermethylated locus, re-activation was only transient. Yet, the precise contribution of these genomic features are to be determined. Although this study links H3K4me3 to gene (re-)activation, the chosen HMT possesses other targets on histones linked to transcription, for example H3K36 *in vivo*, and H3K9 at least *in vitro* [Koh-Stenta et al., 2014, Powers et al., 2016], none of which were examined. Further studies are required to elucidate if these observations are reproducible at other targets and organisms, particularly in those without DNA methylation like *Drosophila*.

Why is it difficult to study the impact of H3K4me3 on transcription? In yeast the Set1 complex is in charge of mono-, di- and trimethylation of H3K4, therefore altering this enzyme would also impact histone marks other than H3K4me3 (Gu and Lee, 2013). In contrast, human possesses several enzymes catalyzing H3K4 methylation, six Set1 homologs (SET1A, SET1B, MLL1 to 4) but also other enzymes non-related to Set1 (MLL5, SET7 (also called SET9), SMYD1-3, SETMAR, and PRDM9). In *Drosophila*, three Set1 homologs have been identified dSet1, Trithorax (Trx), and Trithorax-related (Trr). Deletion of any of their genes results in lethality in flies, indicating that their target genes may not be redundant. Additionally, loss of *dSet1*, but not *Trx* or *Trr*, leads to a global reduction of H3K4me2/3, suggesting that *Trx* and *Trr* have more specialized functions (Ardehali et al., 2011; Mohan et al., 2011). This diversity complexifies the study of the direct implication of only the H3K4me3 mark due to possible overlapping functions and/or indirect effects on other marks. Indeed, the field is still lacking a conserved model mechanism to support causality between

H3K4me3 and transcriptional activity and accumulating evidence has challenged this causal link.

Several studies in yeast revealed that absence of H3K4me3 has little effect on gene transcription even at genes where H3K4me3 is highly enriched (Margaritis et al., 2012; Ramakrishnan et al., 2016; Weiner et al., 2012). Accumulating evidence in *Drosophila* has also questioned the relevance of H3K4 methylation in transcriptional activation. One of *Drosophila*'s H3K4 HMT, Trx can be cleaved into two proteins Trx-C and Trx-N. Trx-N lacks methyltransferase activity and is associated with broad regions of active genes (Schuettengruber et al., 2009; Schwartz et al., 2010), suggesting that it activates transcription via mechanisms other than histone methylation. Furthermore, the replacement of H3K4 with a non-methylable arginine, revealed that despite the absence of H3K4 methylation, transcriptional activation was still possible and only minimal changes in developmental gene expression were observed (Hödl and Basler, 2012). Methylation of H3K4 is thus dispensable for transcriptional activation and this mark is likely to have a more complex role in chromatin regulation. Furthermore, a recent study in mouse ESCs showed that gene reactivation can occur without reacquisition of H3K4me3 (Douillet et al., 2020). These findings showed thus an uncoupling between transcriptional activation and the histone mark H3K4me3.

Overall, these data show that the role of H3K4me3 cannot be exclusively reduced to that of transcriptional activation.

## 8. Bivalent promoters

A peculiar class of promoters, known as bivalent promoters, were originally identified in ES cells and are characterized by the simultaneous enrichment of both H3K27me3, associated to gene repression and H3K4me3, commonly associated to gene activation (Berstein et al., 2006, Mikkelsen et al., 2007). The enrichment of these opposing modifications correlates with a low-level expression or no expression (Bernstein et al., 2006). During cell differentiation, these bivalent regions are resolved as they undergo either full transcriptional activation, in which case they preserve H3K4me3 and lose H3K27me3, or stable silencing where they preserve H3K27me3 and lose H3K4me3 (Gaertner et al., 2012; Mikkelsen et al., 2007; Pan et al., 2007; Zhao et al., 2007). Interestingly, in more committed cells, neural progenitors and embryonic fibroblasts, bivalent domains were still present in

different proportions, 8% and 43% respectively (Mikkelsen et al., 2007). To explain this difference the authors proposed that the high number of bivalent domains in embryonic fibroblasts may reflect a less differentiated state and/or heterogeneity in the population analyzed. Nevertheless, at least in neural progenitors, genes where bivalent domains were not resolved, continued to be repressed. These data suggest thus a functional role for bivalent domains.

Genome-wide mapping of bivalent chromatin revealed it is frequently found within promoter regions of developmentally important genes (Bernstein et al., 2006; Lesch et al., 2013), providing a silencing system for these genes while keeping them poised for activation. Like this, during development, certain genes become active in a tissue-specific manner leading to cell lineage specification. These regions have been suggested to “safeguard differentiation” and their malfunction might have a profound impact on the cell (Voigt et al., 2013). Indeed, bivalent domains identified in human tumors, such as ovarian cancer, colon cancer, and glioblastomas, coincide with genomic regions decorated with H3K4me3/H3K27me3 in ESCs (Curry et al., 2018; Hall et al., 2018; Rodriguez et al., 2008). However, the extent of this overlap and the biological significance of these recovered bivalent domains in cancerous cells remains to be investigated.

Despite its apparent importance, bivalency is functionally and mechanistically not well understood. A study in ESCs revealed however that nucleosomes carrying H3K4me3 along with H3K27me3 did so on opposite H3 tails. PRC2-mediated methylation of H3K27 was inhibited when nucleosomes contained symmetrically, but not asymmetrically, positioned H3K4me3, showing that the location of the “active” mark can be decisive for establishment of bivalency (Voigt et al., 2012). Further studies should elucidate the requirements for establishment of these chromatin domains.

Until recently, bivalent domains had not been identified in *Drosophila*. Akmammedov and colleagues used re-ChIP to confirm the co-occurrence of H3K27me3 and H3K4me3 in fly embryos, leading to the uncovering of such bivalent domains (Akmammedov et al., 2019). However, only a handful of endogenous sites, all members of the *Hox* genes, were tested. More studies will be needed to see if these domains are present across the genome of *Drosophila* at key developmental genes and if their state of bivalency changes during differentiation.

## 9. Genome folding and transcription

DNA and its associated proteins are confined within the nucleus. This is a topologically constrained and a highly crowded environment. The 3D folding of the eukaryotic genome compatible with all the activities described above is thus a major requirement.

The study of a functional link between higher-order chromatin arrangements and transcription has greatly increased thanks to the rapid development on new techniques. In the mid-2000s, FISH experiments in human fibroblasts, showed the existence of chromosome territories (Bolzer et al., 2005). These territories segregate in regions rich in active genes, typically located in the interior of the nucleus, and regions rich in inactive genes, found at the nuclear periphery. The rapid development of chromosome capture techniques, namely C-based techniques, now allow to assay contact frequency at a genome-wide level. At large scales, Hi-C confirmed two major types of structural domains: A and B compartments. The A compartment corresponds to active chromatin, presents transcriptional activity, higher chromatin accessibility and H3K36me3 deposition. Compartment B contains repressed chromatin in a more compacted state, with low transcriptional activity, associated with the nuclear lamina and presenting H3K27me3 deposition (Lieberman-Aiden et al., 2009; Rao et al., 2014). At a lower scale, chromosomes fold into domains of 100kb-1Mb, with preferential intradomain interactions compared to interdomain interactions. These contact domains are partitioned by boundaries between them and are referred to as topologically associating domains (TADs) (Fig15) (Dixon et al., 2012). The presence of TADs has been confirmed across cell lines and species, indicating that they may represent a conserved feature of genome organization. Importantly, a conserved characteristic across species, is the relationship between gene activity and genome folding (Szabo et al., 2019). Overall, these observations point towards a functional implication of chromosomal organization within the nucleus.

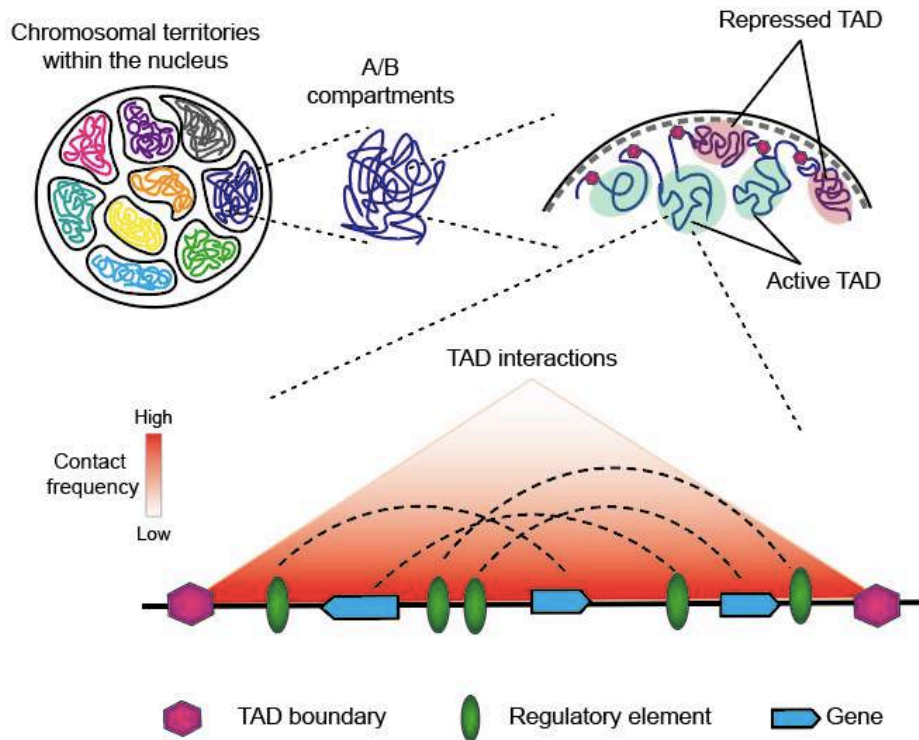


**Fig15-Hierarchical organization of the eukaryotic genome**

Individual chromosomes occupy specific nuclear spaces, forming chromosomes territories, shown schematically in different colors. At the chromosomal scale, chromatin is segregated into active “A” and repressed “B” compartments. At a finer scale the chromatin fibers are partitioned into higher-order domains of preferential internal interactions defined by boundaries referred to as Topologically Associating Domains (TADs). An example of an active TAD with several interactions between distal regulatory elements and genes within it is shown (Matharu and Ahituv, 2015).

Studies in mammalian cells have shown that disruption of TADs can lead to *de novo* interactions between regulatory elements, such as enhancers, and promoters, resulting in gene misexpression and disease (Flavahan et al., 2016; Franke et al., 2016; Lupiáñez et al., 2015). To fully understand the role of TADs in transcriptional regulation it is thus necessary to understand their formation and maintenance. Notably, TAD boundaries in mammals are frequently enriched in both the transcription factor and insulator CTCF and the structural maintenance of chromosomes (SMC) cohesin complex (Dixon et al., 2012; Phillips-Cremins et al., 2013; Rao et al., 2014) Hi-C maps indicate a strong contact between the CTCF- and cohesin-bound TAD boundaries *i.e.*, “corner peaks”, suggesting a model wherein CTCF binds its cognate sites and recruits cohesin, which then folds the in-between chromatin into a loop structure. Interestingly, removal or change in orientation of a single CTCF site can abolish or

shift the position of the TAD boundary (de Wit et al., 2015; Guo et al., 2015; Lupiáñez et al., 2015), suggesting that not only the presence of CTCF but also a convergent orientation is important for TAD boundaries in mammals. A loop extrusion model has been proposed (Fig16), in which extruding factors, the engaged cohesin SMC complex, progressively forms larger chromatin loops until it encounters boundary proteins, including CTCF, or until the complex is dissociated (Fudenberg et al., 2017, 2016). This model has been reinforced by recent studies that show that depletion of CTCF, cohesin or its loading factor disrupt loop domains while depletion of the cohesin release factor reinforces the strength of the loops at TAD borders (Nora et al., 2017; Rao et al., 2017; Wutz et al., 2017), suggesting a determinant role for cohesion in loop formation.

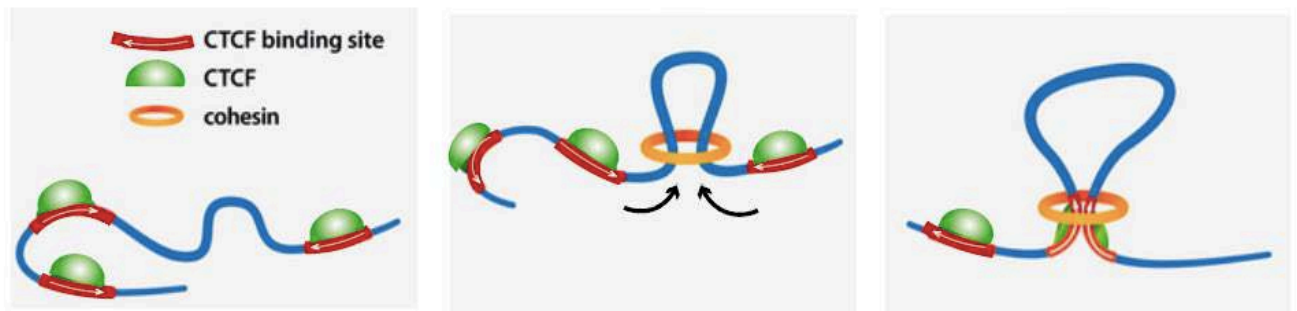


**Fig16-Model for loop extrusion**

Cohesin binds to chromatin, extrudes a chromatin loop and stalls upon encountering CTCF bound at convergently oriented CTCF sites (Wutz et al., 2017).

TADs are also present in the *Drosophila* genome; however, differences have been observed compared to mammalian TADs. Cohesin is also enriched at TAD borders but there are no interaction loops at these borders and enrichment of dCTCF is minor (Van Bortle et al., 2014). Nonetheless, various insulator proteins have been found enriched at boundaries, including Beaf-32, CP190, Pita, M1BP and Chromator (Cubeñas-Potts et al., 2017; Ramírez et al., 2018; Sexton et al., 2012). Also, combinations of these proteins such as Beaf-32/Chromator or Beaf-32/CP190 are good predictors of boundaries (Wang et al., 2018). Surprisingly, siRNA-mediated depletion of Beaf-32 does not abolish boundaries nor has a significant effect on chromatin interactions (Ramírez et al., 2018). A possibility evoked by the authors is that the transcription factor Dref, who binds almost the exact motif as Beaf-32,

could also play a role in chromatin organization. However, no data to support this hypothesis was presented. It is also possible that depletion of a combination of factors is required to disrupt TAD boundaries in *Drosophila*. Further work is thus needed to determine the role of insulator proteins and of other proteins, such as Dref, at *Drosophila* TAD boundaries.

Other mechanisms could also be responsible for 3D organization of chromosomes. Indeed, in mammals even though a majority of TAD boundaries were associated to CTCF, a fraction turned out to be resistant to CTCF loss (Nora et al., 2017). It was observed in mammals and *Drosophila* that TAD borders were enriched for housekeeping genes (Cubebñas-Potts et al., 2017; Dixon et al., 2012; Rennie et al., 2018; Ulianov et al., 2016), those are zones of active transcription hinting thus on a possible role for this process at TAD boundaries. Furthermore, modeling of chromatin fibers proposes that transcription-associated supercoiling could be involved in driving loop extrusion (Racko et al., 2018), suggesting a role for transcription in TAD formation. Based on Hi-C and RNA-seq data in four fly cell lines of various origins, Ulianov and colleagues proposed that inactive TADs are separated by active chromatin regions (Ulianov et al., 2016). In agreement, super-resolution analysis of immunolabeled repressive H3K27me3 or “active” H3K4me3 marks showed active domains at the borders of repressed ones (Boettiger et al., 2016; Cattoni et al., 2017). Moreover, a recent study observed that the degree of transcriptional activity correlates with the strength of TAD insulation (Luzhin et al., 2019). However, inhibition of transcription in mammals and *Drosophila*, does not abolish TAD boundaries (Du et al., 2017; Hug et al., 2017; Ke et al., 2017) nor its induction is sufficient to create TAD boundaries *de novo* (Bonev et al., 2017). It is therefore likely that additional factors are necessary for TAD formation.

Interestingly, polymer simulations using as single input the experimentally derived epigenome from *Drosophila* embryonic cells, agreed with the folding patterns observed in chromosome conformation capture experiments (Ghosh and Jost, 2018; Jost et al., 2014). Additionally, Ulianov and colleagues proposed a “self-assembly” model where nonacetylated nucleosomes from inactive chromatin aggregate whereas acetylated nucleosomes in inter-TADs and TAD boundaries are less prone to interact (Ulianov et al., 2016). These data suggests that the epigenome is a primary driver of chromosome folding in *Drosophila*. Various factors including, transcription, insulator/architectural proteins, epigenetic marks seem to have a role in TAD formation. Further study is thus necessary to determine which

elements are required to form and maintain these compartments separating transcriptional states. This will also help to understand the transition from one domain to another.

As mentioned before, at a larger scale, chromatin in the nucleus is also segregated according to its transcriptional state. Recent research suggests that liquid-liquid phase separation can result in these non-membrane bound compartments in cells. These studies propose that the nucleus is a phase separated compartment containing several different immiscible liquid-like sub-compartments. Segregation of heterochromatin is driven by phase separation mediated, at least in part, by multivalent hydrophobic interactions of HP1a (Larson et al., 2017; Strom et al., 2017). Additionally, clusters of enhancers, regulating cooperatively gene expression can undergo phase separation by transcriptional coactivators suggesting that active domains may also generate phase-separated compartments (Sabari et al., 2018). Together, these physical forces may account at least in part for the compartmentalization of the nucleus.

Importantly, most data gathered from C-based techniques come from a large number of cells and therefore, only averages are observed. To overcome this, chromatin conformation capture-based techniques have been extended to single cell analysis. These studies have revealed heterogeneity in contacts at the TAD scale from cell to cell, with domains appearing as tendencies that become more visible when averaged over a population of cells (Nagano et al., 2013; Stevens et al., 2017; Szabo et al., 2019). This raises the question of the physical reality of TADs rather than just the result of statistical averages. Also, of their functional relevance if such heterogeneity between cells is confirmed. Further single-cell studies are required to elucidate the conservation of TADs at this scale.

There is still much we do not know about nuclear compartments formation and their role in genomic functions. Nonetheless, data gathered in the last few years indicate that these compartments correspond to a functional subdivision of the genome. However, the need of partition the genome into domains to ensure proper gene regulation is still a mystery that hopefully the combination and continuous improvement of new technologies (single-cell omics, super resolution microscopy, modeling of the chromatin fiber...) will be able to elucidate.

In conclusion, eukaryotic transcription is a complex multistep process subject to numerous modes of regulation. This regulation involves the controlled interaction between regulatory elements in the DNA sequence and proteins with a variety of biochemical activities. Interestingly, regulatory elements in the DNA sequence seem to correlate with gene function, however the molecular mechanisms underlying this apparent specificity are yet to be elucidated. In the nucleus, DNA is organized as a chromatin fiber. Therefore, the structure, composition and folding of chromatin represent a major point of control of gene expression. These chromatin features can be dynamically regulated by the concerted action of epigenomic effectors to achieve specific transcriptional outcomes. Indeed, the establishment of specific and highly regulated transcriptional programs determines cell identity and function. During my PhD I particularly focused in the epigenetic control of the *Drosophila melanogaster* ovarian transcriptome. In the next part I will thus describe this particular system.

### **III. Part III Epigenomic regulation during *D. melanogaster* oogenesis**

Fertilization involves the union of two highly different gametes followed by the formation of a totipotent embryo. This implicates a series of complex nuclear and cellular events (Loppin et al., 2015). Remarkably, this occurs in the absence of zygotic transcription which means that these processes are almost entirely controlled by factors already present in the mature oocyte (Avilés-Pagán and Orr-Weaver, 2018; Stitzel and Seydoux, 2007). This developmental strategy is used by a nearly every animal and requires thus the accumulation and deposition of maternal stores during oogenesis. Maternal stockpiles include mRNAs, proteins, and nutrients which permit early embryogenesis to occur in the absence of zygotic transcription.

Preparation of the fertilized oocyte includes profound changes such as completion of female meiosis, formation of male and female pronuclei and the selective translation of

maternal RNAs. The ensemble of events required for the transition from mature oocyte to developing embryo are collectively known as egg activation. Great efforts have been deployed to identify the factors needed for the oocyte-to-zygote transition. (Avilés-Pagán et al., 2020; Avilés-Pagán and Orr-Weaver, 2018; Horner and Wolfner, 2008; Stitzel and Seydoux, 2007). For example, maternal mRNAs synthesized during oogenesis and loaded into the oocyte need to be stably maintained for prolonged periods yet not translated until the right time. Dynamic changes of the poly(A) tail have been involved in the translational control of maternal mRNAs (Eichhorn et al., 2016; Lim et al., 2016; Tadros et al., 2007). These changes depend at least on the kinase Png, the RNA binding protein Smaug and the noncanonical poly(A) polymerase Wispy. However, translational control has not been fully elucidated indicating that more factors are involved. Overall, the oocyte-to-zygote transition requires complex regulation to link developmental signals with profound changes in mRNA translation, cell cycle control, and metabolism. These are complex processes that depend therefore on a wide range of factors with different biochemical properties.

The control of the oocyte-to-embryo transition in *Drosophila* parallels that of other animals, but *Drosophila* offers experimental advantages as a model. In addition to the numerous genetic tools available, the oocyte is the single largest cell and a single ovary contains every stage of oocyte maturation, from stem cell to mature oocyte, and each stage is morphologically distinct (Bastock and St Johnston, 2008; McLaughlin and Bratu, 2015).

## 1. Main steps of *Drosophila* oogenesis

Oogenesis denominates the process of female gamete formation. In insects, this process occurs in the ovarioles of an ovary. *Drosophila melanogaster* females have two ovaries, each containing 16 to 20 autonomous ovarioles, each composed of their own stem cell populations and egg chambers at varying developmental stages (Fig17-A). Each egg chamber gives rise to a single egg. The process of oogenesis has been arbitrarily divided into 14 stages based on morphological criteria (Fig17-B) (King, RC, 1970; Spradling, 1993).

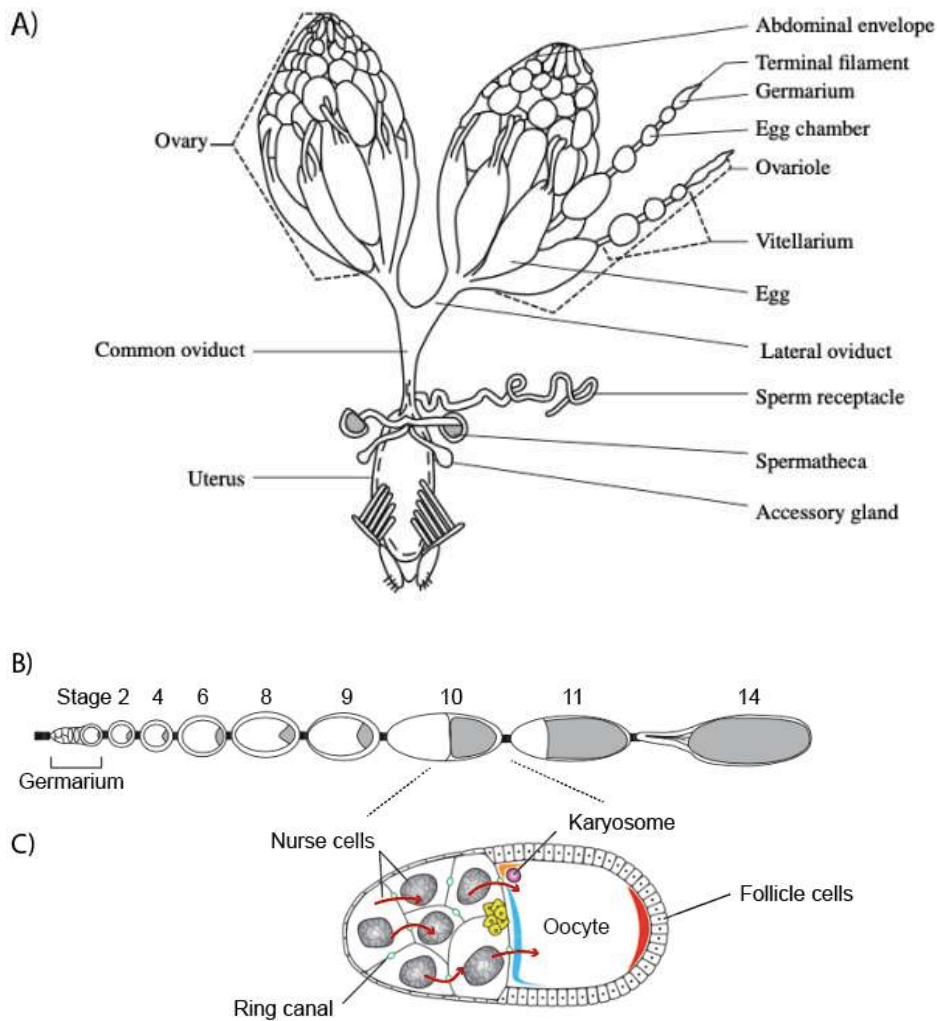


**Fig 17-Oogenesis process in *D. melanogaster***

(A) Organization of the reproductive system in a mature *D. melanogaster* female. The two ovaries are composed of ovarioles each composed of the germarium and egg chambers at varying developmental stages. (B) Scheme of the ovariole with all stages of oogenesis. Egg chambers are formed at the anterior tip, in the germarium and bud at stage 2. The egg chamber grows until stage 10 where the nurse cells empty their content into the oocyte (dumping). Finally at stage 14, the mature egg is enveloped by the vitelline membrane and the chorion and is ready for fertilization. The oocyte is in gray. (C) Detail of an egg chamber at stage 10 where the process of dumping occurs indicated by red arrows (McLaughlin and Bratu, 2015; Ogienko et al., 2007).

Oogenesis progresses from the anterior to the posterior of the ovariole (McLaughlin and Bratu, 2015; Ogienko et al., 2007). The latter can be divided into three regions: a terminal filament, a germarium and a vitellarium. The germarium contains somatic and

germline stem cells (GSC). From there, egg chambers bud off and mature as they pass down the ovariole. Processes like vitellogenesis and choriogenesis are completed in the vitellarium. These constitute the synthesis of protective layers around the egg: the vitelline membrane and the chorion to jointly form the eggshell (Pascucci et al., 1996). Finally, mature eggs reach the posterior part of the ovariole competent for fertilization.

At the anterior tip of the germarium GSCs divide asymmetrically to produce a cystoblast and a new stem cell. Next, the cystoblast undergoes a total of four divisions, producing a 16-cell cyst. Each mitotic division is accompanied by incomplete cytokinesis, forming inter-cellular cytoplasmic bridges known as ring canals. One out of the 16 cells of the cyst becomes the oocyte and the other 15 cells differentiate into nurse cells (Fig18). The oocyte and nurse cells enveloped by somatic follicle cells constitute an egg chamber. Before the egg chamber leaves the germarium, DNA in the oocyte condenses into a compact structure called karyosome. Additionally, meiosis is arrested in prophase I and it will not be continued until late oogenesis, at which point meiosis progresses to metaphase I and is arrested again until egg activation.

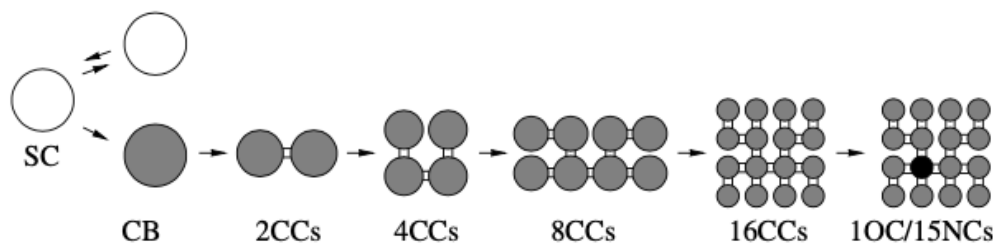


**Fig18-Scheme of germline cell division from a stem cell to a 16-cell cyst.**

Abbreviations: SC= stem cell, CB= cystoblast; CC= cystocyte; OC= oocyte; NC= nurse cell (Ogienko et al., 2007).

The egg chamber buds from the germarium to the vitellarium, marking stage 1 of oogenesis. Developing egg chambers move along the ovariole to the posterior end. The oocyte and nurse cells grow while follicle cells undergo active mitotic divisions. Both nurse cells and follicle cells undergo several rounds of endocycles to synthesize nutrients, mRNAs and proteins essential for oocyte growth and development (see next section). By the end of stage 10, nurse cells empty their content into the oocyte (Fig17-B,C), only nuclei, some actin filaments and a minor amount of cytoplasm remains in the nurse cell. This process is known as “dumping”. It ends with the formation of mature egg, ready for fertilization. Simultaneously, follicle cells

secrete the chorion and the vitelline membrane to protect the mature oocyte. Finally, both nurse cells and follicle cells experience apoptosis at the end of egg chamber development.

## 2. Transcriptional programs of nurse and follicle cells are essential for oocyte nutrition and maturation

In *Drosophila*, germ line transcriptional activity is ensured by the nurse cells, directly connected to the oocyte by cytoplasmic junctions to provide it with large amounts of mRNAs, proteins and other cellular material (Bastock and St Johnston, 2008; Spradling, 1993). This strategy ensures gene expression while maintaining chromosome condensation in the oocyte (Davidson, E, 1986). During early development of egg chamber, certain mRNAs, proteins, and organelles are preferentially transported from nurse cells into the oocyte, in a process known as selective transport. This is a slow and highly selective transport and is essential for oocyte determination and polarity. This process is dependent on the microtubule network and leads to the asymmetric distribution of proteins and mRNAs (Ogienko et al., 2007). After stage 10, rapid transport starts and nonselective dumping of the nurse cell content takes place. This substantial supply is possible thanks to the massive RNA synthesis occurring in the nurse cells. In these cells DNA undergoes 10 to 12 rounds of endoreplication cycles (Dej and Spradling, 1999) and as a result, polyploidy reaches 2048C in cells adjacent to the oocyte. Interestingly, genomic intervals are differentially replicated during the endocycle S phase such that some regions are under-replicated, while others can be amplified (Royzman and Orr-Weaver, 1998). For example, during polyploidization of the nurse cell nuclei, satellite DNA is differentially lost and ribosomal DNA increases in content in their genome (Hammond and Laird, 1985). This bias certainly reflects the needs of the mature oocyte, where great amounts of translation of maternal mRNAs will be needed.

Follicle cells surround the developing oocyte and are also essential for oocyte maturation. Until stage 6 of oogenesis, these cells proliferate by mitosis giving rise to a maximum number of ~1000 cells surrounding the egg chamber (Deng et al., 2001). At stage 6, follicle cells stop a normal mitotic cycle and enter several rounds of endocycles (Nordman and Orr-Weaver, 2012). At stage 10, follicle cells exit the endocycle and begin gene amplification cycles. this event is known as E/A switch. During this amplification, four specific genomic loci, encoding genes involved in chorion and vitelline membrane synthesis,

are amplified from 4 to 80-fold. The four amplified loci are known as a *Drosophila* amplicon in the follicle cells (Claycomb and Orrweaver, 2005). Amplification of two clusters of chorion protein genes allows the production of high-levels of chorion-related proteins, required for egg maturation. Egg chambers are composed of morphologically, genetically and functionally different cells and transcriptional regulation of each of them is important for correct oogenesis.

In conclusion, DNA endoreplication and gene amplification constitute an effective strategy to supply the high demand that represents nourishment and maturation of the oocyte.

### 3. Mechanisms of epigenomic regulation in the female germline

#### A. Silencing of bulk chromatin by the piRNA system

Additional to the silencing of bulk chromatin (described in section II-4) mediated by the H3K9me3/HP1 pathway, the metazoan germline developed the piRNA (PIWI-interacting RNA) system. This is a small RNA silencing system that acts in animal gonads and protects the genome against the deleterious influence of transposable elements (TEs). Indeed, TEs are DNA pieces that can move within the genome potentially compromising faithful transmission of the genetic information in the germline. Loss of piRNAs is associated with significant over expression of retrotransposons (Aravin et al., 2001; Malone et al., 2009), suggesting thus that the mechanism silencing them is piRNA-dependent.

Two types of silencing can be achieved with this pathway, transcriptional silencing mediated by the nuclear Piwi protein in *Drosophila*, or post-transcriptional silencing mediated by cytoplasmic proteins such as Aubergine and Argonaute3. One of the prevalent models for Piwi-mediated transcriptional silencing proposes that the Piwi-piRNA complex binds to the nascent transposon transcript and recruits several proteins ultimately tethering the H3K9 histone methyltransferase Eggless/dSETDB1. This results in the establishment of a repressive chromatin state, silencing thus transposon expression (Fig19). Alternatively, it has also been proposed that Piwi can directly recruit HP1a to initiate the heterochromatinization process. These models are not mutually exclusive and share two features, the binding of a Piwi-piRNA complex at the target site to recruit chromatin factors and transcriptional

repression mediated by chromatin structure modification. Post-transcriptional silence takes place in the cytoplasm where a Piwi-piRNA complex binds the complementary transposon RNA and the latter is cleaved by the Piwi protein. This also promotes piRNA biogenesis and amplifies the system (Ozata et al., 2019; Wang and Lin, 2021), maintaining thereby a solid repression.

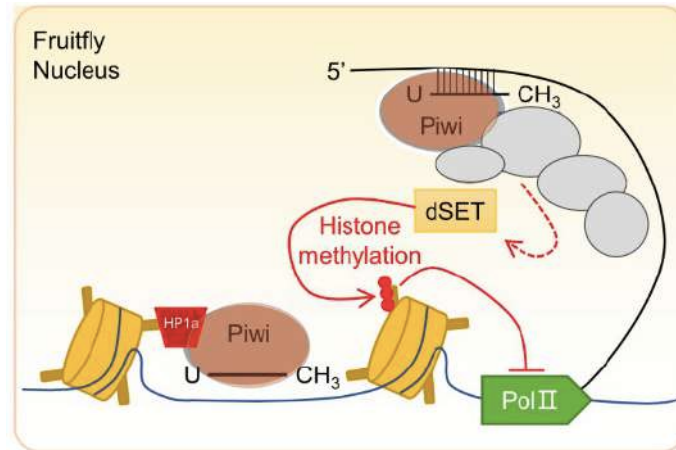


**Fig19-Model for Piwi-mediated transcriptional silencing of transposons in *D. melanogaster* nucleus.**

Piwi-piRNA complex binds to a nascent transposon transcript ultimately recruiting to the vicinity of the target chromatin region the H3K9 methyltransferase Eggless/dSetDB1 which establishes a repressive chromatin state to suppress transposon expression. Alternative model proposes that Piwi can directly recruit HP1a (Wang and Lin, 2021).

piRNA biogenesis can be divided into two stages. First, long RNA precursors are transcribed in the nucleus and exported into the cytoplasm. In the cytoplasm, piRNA precursors are further processed to generate mature piRNAs that get loaded into Piwi proteins. In flies, piRNA precursors come from heterochromatic loci. In the germline, majority of piRNAs are produced in “dual-strand” clusters. They produce sense and antisense piRNAs regardless of transposon orientation and their transcription requires both the repressive chromatin mark H3K9me3 and the transcriptional silencing protein Piwi (Akkouche et al., 2017; Rangan et al., 2011). Dual-strand clusters give rise to piRNA precursor RNAs via non-canonical transcription facilitated by the Rhino protein, a germline-specific HP1 variant (Klattenhoff et al., 2009). Rhino binds H3K9me3 and tethers a specific transcription factor initiator, Moonshiner, on both strands of DNA. In turn, Moonshiner forms an alternative pre-initiation complex, allowing RNA Pol II to initiate transcription from many

sites on both DNA strands. Rhino is thus able to bypass the need of specific DNA regulatory sequences such as promoters (Andersen et al., 2017). To conclude, the piRNA-Piwi silencing system provides a potent chromatin-based defense against potential deleterious effects from TEs, thereby guarding genome integrity in the future gametes.

## B. The importance of fine transcriptional regulation during oogenesis

The products contained in the oocyte ensure a successful oocyte-to-zygote transition and early embryogenesis. However, most of our knowledge of this process is centered on the post-transcriptional regulation of gene expression (Kronja et al., 2014). Polyploid nurse cells are capable of mass-producing the necessary factors for the onset of development. Yet, transcriptional regulation during oogenesis has been largely overlooked. Focus on the fundamental importance of proper regulation of transcriptional programs during oogenesis has just recently emerged.

### *a. Targeted silencing is essential for female germline determination*

In part II of this introduction, I described a series of mechanisms to ensure fine gene regulation based on chromatin-related mechanisms. Nonetheless, knowledge on how these mechanisms are used in the female germline is very limited. As said before, a unique germ stem cell (GSC) gives rise to different lineages of the germline, the nurse cells and the oocyte. This unique cell must thus undergo major changes in gene expression and chromatin organization.

New insights underlying epigenomic changes during oogenesis came from a recent study, from the Spradling lab, where they used *Drosophila* oogenesis to study Polycomb repression. Implication of Polycomb proteins in gene regulation during *Drosophila* oogenesis had already been observed. A mutation in E(z), the catalytic subunit of the PRC2 complex, impairs gene silencing of *Cyclin E* and *dacapo*, a cyclin-dependent kinase inhibitor. This results in the oocyte-to-be entering a nurse cell-like endoreplicative program and failing to be determined as the oocyte (Iovino et al., 2013). In the new study by DeLuca *et al.*, authors unveiled a role for Polycomb silencing in the transition from GSC to nurse cell (DeLuca et

al., 2020). They first noticed that the patterns of H3K27me3 between these two cell types were different. Indeed, nurse cell progenitors lack silencing and H3K27me3 shows a broad distribution, referred to by the authors as non-canonical H3K27me3 pattern. As nurse cells differentiate, the H3K27me3 pattern becomes focused on common PcG domains. The authors proposed a model where association of PRC2 with the PcG protein Pcl, prevents it from sampling at many sites, resulting in infrequent and stochastic silencing. As differentiation occurs, Pcl levels drop and core-PRC2 is freed to sample and silence more sites. This study shows how Polycomb-mediated reshaping of chromatin is essential for female germline development in *Drosophila*.

Interestingly, it was also observed that female germ cell fate is maintained by an epigenetic regulatory pathway depending on H3K9me3/HP1a silencing of key spermatogenesis genes (Smolko et al., 2018). Female germ line specific knockdown of the H3K9 methyltransferase *eggless/dSETDB1* and its partners *HP1a* and *windei* results in ectopic expression of testis-specific genes. Mapping of H3K9me3 revealed the accumulation of this mark on 21 of the ectopically expressed genes. Remarkably, and contrary to the general vision of H3K9me3 as broad heterochromatin blocks, the mark was highly localized and did not spread into neighboring loci. A striking example the authors described was the *phf7* gene, where in ovaries, H3K9me3 is restricted to the region surrounding the silent testis-specific TSS. The mechanisms through which H3K9me3 is targeted and restricted in such a specific manner are not fully elucidated. Nevertheless, this study provides a non-common usage of the H3K9me3/HP1a silencing pathway in the female germline.

Overall, these data emphasize the importance of fine chromatin-based regulation of transcription in the female germline for correct gamete production.

#### *b. Histone modifiers play an important role in transcription activation during oogenesis*

Different studies found an important role for histone modifiers during oogenesis, pointing out the importance of an epigenetic mode of regulation during this process. The importance of the H3K4me3 histone demethylase *Lid/dKDM5* during oogenesis was observed by two different groups in addition to ours (see Results). Zhaunova and colleagues observed that absence of *Lid/dKDM5* in the female germline leads to a series of defects in meiotic chromatin organization in oocytes, including instability of the recombination

machinery (Zhaunova et al., 2016). Oocytes remain arrested in prophase I of meiosis for a significant amount of time. They are transcriptionally silent throughout this arrest but they reactivate transcription prior to the resumption of meiosis (Mahowald and Tiefert, 1970). Navarro-Costa and colleagues characterized the epigenome of the prophase I-arrested oocyte and found that it is highly dynamic and contains both euchromatic and heterochromatic marks that vary during oocyte quiescence and reactivation (Navarro-Costa et al., 2016). Female germ-line depletion of Lid/dKDM5, led to a significant increase in the levels of H3K4me3 and to precocious transcriptional reactivation of the quiescent prophase I-arrested oocytes. On the contrary, no changes in H3K27me3 levels were detected. Importantly, the demethylase activity of Lid/dKDM5 was required for correct transcriptional reactivation of the oocyte and meiotic progression, suggesting a role of this histone demethylase in the regulation of the oocyte epigenome. These data support the hypothesis that correct reactivation of the dormant primary oocyte is epigenetically regulated. They also observed that loss of Lid/dKDM5 severely affects meiotic completion and accordingly, most fertilized eggs fail to initiate mitotic divisions.

Furthermore, a recent study identified the H3K4 methyltransferase Trr as essential for the oocyte-to-zygote transition. Interestingly, in the absence of Trr, oocytes develop normally but fail to complete maternal meiosis and to form the paternal pronucleus. The proposed model is that during oocyte development, Trr promotes the expression of a subset of genes that are not required during oogenesis but their presence in the mature oocyte is critical for proper zygote formation (Fig20). One of the identified genes under direct control of Trr and necessary for the oocyte-to-zygote transition coded for the IDGF4 glycoprotein (Prudêncio et al., 2018) but its specific role at zygote formation is yet to be determined. Overall, these data emphasize the important role of chromatin regulation during female gametogenesis.

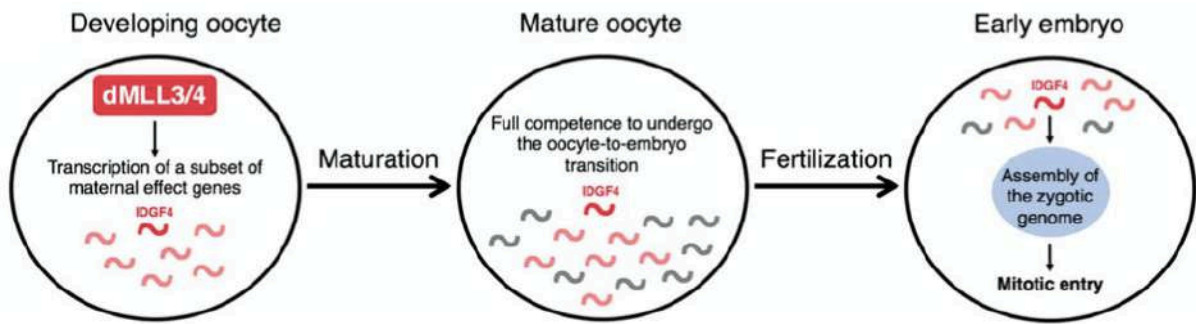


**Fig20-Proposed model for Trr-regulated acquisition of embryo fate at fertilization.**

During oocyte maturation, Trr promotes the expression of a subset of genes, which products are not required for normal oogenesis but will be indispensable for zygotic genome assembly at fertilization (Prudêncio et al., 2018).

Emergent evidence suggests that transcriptional regulation during oogenesis is mediated, at least in part, by epigenetic mechanisms that define specific gene expression modules. This allows the establishment of the molecular basis of the crucial and complex oocyte-to-zygote transition.

#### **IV. Part IV The peculiar case of *dhd* regulation**

My PhD project was based on the discovery of a specific functional connection between a series of epigenomic effectors and the highly regulated terminal effector of zygote formation, the maternal thioredoxin Deadhead (Dhd). The different effectors involved are: the histone demethylase Lid/dKDM5, the histone deacetylase complex scaffold Sin3A, the Brahma chromatin remodeler sub-unit Snr1 and the insulator component Mod(mdg4). The case of *dhd* represented thus an opportunity to study the molecular mechanisms underneath transcriptional regulation by chromatin factors. I will first introduce the role of Dhd at fertilization and the specific features of this protein and of the gene that encodes it. This will be followed by a state-of-the art on the epigenomic effectors that regulate this singular gene.

## 1. The essential role of Deadhead at fertilization

The *dhd* gene encodes an egg specific thioredoxin required for female fertility and development of viable embryos (Emelyanov and Fyodorov, 2016; Salz et al., 1994; Tirmarche et al., 2016). Thioredoxins are small, highly conserved redox proteins that catalyze the reduction of disulfide bonds on target proteins (Arnér and Holmgren, 2000). At fertilization, Dhd is critically required for sperm chromatin remodeling. DNA in the sperm nucleus is highly compacted due to the almost total replacement of histones by sperm nuclear basic proteins (SNBPs), including protamines (Miller et al., 2010). This level of compaction is incompatible with basic nuclear activities such as transcription, replication or repair. One of the first key events at fertilization is thus remodeling of this nucleus so that paternal chromosomes can be integrated into the zygote (Fig21-A) (Loppin et al., 2015). This process depends on Dhd reducing disulfide bonds between protamines thus allowing sperm nuclear decondensation. Indeed, in eggs laid by *dhd* null mutant females, the sperm nucleus retains protamines and remains needle-shaped, reminiscent of its ultra-compacted DNA (Fig21-B,C) (Emelyanov and Fyodorov, 2016; Tirmarche et al., 2016). A catalytic mutant is unable to rescue the *dhd* mutant phenotype showing that this process depends on Dhd catalytic reducing activity (Emelyanov and Fyodorov, 2016; Tirmarche et al., 2016). Dhd has also been involved in the redox balance at the oocyte-to-embryo transition (Petrova et al., 2018). The study of redox state changes during this process revealed that early embryos have a more oxidized state than mature oocytes. It was observed that *dhd* mutant oocytes are prematurely oxidized and exhibit meiotic delay. A highly specific list of Dhd substrates was established and a major fraction of Dhd's interactors are ribosomes or ribosome-associated. These data show that Dhd has crucial roles during the oocyte-to-zygote transition.

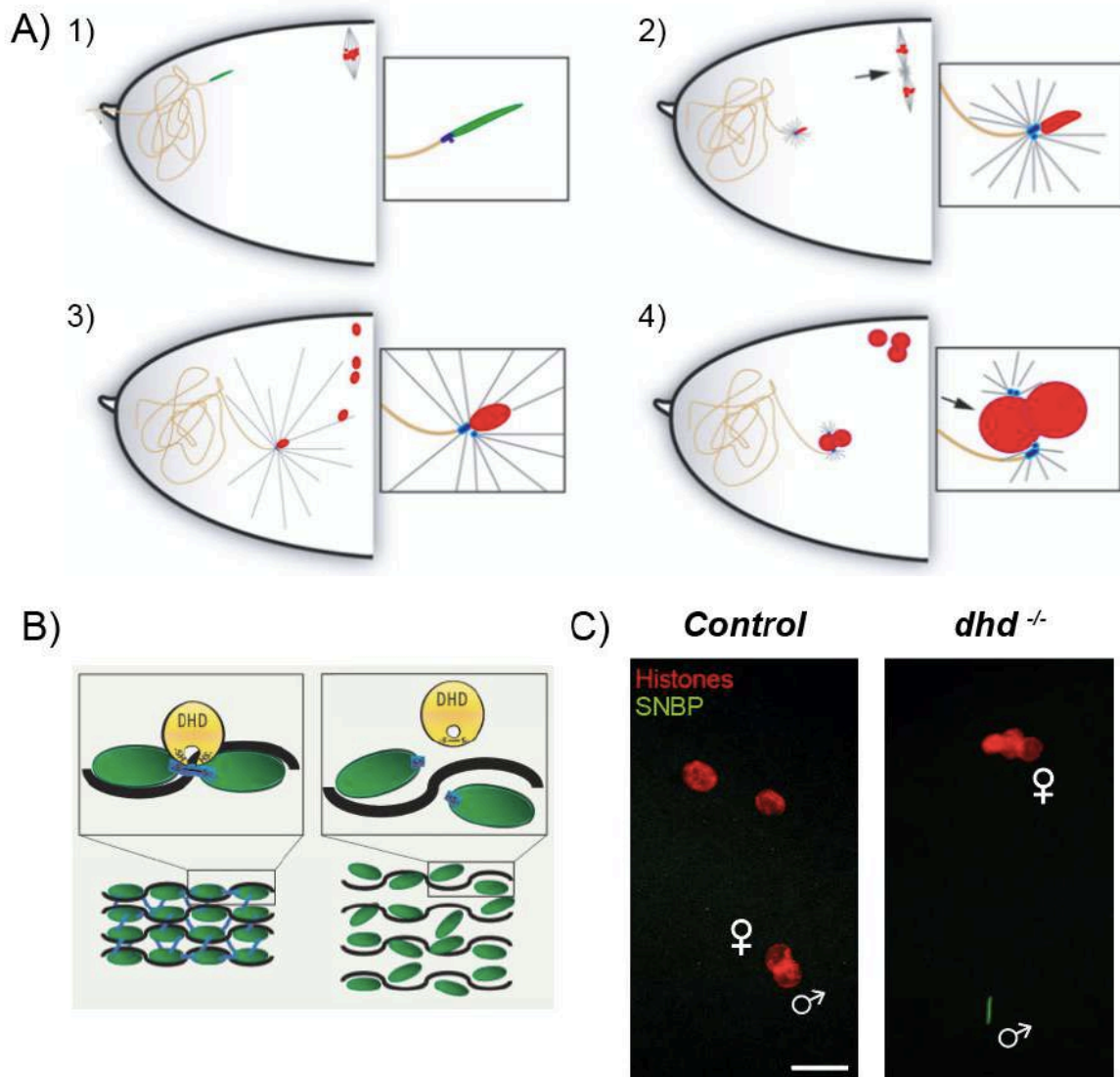


**Fig 21: The essential role of Deadhead at fertilization.**

(A) First steps of zygote formation in *Drosophila melanogaster*. (1) Sperm enters the egg. At fertilization, maternal chromosomes are arrested in metaphase I of meiosis I. Sperm nucleus is ultra-compact and packed with sperm nuclear basic proteins (SNBPs) (green). (2) Maternal chromosomes progressed to metaphase of meiosis II. Remodeling of the sperm chromatin took place: SNBPs were replaced by maternally provided histones (red) and the nucleus is decondensed. (3) Pronuclei migration. The inner most product of female meiosis migrates towards its male counterpart. (4) Apposition of female and male pronuclei. The first zygotic replication begins (Loppin et al., 2015). (B) Schematic representation of the role of Deadhead at fertilization. The thioredoxin DHD reduces disulfide bonds between SNBPs (left) allowing their eviction and chromatin decondensation (right) (Horard and Loppin, 2017). (C) Confocal images of eggs at the apposition stage, laid by control (left) and *dhd* null (right) mutant females. In control eggs both male and female pronuclei are round and

contain only histones. In *dhd* mutant eggs, the sperm nucleus retains SNBPs and is needle-shaped, reminiscent of compacted DNA. Scale bar 10  $\mu$ m.

Dhd is exclusively found in ovaries, its levels increase during oocyte maturation and start decreasing at egg activation (Kronja et al., 2014; Tirmarche et al., 2016). At fertilization, Dhd is abundant and homogeneously distributed throughout the egg cytoplasm. Strikingly, it becomes rapidly undetectable after completion of the first zygotic cycle (Fig22) (Tirmarche et al., 2016). This indicates that likely Dhd plays no other role after zygote formation and it is possible that its continued presence is detrimental to embryogenesis.

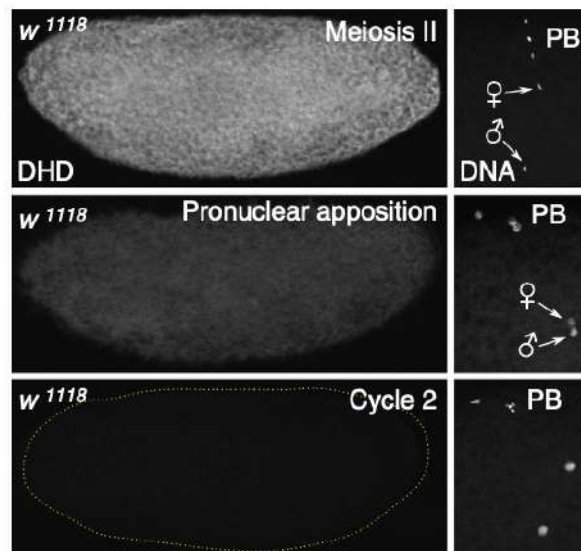


**Fig22-Deadhead is rapidly degraded after fertilization**

Confocal images of control eggs stained for DHD (left) and DNA (right). DHD is abundant and homogeneously distributed at fertilization but is rapidly undetectable (Tirmarche et al., 2016).

The role of Dhd is thus essential for the oocyte-to-zygote transition and the onset of embryonic development. Interestingly, *dhd* stands out for a series of unusual features at the protein level as well as at its genomic locus.

## 2. Dhd, a thioredoxin not like the others

As mentioned before, Dhd is a thioredoxin. Thioredoxins constitute a family of small thiol proteins that are present in all organisms studied so far, and are characterized by the sequence of their conserved active site (WCGPC). In addition to their role maintaining redox homeostasis in the cell, they have been implicated in DNA synthesis, regulation of transcription factors or programmed cell death (Arnér and Holmgren, 2000), indicating a wide variety of roles for these proteins.

*Drosophila melanogaster* possesses three true thioredoxins, the testis-specific TrxT, the ovary-specific Dhd and the ubiquitous Trx2. Alignment of the protein sequences revealed that Dhd is less related to Trx2 than TrxT (J. Svensson and Larsson, 2007). Accordingly, *in vitro* Trx2 is not able to substitute Dhd's role in reducing protamine disulfide bonds (Emelyanov and Fyodorov, 2016; Tirmarche et al., 2016). Interestingly, a recent characterization of the structure of the *Drosophila melanogaster* thioredoxins revealed that Dhd has an atypical structure for a thioredoxin (Freier et al., 2021). In contrast to the negatively charged surfaces commonly found in most thioredoxins, it was observed that Dhd has positively charged patches on its surface. Dhd is in charge of reducing protamine disulfide bonds in sperm chromatin and was found associated with ribosomes (Petrova et al., 2018; Tirmarche et al., 2016). The unusual positive patches on its surface might thus help Dhd in selecting proteins and DNA/RNA partners by complementarity with their negatively charged backbone. This distinctive charge distribution helps to define the initial encounter with DNA/RNA complexes that will lead to final specific interactions with cofactors to promote chromatin remodeling (Freier et al., 2021). Specific and unusual features of the Dhd thioredoxin are thus important for its role at fertilization.

### 3. The intricate *dhd* locus

Dhd protein is present exclusively in ovaries (Salz et al., 1994; Tirmarche et al., 2016). Accordingly, RNA *in situ* hybridization experiments show that the gene is transcribed in nurse cells and the transcript is highly present at stage 10 and then deposited in the oocyte (Salz et al., 1994; Svensson et al., 2003; Tirmarche et al., 2016).

Data from Flybase (<http://flybase.org>), and our own RNA-seq analyses, indicate that *dhd* is among the most highly expressed genes in ovaries (Fig23-A). This is all the more

surprising due to the genomic context of this gene. *dhd* is a small, intronless gene located in the middle of a cluster of fifteen densely packed genes spanning about 40 kb of genomic DNA (Fig23-B). Commonly, *Drosophila* genes with tissue-, temporally-biased expression patterns have been shown to be concentrated in neighborhoods of contiguous genes (Parisi et al., 2004; Spellman and Rubin, 2002). However, the *dhd* gene lies within a 1.4 kb region that is immediately flanked by two genes with testis-specific expression, the thioredoxin *Trx-T* and the *CG4198* gene of unknown function. *TrxT* and *dhd* are arranged as a gene pair, transcribed in opposite directions separated by 282 bp. These two genes have thus closely spaced promoters and are differentially regulated by a short common control region. A transgene including the *TrxT-dhd* region and an additional 2 kb and 1 kb downstream of *TrxT* and *dhd* respectively ( $P[w^+ snf^+ TrxT^+ dhd^+]$ ) (Fig23-B), inserted at the X chromosome or at an autosome was able to recreate the expression pattern of *TrxT* and *dhd*. This shows that the endogenous X chromosome location of *TrxT-dhd* is not essential for tissue-specific transcription (Svensson et al., 2007). Furthermore, an even smaller transgene spanning only *Trx-T*, *dhd* and part of *CG4198* ( $pW8-attB-dhd^{WT}$ ) (Fig23-B), fully rescues *dhd* maternal effect embryonic lethal phenotype (Tirmarche et al., 2016), showing that this 4.3 kb region is capable of recapitulating *dhd* expression. The necessary regulatory signals for *dhd* activation are thus contained within this restricted region.

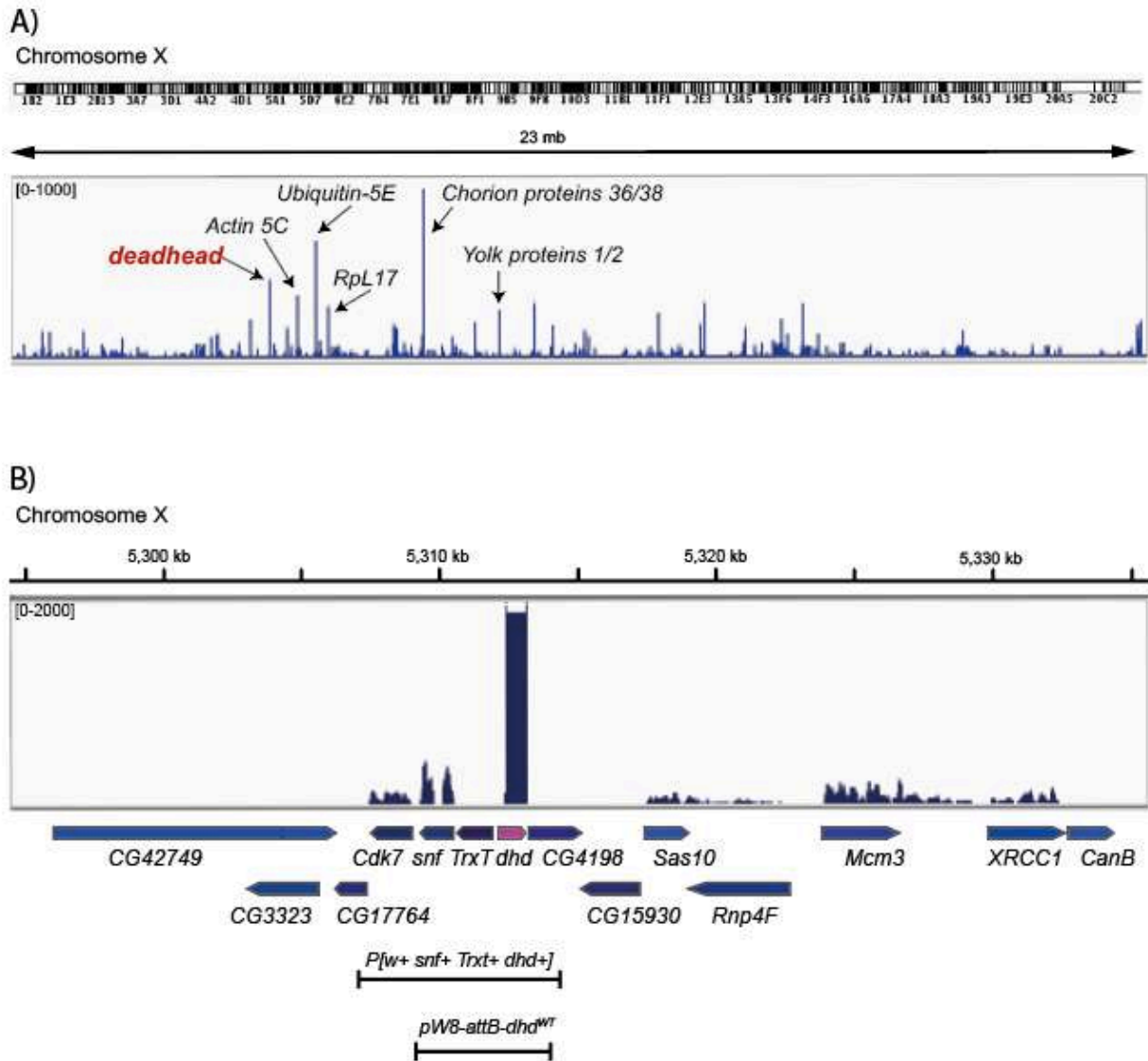


**Fig 23-*deadhead* is massively expressed in ovaries**

*dhd* is amongst the highest expressed genes in ovaries. (A) Genome browser view of control ovarian RNA-seq signal of the X-chromosome showing the high level of transcription of *dhd*. Examples of other highly expressed genes are indicated by arrows. (B) Genome browser view of control ovarian RNA-seq signal at the *dhd* region. Signal coming from the *dhd* locus was truncated for readability. The genomic region covered by two different transgenes are shown: (i) the *P[w+ snf+ Trxt+ dhd+]* transgene, capable of recreating *dhd* expression pattern (Svensson et al., 2003) and (ii) the *pWB-attB-dhd<sup>WT</sup>* transgene, capable of restoring *dhd* expression and rescue female sterility [Tirmarche et al., 2016].

Svensson and colleagues did a thorough analysis of the organization of the *TrxT* and *dhd* locus across several *Drosophilid* species (Svensson et al., 2007). The intriguing gene organization and regulation of *TrxT* and *dhd* is remarkably well conserved. For both of these

genes, the lack of introns in the coding region is conserved across species. Additionally, predictions of TSSs for *dhd* and *TrxT* in different *Drosophilid* species revealed that the closer to the transcription start sites, the higher the conservation level of the sequence. Conserved motif analysis within 150 bp upstream of the predicted TSSs revealed 9 different motifs however, none of them had obvious similarities with known common target sequences for transcription factors. The motifs identified were also compared to the 5' flanking regions of ovary- and testis-specific genes. They were detected in less than 1% of the genes in both ovary and testes sets indicating that they are neither ovary- nor testis-specific. Finally, the search for gene pairs including a testis-specific gene and an ovary- specific gene transcribed in opposite directions and separated by no more than 1000 bp, showed only 8 additional gene pairs in this configuration. None of the nine motifs previously identified were found in the 5' flanking regions of any of the other gene pairs. Importantly, none had such extreme ovary- or testes-specific expression as *dhd* and *TrxT* when expressed as a ratio, showing thus the rareness of this organization.

In conclusion, the genomic organization and regulation of *TrxT* and *dhd* is unique and well conserved in evolution. Strikingly, the *dhd* locus accumulates a series of counterintuitive features when considering its high expression.

#### 4. State-of-the art of *dhd* regulators in transcription regulation

My PhD project focused on the epigenetic regulation of the *dhd* singular gene which led me to focus on the role of particular epigenomic effectors so in this section I will more precisely lay out the current literature on their roles in transcription regulation.

##### A. The histone demethylase Lid/dKDM5

Lid/dKDM5 is the sole member of the KDM5 histone demethylases in *Drosophila*. It specifically targets H3K4me3 *in vivo* (Secombe et al., 2007). Lid/dKDM5 has been found enriched at promoter regions in embryonic cells, whole adults and wing discs (Gajan et al., 2016; Liu and Secombe, 2015; Lloret-Llinares et al., 2012; Zamurrad et al., 2018), hinting about a role in transcriptional regulation.

Since H3K4me3 has long been associated with transcriptional activation and Lid/dKDM5 removes this mark, this enzyme could have been expected to have a role in global repression rather than activation. Nonetheless, RNA-seq analyses in mutants and Lid/dKDM5-depleted cultured cells, show equivalent up-regulated and down-regulated genes (Drelon et al., 2018; Gajan et al., 2016; Liu and Secombe, 2015). A global increase in H3K4me3 is consistently observed upon Lid/dKDM5 depletion or mutation, however the impact on transcription has been found mild (Drelon et al., 2018; Liu et al., 2014; Lloret-Llinares et al., 2012; Zamurrad et al., 2018). This reinforces the enigmatic role of H3K4me3 in transcriptional activation discussed in section II-7-B.

The impact of H3K4me3 on transcription is not clear however Lid/dKDM5 possesses additional domains with other functions. Indeed, the family of KDM5 proteins contain the following domains: JmjN domain (unknown function), JmjC domain (H3K4me3 demethylase activity), ARID (implicated in DNA binding), C5HC2 zinc finger and two or three PHD domains (protein-protein interaction). Interestingly, null *lid* mutants are lethal but can be rescued with a demethylase-dead transgene (Drelon et al., 2018; Li et al., 2010; Liu and Secombe, 2015), showing thus that Lid/dKDM5 has catalytic-independent crucial roles. Indeed, in whole adults, Lid/dKDM5 proved to be a critical regulator of genes associated with mitochondrial structure and function. This regulation was independent from its demethylase JmjC domain however the C-terminal PHD motif, capable of binding di- and trimethylated H3K4 was essential (Liu and Secombe, 2015). Nonetheless, in a study where only fly brains were analyzed, it was observed that Lid/dKDM5 can directly activate or repress transcription in a demethylase-dependent manner (Zamurrad et al., 2018). These data indicates thus that Lid/dKDM5 regulates genes involved in different cellular processes and that this regulation can depend or not on its demethylase activity.

An extra layer of complexity comes from the fact that Lid/dKDM5 can act with different partners, probably due to its different protein domains. These interactions can lead to different outcomes on gene transcription. In *Drosophila* embryos, Lid/dKDM5 was found in a complex with the histone deacetylase Rpd3, the scaffold Sin3A, the histone chaperones (Asf1 or Nap-1) and other proteins. The resulting complexes acted as repressors of Notch target genes (Moshkin et al., 2009). However, in embryonic fly cells, Lid/dKDM5 interaction with the transcription factor Foxo and the histone deacetylase dHDAC4 leads to the activation of a subset of Foxo target genes (Liu et al., 2014), showing the versatility of Lid/dKDM5 on transcriptional outcomes. It has been also observed that Lid/dKDM5

genetically interacts with the H3K4me1/2 demethylase dLsd1 (Di Stefano et al., 2011). Lid/dKDM5 opposes the functions of dLsd1 and the H3K9 methyltransferase Su(var)3–9 in promoting heterochromatin spreading at heterochromatin–euchromatin boundaries. However, Lid/dKDM5 cooperates with dLsd1 in regulating certain Notch target genes in euchromatic contexts, illustrating that the activity of histone demethylases is context-dependent. Lid/dKDM5 has thus a complex and intricate role in gene transcription regulation that depends on several factors such as cell-type and interactors.

## B. The Sin3-HDAC complex

The Sin3 protein is highly conserved from yeast to mammals and has different isoforms in metazoans (Chaubal and Pile, 2018). Sin3, through its interaction with DNA-binding factors, acts as a scaffold protein that recruits histone deacetylases (HDACs) and other chromatin-modifying enzymes onto target promoters (Silverstein and Ekwall, 2005).

Classically, Sin3-HDAC complexes have been associated with transcriptional repression via direct recruitment of transcriptional repressors mediated by Sin3 and nucleosome deacetylation (Kadamb et al., 2013; McDonel et al., 2009; van Oevelen et al., 2008; Sahu et al., 2008). Accumulating evidence, however, points to a dual role of the SIN3 complex in transcriptional regulation. The Sin3A protein in *Drosophila* was found to bind promoters at euchromatic regions, preferentially at TSSs (Das et al., 2013; Saha et al., 2016). The transcriptional profile of a Sin3-deleted yeast strain showed both gene upregulation (173) and downregulation (269), suggesting thus a dual role of this protein in transcription (Bernstein et al., 2000). This tendency was also observed in *Drosophila* cultured cells upon depletion of Sin3A (Gajan et al., 2016; Saha et al., 2016). Sin3 can then positively or negatively influence transcription.

Studies integrating transcriptome and genome-wide binding data in human kidney and fly embryonic cells provided evidence of a direct role of SIN3A in gene transcription. For human SIN3A, 42% of activated genes and 61% of repressed genes were directly bound by this protein (Williams et al., 2011). In *Drosophila* embryonic cells, 92 % and 46 % of the genes repressed and activated by Sin3A, respectively, are direct targets (Saha et al., 2016).

These results suggest thus a direct role of SIN3A both in activation and repression and at least for *Drosophila*, repressed genes are more likely to be direct targets. The corepressor activity of Sin3A is commonly attributed to its association with histone deacetylases. However, the mechanisms through which Sin3A could mediate gene activation are not known. One possibility is that the deacetylase component of the SIN3 complex could act on transcription factors thereby altering DNA-binding capability or protein interactions. For example, it has been observed that acetylation of the transcription factor FoxO1 reduces DNA-binding affinity (Brent et al., 2008). These data show that at least a subset of genes can be direct targets of Sin3A, however the Sin3A-dependent molecular mechanisms regulating transcription are fully understood. Much work remains to determine the network of interactors of Sin3 proteins which will help elucidate how a single complex can have opposite effects on transcription.

### C. The nucleosome remodeler subunit Snr1

The conserved SWI/SNF family contains multi-subunit chromatin-remodeling complexes. These are large protein complexes usually formed around Brm (Brahma) in *Drosophila* or BRG1 in Humans, which confer the ATP-hydrolysis catalytic activity. In *Drosophila*, two Swi/Snf complexes exist: the BRM-associated protein complex (BAP) and the polybromo-containing BAP complex (PBAP). These complexes share a common core and differ by signature subunits (Mohrmann et al., 2004). Snr1 is part of the common core of the BAP/PBAP complexes and was found essential for fly viability (Dingwall et al., 1995).

First indications that *snr1* might have a role in gene expression came from its genetic interaction with the TrxG genes *brahma* and *trithorax* (Dingwall et al., 1995). Furthermore, staining in polytene chromosomes showed that a subset of Snr1 overlaps with a fraction of RNA Pol II, suggesting a wide array of potential *in vivo* targets for gene regulation (Zrally et al., 2003). Additionally, an upregulation of the clustered *Ecdysone induced genes* (*Eig*) was observed in loss of function *snr1* mutants and *snr1*-depleted cultured cells. The proposed model by the authors was that upon Snr1 loss, nucleosome accessibility increases and minimizes barriers to transcription. Like this, RNA Pol II proceeds elongation with little or no stalling (Zrally et al., 2006; Zrally and Dingwall, 2012). This suggests thus a function for Snr1 within remodeler activities.

Moreover, it was observed that Snr1 is not required or expressed in all tissues dependent on BAP/PBAP complex activities (Zraly et al., 2003). Snr1 is thus not necessary for all BAP/PBAP functions. Since Snr1 is essential for viability it likely has regulatory functions independent from the BAP/PBAP complexes. RNA-seq analysis in control and Snr1-depleted tumorigenic wing imaginal discs revealed hundreds of misregulated genes upon *snr1* loss and most of them (336 vs 57) were upregulated (Xie et al., 2017). In contrast to *Eig* genes, in this case Snr1, mostly had a repressive role. Strikingly, this study also described a cytoplasmic localization of Snr1 in wing disc cells and salivary gland cells contrary to other core subunits of the BAP/PBAP complexes. This location was required for its tumor-suppressor role. Overall, these data show that Snr1 has gene regulatory functions within and outside the BAP/PBAP complexes. These functions can favor or repress transcription depending on the targets.

#### D. The multifaceted protein Mod(mdg4)

Between 1993 and 1997, the *mod(mdg4)* gene was cloned three separate times, each time by a different laboratory and was associated to different functions. First, as an enhancer of position-effect variegation, a protein involved in establishing and/or maintaining an open chromatin conformation (Dorn et al., 1993). Next, as a chromatin insulator by directing the repressive effect of Su(Hw) (Gerasimova et al., 1995). Finally, as a protein that induces apoptosis (Harvey et al., 1997). Around the same time, it was also observed that in *mod(mdg4)* mutant larvae, expression of some homeotic genes was decreased, suggesting a positive role for Mod(mdg4) in their regulation (Gerasimova and Corces, 1998). The multifaceted character of Mod(mdg4) could be due to the wide variety of isoforms that come from the single gene. Indeed, at least 31 isoforms sharing a common N-terminal region have been identified from the *mod(mdg4)* gene (Büchner et al., 2000). To date, the most well-studied isoform is the 67.2 for its essential role along with Su(Hw) and CP190 at the *gypsy* insulator (Gerasimova et al., 1995; Melnikova et al., 2017, 2004). However, polytene chromosome staining and ChIP experiments of the 67.2 isoform do not account for all Mod(mdg4) recruitment to DNA (Büchner et al., 2000; Melnikova et al., 2019; Van Bortle et al., 2012). Additionally, a null allele of *mod(mdg4)* showed that this gene is essential but mutations disrupting only the 67.2 isoform are viable (Savitsky et al., 2016) indicating that the roles of Mod(mdg4) go beyond its insulator function.

Little is known about the mechanisms of action of Mod(mdg4) and its influence on gene transcription but mapping of the protein revealed its enrichment at gene promoters in fly embryos (Nègre et al., 2010). Mod(mdg4) does not have sequence specificity and may not be able to bind DNA directly but can mediate homotypic and heterotypic protein–protein interactions via its BTB/POZ domain. This in turn could support pairing between distant regions in the chromosomes (Gurudatta and Corces, 2009; Kyrchanova and Georgiev, 2014). Studies of the role of Mod(mdg4) at the BX-C complex revealed that it promotes *Abd-B* expression in the posterior abdominal segments (Büchner et al., 2000; Dorn et al., 1993; Savitsky et al., 2016) but no mechanism has been proposed. It was observed that *mod(mdg4)* mutations enhance transformations caused by dCTCF deficiency. Also, dCTCF and Mod(mdg4) share many sites at the bithorax complex and genome-wide (Nègre et al., 2010; Savitsky et al., 2016; Van Bortle et al., 2012), favoring a scenario where these two proteins are part of the same molecular pathway. One possibility is that Mod(mdg4) and dCTCF promote the interaction of *Abd-B* promoter with the corresponding enhancers. Since both proteins bind the vicinity of some of the *Abd-B* TSSs, a direct role promoting transcription is also worth considering (Savitsky et al., 2016). Mod(mdg4) has also been found at the borders of H3K27me3 domains. Its depletion led to a decrease of the mark within the domain. Surprisingly, there was no significant effect on expression at genes flanking the domain nor at those embedded in the domain (Schwartz et al., 2012; Van Bortle et al., 2012). However, this was only assessed at a limited number of genes, a genome-wide study would help to evaluate the impact of Mod(mdg4) depletion on transcription. It is well-documented that Mod(mdg4) can affect gene expression when it is part of an insulator complex. However, there is limited data concerning the roles that other isoforms may have in gene transcriptional regulation. Further work is needed to clarify this potential role and to unveil the molecular mechanisms underneath it.

The accumulation of specific features makes Deadhead truly unique. The *dhd* locus is located in an unfavorable genomic environment but achieves high ovary-specific expression, which makes its regulation even more intriguing. Additionally, the epigenomic effectors at play have been shown capable of favoring repression as well as activation of transcription in a context-dependent manner. The *dhd* locus represents thus a paradigmatic gene exquisitely

regulated by chromatin factors and offering a unique opportunity to study the molecular mechanisms at play in epigenetic transcriptional regulation.

# RESULTS & DISCUSSION

<b>I. AN SHRNA SCREEN IDENTIFIES MATERNAL CHROMATIN FACTORS REQUIRED FOR THE OOCYTE-TO-ZYGOTE TRANSITION .....</b>	<b>84</b>
1. ARTICLE PRESENTATION .....	84
<b>II. THE CONCERTED ACTIVITY OF EPIGENOMIC EFFECTORS IS ESSENTIAL TO ESTABLISH TRANSCRIPTIONAL PROGRAMS DURING OOGENESIS.....</b>	<b>137</b>
1. ARTICLE PRESENTATION .....	137
<b>III. ADDITIONAL RESULTS AND DISCUSSION .....</b>	<b>200</b>
1. IS THERE AN “OVARIAN HYPERACTIVATION CODE”?.....	200
2. AN UNUSUAL HETEROCHROMATIC DOMAIN.....	205
3. DIFFERENT ROLES FOR EPIGENOMIC REGULATORS.....	207
4. AN APPROACH TO PROFILE REGULATORY ARCHITECTURE OF CHROMATIN DOMAINS. ....	209
<b>GENERAL CONCLUSION .....</b>	<b>211</b>
<b>REFERENCES:.....</b>	<b>212</b>

## **I. An shRNA screen identifies maternal chromatin factors required for the oocyte-to-zygote transition**

### **1. Article presentation**

This first article published in PLOS Genetics presents an shRNA-based genetic screen designed to identify maternal chromatin factors required for the integration of paternal chromosomes into the zygote. This consisted on expressing shRNAs specifically in the female germline and identify embryos that lost paternal chromosomes and developed as gynohaploids. Like this, we identified the histone demethylase Lid/dKDM5 and the members of the HDAC complex Sin3A and Rpd3 as essential for the activation of a critical effector of the oocyte-to-zygote transition: the maternal thioredoxin Deadhead.

To investigate the mechanism underneath this regulation, we focused mainly on Lid/dKDM5. As mentioned in the introduction, H3K4me3 is a hallmark of active transcription and is also the target of the demethylase Lid/dKDM5, therefore we assessed the impact of depletion of *lid* on this mark in ovaries.

Finally, we tested to what extent the phenotype observed in eggs laid by Lid-depleted females was caused by *dhd* loss.

RESEARCH ARTICLE

# The Lid/KDM5 histone demethylase complex activates a critical effector of the oocyte-to-zygote transition

Daniela Torres-Campana<sup>1</sup>\*, Shuhei Kimura<sup>2</sup>\*, Guillermo A. Orsi<sup>1</sup>, Béatrice Horard<sup>1</sup>, Gérard Benoit<sup>1</sup>, Benjamin Loppin<sup>1</sup>\*

**1** Laboratoire de Biologie et de Modélisation de la Cellule, CNRS UMR5239, Ecole Normale Supérieure de Lyon, University of Lyon, France, **2** Laboratoire de Biométrie et Biologie Evolutive, Université Lyon 1, CNRS, UMR 5558, Villeurbanne F-69622, France

\* These authors contributed equally to this work.

† Current address: Seto Hospital, Kanayama-cho, Tokorozawa-shi, Saitama-ken, Japan

\* benjamin.loppin@ens-lyon.fr



**OPEN ACCESS**

**Citation:** Torres-Campana D, Kimura S, Orsi GA, Horard B, Benoit G, Loppin B (2020) The Lid/KDM5 histone demethylase complex activates a critical effector of the oocyte-to-zygote transition. *PLoS Genet* 16(3): e1008543. <https://doi.org/10.1371/journal.pgen.1008543>

**Editor:** Giovanni Bosco, Geisel School of Medicine at Dartmouth, UNITED STATES

**Received:** June 28, 2019

**Accepted:** November 26, 2019

**Published:** March 5, 2020

**Copyright:** © 2020 Torres-Campana et al. This is an open access article distributed under the terms of the [Creative Commons Attribution License](https://creativecommons.org/licenses/by/4.0/), which permits unrestricted use, distribution, and reproduction in any medium, provided the original author and source are credited.

**Data Availability Statement:** The DNA sequencing data from this publication have been deposited to the Gene Expression Omnibus database [<https://www.ncbi.nlm.nih.gov/geo/>] and assigned the identifier GSE133064 (RNA-Seq) and GSE133202 (ChIP-Seq).

**Funding:** SK was supported by a fellowship from the Agence Nationale de la Recherche (<https://anr.fr/>, I) (ZygePal ANR-12-BSV5-0014). The funders had no role in study design, data collection and

## Abstract

Following fertilization of a mature oocyte, the formation of a diploid zygote involves a series of coordinated cellular events that ends with the first embryonic mitosis. In animals, this complex developmental transition is almost entirely controlled by maternal gene products. How such a crucial transcriptional program is established during oogenesis remains poorly understood. Here, we have performed an shRNA-based genetic screen in *Drosophila* to identify genes required to form a diploid zygote. We found that the Lid/KDM5 histone demethylase and its partner, the Sin3A-HDAC1 deacetylase complex, are necessary for sperm nuclear decompaction and karyogamy. Surprisingly, transcriptomic analyses revealed that these histone modifiers are required for the massive transcriptional activation of *deadhead* (*dhd*), which encodes a maternal thioredoxin involved in sperm chromatin remodeling. Unexpectedly, while *lid* knock-down tends to slightly favor the accumulation of its target, H3K4me3, on the genome, this mark was lost at the *dhd* locus. We propose that Lid/KDM5 and Sin3A cooperate to establish a local chromatin environment facilitating the unusually high expression of *dhd*, a key effector of the oocyte-to-zygote transition.

## Author summary

Nuclear enzymes that add or remove epigenetic marks on histone tails potentially control gene expression by affecting chromatin structure and DNA accessibility. For instance, members of the KDM5 family of histone demethylases specifically remove methyl groups on the lysine 4 of histone H3, a mark generally correlated with gene expression. Lid (Little imaginal discs), the *Drosophila* KDM5, is essential for viability but is also required for female fertility. In this paper, we have found that the specific removal of Lid in developing oocytes perturbs the decompaction of the sperm nucleus at fertilization and the integration of paternal chromosomes in the zygote. Sperm nuclear decompaction normally requires the presence of a small redox protein called Deadhead (Dhd), which is massively

analysis, decision to publish, or preparation of the manuscript.

**Competing interests:** The authors have declared that no competing interests exist.

expressed at the end of oogenesis. Strikingly, our analyses of ovarian transcriptomes revealed that the absence of Lid completely abolishes the expression of *dhd*. This direct functional link between a general histone modifier and the expression of an essential terminal effector gene represents a rare finding. We hope that our work will help understanding how histone demethylases function in controlling complex developmental transitions as well as cancer progression.

## Introduction

In sexually reproducing animals, fertilization allows the formation of a diploid zygote through the association of two haploid gametes of highly different origins and structures. Generally, the spermatozoon delivers its compact nucleus within the egg cytoplasm, along with a pair of centrioles, while the egg provides one haploid meiotic product and all resources to sustain zygote formation [1]. In some species, this maternal control extends to early embryo development, as in *Drosophila melanogaster*, where the initial amplification of embryo cleavage nuclei occurs without significant zygotic transcription [2]. Instead, the bulk of transcriptional activity takes place in the fifteen interconnected large polyploid germline nurse cells that deposit gene products in the cytoplasm of the growing oocyte [3]. The developmental potential of the egg is thus initially dependent on the establishment of a highly complex transcriptional program in female germ cells.

One of the earliest events of the oocyte-to-zygote transition is the rapid transformation of the fertilizing sperm nucleus into a functional male pronucleus. In *Drosophila*, the needle-shaped, highly compact sperm nucleus is indeed almost entirely organized with non-histone, Sperm Nuclear Basic Proteins (SNBPs) of the protamine like type [4,5]. Male pronucleus formation begins with the genome-wide replacement of SNBPs with maternally supplied histones, a process called sperm chromatin remodeling, which is followed by extensive pronuclear decondensation [1]. Finally, zygote formation involves the coordinated migration and apposition of male and female pronuclei and the switch from meiotic to mitotic division within the same cytoplasm.

Here, we report the results of a genetic screen specifically designed to find new genes required for the oocyte-to-zygote transition in *Drosophila*. Our screen identified two histone modifiers, the Lid/KDM5 histone H3K4me3 demethylase and the Sin3A-HDAC1 histone deacetylase complex, which are both required for the integration of paternal chromosomes into the zygote. These interacting epigenetic factors are known to regulate the expression of hundreds of genes in somatic tissues but their role in the establishment of the ovarian transcriptome is unknown. Strikingly, RNA-Sequencing analyses revealed that, despite the modest impact of their depletion on ovarian transcripts, Lid and Sin3A are critically required for the massive expression of *deadhead* (*dhd*), a key effector of the oocyte-to-zygote transition [6,7]. Furthermore, we demonstrate that germline knock-down of these histone modifiers specifically prevent sperm chromatin remodeling through a mechanism that depends on the DHD thioredoxin.

## Results & discussion

### A maternal germline genetic screen for gynohaploid embryo development

We performed an *in vivo* RNA interference screen in the female germline to identify genes required for the integration of paternal chromosomes in the zygote. In *Drosophila*, failure to

form a male pronucleus following fertilization is generally associated with the development of haploid embryos that possess only maternally-derived chromosomes (gynohaploid embryos) and that never hatch [8]. We chose to screen transgenic lines from the TRiP collection that express small hairpin RNAs (shRNAs) under the control of the Gal4 activator [9]. We selected shRNA lines that targeted genes with known or predicted chromatin-related function and that show adult ovarian expression (Flybase). Among the 374 tested TRiP lines, 157 (41.9%) induced female sterility or severely reduced fertility when induced with the germline-specific *P*{*GAL4:VP16-nos.UTR*}<sup>MVD1</sup> Gal4 driver (*nos-Gal4*), thus underlying the importance of chromatin regulation for oogenesis and early embryo development (S1 Table). We then specifically searched for shRNAs that induced a maternal effect embryonic lethal phenotype associated with gynohaploid development (Fig 1A). Gynohaploid embryos can be efficiently identified by scoring the zygotic expression of a paternally-transmitted *P*{*g-GFP::cid*} transgene at the gastrulation stage or beyond [10]. Among the sterile lines with late developing embryos (class 4 in Fig 1A and S1 Table) that were identified, four shRNA lines (GLV21071, GL00612, HMS00359 and HMS00607) produced embryos that were negative for GFP::CID (Fig 1B). Note that none of these shRNAs induced complete female sterility and about 1 to 4% of embryos hatched and were thus diploid (Table 1).

Two of the identified lines (GLV21071 and GL00612) express the same shRNA against the *little imaginal disc (lid)* gene, which encodes the single fly member of the KDM5/JARID1A family of histone demethylases [11,12]. KDM5 demethylases specifically target the trimethylation of lysine 4 of histone H3 (H3K4me3), a mark typically enriched around the Transcriptional Start Site (TSS) of transcriptionally active genes [13,14]. The two other shRNAs (HMS00359 and HMS00607) target the *Sm3A* and *HDAC1/ripd3* genes, respectively. The conserved Sin3A protein scaffold interacts with the histone lysine deacetylase HDAC1 to form the core SIN3 histone deacetylase complex, which is generally considered as a transcriptional repressor [15]. The SIN3 complex regulates the expression of genes involved in a number of metabolic and developmental processes [16–19]. Interestingly, Lid and the largest Sin3A isoform were previously shown to physically and functionally interact [16,17,20,21], thus opening the possibility that these histone modifiers could control the same pathway leading to the formation of a diploid zygote.

### Lid and SIN3 are required for sperm chromatin remodeling at fertilization

The Lid demethylase has been previously shown to be required in the female germline for embryo viability [22,23]. Both studies reported a dual phenotype for eggs produced by *lid* KD females (hereafter called *lid* KD eggs): while a majority of eggs fail to initiate development, a variable but significant fraction developed but died at later stages. Our own observations confirmed that about 15% of *lid* KD embryos reach or develop beyond the blastoderm stage (S1 Fig). Furthermore, our analysis of *P*{*g-GFP::cid*} expression (Fig 1B) indicates that most of these late, non viable KD embryos are haploid and develop with maternal chromosomes. To follow the fate of paternal chromosomes in *lid* KD eggs, we crossed *lid* KD females with males expressing the sperm chromatin marker *Mst35Ba::GFP* (*ProtA::GFP*) [24]. In *Drosophila*, protamine-like proteins such as *Mst35Ba* are rapidly removed from sperm chromatin at fertilization [1] and, accordingly, *ProtA::GFP* is never observed in the male nucleus of control eggs. In striking contrast, the vast majority of fertilized *lid* KD eggs contained a needle-shaped sperm nucleus that was still positive for *ProtA::GFP*, indicating that sperm chromatin remodeling was compromised (Fig 1C and 1D). Anti-histone immunostaining indeed revealed that the replacement of SNBPs with maternally supplied histones was variable in KD eggs, ranging from complete absence of histones in the sperm nucleus to the coexistence of variable amounts

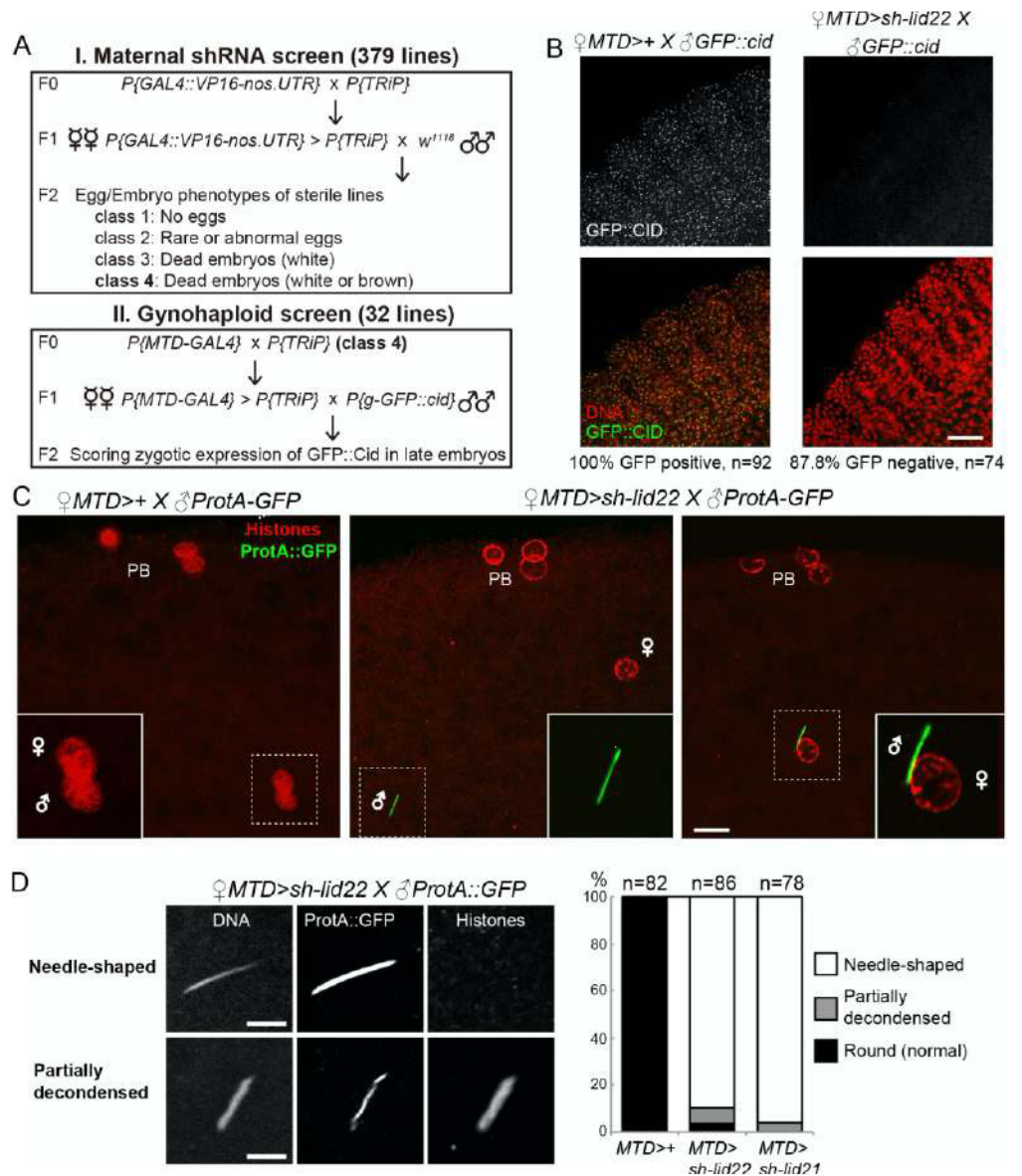


**Fig 1. Lid is required for sperm nuclear decompaction at fertilization.** A—Scheme of shRNA screen in the female germline. B—Left: Zygotic expression of a paternally-derived  $P\{g-GFP::cid\}$  transgene in a control embryo. GFP::Cid marks centromeric chromatin and is visible as nuclear dots. Right: *lid* KD females produce embryos that fail to express the paternally-inherited transgene. Scale bar: 25  $\mu$ m. C—Maternal Lid is required for SNBP removal and sperm nuclear decompaction at fertilization. Left: a control egg at pronuclear apposition. Both pronuclei (inset) appear similar in size and shape and the SNBP marker ProtA::GFP is not detected. Middle: A representative *lid* KD egg containing a needle-shaped sperm nucleus (inset) still packaged with ProtA::GFP. Right: A fertilized *lid* KD egg with the sperm nucleus apposed to the female pronucleus. Scale bar: 10  $\mu$ m. D—SNBP replacement with histones is impaired in *lid* KD eggs. Left: Confocal images of representative sperm nuclei in *lid* KD eggs. Partially decondensed nuclei are positive for histones. Scale bar: 5  $\mu$ m. Right: Quantification of sperm nuclear phenotype in control and *lid* KD eggs.

<https://doi.org/10.1371/journal.pgen.1008543.g001>

Table 1. Embryo hatching rates.

Female genotype	Male genotype	Number of eggs	Hatch. rate (%)
<i>w<sup>1118</sup></i>	<i>w<sup>1118</sup></i>	344	97.67
<i>dhd<sup>Δ5</sup></i>	<i>w<sup>1118</sup></i>	375	0.00
<i>dhd<sup>Δ5</sup>/TM2</i>	<i>w<sup>1118</sup></i>	573	78.36
<i>MTD &gt; +</i>	<i>w<sup>1118</sup></i>	1561	98.27
<i>MTD &gt; sh-lid22</i>	<i>w<sup>1118</sup></i>	1403	2.14
<i>MTD &gt; sh-lid21</i>	<i>w<sup>1118</sup></i>	1144	1.05
<i>MTD &gt; sh-Sin3A</i>	<i>w<sup>1118</sup></i>	1221	0.25
<i>MTD &gt; sh-Rpd3</i>	<i>w<sup>1118</sup></i>	521	4.03
<i>MTD &gt; sh-Hira</i>	<i>w<sup>1118</sup></i>	315	0.00
<b>Rescue with P[<i>dhd<sup>WT</sup></i>] genomic transgene</b>			
<i>dhd<sup>Δ5</sup>; P[<i>dhd</i>]</i>	<i>w<sup>1118</sup></i>	663	85.67
<i>dhd<sup>Δ5</sup>; P[<i>dhd</i>]/TM2</i>	<i>w<sup>1118</sup></i>	884	94.57
<i>MTD &gt; sh-lid22; P[<i>dhd</i>]</i>	<i>w<sup>1118</sup></i>	1159	4.57
<b>Rescue with P[<i>gnu-dhd<sup>WT</sup></i>] transgene</b>			
<i>dhd<sup>Δ5</sup>; P[<i>gnu-dhd</i>]</i>	<i>w<sup>1118</sup></i>	351	7.25
<i>dhd<sup>Δ5</sup>; P[<i>gnu-dhd</i>]/TM2</i>	<i>w<sup>1118</sup></i>	1059	3.40
<i>MTD &gt; sh-lid22; P[<i>gnu-dhd</i>]/+</i>	<i>w<sup>1118</sup></i>	695	7.48
<b>Rescue with P[UASP-<i>dhd</i>] inducible transgenes</b>			
<i>nos &gt; +</i>	<i>w<sup>1118</sup></i>	711	95.36
<i>nos &gt; P[UASP-<i>dhd</i>]/+</i>	<i>w<sup>1118</sup></i>	450	97.33
<i>dhd<sup>Δ5</sup>; nos &gt; P[UASP-<i>dhd</i>]</i>	<i>w<sup>1118</sup></i>	1163	99.28
<i>dhd<sup>Δ5</sup>; nos &gt; P[UASP-<i>dhd</i><sup>XXX3</sup>]</i>	<i>w<sup>1118</sup></i>	702	0.00
<i>MTD &gt; sh-lid22; P[UASP-<i>dhd</i>]</i>	<i>w<sup>1118</sup></i>	1343	28.44
<i>MTD &gt; sh-lid22; P[UASP-<i>dhd</i><sup>XXX3</sup>]</i>	<i>w<sup>1118</sup></i>	315	14.60
<i>nos &gt; sh-lid21</i>	<i>w<sup>1118</sup></i>	1508	1.92
<i>nos &gt; P[UASP-<i>dhd</i>]/sh-lid21</i>	<i>w<sup>1118</sup></i>	385	19.32
<i>nos &gt; sh-Sin3a</i>	<i>w<sup>1118</sup></i>	542	2.03
<i>nos &gt; P[UASP-<i>dhd</i>]/sh-Sin3a</i>	<i>w<sup>1118</sup></i>	621	8.86
<i>nos &gt; sh-Rpd3</i>	<i>w<sup>1118</sup></i>	919	2.94
<i>nos &gt; P[UASP-<i>dhd</i>]/sh-Rpd3</i>	<i>w<sup>1118</sup></i>	395	7.59
<i>nos &gt; sh-Hira</i>	<i>w<sup>1118</sup></i>	514	0.00
<i>nos &gt; P[UASP-<i>dhd</i>]/sh-Hira</i>	<i>w<sup>1118</sup></i>	380	0.00

<https://doi.org/10.1371/journal.pgen.1008543.t001>

of histones and ProtA::GFP (Fig 1D). Notably, we noticed that partially decondensed sperm nuclei in *lid* KD eggs were systematically positive for histones. Taken together, our observations indicate that sperm chromatin remodeling is severely impaired in *lid* KD eggs, thus explaining the absence of paternal chromosomes in most developing embryos.

Germline depletion of Lid was previously shown to affect karyosome morphology and chromosome positioning in metaphase I oocytes [25]. In contrast, another study had previously reported that meiotic progression was not affected in *lid* KD oocytes [22]. Interestingly, although our own observations indeed confirmed the aberrant karyosome structure in *lid* KD oocytes, we observed that the second meiotic division appeared to resume normally in a vast majority of *lid* KD eggs (S2 Fig). We noted, however, that, following meiosis, the female pronucleus frequently (62%, n = 76) failed to appose to the sperm nucleus in *lid* KD eggs (Fig 1C). Thus, we propose that defective pronuclear migration largely accounts for the previously reported failure of *lid* KD embryos to initiate cleavage divisions [23]. Like Navarro-Costa

*et al.*, we noted that the rosette of polar body chromosomes was frequently abnormal in morphology, but this phenotype appeared independent of meiosis *per se*.

Remarkably, we found that germline KD of *Sin3A* also induced a highly penetrant sperm nuclear phenotype with all scored fertilizing sperm nuclei retaining a needle-like shape (100%,  $n = 19$ ) (S3 Fig). Finally, a similar but less penetrant phenotype was also observed in *ripd3* KD eggs (S3 Fig). As this low penetrance could result from less efficient gene knock-down, we chose to mainly focus on *lid* and *Sin3A* in the rest of this study.

### Transcriptomic analysis of *lid* KD and *Sin3A* KD ovaries identifies *deadhead* as a common and major target gene

In eggs from wild-type females, anti-Lid immunostaining failed to detect Lid protein in the male or female pronucleus, thus suggesting that its implication in sperm chromatin remodeling was indirect. In fact, Lid was not detected in embryos before the blastoderm stage (S4 Fig). We thus turned to RNA sequencing (RNA Seq) to analyze the respective impact of *lid* KD and *Sin3A* KD on the ovarian transcriptome.

We compared transcriptomes obtained from *lid* KD or *Sin3A* KD ovaries (using the maternal triple driver MTD-Gal4) with control transcriptomes (MTD-Gal4 only). Globally, our analyses revealed a relatively modest impact of *lid* KD and *Sin3A* KD on ovarian gene expression, with more genes downregulated in both cases (Fig 2B and S5 Fig; S2 Table). Note that these changes are expected to reflect the activity of Lid and Sin3A in germ cells, as ovarian somatic cells (see Fig 2A) do not express the targeting shRNAs. In their transcriptome analysis (based on microarrays) of *lid* KD wing imaginal discs, Azorin and colleagues found a similar number of differentially-expressed genes, most of them being downregulated [14]. However, RNA Seq analyses recently published by Drelon *et al.* in contrast found 1630 genes (FDR<0.05) dysregulated in wing discs from a null *lid* mutant [26]. Moreover, Liu and Secombe [27] found 8,056 genes differentially expressed (60% were down-regulated) in *lid* adult mutant flies (FDR<0.05), a number which could reflect the greater cell type complexity involved in this analysis.

We found that only 29% (139) of the 473 differentially-expressed genes in *lid* KD were also differentially-expressed in *Sin3A* KD, and only 100 genes (21%) were dysregulated in the same direction in both KD (Fig 2B). As a matter of comparison, Gajan *et al.* found a 65% overlap in *Drosophila* S2 cells [17]. As the *Sin3A* shRNA that we used targets all predicted alternatively spliced mRNAs, this suggests that the knock-down affects Sin3A isoforms with Lid-independent functions [16].

Remarkably, however, we noticed that the *deadhead* (*dhd*) gene was by far the most severely impacted gene, downregulated by more than two orders of magnitude in both *lid* KD and *Sin3A* KD transcriptomes (Fig 2C, S6 Fig). The implication of *dhd* appeared particularly interesting because we and others have recently established that this germline specific gene is critically required for sperm nuclear decompaction at fertilization [6,28]. *dhd* indeed encodes a specialized thioredoxin that cleaves disulfide bonds on SNBPs, thus facilitating their removal from sperm chromatin [6,28]. RT-PCR and Western-blot analyses confirmed the severe down-regulation of *dhd* in *lid* KD and *Sin3A* KD (S5 Fig).

*dhd* is a small, intronless gene located in the middle of a cluster of fifteen densely packed genes spanning about 40 kb of genomic DNA. Interestingly, the *dhd* gene lies within a 1.4 kb region that is immediately flanked by two genes with testis-specific expression (*Trx-T* and *CG4198*) (Fig 2D). Despite this apparently unfavorable genomic environment, *dhd* is one of the most highly-expressed genes in ovaries [29], as confirmed by our RNA Seq profiles (Fig 2C and S6 Fig). Interestingly, although this 40 kb region contains six additional genes expressed

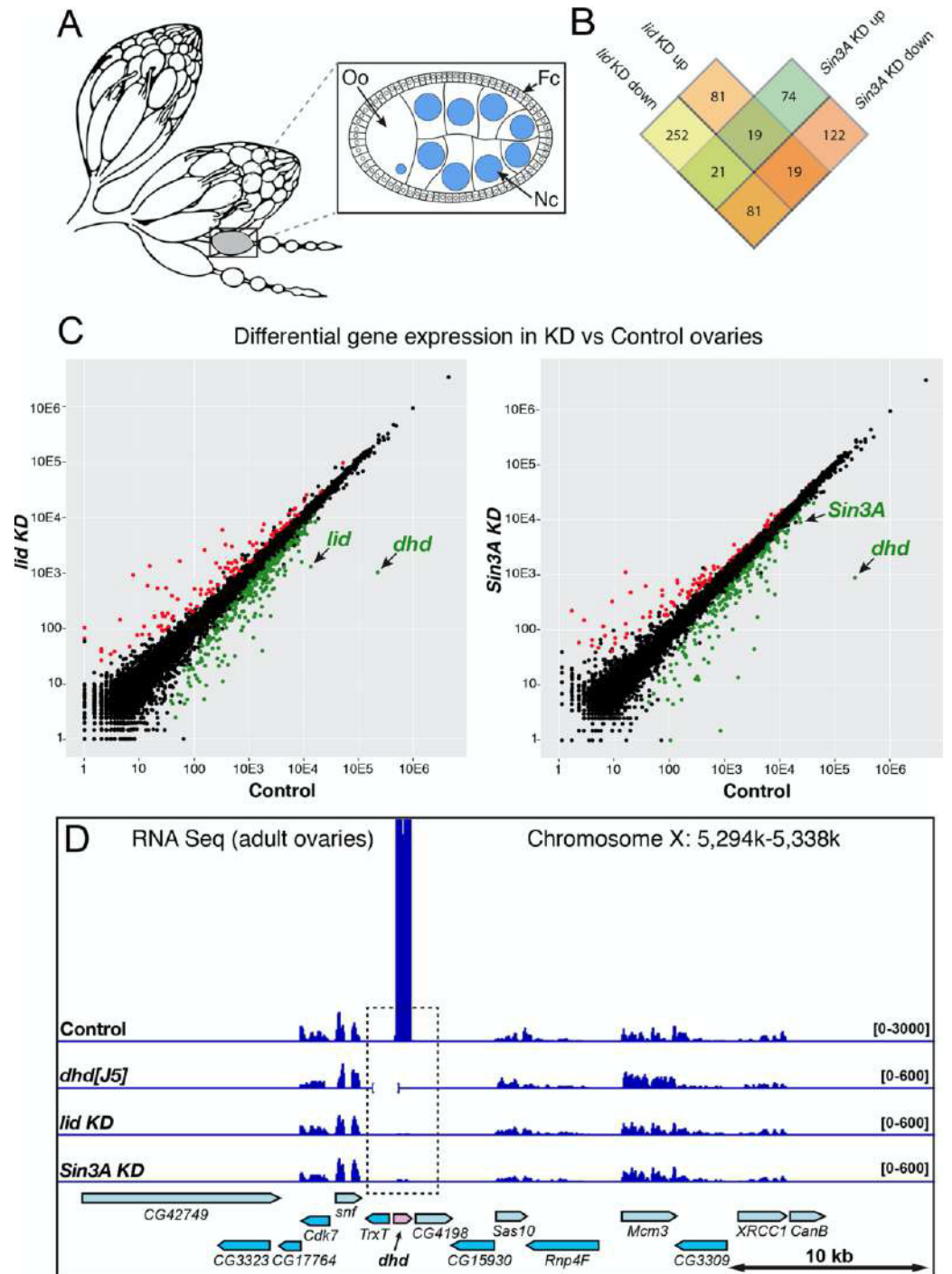


**Fig 2. *deadhead* is strongly downregulated in *lid* KD and *Sin3A* KD ovaries.** A—Scheme of a pair of adult ovaries with two isolated ovarioles and an egg chamber (inset). Germline nuclei are in blue. Oo: Oocyte, Ne: Nurse cells, Fc: Follicle cells. B—Venn diagram showing the number of differentially expressed genes in *lid* KD and *Sin3A* KD ovarian transcriptomes (FDR<0.001). C—Comparison of RNA seq normalized reads per gene (DESeq2) are shown for *lid* KD vs Control (left) and *Sin3A* KD vs Control (right). Genes with a negative foldchange (downregulated in KD) are in green (FDR<0.001). Genes with a positive foldchange (upregulated in KD) are in red (FDR<0.001). D—Integrative Genomics Viewer (igv) view of Control, *dhd*<sup>fl/fl</sup>, *lid* KD and *Sin3A* KD ovarian RNA Seq signal on the *dhd* region. The *Df(1)15* deficiency is indicated as an interrupted baseline on the *dhd*<sup>fl/fl</sup> track.

<https://doi.org/10.1371/journal.pgen.1008543.g002>

in ovaries, *dhd* is the only one affected by *lid* KD or *Sin3A* KD (Fig 2D). Thus, Lid and the SIN3 complex exert a critical and surprisingly specific control on the transcriptional activation of *dhd* in female germ cells.

### Impact of Lid depletion on the distribution of H3K4me3 in ovaries

To evaluate the impact of *lid* KD on the distribution of its target histone mark in the female germline, we performed chromatin immunoprecipitation and sequencing (ChIP-Seq) analyses of H3K4me3 in ovaries from control and *lid* KD females. Consistent with earlier reports of a global increase of H3K4me3 in *lid* mutant tissues [14,23,25,30], we observed that H3K4me3 ChIP peaks in *lid* KD ovaries were globally more pronounced compared to control ovaries (Fig 3A). Our analysis actually revealed that about 10% (1528) of H3K4me3 identified peaks in control ovaries were significantly increased in *lid* KD ovaries (S3 Table; FDR<0.05). For those peaks that were associated with genes, the relative enrichment of H3K4me3 in *lid* KD ovaries mainly affected the promoter region and gene body (Fig 3B). A similar effect was previously observed in *lid* depleted wing imaginal discs, with H3K4me3 abundance specifically increased at the TSS of Lid direct target genes [14]. We nevertheless found 46 H3K4me3 peaks that were significantly decreased in *lid* KD ovaries compared to control ovaries (S3 Table; FDR<0.05). Among these, the H3K4me3 peak on the *dhd* gene was the second most severely affected (S3 Table and Fig 3C). Furthermore, only ten of the negatively affected peaks covered genes that were downregulated in *lid* KD ovaries, including *dhd*. Remarkably, the prominent H3K4me3 peak on *dhd* was almost completely lost in *lid* KD ovaries while other peaks within the *dhd* region remained essentially unchanged. *CG4198*, which lies immediately downstream of *dhd* is a notable exception, as this gene also shows a decrease of H3K4me3 (Fig 3C). In this case, however, it is interesting to note that the presence of the mark is not correlated with transcriptional activity.

At first, the paradoxical loss of H3K4me3 enrichment on the *dhd* gene upon Lid depletion suggests that the demethylase activity of Lid is not locally responsible for this regulation. In fact, it has been established that *lid* mutant females with a catalytic dead JmjC<sup>-</sup> *lid* rescue transgene are viable and at least partially fertile [23,26,31], thus suggesting that the catalytic activity of Lid is not absolutely required to form a viable zygote. To directly test the implication of the Lid demethylase domain in *dhd* regulation, we measured *dhd* expression in JmjC<sup>-</sup> rescued females. Surprisingly, *dhd* transcripts were severely reduced in these females compared to control females rescued with a wild-type *lid* transgene (S7 Fig). We thus conclude that the demethylase activity of Lid is important for *dhd* expression. At least two hypotheses could reconcile this conclusion with our ChIP-Seq results. First, it is possible that the demethylase activity of Lid is only transiently required at the *dhd* locus, perhaps to switch on its transcription at mid oogenesis, while later, massive *dhd* expression would no longer require this activity. Alternatively, Lid could exert a control on *dhd* transcription by restricting the level of H3K4me3 at an enhancer element, similarly to what was previously reported for KDM5 demethylases in different model organisms [32–34]. Although our ChIP-Seq analyses failed to identify any

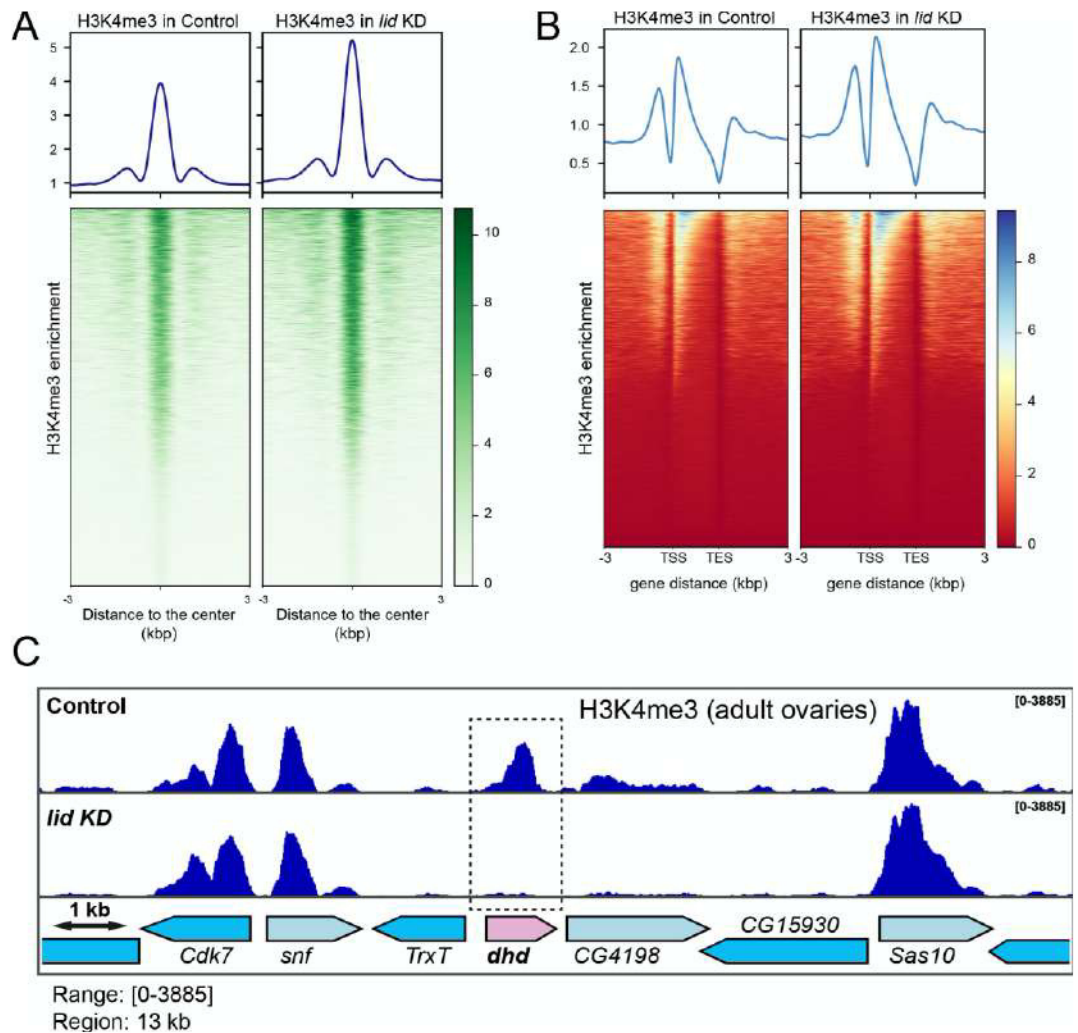


**Fig 3. H3K4me3 ovarian ChIP-Seq analysis.** A—H3K4me3 enrichment around peak center for Control and *lid* KD ovaries. Upper panels show the average profile around detected peak centers. Lower panels show read density heatmaps around the detected peak centers. B—H3K4me3 enrichment around gene loci for Control and *lid* KD ovaries. Upper panels show the average signal profile on genomic loci defined as 3kb upstream of annotated TSS to 3kb downstream of annotated TES. Lower panels show read density heatmaps around the same genomic loci. C—igv view of H3K4me3 occupancy on the *dhd* genomic region in Control and *lid* KD ovaries.

<https://doi.org/10.1371/journal.pgen.1008543.g003>

obvious candidate enhancer element in the vicinity of the *dhd* gene region, we cannot exclude this possibility.

Besides its JmjC demethylase domain, Lid/KDM5 possesses a conserved C-terminal PHD motif capable of binding H3K4me2/3. This binding motif is required for the recruitment of Lid at the promoter of target genes, where it could promote their activation [27]. The local recruitment of Lid, either through its C-terminal PHD motif or through its DNA binding ARID (AT-rich interaction domain) motif, or both, could thus establish a chromatin

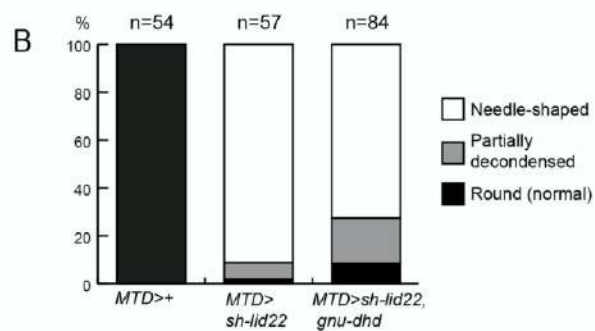
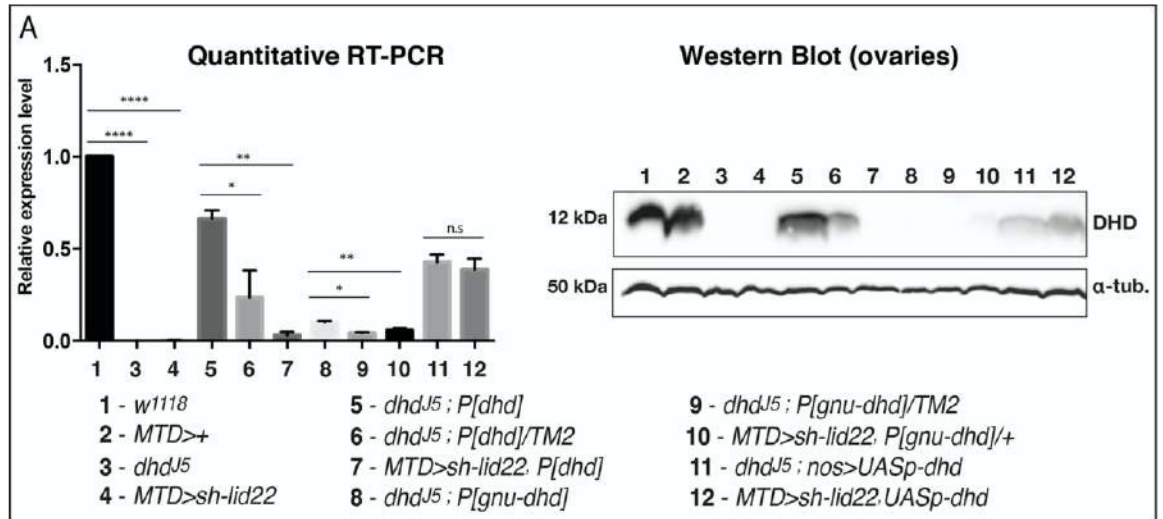
environment permissive to *dhd* massive expression in late oogenesis. In this context, the role of the Sin3A/HDAC1 complex also remains to be clarified. The Sin3A histone deacetylase complex is generally considered as a transcriptional repressor [15], but it also functions as a transcriptional activator in *Drosophila* S2 cells [17]. Lacking an intrinsic DNA binding ability [15], the recruitment of this complex to chromatin requires an additional factor. It is thus tempting to propose that Lid itself could recruit Sin3A/HDAC1 locally to activate *dhd* expression in female germ cells.

### Forced *dhd* expression in *lid* KD ovaries partially restores sperm chromatin remodeling at fertilization

Taken together, our cytological and transcriptomic analyses strongly suggest that the loss of *dhd* expression in *lid* KD ovaries at least contributes to the observed fertilization phenotype. To directly test this possibility, we attempted to restore *dhd* expression in *lid* KD female germ cells through the use of transgenic constructs. A genomic transgene (P[*dhd*]) that fully rescued the fertility of *dhd* mutant females [6] only had a very limited impact on the hatching rate of *lid* KD embryos (Table 1) but quantitative RT-PCR analyses revealed that P[*dhd*] remained essentially silent in *lid* KD ovaries (Fig 4A). This result indicates that the 4.3 kb genomic region present in this transgene is sufficient to recapitulate the endogenous control exerted by Lid on *dhd* transcription. We then designed another transgene expressing *dhd* under the control of the *giant nuclei* (*gnu*) regulatory sequences. Like *dhd*, *gnu* is specifically expressed during oogenesis and is functionally required during zygote formation [35]. In addition, our RNA Seq data indicated that its expression is not controlled by Lid. We observed that the P[*gnu-dhd*] transgene indeed restored fertility to *dhd* homozygous mutant females albeit to modest level (about 7% embryo hatching rate; Table 1). In fact, rescued females only produced about 10% of the normal amount of *dhd* mRNA in their ovaries and the DHD protein remained almost undetectable in Western-blot (Fig 4A). Interestingly, when introduced into *lid* KD females, the P[*gnu-dhd*] transgene also slightly increased embryo hatching rate (Table 1). Furthermore, cytological examination of eggs laid by these females revealed a limited but clear improvement of sperm nuclear decondensation (Fig 4B and 4C). These results thus indicate that forced expression of *dhd* can improve the survival of *lid* KD eggs through its positive impact on sperm chromatin remodeling. Finally, we tried to further increase the level of expression of *dhd* by using a Gal4 inducible transgene, P[UAS-*dhd*<sup>WT</sup>]. Indeed, induction of this transgene in the germline of *dhd*<sup>Δ</sup> mutant females fully restored their fertility (Table 1). We also observed a strong effect on the hatching rate of embryos laid by *lid* KD, P[UAS-*dhd*<sup>WT</sup>] females (about 28%; Table 1). However, a P[UAS-*dhd*<sup>Δ</sup>] transgene expressing a catalytic mutant DHD with no rescuing potential also improved the fertility of *lid* KD females. This effect suggests that Gal4 becomes limiting in the presence of two UAS transgenes, with a negative impact on knock-down efficiency. The fertility of P[UAS-*dhd*<sup>WT</sup>] rescued females was nevertheless doubled compared to P[UAS-*dhd*<sup>Δ</sup>] control females (Table 1), thus supporting the idea that partial *dhd* re-expression in *lid* KD ovaries significantly improved the probability of these eggs to form a viable, diploid zygote. Besides its already established roles in controlling the oocyte epigenome and the architecture of meiotic chromosomes, we show that the transcriptional regulation of *dhd* (and possibly additional early acting genes) is indeed a critical function of Lid and associated factors in female germ cells.

### Trr controls sperm chromatin remodeling through a DHD-independent pathway

Intriguingly, germline KD of the Trithorax group protein Trithorax-related (Trr, also known as dMLL3/4), a histone methyltransferase responsible for monomethylation of H3K4 [36], was



**C** ♀ *MTD>sh-lid22, P[gnu-dhd]*

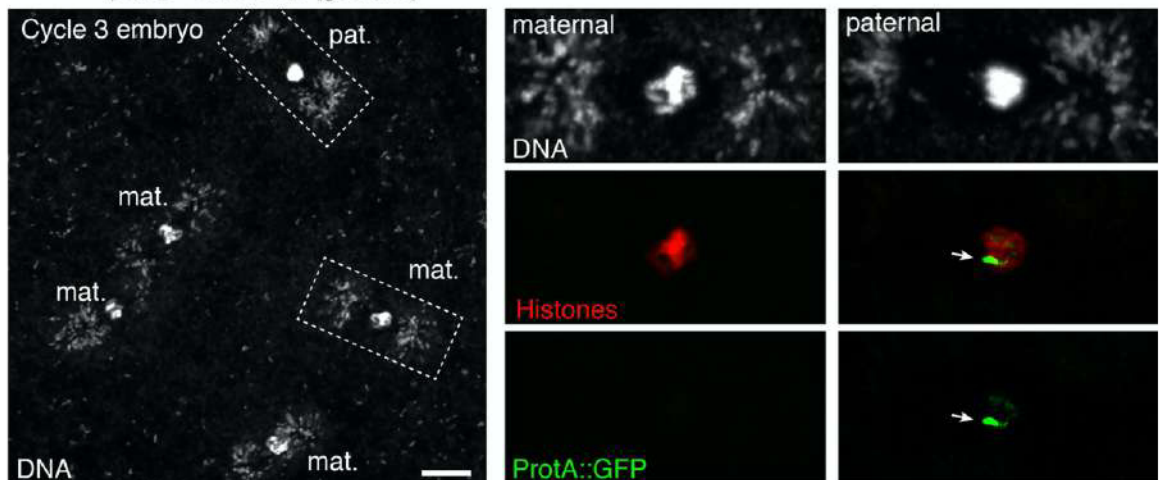


**Fig 4. Forced expression of *dhd* partially rescues the *lid* KD phenotype.** A—Left: RT-qPCR quantification of *dhd* mRNA levels in ovaries of indicated genotypes (normalized to *rp49* and relative to expression in  $w^{1118}$ ). Data are presented as mean  $\pm$  SD of 2 biological replicates. P values indicate one-way ANOVA with Dunnett's multiple comparisons test to a control (\*\*\*)  $P < 0.0001$ ; \*\*  $P < 0.01$ ; \*  $P < 0.05$ ; n.s. = not significant). Right: Western blot analysis of DHD expression in ovaries of indicated genotypes. Alpha-tubulin detection is used as a loading control in Western blotting. B—Quantification of sperm nuclear phenotype in eggs laid by females of indicated genotypes. C—Confocal images of a *MTD>hid22; P[*gou-dhd*]* haploid embryo during the third nuclear division with incompletely remodeled male nucleus. Karyogamy has failed and the embryo contains four haploid nuclei of presumably maternal origin. The paternal nucleus (inset) still contains a region packaged with ProTA::GFP (arrow). Note that DNA positive dots at the spindle poles are *Wolbachia* endosymbionts. Scale bar: 10  $\mu$ m.

<https://doi.org/10.1371/journal.pgen.1008543.g004>

recently shown to induce a sperm decondensation defect at fertilization similar to the one reported here for *lid*, *Sin3a* and *tpd3* KD [37]. In their study, however, Prudêncio *et al.* did not find any significant change in *dhd* mRNA level in *trr* KD early embryos. To more directly exclude any implication of DHD in the *trr* KD phenotypes, we stained control and KD eggs with an anti-DHD antibody. At fertilization, maternally-expressed DHD is abundant throughout the egg cytoplasm (100%,  $n = 41$ ) but is rapidly degraded after pronuclear apposition. As expected, DHD protein remained undetectable in most *lid* KD eggs (92%,  $n = 50$ ), including those that were fixed before the end of meiosis II (S8 Fig). In sharp contrast, DHD protein was normally detected in a majority of *trr* KD eggs, even though these eggs indeed contained a needle-shaped sperm nucleus still packaged with SNBPs (S8 Fig). This result thus confirms that *Trr/dMLL3/4* controls sperm nuclear remodeling through a yet unknown, DHD-independent mechanism. Conversely, *Trr* was shown to control meiosis progression through the activation of *Ldgf4* [37], a gene that is not affected by *lid* or *Sin3a* KD (this study). Thus *Trr* and *Lid/Sin3A* respectively activate a distinct repertoire of genes important for the oocyte-to-zygote transition and sperm chromatin remodeling.

## Conclusion

Our maternal germline genetic screen has unveiled a complex and remarkably specific transcriptional regulation of the *dhd* gene by *Lid/KDM5* and the *Sin3A/HDAC1* complex. In addition to its crucial role in sperm protamine removal at fertilization, DHD was recently involved in the establishment of a redox state balance at the oocyte-to-zygote transition with a number of identified target proteins [7]. This important DHD-dependent thiol proteome remodeling is thus ultimately controlled by *Lid* and the *SIN3* complex, underlying the critical contribution of these transcriptional regulators to this delicate developmental transition. Future work will aim at dissecting the chromatin mechanisms at play in setting up *dhd* specific activation in female germ cells.

## Materials & methods

### Drosophila strains

Flies were raised at 25°C on standard medium. The  $w^{1118}$  strain was used as a wild-type control. shRNAs lines used in this study (see S1 Table) were established by the Transgenic RNAi Project (TRiP) at Harvard Medical School and were obtained from the Bloomington Drosophila Stock Center at Indiana University. The *hid* and *Sin3A* shRNA lines target all predicted isoforms of their respective target genes. Additional stocks were *EGFP-Cid* [38], *P[otu-GAL4::VP16.R]1*; *P[GAL4-nos.NGT]40*; *P[GAL4::VP16-nos.UTR]MVD1* ("MTD-Gal4"), *P[GAL4::VP16-nos.UTR]MVD1* ("nos-Gal4"), *P[Mst35Ba-EGFP]* [24] and *Df(1)J5/EM7c* [39]. The *pUASP-dhd[WI]* and *pUASP-dhd[SXXS]* transgenic flies were a gift from C. Gonzalez and C. Molnar. The *PatB[gLid-WT-HA]* and *PatB[gLid-JMJC-HA]* transgenic flies were kindly provided by P. Navarro-Costa [23].

### Germline knock-down and fertility tests

To obtain *KD* females, virgin shRNA transgenic females were mass crossed with transgenic Gal4 males at 25°C and females of the desired genotype were recovered in the F1 progeny. To measure fertility, virgin females of different genotypes were aged for 2 days at 25°C in the presence of males and were then allowed to lay eggs on standard medium for 24 hours. Embryos were counted and then let to develop for at least 36 hours at 25°C. Unhatched embryos were counted to determine hatching rates.

### Immunofluorescence and imaging

Early (0–30 min) and late (about 6 hours) embryos laid by randomly selected females were collected on agar plates. Embryos were dechorionated in bleach, fixed in a 1:1 heptane:methanol mixture and stored at -20°C. Embryos were washed three times (10 min each) with PBS1X 0.1%, Triton X-100 and were then incubated with primary antibodies in the same buffer on a wheel overnight at 4°C. They were then washed three times (20 min each) with PBS 0.1%, Triton X-100. Incubations with secondary antibodies were performed identically. Embryos were mounted in Dako mounting medium containing DAPI.

Ovaries were dissected in PBS-Triton 0.1% and fixed at room temperature in 4% formaldehyde in PBS for 25 minutes. Immunofluorescence was performed as for embryos except for secondary antibodies that were incubated four hours at room temperature. Ovaries were then mounted as described above.

Primary antibodies used were mouse monoclonal anti-histones (Sigma #MABE71; 1:1000), rabbit polyclonal anti-DHD (1:1000) [6], rat polyclonal anti-Lid (1:500) [14], mouse monoclonal anti-GFP (Roche #11814460001; 1:200) and Rat monoclonal anti  $\alpha$ -tubulin (Abcam #ab6160; 1:50). Secondary antibodies were goat anti-rabbit antibodies (ThermoFisher Scientific, 1:500), goat anti-mouse or anti-rat antibodies (Jackson ImmunoResearch, 1:500) conjugated to AlexaFluor. Images were acquired on an LSM 800 confocal microscope (Carl Zeiss). Images were processed with Zen imaging software (Carl Zeiss) and Photoshop (Adobe).

### Western blotting

Ovaries from 30 females were collected and homogenized in lysis buffer (20mM Hepes pH7.9, 100mM KCl, 0.1mM EDTA, 0.1mM EGTA, 5% Glycerol, 0.05% Igepal and protease inhibitors (Roche)). The protein extracts were cleared by centrifugation and stored at -80°C.

Eggs were collected every 30 min, dechorionated in bleach and quickly frozen in liquid nitrogen. Protein extracts were prepared from ca. 10  $\mu$ l of embryos. Protein samples were run on 15% SDS polyacrylamide gel and transferred to Immun-Blot<sup>®</sup> PVDF membrane (Bio-Rad) for 1h at 60V. Membranes were blocked for 1h at room temperature in 5% non-fat milk in PBS 1X-Tween20 0.05%, followed by an overnight incubation with the primary antibody at 4°C in 5% non-fat milk in PBS1X-Tween20 0.05%. Secondary antibodies used were added and incubated for 2 hours at room temperature. Protein detection was performed using ECL solution according manufacturer's instruction (GE Healthcare). Antibodies used were: rabbit polyclonal anti-DHD (1/1000) [6], mouse monoclonal anti- $\alpha$ -Tubulin (Sigma Aldrich #T9026, 1:500), HRP-conjugated goat anti-mouse (Biorad #170-5047; 1:50 000) and peroxidase-conjugated goat anti-rabbit (Thermoscientific #32460; 1:20 000).

### Gene expression analysis by RT-QPCR

Total RNA was extracted from ovaries of 3-day-old females using the NucleoSpin<sup>®</sup> RNA isolation kit (Macherey-Nagel), following the instructions of the manufacturer. Duplicates were

processed for each genotype. cDNAs were generated from 1µg of purified RNA with oligo (dT) primers using the SuperScript™ II Reverse Transcriptase kit (Invitrogen).

Generated cDNAs were diluted to 1/5 and were used as template in a real time quantitative PCR assay using SYBR® Premix Ex Taq™ II (Tli RNaseH Plus) (Takara). All qRT-PCR reactions were performed in duplicate using Bio-Rad CFX-96 Connect system with the following conditions: 95°C for 1 min followed by 40 cycles of denaturation at 95°C for 10 s, annealing at 59°C for 30 s and extension at 72°C for 30 s. Relative fold change in gene expression was determined by the comparative quantification ΔΔCT method of analysis [40]. The housekeeping gene *rp49* was used to normalize cDNA amounts in the comparative analysis. The primer sets used in the PCR reactions were: *dhd*-forward 5'-TCTATGCGACATGGTGTGGT-3' and *dhd*-reverse 5'-TCCACATCGATCTTGAGCAC-3'; *lid*-forward 5'-ATTGGTTTCACGAGGATTGC-3' and *lid*-reverse 5'-CATAGCCACTTGGGTCGATT-3'; *Rp49*-forward 5'-AAGATCGTGAAGAA GCGCAC-3' and *Rp49*-reverse 5'-GATACTGTCCCTTGAAGCGG-3'. Statistical tests were performed using GraphPad Prism version 6.00 for Mac OS X (GraphPad Software).

### Ovarian RNA sequencing and analysis

For each samples, 8 pairs of ovaries were dissected from 6 day old virgin females and total RNA were extracted using the NucleoSpin® RNA isolation kit (Macherey-Nagel), following the instructions of the manufacturer. Extracted RNAs were treated with Turbo™ DNase (Ambion #AM2238). After DNase inactivation, RNAs were purified using the NucleoSpin® RNA Clean-up XS kit (Macherey-Nagel) according to manufacturer's instructions. Sequencing was completed on two biological replicates of each genotype:

Control KD (*MTD-Gal4>+*)

$P\{w[+mC] = \text{otu-GAL4:VP16.R}1, w[\ ]/y[1] v[1]; P\{w[+mC] = \text{GAL4-nos.NGT}1/40/+; P\{w[+mC] = \text{GAL4:VP16-nos.UTR}CG6325[MVD1]/P\{y[+7.7] = \text{CaryP}attP2$

*lid* KD (*MTD-Gal4>shRNA lid*)

$P\{w[+mC] = \text{otu-GAL4:VP16.R}1, w[\ ]/y[1] sc[\ ] v[1]; P\{w[+mC] = \text{GAL4-nos.NGT}1/40/+; P\{w[+mC] = \text{GAL4:VP16-nos.UTR}CG6325[MVD1]/P\{y[+7.7] v[+1.8] = \text{TRiP.GLV21071}attP2$

*Sin3A* KD (*MTD-Gal4>shRNA Sin3A*)

$P\{w[+mC] = \text{otu-GAL4:VP16.R}1, w[\ ]/y[1] sc[\ ] v[1]; P\{w[+mC] = \text{GAL4-nos.NGT}1/40/+; P\{w[+mC] = \text{GAL4:VP16-nos.UTR}CG6325[MVD1]/P\{y[+7.7] v[+1.8] = \text{TRiP.HMS00359}attP2$

Sequencing libraries for each sample were synthesized using TruSeq Stranded mRNA kit (Illumina) following supplier recommendations (Sample Preparation Guide—PN 15031047, version Rev.E Oct 2013) and were sequenced on Illumina HiSeq 4000 sequencer as Single-Reads 50 base reads following Illumina's instructions (GenomEast platform, IGBM, Strasbourg, France). Image analysis and base calling were performed using RTA 2.7.3 and bcl2fastq 2.17.1.14. Adapter dimer reads were removed using DimerRemover. Sequenced reads were mapped to the *Drosophila melanogaster* genome assembly dm6 using TopHat (version 2.1.1) with default option. The aligned reads were assigned to genes by FeatureCounts, run with default options on the dmel-all-r6.15 version of the *Drosophila melanogaster* genome annotation. Differentially expressed genes were identified using the R-package DESeq2 (version 1.14.1). The annotated genes exhibiting an adjusted-P < 0.001 were considered differentially expressed compared to Control.

### Chromatin immunoprecipitation, sequencing and analysis

ChIP assays were performed as previously described [41]. Two biological replicates for *control* KD and *lid* KD ovaries (same genotypes as for RNA Seq) were processed and analyzed. For

each biological replicate, eighty ovary pairs were dissected from 2 day-old females and flash frozen. Dissected ovaries were fixed in 1.8% formaldehyde at room temperature for 10 minutes. Chromatin was sonicated using a Diagenod Bioruptor (18 cycles, high intensity, 30s on/30s off) to generate random DNA fragments from 100 to 800 base pairs. Sheared chromatin was incubated overnight at 4°C with H3K4me3 antibody (ab8580 Abcam). Immunoprecipitated samples were treated with RNase A, proteinase K and DNA purified using the ChIP DNA Purification kit (Active Motif #58002) following the manufacturer's instructions. Quantification assessment of purified DNA was done using Qbit dsDNA HS Assay on the Qbit fluorometer (Invitrogen). Immunoprecipitated DNA quality was evaluated on a Bioanalyzer 2100 (Agilent).

Sequencing libraries for each sample were synthesized using Diagenode MicroPlex Library Preparation kit according to supplier recommendations (version 2.02.15) and were sequenced on Illumina HiSeq 4000 sequencer as Paired-End 50 base reads following Illumina's instructions (GenomEast platform, IGBM, Strasbourg, France). Image analysis and base calling were performed using RTA 2.7.3 and bcl2fastq 2.17.1.14. Adapter dimer reads were removed using DimerRemover. Sequenced reads were mapped to the *Drosophila melanogaster* genome assembly dm6 using Bowtie (version 2.3.3) with default option. Only uniquely aligned reads have been retained for further analyses. Duplicated reads were removed using picard-tools (version 2.17.10). Peak calling was performed for each individual samples and on merged biological replicates using MACS algorithm (version 2.1.1) with default option and a relaxed q-value cut-off of 0.1. Consistent peaks between biological replicates were identified using irreproducible discovery rate (IDR version 2.0.3) with a 0.05 cut-off. Differentially modified H3K4me3 peaks between Control and *lid* Knock-down ovaries were identified using the R-package DiffBind (version 2.2.12) with a 0.05 FDR cut-off.

## Data visualization

The Deeptools software was used to convert alignment files to bigwig (bamCoverage) and to generate H3K4me3 heatmap and density profiles (computeMatrix and plotHeatmap). The generated bigwig files were visualized using IGV software.

## Supporting information

**S1 Fig. Developmental defects of *lid* KD embryos.** Embryos were collected for four hours and aged for another four hours at 25°C before DAPI staining and examination in fluorescent microscopy. More than 85% of *lid* KD embryos arrest development before the blastoderm stage. In contrast, 100% of control embryos had reached gastrula or later stages. (TIF)

**S2 Fig. Meiosis II is not visibly affected in eggs from *lid* KD females.** A—Representative confocal images of eggs in metaphase of meiosis II stained for DNA (blue), alpha-tubulin (red) and ProtA::GFP (green). The tandem of meiotic spindles is shown on the left, the corresponding male nucleus from the same egg is on the right. Bars: 5 μm. B—Quantification of meiosis II phenotypes (normal or abnormal chromosome segregation). (TIF)

**S3 Fig. Phenotype of *Sim3A* KD and *rpd3* KD eggs/embryos.** A—Confocal images of *Sim3A* KD eggs stained for DNA at the indicated stages. The sperm nucleus in the left panel is indicated (arrow). Bar: 10 μm. PB: Polar bodies. B—Confocal images of *rpd3* KD early embryos (from ProtA::GFP fathers) stained for DNA and anti-GFP. The sperm nucleus is indicated

(arrows). Bar: 10  $\mu$ m. PB: Polar bodies.

(TIF)

**S4 Fig. Lid is not directly involved in sperm chromatin remodeling at fertilization.** A—Top row: confocal images of stage 10 egg chambers from control (left) and lid KD (right) females stained for DNA (red) and anti-Lid (green). Middle row: detail of a nurse cell nucleus. Bottom row: detail of the oocyte germinal vesicle (oocyte nucleus). Bar: 20  $\mu$ m. B—Confocal images of the male pronucleus and the female pronucleus from a control egg in meiosis II stained for DNA and anti-Lid. Bar: 10  $\mu$ m. Quantification of Lid positive nuclei is indicated. C—Confocal images of a control (left) and lid KD (right) blastoderm embryo with same staining as in B. Bar: 10  $\mu$ m. Quantifications of embryos with a positive/negative nuclear Lid staining are indicated for each genotype.

(JPG)

**S5 Fig. Lid and Sin3A control *dhd* expression in female germ cells.** A—Principal Component Analysis of Control, *lid* KD and *Sin3A* KD ovarian transcriptomes (two biological replicates for each genotype). B—Volcano plot representations of Differentially-Expressed genes in Control vs *lid* KD (left) and Control vs *Sin3A* KD (right). C—RT-qPCR quantification of *dhd* mRNA levels in ovaries of indicated genotypes. mRNA levels were normalized to *rp49* and shown as relative expression in MTD>+ control. Error bars represent SD (Dunnett's multiple comparisons test to the control MTD>+, \*\*\*  $P < 0.0001$ ). D—Western blot analysis of DHD in adult ovaries (left) and 0-30min postfertilization embryos (right).  $\alpha$ -tubulin was used as a loading control. E—Western blot analysis of DHD in adult ovaries of indicated genotypes.  $\alpha$ -tubulin was used as a loading control.

(TIF)

**S6 Fig. Top twelve most downregulated and upregulated genes in *lid* KD and *Sin3A* KD transcriptomes.**

(TIF)

**S7 Fig. The JmjC domain of Lid is required for normal *dhd* expression.** A—Embryo hatching rates from females of indicated genotypes. B—RT-qPCR quantification of *dhd* (left) and *lid* (right) mRNA levels in ovaries of indicated genotypes. mRNA levels were normalized to *rp49* and shown as relative expression in *w<sup>1118</sup>* control. Error bars represent SD (Dunnett's multiple comparisons test to the control (\*\*  $P < 0.01$ ; \*\*\*  $P = 0.0002$ ). C—Analysis of paternal GFP::Cid expression in late embryos from indicated females (as in Fig 1B).

(TIF)

**S8 Fig. *trr* KD does not affect *dhd* expression.** A—Confocal images of representative embryos of the indicated genotypes stained for DNA and anti-DHD. The fertilizing sperm nucleus is magnified in insets. Bar: 20  $\mu$ m. B—Details of maternal chromosomes (top row) and sperm nucleus (bottom row) from a representative *trr* KD egg stained for ProtA::GFP and histones.

(JPG)

**S1 Table. Haploid TRiP genetic screen.**

(XLSX)

**S2 Table. Differentially expressed genes in *lid* KD and *Sin3A* KD ovaries.**

(XLSX)

**S3 Table. Quantitative analysis of H3K4me3 differential enrichment in Control vs *lid* KD ovarian ChIP-Seq.**

(XLSX)

## Acknowledgments

We thank Ferran Azorin, Cayetano Gonzalez, Cristina Molnar and Paulo Navarro-Costa for sharing fly stocks and antibodies. We are grateful to the TRIP projects and Bloomington Drosophila Stock Center for shRNA stocks. The authors would like to thank the members of the IGBMC GenomEast platform for their help. We also thank Raphaëlle Dubruielle for her helpful comments on the manuscript.

## Author Contributions

**Conceptualization:** Daniela Torres-Campana, Shuhei Kimura, Guillermo A. Orsi, Benjamin Loppin.

**Data curation:** Guillermo A. Orsi, Gérard Benoit.

**Formal analysis:** Gérard Benoit.

**Funding acquisition:** Benjamin Loppin.

**Investigation:** Daniela Torres-Campana, Shuhei Kimura, Béatrice Horard, Benjamin Loppin.

**Methodology:** Gérard Benoit.

**Supervision:** Béatrice Horard, Benjamin Loppin.

**Validation:** Daniela Torres-Campana, Guillermo A. Orsi, Béatrice Horard, Gérard Benoit, Benjamin Loppin.

**Writing – original draft:** Benjamin Loppin.

**Writing – review & editing:** Daniela Torres-Campana, Guillermo A. Orsi, Béatrice Horard, Gérard Benoit, Benjamin Loppin.

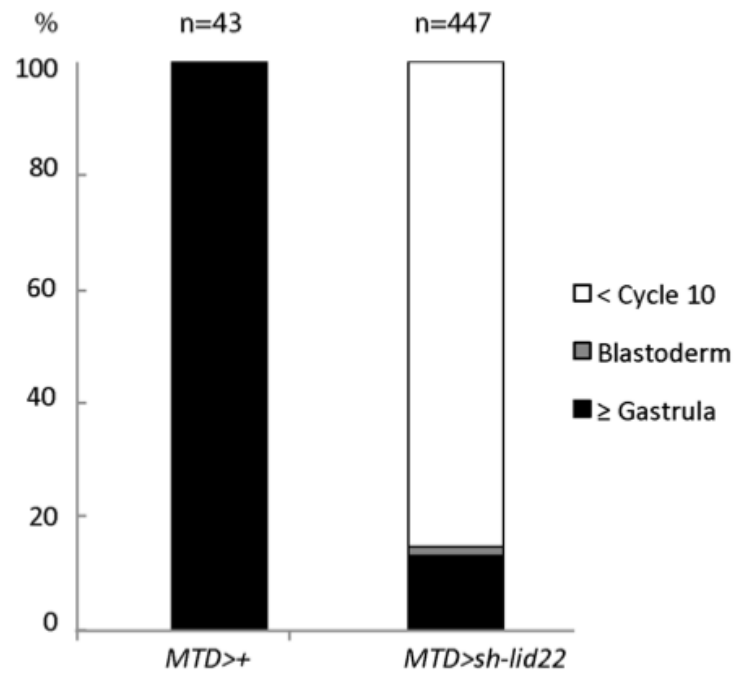
## References

1. Loppin B, Dubruielle R, Horard B (2015) The intimate genetics of *Drosophila* fertilization. *Open Biol* 5: 150076. <https://doi.org/10.1098/rsob.150076> PMID: 26246493
2. Hamm DC, Harrison MM (2018) Regulatory principles governing the maternal-to-zygotic transition: insights from *Drosophila melanogaster*. *Open Biol* 8: 180183. <https://doi.org/10.1098/rsob.180183> PMID: 30977698
3. Spradling AC (1993) Developmental genetics of oogenesis. *The Development of Drosophila melanogaster*—Cold Spring Harbor Laboratory Press. 1–69.
4. Eirin-López JM, Ausió J (2009) Origin and evolution of chromosomal sperm proteins. *Bioessays* 31: 1062–1070. <https://doi.org/10.1002/bies.200900050> PMID: 19708021
5. Rathke C, Baarends WM, Awe S, Renkawitz-Pohl R (2014) Chromatin dynamics during spermiogenesis. *Biochim Biophys Acta* 1839: 155–168. <https://doi.org/10.1016/j.bbaggm.2013.08.004> PMID: 24091090
6. Tirmarche S, Kimura S, Dubruielle R, Horard B, Loppin B (2016) Unlocking sperm chromatin at fertilization requires a dedicated egg thiorodexin in *Drosophila*. *Nature Commun* 7: 13539. <https://doi.org/10.1038/ncomms13539>
7. Petrova B, Liu K, Tian C, Kitaoka M, Freinkman E, Yang J, et al. (2018) Dynamic redox balance directs the oocyte-to-embryo transit via developmentally controlled reactive cysteine changes. *Proc Natl Acad Sci USA* 115: E7978–E7986. <https://doi.org/10.1073/pnas.1807918115> PMID: 30082411
8. Horard B, Sapey-Triomphe L, Bonnefoy E, Loppin B (2018) ASF1 is required to load histones on the HIRA complex in preparation of paternal chromatin assembly at fertilization. *Epigenetics Chromatin* 11: 19. <https://doi.org/10.1186/s13072-018-0189-x> PMID: 29751347
9. Ni J-Q, Zhou R, Czech B, Liu L-P, Holdersbaum L, Yang-Zhou D, et al. (2011) A genome-scale shRNA resource for transgenic RNAi in *Drosophila*. *Nat Meth* 8: 405–407. <https://doi.org/10.1038/nmeth.1592>
10. Delabaere L, Orsi GA, Sapey-Triomphe L, Horard B, Couble P, Loppin B (2014) The Spartan Ortholog Maternal Haploid Is Required for Paternal Chromosome Integrity in the *Drosophila* Zygote. *Curr Biol* 24: 2281–2287. <https://doi.org/10.1016/j.cub.2014.08.010> PMID: 25242033

11. Gildea JJ, Lopez R, Shearn A (2000) A screen for new trithorax group genes identified little imaginal discs, the *Drosophila melanogaster* homologue of human retinoblastoma binding protein 2. *Genetics* 156: 645–663. PMID: 11014813
12. Secombe J, Li L, Carlos L, Eisenman RN (2007) The Trithorax group protein Lid is a trimethyl histone H3K4 demethylase required for dMyc-induced cell growth. *Genes & Dev* 21: 537–551. <https://doi.org/10.1101/gad.1523007>
13. Lloret-Linares M, Carr CM, Vaquero A, de Olano N, Azorin F (2008) Characterization of *Drosophila melanogaster* JmjC+N histone demethylases. *Nucleic Acids Res*. 36: 2852–2863. <https://doi.org/10.1093/nar/gkn098> PMID: 18375980
14. Lloret-Linares M, Perez-Lluch S, Rossell D, Moran T, Ponsa-Cobas J, Auer H, et al. (2012) dKDM5/LID regulates H3K4me3 dynamics at the transcription-start site (TSS) of actively transcribed developmental genes. *Nucleic Acids Res*. 40: 9493–9505. <https://doi.org/10.1093/nar/gks773> PMID: 22904080
15. Grzenda A, Lombark G, Zhang J-S, Urrutia R (2009) Sin3: Master scaffold and transcriptional corepressor. *Biochim Biophys Acta* 1789: 443–450. <https://doi.org/10.1016/j.bbagr.2009.05.007> PMID: 19505602
16. Spain MM, Caruso JA, Swaminathan A, Pile LA (2010) *Drosophila* SIN3 Isoforms Interact with Distinct Proteins and Have Unique Biological Functions. *J Biol Chem* 285: 27457–27467. <https://doi.org/10.1074/jbc.M110.130245> PMID: 20566628
17. Gajan A, Barnes VL, Liu M, Saha N, Pile LA (2016) The histone demethylase dKDM5/LID interacts with the SIN3 histone deacetylase complex and shares functional similarities with SIN3. *Epigenetics Chromatin* 9:4 <https://doi.org/10.1186/s13072-016-0053-9> PMID: 26848313
18. Liu M, Pile LA (2017) The Transcriptional Corepressor SIN3 Directly Regulates Genes Involved in Methionine Catabolism and Affects Histone Methylation, Linking Epigenetics and Metabolism. *J Biol Chem* 292: 1970–1976. <https://doi.org/10.1074/jbc.M116.749754> PMID: 28028175
19. Barnes VL, Bhat A, Unnikrishnan A, Heydari AR, Arking R, Pile LA (2014) SIN3 is critical for stress resistance and modulates adult lifespan. *Aging* 6: 645–660. <https://doi.org/10.18632/aging.100684> PMID: 25133314
20. Moshkin YM, Kan TW, Goodfellow H, Bezstarosti K, Maeda RK, Pilyugin M, et al. (2009) Histone Chaperones ASF1 and NAP1 Differentially Modulate Removal of Active Histone Marks by LID-RPD3 Complexes during NOTCH Silencing. *Mol Cell* 35: 782–793. <https://doi.org/10.1016/j.molcel.2009.07.020> PMID: 19782028
21. Lee N, Erdjument-Bromage H, Tempst P, Jones RS, Zhang Y (2009) The H3K4 Demethylase Lid Associates with and Inhibits Histone Deacetylase Rpd3. *Mol Cell Biol* 29: 1401–1410. <https://doi.org/10.1128/MCB.01643-08> PMID: 19114561
22. Kronja J, Yuan B, Eichhorn SW, Dzeyk K, Kringsvold J, Bartel DP, et al. (2014) Widespread Changes in the Posttranscriptional Landscape at the *Drosophila* Oocyte-to-Embryo Transition. *Cell Reports* 7: 1495–1508. <https://doi.org/10.1016/j.celrep.2014.05.002> PMID: 24882012
23. Navarro-Costa P, McCarthy A, Prudêncio P, Greer C, Guilgur LG, Becker JORD, et al. (2016) Early programming of the oocyte epigenome temporally controls late prophase I transcription and chromatin remodelling. *Nature Commun* 7: 1–15. <https://doi.org/10.1038/ncomms12331>
24. Manier MK, Belote JM, Berben KS, Novikov D, Stuart WT, Pitnick S (2010) Resolving Mechanisms of Competitive Fertilization Success in *Drosophila melanogaster*. *Science* 328: 354–357. <https://doi.org/10.1126/science.1187096> PMID: 20299550
25. Zhaunova L, Ohkura H, Breuer M (2016) Kdm5/Lid Regulates Chromosome Architecture in Meiotic Prophase I Independently of Its Histone Demethylase Activity. *PLoS Genet*. 12: e1006241. <https://doi.org/10.1371/journal.pgen.1006241> PMID: 27494704
26. Dreton C, Belalcazar HM, Secombe J. The Histone Demethylase KDM5 Is Essential for Larval Growth in *Drosophila* (2018) *Genetics* 209: 773–787. <https://doi.org/10.1534/genetics.118.301004> PMID: 29764801
27. Liu X, Secombe J (2015) The Histone Demethylase KDM5 Activates Gene Expression by Recognizing Chromatin Context through Its PHD Reader Motif. *Cell Reports* 13: 2219–2231. <https://doi.org/10.1016/j.celrep.2015.11.007> PMID: 26673323
28. Emelyanov AV, Fyodorov DV (2016) Thioredoxin-dependent disulfide bond reduction is required for protamine eviction from sperm chromatin. *Genes & Dev* 30: 2651–2656. <https://doi.org/10.1101/gad.290916.116>
29. Sandler JE, Stathopoulos A (2016) Quantitative Single-Embryo Profile of *Drosophila* Genome Activation and the Dorsal-Ventral Patterning Network. *Genetics* 202: 1575–1584. <https://doi.org/10.1534/genetics.116.186783> PMID: 26896327

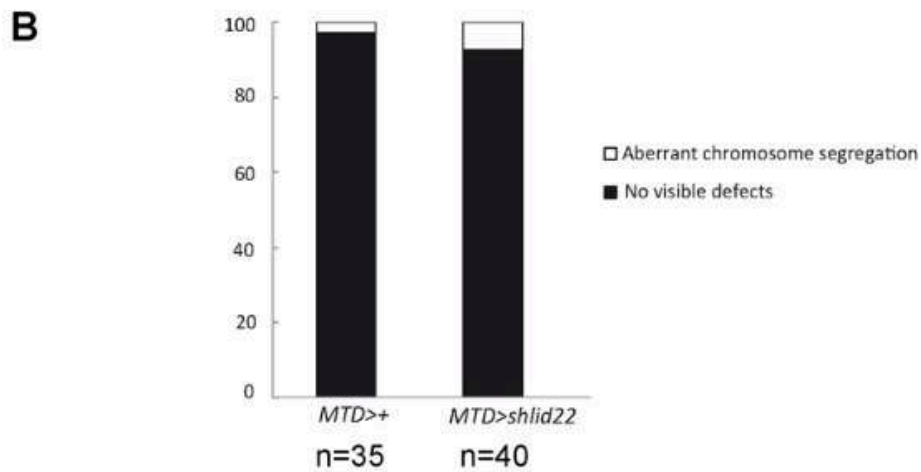
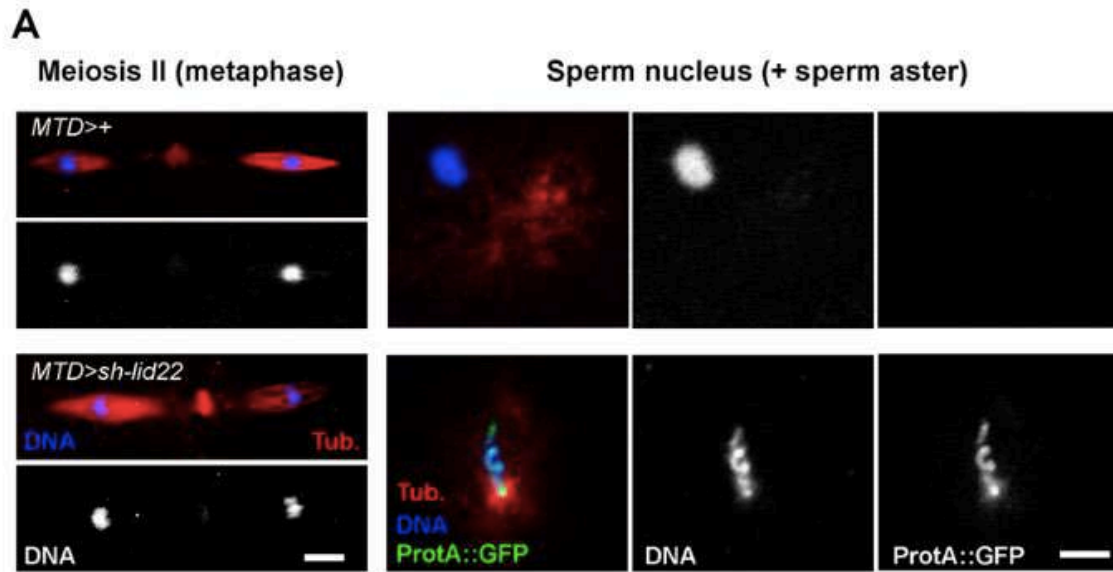
30. Zamurrad S, Hatch HAM, Drelon C, Belalcazar HM, Secombe J (2018) A *Drosophila* Model of Intellectual Disability Caused by Mutations in the Histone Demethylase KDM5. *Cell Reports* 22: 2359–2369. <https://doi.org/10.1016/j.celrep.2018.02.018> PMID: 29490272
31. Li L, Greer C, Eisenman RN, Secombe J (2010) Essential functions of the histone demethylase lid. *PLoS Genet* 6: e1001221. <https://doi.org/10.1371/journal.pgen.1001221> PMID: 21124823
32. Lussi YC, Mariani L, Friis C, Pelltonen J, Myers TR, Krag C, et al. (2016) Impaired removal of H3K4 methylation affects cell fate determination and gene transcription. *Development* 143: 3751–3762. <https://doi.org/10.1242/dev.139139> PMID: 27578789
33. Kidder B., Hu G, Zhao K (2014) KDM5B focuses H3K4 methylation near promoters and enhancers during embryonic stem cell self-renewal and differentiation. *Genome Biol* 15: R32. <https://doi.org/10.1186/gb-2014-15-2-r32> PMID: 24495580
34. Outchkourov NS, Muñio JM, Kaufmann K, van Ijcken WFJ, Koerkamp MJG, van Leenen D, et al. (2013) Balancing of Histone H3K4 Methylation States by the Kdm5c/SMCX Histone Demethylase Modulates Promoter and Enhancer Function. *Cell Reports* 3: 1071–1079. <https://doi.org/10.1016/j.celrep.2013.02.030> PMID: 23545502
35. Freeman M, Nüsslein-Volhard C, Glover DM (1986) The dissociation of nuclear and centrosomal division in *gnu*, a mutation causing giant nuclei in *Drosophila*. *Cell* 46: 457–468. [https://doi.org/10.1016/0092-8674\(86\)90666-5](https://doi.org/10.1016/0092-8674(86)90666-5) PMID: 3089628
36. Herz HM, Mohan M, Garruss AS, Liang K, Takahashi YH, Mickey K, et al. (2012) Enhancer-associated H3K4 monomethylation by Trithorax-related, the *Drosophila* homolog of mammalian Mll3/Mll4. *Genes & Dev* 26: 2604–2620. <https://doi.org/10.1101/gad.201327.112>
37. Prudêncio P, Guilgur LG, Sobral J, Becker JD, Martinho RG, Navarro-Costa P (2018) The Trithorax group protein dMLL3/4 instructs the assembly of the zygotic genome at fertilization. *EMBO Rep* 19: e45728. <https://doi.org/10.15252/embr.201845728> PMID: 30037897
38. Schuth M, Lehner CF, Heidmann S (2007) Incorporation of *Drosophila* CID/CENP-A and CENP-C into centromeres during early embryonic anaphase. *Curr Biol* 17: 237–243. <https://doi.org/10.1016/j.cub.2006.11.051> PMID: 17222555
39. Salz HK, Flickinger TW, Mitterdorf E, Pellicena-Palle A, Petschek JP, Brown Abrecht E (1994) The *Drosophila* Maternal Effect Locus deadhead Encodes a Thioredoxin Homolog Required for Female Meiosis and Early Embryonic Development. *Genetics* 136: 1075–1086. PMID: 7516301
40. Livak KJ, Schmittgen TD (2001) Analysis of Relative Gene Expression Data Using Real-Time Quantitative PCR and the 2<sup>-ΔΔCT</sup> Method. *Methods* 25: 402–408. <https://doi.org/10.1006/meth.2001.1262> PMID: 11846609
41. Grentzinger T, Armenise C, Brun C, Mugat B, Serrano V, Pelisson A, et al. (2012) piRNA-mediated transgenerational inheritance of an acquired trait. *Genome Res* 22: 1877–1888. <https://doi.org/10.1101/gr.136614.111> PMID: 22555593

## Supplemental data:



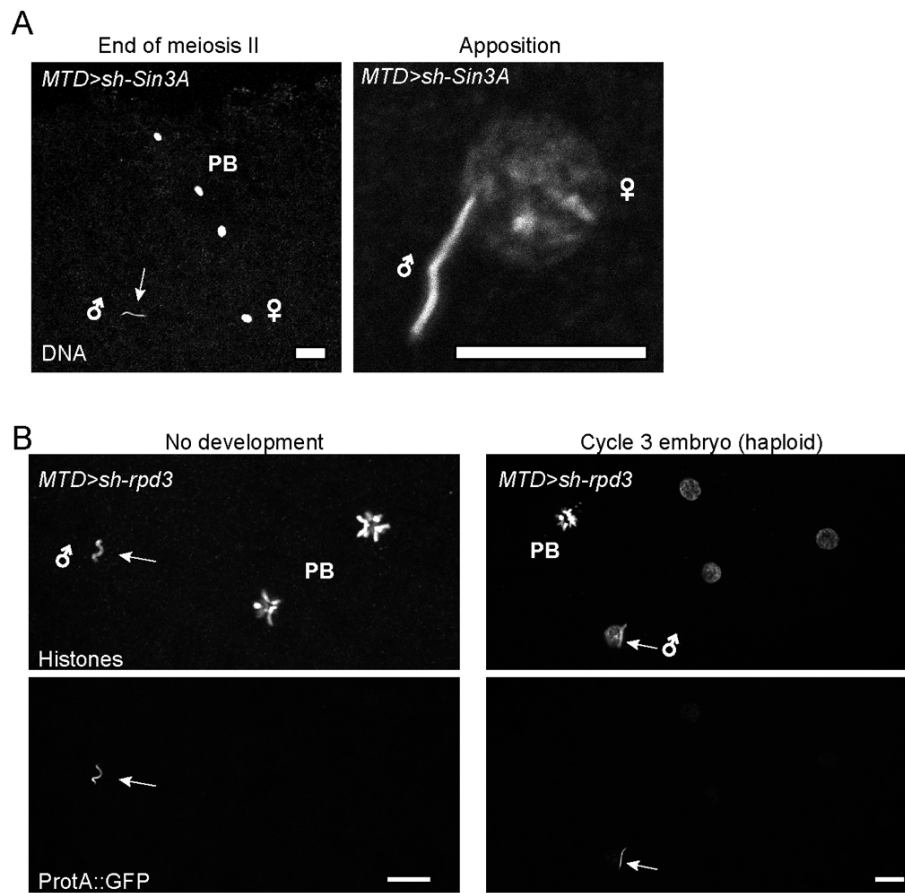
**Fig S1. Developmental defects of *lid* KD embryos.**

Embryos were collected for four hours and aged for another four hours at 25°C before DAPI staining and examination in fluorescent microscopy. More than 85% of *lid* KD embryos arrest development before the blastoderm stage. In contrast, 100% of control embryos had reached gastrula or later stages.



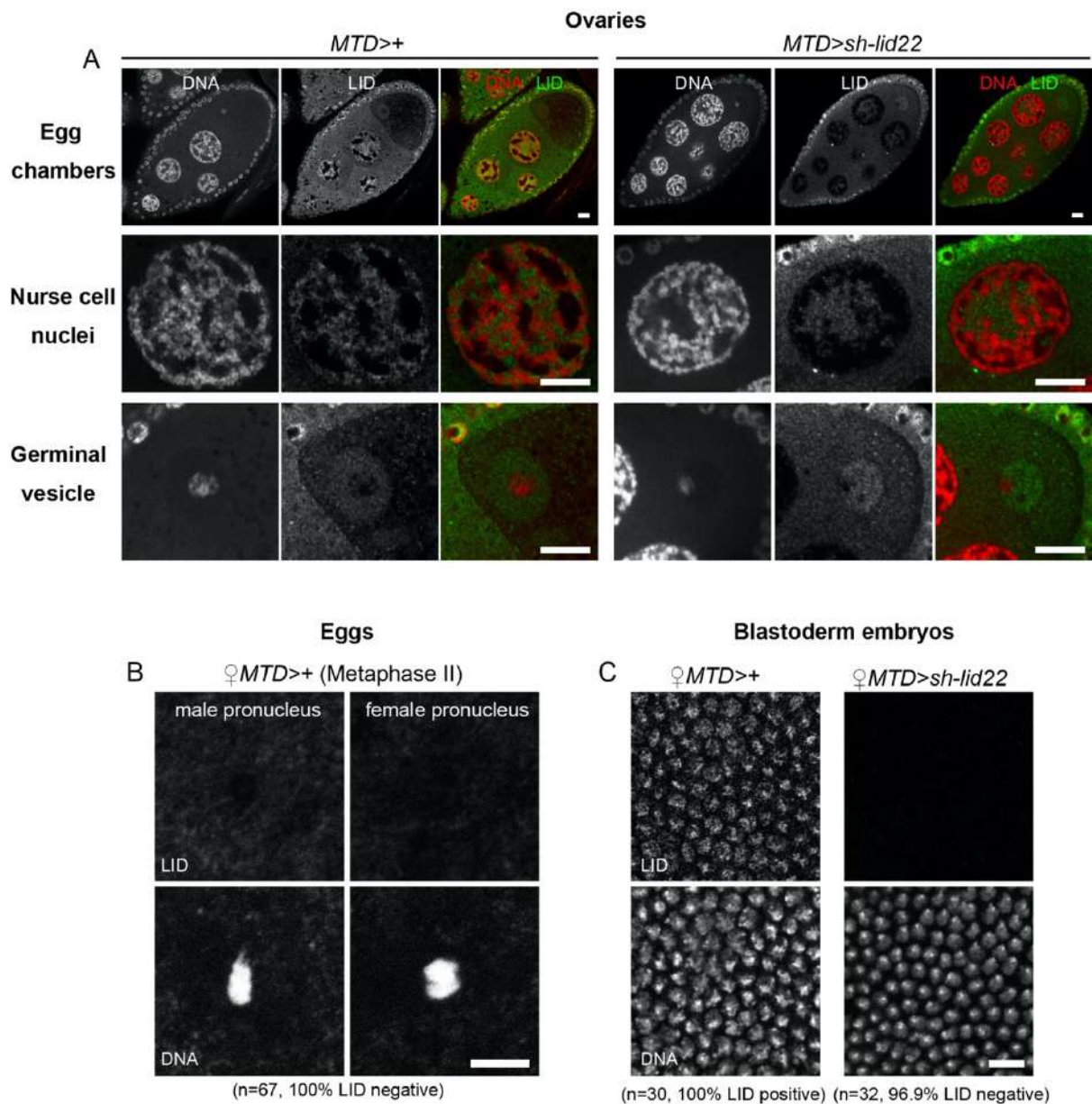
**Fig S2. Meiosis II is not visibly affected in eggs from *lid* KD females.**

A-Representative confocal images of eggs in metaphase of meiosis II stained for DNA (blue), alpha-tubulin (red) and ProtA::GFP (green). The tandem of meiotic spindles is shown on the left, the corresponding male nucleus from the same egg is on the right. Bars: 5  $\mu$ m. B-Quantification of meiosis II phenotypes (normal or abnormal chromosome segregation).



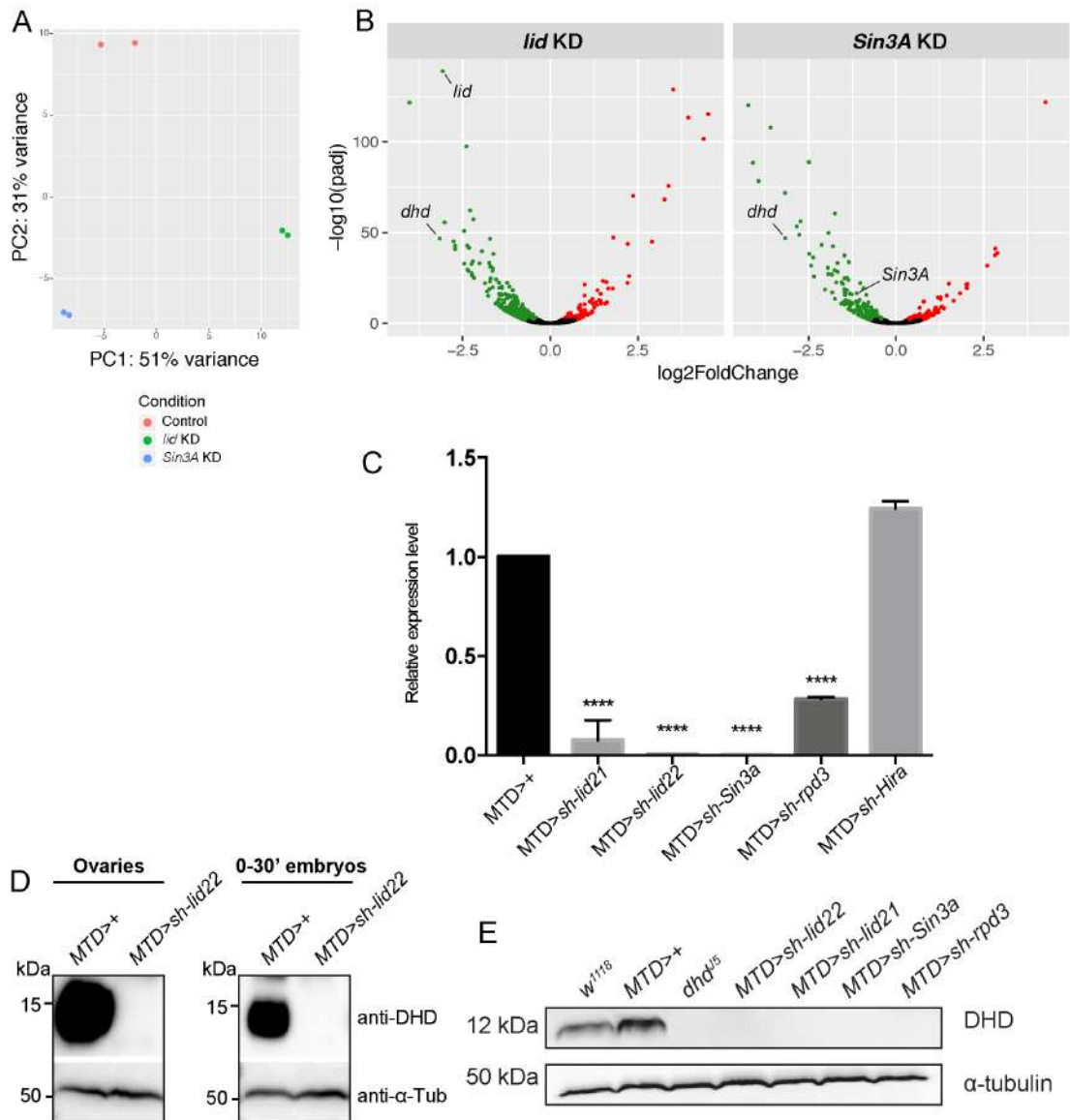
**Fig S3. Phenotype of *Sin3A* KD and *rpd3* KD eggs/embryos.**

A-Confocal images of *Sin3A* KD eggs stained for DNA at the indicated stages. The sperm nucleus in the left panel is indicated (arrow). Bar: 10  $\mu$ m. PB: Polar bodies. B-Confocal images of *rpd3* KD early embryos (from ProtA::GFP fathers) stained for DNA and anti-GFP. The sperm nucleus is indicated (arrows). Bar: 10  $\mu$ m. PB: Polar bodies.



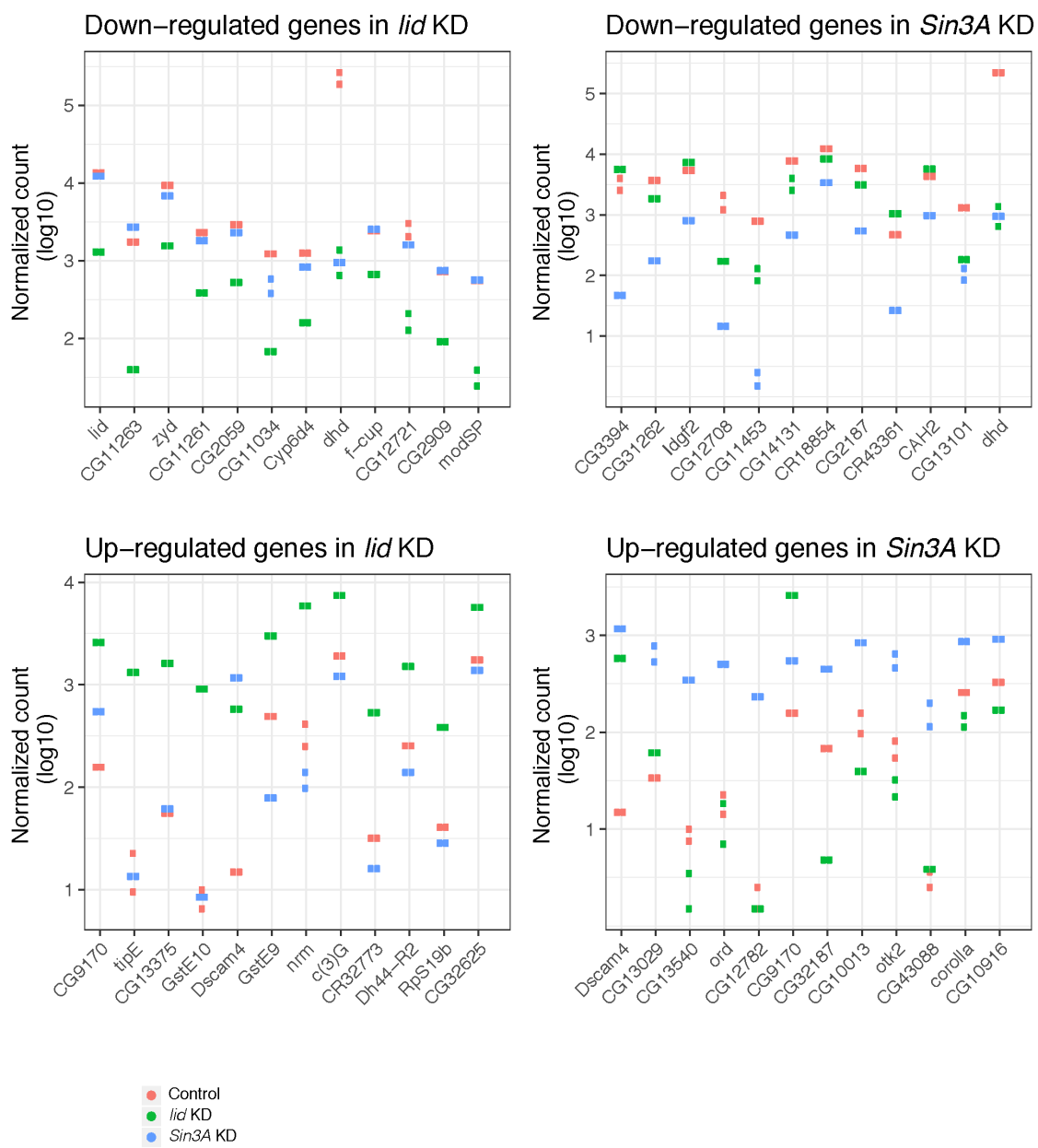
**Fig S4. Lid is not directly involved in sperm chromatin remodeling at fertilization.**

A-Top row: confocal images of stage 10 egg chambers from control (left) and lid KD (right) females stained for DNA (red) and anti-Lid (green). Middle row: detail of a nurse cell nucleus. Bottom row: detail of the oocyte germinal vesicle (oocyte nucleus). Bar: 20  $\mu$ m. B-Confocal images of the male pronucleus and the female pronucleus from a control egg in meiosis II stained for DNA and anti-Lid. Bar: 10  $\mu$ m. Quantification of Lid positive nuclei is indicated. C-Confocal images of a control (left) and lid KD (right) blastoderm embryo with same staining as in B. Bar: 10  $\mu$ m. Quantifications of embryos with a positive/negative nuclear Lid staining are indicated for each genotype.



**Fig S5. Lid and Sin3A control *dhd* expression in female germ cells.**

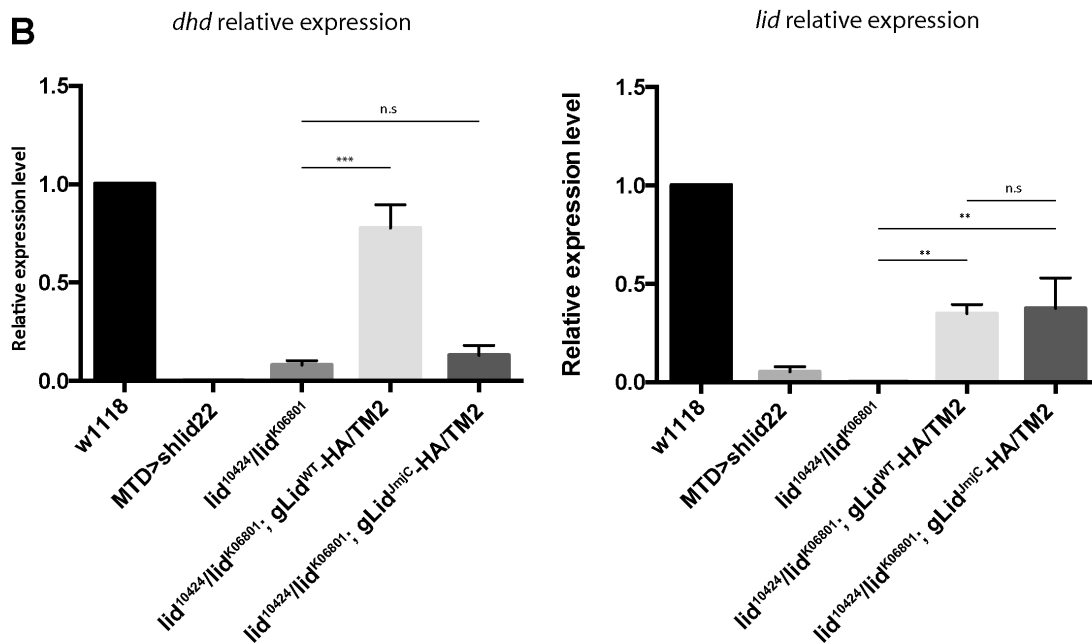
A-Principal Component Analysis of Control, *lid* KD and *Sin3A* KD ovarian transcriptomes (two biological replicates for each genotype). B-Volcano plot representations of Differentially-Expressed genes in Control vs *lid* KD (left) and Control vs *Sin3A* KD (right). C-RT-qPCR quantification of *dhd* mRNA levels in ovaries of indicated genotypes. mRNA levels were normalized to rp49 and shown as relative expression in MTD>+ control. Error bars represent SD (Dunnett's multiple comparisons test to the control MTD>+, \*\*\*\* P < 0.0001). D—Western blot analysis of DHD in adult ovaries (left) and 0-30min postfertilization embryos (right).  $\alpha$ -tubulin was used as a loading control. E—Western blot analysis of DHD in adult ovaries of indicated genotypes.  $\alpha$ -tubulin was used as a loading control.



**Fig S6. Top twelve most downregulated and upregulated genes in *lid* KD and *Sin3A* KD transcriptomes.**

**A**

Female Genotype	No. eggs	Hatching rate
<i>w<sup>1118</sup></i>	330	97.2
<i>lid<sup>10424</sup>/lid<sup>K06801</sup>; gLid<sup>WT</sup>-HA/TM2</i>	921	63.4
<i>lid<sup>10424</sup>/lid<sup>K06801</sup>; gLid<sup>JmjC</sup>-HA/TM2</i>	117	16.2

**B****C**

Female Genotype	No. eggs	Gastrula or beyond	GFP neg.	GFP pos.
<i>lid<sup>10424</sup>/lid<sup>K06801</sup>; gLid<sup>WT</sup>-HA/TM2</i>	53	34	0	34
<i>lid<sup>10424</sup>/lid<sup>K06801</sup>; gLid<sup>JmjC</sup>-HA/TM2</i>	14	6	3	3

**Fig S7. The JmjC domain of Lid is required for normal *dhd* expression.**

A-Embryo hatching rates from females of indicated genotypes. B-RT-qPCR quantification of *dhd* (left) and *lid* (right) mRNA levels in ovaries of indicated genotypes. mRNA levels were normalized to rp49 and shown as relative expression in *w<sup>1118</sup>* control. Error bars represent SD (Dunnett's multiple comparisons test to the control (\*\* P < 0.01; \*\*\* P = 0.0002). C-Analysis of paternal GFP::Cid expression in late embryos from indicated females (as in Fig 1B).

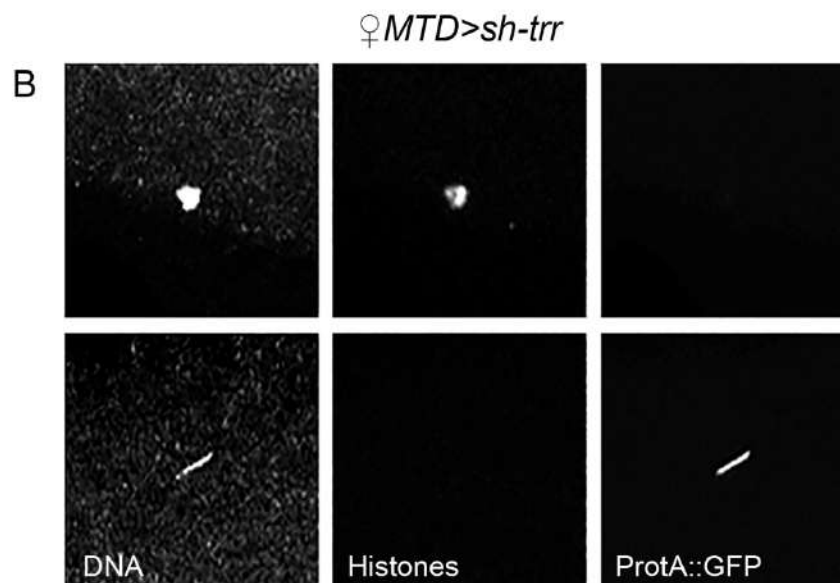
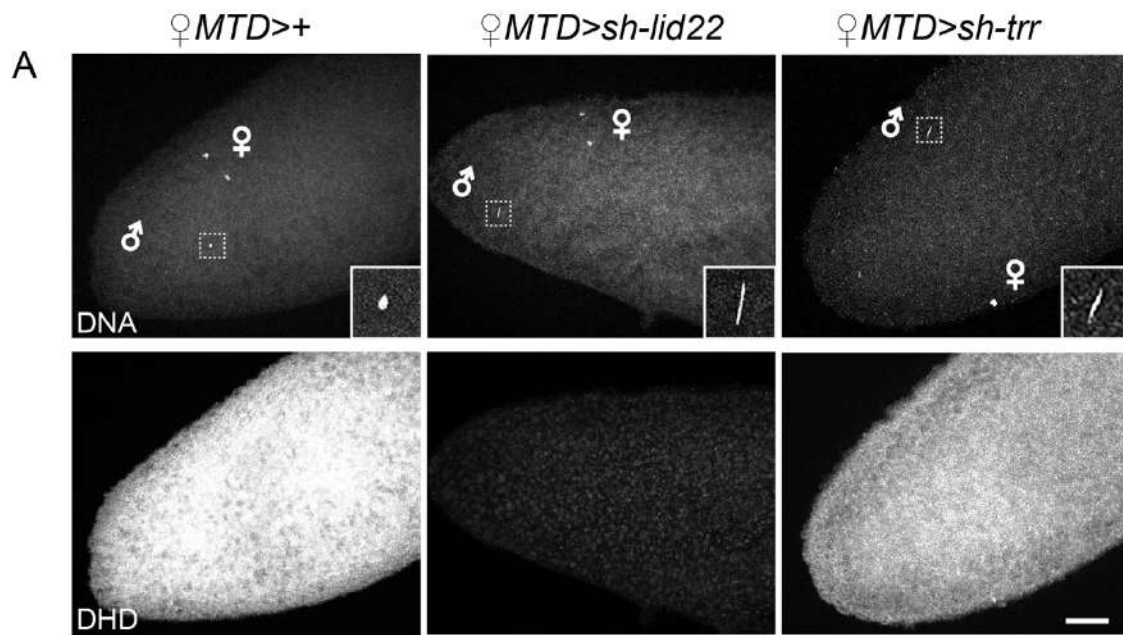


**Fig S8. *trr* KD does not affect *dhd* expression.**

A-Confocal images of representative embryos of the indicated genotypes stained for DNA and anti-DHD. The fertilizing sperm nucleus is magnified in insets. Bar: 20  $\mu$ m. B-Details of maternal chromosomes (top row) and sperm nucleus (bottom row) from a representative *trr* KD egg stained for ProtA::GFP and histones.



<b>S1 Table - Haploid TRIP screen</b>							
	<b>Fertile</b>						<b>"dhd-like": needle-shaped sperm nucleus, as in <i>dhdJ5</i> mutant.</b>
	<b>Sterile, class 1: No egg laying.</b>						<b>"ssm-like": small, round male nucleus, as in <i>Hira(ssm)</i> mutant.</b>
	<b>Sterile, class 2: Few abnormal eggs, no hatching.</b>						
	<b>Sterile, class 3: Eggs do not hatch (HR&lt;5%) and remain white.</b>						
	<b>Sterile, class 4: Eggs do not hatch (HR&lt;5%), some turn brown.</b>						
BDSC#	TRIP#	CG#	Gene Symbol	Vector	Female fertility	GFP::Cid expression	Sperm nuclear phenotype
35334	GL00243	CG9638	Ada2b	pVALIUM22	Fertile	Not tested	Not tested
35232	GL00117	CG40300	AGO3	pVALIUM22	Fertile	Not tested	Not tested
36803	GL01012	CG8887	ash1	pVALIUM22	Fertile	Not tested	Not tested
32503	HMS00507	CG4303	Bap60	pVALIUM20	Fertile	Not tested	Not tested
36781	GL00127	CG6046	Bin1	pVALIUM22	Fertile	Not tested	Not tested
43174	GL01516	CG2009	bip2	pVALIUM22	Fertile	Not tested	Not tested
42502	HMJ02067	CG1845	Br140	pVALIUM20	Fertile	Not tested	Not tested
42658	HMS02494	CG14514	Brd8	pVALIUM20	Fertile	Not tested	Not tested
35623	GL00467	CG31256	Brf	pVALIUM22	Fertile	Not tested	Not tested
35211	GL00090	CG5942	brm	pVALIUM22	Fertile	Not tested	Not tested
35163	GL00031	CG7597	Cdk12	pVALIUM22	Fertile	Not tested	Not tested
33701	HMS00578	CG10133	CG10133	pVALIUM20	Fertile	Not tested	Not tested
43137	GL01475	CG10445	CG10445	pVALIUM22	Fertile	Not tested	Not tested
41847	GL01275	CG11329	CG11329	pVALIUM22	Fertile	Not tested	Not tested
36834	GL01075	CG12877	CG12877	pVALIUM22	Fertile	Not tested	Not tested
33731	HMS00614	CG13900	CG13900	pVALIUM20	Fertile	Not tested	Not tested
36914	GL01123	CG14352	CG14352	pVALIUM22	Fertile	Not tested	Not tested
36812	GL01030	CG1815	CG1815	pVALIUM22	Fertile	Not tested	Not tested
42488	HMJ02050	CG2051	CG2051	pVALIUM20	Fertile	Not tested	Not tested
35803	GL00427	CG32772	CG32772	pVALIUM22	Fertile	Not tested	Not tested
35475	GL00403	CG33694,CG33695	cana,CG33695	pVALIUM22	Fertile	Not tested	Not tested
38211	GL00652	CG3509	CG3509	pVALIUM20	Fertile	Not tested	Not tested
34077	HMS00584	CG4049	CG4049	pVALIUM20	Fertile	Not tested	Not tested
32973	HMS00770	CG4078	CG4078	pVALIUM20	Fertile	Not tested	Not tested
41976	HMS02374	CG4203	CG4203	pVALIUM20	Fertile	Not tested	Not tested
34606	HMS00577	CG43320	CG43320	pVALIUM20	Fertile	Not tested	Not tested
42533	HMJ02100	CG4400	CG4400	pVALIUM20	Fertile	Not tested	Not tested
33696	HMS00568	CG4747	CG4747	pVALIUM20	Fertile	Not tested	Not tested
42833	HMS02525	CG4854	CG4854	pVALIUM20	Fertile	Not tested	Not tested
32441	HMS00439	CG6418	CG6418	pVALIUM20	Fertile	Not tested	Not tested
42552	HMJ02125	CG6506	CG6506	pVALIUM20	Fertile	Not tested	Not tested
41824	GL01252	CG6937	CG6937	pVALIUM22	Fertile	Not tested	Not tested
32485	HMS00488	CG7200	CG7200	pVALIUM20	Fertile	Not tested	Not tested
35229	GL00113	CG7878	CG7878	pVALIUM22	Fertile	Not tested	Not tested
35593	GL00430	CG7911	CG7911	pVALIUM22	Fertile	Not tested	Not tested
41874	GL01305	CG8223	CG8223	pVALIUM22	Fertile	Not tested	Not tested
33361	HMS00233	CG8289	CG8289	pVALIUM20	Fertile	Not tested	Not tested
41649	GL01231	CG9272	CG9272	pVALIUM22	Fertile	Not tested	Not tested
42766	GL00722	CG9418	CG9418	pVALIUM22	Fertile	Not tested	Not tested
35807	GL00455	CG9576	CG9576	pVALIUM22	Fertile	Not tested	Not tested
35652	GLV21017	CG10890,CG13399	mus201,Chrac-14	pVALIUM21	Fertile	Not tested	Not tested
36084	GL00503	CG10712	Chro	pVALIUM22	Fertile	Not tested	Not tested
35387	GL00306	CG2714	cm	pVALIUM22	Fertile	Not tested	Not tested
35354	GL00266	CG8591	CTCF	pVALIUM22	Fertile	Not tested	Not tested
34732	HMS01212	CG7405	CycH	pVALIUM20	Fertile	Not tested	Not tested
35168	GL00037	CG6292	CycT	pVALIUM22	Fertile	Not tested	Not tested
32451	HMS00450	CG7098	dik	pVALIUM20	Fertile	Not tested	Not tested
32397	HMS00391	CG42799	dikar	pVALIUM20	Fertile	Not tested	Not tested
33410	HMS00290	CG7143	DNApol-eta	pVALIUM20	Fertile	Not tested	Not tested
36648	GL00608	CG7602	DNApol-iota	pVALIUM22	Fertile	Not tested	Not tested
35353	GL00265	CG32346	E(bx)	pVALIUM22	Fertile	Not tested	Not tested
32346	HMS00337	CG12238	e(y)3	pVALIUM20	Fertile	Not tested	Not tested
33904	HMS00846	CG12756	Eaf6	pVALIUM20	Fertile	Not tested	Not tested
37017	HMS01255	CG6755	EloA	pVALIUM20	Fertile	Not tested	Not tested
36906	GL01110	CG10215	Ercc1	pVALIUM22	Fertile	Not tested	Not tested
43285	HMS02657	CG1474	Es2	pVALIUM20	Fertile	Not tested	Not tested
33891	HMS00829	CG5899	Etl1	pVALIUM20	Fertile	Not tested	Not tested
35805	GL00442	CG4274	fzy	pVALIUM22	Fertile	Not tested	Not tested
42787	GL01157	CG10670	Gen	pVALIUM22	Fertile	Not tested	Not tested
41893	GL01325	CG42803	gpp	pVALIUM20	Fertile	Not tested	Not tested
33705	HMS00582	CG8887	ash1	pVALIUM20	Fertile	Not tested	Not tested
34817	HMS00127	CG2995	G9a	pVALIUM20	Fertile	Not tested	Not tested
34727	HMS01206	CG6662	GstO1	pVALIUM20	Fertile	Not tested	Not tested
34033	HMS01004	CG4976	NSD	pVALIUM20	Fertile	Not tested	Not tested
33703	HMS00580	CG8651	lrx	pVALIUM20	Fertile	Not tested	Not tested
40931	HMS02179	CG40351	Set1	pVALIUM20	Fertile	Not tested	Not tested
35276	GL00176	CG40080	Haspin	pVALIUM22	Fertile	Not tested	Not tested
42620	HMS02455	CG5825	His3.3A	pVALIUM20	Fertile	Not tested	Not tested
36639	GL00599	CG13363	Hmt4-20	pVALIUM22	Fertile	Not tested	Not tested
32401	HMS00396	CG7041	HP1b	pVALIUM20	Fertile	Not tested	Not tested
33962	HMS00919	CG6990	HP1c	pVALIUM20	Fertile	Not tested	Not tested
37473	GL00616	CG31212	Ino80	pVALIUM22	Fertile	Not tested	Not tested
35819	GL00286	CG5247	Irbp	pVALIUM22	Fertile	Not tested	Not tested
37545	GLV21092	CG13201	ix	pVALIUM21	Fertile	Not tested	Not tested
40855	HMS02022	CG3654	Jarid2	pVALIUM20	Fertile	Not tested	Not tested
35438	GL00363	CG4029	jumu	pVALIUM22	Fertile	Not tested	Not tested
33699	HMS00574	CG11033	Kdm2	pVALIUM20	Fertile	Not tested	Not tested
34629	HMS01304	CG15835	Kdm4A	pVALIUM20	Fertile	Not tested	Not tested
34912	HMS01260	CG10080	mahj	pVALIUM20	Fertile	Not tested	Not tested
33709	HMS00587	CG3753	Marcal1	pVALIUM20	Fertile	Not tested	Not tested
34012	HMS00978	CG5465	MED16	pVALIUM20	Fertile	Not tested	Not tested
42634	HMS02470	CG14802	MED18	pVALIUM20	Fertile	Not tested	Not tested
33710	HMS00588	CG5546	MED19	pVALIUM20	Fertile	Not tested	Not tested
34577	HMS01051	CG18780	MED20	pVALIUM20	Fertile	Not tested	Not tested
34573	HMS01047	CG3034	MED22	pVALIUM20	Fertile	Not tested	Not tested



33755	HMS01097	CG7999	MED24	pVALIUM20	Fertile	Not tested	Not tested
42501	HMJ02066	CG12254	MED25	pVALIUM20	Fertile	Not tested	Not tested
32459	HMS00458	CG5121	MED28	pVALIUM20	Fertile	Not tested	Not tested
34697	HMS01176	CG8609	MED4	pVALIUM20	Fertile	Not tested	Not tested
35371	GL00284	CG4252	mer-41	pVALIUM22	Fertile	Not tested	Not tested
36605	GL00565	CG11301	Mes4	pVALIUM22	Fertile	Not tested	Not tested
36870	GL01011	CG3025	mof	pVALIUM22	Fertile	Not tested	Not tested
35241	GL00128	CG6363	MRG15	pVALIUM22	Fertile	Not tested	Not tested
35737	HMS01479	CG7003	Msh6	pVALIUM20	Fertile	Not tested	Not tested
35345	GL00256	CG10385	msl-1	pVALIUM22	Fertile	Not tested	Not tested
35272	GL00170	CG8631	msl-3	pVALIUM22	Fertile	Not tested	Not tested
42906	HMS02599	CG10692	Mt2	pVALIUM20	Fertile	Not tested	Not tested
34905	HMS01251	CG2244	MTA1-like	pVALIUM20	Fertile	Not tested	Not tested
32941	HMS00735	CG8274	Mtor	pVALIUM20	Fertile	Not tested	Not tested
35430	GL00354	CG18543	mtm	pVALIUM22	Fertile	Not tested	Not tested
35732	GLC01346	CG4644	mtRNApol	pVALIUM22	Fertile	Not tested	Not tested
43244	GLC01431	CG11156	mus101	pVALIUM22	Fertile	Not tested	Not tested
32446	HMS00444	CG12124	mx	pVALIUM20	Fertile	Not tested	Not tested
34741	HMS01221	CG42279	Nedd4	pVALIUM20	Fertile	Not tested	Not tested
36682	HMS01570	CG15319	nej	pVALIUM20	Fertile	Not tested	Not tested
35328	GL00235	CG17256	Nek2	pVALIUM22	Fertile	Not tested	Not tested
32897	HMS00686	CG5874	Nelf-A	pVALIUM20	Fertile	Not tested	Not tested
42547	HMJ02119	CG32721	NELF-B	pVALIUM20	Fertile	Not tested	Not tested
32835	HMS00525	CG5994	Nelf-E	pVALIUM20	Fertile	Not tested	Not tested
35595	GL00432	CG33554	Nipped-A	pVALIUM22	Fertile	Not tested	Not tested
32837	HMS00527	CG4453	Nup153	pVALIUM20	Fertile	Not tested	Not tested
32391	HMS00385	CG4738	Nup160	pVALIUM20	Fertile	Not tested	Not tested
33707	HMS00585	CG3736	okr	pVALIUM20	Fertile	Not tested	Not tested
35447	GL00372	CG7467	osa	pVALIUM22	Fertile	Not tested	Not tested
43263	GLC01452	CG11237	Oseg6	pVALIUM22	Fertile	Not tested	Not tested
39009	HMS01926	CG5581	Ote	pVALIUM20	Fertile	Not tested	Not tested
35792	GL00229	CG40411	Parp	pVALIUM22	Fertile	Not tested	Not tested
33972	HMS00929	CG1800	pasha	pVALIUM20	Fertile	Not tested	Not tested
34667	HMS01144	CG5208	Patr-1	pVALIUM20	Fertile	Not tested	Not tested
36070	GL00488	CG32443	Pc	pVALIUM22	Fertile	Not tested	Not tested
35601	GL00439	CG4107	Pcaf	pVALIUM22	Fertile	Not tested	Not tested
33946	HMS00897	CG5109	Pcl	pVALIUM20	Fertile	Not tested	Not tested
34690	HMS01169	CG3291	pcm	pVALIUM20	Fertile	Not tested	Not tested
35632	GL00479	CG17509	pds5	pVALIUM22	Fertile	Not tested	Not tested
35206	GL00082	CG17743	pho	pVALIUM22	Fertile	Not tested	Not tested
35724	GLV21089	CG3941	pita	pVALIUM21	Fertile	Not tested	Not tested
35178	GL00049	CG7001	Pk17E	pVALIUM22	Fertile	Not tested	Not tested
32840	HMS00531	CG11375	polybromo	pVALIUM20	Fertile	Not tested	Not tested
35322	GL00228	CG3307	pr-set7	pVALIUM22	Fertile	Not tested	Not tested
34622	HMS01297	CG8877	Ptp8	pVALIUM20	Fertile	Not tested	Not tested
35297	GL00199	CG3886	Psc	pVALIUM22	Fertile	Not tested	Not tested
33700	HMS00576	CG5383	PSR	pVALIUM20	Fertile	Not tested	Not tested
35269	GL00167	CG32133	ptip	pVALIUM22	Fertile	Not tested	Not tested
34784	HMS00093	CG7138	r2d2	pVALIUM20	Fertile	Not tested	Not tested
32882	HMS00670	CG9862	Rae1	pVALIUM20	Fertile	Not tested	Not tested
33005	HMS00805	CG5252	Ranbp9	pVALIUM20	Fertile	Not tested	Not tested
32466	HMS00466	CG4879	RecQ5	pVALIUM20	Fertile	Not tested	Not tested
36654	GL00614	CG12189	Rev1	pVALIUM22	Fertile	Not tested	Not tested
34684	HMS01162	CG30149	rig	pVALIUM20	Fertile	Not tested	Not tested
43259	GLC01448	CG18145	Ripalpha	pVALIUM22	Fertile	Not tested	Not tested
32472	HMS00472	CG5422	Rox8	pVALIUM20	Fertile	Not tested	Not tested
34587	HMS01061	CG9273	RPA2	pVALIUM20	Fertile	Not tested	Not tested
36800	GL01005	CG7471	Rpd3	pVALIUM22	Fertile	Not tested	Not tested
43282	HMC02681	CG3180	Rpil140	pVALIUM20	Fertile	Not tested	Not tested
35420	GL00343	CG3178	Rrp1	pVALIUM22	Fertile	Not tested	Not tested
42604	HMS02437	CG7292	Rrp6	pVALIUM20	Fertile	Not tested	Not tested
38914	GL00686	CG4385	S	pVALIUM22	Fertile	Not tested	Not tested
35446	GL00371	CG5595	Sce	pVALIUM22	Fertile	Not tested	Not tested
36637	GL00597	CG30390	Sg29	pVALIUM22	Fertile	Not tested	Not tested
34630	HMS01305	CG9936	skd	pVALIUM20	Fertile	Not tested	Not tested
34949	HMS00313	CG18271	slx1	pVALIUM20	Fertile	Not tested	Not tested
36598	GL00558	CG6057	SMC1	pVALIUM22	Fertile	Not tested	Not tested
35477	GL00406	CG5263	smg	pVALIUM22	Fertile	Not tested	Not tested
34087	HMS00842	CG4013	Smr	pVALIUM20	Fertile	Not tested	Not tested
36125	HMS01540	CG4494	smt3	pVALIUM20	Fertile	Not tested	Not tested
36881	GL01045	CG31755	SoYb	pVALIUM22	Fertile	Not tested	Not tested
38898	GL00669	CG7948	spn-A	pVALIUM22	Fertile	Not tested	Not tested
43158	GL01500	CG3325	spn-B	pVALIUM22	Fertile	Not tested	Not tested
35148	GL00016	CG3169	Spt3	pVALIUM22	Fertile	Not tested	Not tested
35437	GL00362	CG8396	Ssb-c31a	pVALIUM22	Fertile	Not tested	Not tested
38344	HMS01811	CG14216	Ssu72	pVALIUM20	Fertile	Not tested	Not tested
34996	HMS01406	CG11268	ste14	pVALIUM20	Fertile	Not tested	Not tested
36867	GL01006	CG17149	Su(var)3-3	pVALIUM22	Fertile	Not tested	Not tested
33402	HMS00280	CG8013	Su(z)12	pVALIUM20	Fertile	Not tested	Not tested
33403	HMS00281	CG3905	Su(z)2	pVALIUM20	Fertile	Not tested	Not tested
36893	GL01080	CG7869	SuUR	pVALIUM22	Fertile	Not tested	Not tested
42770	GL00726	CG9874	Tbp	pVALIUM22	Fertile	Not tested	Not tested
35429	GL00353	CG3710	Tfls	pVALIUM22	Fertile	Not tested	Not tested
42931	HMS02624	CG9984	TH1	pVALIUM20	Fertile	Not tested	Not tested
41843	GL01271	CG1981	Thd1	pVALIUM22	Fertile	Not tested	Not tested
35603	GL00443	CG10387	tos	pVALIUM22	Fertile	Not tested	Not tested
35790	GL00397	CG10897	tou	pVALIUM22	Fertile	Not tested	Not tested
35794	GL00258	CR34649	tre-1	pVALIUM22	Fertile	Not tested	Not tested
41582	GL00699	CG33261,CG42507	Trf,CG42507	pVALIUM22	Fertile	Not tested	Not tested
36116	HMS01492	CG42595	uex	pVALIUM20	Fertile	Not tested	Not tested
34076	HMS00575	CG5640	Utx	pVALIUM20	Fertile	Not tested	Not tested
35468	GL00394	CG12701	vfl	pVALIUM22	Fertile	Not tested	Not tested
36877	GL01036	CG10728	vis	pVALIUM22	Fertile	Not tested	Not tested
36616	GL00576	CG3707	wapl	pVALIUM22	Fertile	Not tested	Not tested



32469	HMS00469	CG4448	wda	pVALIUM20	Fertile	Not tested	Not tested
33363	GLC01357	CG9226	WDR79	pVALIUM20	Fertile	Not tested	Not tested
35680	GLV21045	CG4148	wek	pVALIUM21	Fertile	Not tested	Not tested
32894	HMS00683	CG4548	XNP	pVALIUM20	Fertile	Not tested	Not tested
35208	GL00084	CG7803	z	pVALIUM22	Fertile	Not tested	Not tested
35228	GL00112	CG12314	zuc	pVALIUM22	Fertile	Not tested	Not tested
34846	HMS00164	CG7471	Rpd3	pVALIUM20	Fertile	Not tested	Not tested
32853	HMS00638	CG17149	Su(var)3-3	pVALIUM20	Fertile	Not tested	Not tested
33726	HMS00608	CG17149	Su(var)3-3	pVALIUM20	Fertile	Not tested	Not tested
38285	HMS01738	CG7467	osa	pVALIUM20	Fertile	Not tested	Not tested
33954	HMS00909	CG4303	Bap60	pVALIUM20	Fertile	Not tested	Not tested
34520	HMS00050	CG5942	brm	pVALIUM20	Fertile	Not tested	Not tested
41857	GL01285	CG4193	dhd	pVALIUM22	Fertile	Not tested	Not tested
36867	GL01006	CG17149	Su(var)3-3	pVALIUM22	Fertile	Not tested	Not tested
32993	HMS00793	CG3143	foxo	pVALIUM20	Fertile	Not tested	Not tested
32427	HMS00422	CG3143	foxo	pVALIUM20	Fertile	Not tested	Not tested
34774	HMS00083	CG1770	HDAC4	pVALIUM20	Fertile	Not tested	Not tested
44103	HMS02823	CG44132	mamo	pVALIUM20	Fertile	Not tested	Not tested
37486	GLV21091	CG44132	mamo	pVALIUM21	Fertile	Not tested	Not tested
40850	HMS02017	CG8591	CTCF	pVALIUM20	Fertile	Not tested	Not tested
42536	HMJ02105	CG6384	Cp190	pVALIUM20	Fertile	Not tested	Not tested
33944	HMS00895	CG6384	Cp190	pVALIUM20	Fertile	Not tested	Not tested
33903	HMS00845	CG6384	Cp190	pVALIUM20	Fertile	Not tested	Not tested
35642	GLV21006	CG10159	BEAF-32	pVALIUM21	Fertile	Not tested	Not tested
34006	HMS00970	CG8573	su(Hw)	pVALIUM20	Fertile	Not tested	Not tested
33906	HMS00848	CG8573	su(Hw)	pVALIUM20	Fertile	Not tested	Not tested
34351	HMS01340	CG6057	SMC1	pVALIUM20	Fertile	Not tested	Not tested
33431	HMS00318	CG9802	Cap	pVALIUM20	Fertile	Not tested	Not tested
33622	HMS00016	CG32443	Pc	pVALIUM20	Fertile	Not tested	Not tested
33964	HMS00921	CG32443	Pc	pVALIUM20	Fertile	Not tested	Not tested
42926	HMS02619	CG17743	pho	pVALIUM20	Fertile	Not tested	Not tested
38261	HMS01706	CG3886	Psc	pVALIUM20	Fertile	Not tested	Not tested
40940	HMS02188	CG33261,CG42507	Tri,CG42507	pVALIUM20	Fertile	Not tested	Not tested
43962	GL01314	CG10798	dm	pVALIUM22	Fertile	Not tested	Not tested
36126	HMS01541	CG6376	E2f	pVALIUM20	Fertile	Not tested	Not tested
33669	HMS00082	CG18412	ph-p	pVALIUM20	Fertile	Not tested	Not tested
35207	GL00083	CG18412	ph-p	pVALIUM22	Fertile	Not tested	Not tested
36720	HMS01610	CG1772	dap	pVALIUM20	Fertile	Not tested	Not tested
32890	HMS00678	CG10414	Atac2	pVALIUM20	Sterile, class 1	N/A	N/A
36624	GL00584	CG10726	barr	pVALIUM22	Sterile, class 1	N/A	N/A
35185	GL00057	CG9748	bel	pVALIUM22	Sterile, class 1	N/A	N/A
36067	GL00485	CG10480	Bj1	pVALIUM22	Sterile, class 1	N/A	N/A
33421	HMS00304	CG31132	BRWD3	pVALIUM20	Sterile, class 1	N/A	N/A
32989	HMS00789	CG7581	Bub3	pVALIUM20	Sterile, class 1	N/A	N/A
35199	GL00073	CG3319	Cdk7	pVALIUM22	Sterile, class 1	N/A	N/A
34857	HMS00175	CG10333	CG10333	pVALIUM20	Sterile, class 1	N/A	N/A
43205	GL01550	CG10565	CG10565	pVALIUM22	Sterile, class 1	N/A	N/A
42810	GL01184	CG3430	CG3430	pVALIUM22	Sterile, class 1	N/A	N/A
35020	HMS01433	CG5033	CG5033	pVALIUM20	Sterile, class 1	N/A	N/A
43254	GLC01443	CG5290	CG5290	pVALIUM22	Sterile, class 1	N/A	N/A
32334	HMS00325	CG5589	CG5589	pVALIUM20	Sterile, class 1	N/A	N/A
43206	GL01551	CG5800	CG5800	pVALIUM22	Sterile, class 1	N/A	N/A
34565	HMS01037	CG6015	CG6015	pVALIUM20	Sterile, class 1	N/A	N/A
34804	HMS00113	CG7185	CG7185	pVALIUM20	Sterile, class 1	N/A	N/A
36609	GL00589	CG8142	CG8142	pVALIUM22	Sterile, class 1	N/A	N/A
36589	GL00549	CG9253	CG9253	pVALIUM22	Sterile, class 1	N/A	N/A
41679	HMS02243	CG9422	CG9422	pVALIUM20	Sterile, class 1	N/A	N/A
34564	HMS01036	CG5602	DNA-lig1	pVALIUM20	Sterile, class 1	N/A	N/A
34827	HMS00142	CG9696	dom	pVALIUM20	Sterile, class 1	N/A	N/A
35149	GL00017	CG1828	dre4	pVALIUM22	Sterile, class 1	N/A	N/A
35271	GL00169	CG7776	E(Pc)	pVALIUM22	Sterile, class 1	N/A	N/A
32345	HMS00336	CG6474	e(y)1	pVALIUM20	Sterile, class 1	N/A	N/A
35764	HMS01512	CG8648	Fen1	pVALIUM20	Sterile, class 1	N/A	N/A
41716	HMS02281	CG5148	cal1	pVALIUM20	Sterile, class 1	N/A	N/A
33666	HMS00076	CG7269	Hel25E	pVALIUM20	Sterile, class 1	N/A	N/A
41988	HMS02387	CG33882,CG33880,CG33876,C	His2B	pVALIUM20	Sterile, class 1	N/A	N/A
35299	GL00202	CG6620	ial	pVALIUM22	Sterile, class 1	N/A	N/A
34552	HMS01024	CG10850	ida	pVALIUM20	Sterile, class 1	N/A	N/A
35366	GL00279	CG12165	Incnp	pVALIUM22	Sterile, class 1	N/A	N/A
41916	HMS02313	CG6189	l(1)1Bi	pVALIUM20	Sterile, class 1	N/A	N/A
43981	GL01591	CG10563	l(2)37Cd	pVALIUM22	Sterile, class 1	N/A	N/A
33002	GLC01635	CG8426	l(2)NC136	pVALIUM22	Sterile, class 1	N/A	N/A
34024	HMS02950	CG5931	l(3)72Ab	pVALIUM20	Sterile, class 1	N/A	N/A
34575	HMS01049	CG12031	MED14	pVALIUM20	Sterile, class 1	N/A	N/A
34664	HMS01141	CG7957	MED17	pVALIUM20	Sterile, class 1	N/A	N/A
34731	HMS01211	CG17397	MED21	pVALIUM20	Sterile, class 1	N/A	N/A
33743	HMS01081	CG9473	MED6	pVALIUM20	Sterile, class 1	N/A	N/A
34926	HMS01275	CG13867	MED8	pVALIUM20	Sterile, class 1	N/A	N/A
35398	GL00318	CG8103	Mi-2	pVALIUM22	Sterile, class 1	N/A	N/A
35150	GL00018	CG13778	Mnn1	pVALIUM22	Sterile, class 1	N/A	N/A
34990	HMS01400	CG12202	Nat1	pVALIUM20	Sterile, class 1	N/A	N/A
37482	GL00625	CG9938	Ndc80	pVALIUM22	Sterile, class 1	N/A	N/A
33694	HMS00564	CG7421	Nopp140	pVALIUM20	Sterile, class 1	N/A	N/A
32836	HMS00526	CG34407	Not1	pVALIUM20	Sterile, class 1	N/A	N/A
34710	HMS01189	CG4579	Nup154	pVALIUM20	Sterile, class 1	N/A	N/A
33897	HMS00837	CG3820	Nup214	pVALIUM20	Sterile, class 1	N/A	N/A
33003	HMS00803	CG11856	Nup358	pVALIUM20	Sterile, class 1	N/A	N/A
35695	GLV21060	CG6251	Nup62	pVALIUM21	Sterile, class 1	N/A	N/A
32409	GLC01628	CG2917	Orc4	pVALIUM22	Sterile, class 1	N/A	N/A
32838	HMS00528	CG8241	pea	pVALIUM20	Sterile, class 1	N/A	N/A
41997	HMS02398	CG7769	pic	pVALIUM20	Sterile, class 1	N/A	N/A
43984	GLC01465	CG6375	pit	pVALIUM22	Sterile, class 1	N/A	N/A
32865	HMS00652	CG5519	Prp19	pVALIUM20	Sterile, class 1	N/A	N/A
41912	HMS02306	CG4320	raptor	pVALIUM20	Sterile, class 1	N/A	N/A

32415	HMS00410	CG9750	rept	pVALIUM20	Sterile, class 1	N/A	N/A
41861	GL01291	CG11979	Rpb5	pVALIUM22	Sterile, class 1	N/A	N/A
36830	GL01068	CG1554	RplI215	pVALIUM22	Sterile, class 1	N/A	N/A
34567	HMS01040	CG7885	RplI33	pVALIUM20	Sterile, class 1	N/A	N/A
32363	HMS00354	CG2173	Rs1	pVALIUM20	Sterile, class 1	N/A	N/A
38531	HMS01744	CG9198	shtd	pVALIUM20	Sterile, class 1	N/A	N/A
35602	GL00440	CG10212	SMC2	pVALIUM22	Sterile, class 1	N/A	N/A
38371	HMS01840	CG13570	spag	pVALIUM20	Sterile, class 1	N/A	N/A
33914	HMS00857	CG9809	Spargel	pVALIUM20	Sterile, class 1	N/A	N/A
35466	GL00392	CG11451	Spc105R	pVALIUM22	Sterile, class 1	N/A	N/A
32896	HMS00685	CG12372	spt4	pVALIUM20	Sterile, class 1	N/A	N/A
34837	HMS00153	CG7626	Spt5	pVALIUM20	Sterile, class 1	N/A	N/A
32373	HMS00364	CG12225	Spt6	pVALIUM20	Sterile, class 1	N/A	N/A
38948	HMS01862	CG6238	ssh	pVALIUM20	Sterile, class 1	N/A	N/A
41648	GL01230	CG8592	stil	pVALIUM22	Sterile, class 1	N/A	N/A
35415	GL00337	CG3836	stwl	pVALIUM22	Sterile, class 1	N/A	N/A
38255	HMS01699	CG12864	Su(var)2-HP2	pVALIUM20	Sterile, class 1	N/A	N/A
35314	GL00219	CG17603	TafI	pVALIUM22	Sterile, class 1	N/A	N/A
35367	GL00280	CG7704	Taf5	pVALIUM22	Sterile, class 1	N/A	N/A
35428	GL00352	CG10281	TflIFalpha	pVALIUM22	Sterile, class 1	N/A	N/A
35462	GL00388	CG3278	Tif-IA	pVALIUM22	Sterile, class 1	N/A	N/A
36307	GL00491	CG1782	Uba1	pVALIUM22	Sterile, class 1	N/A	N/A
35806	GL00452	CG7528	Uba2	pVALIUM22	Sterile, class 1	N/A	N/A
42642	HMS02478	CG7989	wcd	pVALIUM20	Sterile, class 1	N/A	N/A
32952	HMS00746	CG17437	wds	pVALIUM20	Sterile, class 1	N/A	N/A
38297	HMS01758	CG7670	WRNexo	pVALIUM20	Sterile, class 1	N/A	N/A
36123	HMS01538	CG10798	dm	pVALIUM20	Sterile, class 1	N/A	N/A
51454	HMC03189	CG10798	dm	pVALIUM20	Sterile, class 1	N/A	N/A
34069	HMS00051	CG4236	Caf1	pVALIUM20	Sterile, class 1	N/A	N/A
35139	GL00006	CG2252	fs(1)h	pVALIUM22	Sterile, class 1	N/A	N/A
52111	HMC03356	CG4039	Mcm6	pVALIUM20	Sterile, class 1	N/A	N/A
41842	GL01270	CG4039	Mcm6	pVALIUM22	Sterile, class 1	N/A	N/A
36092	GL00511	CG3938	CycE	pVALIUM22	Sterile, class 1	N/A	N/A
38902	GL00673	CG3938	CycE	pVALIUM22	Sterile, class 1	N/A	N/A
41693	HMS02257	CG2252	fs(1)h	pVALIUM20	Sterile, class 1	N/A	N/A
41943	HMS02340	CG2252	fs(1)h	pVALIUM20	Sterile, class 1	N/A	N/A
44009	HMS02723	CG2252	fs(1)h	pVALIUM20	Sterile, class 1	N/A	N/A
35388	GL00307	CG6677	ash2	pVALIUM22	Sterile, class 2	N/A	Not tested
34390	HMS01384	CG13192	CG13192	pVALIUM20	Sterile, class 2	N/A	Not tested
33704	HMS00581	CG40351	Set1	pVALIUM20	Sterile, class 2	N/A	Not tested
35460	GL00386	CG2161	Rga	pVALIUM22	Sterile, class 2	N/A	Not tested
32473	HMS00473	CG16975	Sfmbt	pVALIUM20	Sterile, class 2	N/A	Not tested
35454	GL00379	CG4735	shu	pVALIUM22	Sterile, class 2	N/A	Not tested
35303	GL00206	CG3158	spn-E	pVALIUM22	Sterile, class 2	N/A	Not tested
35592	GL00429	CG42373,CG31917	Tfb5,CG31917	pVALIUM22	Sterile, class 2	N/A	Not tested
32926	HMS00718	CG17293	Wdr82	pVALIUM20	Sterile, class 2	N/A	Not tested
35240	GL00126	CG3733	Chd1	pVALIUM22	Sterile, class 2	N/A	Not tested
36068	GL00486	CG6502	E(z)	pVALIUM22	Sterile, class 2	N/A	Not tested
35323	GL00230	CG5179	Cdk9	pVALIUM22	Sterile, class 2	N/A	Not tested
35201	GL00076	CG6137	aub	pVALIUM22	Sterile, class 3	N/A	Not tested
35443	GL00368	CG10542	Bre1	pVALIUM22	Sterile, class 3	N/A	Not tested
36783	GL00518	CG9802	Cap	pVALIUM22	Sterile, class 3	N/A	Not tested
35324	GL00231	CG10572	Cdk8	pVALIUM22	Sterile, class 3	N/A	Not tested
36899	GL01093	CG14222	CG14222	pVALIUM22	Sterile, class 3	N/A	Not tested
36916	HMS01019	CG3848	trr	pVALIUM20	Sterile, class 3	N/A	Not tested
32517	HMS00522	CG4184	MED15	pVALIUM20	Sterile, class 3	N/A	Not tested
32995	HMS00795	CG32491	mod(mdg4)	pVALIUM20	Sterile, class 3	N/A	Not tested
35630	GL00477	CG18740	mor	pVALIUM22	Sterile, class 3	N/A	Not tested
38190	GL00629	CG12047	mud	pVALIUM22	Sterile, class 3	N/A	Not tested
34580	HMS01054	CG2158	Nup50	pVALIUM20	Sterile, class 3	N/A	Not tested
43215	GL01560	CG3041	Orc2	pVALIUM22	Sterile, class 3	N/A	Not tested
42803	GL01176	CG9183	plu	pVALIUM22	Sterile, class 3	N/A	Not tested
42482	GL01341	CG1404	ran	pVALIUM22	Sterile, class 3	N/A	Not tested
35171	GL00041	CG10683	rhi	pVALIUM22	Sterile, class 3	N/A	Not tested
36794	GL00534	CG3423	SA	pVALIUM22	Sterile, class 3	N/A	Not tested
32372	HMS00363	CG1064	Snr1	pVALIUM20	Sterile, class 3	N/A	Not tested
36095	GL00514	CG13109	tai	pVALIUM22	Sterile, class 3	N/A	Not tested
36786	GL00522	CG17436	vtd	pVALIUM22	Sterile, class 3	N/A	Not tested
43141	GL01482	CG15737	wisp	pVALIUM22	Sterile, class 3	N/A	Not tested
32845	HMS00628	CG8625	lswi	pVALIUM20	Sterile, class 3	N/A	Not tested
33907	HMS00849	CG32491	mod(mdg4)	pVALIUM20	Sterile, class 3	N/A	Not tested
33395	HMS00272	CG3423	SA	pVALIUM20	Sterile, class 3	N/A	Not tested
33659	HMS00066	CG6502	E(z)	pVALIUM20	Sterile, class 3	N/A	Not tested
33654	HMS00060	CG3938	CycE	pVALIUM20	Sterile, class 3	N/A	No tested
33739	HMS01075	CG5451	Smu1	pVALIUM20	Sterile, class 4	Yes	WT
32889	HMS00677	CG7583	CtBP	pVALIUM20	Sterile, class 4	Yes	WT
35242	GL00129	CG7055	dalao	pVALIUM22	Sterile, class 4	Yes	WT
43185	GL01529	CG2207	Df31	pVALIUM22	Sterile, class 4	Yes	WT
35488	GL00417	CG15433	Elp3	pVALIUM22	Sterile, class 4	Yes	WT
33706	HMS00583	CG1716	Set2	pVALIUM20	Sterile, class 4	Yes	WT
35399	GL00319	CG42245,CG1244	CG42245.MEP-1	pVALIUM22	Sterile, class 4	Yes	WT
35759	HMS01506	CG8384	gro	pVALIUM20	Sterile, class 4	Yes	WT
34778	HMS00087	CG2128	Hdac3	pVALIUM20	Sterile, class 4	Yes	WT
35238	GL00123	CG11990	hyx	pVALIUM22	Sterile, class 4	Yes	WT
36597	GL00557	CG3696	kis	pVALIUM22	Sterile, class 4	Yes	WT
34980	HMS01389	CG2684	lds	pVALIUM20	Sterile, class 4	Yes	WT
36652	GL00612	CG9088	lid	pVALIUM22	Sterile, class 4	No	dhd-like
35152	GL00020	CG10895	lok	pVALIUM22	Sterile, class 4	Yes	WT
36829	GL01067	CG1793	MED26	pVALIUM22	Sterile, class 4	Yes	WT
39028	HMS01947	CG16928	mre11	pVALIUM20	Sterile, class 4	Yes	WT
36614	GL00574	CG17704	Nipped-B	pVALIUM22	Sterile, class 4	Yes	WT
33985	HMS00945	CG4118	nxft2	pVALIUM20	Sterile, class 4	Yes	WT
37483	GL00626	CG6122	piwi	pVALIUM22	Sterile, class 4	Yes	WT
35419	GL00342	CG2368	psq	pVALIUM22	Sterile, class 4	Yes	WT

36632	GL00592	CG12352	san	pVALIUM22	Sterile, class 4	Yes	WT
35389	GL00308	CG9495	Scm	pVALIUM22	Sterile, class 4	Yes	WT
32368	HMS00359	CG8815	Sin3A	pVALIUM20	Sterile, class 4	No	dhd-like
40881	HMS02049	CG4413	trem	pVALIUM20	Sterile, class 4	Yes	WT
36835	GL01076	CG18009	Trf2	pVALIUM22	Sterile, class 4	Yes	WT
35706	GLV21071	CG9088	lid	pVALIUM21	Sterile, class 4	No	dhd-like
33725	HMS00607	CG7471	Rpd3	pVALIUM20	Sterile, class 4	No	dhd-like
Control	GL00257	CG12153	Hira	pVALIUM22	Sterile, class 4	No	ssm-like
Control	MTD>attP2				Fertile	Yes	WT
Control	w [1118]				Fertile	Yes	WT
					<b>Female fertility</b>	<b>GFP::Cid expression</b>	<b>Sperm nuclear phenotype</b>

S2 Table - Differentially expressed genes in *lid* KD and *Sin3A* KD ovaries

		<i>lid</i> KD					<i>Sin3A</i> KD		
gene ID	Flybase record	log2FC	pvalue	fcdr	gene ID	Flybase record	log2FC	pvalue	fcdr
F8gn0031759	<a href="#">lid</a>	-3.0712584	1.19E-143	1.09E-139	F8gn0034999	<a href="#">CG3394</a>	-4.2202683	1.06E-124	4.49E-121
F8gn0036330	<a href="#">CG11263</a>	-4.0238806	8.08E-126	2.47E-122	F8gn0051262	<a href="#">CG31262</a>	-3.585744	5.36E-112	1.51E-108
F8gn0265767	<a href="#">zyl</a>	-2.3911626	2.14E-101	2.80E-98	F8gn0020415	<a href="#">ldgl2</a>	-2.4924243	6.00E-93	1.27E-89
F8gn0036332	<a href="#">CG11261</a>	-2.289144	6.93E-66	5.77E-63	F8gn0030666	<a href="#">CG12708</a>	-4.091286	1.57E-92	2.65E-89
F8gn0029942	<a href="#">CG2059</a>	-2.1961104	5.04E-61	3.85E-58	F8gn0038734	<a href="#">CG11453</a>	-3.9323184	2.36E-82	3.32E-79
F8gn0031741	<a href="#">CG11034</a>	-3.0166023	2.50E-59	1.76E-56	F8gn0036205	<a href="#">CG14131</a>	-3.1718177	1.08E-75	1.30E-72
F8gn0039006	<a href="#">Cyp64A</a>	-2.4571248	1.69E-54	1.11E-51	F8gn0042174	<a href="#">CR1885A</a>	-1.7444457	2.48E-64	2.61E-61
F8gn0011761	<a href="#">dhd</a>	-3.1639711	2.36E-50	1.35E-47	F8gn0017448	<a href="#">CG2187</a>	-2.7282585	6.16E-60	5.77E-57
F8gn0028487	<a href="#">F-cup</a>	-1.7169553	4.48E-50	2.42E-47	F8gn0263093	<a href="#">CR43361</a>	-2.8379209	4.08E-57	3.44E-54
F8gn0030373	<a href="#">CG12721</a>	-2.759553	1.23E-48	6.24E-46	F8gn0027843	<a href="#">CAH2</a>	-1.9318723	2.16E-53	1.66E-50
F8gn0030189	<a href="#">CG2909</a>	-2.3738814	2.85E-46	1.24E-43	F8gn0032084	<a href="#">CG13101</a>	-2.7702721	1.67E-52	1.17E-49
F8gn0051217	<a href="#">modSP</a>	-2.7201402	4.00E-46	1.67E-43	F8gn0011761	<a href="#">dhd</a>	-3.1714692	1.39E-50	8.99E-48
F8gn0010549	<a href="#">l(2)03659</a>	-2.3208622	5.27E-45	2.10E-42	F8gn0063491	<a href="#">GstE9</a>	-2.1325219	9.01E-47	5.43E-44
F8gn0031157	<a href="#">CG1503</a>	-2.7196155	2.06E-44	7.85E-42	F8gn0264385	<a href="#">CR43837</a>	-1.8051528	5.23E-46	2.94E-43
F8gn0030757	<a href="#">CG9902</a>	-1.9505708	4.17E-43	1.53E-40	F8gn0038098	<a href="#">CG7381</a>	-2.4840253	8.69E-42	4.07E-39
F8gn0037205	<a href="#">BoYb</a>	-1.6205084	1.34E-41	4.72E-39	F8gn0028516	<a href="#">Znf35C</a>	-1.4720133	7.88E-41	3.32E-38
F8gn0030799	<a href="#">CG4872</a>	-2.2114932	1.87E-37	6.33E-35	F8gn0003285	<a href="#">rst</a>	-2.3689615	1.14E-39	4.57E-37
F8gn0032449	<a href="#">CG17036</a>	-1.7420374	1.28E-36	4.18E-34	F8gn0016054	<a href="#">plrf-4</a>	-1.3532928	3.77E-37	1.44E-34
F8gn0034270	<a href="#">PIG-A</a>	-2.0221889	2.63E-36	8.03E-34	F8gn0036824	<a href="#">CG3902</a>	-1.6753711	1.50E-36	5.48E-34
F8gn0030666	<a href="#">CG12708</a>	-2.4559175	3.98E-36	1.18E-33	F8gn0259224	<a href="#">CG42324</a>	-2.4297305	3.97E-35	1.34E-32
F8gn0032084	<a href="#">CG13101</a>	-2.2464821	6.86E-36	1.96E-33	F8gn0034270	<a href="#">PIG-A</a>	-1.9494089	7.37E-34	2.39E-31
F8gn0034179	<a href="#">CG6805</a>	-1.718645	1.81E-34	5.04E-32	F8gn0010039	<a href="#">GstIIb</a>	-1.7549245	1.77E-32	5.54E-30
F8gn0029831	<a href="#">CG5966</a>	-1.6877179	2.77E-34	7.47E-32	F8gn0029866	<a href="#">CG3842</a>	-1.6741608	1.07E-31	3.23E-29
F8gn0038115	<a href="#">CG7966</a>	-1.6351573	2.76E-33	7.22E-31	F8gn0031894	<a href="#">CG4496</a>	-1.9342072	2.22E-30	6.46E-28
F8gn0264676	<a href="#">CR43961</a>	-2.3616771	7.97E-33	2.03E-30	F8gn0265810	<a href="#">CR4959</a>	-1.827715	4.24E-30	1.19E-27
F8gn0039941	<a href="#">CG17167</a>	-2.3378925	3.56E-32	8.82E-30	F8gn0050046	<a href="#">CG30046</a>	-2.3477317	5.95E-29	1.62E-26
F8gn0037617	<a href="#">nom</a>	-1.6497844	4.41E-32	1.06E-29	F8gn0263607	<a href="#">l(3)720p</a>	-1.4039175	2.14E-28	5.64E-26
F8gn0003950	<a href="#">unc</a>	-2.2472133	8.29E-31	1.95E-28	F8gn0034406	<a href="#">Jhed3</a>	-1.4772969	5.73E-28	1.47E-25
F8gn0029710	<a href="#">CG3568</a>	-2.2292889	1.66E-29	3.80E-27	F8gn0000251	<a href="#">cad</a>	-1.3652224	4.24E-27	1.05E-24
F8gn0038734	<a href="#">CG11453</a>	-2.1747893	3.40E-28	7.42E-26	F8gn0260388	<a href="#">CG4514</a>	-1.5594298	9.97E-26	2.40E-23
F8gn0033051	<a href="#">Strica</a>	-1.6975548	6.51E-28	1.39E-25	F8gn0010549	<a href="#">l(2)03659</a>	-1.7120513	1.18E-25	2.76E-23
F8gn0035955	<a href="#">CG5194</a>	-1.5455268	2.56E-27	5.33E-25	F8gn0037203	<a href="#">sbl</a>	-1.0254701	2.49E-25	5.67E-23
F8gn0051075	<a href="#">CG31075</a>	-1.7191968	3.57E-26	7.11E-24	F8gn0025739	<a href="#">pen</a>	-1.5225974	6.70E-25	1.45E-22
F8gn0031814	<a href="#">retm</a>	-1.4618361	1.84E-25	3.45E-23	F8gn0016034	<a href="#">maei</a>	-0.9278028	2.30E-22	4.51E-20
F8gn0030421	<a href="#">CG3812</a>	-1.2307055	2.69E-25	4.93E-23	F8gn0250785	<a href="#">varl</a>	-1.4747975	7.39E-22	1.42E-19
F8gn0040964	<a href="#">CG18661</a>	-1.8630762	3.82E-25	6.73E-23	F8gn0265203	<a href="#">CR44263</a>	-2.032906	1.25E-21	2.34E-19
F8gn0020379	<a href="#">Rfx</a>	-1.1649689	3.12E-23	5.30E-21	F8gn0262524	<a href="#">vex</a>	-1.4075366	1.84E-21	3.38E-19
F8gn0035102	<a href="#">CG7049</a>	-1.3835219	3.70E-23	6.16E-21	F8gn0028369	<a href="#">kirre</a>	-1.8269137	5.43E-20	9.74E-18
F8gn0034706	<a href="#">CG11275</a>	-1.6436042	6.46E-23	1.06E-20	F8gn0029881	<a href="#">pig3</a>	-1.465781	6.39E-20	1.12E-17
F8gn0015714	<a href="#">Cyp6a12</a>	-1.4470292	1.14E-22	1.84E-20	F8gn0022764	<a href="#">Sin3A</a>	-1.1227377	1.72E-19	2.90E-17
F8gn0264745	<a href="#">CR44003</a>	-1.3760264	2.39E-22	3.77E-20	F8gn0015714	<a href="#">Cyp6a12</a>	-1.3288249	2.14E-19	3.53E-17
F8gn0052243	<a href="#">CG32243</a>	-1.7389495	7.42E-22	1.11E-19	F8gn0032891	<a href="#">Osep3</a>	-1.272665	6.30E-19	1.02E-16
F8gn0261859	<a href="#">CG42788</a>	-1.0677649	3.11E-21	4.60E-19	F8gn0033232	<a href="#">CG12159</a>	-0.8479804	1.22E-18	1.94E-16
F8gn0036324	<a href="#">CG12520</a>	-1.8023267	1.57E-20	2.25E-18	F8gn0034706	<a href="#">CG11275</a>	-1.4584788	1.85E-18	2.89E-16
F8gn0038296	<a href="#">CG6752</a>	-1.4303478	4.08E-19	5.58E-17	F8gn0063923	<a href="#">Kaz1-ORF.B</a>	-1.7465855	2.41E-16	3.50E-14
F8gn0028746	<a href="#">CG18508</a>	-1.2806776	4.03E-19	5.58E-17	F8gn0035517	<a href="#">CG1205</a>	-1.0430897	7.24E-16	1.02E-13
F8gn0047199	<a href="#">CG31517</a>	-1.4214417	4.55E-19	6.14E-17	F8gn0036821	<a href="#">CG3961</a>	-1.4377702	8.61E-16	1.19E-13
F8gn0023094	<a href="#">eye</a>	-1.4563032	4.75E-19	6.31E-17	F8gn0040396	<a href="#">CrebA</a>	-1.3364748	5.14E-15	6.88E-13
F8gn0032820	<a href="#">lho</a>	-1.4464475	1.14E-18	1.50E-16	F8gn0033978	<a href="#">Cyp6a23</a>	-1.141044	7.33E-15	9.65E-13
F8gn0038190	<a href="#">CG9926</a>	-1.3835824	1.75E-18	2.26E-16	F8gn0085212	<a href="#">CG34183</a>	-1.0941979	9.69E-15	1.24E-12
F8gn0035151	<a href="#">CG17129</a>	-1.1841525	1.99E-18	2.53E-16	F8gn0028523	<a href="#">CG5888</a>	-1.4984311	1.42E-14	1.79E-12
F8gn0260902	<a href="#">cuff</a>	-1.3874404	2.38E-18	2.98E-16	F8gn0013995	<a href="#">Calk</a>	-0.7936823	3.03E-14	3.76E-12
F8gn0050440	<a href="#">CG30440</a>	-1.0217497	4.41E-18	5.39E-16	F8gn0034262	<a href="#">swi2</a>	-1.4987164	3.95E-14	4.82E-12
F8gn0032382	<a href="#">Mal-B2</a>	-1.0646868	4.70E-18	5.66E-16	F8gn0036369	<a href="#">CG10089</a>	-1.2616404	6.11E-14	7.36E-12
F8gn0031313	<a href="#">CG5080</a>	-1.7721223	5.47E-18	6.51E-16	F8gn0010225	<a href="#">Gcl</a>	-0.9302227	9.01E-14	1.07E-11
F8gn0037838	<a href="#">CG4089</a>	-1.1250484	1.95E-17	2.29E-15	F8gn0263492	<a href="#">CR43481</a>	-1.3214228	1.01E-13	1.19E-11
F8gn0037921	<a href="#">CG6808</a>	-1.226594	1.99E-17	2.30E-15	F8gn0260435	<a href="#">CR42530</a>	-1.5741372	1.16E-13	1.35E-11
F8gn0038815	<a href="#">CG5466</a>	-0.9670653	2.51E-17	2.88E-15	F8gn0034126	<a href="#">jhb</a>	-1.2521974	1.26E-13	1.44E-11
F8gn0085245	<a href="#">CG34216</a>	-1.2301847	1.39E-16	1.57E-14	F8gn0036765	<a href="#">CG7408</a>	-1.4021843	1.42E-13	1.60E-11
F8gn0032343	<a href="#">CG6201</a>	-1.0192506	4.46E-16	4.92E-14	F8gn0033979	<a href="#">Cyp6a19</a>	-0.8188227	3.12E-13	3.46E-11
F8gn0001224	<a href="#">Hsp23</a>	-1.4714794	5.23E-16	5.70E-14	F8gn0034322	<a href="#">CG18536</a>	-1.4809179	3.86E-13	4.23E-11
F8gn0022202	<a href="#">Chi2</a>	-1.4310409	7.08E-16	7.63E-14	F8gn0035084	<a href="#">CG15861</a>	-1.1101584	6.72E-13	7.26E-11
F8gn0261393	<a href="#">alpha-Es15</a>	-1.3211846	1.68E-15	1.77E-13	F8gn0034729	<a href="#">CG10344</a>	-0.8888346	1.75E-12	1.86E-10
F8gn0011770	<a href="#">Glp</a>	-0.9263151	2.95E-15	3.07E-13	F8gn0025628	<a href="#">CG4199</a>	-0.9498517	1.92E-12	2.02E-10
F8gn0035641	<a href="#">CG5568</a>	-0.988897	9.04E-15	9.10E-13	F8gn0036620	<a href="#">CG4842</a>	-1.3062619	2.41E-12	2.51E-10
F8gn0037583	<a href="#">CG9684</a>	-1.0702856	1.24E-14	1.23E-12	F8gn0050440	<a href="#">CG30440</a>	-0.8206139	3.28E-12	3.38E-10
F8gn0033917	<a href="#">SmydA-1</a>	-0.943787	1.57E-14	1.53E-12	F8gn0030968	<a href="#">CG7322</a>	-1.1011257	5.10E-12	5.12E-10
F8gn0029137	<a href="#">Palsas</a>	-1.5041647	1.94E-14	1.88E-12	F8gn0003353	<a href="#">sei</a>	-0.8772684	5.09E-12	5.12E-10
F8gn0034262	<a href="#">swi2</a>	-1.509625	2.73E-14	2.55E-12	F8gn0029723	<a href="#">Pnc-R</a>	-1.0504156	1.19E-11	1.17E-09
F8gn0000346	<a href="#">cnrmf</a>	-1.3234813	3.14E-14	2.91E-12	F8gn0031182	<a href="#">CypR1</a>	-1.0634995	1.31E-11	1.27E-09
F8gn0029866	<a href="#">CG3842</a>	-1.076243	3.26E-14	2.99E-12	F8gn0024194	<a href="#">rasp</a>	-0.7121256	1.39E-11	1.33E-09
F8gn0036843	<a href="#">Slsn2</a>	-0.9270425	5.61E-14	5.09E-12	F8gn0037664	<a href="#">CG6420</a>	-0.9313398	2.16E-11	2.02E-09
F8gn0051320	<a href="#">HicA1R2</a>	-1.1200264	9.20E-14	8.26E-12	F8gn0262987	<a href="#">CG43295</a>	-1.0673364	5.73E-11	5.20E-09
F8gn0029753	<a href="#">CG4198</a>	-1.5619893	1.28E-13	1.13E-11	F8gn0026263	<a href="#">bip1</a>	-0.8522921	6.42E-11	5.70E-09
F8gn0027865	<a href="#">Tsc6B</a>	-0.9262642	2.08E-13	1.76E-11	F8gn0030598	<a href="#">CG9503</a>	-1.0489086	8.19E-11	7.19E-09
F8gn0025739	<a href="#">pen</a>	-1.0767554	2.19E-13	1.84E-11	F8gn0033079	<a href="#">Fmo-2</a>	-1.3682329	1.11E-10	9.66E-09
F8gn0037186	<a href="#">CG11241</a>	-1.390111	2.65E-13	2.21E-11	F8gn0039099	<a href="#">Gll1T2</a>	-0.7327631	4.47E-10	3.85E-08
F8gn0040402	<a href="#">Roc2</a>	-0.9693241	3.79E-13	3.13E-11	F8gn0029114	<a href="#">Tdllo</a>	-1.1827078	4.82E-10	4.10E-08
F8gn0003210	<a href="#">rlb</a>	-0.7951324	4.49E-13	3.67E-11	F8gn0029603	<a href="#">CG14053</a>	-1.2936781	6.45E-10	5.38E-08
F8gn0051373	<a href="#">CG31373</a>	-1.1418253	5.61E-13	4.51E-11	F8gn0034351	<a href="#">rs-wl</a>	-0.6549448	8.01E-10	6.55E-08
F8gn0014342	<a href="#">mia</a>	-1.4117988	1.53E-12	1.20E-10	F8gn0250907	<a href="#">Chi10</a>	-1.2916825	9.00E-10	7.30E-08
F8gn0010194	<a href="#">Wnt5</a>	-0.9969608	1.95E-12	1.51E-10	F8gn0038099	<a href="#">CG7091</a>	-0.5724301	1.01E-09	8.15E-08
F8gn0050046	<a href="#">CG30046</a>	-1.4641854	2.18E-12	1.68E-10	F8gn0031435	<a href="#">Elba2</a>	-0.8698732	1.04E-09	8.30E-08
F8gn0037696	<a href="#">GstZ1</a>	-1.1641738	2.95E-12	2.25E-10	F8gn0032034	<a href="#">Roi4</a>	-0.8422531	1.71E-09	1.33E-07
F8gn0036901	<a href="#">CG772</a>	-1.1433254	4.51E-12	3.42E-10	F8gn0031741	<a href="#">CG11034</a>	-1.0844981	2.10E-09	1.62E-07
F8gn0030883	<a href="#">CG772</a>	-1.1675829	4.84E-12	3.63E-10	F8gn				

FBgn0029881	<a href="#">pigs</a>	-1.0651714	2.06E-11	1.45E-09	FBgn0033233	<a href="#">KlnrMA</a>	-0.6829652	1.01E-06	7.14E-07
FBgn0052641	<a href="#">CG32641</a>	-1.2247928	2.38E-11	1.67E-09	FBgn0030187	<a href="#">lpnd</a>	-1.2043668	1.53E-08	1.06E-06
FBgn0260874	<a href="#">Jr76a</a>	-1.0911372	2.74E-11	1.90E-09	FBgn0031948	<a href="#">CG17149</a>	-1.0429932	1.63E-08	1.12E-06
FBgn0050414	<a href="#">CG30414</a>	-1.2153351	3.13E-11	2.14E-09	FBgn0031645	<a href="#">CG30336</a>	-0.8406185	2.05E-08	1.38E-06
FBgn001987	<a href="#">Gli</a>	-0.9659603	3.59E-11	2.44E-09	FBgn0034046	<a href="#">tan</a>	-0.55626	2.04E-08	1.38E-06
FBgn0035833	<a href="#">CG7565</a>	-0.8088702	4.12E-11	2.78E-09	FBgn002736	<a href="#">mago</a>	-0.5731716	2.58E-08	1.70E-06
FBgn0033257	<a href="#">sard</a>	-1.3823352	5.66E-11	3.79E-09	FBgn0039914	<a href="#">max</a>	-0.7934145	2.68E-08	1.75E-06
FBgn0034117	<a href="#">CG7997</a>	-0.763632	5.86E-11	3.89E-09	FBgn0039251	<a href="#">Irf4-2</a>	-0.7011303	2.87E-08	1.86E-06
FBgn0033903	<a href="#">CG8323</a>	-1.1131696	7.96E-11	5.21E-09	FBgn0058006	<a href="#">CG40006</a>	-0.7958262	3.01E-08	1.94E-06
FBgn0036764	<a href="#">CG5535</a>	-0.7545567	8.88E-11	5.77E-09	FBgn0031434	<a href="#">inv</a>	-0.6828101	5.73E-08	3.64E-06
FBgn0266619	<a href="#">Q45126</a>	-1.2911846	1.32E-10	8.52E-09	FBgn0261016	<a href="#">clou</a>	-0.8133906	7.24E-08	4.56E-06
FBgn0034321	<a href="#">CG14502</a>	-1.3268889	1.64E-10	1.05E-08	FBgn0041629	<a href="#">Hm20</a>	-0.8525238	9.62E-08	6.01E-06
FBgn0037031	<a href="#">CG11456</a>	-0.7363562	2.42E-10	1.53E-08	FBgn0036857	<a href="#">CG9629</a>	-1.0935355	1.27E-07	7.83E-06
FBgn0026315	<a href="#">Ugt35a</a>	-0.8958298	2.86E-10	1.80E-08	FBgn0058298	<a href="#">CG40298</a>	-1.0896436	1.33E-07	8.12E-06
FBgn0037999	<a href="#">CG4860</a>	-0.914685	2.89E-10	1.80E-08	FBgn0051999	<a href="#">CG31999</a>	-1.0118804	1.68E-07	1.02E-05
FBgn0037717	<a href="#">CG8301</a>	-0.7261462	2.98E-10	1.84E-08	FBgn0039094	<a href="#">CG10184</a>	-0.8494729	1.89E-07	1.13E-05
FBgn0026263	<a href="#">hpl1</a>	-0.8163696	3.82E-10	2.35E-08	FBgn0031263	<a href="#">Tspo</a>	-0.8185505	1.95E-07	1.16E-05
FBgn0031961	<a href="#">CG7102</a>	-1.2412474	3.92E-10	2.39E-08	FBgn0262509	<a href="#">rrm</a>	-0.9612758	2.34E-07	1.37E-05
FBgn0031488	<a href="#">CG17265</a>	-1.059634	5.31E-10	3.22E-08	FBgn0037186	<a href="#">CG11241</a>	-0.9780927	2.48E-07	1.44E-05
FBgn0014395	<a href="#">tllb</a>	-1.3194748	5.85E-10	3.53E-08	FBgn0264822	<a href="#">CG44030</a>	-1.0195041	2.95E-07	1.70E-05
FBgn0051119	<a href="#">HDAC11</a>	-1.205338	6.74E-10	4.03E-08	FBgn0069699	<a href="#">CG40498</a>	-1.0623555	3.45E-07	1.97E-05
FBgn0030387	<a href="#">pm</a>	-0.8624825	7.25E-10	4.28E-08	FBgn0040260	<a href="#">Ugt130bc</a>	-0.8753219	4.38E-07	2.45E-05
FBgn0038243	<a href="#">CG8066</a>	-0.8549971	1.04E-09	6.10E-08	FBgn0266319	<a href="#">CG44984</a>	-1.0737286	4.51E-07	2.50E-05
FBgn0037819	<a href="#">CG14688</a>	-0.721363	1.05E-09	6.16E-08	FBgn0058803	<a href="#">CG5191</a>	-0.6495903	4.67E-07	2.58E-05
FBgn0015558	<a href="#">tly</a>	-1.2965917	1.14E-09	6.60E-08	FBgn0040823	<a href="#">dwp6</a>	-0.70335	6.86E-07	3.73E-05
FBgn0035904	<a href="#">GstO3</a>	-1.1528477	1.30E-09	7.47E-08	FBgn0035999	<a href="#">CG3552</a>	-0.6534192	7.51E-07	4.06E-05
FBgn0037960	<a href="#">mth5</a>	-1.0338692	1.39E-09	7.97E-08	FBgn0037578	<a href="#">CG9601</a>	-0.6525109	8.02E-07	4.31E-05
FBgn0031419	<a href="#">CG15390</a>	-0.8367551	1.50E-09	8.51E-08	FBgn0036294	<a href="#">CG10654</a>	-0.73282	8.44E-07	4.51E-05
FBgn0040551	<a href="#">CG11686</a>	-1.0442442	1.64E-09	9.30E-08	FBgn0032645	<a href="#">CG15142</a>	-0.9543489	1.07E-06	5.68E-05
FBgn0264561	<a href="#">Glg1</a>	-0.6445743	1.78E-09	9.99E-08	FBgn0261794	<a href="#">loc</a>	-0.5784062	1.12E-06	5.89E-05
FBgn0036205	<a href="#">CG14131</a>	-1.0276741	1.85E-09	1.04E-07	FBgn0050005	<a href="#">GstT2</a>	-0.655386	1.33E-06	6.85E-05
FBgn0029588	<a href="#">CG14798</a>	-1.0967802	2.18E-09	1.21E-07	FBgn000246	<a href="#">g[3]G</a>	-0.5895323	1.3619E-06	6.9605E-05
FBgn0030968	<a href="#">CG7322</a>	-0.949729	2.50E-09	1.38E-07	FBgn0031117	<a href="#">GstT3</a>	-0.6273411	1.65E-06	8.3189E-05
FBgn0030347	<a href="#">CG15739</a>	-1.2401826	2.76E-09	1.51E-07	FBgn0031031	<a href="#">CG14218</a>	-0.9280998	1.73E-06	8.63E-05
FBgn0030357	<a href="#">Scjn</a>	-1.0122455	3.06E-09	1.67E-07	FBgn0035151	<a href="#">CG17129</a>	-0.6414527	1.91E-06	9.48E-05
FBgn0034322	<a href="#">CG18536</a>	-1.2110539	3.50E-09	1.90E-07	FBgn0039938	<a href="#">Snx102F</a>	-0.8740615	2.3254E-06	0.0001401
FBgn0030187	<a href="#">lpnd</a>	-1.2385667	5.95E-09	3.15E-07	FBgn0020908	<a href="#">Snpl</a>	-0.9771089	2.64E-06	1.28E-04
FBgn0030745	<a href="#">CG4239</a>	-0.8448908	6.13E-09	3.23E-07	FBgn0026593	<a href="#">CG5707</a>	-0.8438915	2.65E-06	1.28E-04
FBgn0039525	<a href="#">CG5646</a>	-1.2155351	7.04E-09	3.69E-07	FBgn0038331	<a href="#">Qm3</a>	-0.5150585	2.67E-06	1.29E-04
FBgn0037092	<a href="#">M6</a>	-0.963899	7.52E-09	3.90E-07	FBgn0035186	<a href="#">GstT1</a>	-0.987372	3.11E-06	1.47E-04
FBgn0002778	<a href="#">mnd</a>	-0.806747	9.72E-09	5.00E-07	FBgn0050000	<a href="#">GstT1</a>	-0.523767	3.10E-06	1.47E-04
FBgn0031530	<a href="#">pgant2</a>	-1.1444054	9.96E-09	5.10E-07	FBgn003249	<a href="#">TBC1D16</a>	-0.7023452	3.35E-06	1.56E-04
FBgn0264494	<a href="#">CG17646</a>	-0.9205579	1.05E-08	5.33E-07	FBgn0031814	<a href="#">rlm</a>	-0.64624	3.35E-06	1.56E-04
FBgn0034371	<a href="#">SP2637</a>	-0.6113293	1.33E-08	6.72E-07	FBgn0265362	<a href="#">CG44303</a>	-0.8715818	3.66E-06	1.69E-04
FBgn0030457	<a href="#">CG12096</a>	-0.894159	1.59E-08	7.98E-07	FBgn001987	<a href="#">Gli</a>	-0.6662484	4.66E-06	2.14E-04
FBgn0035356	<a href="#">CG16986</a>	-0.9019828	1.61E-08	8.03E-07	FBgn0063492	<a href="#">GstF8</a>	-0.727191	4.75E-06	2.17E-04
FBgn0031031	<a href="#">CG14218</a>	-1.0942315	1.62E-08	8.04E-07	FBgn0266982	<a href="#">Q45433</a>	-0.9637767	5.92E-06	2.63E-04
FBgn0036689	<a href="#">CG7730</a>	-0.6978042	1.73E-08	8.50E-07	FBgn0046776	<a href="#">CH14033</a>	-0.7082347	8.32E-06	0.0003589
FBgn0040259	<a href="#">Ugt186Da</a>	-0.6475277	1.88E-08	9.24E-07	FBgn003205	<a href="#">Ras850</a>	-0.4664327	8.34E-06	3.59E-04
FBgn0024179	<a href="#">wit</a>	-0.9130951	2.02E-08	9.85E-07	FBgn0032775	<a href="#">CG17544</a>	-0.7913098	8.46E-06	3.62E-04
FBgn0051262	<a href="#">CG31262</a>	-0.861913	2.33E-08	1.12E-06	FBgn0040262	<a href="#">Ugt30Ba</a>	-0.8297009	1.03E-05	4.34E-04
FBgn0032452	<a href="#">CG15484</a>	-1.0295249	2.48E-08	1.19E-06	FBgn0035082	<a href="#">CG2811</a>	-0.5063722	1.11E-05	4.60E-04
FBgn0264744	<a href="#">CG44002</a>	-0.8415038	2.53E-08	1.21E-06	FBgn0263746	<a href="#">CG46671</a>	-0.9226564	1.17E-05	0.00048167
FBgn0035957	<a href="#">CG5144</a>	-1.0227201	2.87E-08	1.36E-06	FBgn0028400	<a href="#">Syt4</a>	-0.69069	1.18E-05	0.00048695
FBgn0036463	<a href="#">Reck</a>	-1.1572904	3.73E-08	1.76E-06	FBgn0028499	<a href="#">CG7985</a>	-0.7328768	1.43E-05	5.81E-04
FBgn0029648	<a href="#">CG3603</a>	-0.745846	4.08E-08	1.91E-06	FBgn0031032	<a href="#">CG14204</a>	-0.7709141	1.44E-05	5.83E-04
FBgn0052512	<a href="#">CG32512</a>	-0.6016979	4.21E-08	1.96E-06	FBgn0029975	<a href="#">spidy</a>	-0.4900255	1.64E-05	6.57E-04
FBgn0027070	<a href="#">CG17322</a>	-0.7492832	4.28E-08	1.98E-06	FBgn0266096	<a href="#">CG44833</a>	-0.8551666	1.71E-05	0.00067917
FBgn0041182	<a href="#">Tep2</a>	-0.7242566	4.63E-08	2.12E-06	FBgn0038047	<a href="#">CG5245</a>	-0.618797	1.75E-05	6.89E-04
FBgn0039250	<a href="#">Mirk</a>	-0.639282	5.95E-08	2.70E-06	FBgn001224	<a href="#">Hsp23</a>	-0.7763302	1.79E-05	6.97E-04
FBgn0039098	<a href="#">GIL13</a>	-0.7013264	6.00E-08	2.71E-06	FBgn0027865	<a href="#">Tsp96F</a>	-0.5401966	1.79E-05	6.97E-04
FBgn0035167	<a href="#">Gr61a</a>	-1.1497859	6.74E-08	3.03E-06	FBgn0033258	<a href="#">G8t712</a>	-0.4730603	1.81E-05	7.00E-04
FBgn0031245	<a href="#">CG3625</a>	-0.971262	7.57E-08	3.39E-06	FBgn0028743	<a href="#">Dhit</a>	-0.7528332	2.00E-05	7.67E-04
FBgn0033274	<a href="#">CG14757</a>	-1.090869	7.70E-08	3.39E-06	FBgn0032620	<a href="#">CG12288</a>	-0.553131	2.02E-05	7.73E-04
FBgn0037623	<a href="#">CG9801</a>	-0.6974149	7.67E-08	3.39E-06	FBgn0036927	<a href="#">Galat</a>	-0.428105	2.17E-05	8.12E-04
FBgn0031484	<a href="#">CG3165</a>	-0.6795141	7.67E-08	3.39E-06	FBgn0033744	<a href="#">HD44-R2</a>	-0.6829629	2.32E-05	8.62E-04
FBgn0038047	<a href="#">CG5245</a>	-0.7751217	7.74E-08	3.39E-06	FBgn0035243	<a href="#">CG17226</a>	-0.5272733	2.74E-05	9.93E-04
FBgn0031678	<a href="#">CG31918</a>	-0.8319058	7.94E-08	3.47E-06	FBgn0036152	<a href="#">CG6125</a>	-0.4987982	2.74E-05	9.93E-04
FBgn0031968	<a href="#">CG7231</a>	-0.6421679	8.08E-08	3.51E-06	FBgn0263219	<a href="#">Dexam4</a>	4.2657635	1.54E-126	1.30E-122
FBgn0037654	<a href="#">CG11983</a>	-1.0667257	8.28E-08	3.58E-06	FBgn0036670	<a href="#">CG13029</a>	2.83424902	1.19E-44	6.28E-42
FBgn0028504	<a href="#">CG12182</a>	-0.6690131	8.84E-08	3.80E-06	FBgn0034839	<a href="#">CG13540</a>	2.89163461	3.44E-42	1.70E-39
FBgn0036777	<a href="#">CG7341</a>	-0.6764114	1.15E-07	4.92E-06	FBgn0030009	<a href="#">ord</a>	2.82783356	5.85E-41	2.60E-38
FBgn0036333	<a href="#">MICAL-like</a>	-0.6050858	1.27E-07	5.37E-06	FBgn0034838	<a href="#">CG12782</a>	2.6054219	3.33E-35	1.17E-32
FBgn0033174	<a href="#">CG11125</a>	-0.744251	1.54E-07	6.47E-06	FBgn0030716	<a href="#">CG9178</a>	1.50784841	4.94E-25	1.10E-22
FBgn0030749	<a href="#">Arnd11</a>	-0.6167345	1.74E-07	7.25E-06	FBgn0052187	<a href="#">CG32187</a>	2.04105356	7.36E-25	1.55E-22
FBgn0023531	<a href="#">CG32809</a>	-0.8578439	1.77E-07	7.33E-06	FBgn0038012	<a href="#">CG10013</a>	2.0095881	1.55E-24	3.20E-22
FBgn0262987	<a href="#">CG43295</a>	-0.8451577	1.91E-07	7.87E-06	FBgn0267728	<a href="#">otk</a>	2.02130435	1.56E-22	3.12E-20
FBgn0031227	<a href="#">CG3709</a>	-0.766059	2.02E-07	8.31E-06	FBgn0262534	<a href="#">CG43088</a>	1.82971272	1.54E-19	2.65E-17
FBgn0042174	<a href="#">QR18854</a>	-0.5297378	2.27E-07	9.31E-06	FBgn0267967	<a href="#">carula</a>	1.44841679	3.13E-18	4.80E-16
FBgn0010039	<a href="#">Gsd3</a>	-0.7605547	2.48E-07	1.01E-05	FBgn0036196	<a href="#">CG11658</a>	1.20258103	3.60E-17	5.37E-15
FBgn0035570	<a href="#">pst</a>	-0.5961126	2.54E-07	1.03E-05	FBgn0034312	<a href="#">CG10916</a>	1.2776931	3.63E-17	5.37E-15
FBgn0037215	<a href="#">beta-Man</a>	-0.4990579	3.24E-07	1.30E-05	FBgn0032899	<a href="#">CG93338</a>	1.27676094	4.27E-16	6.10E-14
FBgn0037203	<a href="#">slif</a>	-0.5000146	3.72E-07	1.48E-05	FBgn0052364	<a href="#">lut</a>	1.64735177	2.53E-15	3.44E-13
FBgn0038381	<a href="#">Endo11</a>	-0.5336266	3.99E-07	1.57E-05	FBgn0085370	<a href="#">Pkle11</a>	0.79023517	9.19E-15	1.19E-12
FBgn0026570	<a href="#">CG5704</a>	-0.6871541	4.23E-07	1.66E-05	FBgn0014342	<a href="#">mia</a>	1.31881784	6.68E-12	6.63E-10
FBgn0030876	<a href="#">CG6762</a>	-1.0198113	4.43E-07	1.73E-05	FBgn0039941	<a href="#">CG17167</a>	2.29442172	1.58E-11	1.50E-09
FBgn0265362	<a href="#">CG44303</a>	-0.9489117	4.64E-07	1.80E-05	FBgn0085638	<a href="#">CG41378</a>	1.13276183	2.51E-11	2.33E-09

FBgn0260027	<a href="#">CG42495</a>	-0.968787	8.35E-07	3.10E-05	FBgn0283427	<a href="#">FASN1</a>	0.86975756	2.30E-08	1.52E-06
FBgn0030598	<a href="#">CG9903</a>	-0.7904792	8.51E-07	3.14E-05	FBgn0050401	<a href="#">dary</a>	1.11817354	2.28E-08	1.52E-06
FBgn0031998	<a href="#">SLSA11</a>	-0.7290666	9.82E-07	3.615E-05	FBgn0263705	<a href="#">Mho10A</a>	0.98315534	3.45E-08	2.20E-06
FBgn0031589	<a href="#">CG3714</a>	-0.522241	1.01E-06	3.71E-05	FBgn0075676	<a href="#">Cblalpha-3</a>	0.67693092	1.26E-07	7.83E-06
FBgn0033205	<a href="#">CG2064</a>	-0.7867165	1.04E-06	3.79E-05	FBgn0039927	<a href="#">CG11355</a>	0.90203488	1.71E-07	1.03E-05
FBgn0037581	<a href="#">CG7352</a>	-0.8753558	1.08E-06	3.92E-05	FBgn0037623	<a href="#">CG9801</a>	0.6640328	2.35E-07	1.37E-05
FBgn0028468	<a href="#">riet</a>	-0.6723628	1.43E-06	5.16E-05	FBgn0031157	<a href="#">CG1503</a>	0.93002568	3.29E-07	1.88E-05
FBgn0015569	<a href="#">alpha-Est10</a>	-0.8392161	1.44E-06	5.18E-05	FBgn0004895	<a href="#">Fnd1</a>	1.0757224	4.27E-07	2.42E-05
FBgn0031117	<a href="#">GstE3</a>	-0.6298817	1.48E-06	5.2882E-05	FBgn0266710	<a href="#">hng</a>	0.83815038	4.39E-07	2.45E-05
FBgn0265761	<a href="#">CR44568</a>	-0.9108888	1.88E-06	6.72E-05	FBgn0000038	<a href="#">nAcHbeta1</a>	1.04459491	6.48E-07	3.55E-05
FBgn0030668	<a href="#">CG8128</a>	-0.6943842	1.92E-06	6.81E-05	FBgn0039118	<a href="#">CG10208</a>	0.80955118	1.20E-06	6.26E-05
FBgn0050005	<a href="#">GstI2</a>	-0.6438248	2.01E-06	7.11E-05	FBgn0033458	<a href="#">CG18446</a>	0.58308966	1.28E-06	6.64E-05
FBgn0034032	<a href="#">CG8195</a>	-0.5408707	2.05E-06	7.22E-05	FBgn0033520	<a href="#">Pnc2540-1</a>	0.74375135	1.29E-06	6.66E-05
FBgn0030925	<a href="#">Hayan</a>	-0.9826592	2.15E-06	7.55E-05	FBgn0031689	<a href="#">Cpr28d1</a>	0.80053352	1.58E-06	8.04E-05
FBgn0037000	<a href="#">ZnT7C</a>	-0.6746768	2.26E-06	7.89E-05	FBgn0032729	<a href="#">L2HG0H</a>	0.52320052	1.72E-06	8.62E-05
FBgn0004108	<a href="#">Nrt</a>	-0.6964366	2.36E-06	8.20E-05	FBgn0037717	<a href="#">CG8301</a>	0.54410035	1.94E-06	9.55E-05
FBgn0032749	<a href="#">TBC1D16</a>	-0.7115413	2.42E-06	8.36E-05	FBgn0033205	<a href="#">CG2064</a>	0.73749884	3.06E-06	1.47E-04
FBgn0259224	<a href="#">CG42324</a>	-0.8959483	2.45E-06	8.44E-05	FBgn0027621	<a href="#">Pfxz</a>	0.72002681	3.25E-06	1.53E-04
FBgn0033233	<a href="#">Kdm4A</a>	-0.5605395	2.53E-06	8.70E-05	FBgn0050460	<a href="#">CG30460</a>	0.62944429	3.81E-06	1.76E-04
FBgn0262902	<a href="#">CR43257</a>	-0.957284	2.61E-06	8.94E-05	FBgn0035094	<a href="#">CG9380</a>	0.93844635	4.81E-06	0.0021789
FBgn0038012	<a href="#">CG10013</a>	-0.9437117	2.77E-06	9.36E-05	FBgn0051793	<a href="#">CG31793</a>	0.65755611	4.93E-06	2.23E-04
FBgn0039094	<a href="#">CG10184</a>	-0.7620824	2.77E-06	9.36E-05	FBgn0258885	<a href="#">hnc</a>	0.61521329	5.50E-06	2.47E-04
FBgn0033875	<a href="#">CG6357</a>	-0.8296114	2.97E-06	9.98E-05	FBgn0037326	<a href="#">CG14669</a>	0.84098198	5.58E-06	2.49E-04
FBgn0011660	<a href="#">Pms2</a>	-0.6191626	4.01E-06	1.33E-04	FBgn0032719	<a href="#">CG17321</a>	0.73961713	6.03E-06	2.66E-04
FBgn0023540	<a href="#">CG3630</a>	-0.7750882	4.38E-06	1.44E-04	FBgn0037606	<a href="#">CG8032</a>	0.48037173	6.10E-06	2.68E-04
FBgn0040260	<a href="#">Ugt36a</a>	-0.7920914	4.55E-06	1.49E-04	FBgn026417	<a href="#">Hus1-like</a>	0.61835828	6.46E-06	2.82E-04
FBgn0032744	<a href="#">Ttc19</a>	-0.7666054	4.63E-06	1.52E-04	FBgn0001085	<a href="#">fz</a>	0.60208374	6.78E-06	2.95E-04
FBgn0034399	<a href="#">CG15083</a>	-0.6891411	4.71E-06	1.54E-04	FBgn0267347	<a href="#">sqd</a>	0.60195776	6.58E-06	3.66E-04
FBgn0031161	<a href="#">CG15446</a>	-0.5597497	5.16E-06	1.66E-04	FBgn0033257	<a href="#">sand</a>	0.9250535	8.99E-06	3.81E-04
FBgn0034569	<a href="#">dgl3</a>	-0.5100777	5.16E-06	1.66E-04	FBgn0003071	<a href="#">Pfk</a>	0.57585055	9.37E-06	3.95E-04
FBgn0031011	<a href="#">CG8034</a>	-0.5605182	5.44E-06	0.00017485	FBgn0261041	<a href="#">sil</a>	0.81342642	1.07E-05	4.47E-04
FBgn0027499	<a href="#">wde</a>	-0.4701503	5.51E-06	1.77E-04	FBgn0051676	<a href="#">CG31676</a>	0.89263646	1.42E-05	5.81E-04
FBgn0053170	<a href="#">CG33170</a>	-0.7056534	5.85E-06	0.00018566	FBgn0038296	<a href="#">CG6752</a>	0.66542534	1.56E-05	6.28E-04
FBgn0000152	<a href="#">Axs</a>	-0.6035714	5.84E-06	1.86E-04	FBgn0022709	<a href="#">Auk1</a>	0.55981758	1.65E-05	6.58E-04
FBgn0017448	<a href="#">CG2187</a>	-0.7509568	5.90E-06	1.86E-04	FBgn0032161	<a href="#">CG4594</a>	0.57432263	1.75E-05	6.89E-04
FBgn0024222	<a href="#">lR3beta</a>	-0.5333447	6.15E-06	1.94E-04	FBgn0023535	<a href="#">arg</a>	0.90279534	1.76E-05	6.89E-04
FBgn0011642	<a href="#">Zyx</a>	-0.6685735	6.47E-06	0.00020304	FBgn0033246	<a href="#">ACC</a>	0.51387976	1.98E-05	7.62E-04
FBgn0034928	<a href="#">CG13562</a>	-0.9576823	6.71E-06	2.10E-04	FBgn0017482	<a href="#">13dh</a>	0.78501069	2.08E-05	7.91E-04
FBgn0025702	<a href="#">Sprk9D</a>	-0.9076152	6.96E-06	2.17E-04	FBgn0014417	<a href="#">CG13397</a>	0.40989893	2.1026E-05	0.00079514
FBgn0032210	<a href="#">CYD</a>	-0.6022837	6.93E-06	2.58E-04	FBgn0031703	<a href="#">CG12512</a>	0.55306249	2.15E-05	8.08E-04
FBgn0035160	<a href="#">hng3</a>	-0.7523256	8.55E-06	2.63E-04	FBgn0264816	<a href="#">hshn</a>	0.43906737	2.28E-05	8.50E-04
FBgn0040384	<a href="#">CG2795</a>	-0.5216919	8.89E-06	2.72E-04	FBgn0037742	<a href="#">lgt3R</a>	0.90083167	2.34E-05	8.66E-04
FBgn0030683	<a href="#">CG8239</a>	-0.5479759	1.16E-05	3.53E-04	FBgn0033815	<a href="#">CG4676</a>	0.88304551	2.39E-05	8.80E-04
FBgn0038704	<a href="#">CG5316</a>	-0.5674446	1.19E-05	3.59E-04	FBgn0085339	<a href="#">CG34310</a>	0.71342358	2.46E-05	9.03E-04
FBgn0261794	<a href="#">lcc</a>	-0.5170776	1.31E-05	3.96E-04	FBgn0263665	<a href="#">CR43656</a>	0.67340873	2.72E-05	9.93E-04
FBgn0267967	<a href="#">orocilla</a>	-0.7468133	1.40E-05	4.20E-04					
FBgn0034985	<a href="#">CG3328</a>	-0.9088474	1.42E-05	4.23E-04					
FBgn0058160	<a href="#">CG40160</a>	-0.5573892	1.44E-05	0.00042856					
FBgn0263001	<a href="#">CR43309</a>	-0.9140864	1.55E-05	4.59E-04					
FBgn0035264	<a href="#">Osep4</a>	-0.8324113	1.58E-05	4.66E-04					
FBgn0030467	<a href="#">CG1764</a>	-0.6086858	1.68E-05	4.94E-04					
FBgn0031224	<a href="#">CG11454</a>	-0.6511044	1.79E-05	5.23E-04					
FBgn0261363	<a href="#">PPO3</a>	-0.908642	1.87E-05	5.43E-04					
FBgn0036765	<a href="#">CG7408</a>	-0.8043628	1.92E-05	5.57E-04					
FBgn0038966	<a href="#">pinta</a>	-0.6002371	1.93E-05	5.57E-04					
FBgn0264979	<a href="#">CG4267</a>	-0.5921441	1.95E-05	5.62E-04					
FBgn0031974	<a href="#">CG12560</a>	-0.6468851	2.10E-05	5.99E-04					
FBgn0030349	<a href="#">CG10353</a>	-0.5110312	2.26E-05	6.42E-04					
FBgn0046685	<a href="#">WscK</a>	-0.554038	2.39E-05	6.80E-04					
FBgn0036196	<a href="#">CG11658</a>	-0.6157453	2.51E-05	7.08E-04					
FBgn0029332	<a href="#">neur</a>	-0.5215054	2.55E-05	7.16E-04					
FBgn0038490	<a href="#">CG5285</a>	-0.6202791	2.59E-05	7.25E-04					
FBgn0027535	<a href="#">hstv</a>	-0.5633173	2.64E-05	7.39E-04					
FBgn0011676	<a href="#">Nus</a>	-0.882868	2.73E-05	7.61E-04					
FBgn0052109	<a href="#">CG32109</a>	-0.6631842	2.96E-05	0.00082025					
FBgn0266211	<a href="#">CR44906</a>	-0.84417	3.08E-05	8.49E-04					
FBgn0032079	<a href="#">CG31886</a>	-0.7657233	3.21E-05	8.78E-04					
FBgn0086898	<a href="#">dgo</a>	-0.6488394	3.30E-05	9.01E-04					
FBgn0036331	<a href="#">CG14117</a>	-0.7419989	3.32E-05	9.02E-04					
FBgn0033715	<a href="#">CG8490</a>	-0.565824	3.39E-05	9.17E-04					
FBgn0034578	<a href="#">CG15653</a>	-0.6741581	3.52E-05	9.50E-04					
FBgn0033261	<a href="#">ucll</a>	-0.5640484	3.64E-05	0.00097761					
FBgn0085212	<a href="#">CG34183</a>	-0.5802033	3.68E-05	0.00098506					
FBgn0030716	<a href="#">CG9170</a>	3.51543874	2.73E-133	1.25E-129					
FBgn0037710	<a href="#">tipe</a>	4.51536274	2.28E-119	5.23E-116					
FBgn0040370	<a href="#">CG13375</a>	3.94270954	2.25E-117	4.12E-114					
FBgn0063499	<a href="#">GstE10</a>	4.38522941	1.29E-105	1.96E-102					
FBgn0263219	<a href="#">Dscam4</a>	3.38390085	1.29E-79	1.48E-76					
FBgn0063491	<a href="#">GstE9</a>	2.37209129	5.43E-74	5.53E-71					
FBgn0262509	<a href="#">nrm</a>	3.26989536	5.19E-72	4.76E-69					
FBgn0000246	<a href="#">o3jG</a>	1.80256044	7.60E-51	4.64E-48					
FBgn0052773	<a href="#">CR32773</a>	2.91153609	2.21E-48	1.06E-45					
FBgn0033744	<a href="#">DM4-R2</a>	2.21228708	3.41E-47	1.56E-44					
FBgn0004034	<a href="#">y</a>	2.3656636	1.46E-36	4.63E-34					
FBgn0039129	<a href="#">Rpf19b</a>	2.25634285	4.45E-29	9.94E-27					
FBgn0052625	<a href="#">CG32625</a>	1.50639584	1.75E-26	3.56E-24					
FBgn0003965	<a href="#">v</a>	2.2137325	8.01E-26	1.56E-23					
FBgn0028400	<a href="#">Syt4</a>	1.60413573	8.45E-26	1.61E-23					
FBgn0035086	<a href="#">CG12851</a>	2.20739805	3.06E-25	5.51E-23					
FBgn0014417	<a href="#">CG13397</a>	0.9799056	2.34E-24	4.05E-22					
FBgn0052373	<a href="#">CG32373</a>	1.65820956	3.79E-22	5.89E-20					
FBgn0039683	<a href="#">RhoGAP100F</a>	1.78355414	4.14E-22	6.32E-20					
FBgn0052816	<a href="#">CG32816</a>	1.34949326	3.29E-21	4.78E-19					
FBgn0036369	<a href="#">CG10089</a>	1.43828569	3.97E-19	5.58E-17					
FBgn0035083	<a href="#">Tina-1</a>	0.97905168	3.91E-18	4.84E-16					
FBgn0031645	<a href="#">CG3086</a>	1.20681255	3.21E-16	3.59E-14					

FBgn0028743	<a href="#">Uhit</a>	1,400557	1,35E-15	1,44E-13
FBgn0264439	<a href="#">CG43857</a>	1,44206442	3,80E-15	3,91E-13
FBgn0029723	<a href="#">Prnc-R</a>	1,16467501	8,98E-15	9,10E-13
FBgn0036368	<a href="#">CG10738</a>	1,12952567	1,06E-14	1,05E-12
FBgn0267733	<a href="#">CR46064</a>	1,30463417	2,70E-14	2,55E-12
FBgn0266258	<a href="#">CG44953</a>	1,61734556	2,70E-14	2,55E-12
FBgn0038204	<a href="#">CG14357</a>	1,45024866	1,17E-13	1,04E-11
FBgn0039900	<a href="#">Syt7</a>	1,57434289	1,36E-13	1,18E-11
FBgn0031275	<a href="#">GABA-B-R3</a>	1,56925587	1,55E-13	1,34E-11
FBgn0039118	<a href="#">CG10208</a>	1,225912	1,70E-13	1,45E-11
FBgn0267347	<a href="#">sqn</a>	0,97779595	4,75E-13	3,85E-11
FBgn0003866	<a href="#">tsh</a>	1,33447888	7,38E-13	5,88E-11
FBgn0033458	<a href="#">CG18446</a>	0,8595366	9,18E-13	7,25E-11
FBgn0050403	<a href="#">CG30403</a>	0,83287764	1,55E-11	1,10E-09
FBgn0032645	<a href="#">CG15142</a>	1,25685861	2,82E-11	1,94E-09
FBgn0264385	<a href="#">CG43837</a>	0,80630682	7,48E-11	4,93E-09
FBgn0038038	<a href="#">CG5167</a>	0,86009134	2,30E-10	1,46E-08
FBgn0263093	<a href="#">CR43361</a>	0,98968277	7,16E-10	4,26E-08
FBgn0284435	<a href="#">lyn</a>	0,90935674	3,67E-09	1,9771E-07
FBgn0259229	<a href="#">CG42329</a>	0,99577599	4,2094E-09	2,2561E-07
FBgn0035317	<a href="#">Osep2</a>	1,2035749	4,82E-09	2,57E-07
FBgn0030723	<a href="#">dpr18</a>	1,20750721	7,53E-09	3,90E-07
FBgn0266005	<a href="#">CR44779</a>	0,91939442	1,40E-08	7,03E-07
FBgn0283427	<a href="#">FASN1</a>	0,86971339	2,30E-08	1,11E-06
FBgn0037902	<a href="#">CG5281</a>	1,01450627	2,83E-08	1,35E-06
FBgn0261266	<a href="#">zuc</a>	0,59100256	4,51E-08	2,07E-06
FBgn0040001	<a href="#">FASN3</a>	1,15849921	5,08E-08	2,32E-06
FBgn0039341	<a href="#">CG5112</a>	0,52776631	9,83E-08	4,21E-06
FBgn0039938	<a href="#">Sox102F</a>	0,96839303	1,34E-07	5,6477E-06
FBgn0051997	<a href="#">CG31997</a>	1,08525441	1,72E-07	7,21E-06
FBgn0042696	<a href="#">Nfl</a>	1,08171827	2,65E-07	1,07E-05
FBgn0263617	<a href="#">CR43626</a>	1,0436084	3,50E-07	1,40E-05
FBgn0023535	<a href="#">arg</a>	1,07140257	3,57E-07	1,42E-05
FBgn0039543	<a href="#">CG12428</a>	0,51181318	3,79E-07	1,50E-05
FBgn0263660	<a href="#">CR43651</a>	0,94475809	5,01E-07	1,94E-05
FBgn0033246	<a href="#">ACC</a>	0,58306679	1,27E-06	4,62E-05
FBgn0265168	<a href="#">CR44237</a>	0,75743644	2,18E-06	7,63E-05
FBgn0039927	<a href="#">CG11155</a>	0,81040266	2,64E-06	9,00E-05
FBgn0260745	<a href="#">mfaf</a>	0,73309962	2,88E-06	9,71E-05
FBgn0260812	<a href="#">mfaf-D</a>	0,94838747	3,51E-06	1,17E-04
FBgn0027611	<a href="#">LMan1l</a>	0,78767635	3,80E-06	1,27E-04
FBgn0002905	<a href="#">rnas.306</a>	0,63117721	3,93E-06	1,30E-04
FBgn0004047	<a href="#">Yp3</a>	0,86055593	4,75E-06	1,54E-04
FBgn0025629	<a href="#">CG4045</a>	0,61428341	5,64E-06	1,80E-04
FBgn0264265	<a href="#">CG43765</a>	0,89472755	7,33E-06	2,28E-04
FBgn0004895	<a href="#">foad1</a>	0,94745812	8,43E-06	2,60E-04
FBgn0031703	<a href="#">CG12512</a>	0,57709695	9,14E-06	2,79E-04
FBgn0041581	<a href="#">Att18</a>	0,94032658	9,6168E-06	0,00029282
FBgn0025382	<a href="#">Rab27</a>	0,84551951	1,32E-05	0,000398
FBgn0030583	<a href="#">CG14410</a>	0,57134888	1,4142E-05	0,00042218
FBgn0263916	<a href="#">Enr12</a>	0,54077834	1,78E-05	5,21E-04
FBgn0030660	<a href="#">CG8097</a>	0,47918563	1,96E-05	5,64E-04
FBgn0016926	<a href="#">Hrno</a>	0,5721965	2,07E-05	5,92E-04
FBgn0267001	<a href="#">Ten-a</a>	0,80076692	2,42E-05	6,84E-04
FBgn0037577	<a href="#">CG1443</a>	0,82607808	2,8441E-05	0,00078987
FBgn0026361	<a href="#">Sep6</a>	0,58579619	3,19E-05	8,77E-04
FBgn0085370	<a href="#">Pde11</a>	0,4243612	3,21E-05	8,78E-04
FBgn0052702	<a href="#">Gdm</a>	0,56358184	3,33E-05	0,00090215

S3 Table. Quantitative analysis of H3K4me3 differential enrichment in Control vs *lid* KD ovarian ChIP-Seq.

chromosome	start	end	Corr_WF1	Corr_LiKD	Fold	p-value	FDR	Annotation	Detailed Annotation	Distance to TSS	Nearest PromoterID
chr2R	13409200	13409700	8.65	1.25	-7.35	4.80E-93	1.41E-49	TTS (H3p02G705)	exon (NM_362983, exon 2 of 4)	437	Fly0033836 Fly003716
chr2R	1310648	5102148	10.01	6.75	-3.25	2.10E-14	8.05E-12	Intergenic	NC9049: 1st UTR Gyro	13949	Fly0033836 Fly0038648
chrX	5312452	5312952	11.66	8.54	-3.11	5.61E-52	2.40E-34	Intergenic	promoter-TSS (NM_131386)	349	Fly0033836 Fly0037449
chr2R	5106392	5106892	9.02	6.14	-2.89	2.69E-09	2.97E-07	Intergenic	FM2_DM1[DM1]Jockey	14758	Fly0033836 Fly0031280
chr3R	10957690	10958190	9.47	6.85	-2.62	2.76E-13	8.13E-11	Intergenic	CpG	7657	Fly0033836 Fly0032326
chr2R	5105620	5106120	10.35	8.1	-2.25	8.30E-28	8.15E-25	Intergenic	NM1A_1stUTR[1A]	13986	Fly0033836 Fly0031128
chr2L	20292285	20292785	9.44	7.94	-2.08	3.58E-14	1.27E-11	Intergenic	(CA) [Simple_repeat] [Simple_repeat]	2257	Fly0040996 Fly0038351
chr2L	18685896	18686396	10.01	7.9	-2.07	8.83E-13	2.36E-10	Intergenic	promoter-TSS (NM_340795, exon 2 of 2)	1371	Fly0033836 Fly0034632
chr3R	29925218	29925718	8.21	7.69	-1.12	4.83E-07	2.26E-05	Intergenic	exon (NM_103162954, exon 2 of 2)	394	Fly0033836 Fly0035873
chr2R	7681134	7681634	10.71	9.34	-1.38	1.97E-07	1.06E-05	Intergenic	promoter-TSS (NM_10313212)	134	Fly0033836 Fly0031078
chr3R	31196793	31197293	8.9	7.59	-1.3	1.03E-08	9.30E-07	Intergenic	exon (NM_343922, exon 3 of 12)	128	Fly0033836 Fly0038755
chrX	12072279	12072779	10.45	9.3	-1.15	3.92E-08	2.86E-06	Intergenic	exon (Fly0030373, exon 3 of 1)	289	Fly0033836 Fly0032637
chr2L	17990861	17991361	9.1	7.95	-1.15	9.50E-07	4.10E-05	Intergenic	exon (NM_365234, exon 3 of 1)	694	Fly0033836 Fly0030825
chr2L	7791670	7792170	7.94	7.94	-1.14	2.30E-08	1.80E-06	Intergenic	intron (Fly0025687, intron 7 of 7)	1363	Fly0033836 Fly0032496
chr2R	6022744	6023244	10.14	9.04	-1.11	9.50E-05	0.00162	Intergenic	promoter-TSS (NM_1030395)	353	Fly0033836 Fly0032851
chr2R	4674779	4675279	9.36	8.25	-1.11	6.54E-05	0.00126	Intergenic	exon (NM_10313053, exon 3 of 3)	3177	Fly0040005 Fly0031129
chrX	18359008	18359508	9.3	8.21	-1.09	1.89E-05	0.000434	Intergenic	exon (NM_330254, exon 2 of 4)	3388	Fly0033836 Fly0034553
chr2L	1189844	1190344	10.23	9.15	-1.08	3.95E-08	2.86E-06	TTS (Fly0035387)	TTS (NM_138236)	507	Fly0033836 Fly0032625
chr2L	9996097	9996597	9.91	8.88	-1.03	0.000117	0.00019	TTS (Fly0035395)	TTS (NM_10323384)	225	Fly0033836 Fly0032973
chr2R	6769814	6770314	9.26	8.24	-1.02	0.00126	0.00106	Intergenic	5' UTR (NM_10323384, exon 3 of 10)	438	Fly0033836 Fly0032951
chr2L	22502445	22502945	11.56	10.58	-1.02	9.57E-06	4.02E-05	Intergenic	exon (Fly0032205, exon 3 of 1)	298	Fly0033836 Fly0032859
chrX	946167	946667	8.4	7.45	-0.96	6.79E-06	0.00019	Intergenic	exon (Fly0032985, exon 8 of 8)	9920	Fly0033836 Fly0032959
chrX	23222211	23222711	9.81	8.85	-0.96	0.00512	0.033	Intergenic	R2_DM1[DM1]R2	7920	Fly0033836 Fly0034689
chr2R	4833428	4833928	9.12	8.19	-0.93	1.21E-05	0.000304	Intergenic	Buggen3[LINE]LDA	4433	Fly0033836 Fly0022923
chr2R	429786	429836	9.7	8.77	-0.93	0.00224	0.0181	Intergenic	(CGCG) [Simple_repeat] [Simple_repeat]	-56702	Fly0033836 Fly0031128
chrX_D5483928v1_random	2011	2511	8.66	7.76	-0.91	0.000582	0.00667	Intergenic	NA	NA	NA
chr2L	1670372	1670872	9.38	8.49	-0.89	0.00813	0.0459	Intergenic	Intergenic	NA	NA
chr2R	6716557	6717057	9.96	9.09	-0.87	0.00492	0.0321	Intergenic	promoter-TSS (Fly0033095)	900	Fly0033836 Fly0031329
chr3L	217378	217878	9.44	8.62	-0.82	5.78E-05	0.00109	Intergenic	promoter-TSS (NM_138110)	253	Fly0033836 Fly0032488
chr2R	14910246	14910746	8.82	8.04	-0.78	0.00692	0.0416	Intergenic	exon (NM_10313048, exon 4 of 13)	373	Fly0027596 Fly0030834
chr3L	1928025	1928075	8.74	7.97	-0.77	0.000339	0.00444	Intergenic	TTS (NM_140886)	345	Fly0033836 Fly0032015
chrX	8039588	8039638	9.21	8.43	-0.77	0.00445	0.00555	Intergenic	exon (NM_332205, exon 4 of 5)	1279	Fly0027596 Fly0031323
chrX	1567620	1567670	9.2	8.54	-0.67	0.00455	0.0307	Intergenic	5' UTR (NM_10314122, exon 2 of 2)	3025	Fly0033836 Fly0032952
chr2L	22491784	22492284	9.72	9.01	-0.71	0.00325	0.0122	Intergenic	exon (NM_326779, exon 3 of 11)	1449	Fly0027596 Fly0032923
chr2R	12314643	12315143	8.97	8.27	-0.7	0.00675	0.0407	Intergenic	exon (NM_365878, exon 2 of 6)	777	Fly0033836 Fly0030895
chrX_D5483928v1_random	617	1117	8.73	8.04	-0.69	0.00826	0.0475	Intergenic	R1_DM1[DM1]R1	NA	NA
chr2R	6705730	6706230	8.82	8.15	-0.68	0.00161	0.014	Intergenic	5' UTR (NM_10316952, exon 2 of 2)	1267	Fly0026552 Fly0030849
chr2L	22448885	22449385	10.38	9.71	-0.67	0.000683	0.00735	Intergenic	promoter-TSS (NM_134614)	458	Fly0033836 Fly0030987
chr2L	718187	718687	9.2	8.54	-0.67	0.00455	0.0307	TTS (Fly0028232)	TTS (NM_100103120)	367	Fly0033836 Fly0030958
chr2L	7785117	7785617	10.62	10.06	-0.56	0.00265	0.0178	TTS (Fly0028232)	TTS (NM_103102853)	305	Fly0027596 Fly0032626
chr2L	7789510	7790010	10.4	9.83	-0.57	0.00219	0.0178	Intergenic	5' UTR (NM_138205, exon 1 of 8)	397	Fly0033836 Fly0029496
chr3L	14219569	14220069	8.81	8.17	-0.63	0.00416	0.0268	Intergenic	promoter-TSS (NM_1031378)	78	Fly0033836 Fly0031004
chr3R	17059672	17060172	8.67	8.04	-0.63	0.00581	0.0383	Intergenic	intron (Fly0020493, intron 3 of 2)	5026	Fly0020493 Fly0030834
chrX	709187	709687	8.44	7.83	-0.61	0.00521	0.0334	Intergenic	promoter-TSS (NM_1032238)	52	Fly0029504 Fly0033027
chrX	5037817	5038317	8.99	8.42	-0.58	0.00481	0.0317	Intergenic	Intergenic	-1488	Fly0033836 Fly0030832
chr2L	6317817	6318317	11.69	10.73	-0.97	0.00173	0.0129	Intergenic	5' UTR (NM_10315623)	309	Fly0033836 Fly0032952
chr2R	4311476	4311976	11.7	11.2	-0.59	0.00738	0.0435	Intergenic	promoter-TSS (Fly0033721)	219	Fly0033836 Fly0031628
chr2R	24034534	24035034	11.64	11.94	0.3	0.00488	0.032	Intergenic	promoter-TSS (Fly0033764)	560	Fly0033836 Fly0022166
chr2L	13549543	13550043	11.23	11.53	0.3	0.00797	0.0463	Intergenic	exon (NM_10313812, exon 2 of 4)	465	Fly0033836 Fly0030834
chr2L	6490282	6490782	11.72	12.01	0.3	0.00852	0.0484	Intergenic	promoter-TSS (NM_10310629)	331	Fly0033836 Fly0029264
chr2R	18141277	18141777	11.39	11.7	0.31	0.00464	0.0261	Intergenic	exon (NM_362205, exon 2 of 5)	151	Fly0026552 Fly0030834
chr3L	25324370	25324870	11.45	11.75	0.3	0.00495	0.0313	TTS (Fly0028232)	TTS (NM_103102853)	341	Fly0033836 Fly0032952
chr2L	7789510	7790010	11.21	11.52	0.31	0.0045	0.0304	Intergenic	promoter-TSS (NM_10323022)	130	Fly0033836 Fly0031078
chr3L	9398699	9399199	11.17	11.48	0.31	0.00508	0.0329	Intergenic	promoter-TSS (Fly0035928)	221	Fly0033836 Fly0031004
chrX	19730950	19731450	11.75	12.07	0.31	0.0056	0.0353	Intergenic	intron (Fly0020381, intron 1 of 2)	159	Fly0033836 Fly0030834
chrX	189930	189980	11.17	11.48	0.31	0.00612	0.0377	Intergenic	promoter-TSS (Fly0000137)	26	Fly0000137 Fly0030898
chrX	8993122	8993622	11.73	12.05	0.31	0.00656	0.0398	Intergenic	promoter-TSS (Fly0020243)	120	Fly0033836 Fly0030986
chr3R	21076010	21076510	11.41	11.71	0.31	0.00891	0.0411	Intergenic	TTS (Fly0028232)	425	Fly0033836 Fly0030987
chr2L	13930802	13931302	11.12	11.54	0.31	0.00761	0.0446	Intergenic	exon (NM_362003, exon 2 of 6)	356	Fly0033836 Fly0034659
chr2R	17666487	17666987	11.62	11.94	0.32	0.00296	0.0225	TTS (Fly0028232)	TTS (NM_103102853)	357	Fly0033836 Fly0030834
chr3L	21343327	21343827	11.38	11.7	0.32	0.00411	0.0285	Intergenic	promoter-TSS (Fly0025243)	139	Fly0033836 Fly0033797
chr2R	23698390	23698890	11.13	11.45	0.32	0.00433	0.0297	Intergenic	promoter-TSS (NM_103144273)	536	Fly0033836 Fly0032084
chr2L	16258108	16258608	11.11	11.43	0.32	0.00456	0.0307	Intergenic	promoter-TSS (NM_138293)	254	Fly0028555 Fly0030834
chr2L	18446572	18447072	11.82	12.14	0.32	0.00585	0.0365	TTS (Fly0028232)	TTS (NM_103102853)	376	Fly0033836 Fly0030834
chr2L	16259128	16259628	11.36	11.67	0.32	0.00429	0.0287	Intergenic	promoter-TSS (Fly0025243)	102	Fly0033836 Fly0030834
chrX	16440882	16441382	11.34	11.67	0.33	0.00233	0.0187	Intergenic	promoter-TSS (Fly0030752)	64	Fly0033836 Fly0034350
chr2L	8082353	8082853	11.23	11.56	0.33	0.00286	0.0218	Intergenic	promoter-TSS (NM_364789)	-255	Fly0027596 Fly0034551
chr2L	4854741	4855241	11.64	11.97	0.33	0.00355	0.0257	TTS (Fly0028232)	TTS (NM_103123053)	247	Fly0033836 Fly0027462
chr3L	6193522	6194022	11.37	11.7	0.33	0.00434	0.0297	Intergenic	promoter-TSS (NM_103102853)	371	Fly0027596 Fly0030834
chr3R	21364469	21364969	11.84	12.17	0.33	0.00471	0.0313	Intergenic	promoter-TSS (Fly0025243)	120	Fly0027596 Fly0033797
chr2L	8513396	8513896	11.34	11.67	0.33	0.00429	0.0287	Intergenic	promoter-TSS (NM_103144273)	373	Fly0033836 Fly0030834
chrX	11454835	11455335	11.58	11.92	0.33	0.00541	0.0343	Intergenic	promoter-TSS (NM_103102853)	300	Fly0033836 Fly0030834
chr2R	6213680	6214180	11.91	12.24	0.33	0.00602	0.0373	Intergenic	promoter-TSS (Fly0025243)	132	Fly0027596 Fly0030834
chr2L	15005806	15006306	11.16	11.49	0.33	0.00606	0.0374	TTS (Fly0028232)	TTS (NM_138293)	354	Fly0040228 Fly0030834
chr3L	851243	851743	11.3	11.62	0.33	0.00603	0.0374	TTS (Fly0035388)	TTS (NM_138236)	188	Fly0033836 Fly0032567
chr3R	2905857	2906357	11.5	11.83	0.33	0.00627	0.038				

chr2R	24130383	24130383	11.83	12.09	0.36	0.00235	0.0188	promoter-TSS (FBgn0039153)	promoter-TSS (NM_142960)	327	FBgn0036317 (FB0008546)
chr2R	22174874	22175374	11.65	12.01	0.36	0.00247	0.0196	promoter-TSS (NM_137802)	promoter-TSS (NM_137802)	203	FBgn0037176 (FB0007176)
chr2R	24940004	24940504	10.91	11.27	0.36	0.0026	0.0203	TTS (FBgn0022343)	TTS (NM_001038855)	126	FBgn0050821 (FB0034555)
chr3L	18745922	18746422	11.72	12.08	0.36	0.00255	0.0242	TTS (FBgn0036810)	TTS (NM_140799)	317	FBgn0036811 (FB0007504)
chrX	529325	529825	11.89	12.26	0.36	0.00357	0.0259	promoter-TSS (FBgn0001008)	promoter-TSS (NM_057278)	274	FBgn0004983 (FB0007089)
chr3R	10042537	10043037	10.91	11.27	0.36	0.00416	0.0288	promoter-TSS (FBgn0053208)	promoter-TSS (NM_176455)	34	FBgn0053208 (FB0008276)
chr2R	13521301	13521601	11.66	12.02	0.36	0.00466	0.0311	TTS (FBgn0020370)	TTS (NM_162956)	326	FBgn0020370 (FB0003029)
chrX	13059411	13059411	11.84	12.2	0.36	0.00483	0.0318	TTS (FBgn0021524)	TTS (NM_057814)	194	FBgn0021524 (FB0007121)
chrX	19589927	19590427	11.86	12.22	0.36	0.00467	0.0385	TTS (FBgn0005286)	TTS (NM_079482)	247	FBgn0005286 (FB0007471)
chr3R	10049257	10049757	11.88	12.24	0.36	0.00673	0.0407	promoter-TSS (FBgn0037779)	promoter-TSS (NM_141715)	309	FBgn0037779 (FB0008214)
chr2L	4976585	4977085	11.75	12.11	0.36	0.00695	0.0416	promoter-TSS (FBgn0031662)	promoter-TSS (NM_135045)	188	FBgn0031661 (FB0007949)
chr2R	15570964	15571464	11.54	11.91	0.36	0.00734	0.0434	promoter-TSS (FBgn0050466)	promoter-TSS (NM_166103)	203	FBgn0050466 (FB0008725)
chr2R	12692259	12692759	11.79	12.15	0.36	0.00812	0.0469	exon (FBgn0031267, exon 2 of 4)	exon (NM_136929, exon 2 of 4)	181	FBgn0031267 (FB0008781)
chr2L	11282009	11282509	11.01	11.38	0.36	0.0082	0.0473	TTS (FBgn0032358)	TTS (NM_136566)	170	FBgn0032358 (FB0008023)
chr3R	11407832	11408332	11.78	12.14	0.36	0.00828	0.0475	exon (FBgn0034447, exon 2 of 4)	exon (NM_134810)	165	FBgn0034447 (FB0008234)
chr2R	19452653	19453153	12.14	12.5	0.36	0.00847	0.0482	exon (FBgn004852, exon 1 of 2)	5' UTR (NM_137578, exon 1 of 2)	400	FBgn004852 (FB0008635)
chr2R	16452264	16452764	10.87	11.23	0.36	0.00894	0.0487	promoter-TSS (FBgn0050493)	promoter-TSS (NM_165351)	331	FBgn0050493 (FB0032911)
chr3R	31985153	31985653	11.26	11.64	0.37	0.00489	0.0586	exon (FBgn001224, exon 1 of 14)	5' UTR (NM_001104524, exon 1 of 14)	365	FBgn001224 (FB0011286)
chr2L	19533466	19533966	11.17	11.54	0.37	0.00598	0.0683	TTS (FBgn0032800)	TTS (NM_144467)	238	FBgn0032800 (FB0008129)
chr3R	8561149	8561649	11.33	11.7	0.37	0.00866	0.0891	TTS (FBgn0051450)	TTS (NM_169226)	365	FBgn0051453 (FB0033930)
chr3L	1303001	13030501	11.75	12.12	0.37	0.00955	0.0944	promoter-TSS (FBgn0010333)	promoter-TSS (NM_057602)	308	FBgn0095203 (FB0007267)
chr2L	16300406	16300906	11.37	11.75	0.37	0.00969	0.0958	promoter-TSS (FBgn0028375)	promoter-TSS (NM_078857)	443	FBgn0028375 (FB0008029)
chr2L	14362258	14362758	11.71	12.08	0.37	0.0014	0.0125	exon (NM_001014482, exon 3 of 6)	exon (NM_001014482, exon 3 of 6)	440	FBgn0014482 (FB0008030)
chr2R	19759085	19759585	11.39	11.77	0.37	0.00206	0.017	promoter-TSS (FBgn0032818)	promoter-TSS (NM_136355)	457	FBgn0032818 (FB0008129)
chr2R	16170376	16170876	11.74	12.1	0.37	0.00235	0.0188	TTS (FBgn0034083)	TTS (NM_137249)	435	FBgn0034083 (FB0008749)
chr2R	6749577	6750077	11.75	12.12	0.37	0.00286	0.0218	TTS (FBgn0020370)	TTS (NM_144467)	311	FBgn0020370 (FB0008129)
chr3R	15361138	15361638	11.88	12.26	0.37	0.00376	0.0268	promoter-TSS (FBgn0028327)	promoter-TSS (NM_169505)	269	FBgn0028327 (FB0008314)
chr3L	5139881	5139931	11.52	11.89	0.37	0.00393	0.0277	promoter-TSS (FBgn0055289)	promoter-TSS (NM_139690)	164	FBgn0055289 (FB0007180)
chr3R	15274489	15274989	11.93	12.3	0.37	0.00421	0.029	promoter-TSS (FBgn0038131)	promoter-TSS (NM_169632)	51	FBgn0038131 (FB0008317)
chr2L	11807766	11808266	10.97	11.34	0.37	0.00426	0.0294	exon (FBgn0022805, exon 1 of 8)	5' UTR (NM_057897, exon 1 of 7)	956	FBgn0022805 (FB0008026)
chr2R	11223032	11223532	10.76	11.13	0.37	0.00481	0.0317	promoter-TSS (FBgn0033584)	promoter-TSS (NM_00129379)	162	FBgn0033584 (FB0039479)
chrX	12611093	12611593	11.93	12.31	0.37	0.00488	0.032	promoter-TSS (FBgn0030407)	promoter-TSS (NM_132586)	265	FBgn0030407 (FB0007367)
chr3L	14786895	14787395	12.05	12.42	0.37	0.00498	0.0324	promoter-TSS (FBgn0036449)	promoter-TSS (NM_001169974)	355	FBgn0036449 (FB0007561)
chrX	1236282	1236782	11.31	11.67	0.37	0.00532	0.0339	TTS (FBgn0076876)	TTS (NM_130542)	152	FBgn0076876 (FB0036978)
chr2R	18421492	18421992	11.54	11.91	0.37	0.00682	0.0411	TTS (FBgn0027835)	TTS (NM_206164)	330	FBgn0027835 (FB0008148)
chrX	11869991	11870491	11.57	11.94	0.37	0.00686	0.0416	promoter-TSS (FBgn0030344)	promoter-TSS (NM_132529)	370	FBgn0030344 (FB0007567)
chr3R	3470656	3471156	11.27	11.64	0.37	0.00707	0.0422	TTS (FBgn0052857)	TTS (NM_168932)	263	FBgn0052857 (FB0007343)
chr3R	4387694	4388194	11.81	12.18	0.37	0.00747	0.044	TTS (FBgn0037240)	TTS (NM_141204)	203	FBgn0037240 (FB0032038)
chr2L	13782925	13783425	11.68	12.05	0.37	0.0078	0.0454	promoter-TSS (FBgn0028539)	promoter-TSS (NM_001042895)	285	FBgn0028539 (FB0008028)
chr3R	28812222	28812722	12.18	12.56	0.37	0.00842	0.048	promoter-TSS (FBgn005070)	promoter-TSS (NM_002503)	95	FBgn005070 (FB0009165)
chr3R	7082279	7082779	11.29	11.66	0.37	0.00847	0.0482	TTS (FBgn0037470)	TTS (NM_169169)	348	FBgn0037470 (FB0008138)
chr2L	4459087	4459587	11.84	12.22	0.37	0.0085	0.0483	promoter-TSS (FBgn0031608)	promoter-TSS (NM_001201760)	265	FBgn0031608 (FB0035135)
chr3L	7356086	7356586	12.22	12.59	0.37	0.00881	0.0496	TTS (FBgn0035770)	TTS (NM_168209)	336	FBgn0035770 (FB0034683)
chr2R	17786200	17786700	11.68	12.06	0.38	0.000676	0.0075	exon (FBgn0026895, exon 2 of 3)	exon (NM_058065, exon 2 of 3)	316	FBgn0026895 (FB0008949)
chr2L	9575985	9576485	11.56	11.94	0.38	0.00109	0.0104	exon (FBgn0029873, exon 2 of 5)	5' UTR (NM_164860, exon 2 of 5)	534	FBgn0029873 (FB0007957)
chr3R	7073857	7074357	11.67	12.05	0.38	0.00151	0.0151	promoter-TSS (FBgn0037468)	promoter-TSS (NM_141484)	345	FBgn0037468 (FB0008169)
chr3L	16229251	16229751	10.92	11.3	0.38	0.00159	0.0158	promoter-TSS (FBgn0026305)	promoter-TSS (NM_140589)	402	FBgn0026305 (FB0007547)
chr3R	11620031	11620531	11.48	11.86	0.38	0.00188	0.0158	promoter-TSS (FBgn0013631)	promoter-TSS (NM_169406)	192	FBgn0013631 (FB0009956)
chr3L	19063069	19063569	10.8	11.18	0.38	0.00191	0.016	promoter-TSS (FBgn0036842)	promoter-TSS (NM_140828)	155	FBgn0036842 (FB0007505)
chr2R	15311626	15312126	11.46	11.83	0.38	0.00192	0.0161	promoter-TSS (FBgn0034008)	promoter-TSS (NM_137184)	367	FBgn0034008 (FB0030870)
chr3R	22462477	22462977	11.63	12.01	0.38	0.00195	0.0163	promoter-TSS (FBgn0028688)	promoter-TSS (NM_142791)	273	FBgn0028688 (FB0008425)
chr3L	13512559	13513059	11.64	12.03	0.38	0.00212	0.0173	promoter-TSS (FBgn0036376)	promoter-TSS (NM_168556)	303	FBgn0036376 (FB0007518)
chr3R	20550347	20550847	10.8	11.18	0.38	0.00211	0.0173	intron (FBgn0036917, intron 1 of 8)	intron (NM_001275830, intron 1 of 9)	510	FBgn0036917 (FB0008948)
chrX	8412111	8411711	10.89	11.28	0.38	0.00225	0.0197	exon (FBgn0026725, exon 1 of 4)	5' UTR (NM_00125850, exon 1 of 4)	197	FBgn0026725 (FB0008226)
chr3L	7976525	7977025	11.77	12.15	0.38	0.00256	0.0201	promoter-TSS (FBgn0035299)	promoter-TSS (NM_168291)	172	FBgn0035299 (FB0007673)
chr3L	19979238	19979738	11.84	12.22	0.38	0.00273	0.0211	exon (FBgn004892, exon 2 of 2)	exon (NM_140926, exon 2 of 2)	334	FBgn004892 (FB0034524)
chr3L	9887996	9888496	11.85	12.23	0.38	0.00324	0.0241	promoter-TSS (NM_0007586)	promoter-TSS (NM_079292)	437	FBgn0007586 (FB0007631)
chr2R	24534711	24535211	11.37	11.74	0.38	0.00328	0.0244	exon (FBgn003021, exon 2 of 4)	exon (NM_001038882, exon 4 of 6)	466	FBgn003021 (FB0007234)
chr3R	9260852	9261352	12.11	12.49	0.38	0.00374	0.0266	TTS (FBgn0037670)	TTS (NM_141618)	465	FBgn0037671 (FB0008198)
chr3L	9457963	9458463	11.27	11.65	0.38	0.00424	0.0291	promoter-TSS (FBgn0039598)	promoter-TSS (NM_140061)	302	FBgn0039599 (FB0007643)
chr2R	21282667	21283167	10.72	11.1	0.38	0.00455	0.0307	promoter-TSS (FBgn0034611)	promoter-TSS (NM_001299742)	80	FBgn0034611 (FB0034284)
chr3R	22879287	22879787	11.93	12.31	0.38	0.0047	0.0312	promoter-TSS (FBgn0044324)	promoter-TSS (NM_168976)	292	FBgn0044324 (FB0032051)
chr3R	10143547	10144047	11.68	12.07	0.38	0.0047	0.0312	promoter-TSS (NM_0006359)	promoter-TSS (NM_143815)	387	FBgn0006359 (FB0033825)
chr3L	1348692	1348692	12.12	12.5	0.38	0.0052	0.0333	promoter-TSS (FBgn0005194)	promoter-TSS (NM_138242)	323	FBgn0005194 (FB0007652)
chr3R	6404938	6405438	11.24	11.62	0.38	0.00573	0.0373	exon (FBgn0011706, exon 1 of 11)	TTS (NM_00117066, exon 1 of 11)	252	FBgn0011706 (FB0028939)
chr3R	20577097	20577597	11.27	11.6	0.38	0.00724	0.0429	TTS (FBgn0034565)	TTS (NM_001043099)	292	FBgn0034565 (FB0007120)
chr3R	14511927	14512427	11.42	11.8	0.38	0.00801	0.0464	promoter-TSS (FBgn0038233)	promoter-TSS (NM_142109)	340	FBgn0038233 (FB0008293)
chrX	23082875	23083375	12.14	12.52	0.38	0.00887	0.0499	promoter-TSS (FBgn0039942)	promoter-TSS (NM_001015255)	388	FBgn0039943 (FB0011370)
chrX	10010581	10011081	11.48	11.86	0.38	0.00238	0.0341	TTS (FBgn0053575)	TTS (NM_001014730)	351	FBgn0010147 (FB0007145)
chrX	12902720	12903220	11.21	11.6	0.39	0.000276	0.0038	TTS (FBgn0030432)	TTS (NM_132610)	192	FBgn0030431 (FB0007366)
chr3R	31748482	31748982	11.5	11.89	0.39	0.000564	0.0065	promoter-TSS (FBgn0039870)	promoter-TSS (NM_143620)	243	FBgn0039870 (FB0008536)
chrX	10365208	10365708	11.29	11.68	0.39	0.000564	0.0065	TTS (FBgn0076729)	TTS (NM_167225)	815	FBgn0076729 (FB0034709)
chr2L	106338	106338	11.45	11.84	0.39	0.000576	0.00662	promoter-TSS (FBgn0005278)	promoter-TSS (NM_206580)	144	FBgn0005278 (FB0030152)
chr3L	2553699	2553699	10.99	11.38	0.39	0.000666	0.0066	intron (FBgn0025947, intron 1 of 15)	intron (NM_001259411, intron 1 of 15)	443	FBgn0025947 (FB0008414)
chr3L	11164870	11165370	11.37	11.76	0.39	0.00071	0.00775	promoter-TSS (FBgn0047421)	promoter-TSS (NM_00129293)	150	FBgn0047421 (FB0007617)
chr2R	23809307	23809807	11.72	12.11	0.39	0.000736	0.00795	promoter-TSS (FBgn0010278)	promoter-TSS (NM_079106)	322	FBgn0010278 (FB0007124)
chr2R	6971034	6971534	11.35	11.74	0.39	0.00074	0.00797	TTS (FBgn0033121)	TTS (NM_136408)	353	FBgn0033121 (FB0032942)
chr2L	19444310	19444810	11.8	12.2	0.39	0.000806	0.00843	promoter-TSS (FBgn0033346)	promoter-TSS (NM_001273649)		

chr2R	12490527	12491027	11.93	12.34	0.4	0.00649	0.0395	TTS (Fg0033738)	TTS (NM_165900)	183	Fg0262840   Fb0306802
chr3R	25262806	25263306	11.46	11.87	0.41	0.00012	0.00194	promoter-TSS (Fg0039304)	promoter-TSS (NM_143106)	316	Fg0303305   Fb0094815
chrX	20429002	20429502	11.67	12.08	0.41	0.00033	0.00690	promoter-TSS (NM_078690)	promoter-TSS (NM_1339682)	426	Fg0303115   Fb0339682
chr3L	2651246	2651746	11.59	12.01	0.41	0.000256	0.00359	promoter-TSS (Fg0025919)	promoter-TSS (NM_001144405)	356	Fg0202702   Fb0072948
chr3L	15576795	15577295	11.6	12.01	0.41	0.000274	0.00378	TTS (NM_140521)	TTS (NM_140521)	474	Fg0305371   Fb0075563
chr2R	11493454	11493954	10.82	11.23	0.41	0.000533	0.00624	promoter-TSS (Fg0026574)	promoter-TSS (NM_206868)	234	Fg0305266   Fb0340295
chr2R	9122299	9122799	10.95	11.36	0.41	0.000739	0.00797	TTS (Fg0027541)	TTS (NM_145673)	110	Fg0303381   Fb0098579
chr3L	9364800	9365300	11.82	12.23	0.41	0.0011	0.0105	exon (Fg0025991, exon 1 of 1)	exon (NM_140045, exon 1 of 1)	281	Fg0303580   Fb0005444
chr3L	7902201	7902701	11.82	12.23	0.41	0.00117	0.0109	exon (Fg0030292, exon 3 of 5)	exon (NM_078515, exon 3 of 5)	572	Fg0301022   Fb0071050
chr3R	31616386	31616886	11.56	11.97	0.41	0.00131	0.012	promoter-TSS (Fg0039850)	promoter-TSS (NM_143620)	334	Fg0303980   Fb0090810
chr3L	3035517	3036017	10.9	11.31	0.41	0.00135	0.0123	intron (Fg0035385, intron 1 of 9)	(ACA)n Simple_repeat (Simple_repeat	572	Fg0303388   Fb0072981
chr2L	5096469	5096969	11.46	11.87	0.41	0.00142	0.0126	TTS (Fg0031602)	TTS (NM_01273156)	349	Fg0303163   Fb0032982
chr3L	15099712	15100212	11.66	12.07	0.41	0.00153	0.0135	TTS (Fg0036849)	TTS (NM_140834)	393	Fg0303850   Fb0075032
chr3R	19876884	19877384	11.83	12.24	0.41	0.00164	0.0142	promoter-TSS (NM_141283)	promoter-TSS (NM_142583)	280	Fg0303741   Fb0092858
chrX	16886915	16887415	11.53	11.94	0.41	0.0018	0.0153	promoter-TSS (Fg0030802)	promoter-TSS (NM_001272701)	345	Fg0303803   Fb0031051
chrX	5673862	5674362	10.66	11.07	0.41	0.00223	0.0181	TTS (Fg0029275)	TTS (NM_167043)	139	Fg0202975   Fb0070780
chr2L	1899772	1899822	11.61	12.02	0.41	0.00235	0.02	promoter-TSS (Fg0030299)	promoter-TSS (NM_136055)	292	Fg0303700   Fb0091096
chr2L	12652964	12653464	11.93	12.35	0.41	0.00259	0.0208	promoter-TSS (Fg0033751)	promoter-TSS (NM_136961)	430	Fg0303762   Fb0092684
chr2L	21102780	21103280	11.85	12.26	0.41	0.00319	0.0239	promoter-TSS (Fg0028421)	promoter-TSS (NM_136292)	218	Fg0303916   Fb0091465
chr3L	8522871	8523371	11.36	11.77	0.41	0.0032	0.0239	TTS (Fg0039507)	TTS (NM_139983)	380	Fg0303906   Fb0076564
chr3R	22380199	22380699	11.7	12.11	0.41	0.00346	0.0253	promoter-TSS (NM_01263047)	promoter-TSS (NM_001260309)	322	Fg0303985   Fb0113489
chr2R	18095234	18095734	11.6	12.02	0.41	0.00367	0.0263	promoter-TSS (Fg0034300)	promoter-TSS (NM_001103893)	80	Fg0303430   Fb0113092
chr2L	4971737	4972237	12.1	12.51	0.41	0.00377	0.0268	promoter-TSS (NM_164605)	promoter-TSS (NM_164605)	286	Fg0303169   Fb0078995
chr3R	13265926	13266426	11.89	12.3	0.41	0.00396	0.0279	promoter-TSS (Fg0030598)	promoter-TSS (NM_001170130)	295	Fg0303171   Fb0092779
chr3R	20448889	20449389	11.48	11.89	0.41	0.00403	0.0282	promoter-TSS (Fg0030549)	promoter-TSS (NM_170119)	342	Fg0304945   Fb0032261
chr3L	13943266	13943766	11.83	12.24	0.41	0.00436	0.0298	promoter-TSS (Fg0036341)	promoter-TSS (NM_079330)	346	Fg0306261   Fb0091754
chr3L	20392892	20393392	11.17	11.57	0.41	0.00489	0.032	exon (Fg003952, exon 2 of 3)	exon (NM_001038946, exon 2 of 3)	413	Fg0305959   Fb0090010
chr3R	13964881	13965381	11.81	12.22	0.41	0.00489	0.032	promoter-TSS (Fg0038191)	promoter-TSS (NM_142067)	247	Fg0303720   Fb0090826
chr2L	6062897	6063397	11.45	11.86	0.41	0.00555	0.035	promoter-TSS (Fg0031771)	promoter-TSS (NM_135143)	179	Fg0303172   Fb0091312
chr3L	15144281	15144781	11.78	12.19	0.41	0.00563	0.0354	promoter-TSS (NM_0147178)	promoter-TSS (NM_168616)	197	Fg0303644   Fb0092640
chr3L	21030861	21031361	10.86	11.26	0.41	0.00688	0.0413	promoter-TSS (Fg0028402)	promoter-TSS (NM_001170015)	240	Fg0303704   Fb0078327
chr2R	9292558	9293058	10.45	10.86	0.41	0.00739	0.0436	promoter-TSS (Fg0022808)	promoter-TSS (NM_001278091)	400	Fg0302408   Fb0032998
chr3L	19913085	19913585	11.91	12.33	0.41	0.00767	0.0448	exon (Fg0036915)	TTS (NM_168625)	259	Fg0306916   Fb0091718
chr3R	5598889	5599389	11.9	12.31	0.41	0.00859	0.0487	exon (Fg0040381, exon 1 of 1)	exon (NM_079210, exon 1 of 1)	280	Fg0300438   Fb0077157
chr2R	16149239	16149739	11.8	12.21	0.41	0.00888	0.0489	promoter-TSS (Fg0029175)	promoter-TSS (NM_166250)	350	Fg0303585   Fb0034652
chr3R	6042223	6042723	11.41	11.82	0.41	0.0116	0.05	exon (Fg0030375, exon 1 of 5)	exon (NM_236024, exon 1 of 5)	434	Fg0303762   Fb0092684
chr3R	15350321	15350821	11.19	11.61	0.42	9.30E-05	0.00159	promoter-TSS (Fg0038324)	exon (NM_142194)	430	Fg0262722   Fb0093116
chrX	15075602	15076102	11.04	11.47	0.42	0.000145	0.00229	exon (Fg0030061, exon 1 of 4)	exon (NM_001042912, exon 1 of 4)	369	Fg0303608   Fb0091600
chr3R	15277500	15278000	11.65	12.07	0.42	0.000173	0.00266	TTS (Fg0011476)	TTS (NM_142186)	358	Fg0302738   Fb0093125
chrX	16303935	16304435	11.56	11.99	0.42	0.000185	0.0028	TTS (Fg0030735)	TTS (NM_001103529)	316	Fg0202751   Fb0074222
chrX	6742782	6743282	11.42	11.84	0.42	0.00021	0.00309	promoter-TSS (Fg0086668)	promoter-TSS (NM_0037229)	331	Fg0303013   Fb0091356
chrX	2180424	2180924	11.7	12.13	0.42	0.000281	0.00385	promoter-TSS (Fg0030316)	promoter-TSS (NM_057336)	342	Fg0265901   Fb0091273
chr2L	21180297	21180797	11.72	12.14	0.42	0.000377	0.00483	promoter-TSS (Fg0000239)	promoter-TSS (NM_138759)	615	Fg0303529   Fb0091874
chr2R	24196163	24196663	11.62	12.04	0.42	0.000566	0.00436	TTS (Fg0026053)	TTS (NM_138050)	436	Fg0303261   Fb0091261
chr2R	10230331	10230831	11.28	11.7	0.42	0.000594	0.00601	exon (Fg0029787, exon 1 of 14)	exon (NM_001104048, exon 1 of 15)	472	Fg0303741   Fb0091749
chr2R	17716633	17717133	10.81	11.22	0.42	0.000669	0.00745	promoter-TSS (Fg0028494)	promoter-TSS (NM_137405)	387	Fg0202844   Fb0091023
chr3L	19805662	19806162	11.56	11.98	0.42	0.00096	0.0095	promoter-TSS (Fg0036909)	promoter-TSS (NM_168191)	134	Fg0303952   Fb0091016
chr2R	12037377	12037877	12.02	12.44	0.42	0.000992	0.00974	promoter-TSS (NM_0125934)	promoter-TSS (NM_0125934)	230	Fg0301939   Fb0091676
chr3L	17622039	17622539	11.49	11.91	0.42	0.00117	0.0109	promoter-TSS (Fg0036740)	promoter-TSS (NM_140740)	366	Fg0303704   Fb0092512
chr3L	8524310	8524810	11.08	11.5	0.42	0.00155	0.0136	promoter-TSS (Fg0024236)	promoter-TSS (NM_079250)	405	Fg0303907   Fb0076852
chr3L	12849562	12850062	10.89	11.31	0.42	0.00188	0.0158	promoter-TSS (Fg0036318)	promoter-TSS (NM_001144473)	21	Fg0303317   Fb0073237
chr3R	5218930	5219430	11.66	12.08	0.42	0.0023	0.0185	TTS (Fg0037296)	TTS (NM_141298)	276	Fg0259212   Fb0091363
chr3R	21855610	21856110	12.01	12.44	0.42	0.0025	0.0197	exon (Fg0035225, exon 1 of 2)	exon (NM_079719, exon 1 of 2)	406	Fg0303192   Fb0091457
chrX	6597354	6597854	11.33	11.75	0.42	0.00258	0.0204	TTS (Fg0029787)	TTS (NM_00127257)	423	Fg0303678   Fb0092994
chr3R	5975595	5976095	11.92	12.34	0.42	0.00316	0.0238	promoter-TSS (Fg0086695)	promoter-TSS (NM_001316495)	288	Fg0303717   Fb0091043
chr3L	16105087	16105587	11.34	11.75	0.42	0.00327	0.0243	promoter-TSS (Fg0026287)	promoter-TSS (NM_001258959)	290	Fg0303205   Fb0091549
chr3L	18867821	18868321	11.83	12.25	0.42	0.00356	0.0258	TTS (Fg0036818)	TTS (NM_00125897)	301	Fg0303810   Fb0091707
chr2L	8196379	8196879	11.38	11.8	0.42	0.0043	0.0295	promoter-TSS (Fg0031996)	promoter-TSS (NM_135346)	281	Fg0303199   Fb0093518
chrX	15710947	15711447	11.6	12.02	0.42	0.00441	0.03	promoter-TSS (Fg0030672)	promoter-TSS (NM_132299)	149	Fg0303073   Fb0091405
chrX	5689047	5689547	11.72	12.14	0.42	0.00447	0.0303	promoter-TSS (Fg0000394)	promoter-TSS (NM_080525)	176	Fg0202789   Fb0092084
chr2R	10074941	10075441	11.12	11.54	0.42	0.00449	0.0304	exon (Fg0033945, exon 2 of 6)	exon (NM_136707, exon 2 of 6)	340	Fg0303492   Fb0091676
chr3R	11520349	11520849	10.95	11.38	0.42	0.00454	0.0307	TTS (Fg0042255)	TTS (NM_144455)	434	Fg0303281   Fb0092818
chr2R	16017704	16018204	10.99	11.41	0.42	0.00479	0.0317	promoter-TSS (Fg0034066)	promoter-TSS (NM_137294)	238	Fg0304067   Fb0091707
chr3L	7320286	7320786	11.75	12.17	0.42	0.00505	0.0328	TTS (Fg0035761)	TTS (NM_168199)	469	Fg0303760   Fb0091037
chr3R	18241602	18242102	11.85	12.27	0.42	0.00525	0.0336	promoter-TSS (Fg0020238)	promoter-TSS (NM_169799)	307	Fg0303585   Fb0093606
chr2L	8514222	8514722	12.18	12.59	0.42	0.00567	0.0356	promoter-TSS (Fg0032052)	promoter-TSS (NM_135394)	396	Fg0303205   Fb0091769
chr3L	654427	654927	11.07	11.48	0.42	0.00809	0.0468	promoter-TSS (Fg0035149)	promoter-TSS (NM_138202)	325	Fg0303150   Fb0092252
chr3R	14125967	14126467	11.81	12.24	0.43	0.00243	0.00346	promoter-TSS (Fg0010340)	promoter-TSS (NM_057603)	437	Fg0262955   Fb0092892
chrX	16586554	16587054	10.8	11.23	0.43	0.000593	0.00678	promoter-TSS (Fg00267912)	promoter-TSS (NM_167524)	-139	Fg0267912   Fb0093198
chr3L	9073188	9073688	11.51	11.95	0.43	0.000659	0.00739	promoter-TSS (Fg0039599)	promoter-TSS (NM_1400298)	334	Fg0303960   Fb0091624
chr3L	1312719	1313219	11.63	12.06	0.43	0.000768	0.00816	promoter-TSS (Fg0030520)	promoter-TSS (NM_167868)	236	Fg0303572   Fb0091728
chr2L	6780162	6780662	11.71	12.13	0.43	0.00082	0.00649	promoter-TSS (Fg0040280)	promoter-TSS (NM_1391280)	347	Fg0303458   Fb0091709
chr2L	21101727	21102227	11.65	12.08	0.43	0.000921	0.00929	promoter-TSS (Fg0039916)	promoter-TSS (NM_1362943)	452	Fg0262951   Fb0091415
chrX	13617175	13617675	10.91	11.34	0.43	0.000944	0.0094	promoter-TSS (Fg0030502)	promoter-TSS (NM_001298287)	453	Fg0303053   Fb0093864
chr2R	9860156	9860656	10.97	11.41	0.43	0.00112	0.0106	promoter-TSS (Fg00265339)	promoter-TSS (NM_124490)	357	Fg0202750   Fb0091654
chr3L	22727428	22727928	11.91	12.34	0.43	0.00119	0.0111	promoter-TSS (Fg0037185)	promoter-TSS (NM_141155)	291	Fg0303784   Fb0092837
chrX	13821615	13822115	10.97	11.4	0.43	0.00131	0.012	promoter-TSS (Fg0027537)	promoter-TSS (NM_132701)	442	Fg0303250   Fb0091385
chr2L	1166477	1166977	11.07	11.5	0.43	0.00204	0.0169	TTS (Fg0024314)	TTS (NM_134735)	22	

chrX	6086661	6087131	1146	1191	0.45	3.92E-05	0.000787	exon (Fg)0003302, exon 3 of 3	exon (NM_076498, exon 2 of 2)	381	Fg0003302   Fg00070889
chrX	20430219	20430719	1127	1173	0.45	4.35E-05	0.000858	promoter-TSS (Fg)0031115	promoter-TSS (NM_167704)	335	Fg0000261   Fg00077306
chr2R	16150071	16150771	1116	1161	0.45	5.09E-05	0.000976	promoter-TSS (NM_001032251)	promoter-TSS (NM_001032251)	199	Fg00034083   Fg000302084
chr3L	8514309	8514809	1109	1155	0.45	7.98E-05	0.00139	exon (Fg)0005902, exon 2 of 2	exon (NM_139975, exon 2 of 2)	362	Fg00035502   Fg00076655
chr3R	5793722	5794222	1178	1223	0.45	0.000119	0.00192	promoter-TSS (Fg)0037379	promoter-TSS (NM_141334)	345	Fg00037379   Fg00078668
chr3R	24876774	24881774	1215	1261	0.45	0.000123	0.00192	promoter-TSS (Fg)0036280	promoter-TSS (NM_140959)	463	Fg00036280   Fg00078668
chr3L	20375338	20375838	1171	1216	0.45	0.000215	0.00314	promoter-TSS (Fg)0036280	promoter-TSS (NM_140959)	308	Fg0000127   Fg00073273
chr3L	3937452	3937952	1182	1228	0.45	0.000394	0.00439	TTS (Fg)0035475	TTS (NM_139552)	290	Fg00035475   Fg000345342
chr3L	22877459	22877959	1108	1154	0.45	0.000344	0.00444	exon (Fg)0044324, exon 1 of 6	exon (NM_162976, exon 3 of 6)	475	Fg00044324   Fg00078570
chr3R	29112347	29112947	1135	1181	0.45	0.000344	0.00444	promoter-TSS (Fg)0039637, exon 1 of 3	promoter-TSS (NM_057545)	308	Fg00039637   Fg00085372
chr3R	16435923	16436423	1165	1211	0.45	0.000473	0.0057	TTS (Fg)0038472	TTS (NM_001038969)	424	Fg00038472   Fg00083316
chr3R	19863776	19864276	1191	1237	0.45	0.000514	0.0061	promoter-TSS (NM_142580)	promoter-TSS (NM_142580)	367	Fg00038738   Fg00083366
chr3L	19261554	19262054	1162	1207	0.45	0.000584	0.00668	0.00668	TTS (NM_140840)	411	Fg00026057   Fg00074989
chrX	17421350	17421850	1177	1222	0.45	0.00105	0.0102	TTS (Fg)0040877	TTS (NM_144231)	545	Fg00027002   Fg00074440
chr3L	13929484	13929984	1213	1258	0.45	0.00115	0.0109	promoter-TSS (Fg)0036386	promoter-TSS (NM_140412)	348	Fg00001208   Fg00075756
chr2R	13941505	13942005	1089	1134	0.45	0.00126	0.0116	TTS (Fg)0038855	TTS (NM_133072)	355	Fg00038855   Fg00076156
chr2R	19310057	19310557	115	1195	0.45	0.00141	0.0126	TTS (NM_001274158)	TTS (NM_001274158)	358	Fg00034433   Fg00085538
chr3L	14001155	14001655	1101	1146	0.45	0.0018	0.0153	promoter-TSS (Fg)0036395	promoter-TSS (NM_140424)	406	Fg00036397   Fg00033025
chr2L	18709003	18709503	1157	1202	0.45	0.00192	0.0161	promoter-TSS (Fg)0025605	promoter-TSS (NM_058040)	408	Fg00025605   Fg00081099
chr2R	13197504	13198004	1182	1227	0.45	0.00208	0.0171	exon (Fg)00053182, exon 2 of 7	5' UTR (NM_001169668, exon 2 of 7)	583	Fg00053182   Fg00087770
chr3R	13970746	13971246	1108	1153	0.45	0.00223	0.0181	promoter-TSS (Fg)0036314	promoter-TSS (NM_048388)	736	Fg00026341   Fg00083198
chr2L	7026537	7027037	1182	1227	0.45	0.00251	0.0198	promoter-TSS (Fg)0031881	promoter-TSS (NM_135249)	300	Fg00031881   Fg00079429
chr3R	5613441	5613941	1192	1237	0.45	0.00261	0.0204	promoter-TSS (Fg)0017550	promoter-TSS (NM_169090)	534	Fg00017550   Fg00078704
chr3L	7348360	7348860	1138	1183	0.45	0.00271	0.0211	promoter-TSS (Fg)0032989	promoter-TSS (NM_057778)	288	Fg00032989   Fg00045392
chr3L	19792989	19793489	1072	1117	0.45	0.00273	0.0211	promoter-TSS (Fg)00261283	promoter-TSS (NM_168816)	430	Fg000261283   Fg000302778
chr2R	20622767	20623267	1214	1259	0.45	0.0031	0.0234	promoter-TSS (Fg)0034529	promoter-TSS (NM_137652)	312	Fg00034529   Fg000808254
chr3R	23957678	23958178	121	1255	0.45	0.00322	0.024	promoter-TSS (Fg)0039132	promoter-TSS (NM_142941)	463	Fg00039132   Fg00085111
chr2R	13133212	13133712	1174	1219	0.45	0.00352	0.0256	exon (Fg)00259876, exon 1 of 5	exon (NM_001169664, exon 1 of 5)	321	Fg00025976   Fg00029507
chr3L	15836660	15837160	1084	1129	0.45	0.00387	0.0275	TTS (Fg)0052150	TTS (NM_168635)	572	Fg00036538   Fg00030654
chrX	5916001	5916501	107	1115	0.45	0.00406	0.0283	promoter-TSS (Fg)0029823	promoter-TSS (NM_001144690)	66	Fg00029823   Fg000345317
chr2L	143872	143872	1178	1223	0.45	0.00634	0.0388	promoter-TSS (Fg)0051974	promoter-TSS (NM_001272671)	300	Fg00031224   Fg00078116
chrX	10745555	10746055	1186	1231	0.45	0.00674	0.0407	promoter-TSS (Fg)0052675	promoter-TSS (NM_001274957)	352	Fg00030384   Fg00073494
chr2R	15420235	15420735	1112	1157	0.45	0.00682	0.0411	exon (Fg)00034021, exon 1 of 5	exon (NM_137125, exon 1 of 5)	548	Fg00034021   Fg00045392
chr2R	9732678	9733178	1137	1182	0.45	0.00722	0.0439	exon (Fg)00032171, exon 1 of 4	exon (NM_135469, exon 1 of 4)	545	Fg00032171   Fg00073969
chr3R	26965818	26966318	1124	1169	0.45	0.00793	0.0462	promoter-TSS (Fg)0041224	promoter-TSS (NM_178570)	139	Fg00039466   Fg00082059
chrX	17710050	17710550	1013	1058	0.45	0.00826	0.0475	promoter-TSS (Fg)0030864	promoter-TSS (NM_133011)	157	Fg00026150   Fg00030235
chrX	5419768	5420268	1136	1181	0.45	0.00877	0.0495	promoter-TSS (Fg)0029877	promoter-TSS (NM_167033)	318	Fg00029877   Fg00070795
chr2L	2780006	2780506	1203	1248	0.45	0.00889	0.0499	promoter-TSS (Fg)0031455	promoter-TSS (NM_001032050)	333	Fg00031456   Fg00077125
chr3L	22071345	22071845	1136	1181	0.45	0.02025	0.00457	promoter-TSS (Fg)00364727	promoter-TSS (NR_073073)	253	Fg00027332   Fg00078486
chr3R	8032590	8033090	1122	1167	0.45	0.00825	0.00825	promoter-TSS (NM_001031081)	promoter-TSS (NM_001031696)	169	Fg00037544   Fg00034760
chr2R	18706189	18706689	1126	1171	0.46	8.83E-05	0.00144	TTS (Fg)0026103	TTS (NM_001103899)	463	Fg00031379   Fg00086607
chrX	6547453	6547953	1157	1202	0.46	0.00138	0.00216	exon (Fg)0002987, exon 1 of 1	exon (NM_163209, exon 1 of 1)	601	Fg00029876   Fg00070905
chr2R	21282880	21283380	1137	1182	0.46	0.00165	0.00251	exon (Fg)00025890, exon 1 of 2	exon (NM_167460, exon 1 of 2)	541	Fg00025890   Fg00071611
chrX	15878475	15878975	1189	1234	0.46	0.000239	0.00342	promoter-TSS (Fg)0035040	promoter-TSS (NM_001299221)	243	Fg00035039   Fg00034457
chr2R	24611874	24612374	1143	1188	0.46	0.000282	0.00386	exon (Fg)00036302, exon 2 of 13	exon (NM_001144471, exon 2 of 10)	482	Fg00036302   Fg00030087
chr3L	1257810	1257810	1148	1193	0.46	0.000425	0.00526	promoter-TSS (Fg)0051626	promoter-TSS (NM_165362)	281	Fg00026129   Fg00081478
chr2L	21237280	21237780	1083	1128	0.46	0.00075	0.00829	promoter-TSS (Fg)0036090	promoter-TSS (NM_168415)	314	Fg0000029   Fg00027338
chr3L	10637255	10637755	1122	1167	0.46	0.000786	0.00829	promoter-TSS (Fg)00264378	promoter-TSS (NR_073877)	270	Fg00033990   Fg000332259
chr2R	14993315	14993815	1145	1190	0.46	0.00127	0.0117	promoter-TSS (NM_00113444)	promoter-TSS (NM_00113444)	351	Fg00026174   Fg000339071
chr3R	16955558	16956058	1183	1228	0.46	0.00134	0.0122	promoter-TSS (Fg)0038544	promoter-TSS (NM_169580)	498	Fg00038544   Fg00083854
chr3R	19904120	19904620	118	1225	0.46	0.00134	0.0136	promoter-TSS (Fg)0038544	promoter-TSS (NM_169580)	498	Fg00038544   Fg00083854
chr3R	23758424	23758924	117	1216	0.46	0.00157	0.0164	promoter-TSS (Fg)0027264	promoter-TSS (NM_00129353)	67	Fg00029303   Fg000345021
chr2L	10423554	10424054	1212	1257	0.46	0.00393	0.0278	exon (Fg)0003246, exon 3 of 7	exon (NM_135556, exon 2 of 6)	471	Fg0003246   Fg00080020
chr2R	12515492	12515992	1164	1209	0.46	0.00395	0.0278	promoter-TSS (Fg)0033749	promoter-TSS (NM_165912)	308	Fg00033750   Fg00087939
chrX	2609322	2609322	1161	1207	0.46	0.00641	0.0392	promoter-TSS (Fg)0004643	promoter-TSS (NM_080126)	331	Fg00011016   Fg00034003
chr2L	15270835	15271335	1085	1131	0.46	0.00705	0.0421	promoter-TSS (Fg)00216285	promoter-TSS (NM_165112)	543	Fg00021628   Fg000302158
chr3L	22263471	22263971	1182	1228	0.46	0.00772	0.045	promoter-TSS (Fg)0027500	promoter-TSS (NM_001275276)	353	Fg00027505   Fg00078492
chr2L	10412870	10413370	1124	1169	0.46	0.00797	0.0483	promoter-TSS (Fg)0032943	promoter-TSS (NM_001169466)	343	Fg00032942   Fg00080047
chr3L	9722587	9723087	1173	1218	0.46	0.00812	0.0489	promoter-TSS (Fg)0034038	promoter-TSS (NM_140075)	357	Fg00034038   Fg00030639
chr3R	18742075	18742575	1127	1172	0.46	0.00825	0.0493	exon (Fg)00027275, exon 1 of 4	promoter-TSS (NM_0012141)	317	Fg00027275   Fg000305174
chr2R	10051544	10052044	1158	1203	0.47	2.09E-05	0.00407	promoter-TSS (Fg)0022169	promoter-TSS (NM_00129353)	373	Fg00022169   Fg00083433
chr2R	17027772	17027772	1137	1184	0.47	2.45E-05	0.000539	promoter-TSS (Fg)00265540	promoter-TSS (NM_134587)	333	Fg00023172   Fg00080690
chrX	7965754	7966254	1102	1147	0.47	2.60E-05	0.000563	exon (Fg)0003656, exon 1 of 11	5' UTR (NM_167140, exon 1 of 11)	412	Fg0003656   Fg000712125
chr3R	16646364	16646864	1106	1151	0.47	3.68E-05	0.000749	promoter-TSS (Fg)0015019	promoter-TSS (NM_169727)	390	Fg00026154   Fg00083356
chr3L	9863660	9864160	1121	1166	0.47	3.89E-05	0.000783	promoter-TSS (Fg)00027567	promoter-TSS (NM_168386)	439	Fg00027567   Fg00076362
chrX	16287975	16288475	1101	1146	0.47	4.59E-05	0.00104	promoter-TSS (Fg)0011571	promoter-TSS (NM_001272673)	308	Fg00025256   Fg00074245
chr3L	7347919	7348419	1161	1206	0.47	5.82E-05	0.00109	promoter-TSS (Fg)0019662	promoter-TSS (NM_001169899)	446	Fg00035768   Fg00076880
chr3R	24134958	24135458	1162	1207	0.47	5.91E-05	0.0011	TTS (Fg)0026317	TTS (NM_058007)	459	Fg00026673   Fg00084547
chr3R	18908035	18908535	1137	1182	0.47	6.89E-05	0.00127	promoter-TSS (Fg)00036027	promoter-TSS (NM_140815)	368	Fg00033992   Fg000757075
chrX	477461	477961	1117	1162	0.47	7.52E-05	0.00133	exon (NM_00103388, exon 2 of 3)	exon (NM_00103388, exon 2 of 3)	344	Fg00003128   Fg00070786
chr3R	10761423	10761923	1168	1213	0.47	8.04E-05	0.0014	promoter-TSS (Fg)0051390	promoter-TSS (NM_206471)	98	Fg00037851   Fg00082723
chr2L	1704977	1705477	1153	1198	0.47	0.000176	0.00268	promoter-TSS (Fg)0011570	promoter-TSS (NM_001272948)	304	Fg00011570   Fg000331630
chr3L	24851805	24852305	1171	1216	0.47	0.000182	0.00276	TTS (Fg)0039233	TTS (NM_143039)	455	Fg00029234   Fg000804705
chr3L	11122718	11123218	1184	1229	0.47	0.000283	0.00386	promoter-TSS (Fg)00260795	promoter-TSS (NM_140194)	248	Fg00026136   Fg00076223
chr3L	1517965	1518465	1177	1222	0.47	0.000287	0.00391	promoter-TSS (Fg)0011204	promoter-TSS (NM_138269)	363	Fg00026123   Fg00072702
chr3R	30056983	30057483	1192	1237	0.47	0.000317	0.00423	TTS (Fg)0039744	TTS (NM_143512)	375	Fg00026168   Fg00085563
chrX	190153										

chr3R	8806260	8807060	11.52	12.01	0.49	4.53E-06	0.000139	TIS (#Rgn0037622)	TIS (NM_141578)	489	Fgpn0037624   Fba0081919
chr3R	7919439	7919939	11.01	11.51	0.49	7.23E-06	0.000201	paramoter-TSS (#Rgn002542)	paramoter-TSS (NM_080111)	422	Fgpn0037531   Fba0030625
chr3L	8340955	8341455	11.41	11.91	0.49	8.22E-06	0.000221	TIS (NM_139953)	TIS (#Rgn0035876)	461	Fgpn0037507   Fba0076604
chrX	54093	54593	11.44	11.94	0.49	1.58E-05	0.000036	Intergenic	HEJ ALINE Jockey	682	Fgpn0058669   Fba00307354
chr3L	13411941	13412441	11.67	12.16	0.49	1.74E-05	0.000046	paramoter-TSS (#Rgn026049)	paramoter-TSS (NM_168543)	2619	Fgpn0036566   Fba0039454
chr2R	15577076	15577576	11.61	12.11	0.49	1.87E-05	0.000073	TIS (#Rgn005183)	TIS (NM_142248)	144	Fgpn0046761   Fba0003158
chr3L	19257015	19260425	11.22	11.71	0.49	2.15E-05	0.000047	exon (#Rgn0010315, exon 2 of 4)	exon (NM_167473, exon 2 of 4)	138	Fgpn0046761   Fba00495271
chrX	15508598	15509098	11.54	12.03	0.49	3.18E-05	0.000065	exon (#Rgn0010315, exon 2 of 6)	exon (NM_167473, exon 2 of 6)	828	Fgpn0010315   Fba00300391
chr2R	10680200	10680700	11.18	11.67	0.49	5.68E-05	0.000107	paramoter-TSS (#Rgn010356)	paramoter-TSS (NM_057609)	477	Fgpn0033564   Fba00289471
chr3R	8663253	8663753	11.88	12.37	0.49	6.81E-05	0.000124	paramoter-TSS (#Rgn0127606)	paramoter-TSS (NM_141554)	396	Fgpn0066679   Fba0001857
chr3L	5751294	5751794	11.64	12.13	0.49	6.89E-05	0.000126	exon (#Rgn0263106, exon 1 of 3)	exon (NM_168128, exon 1 of 3)	643	Fgpn0263106   Fba0007123
chr3R	8344822	8345322	11.13	11.62	0.49	7.53E-05	0.000133	TIS (#Rgn014536)	TIS (NM_141536)	675	Fgpn0037540   Fba0001850
chr3R	27112672	27113172	11.85	12.34	0.49	8.94E-05	0.000154	paramoter-TSS (#Rgn039487)	paramoter-TSS (NM_13136513)	352	Fgpn0027564   Fba0008510
chr2R	11452320	11452820	11.18	11.67	0.49	9.77E-05	0.000166	exon (#Rgn0000581, exon 2 of 10)	5'UTR (NM_001273968, exon 2 of 11)	207	Fgpn0000581   Fba0008146
chr3R	16412818	16413318	11.63	12.12	0.49	0.00017	0.000261	paramoter-TSS (#Rgn028429)	paramoter-TSS (NM_142956)	325	Fgpn0038491   Fba0003289
chr3R	27273763	27274263	11.99	12.47	0.49	0.000233	0.000497	paramoter-TSS (#Rgn046247)	paramoter-TSS (NM_001104477)	309	Fgpn0039255   Fba0005158
chr2R	23556490	23556990	11.33	11.81	0.49	0.000441	0.00041	paramoter-TSS (#Rgn018450)	paramoter-TSS (NM_001160791)	651	Fgpn0034891   Fba00129860
chr2R	9290949	9291449	11.61	12.11	0.49	0.000453	0.00054	paramoter-TSS (#Rgn028408)	paramoter-TSS (NM_136624)	366	Fgpn0026266   Fba0008859
chr3R	25292521	25293021	10.92	11.41	0.49	0.000453	0.00054	TIS (#Rgn051102)	TIS (NM_120213)	206	Fgpn0051089   Fba0004863
chr2R	20644166	20644666	11.82	12.31	0.49	0.000604	0.000687	paramoter-TSS (#Rgn061361)	paramoter-TSS (NM_001032273)	381	Fgpn0034573   Fba0006232
chr3R	14662572	14663072	11.77	12.26	0.49	0.000665	0.000744	paramoter-TSS (#Rgn038252)	paramoter-TSS (NM_142126)	375	Fgpn0025808   Fba0002974
chr2L	20797873	20798373	10.44	10.92	0.49	0.000731	0.000792	exon (#Rgn002886, exon 1 of 3)	5'UTR (NM_165344, exon 1 of 3)	209	Fgpn002886   Fba0004115
chr3L	16419643	16420143	11.95	12.44	0.49	0.000791	0.000959	exon (#Rgn0027080)	paramoter-TSS (NM_140638)	497	Fgpn0033583   Fba0007530
chr2L	4459825	4460325	11.88	12.37	0.49	0.00103	0.00116	paramoter-TSS (#Rgn051002)	paramoter-TSS (NM_001173099)	276	Fgpn0034501   Fba0007444
chr2R	23363474	23363974	11.44	11.93	0.49	0.00109	0.00105	exon (#Rgn0266011)	exon (NM_140580, exon 1 of 5)	788	Fgpn0040660   Fba0002233
chr3R	23762634	23763134	12.03	12.52	0.49	0.00109	0.00105	paramoter-TSS (#Rgn031114)	paramoter-TSS (NM_142926)	370	Fgpn0039111   Fba0004644
chr2R	8950319	8950819	12.04	12.53	0.49	0.0011	0.00111	exon (#Rgn003356, exon 2 of 3)	exon (NM_165638, exon 2 of 2)	517	Fgpn0053919   Fba0030734
chr2L	469220	4692720	12.17	12.66	0.49	0.00128	0.00118	paramoter-TSS (#Rgn_135040)	paramoter-TSS (NM_135040)	467	Fgpn0031657   Fba0007894
chr3R	24187998	24188498	11.93	12.43	0.49	0.00149	0.00132	TIS (#Rgn029503)	TIS (NM_142971)	515	Fgpn0039361   Fba00345215
chr2R	17733502	17734002	11.45	11.94	0.49	0.00168	0.00145	TIS (#Rgn034266)	TIS (NM_00116912)	515	Fgpn0025808   Fba0011288
chr3L	15512053	15512553	10.52	11.01	0.49	0.00183	0.00155	exon (#Rgn0000565, exon 2 of 4)	exon (NM_206271, exon 2 of 4)	415	Fgpn0000565   Fba00180176
chr3R	29867066	29867566	11.79	12.28	0.49	0.00203	0.00185	paramoter-TSS (#Rgn039714)	paramoter-TSS (NM_170444)	452	Fgpn0033583   Fba00010888
chrX	91427768	91432768	11.69	12.19	0.49	0.00232	0.00246	exon (#Rgn000001, exon 2 of 3)	exon (NM_132931, exon 2 of 3)	526	Fgpn000001   Fba0011279
chr2L	19083988	19084488	11.52	12.01	0.49	0.00444	0.0032	exon (#Rgn003614, exon 1 of 5)	exon (NM_140580, exon 1 of 5)	456	Fgpn0034501   Fba0003220
chr2L	18831434	18831934	10.97	11.47	0.49	0.00548	0.00346	paramoter-TSS (#Rgn032125)	paramoter-TSS (NM_00125912)	526	Fgpn0015808   Fba0001109
chr3L	21633723	21634223	12.23	12.71	0.49	0.00698	0.00417	exon (#Rgn0037109, exon 2 of 4)	exon (NM_143084, exon 2 of 4)	473	Fgpn0037109   Fba0007864
chr3R	17671866	17672366	9.75	10.24	0.49	0.00732	0.00433	exon (#Rgn0000063, exon 2 of 4)	exon (NM_142887, exon 2 of 4)	846	Fgpn0000063   Fba0003478
chr3R	16456267	16456767	11.34	11.84	0.5	2.13E-06	7.80E-05	TIS (#Rgn038413)	TIS (NM_001043252)	466	Fgpn0038413   Fba0003129
chr2R	17569013	17569513	11.44	11.94	0.5	3.06E-06	0.000102	paramoter-TSS (#Rgn034243)	paramoter-TSS (NM_137388)	532	Fgpn0040249   Fba0006828
chr3R	10045008	10046008	11.61	12.11	0.5	3.50E-06	0.000113	paramoter-TSS (#Rgn037777)	paramoter-TSS (NM_141713)	385	Fgpn0037778   Fba0002173
chr2L	20925542	20926042	11.39	11.88	0.5	4.94E-06	0.000147	TIS (#Rgn029077)	TIS (NM_136234)	155	Fgpn0029077   Fba0001438
chr3R	14328922	14329422	11.55	12.05	0.5	5.10E-06	0.000145	TIS (#Rgn038224)	TIS (NM_162512)	292	Fgpn0038224   Fba0003233
chr3L	13236602	13237102	11.57	12.06	0.5	5.53E-06	0.000015	TIS (#Rgn036407)	TIS (NM_00114471)	460	Fgpn0036407   Fba0007965
chr2R	13593843	13594343	11.71	12.22	0.5	8.66E-06	0.000227	paramoter-TSS (#Rgn027581)	paramoter-TSS (NM_001274029)	450	Fgpn0038519   Fba00087623
chr2R	8168111	8168611	11.21	11.71	0.5	9.76E-06	0.000253	TIS (#Rgn021995)	TIS (NM_141713)	314	Fgpn0033273   Fba0008679
chr3L	20426982	20427482	11.35	11.85	0.5	2.82E-05	0.000064	TIS (#Rgn029888)	TIS (NM_140966)	492	Fgpn0026987   Fba0007832
chr3R	5606001	5606501	11.69	12.19	0.5	2.90E-05	0.000064	exon (#Rgn0261004, exon 2 of 3)	exon (NM_141300, exon 2 of 3)	282	Fgpn0261004   Fba0007843
chr3R	10043306	10043806	11.57	12.07	0.5	6.07E-05	0.000112	paramoter-TSS (#Rgn0033208)	paramoter-TSS (NM_001316573)	297	Fgpn0072574   Fba0002172
chr3L	19062658	19063158	11.37	11.87	0.5	7.19E-05	0.000129	exon (#Rgn0036846, exon 1 of 3)	exon (NM_079300, exon 1 of 3)	239	Fgpn0036846   Fba0007506
chr2R	12985752	12986252	11.63	12.13	0.5	0.000103	0.000172	paramoter-TSS (#Rgn033785)	paramoter-TSS (NM_176160)	533	Fgpn0033785   Fba0006783
chr2L	2717099	2717599	10.75	11.25	0.5	0.000134	0.000279	TIS (#Rgn068912)	TIS (NM_134667)	784	Fgpn0031238   Fba0007840
chr2L	2771774	2772274	12.38	12.88	0.5	0.000135	0.000279	paramoter-TSS (#Rgn0288255)	paramoter-TSS (NM_001127882)	211	Fgpn0034501   Fba0001804
chr2R	9712774	9713274	11.46	11.96	0.5	0.00048	0.00079	exon (#Rgn0010316, exon 1 of 3)	exon (NM_057400, exon 1 of 3)	405	Fgpn0010316   Fba0008469
chr3R	16433085	16433585	11.86	12.36	0.5	0.000686	0.000758	TIS (#Rgn051272)	TIS (NM_001170159)	338	Fgpn0038424   Fba00083286
chr3L	1731078	1731578	10.49	10.99	0.5	0.000801	0.00088	paramoter-TSS (#Rgn_167911)	paramoter-TSS (NM_167911)	221	Fgpn0027974   Fba0007728
chr3R	21130471	21130971	11.63	12.13	0.5	0.00106	0.00103	exon (#Rgn0038860, exon 1 of 1)	exon (NM_142689, exon 1 of 1)	506	Fgpn0038860   Fba0004015
chr3L	11065187	11065687	11.41	11.91	0.5	0.00116	0.00109	paramoter-TSS (#Rgn0052075)	paramoter-TSS (NM_140171)	447	Fgpn0025755   Fba0006203
chr2R	16287275	16287775	10.93	11.43	0.5	0.00118	0.0011	paramoter-TSS (#Rgn040079)	paramoter-TSS (NM_135939)	290	Fgpn0019949   Fba00034814
chr2L	14161465	14161965	11.68	12.18	0.5	0.00135	0.00122	paramoter-TSS (#Rgn033900)	paramoter-TSS (NM_137086)	286	Fgpn0033911   Fba0006750
chr2L	943050	9431000	10.25	10.75	0.5	0.0014	0.00126	paramoter-TSS (#Rgn023117)	paramoter-TSS (NM_080166)	302	Fgpn0032171   Fba00046223
chr2R	20618774	20619274	11.89	12.39	0.5	0.00128	0.00129	exon (#Rgn0038114)	exon (NM_164640)	399	Fgpn0034501   Fba0006225
chr3R	9401579	9402079	11.59	12.09	0.5	0.00279	0.00214	paramoter-TSS (#Rgn032686)	paramoter-TSS (NM_160977)	375	Fgpn0032671   Fba00062029
chrX	4319756	4320256	11.8	12.3	0.5	0.00323	0.00241	exon (#Rgn0266570, exon 2 of 2)	exon (NM_167007, exon 2 of 2)	560	Fgpn0266570   Fba00070648
chr3R	22042895	22043395	11.1	11.6	0.5	0.0033	0.00244	exon (NM_001170213, exon 2 of 9)	exon (NM_164449   Fba0008178)	959	Fgpn0026449   Fba0008178
chr2L	1048062	1048562	11.99	12.49	0.5	0.00348	0.00254	paramoter-TSS (#Rgn032259)	paramoter-TSS (NM_001038806)	410	Fgpn0032259   Fba00080038
chr2L	10427068	10427568	12.28	12.78	0.5	0.00366	0.00263	paramoter-TSS (#Rgn_00120181)	paramoter-TSS (NM_00120181)	332	Fgpn0267310   Fba00080021
chrX	16654426	16654926	12.01	12.51	0.5	0.00464	0.0031	paramoter-TSS (#Rgn003189)	paramoter-TSS (NM_078653)	339	Fgpn0030468   Fba00074736
chrX	21027902	21028402	11	11.5	0.5	0.00478	0.00316	TIS (NM_001144751)	TIS (NM_001144751)	209	Fgpn0031134   Fba00039633
chr3L	1546800	1546850	11.61	12.12	0.5	0.00495	0.00329	paramoter-TSS (#Rgn025213)	paramoter-TSS (NM_167894)	429	Fgpn0041381   Fba0007278
chr2R	17682113	17682613	11.17	11.67	0.5	0.00511	0.00311	exon (#Rgn0038114)	exon (NM_164640)	21	Fgpn0034501   Fba0008621
chr2L	6921813	6922313	10.7	11.2	0.5	0.00718	0.00427	intron (#Rgn0004838, intron 1 of 4)	intron (NM_164722, intron 1 of 4)	475	Fgpn0004838   Fba00091404
chr2R	10478058	10478558	10.31	10.81	0.5	0.00823	0.00473	TIS (#Rgn033528)	TIS (NM_136747)	259	Fgpn0261862   Fba00088307
chr2R	17444193	17444693	11.59	12.09	0.5	0.0087	0.00491	TIS (NM_176214)	TIS (NM_176214)	495	Fgpn0027516   Fba0006958
chr2R	959977	9600277	11.45	11.95	0.51	3.40E-06	0.000111	paramoter-TSS (#Rgn033467)	paramoter-TSS (NM_136694)	230	Fgpn0283501   Fba00039422
chr3R	5623641	5624141	11.03	11.54	0.51	4.81E-06	0.000146	paramoter-TSS (#Rgn0337351)	paramoter-TSS (NM_141303)	154	Fgpn0044823   Fba00028729
chr3R	22025026	22025526	11.09	11.61	0.51	5.28E-06	0.000155	TIS (#Rgn038923)	TIS (NM_142746)	430	Fgpn0038924   Fba0004186
chr3R	16650490	16650990	11.47	11.98	0.51						

ch2L	568439	568939	12.09	12.6	0.52	0.00659	0.0389	promoter-TSS #Bp0021874)	promoter-TSS #Bp_057946)	350	Fb00031266 Fb00078068
chrX	18402490	18409990	10.92	11.44	0.52	0.00802	0.0465	intron #Bp0057529, intron 1 of 9)	intron #Bp_206726, intron 1 of 9)	351	Fb00052594 Fb00074570
chr2L	16943230	16943730	10.88	11.41	0.53	0.00336	0.0239	TSS #Bp0036837)	TSS #Bp_134346	352	Fb00075043
chr3R	17373772	17374272	11.96	12.48	0.52	0.00841	0.048	TSS #Bp0037829)	TTS (NM_001120041)	410	Fb00073618 Fb00078720
chr2L	1740373	1740373	11.22	11.75	0.53	9.39E-07	3.93E-05	promoter-TSS #Bp00031450)	promoter-TSS (NM_164497)	371	Fb00001001 Fb00089249
chr3L	13966631	13967131	10.94	11.47	0.53	2.48E-06	8.66E-05	exon #Bp0263232, exon 2 of 5)	exon (NM_162566, exon 2 of 5)	167A	Fb00036389 Fb00075759
chrX	19605348	19605848	11.05	11.58	0.53	5.75E-06	0.000165	exon #Bp001037, exon 1 of 4)	exon (NM_167669, exon 1 of 5)	397	Fb0001037 Fb00074733
chr3L	1466574	14667074	11.49	12.03	0.53	9.25E-06	0.000242	TTS #Bp00411614)	TTS (NM_00014556)	400	Fb0000317 Fb00073127
chr3L	19845655	19845655	11.55	12.08	0.53	1.34E-05	0.000327	promoter-TSS #Bp00037444)	promoter-TSS (NM_079446)	349	Fb0005272 Fb00030108
chrX	16942262	16942762	11.87	12.4	0.53	2.64E-05	0.000569	promoter-TSS #Bp0030808)	promoter-TSS (NM_001042817)	156	Fb00030806 Fb00074417
chr2R	6015060	6015060	11.35	11.89	0.53	2.65E-05	0.000571	exon #Bp000004, exon 2 of 2)	exon (NM_078931, exon 2 of 2)	450	Fb0000043 Fb00086029
chr2R	17431148	17431648	11.37	11.9	0.53	0.000293	0.000625	5' UTR (NM_136673, exon 1 of 11)	5' UTR (NM_136673, exon 1 of 11)	375	Fb0002723 Fb00042929
chr2R	24767202	24767702	11.06	11.6	0.53	3.08E-05	0.000664	TTS #Bp0025860)	TTS (NM_166687)	259	Fb00027500 Fb00034296
chr3L	12193004	12193504	11.68	12.21	0.53	0.00012	0.00193	TTS #Bp000594)	TTS (NM_176323)	434	Fb00036313 Fb00031601
chr2R	22421070	22421570	11.5	12.04	0.53	0.00016	0.00248	promoter-TSS #Bp0034727)	promoter-TSS (NM_079087)	308	Fb00034728 Fb00036618
chr2L	13829887	13830387	11.79	12.32	0.53	0.00023	0.00333	promoter-TSS #Bp001961)	promoter-TSS (NM_165063)	401	Fb0005271 Fb00080543
chr3R	9015608	9015608	11.59	12.12	0.53	0.000237	0.00341	promoter-TSS #Bp007655)	promoter-TSS (NM_001370091)	413	Fb00037656 Fb00083967
chr3L	18819945	18820445	10.96	11.49	0.53	0.00039	0.00494	promoter-TSS #Bp0036815)	promoter-TSS (NM_168777)	480	Fb00036814 Fb00075084
chr2L	7222445	7222445	12.08	12.61	0.53	0.000527	0.00621	TTS #Bp0259111)	TTS (NM_00127254)	386	Fb00026313 Fb00037913
chrX	2704802	2705302	12.06	12.59	0.53	0.000554	0.00642	exon #Bp0024936, exon 3 of 5)	exon (NM_130664, exon 3 of 5)	412	Fb00004936 Fb00070479
chr2L	9750963	9751463	11.88	12.41	0.53	0.000576	0.00693	promoter-TSS #Bp00421214)	promoter-TSS (NM_137365)	367	Fb00034217 Fb00089317
chr3L	85901	859401	11.76	12.3	0.53	0.00109	0.0104	TTS #Bp0260755)	TTS (NM_138217)	467	Fb00026313 Fb00031253
chr2R	6613924	6614424	11.58	12.08	0.53	0.00122	0.0113	exon #Bp0086655, exon 2 of 7)	exon (NM_001103730, exon 2 of 7)	400	Fb00036728 Fb000301636
chr2R	10724558	10724958	11.19	11.72	0.53	0.00137	0.0124	promoter-TSS #Bp0263345)	promoter-TSS (NR_124506)	161	Fb00023144 Fb00082854
chr2L	13219080	13219580	11.58	12.11	0.53	0.00168	0.0145	promoter-TSS #Bp0032486)	promoter-TSS (NM_135773)	593	Fb00032485 Fb00080254
chr3R	29033410	29033910	12	12.53	0.53	0.00346	0.0254	promoter-TSS #Bp0027873)	promoter-TSS (NM_134301)	348	Fb00039265 Fb00085419
chr2L	1610735	1611235	11.37	11.91	0.53	0.00366	0.0263	promoter-TSS #Bp0031951)	promoter-TSS (NM_134765)	172	Fb00050195 Fb00079716
chr2R	9139167	9139667	10.55	11.08	0.53	0.00367	0.0269	exon #Bp0265313, exon 2 of 3)	5' UTR (NM_001299305, exon 2 of 3)	356	Fb00076531 Fb00034448
chr3R	25126967	25127467	11.24	11.74	0.53	0.00392	0.0277	promoter-TSS #Bp0259152)	promoter-TSS (NM_001170250)	142	Fb00038280 Fb0008482
chr3R	15837321	15837821	11.08	11.6	0.53	0.00507	0.0328	promoter-TSS #Bp0017567)	promoter-TSS (NM_079989)	355	Fb00032483 Fb00031813
chr2L	4882066	4882566	11.59	12.12	0.53	0.00597	0.0372	promoter-TSS #Bp0031643)	promoter-TSS (NM_135027)	791	Fb00000286 Fb00030488
chr3R	6629823	6630323	12.01	12.54	0.53	0.00724	0.0429	exon #Bp0005585, exon 3 of 4)	exon (NM_079569, exon 3 of 4)	728	Fb00000585 Fb000334618
chr2R	24786678	24787178	10.96	11.5	0.54	1.71E-06	6.45E-05	exon #Bp0041205, exon 2 of 6)	exon (NM_079132, exon 2 of 6)	443	Fb00041205 Fb00072428
chrX	496681	497181	11.47	12.01	0.54	2.89E-06	9.79E-05	TTS #Bp0022534)	TTS (NM_130490)	483	Fb00026313 Fb00034373
chr3L	18901669	18902169	11.73	12.27	0.54	3.01E-06	0.000101	promoter-TSS #Bp0036826)	promoter-TSS (NM_140814)	326	Fb00036827 Fb00075067
chr2L	7800638	7801138	11.17	11.71	0.54	3.17E-06	0.000105	promoter-TSS #Bp0031950)	promoter-TSS (NM_135300)	507	Fb00031951 Fb00030129
chr2R	13205559	13206059	11.38	11.92	0.54	3.90E-06	0.000124	promoter-TSS #Bp0038812)	promoter-TSS (NM_133006)	227	Fb00038813 Fb00087744
chr3R	17305148	17305648	11.24	11.78	0.54	0.00121	0.00814	exon #Bp0038865, exon 1 of 4)	exon (NM_142322)	727	Fb00038864 Fb00083374
chr3L	21317321	21317821	11.77	12.31	0.54	4.85E-05	0.00094	TTS #Bp0267234)	TTS (NR_125033)	472	Fb00032172 Fb00078405
chr3R	29933778	29934278	11.64	12.17	0.54	6.25E-05	0.00115	promoter-TSS #Bp0051040)	promoter-TSS (NM_134933)	342	Fb00026313 Fb000301256
chr3L	4826006	4826506	12.06	12.59	0.54	0.000131	0.00208	promoter-TSS #Bp0261797)	promoter-TSS (NM_168103)	404	Fb00027085 Fb000334618
chr2R	13509669	13510169	11.03	11.56	0.54	0.000161	0.00248	TTS #Bp0247556)	TTS (NM_001169673)	382	Fb00033846 Fb000301388
chr3R	8085066	8085566	11.17	11.71	0.54	0.000272	0.00377	exon #Bp0037633, exon 2 of 3)	exon (NM_141579, exon 1 of 2)	203	Fb00037633 Fb00081934
chr2R	8939142	8939642	11	11.55	0.54	0.000284	0.00388	exon #Bp0033354, exon 2 of 13)	exon (NM_136585, exon 2 of 13)	397	Fb0003354 Fb00080675
chr2R	8444632	8445132	10.32	10.86	0.54	0.00044	0.00541	exon #Bp0014463, exon 2 of 7)	exon (NM_084064)	117	Fb000262313 Fb000304480
chrX	11887458	11887958	11.99	12.53	0.54	0.000562	0.0065	promoter-TSS #Bp0030349)	promoter-TSS (NM_001272545)	472	Fb00040350 Fb00087350
chr3R	18301005	18301505	11.61	12.15	0.54	0.00052	0.00792	TTS #Bp0028602)	TTS (NM_142452)	423	Fb00028602 Fb00082594
chrX	19601255	19601755	11.89	12.43	0.54	0.00094	0.0094	exon #Bp0031036, exon 2 of 4)	exon (NM_134481, exon 2 of 4)	349	Fb00031016 Fb00070762
chr3R	28337137	28337637	10.68	11.22	0.54	0.00117	0.0109	promoter-TSS #Bp0261618)	promoter-TSS (NM_170365)	498	Fb0002773 Fb000347337
chr2R	6675204	6675704	11.55	12.08	0.54	0.00154	0.0136	promoter-TSS #Bp0033092)	promoter-TSS (NM_165844)	351	Fb00033092 Fb00080502
chr2R	20258031	20258531	11.29	11.84	0.54	0.00271	0.0209	promoter-TSS #Bp0025720)	promoter-TSS (NM_001274172)	289	Fb00034722 Fb00086272
chr2R	10820311	10820811	12.25	12.79	0.54	0.0043	0.0295	promoter-TSS #Bp0086898)	promoter-TSS (NM_165800)	404	Fb00029134 Fb00082824
chr2R	19496158	19496658	12.24	12.78	0.54	0.00456	0.0307	exon #Bp0261456, exon 1 of 2)	exon (NM_001274163, exon 1 of 2)	448	Fb000261456 Fb000331920
chrX	18099932	18100432	9.33	9.88	0.54	0.00512	0.033	promoter-TSS #Bp0030894)	promoter-TSS (NM_167602)	279	Fb00030894 Fb00030272
chr3R	6065268	6065768	10.24	10.78	0.54	0.00536	0.034	exon #Bp0038285, exon 4 of 4)	exon (NM_148232, exon 4 of 4)	76	Fb00038285 Fb00082882
chrX	10890154	10890654	9.69	10.23	0.54	0.00566	0.0356	exon #Bp0017561, exon 1 of 7)	5' UTR (NM_078557, exon 1 of 7)	416	Fb00017561 Fb00073404
chr2L	245546	246046	9.23	9.77	0.54	0.00759	0.0445	intron #Bp0266657, intron 1 of 16)	intron (NM_001258891, intron 1 of 16)	-2720	Fb00026252 Fb000304344
chrX	1557347	1557847	11.23	11.78	0.55	9.94E-07	4.10E-05	promoter-TSS #Bp0030658)	promoter-TSS (NM_132816)	405	Fb00030657 Fb00089270
chr2R	9093883	9094383	11.44	11.98	0.55	1.06E-06	4.33E-05	exon #Bp0033374, exon 2 of 3)	exon (NM_176109, exon 2 of 3)	521	Fb0003374 Fb00082832
chr2R	7924303	7924803	11.24	11.79	0.55	2.67E-06	9.17E-05	intron #Bp0033233, intron 2 of 3)	intron (NM_00129265, intron 2 of 3)	335	Fb00033233 Fb00082866
chr3R	18685927	18686427	11.8	12.35	0.55	2.66E-06	9.17E-05	promoter-TSS #Bp0051294)	promoter-TSS (NM_169826)	460	Fb0002794 Fb00038360
chr2R	14871627	14872127	10.86	11.41	0.55	5.29E-06	0.000155	promoter-TSS #Bp0264962)	promoter-TSS (NM_001169633)	390	Fb0003773 Fb00087450
chr3R	2713531	2714031	11.21	11.75	0.55	8.66E-06	0.00021	exon #Bp0034991)	exon (NM_164649)	150	Fb00034991 Fb00084930
chr3L	14163736	14164236	11.74	12.28	0.55	1.15E-05	0.000381	TTS #Bp0023947)	TTS (NM_001299215)	625	Fb00023947 Fb00039964
chrX	15984036	15984536	11.38	11.93	0.55	4.09E-05	0.000814	exon #Bp0030717, exon 3 of 4)	exon (NM_132858, exon 3 of 4)	515	Fb00030717 Fb00074134
chr3R	9555865	9556365	11.76	12.3	0.55	4.14E-05	0.00137	promoter-TSS #Bp0037708)	promoter-TSS (NM_141647)	313	Fb00037708 Fb00082067
chr2R	10124932	10125432	11.12	11.67	0.55	5.10E-05	0.000977	promoter-TSS #Bp0050011)	promoter-TSS (NM_165750)	313	Fb00020111 Fb00082959
chr3R	24161787	24162287	11.5	12.05	0.55	7.17E-05	0.00129	promoter-TSS #Bp0039157)	promoter-TSS (NM_001032017)	-313	Fb00039157 Fb00084551
chr3L	20226638	20227138	11.32	11.87	0.55	0.000135	0.00214	exon #Bp0260397, exon 2 of 4)	exon (NM_168235, exon 2 of 4)	508	Fb000260397 Fb00074825
chr3R	27929793	27930293	11.82	12.38	0.55	0.000178	0.0027	exon #Bp0027573, exon 3 of 8)	exon (NM_170359, exon 3 of 8)	419	Fb00027573 Fb0008251
chr3R	12691934	12692434	11.94	12.49	0.55	0.00021	0.00309	promoter-TSS #Bp0053955)	promoter-TSS (NM_080502)	413	Fb0003954 Fb00082664
chr2R	25686503	25687003	11.95	12.5	0.55	0.000244	0.00347	exon #Bp0036161, exon 2 of 5)	exon (NM_170236, exon 2 of 5)	384	Fb00036161 Fb00089121
chr2R	23063627	23064127	11.71	12.26	0.55	0.000784	0.00817	promoter-TSS #Bp0261361)	promoter-TSS (NM_131751)	142	Fb00039219 Fb00071984
chr2R	14852832	14853332	11.32	11.87	0.55	0.00101	0.00894	promoter-TSS #Bp0027783)	promoter-TSS (NM_137151)	142	Fb00028404 Fb00085748
chr3R	31805711	31806211	11.23	11.78	0.55	0.00136	0.0124	promoter-TSS #Bp0260755)	promoter-TSS (NM_143642)	283	Fb00039385 Fb000305131
chr2L	17496710	17497210	10.37								

chrX	19750986	19751496	11.08	11.69	0.57	0.008995	0.00975	5' UTR (NM_00127295, exon 1 of 8)	477	Hg0101069 FR00274795
chrX	16739878	16808832	10.57	11.13	0.57	0.00158	0.0138	intron (FBgn0036622, exon 2 of 4)	826	Hg0103622 FR0075422
chrX	2187087	2187587	10.7	11.27	0.57	0.00173	0.0148	promoter-TSS (FBgn0024984)	482	Hg01044584 FR0070392
chr2L	20084416	20084916	11.6	12.17	0.57	0.00184	0.0156	exon (NM_001273688, exon 1 of 2)	404	Hg01063773 FR0130560
chrX	8689514	8690014	11.58	12.15	0.57	0.00219	0.0161	promoter-TSS (FBgn0027864)	282	Hg0103057 FR0071225
chr3R	30783554	30784054	10.24	10.8	0.57	0.00211	0.0173	promoter-TSS (NM_125303)	159	Hg01066699 FR01034123
chr2L	20680299	20681429	11.42	12	0.57	0.00301	0.0228	exon (FBgn0032876, exon 1 of 1)	447	Hg01032876 FR0080140
chr2L	3037623	3038123	12.02	12.59	0.57	0.00351	0.0256	promoter-TSS (NM_001273053)	368	Hg01031498 FR008335478
chr2L	6051377	6051877	10.4	10.97	0.57	0.00382	0.0271	exon (FBgn0031769, exon 2 of 4)	789	Hg01031769 FR0079185
chr3L	14762301	14763301	8.8	9.37	0.57	0.00466	0.031	intron (FBgn0036446, exon 1 of 3)	109	Hg01026446 FR0072569
chr3R	10887776	10888276	10	10.57	0.57	0.00478	0.0316	exon (NM_001274918, exon 2 of 4)	1255	Hg01041094 FR0133170
chr3L	9539082	9539582	9.36	9.94	0.57	0.00606	0.0374	exon (FBgn0035392, exon 3 of 7)	674	Hg01029532 FR0072987
chr2R	12917919	12918419	10.05	10.62	0.57	0.00707	0.0422	5' UTR (NM_001033854, exon 2 of 4)	312	Hg01010488 FR0080787
chr2L	7027637	7028137	11.47	12.04	0.57	0.00771	0.045	promoter-TSS (FBgn0051908)	362	Hg01031881 FR0079389
chr2L	16039162	16039662	9.09	9.66	0.57	0.00794	0.0462	exon (FBgn0028644, exon 8 of 9)	2634	Hg01000182 FR0080803
chr2R	18850823	18851323	11.44	12.02	0.58	6.03e-07	2.69e-05	promoter-TSS (FBgn0034401)	230	Hg01026404 FR0080610
chr3L	9968474	9968974	10.96	11.54	0.58	6.15e-07	2.72e-05	promoter-TSS (NM_140119)	246	Hg01026404 FR0076347
chr2L	4883510	4884010	11.51	12.09	0.58	1.14e-06	4.56e-05	promoter-TSS (FBgn0000296)	363	Hg01031643 FR0077389
chr3L	1237595	1238095	11.4	11.98	0.58	1.26e-06	4.95e-05	exon (FBgn0036446, exon 2 of 2)	418	Hg01052100 FR0076506
chr3L	2373956	2374456	11.53	12.11	0.58	1.46e-06	5.64e-05	promoter-TSS (NM_1305335)	479	Hg01026404 FR0133170
chr2L	10229316	10229816	10.67	11.25	0.58	2.46e-06	8.61e-05	TTS (FBgn0058843)	610	Hg01029339 FR0079940
chr3L	21515408	21515908	10.76	11.34	0.58	1.16e-05	0.000294	promoter-TSS (FBgn0037093)	229	Hg01026371 FR0087837
chr2L	12027500	12028000	10.49	11.07	0.58	2.60e-05	0.000563	exon (FBgn0010497, exon 1 of 5)	313	5' UTR (NM_138760, exon 1 of 5)
chrX	7109448	7109948	10.99	11.57	0.58	2.82e-05	0.000604	exon (FBgn0027342, exon 2 of 4)	623	5' UTR (NM_167119, exon 2 of 4)
chr3L	1948711	1948811	11.47	12.05	0.58	2.91e-05	0.000614	exon (FBgn0002928, exon 1 of 4)	278	exon (NM_168799, exon 2 of 2)
chr3R	10144697	10145197	10.59	11.17	0.58	9.98e-05	0.00168	exon (FBgn0006255, exon 1 of 9)	550	5' UTR (NM_143815, exon 1 of 9)
chr2R	11899751	11900251	11.59	12.17	0.58	0.000118	0.00192	exon (FBgn0033605, exon 1 of 1)	405	exon (NM_136088, exon 1 of 1)
chr2L	1981225	1981725	11.47	12.05	0.58	0.000301	0.00404	promoter-TSS (FBgn0031377)	388	Hg01031378 FR0077814
chrX	1874083	1874583	12.02	12.59	0.58	0.000421	0.00522	promoter-TSS (FBgn0022517)	481	Hg01044133 FR0070311
chr2L	8522787	8523287	10.77	11.35	0.58	0.000457	0.00546	TTS (FBgn0030953)	265	Hg01016122 FR0079585
chr3L	11215639	11216139	9.98	10.56	0.58	0.00102	0.00995	exon (FBgn0025153, exon 1 of 7)	111	5' UTR (NM_001300099, exon 1 of 8)
chr3R	15351151	15351651	11.66	12.24	0.58	0.00117	0.0109	promoter-TSS (FBgn0026722)	341	promoter-TSS (NM_142133)
chr2R	9414594	9415094	11.33	11.91	0.58	0.00141	0.0126	exon (FBgn0041087, exon 1 of 6)	503	5' UTR (NM_080252, exon 1 of 6)
chr3R	10863829	10864329	10.44	11.02	0.58	0.00286	0.0219	promoter-TSS (FBgn0037846)	-551	promoter-TSS (NM_141772)
chr2R	17460302	17460802	9.52	10.1	0.58	0.00291	0.0221	promoter-TSS (FBgn0029933)	-45	promoter-TSS (NM_137370)
chr2R	6742865	6743365	9.43	10.01	0.58	0.00306	0.0231	exon (FBgn0028579, exon 4 of 8)	1217	exon (NM_136388, exon 4 of 8)
chr3R	9019134	9019634	12.06	12.64	0.58	0.00404	0.0282	TTS (FBgn0000932)	458	TTS (NM_109257)
chr2R	9478756	9479256	10.37	10.95	0.58	0.00476	0.0315	promoter-TSS (FBgn0009440)	624	promoter-TSS (NM_001169736)
chr2L	108947	108947	11.54	12.12	0.58	0.00506	0.0328	promoter-TSS (FBgn0002378)	228	promoter-TSS (NM_164832)
chrX	8895119	8895619	8.98	9.55	0.58	0.00517	0.0332	intron (FBgn0011661, exon 1 of 8)	1174	intron (NM_001272432, intron 1 of 8)
chrX	21043014	21043514	9.15	9.73	0.58	0.0053	0.0338	TTS (FBgn0026613)	195	TTS (NM_123913)
chr3L	18998900	19000300	11.38	11.97	0.58	5.73e-08	3.75e-08	TTS (FBgn0036039)	558	TTS (NM_140872)
chr3R	669621	669671	10.86	11.45	0.59	3.25e-07	1.64e-05	TTS (FBgn0026280)	229	TTS (NM_141419)
chr3R	17040948	17041448	11.67	12.26	0.59	5.94e-07	2.67e-05	promoter-TSS (NM_142332)	517	promoter-TSS (NM_142332)
chrX	9272333	9272833	11.66	12.26	0.59	1.24e-06	4.90e-05	promoter-TSS (FBgn0030122)	377	promoter-TSS (NM_132329)
chr2L	10270241	10270741	11.51	12.1	0.59	3.72e-06	0.00012	TTS (FBgn0032205)	441	TTS (NM_138522)
chr3R	15794549	15795049	11.06	11.65	0.59	4.63e-06	0.000142	intron (FBgn0026527, exon 1 of 8)	1018	intron (NM_001170151, intron 1 of 8)
chr2L	13782891	13783391	11.77	12.36	0.59	4.79e-06	0.000146	promoter-TSS (FBgn0028540)	453	promoter-TSS (NM_150255)
chrX	5375116	5375616	10.98	11.57	0.59	7.57e-06	0.000208	exon (FBgn0026256, exon 2 of 3)	2208	exon (NM_00127275, exon 2 of 3)
chrX	16271305	16271805	10.75	11.33	0.59	7.65e-06	0.000209	exon (FBgn0030731, exon 1 of 3)	152	exon (NM_132881, exon 2 of 3)
chr3R	29253830	29254330	10.41	11	0.59	2.51e-05	0.000549	intron (FBgn0016135, exon 1 of 1)	1245	intron (NM_001261317, intron 1 of 1)
chr2L	5235752	5236252	11.09	11.68	0.59	2.99e-05	0.000625	promoter-TSS (FBgn0026320)	-501	promoter-TSS (NM_124085)
chr2R	12880531	12881031	11.54	12.13	0.59	3.15e-05	0.000651	promoter-TSS (NM_165959)	350	promoter-TSS (NM_165959)
chr3R	13647828	13648328	11.06	11.65	0.59	4.92e-05	0.000954	promoter-TSS (FBgn0015778)	-743	promoter-TSS (NM_169531)
chr2R	11198823	11199323	10.5	11.09	0.59	0.000104	0.00172	intron (FBgn003396, exon 1 of 6)	798	intron (NM_134279, intron 1 of 6)
chr3R	5789344	5789844	11.28	11.87	0.59	0.00015	0.00234	promoter-TSS (FBgn0028900)	470	promoter-TSS (NM_141331)
chr3R	24582142	24582642	10.62	11.2	0.59	0.000288	0.00391	TTS (FBgn0039210)	482	TTS (NM_143015)
chr2R	9390269	9390769	11.56	12.15	0.59	0.000344	0.00464	exon (FBgn0020874)	294	exon (NM_136640)
chr3R	17545766	17546266	11.36	11.95	0.59	0.00099	0.00973	TTS (FBgn002571)	515	TTS (NM_079915)
chr2L	2769227	2769727	12	12.59	0.59	0.00111	0.0106	promoter-TSS (NM_001273035)	589	promoter-TSS (NM_001273035)
chr2L	19132507	19133007	11.86	12.45	0.59	0.0047	0.0312	promoter-TSS (FBgn0086443)	435	promoter-TSS (NM_001273632)
chr2L	16349154	16349654	8.89	9.48	0.59	0.00502	0.0326	exon (FBgn0003070, exon 2 of 2)	879	exon (NM_001273570, exon 2 of 2)
chrX	7969644	7970144	10.01	10.6	0.59	0.00595	0.0371	exon (FBgn0003447, exon 1 of 6)	192	5' UTR (NM_001162226, exon 1 of 6)
chr2R	25268998	25269498	8.23	8.82	0.59	0.0065	0.0396	Intergenic	13930	TAIR:JL:Jockey
chr3L	18627239	18627739	11.3	11.89	0.59	0.00877	0.0495	promoter-TSS (FBgn0031717)	298	promoter-TSS (NM_079416)
chr3R	9632267	9632767	10.99	11.58	0.6	1.08e-07	6.24e-06	TTS (FBgn0033334)	559	TTS (NM_109259)
chr2R	14877688	14878188	10.95	11.54	0.6	1.56e-07	8.77e-06	TTS (FBgn0033978)	153	TTS (NM_130154)
chr3R	11235216	11235716	11.09	11.67	0.6	3.02e-07	1.82e-05	exon (FBgn0033444)	304	exon (NM_169382)
chr2R	15931355	15931855	11.16	11.75	0.6	4.90e-07	2.28e-05	TTS (FBgn0018247)	194	TTS (NM_136183)
chr2R	10111204	10111704	10.83	11.43	0.6	1.08e-06	4.40e-05	exon (FBgn0003071, exon 1 of 8)	585	exon (NM_165747, exon 1 of 8)
chr3R	4381718	4382218	10.73	11.33	0.6	1.29e-05	0.000318	TTS (FBgn0037239)	663	TTS (NM_169434)
chr3L	10631372	10631872	11.51	12.11	0.6	1.71e-05	0.000402	promoter-TSS (FBgn00260643)	281	promoter-TSS (NM_001169941)
chr3L	16779039	16779539	11.34	11.94	0.6	1.71e-05	0.000402	promoter-TSS (FBgn0033661)	447	promoter-TSS (NM_168683)
chr2R	21482123	21482623	11.52	12.12	0.6	0.000256	0.00359	exon (FBgn0026269, exon 2 of 8)	447	exon (NM_079990, exon 2 of 8)
chr3L	4289079	4289579	10.83	11.43	0.6	0.000389	0.00494	TTS (NM_00116975)	385	TTS (NM_00116975)
chr2R	22940228	22940728	10.59	11.19	0.6	0.000885	0.00905	exon (FBgn0034904, exon 3 of 4)	319	exon (NM_001274217, exon 3 of 4)
chr3R	24253919	24254419	9.51	10.11	0.6	0.00122	0.0113	exon (FBgn0013225, exon 2 of 13)	468	exon (NM_001034649, exon 2 of 13)
chr3L	17534278	17534778	9.79	10.39	0.6	0.00138	0.0124	intron (FBgn0029174, intron 1 of 16)	278	intron (NM_206399, intron 1 of 16)
chr2R	12570599	12571099	10.51	11.11	0.6	0.00144	0.0128	exon (FBgn0003527, exon 2 of 4)	483	exon (NM_057404, exon 2 of 4)
chr2R	8892022	8892522	11.7	12.3	0.6	0.00156	0.0136	promoter-TSS (FBgn0033337)	441	promoter-TSS (NM_001273833)
chr3R	11742240	11742740	11.49	12.09	0.6	0.00162	0.014	promoter-TSS (FBgn0029906)	601	promoter-TSS (NM_079595)
chr4	1304415	1304415	9.13	9.73	0.6	0.00221	0.0179	Intergenic	72513	HEAT LINE Jockey
chr2R	13821258	13821758	9.35	9.95	0.6	0.00229	0.0185	exon (FBgn0000662, exon 3 of 5)	3045	exon (NM_166010, exon 3 of 5)
chr3R	5798288	5798788	11.88	12.48	0.6	0.00238	0.019	promoter-TSS (FBgn0037869)	331	promoter-TSS (NM_001170041)
chrX	2122297	2122797	10.19	10.79	0.6	0.00254	0.02	promoter-TSS (FBgn0004860)	759	promoter-TSS (NM_080055)
chr2R	11358051	11358551	9.91	10.5	0.6	0.00255	0.0235	promoter-TSS (FBgn0011987)	-691	TTS (NM_078973)
chr3L	2953380	2953880	11.02	11.62	0.6	0.00283	0.0249	exon (FBgn0006261, exon 2 of 2)	228	5' UTR (NM_0010410, exon 2 of 2)
chr3R	31581019	31581519	11.34	11.95	0.61	4.59e-09	4.62e-07	promoter-TSS (FBgn0043900)	316	promoter-TSS (NM_143615)
chr2L	7783070	7783570	11.							

chr2L	10857543	10858043	11.41	12.03	0.62	0.00416	0.0288	paramoter-TSS (HepG027363)	paramoter-TSS (NM_058100)	301	Fgpn024227 Fgpn080180
chr2R	23987938	23988438	10.53	11.15	0.62	0.00777	0.045	paramoter-TSS (HepG034990)	paramoter-TSS (NM_138070)	267	Fgpn0785050 Fgpn072203
chrX	11892890	11893590	12.1	12.71	0.63	0.00388	0.0275	paramoter-TSS (HepG02782)	paramoter-TSS (NM_138066)	419	Fgpn0785050 Fgpn072203
chr3L	11117650	11118150	10.17	10.79	0.62	0.00868	0.0491	exon (HepG0296134, exon 2 of 9)	exon (NM_168446, exon 2 of 9)	566	Fgpn036134 Fgpn0300785
chr3R	19447247	19447747	11.6	12.23	0.63	4.09E-08	2.91E-06	exon (HepG022395, exon 1 of 1)	exon (NM_140854, exon 1 of 1)	325	Fgpn023395 Fgpn047998
chr2R	12587015	12587515	10.31	10.94	0.63	4.69E-05	0.000916	intron (HepG022764, intron 1 of 11)	intron (NM_165916, intron 1 of 11)	1887	Fgpn022764 Fgpn030565
chrX	8101130	8101630	10.62	11.25	0.63	0.000101	0.0017	paramoter-TSS (HepG029997)	paramoter-TSS (NM_001298071)	74	Fgpn029997 Fgpn0340140
chr2L	275127	2752657	10.47	11.1	0.63	0.000151	0.00236	paramoter-TSS (HepG031453)	paramoter-TSS (NM_001273031)	37	Fgpn031453 Fgpn0335125
chr3L	21482519	21483019	11.18	11.81	0.63	0.000219	0.00318	paramoter-TSS (HepG005694)	paramoter-TSS (NM_1689004)	365	Fgpn030781 Fgpn0078399
chrX	9552439	9552939	10.14	10.77	0.63	0.000522	0.00617	exon (HepG029527, exon 2 of 2)	exon (NM_132339, exon 2 of 2)	998	Fgpn029527 Fgpn0341412
chr2L	9365424	9365924	11	11.63	0.63	0.000527	0.0062	paramoter-TSS (HepG035981)	paramoter-TSS (NM_140046)	277	Fgpn034395 Fgpn076499
chr2R	5987521	5988021	9.58	10.21	0.63	0.00113	0.0107	exon (HepG001914, exon 2 of 2)	exon (NM_057246, exon 2 of 2)	694	Fgpn001914 Fgpn032599
chrX	15845445	15845945	9.87	10.5	0.63	0.0019	0.016	exon (HepG030699, exon 3 of 7)	exon (NM_132954, exon 3 of 7)	1099	Fgpn030699 Fgpn0340116
chrX	6869281	6869781	11.91	12.54	0.63	0.00254	0.02	exon (HepG0212869, exon 2 of 4)	exon (NM_001222869, exon 2 of 4)	1024	Fgpn026993 Fgpn0330262
chr2R	9185416	9185916	11.26	11.89	0.63	0.00267	0.0207	exon (HepG029567, exon 2 of 5)	exon (NM_165666, exon 2 of 5)	676	Fgpn029567 Fgpn089932
chr2L	17385480	17385980	8.66	9.29	0.63	0.00291	0.0221	paramoter-TSS (HepG025053)	paramoter-TSS (NM_001273598)	415	Fgpn025053 Fgpn033451
chrX	20424662	20427063	11.6	12.24	0.63	0.00306	0.0231	TIS (HepG031115)	TIS (NM_167704)	229	Fgpn040650 Fgpn0340402
chr3L	19898509	19899009	8.27	8.9	0.63	0.00348	0.0254	intron (HepG014037, intron 1 of 4)	intron (NM_140898, intron 1 of 4)	2968	Fgpn0304139 Fgpn0340139
chr2R	12194975	12195475	11.25	11.88	0.63	0.00748	0.044	exon (HepG027504, exon 2 of 5)	exon (NM_001227984, exon 2 of 5)	681	Fgpn027504 Fgpn033063
chrX	9195717	9196217	11.14	11.77	0.64	1.98E-09	2.31E-07	TIS (HepG030100)	TIS (NM_167878)	447	Fgpn030100 Fgpn071399
chr3R	29583858	29588858	11.3	11.94	0.64	4.95E-09	4.85E-07	TIS (HepG005102)	exon (NM_142481, exon 2 of 2)	328	Fgpn005102 Fgpn089922
chr2L	21164125	21164625	11.79	12.44	0.64	2.44E-06	8.61E-05	paramoter-TSS (HepG026215)	paramoter-TSS (NR_124409)	104	Fgpn026215 Fgpn034876
chr3L	5812323	5812823	11.02	11.66	0.64	4.13E-06	0.00013	TIS (HepG009984)	TIS (NM_001014505)	520	Fgpn035640 Fgpn0077113
chr3R	9763910	9764410	11.36	12	0.64	5.08E-06	0.00015	exon (HepG027746, exon 2 of 4)	exon (NM_001170105, exon 2 of 4)	407	Fgpn027746 Fgpn0301870
chr3L	11070655	11071155	10.65	11.29	0.64	1.32E-05	0.000323	exon (HepG026341, exon 1 of 4)	exon (NM_176317, exon 1 of 4)	342	Fgpn026341 Fgpn076204
chr3R	18169579	18170079	10.06	10.69	0.64	0.000162	0.00251	exon (HepG024236, exon 2 of 9)	exon (NM_001144599, exon 2 of 9)	1052	Fgpn042639 Fgpn0305034
chrX	29248106	29248606	10.36	11	0.64	0.000278	0.00383	exon (HepG026323, exon 2 of 7)	exon (NM_170406, exon 2 of 7)	548	Fgpn026323 Fgpn0850400
chrX	653705	654205	11.22	11.86	0.64	0.00391	0.00494	exon (HepG025639, exon 2 of 3)	exon (NM_130497, exon 2 of 3)	983	Fgpn025639 Fgpn0308625
chr2R	26024589	26025089	10.82	11.46	0.64	0.000441	0.00541	5' UTR (NM_141387, exon 1 of 6)	5' UTR (NM_141387, exon 1 of 6)	260	Fgpn035996 Fgpn085319
chr3R	9627884	9628384	10.12	10.76	0.64	0.000593	0.00624	TIS (HepG005585)	TIS (NM_0295628)	814	Fgpn005585 Fgpn082077
chrX	18707513	18708013	10	10.63	0.64	0.000616	0.00699	exon (HepG005608, exon 2 of 3)	exon (NM_088940, exon 2 of 3)	836	Fgpn005608 Fgpn034115
chr2L	2121256	2121756	11	11.65	0.64	0.000624	0.00706	exon (HepG004540, exon 2 of 5)	exon (NM_080950, exon 2 of 5)	286	Fgpn004540 Fgpn070433
chrX	6997670	6998170	9.74	10.37	0.64	0.000838	0.00867	paramoter-TSS (HepG027108)	paramoter-TSS (NM_001169213)	210	Fgpn0264385 Fgpn0332262
chr2R	7548406	7548906	10.48	11.13	0.64	0.000954	0.00945	exon (HepG025895, exon 1 of 5)	exon (NM_080957, exon 1 of 5)	608	Fgpn025895 Fgpn089329
chr2L	8401404	8401904	11.58	12.23	0.64	0.00104	0.0101	paramoter-TSS (HepG026326)	paramoter-TSS (NR_124146)	430	Fgpn026326 Fgpn0344057
chr3R	9548329	9548829	9.07	9.71	0.64	0.00173	0.0148	paramoter-TSS (HepG031421)	paramoter-TSS (NM_001273998)	444	Fgpn031421 Fgpn0310031
chr2L	19791079	19791579	8.58	9.22	0.64	0.00259	0.0199	intron (HepG032922, intron 1 of 6)	intron (NM_136158, intron 1 of 6)	1553	Fgpn032922 Fgpn0332729
chrX	8904846	8905346	9.05	9.69	0.64	0.00264	0.0204	exon (HepG024302, exon 2 of 1)	exon (NM_001168194, exon 2 of 1)	1145	Fgpn024302 Fgpn0302661
chrX	3296546	3297046	7.79	8.43	0.64	0.00266	0.0207	intron (HepG020487, intron 5 of 15)	intron (NM_166969, intron 5 of 15)	1516	Fgpn020487 Fgpn070518
chrX	7681014	7681514	8.09	8.73	0.64	0.00315	0.0237	paramoter-TSS (HepG026225)	paramoter-TSS (NR_123832)	14	Fgpn026225 Fgpn0346397
chr2L	11112521	11113021	11.2	11.84	0.64	0.00319	0.0239	TIS (HepG036133)	TIS (NM_140182)	969	Fgpn036133 Fgpn0076229
chr3L	1463666	14602166	10.92	11.56	0.64	0.00351	0.0256	paramoter-TSS (HepG036406)	paramoter-TSS (NM_140433)	388	Fgpn026736 Fgpn0342956
chr2R	6502135	6502635	9.51	10.15	0.64	0.0036	0.0259	paramoter-TSS (HepG027444)	paramoter-TSS (NR_133106)	380	Fgpn027444 Fgpn0114365
chrX	5736261	5736761	9.1	9.74	0.64	0.00389	0.0275	intron (HepG005278, intron 1 of 5)	intron (NM_167045, intron 1 of 5)	1520	Fgpn005278 Fgpn070843
chr2L	13387902	13388402	8.47	9.11	0.64	0.0042	0.029	paramoter-TSS (HepG026104)	paramoter-TSS (NR_133117)	817	Fgpn026104 Fgpn0346709
chr3L	5901709	5902209	9.93	10.57	0.64	0.00432	0.0296	TIS (HepG009413)	TIS (NM_001104051)	497	Fgpn009413 Fgpn077080
chr2R	2202173	2202673	8.31	8.95	0.64	0.00435	0.031	exon (HepG002221)	exon (NM_001102255, exon 2 of 8)	543	Fgpn002221 Fgpn031444
chrX	12597193	12597693	9.66	10.31	0.64	0.00531	0.0338	exon (HepG005294, exon 2 of 13)	exon (NM_001103944, exon 2 of 13)	543	Fgpn005294 Fgpn0113445
chr3R	31794844	31795344	9.81	10.45	0.64	0.00756	0.0444	exon (HepG026206, exon 2 of 6)	exon (NM_080486, exon 2 of 6)	1114	Fgpn026206 Fgpn0858454
chr3L	18683354	18683854	11.65	12.29	0.65	2.13E-07	1.13E-05	TIS (HepG007820)	TIS (NM_168774)	457	Fgpn007820 Fgpn0345383
chr2L	19114712	19115212	10.56	11.21	0.65	4.58E-07	2.19E-05	TIS (HepG000075)	TIS (NM_165278)	562	Fgpn000075 Fgpn0811155
chr3R	5648858	5649358	10.41	11.06	0.65	3.82E-06	0.000122	exon (HepG027951, exon 1 of 11)	exon (NM_001144539, exon 1 of 11)	802	Fgpn027951 Fgpn0920206
chrX	699109	6991599	11.93	12.57	0.65	3.80E-05	0.000767	paramoter-TSS (HepG027108, exon 1 of 1)	paramoter-TSS (NM_001169213, exon 1 of 1)	688	Fgpn027108 Fgpn0301868
chr2L	19779872	19780372	11.26	11.92	0.65	4.52E-05	0.000887	paramoter-TSS (HepG005672)	paramoter-TSS (NM_134291)	422	Fgpn005672 Fgpn0812520
chr3L	1273669	1273719	9.8	10.46	0.65	0.000235	0.0039	exon (HepG026793, exon 2 of 2)	exon (NM_080935, exon 2 of 2)	692	Fgpn026793 Fgpn079592
chrX	451	451	11.5	12.15	0.65	0.000245	0.0038	paramoter-TSS (HepG024302)	paramoter-TSS (NM_001168194)	441	Fgpn024302 Fgpn071201
chr2R	2402284	2402334	11.7	12.35	0.65	0.00049	0.00531	paramoter-TSS (HepG034995)	paramoter-TSS (NM_166647)	540	Fgpn042959 Fgpn077162
chr2L	26462113	26462613	9.21	9.86	0.65	0.000917	0.00928	intron (HepG039340, intron 1 of 6)	intron (NM_143224, intron 1 of 6)	837	Fgpn039340 Fgpn0850515
chrX	8277733	8278233	10	10.65	0.65	0.00124	0.0114	5' UTR (NM_164805, exon 1 of 10)	5' UTR (NM_164805, exon 1 of 10)	219	Fgpn003502 Fgpn079618
chr2R	14619874	14620374	9.61	10.26	0.65	0.0014	0.0126	TIS (HepG010638)	TIS (NM_143780)	1396	Fgpn033948 Fgpn087500
chr2L	13550610	13551110	10.71	11.36	0.65	0.00185	0.0156	paramoter-TSS (HepG0053156)	paramoter-TSS (NM_176167)	590	Fgpn0053156 Fgpn087683
chrX	15744780	15745280	8.69	9.34	0.65	0.00349	0.0255	intron (HepG001382, intron 1 of 5)	intron (NM_165125, intron 1 of 5)	1296	Fgpn001382 Fgpn0344038
chrX	15046110	15046610	7.52	8.17	0.65	0.0037	0.0265	intron (HepG030683, intron 1 of 4)	intron (NM_206715, intron 1 of 4)	2267	Fgpn030683 Fgpn073959
chr3L	9376778	9377278	11.71	12.36	0.65	0.00524	0.0395	TIS (HepG009692)	TIS (NM_140074)	347	Fgpn009692 Fgpn076496
chr2R	2012258	2012308	10.72	11.37	0.65	0.00521	0.0394	exon (HepG002841)	exon (NM_001103944, exon 2 of 13)	317	Fgpn002841 Fgpn031444
chr3L	16098867	16099367	9.48	10.13	0.65	0.00576	0.0361	TIS (HepG026341)	TIS (NR_047974)	360	Fgpn026341 Fgpn0304346
chr2L	3353016	3353516	9.71	10.35	0.65	0.00653	0.0397	exon (HepG002045, exon 2 of 9)	exon (NM_205900, exon 2 of 9)	1563	Fgpn002045 Fgpn089979
chr3R	19158394	19158894	10.54	11.19	0.65	0.00698	0.0417	exon (HepG002962, exon 3 of 4)	exon (NM_057310, exon 3 of 4)	1234	Fgpn002962 Fgpn0831749
chr2L	223559	2236059	9.91	10.55	0.65	0.00729	0.0432	paramoter-TSS (HepG026494)	paramoter-TSS (NR_073696)	507	Fgpn026494 Fgpn0335158
chr3L	9694021	9694521	10.95	11.61	0.65	3.94E-09	4.10E-07	paramoter-TSS (HepG0266596)	paramoter-TSS (NR_124838)	186	Fgpn026630 Fgpn0345032
chr2R	5927784	5928284	10.84	11.51	0.66	1.12E-08	9.93E-07	paramoter-TSS (HepG003523)	paramoter-TSS (NM_001014568)	253	Fgpn003523 Fgpn091477
chr3R	21388313	21388813	10.66	11.32	0.66	4.15E-08	2.92E-06	paramoter-TSS (HepG036428)	paramoter-TSS (NM_099078)	178	Fgpn036427 Fgpn0071608
chr2R	23972508	23973008	11.11	11.77	0.66	2.10E-07	1.12E-05	TIS (HepG034946)	TIS (NM_166648)	328	Fgpn007291 Fgpn072756
chrX	1659846	1659896	11.67	12.33	0.66	2.88E-06	9.18E-05	exon (HepG001408, exon 2 of 2)	exon (NM_0792695, exon 2 of 2)	380	Fgpn001408 Fgpn074299
chr2L	12914565	12915065	11.79	11.84	0.66	3.20E-06	0.000105	intron (HepG001282, intron 1 of 3)	intron (NM_165961, intron 1 of 3)	802	Fgpn001282 Fgpn07786
chr3R	2793906	2793956	11.55	12.2	0.66	1.51E-05</					



chr3R	1522053	1522053	11.05	11.8	0.75	8.66E-06	0.00227	exon #Fg0000533, exon 2 of 3	exon #NM_079638, exon 2 of 3	5/5	Fg0000533   Fg0008308
chr2L	12028828	12029328	9.99	10.75	0.75	9.75E-06	0.00253	promoter-TSS (NM_164896)	promoter-TSS (NM_164896)	-567	Fg0003297   Fg0008309
chr2L	12098266	12098796	10.25	11	0.75	2.24E-05	5.00E-04	TTS (Fg00028270)	TTS (NM_001042890)	-709	Fg0003409   Fg0008310
chr3R	153191762	15329262	10.16	10.91	0.75	3.02E-05	0.0031	promoter-TSS (NM_1436318)	promoter-TSS (NM_1436318)	-790	Fg0003856   Fg0008311
chr3R	159164293	159164793	9.38	10.13	0.75	0.00014	0.00222	exon #Fg0261461, exon 2 of 6	exon #NM_001144749, exon 2 of 6	804	Fg0261461   Fg0299622
chr3R	17400240	17400740	10.14	10.89	0.75	0.000217	0.00317	intron (Fg0261461, exon 1 of 2)	ICCA[CCCA]Simple_repeat[Simple_re	906	Fg0261461   Fg0299622
chr2L	17440395	17448875	9.37	9.31	0.75	0.000012	0.00017	promoter-TSS (Fg0260632)	promoter-TSS (NM_001269330)	-415	Fg0260632   Fg0299622
chr3R	15893923	15894411	10.38	11.13	0.75	0.000717	0.00761	exon #Fg0260711, exon 2 of 3	exon #NM_001144749, exon 2 of 3	1735	Fg0260711   Fg0299622
chr3R	9281010	9281510	9.28	10.03	0.75	0.00447	0.0303	exon #Fg0260236, exon 3 of 9	exon #NM_144849, exon 3 of 9	1857	Fg0260236   Fg0299622
chr3R	2065330	2065830	11.31	12.07	0.75	6.65E-08	4.12E-06	promoter-TSS (Fg0262626)	promoter-TSS (NM_1300171)	126	Fg0262626   Fg0299622
chr3R	621761	622261	10.97	11.73	0.75	1.07E-07	6.24E-06	promoter-TSS (NM_130493)	promoter-TSS (NM_130493)	206	Fg0262626   Fg0299622
chr3R	8062184	8062684	9.95	10.72	0.75	1.05E-05	0.000271	intron (Fg0260467, intron 1 of 6)	promoter-TSS (NM_206674)	750	Fg0260467   Fg0299622
chr3R	20587192	20587692	10.49	11.25	0.75	1.44E-05	0.00035	promoter-TSS (Fg0267711)	promoter-TSS (NM_133425)	260	Fg0267711   Fg0299622
chr3R	22133745	22134245	10.03	10.79	0.75	1.45E-05	0.00035	TTS (Fg0262936)	TTS (NM_206540)	161	Fg0262936   Fg0299622
chr3R	15289997	15290497	9.62	10.38	0.75	0.000114	0.00186	promoter-TSS (NM_079636)	promoter-TSS (NM_079636)	52	Fg0262936   Fg0299622
chr3R	3447601	3448101	8.07	8.83	0.75	0.000211	0.00339	intron (Fg0262967, intron 2 of 6)	intron (NM_001272776, intron 2 of 6)	1092	Fg0262967   Fg0299622
chr2L	2584076	2584576	9.64	10.4	0.75	0.000258	0.00361	exon #Fg026479, exon 2 of 8	exon #NM_001273017, exon 2 of 8	1104	Fg026479   Fg0299622
chr2R	25262610	25263110	8.09	8.85	0.75	0.000267	0.00371	Intergenic	ICL1[LINE]Jockey	-7542	Fg0262610   Fg0299622
chr2R	12514615	12515115	10.07	10.83	0.75	0.000373	0.00479	promoter-TSS (Fg0003350)	promoter-TSS (NM_136949)	192	Fg0003370   Fg0299622
chr2R	17591098	17591598	11.43	12.19	0.75	0.000407	0.00509	promoter-TSS (Fg00034249)	promoter-TSS (NM_001274131)	357	Fg00034249   Fg0299622
chr3R	2146596	2147096	10.27	11.04	0.75	0.000891	0.00809	intron (Fg0004654, intron 2 of 2)	intron (NM_025712, intron 2 of 2)	1483	Fg0004654   Fg0299622
chr2R	12146652	12147152	9.49	10.25	0.75	0.000917	0.00828	exon #Fg0027504, exon 5 of 5	exon #NM_001273984, exon 5 of 5	1894	Fg0027504   Fg0299622
chr3R	16799231	16799731	9.95	10.72	0.75	0.00122	0.0113	exon #Fg0029791, exon 1 of 3	exon #NM_206768, exon 1 of 3	258	Fg0029791   Fg0299622
chr3R	9354806	9355306	9.09	9.86	0.75	0.00125	0.0115	5' UTR (NM_00103452, exon 2 of 10)	5' UTR (NM_00103452, exon 2 of 10)	1121	Fg0295476   Fg0299622
chr2R	17395514	17396014	8.8	9.56	0.75	0.00162	0.0141	intron (Fg0101067, intron 1 of 1)	intron (NM_079973, intron 1 of 1)	1172	Fg0101067   Fg0299622
chr3L	11396623	11397123	9.86	10.61	0.75	0.000868	0.00668	intron (Fg003614, intron 1 of 7)	intron (NM_001259125, intron 1 of 7)	620	Fg003614   Fg0299622
chr3L	8357616	8358116	9.22	9.99	0.75	0.00086	0.00887	exon #Fg001248, exon 2 of 2	exon #NM_001144749, exon 2 of 2	257	Fg001248   Fg0299622
chr3L	21173387	21173887	11.51	12.28	0.77	2.09E-11	4.68E-09	exon #Fg0270296, exon 1 of 1	exon #NM_206410, exon 1 of 1	506	Fg0270296   Fg0299622
chr2R	23994299	23994799	11.06	11.84	0.77	1.11E-09	1.47E-07	TTS (Fg00014545)	TTS (NM_001014545)	506	Fg00014545   Fg0299622
chr3R	16051946	16052446	10.21	10.99	0.77	6.28E-07	2.76E-05	exon #Fg027948, exon 2 of 15	exon #NM_001170156, exon 2 of 15	319	Fg027948   Fg0299622
chr2R	13952647	13953147	9.99	10.76	0.77	1.03E-05	0.00267	intron (Fg0026279, intron 3 of 7)	intron (NM_001259325, intron 3 of 7)	1128	Fg0026279   Fg0299622
chr3R	10265814	10266314	9.35	10.13	0.77	0.000113	0.00185	intron (Fg0262617, intron 1 of 11)	intron (NM_001260090, intron 1 of 11)	1129	Fg0262617   Fg0299622
chr3R	18747098	18747598	9.6	10.37	0.77	0.000176	0.00268	exon (Fg0260399, exon 2 of 6)	exon (NM_080121, exon 2 of 6)	929	Fg0260399   Fg0299622
chr3R	8419513	8420013	9.13	9.9	0.77	0.000192	0.00288	intron (Fg0261093, intron 1 of 9)	intron (NM_206654, intron 1 of 9)	1018	Fg0261093   Fg0299622
chr3L	2157080	2157580	9.37	10.64	0.77	0.000295	0.004	exon #Fg000485, exon 2 of 8	exon #NM_080203, exon 2 of 8	-3428	Fg000485   Fg0299622
chr2L	8161804	8162304	10.23	11	0.77	0.000414	0.00518	promoter-TSS (Fg0001614)	TTS (NM_125242)	264	Fg0001614   Fg0299622
chr3L	18626350	18626850	9.9	10.68	0.77	0.00077	0.00816	intron (Fg0036801, intron 1 of 8)	intron (NM_001275088, intron 1 of 8)	642	Fg0036801   Fg0299622
chr3R	15645441	15645941	9.61	10.38	0.77	0.000943	0.0094	intron (Fg0003721, intron 1 of 7)	intron (NM_001260191, intron 1 of 7)	395	Fg0003721   Fg0299622
chr3R	8142743	8143243	11.9	12.67	0.77	0.00159	0.0139	promoter-TSS (Fg00025800)	promoter-TSS (NM_078524)	612	Fg00025800   Fg0299622
chr3L	1964852	1965352	9.54	10.31	0.77	0.000362	0.006	promoter-TSS (NM_139424)	promoter-TSS (NM_139424)	634	Fg0003626   Fg0299622
chr2R	21456266	21456766	8.71	9.48	0.77	0.000661	0.004	promoter-TSS (Fg00010470)	promoter-TSS (NM_001299751)	-352	Fg0010470   Fg0299622
chr2L	12207149	12207649	8.2	8.97	0.77	0.000714	0.00424	promoter-TSS (NM_001030114)	promoter-TSS (NM_001030114)	-532	Fg0000114   Fg0299622
chr2L	6069884	6070384	11.17	11.95	0.78	9.44E-13	2.45E-10	promoter-TSS (NM_078766)	promoter-TSS (NM_078766)	512	Fg0001177   Fg0299622
chr3R	11821495	11821995	11.25	12.03	0.78	1.16E-09	1.48E-07	TTS (Fg00017956)	TTS (NM_00114265)	320	Fg00017956   Fg0299622
chr3L	11396623	11397123	9.86	10.61	0.78	2.36E-05	0.00035355	intron (Fg00025355)	intron (NM_139473, exon 1 of 5)	407	Fg00017956   Fg0299622
chr3R	29200641	29201141	11.54	12.32	0.78	2.45E-06	8.61E-05	TTS (Fg00039620)	TTS (NM_143425)	115	Fg00039620   Fg0299622
chr3R	6350886	6351386	9.94	10.72	0.78	5.43E-05	0.00103	intron (Fg0261955, intron 1 of 2)	intron (NM_132051, intron 1 of 2)	488	Fg0261955   Fg0299622
chr2L	6371603	6372103	9.32	10.1	0.78	7.66E-05	0.00135	promoter-TSS (Fg00043854)	promoter-TSS (NM_135176)	546	Fg00043854   Fg0299622
chr3R	25070142	25070642	10.71	11.38	0.78	8.55E-05	0.00147	promoter-TSS (NM_001170247)	promoter-TSS (NM_001170247)	434	Fg0003721   Fg0299622
chr3L	22724569	22725069	9.33	10.12	0.78	0.000185	0.00279	exon #Fg0262451, exon 2 of 5	5' UTR (NM_001100205, exon 2 of 5)	783	Fg0262451   Fg0299622
chr3L	9683125	9683625	11.58	12.37	0.78	0.000292	0.00396	exon (Fg0261617, exon 2 of 14)	5' UTR (NM_001201647, exon 2 of 14)	292	Fg0261617   Fg0299622
chr3L	11293716	11294216	10.82	11.6	0.78	0.000304	0.00408	exon #Fg0003152, exon 1 of 3	exon (NM_143020, exon 1 of 3)	820	Fg0003152   Fg0299622
chr3R	15804917	15805417	10.19	10.97	0.78	0.000396	0.00384	TTS (Fg00038665)	TTS (NM_142236)	228	Fg0003961   Fg0299622
chr3R	13013732	13014232	9.57	10.35	0.78	0.000318	0.00328	intron (Fg0260496, intron 1 of 5)	intron (NM_136491, intron 1 of 5)	234	Fg0260496   Fg0299622
chr3L	7156497	7156997	8.24	9.03	0.78	0.000367	0.00263	exon #Fg0259173, exon 1 of 8	5' UTR (NM_143193, exon 1 of 8)	376	Fg0259173   Fg0299622
chr3R	15856855	15857355	11.14	11.9	0.79	4.51E-11	8.66E-09	exon #Fg026734, exon 2 of 3	exon (NM_206734, exon 2 of 3)	328	Fg026734   Fg0299622
chr3R	2363070	2363570	10.73	11.52	0.79	2.46E-09	2.79E-07	exon #Fg0009673, exon 1 of 1	exon (NM_142884, exon 1 of 1)	248	Fg0009673   Fg0299622
chr3R	19657850	19658350	11.08	11.88	0.79	1.10E-08	9.80E-07	exon #Fg0005411, exon 2 of 5	exon (NM_057543, exon 2 of 5)	355	Fg0005411   Fg0299622
chr2R	23895284	23895784	10.77	11.56	0.79	4.34E-08	3.00E-06	promoter-TSS (Fg00034923)	promoter-TSS (NM_166629)	422	Fg00034924   Fg0299622
chr3R	18083713	18084213	10.38	11.17	0.79	4.41E-08	3.00E-06	intron (Fg0003890, intron 1 of 6)	CpG	1444	Fg0003890   Fg0299622
chr3R	25244418	25244918	10.19	10.99	0.79	2.34E-06	8.41E-05	exon #Fg0000158, exon 1 of 3	exon (NM_057452, exon 1 of 3)	389	Fg0000158   Fg0299622
chr3R	20166773	20167273	11.46	12.25	0.79	6.22E-06	0.000176	exon #Fg0018974, exon 2 of 4	exon (NM_139631, exon 2 of 4)	351	Fg0018974   Fg0299622
chr3R	10416236	10416736	9.75	10.54	0.79	0.000168	0.00149	exon #Fg001698, exon 1 of 2	exon (NM_001273935, exon 1 of 2)	631	Fg001698   Fg0299622
chr3L	12655108	12655608	9.61	10.4	0.79	1.54E-05	0.000368	intron (Fg0015024, intron 2 of 3)	promoter-TSS (NM_165145)	-373	Fg0015024   Fg0299622
chr2L	16043928	16044428	9.59	10.38	0.79	2.22E-05	0.000495	promoter-TSS (NM_00100182)	exon (NM_137428, exon 1 of 1)	896	Fg000182   Fg0299622
chr2R	17847294	17847794	11.28	12.07	0.79	3.75E-05	0.00076	exon #Fg0015522, exon 1 of 1	exon (NM_137428, exon 1 of 1)	896	Fg0015522   Fg0299622
chr3R	20582222	20582722	11.01	11.79	0.79	5.01E-05	0.000967	promoter-TSS (NM_123969)	promoter-TSS (NM_123969)	-754	Fg0267022   Fg0299622
chr3R	5255582	5256082	9.18	9.97	0.79	6.19E-05	0.00114	TTS (Fg00037804)	TTS (NM_141265)	846	Fg00037805   Fg0299622
chr2L	1156937	1157437	10	10.78	0.79	7.49E-05	0.00133	promoter-TSS (Fg0261458)	promoter-TSS (NM_001038781)	879	Fg0261458   Fg0299622
chr3R	5880787	5881287	10.02	10.81	0.79	7.94E-05	0.00139	exon (Fg00029820, exon 2 of 6)	intron (NM_137074, intron 2 of 6)	1297	Fg00029820   Fg0299622
chr2L	19574180	19574680	9.3	10.09	0.79	8.17E-05	0.00142	intron (Fg0005672, intron 1 of 2)	intron (NM_134291, intron 1 of 2)	275	Fg0005672   Fg0299622
chr3R	12806903	12807403	9.96	10.75	0.79	0.000201	0.00149	exon #Fg0262714, exon 2 of 10	exon (NM_168519, exon 2 of 10)	1008	Fg0262714   Fg0299622
chr3L	30013316	30013816	8.87	9.66	0.79	0.000209	0.00143	intron (Fg0005737, intron 1 of 3)	CpG	1589	Fg0005737   Fg0299622
chr3L	222232	222282	9.39	10.18	0.79	0.000691	0.00759	exon (NM_138171, exon 2 of 9)	exon (NM_138171, exon 2 of 9)	592	Fg0005113   Fg0299622
chr2R	1471673	1471723	9.44	10.23	0.79	0.00					

chr3L	15162476	15162976	10.06	10.91	0.84	2.42E-07	1.26E-05	T1S (NM_140500)	902	IRp0036489	IRp0075646
chr2R	2551130	2551630	10.6	11.44	0.84	1.24E-05	0.003099	exon (NM_001104447, exon 2 of 3)	1138	IRp0035766	IRp0084768
chrX	18566494	18566994	10.08	10.92	0.84	2.25E-05	0.000501	T1S (IRp0025246)	439	IRp0265958	IRp0340365
chr2R	18407821	18408321	9.83	10.67	0.84	3.41E-05	0.000701	promoter-TSS (NM_366279)	238	IRp0036492	IRp0086676
chr2R	11614930	11615430	9.76	10.59	0.84	6.25E-05	0.000115	intron (IRp0032366, intron 1 of 16)	865	IRp0032366	IRp0080891
chr3L	16039381	16039881	8.91	9.75	0.84	0.000102	0.000721	intron (NM_001274988, intron 1 of 2)	1661	IRp0266265	IRp0075501
chrX	8151641	8152141	10.25	11.1	0.84	0.000304	0.023	exon (IRp0030011, exon 1 of 3)	384	IRp0030011	IRp0071189
chr2L	6481870	6482370	10.79	11.64	0.85	4.81E-11	9.04E-09	exon (IRp0031810, exon 2 of 4)	1390	IRp0267010	IRp0345975
chr2R	16692226	16692726	10.66	11.51	0.85	1.49E-07	1.24E-05	exon (NM_057763, exon 2 of 3)	776	IRp0131631	IRp0087111
chrX	5905635	5906135	10.38	11.23	0.85	9.18E-07	3.88E-05	promoter-TSS (NM_025822)	4	IRp0025821	IRp0070284
chr3L	24530504	24535504	8.63	9.48	0.85	0.000107	0.00208	exon (IRp0040045, exon 2 of 2)	1215	IRp0040045	IRp0307117
chr3L	1121452	1121952	10.34	10.99	0.85	0.000227	0.0033	promoter-TSS (NM_368443)	856	IRp0036495	IRp0076211
chr2R	18397116	18397616	8.55	9.4	0.85	0.000297	0.00401	exon (IRp0063499, exon 1 of 1)	160	IRp0063499	IRp0086726
chr2R	29766889	29767389	9.02	9.87	0.85	0.000428	0.00528	exon (IRp0010297, exon 1 of 3)	1145	IRp0010297	IRp0099988
chrX	19781974	19782474	11.4	12.25	0.85	0.000458	0.00557	exon (NM_167685, exon 2 of 2)	919	IRp0259789	IRp0345014
chr2L	3630814	3631314	9.41	10.26	0.85	0.000502	0.00601	intron (IRp0000721, intron 1 of 7)	1090	IRp0000721	IRp0089306
chr2R	1477870	1478370	11.98	12.79	0.85	0.000528	0.00634	exon (NM_0010979, exon 4 of 11)	1262	IRp0010979	IRp0304366
chr2R	18128533	18129033	9.86	10.7	0.85	0.000981	0.00967	T1S (NM_180274)	790	IRp0040665	IRp0086739
chr2R	9293515	9294015	9.98	10.85	0.86	1.63E-07	9.06E-06	intron (IRp0002840, intron 1 of 2)	157	IRp0002840	IRp0339998
chrX	49231	492731	11.46	12.32	0.86	1.31E-05	0.000322	exon (NM_166844, exon 2 of 2)	542	IRp0025251	IRp0070091
chr3R	15198453	15198953	9.39	10.25	0.86	1.80E-05	0.000417	intron (NM_00117045, intron 1 of 5)	1762	IRp0266959	IRp0301102
chrX	16067455	16067955	7.06	7.92	0.86	2.71E-05	0.000582	exon (IRp0030269, exon 5 of 9)	3968	IRp0030269	IRp0074206
chrUn_D5484009.1	1823	2323	8.85	9.71	0.86	0.000531	0.00623	NA	642	IRp0005176	IRp0070091
chr2R	13556794	13557294	10.22	11.08	0.86	0.000444	0.00528	T1S (IRp0263459)	NA	IRp0083006	IRp0131500
chrX	1477870	1478370	11.98	12.79	0.86	0.000528	0.00634	promoter-TSS (NM_166808)	631	IRp0025251	IRp0070091
chrX	2727831	2727831	10.35	11.02	0.87	1.60E-07	8.95E-06	promoter-TSS (NM_343295)	892	IRp0027441	IRp0085175
chrX	8713710	8714210	10.88	11.75	0.87	4.93E-06	0.000447	promoter-TSS (IRp0030061)	213	IRp0030061	IRp0339260
chr3R	11195144	11195644	7.16	8.03	0.87	1.78E-05	0.000414	promoter-TSS (IRp0033787)	697	IRp0033787	IRp0082341
chr2L	8410850	8411350	10.4	11.26	0.87	3.73E-05	0.000757	exon (IRp0014417, exon 2 of 2)	508	IRp0014417	IRp0331991
chr3R	12373064	12373564	9.32	10.2	0.87	5.90E-05	0.0011	promoter-TSS (NM_0010040)	247	IRp0010039	IRp0082570
chrX	7138306	7138836	9.08	9.94	0.87	0.000119	0.00192	intron (NM_132315, intron 1 of 4)	564	IRp0029939	IRp0338215
chrX	2104635	21044135	9.4	10.28	0.87	0.000314	0.0037	exon (IRp002814, exon 2 of 2)	139	IRp0265631	IRp0340439
chrX	2052627	2052527	9.52	10.4	0.87	0.000357	0.0043	exon (IRp0015789, exon 2 of 4)	199	IRp0015789	IRp0073755
chr3L	1477870	1478370	11.98	12.79	0.88	3.56E-11	8.50E-10	5' UTR (NM_138264, exon 1 of 1)	1799	IRp0027854	IRp0332625
chr3L	3162507	3163007	11.27	12.15	0.88	4.31E-07	2.08E-05	T1S (NM_167991)	578	IRp0241934	IRp0073029
chr2R	11853385	11853885	9.86	10.74	0.88	4.99E-07	2.28E-05	exon (IRp0031574, exon 2 of 5)	1019	IRp0013156	IRp0080333
chrX	13717259	13717759	10.26	11.14	0.88	7.24E-06	0.000201	exon (IRp0267276, exon 15 of 15)	776	IRp0030512	IRp0072844
chrX	468935	468435	8.75	9.63	0.88	1.09E-05	0.000279	exon (IRp0010019, exon 1 of 1)	150	IRp0010019	IRp0070099
chr3R	29040851	29041351	9.88	10.76	0.88	7.11E-05	0.00128	exon (IRp0003093, exon 2 of 11)	1272	IRp0003093	IRp0339150
chrX	15708559	15709059	10.55	11.43	0.88	0.000215	0.00314	exon (IRp0030672, exon 2 of 5)	295	IRp0036498	IRp0074057
chr3R	31808020	31808520	9.72	10.6	0.88	0.000999	0.0105	exon (IRp0033982, exon 2 of 2)	1916	IRp0033982	IRp0082522
chrX	22533834	22538334	8.94	9.82	0.88	0.004463	0.031	exon (IRp0018194, exon 2 of 3)	1480	IRp0018194	IRp0332786
chr2R	12138682	12139182	10.55	11.43	0.88	7.78E-13	2.15E-10	T1S (NM_136285)	146	IRp0033883	IRp0082582
chrX	16656232	16656732	10.33	11.22	0.89	1.07E-10	1.85E-08	exon (IRp0001189, exon 2 of 8)	392	IRp0001189	IRp0340155
chr3R	24231688	24232188	11.51	12.4	0.89	7.46E-10	1.03E-07	promoter-TSS (IRp0266744)	-574	IRp0266744	IRp0345246
chr3L	1473790	1474290	8.36	9.25	0.89	2.53E-05	0.000551	exon (IRp0267487, exon 3 of 8)	1217	IRp0267487	IRp0340161
chr2L	2749623	2750123	11.01	11.89	0.89	0.000209	0.00308	promoter-TSS (NM_001273030)	274	IRp0250606	IRp0330726
chr2R	25281169	25281669	10.03	10.93	0.89	0.000382	0.00487	Intergenic	26101	IRp0035094	IRp0333172
chr3L	11884472	11889472	9.07	9.95	0.89	0.000203	0.00169	intron (IRp0036191, intron 1 of 5)	1743	IRp0036191	IRp0273362
chr3R	24627304	24627804	9.97	10.86	0.89	0.00024	0.00191	exon (IRp0046685, exon 3 of 3)	1884	IRp0046685	IRp0082636
chr2L	4183850	4184350	8.73	9.62	0.89	0.0004	0.005	Intergenic	1300	IRp0264866	IRp0334786
chr3L	9715688	9716188	10.24	11.12	0.89	0.000343	0.00251	promoter-TSS (IR_002482)	-864	IRp0060081	IRp0091797
chr3L	7591537	7592037	8.84	9.73	0.89	0.000517	0.0032	promoter-TSS (IR_0018500)	-789	IRp0035800	IRp0076524
chr3R	29675872	29676372	10.67	11.57	0.89	1.14E-10	1.93E-08	promoter-TSS (IRp0025457)	472	IRp0035800	IRp0085452
chr2R	16582939	16583439	10.34	11.24	0.9	6.62E-09	6.42E-07	non-coding (NR_124546, exon 1 of 1)	180	IRp0265295	IRp0340074
chr3L	15140142	15140642	9.41	10.31	0.9	3.34E-06	0.000109	intron (NM_001300142, intron 1 of 1)	-1738	IRp0265295	IRp0345844
chr3L	682998	683498	9.6	10.5	0.9	8.25E-06	0.000221	promoter-TSS (IRp0035152)	-728	IRp0035152	IRp0333378
chr3R	9764773	9765273	9.26	10.16	0.9	1.26E-05	0.000183	exon (IRp0036043, intron 1 of 12)	1480	IRp0036043	IRp0076138
chr4	1202084	1202584	7.68	8.58	0.9	0.000396	0.027	HEA1 LINE Jockey	70452	IRp0052853	IRp0016360
chr2R	18591830	18592330	9.85	10.76	0.91	1.18E-06	4.69E-05	T1S (NM_0013829)	1054	IRp0013829	IRp0292922
chr3R	6049920	6050420	10.27	11.18	0.91	1.51E-06	5.78E-05	promoter-TSS (NM_364679)	-629	IRp0031269	IRp0346135
chrX	18844328	18844828	9.93	10.84	0.91	2.94E-06	9.91E-05	exon (IRp0085451, exon 2 of 5)	916	IRp0085451	IRp0330440
chrX	7284612	7285112	9.51	10.42	0.91	2.98E-06	9.99E-05	promoter-TSS (NM_00129941)	15	IRp0029941	IRp0339819
chr2L	21308406	21308906	11.06	11.97	0.91	4.48E-06	0.000139	exon (IRp0032940, exon 2 of 12)	833	IRp0032940	IRp0301461
chrX	14869974	14874974	9.17	10.09	0.91	0.000176	0.00268	T1S (NM_206739)	500	IRp0030981	IRp0073948
chr2R	18613835	18614335	10.39	11.09	0.91	0.000356	0.00458	promoter-TSS (IRp0034362)	933	IRp0034362	IRp0086739
chr2R	11338141	11338641	11.11	11.96	0.91	1.04E-10	1.24E-08	intron (IRp0030851)	112	IRp0030851	IRp0073140
chr3L	3811858	3812358	10.11	11.03	0.92	3.54E-09	3.72E-07	promoter-TSS (IRp0052263)	846	IRp0052263	IRp0073140
chr2L	5005351	5005851	10.89	11.85	0.92	1.15E-08	1.00E-06	promoter-TSS (NM_00116940)	-673	IRp0051113	IRp0070400
chr2L	15050502	15055502	9.27	10.19	0.92	2.50E-06	8.70E-05	exon (IRp0024183, exon 3 of 4)	2726	IRp0024183	IRp0080721
chrX	12908340	12908840	10.2	11.12	0.92	1.48E-05	0.000356	T1S (IRp0030433)	1032	IRp0030433	IRp0073629
chr3L	11821058	11821558	9.89	10.82	0.92	7.51E-05	0.00133	exon (IRp0030212, exon 2 of 2)	897	IRp0030212	IRp0302136
chr3R	2305651	23053151	9.19	10.12	0.92	0.000111	0.00184	promoter-TSS (NM_133432)	-14	IRp0267258	IRp0347322
chr3R	3866226	3866726	8.75	9.67	0.92	0.000155	0.00241	intron (IRp026575, intron 3 of 5)	241	IRp026575	IRp0340205
chr3R	13823889	13824389	7.98	8.91	0.92	0.000205	0.00259	intron (IRp0052676, intron 1 of 8)	2227	IRp0052676	IRp0309745
chrX	15885422	15885922	10.89	11.86	0.93	1.06E-09	1.42E-07	exon (IRp0269398, exon 2 of 14)	1639	IRp00127652	IRp0310065
chrX	7987992	7988492	10.37	11.3	0.93	9.24E-08	5.63E-06	promoter-TSS (NM_365383)	-719	IRp0037271	IRp0088860
chr3L	15100260	15100760	8.81	9.74	0.93	4.87E-06	0.000147	exon (IRp0264703, exon 2 of 2)	-1008	IRp0264704	IRp0339388
chr2L	19436667	19441667	8.9	9.83	0.93	8.08E-06	0.000219	promoter-TSS (IRp0032783)	-951	IRp0032783	IRp0081209
chr3R	18411364	18411864	8.66	9.6	0.93	2.31E-05	0.00051	promoter-TSS (IRp0038621)	17	IRp0038621	IRp0083654
chr3L	15556674	15557174	7.41	8.34	0.93	3.44E-05	0.000705	exon (IRp0087035, exon 1 of 6)	102	IRp0087035	IRp0331933
chr2R	10357576	10358076	11.23	12.16	0.93	3.85E-05	0.000775	exon (IRp0265512, exon 1 of 3)	758	IRp0265512	IRp0339194
chrX	14507	15007	7.54	8.47	0.93	0.000207	0.00259	NA	NA	IRp0029571	IRp0080594
chrX	7248734	7249234	9.59								

chrX	3074350	3074850	8.13	9.13	1	1.77E-06	6.64E-05	intron (Rg0028369, intron 7 of 12)	intron (NM_080320, intron 7 of 12)	-7038	[Rg0029649] [Rf00107561]
chr3R	9545830	9346330	8.85	9.85	1	1.87E-06	6.96E-05	intron (Rg0026410, intron 2 of 5)	intron (NM_001300317, intron 2 of 5)	6214	[Rg0026410] [Rf00107561]
chrX	15813903	15814403	9.53	10.54	1	4.04E-05	0.000806	5' UTR (NM_001039522, exon 3 of 12)	5' UTR (NM_001039522, exon 3 of 12)	4201	[Rg001039522] [Rf001039522]
chr2L	16824161	16824616	9.69	10.69	1.01	3.44E-06	0.00012	intron (Rg0022213, exon 2 of 7)	intron (NM_078864, exon 2 of 7)	2847	[Rg0022213] [Rf001080930]
chr3L	21881613	21882113	7.51	8.52	1.01	0.00406	0.0283	intron (Rg0027677, intron 1 of 9)	intron (NM_001299949, intron 1 of 9)	2287	[Rg0027677] [Rf001080930]
chr3R	30598976	30599476	10	11.02	1.02	2.65E-08	2.01E-05	intron (Rg0035129, exon 4 of 4)	intron (NM_370512, exon 4 of 4)	1197	[Rg0035129] [Rf001080930]
chr3L	11490065	11490565	7.84	8.86	1.02	1.23E-05	8.86E-05	intron (Rg0036365, intron 1 of 3)	intron (NM_1400213, intron 1 of 3)	2186	[Rg0036365] [Rf001076091]
chr3L	3908183	3908683	9.42	10.44	1.02	0.000641	0.00725	TTS (Rg0041147)	TTS (NM_139585)	1159	[Rg0041147] [Rf001076176]
chr2L	4977718	4978218	10.6	11.62	1.03	4.48E-19	3.60E-16	promoter-TSS (Rg0031661)	promoter-TSS (NM_135044)	-657	[Rg0031661] [Rf001078977]
chr3L	1330766	1331266	9.67	10.7	1.03	3.67E-07	1.82E-05	promoter-TSS (NM_138250)	promoter-TSS (NM_138250)	777	[Rg0032097] [Rf001076278]
chrX	12762762	12763262	10.62	11.65	1.03	8.65E-06	0.000227	exon (Rg0030420, exon 1 of 1)	exon (NM_132599, exon 1 of 1)	549	[Rg0030420] [Rf001076278]
chr2L	16690845	16691345	9.09	10.12	1.03	1.72E-05	0.000404	exon (Rg0026127, exon 2 of 7)	exon (NM_165172, exon 2 of 7)	4928	[Rg0026127] [Rf00100459]
chr3R	8347697	8348197	10.07	11.1	1.03	5.49E-05	0.00104	TTS (Rg0032580)	TTS (NM_169218)	229	[Rg0032581] [Rf001081842]
chr3L	2638877	2639377	9.79	10.83	1.04	1.80E-08	1.47E-06	exon (Rg0030535, exon 2 of 7)	5' UTR (NM_001144403, exon 3 of 8)	223	[Rg0030535] [Rf001078977]
chrX	3968984	3969484	10.07	11.11	1.04	4.83E-08	3.22E-06	promoter-TSS (Rg0029689)	promoter-TSS (NM_130792)	202	[Rg0029689] [Rf001076091]
chr2R	1885219	1885719	10.6	11.64	1.04	1.51E-06	5.78E-05	TTS (Rg0024402)	TTS (NM_132529)	255	[Rg0024402] [Rf001076278]
chr3L	1695695	1695745	8.2	9.24	1.04	4.42E-06	0.000138	promoter-TSS (NM_001104159)	promoter-TSS (NM_001104159)	-653	[Rg0010182] [Rf001076278]
chr2L	10977804	10978304	9.94	10.98	1.04	3.35E-05	0.000689	exon (Rg00104781, exon 2 of 5)	exon (NM_001273440, exon 2 of 5)	1283	[Rg00104781] [Rf001080148]
chr3L	19634087	19634587	9.39	10.44	1.05	2.86E-08	2.20E-06	exon (Rg0036366, exon 2 of 8)	exon (NM_176363, exon 2 of 8)	1241	[Rg0036366] [Rf001080148]
chr2L	2288372	2288422	7.43	8.48	1.05	4.73E-07	2.22E-05	intron (Rg0000384, intron 1 of 5)	intron (NM_00127367, intron 1 of 5)	2160	[Rg0000384] [Rf00111326]
chr2R	15479517	15480017	8.97	10.02	1.05	7.13E-06	0.000199	intron (Rg0034021, intron 1 of 4)	intron (NM_001299525, intron 1 of 4)	3067	[Rg0034021] [Rf001034539]
chr2L	21830910	21830960	7.2	8.25	1.05	3.51E-05	0.000715	intron (Rg0003866, intron 1 of 2)	intron (NM_078891, intron 1 of 2)	684	[Rg0003866] [Rf001080930]
chr2R	21314277	21314777	8.73	9.78	1.05	0.000255	0.00359	intron (Rg0034613, exon 2 of 8)	exon (NM_001169764, exon 2 of 8)	1546	[Rg0034613] [Rf001076101]
chr2L	18853009	18853509	10.04	11.1	1.06	8.85E-08	6.13E-06	promoter-TSS (Rg0032723)	promoter-TSS (NM_145269)	680	[Rg0032723] [Rf001080148]
chr2L	2976277	2976777	11.22	12.28	1.06	1.86E-07	1.02E-05	promoter-TSS (Rg0023494)	promoter-TSS (NM_134858)	325	[Rg0023494] [Rf001076176]
chr2L	18967104	18967604	9.46	10.52	1.06	1.99E-07	1.08E-05	intron (Rg0015772, intron 1 of 6)	intron (NM_001291146, intron 1 of 6)	1367	[Rg0015772] [Rf001081189]
chr3L	7361658	7362158	10.28	11.35	1.06	4.08E-06	0.000129	exon (Rg0027485, exon 1 of 1)	exon (NM_139854, exon 2 of 4)	1348	[Rg0027485] [Rf001076847]
chr3L	14415323	14415823	9.14	10.2	1.06	1.66E-05	0.000939	exon (Rg0008700, exon 3 of 7)	exon (NM_001144481, exon 3 of 7)	4875	[Rg0008700] [Rf001034539]
chr2L	12028733	12029233	8.32	9.38	1.06	0.00055	0.0398	intron (Rg0010497, intron 1 of 4)	intron (NM_138760, intron 1 of 4)	1546	[Rg0010497] [Rf001080930]
chr2R	7624073	7624573	8.2	9.26	1.06	0.00879	0.0495	intron (Rg0026527, intron 1 of 14)	intron (NM_001259256, intron 1 of 14)	1082	[Rg0026527] [Rf001080930]
chrX	19123998	19124498	10.05	11.11	1.07	3.77E-07	1.86E-05	promoter-TSS (Rg0002031)	promoter-TSS (NM_001169541)	-379	[Rg0002031] [Rf001076428]
chr2L	5278292	5278792	8.17	9.24	1.07	2.42E-06	8.57E-05	Intergenic	Intergenic	-17523	[Rg00261803] [Rf001030278]
chr2R	7958802	7959302	9.63	10.71	1.08	5.67E-05	0.00107	exon (Rg0033240, exon 3 of 5)	exon (NM_001030375, exon 3 of 5)	903	[Rg0033240] [Rf001113052]
chrX	2274004	2274504	9.68	10.77	1.09	4.49E-05	2.40E-03	exon (Rg0033240, exon 3 of 5)	exon (NM_001169174, exon 2 of 3)	524	[Rg0033240] [Rf001080930]
chrX	22457563	22458063	9.68	10.78	1.09	2.28E-06	8.24E-05	exon (Rg0031187, exon 3 of 11)	exon (NM_163776, exon 3 of 11)	923	[Rg0031187] [Rf00107248]
chr3R	727707	728207	8.28	9.38	1.1	6.83E-08	4.19E-06	intron (Rg0027431, intron 1 of 2)	CpGp12_TIR TIR CpGp	5336	[Rg0027431] [Rf001141258]
chr2L	21170039	21170539	9.86	10.96	1.1	9.77E-08	5.84E-06	exon (Rg0030413, exon 2 of 4)	exon (NM_001030716, exon 2 of 4)	1124	[Rg0030413] [Rf001081473]
chr2R	18406055	18406555	10.25	11.35	1.1	0.000546	0.00634	promoter-TSS (Rg00063493)	promoter-TSS (NM_137485)	297	[Rg0006349] [Rf001080674]
chr3R	27905196	27905696	7.85	8.95	1.11	5.92E-08	3.82E-06	exon (Rg0085282, exon 1 of 12)	5' UTR (NM_001104478, exon 1 of 12)	395	[Rg0085282] [Rf001030529]
chr3R	1580585	1580635	8.3	9.41	1.11	5.04E-07	2.29E-05	intron (Rg0026616, intron 1 of 4)	intron (NM_142237, intron 1 of 4)	1858	[Rg0026616] [Rf001081179]
chr2L	589855	589905	7.68	8.8	1.12	3.55E-08	2.63E-06	TTS (Rg0027627)	TTS (NR_134663)	958	[Rg0027627] [Rf001045834]
chr2L	1862773	1862823	9.07	10.18	1.12	2.76E-07	1.43E-05	intron (Rg0036801, intron 2 of 8)	CpG	2017	[Rg0036801] [Rf001076101]
chr2R	780978	781028	9.48	10.6	1.12	8.15E-10	4.57E-08	promoter-TSS (Rg0051472)	promoter-TSS (NM_169195)	465	[Rg0051472] [Rf001080148]
chr3R	998184	998234	9.22	10.35	1.13	5.35E-08	3.55E-06	Intergenic	Intergenic	-47182	[Rg002969] [Rf001080930]
chr3R	21272495	21272995	9.39	10.53	1.13	1.95E-05	0.000444	exon (Rg0038877, exon 2 of 4)	exon (NM_142706, exon 2 of 4)	1072	[Rg0038877] [Rf001081102]
chrX	3290979	3291479	9.02	10.15	1.13	5.37E-05	0.00102	promoter-TSS (Rg0000479)	promoter-TSS (NM_166967)	-14	[Rg0000479] [Rf001076176]
chr2R	15481016	15481516	9.19	10.32	1.13	0.00478	0.0316	intron (Rg0034021, intron 1 of 4)	intron (NM_001299525, intron 1 of 4)	1568	[Rg0034021] [Rf001034539]
chr3R	15546532	15547032	9.6	10.74	1.14	1.17E-09	1.48E-07	exon (Rg0038349, exon 4 of 9)	exon (NM_001316510, exon 4 of 9)	954	[Rg0038349] [Rf001081351]
chr2L	9915914	9916414	9.88	11.02	1.14	2.34E-06	8.41E-05	exon (Rg0040064, exon 3 of 4)	exon (NM_078804, exon 3 of 4)	912	[Rg0040064] [Rf001076176]
chr3R	29765807	29766307	8.96	10.1	1.14	4.44E-06	0.000138	promoter-TSS (Rg0001297)	promoter-TSS (NM_001032408)	63	[Rg0001297] [Rf001099988]
chr2L	5341671	5342171	9.33	10.47	1.14	0.00102	0.00991	intron (Rg0031703, intron 1 of 2)	intron (NM_135880, intron 1 of 2)	313	[Rg0031703] [Rf001076176]
chr2L	18417001	18417501	9.71	10.85	1.15	2.46E-08	2.97E-07	exon (Rg0027826, exon 2 of 5)	exon (NM_163294, exon 2 of 5)	329	[Rg0027826] [Rf001080148]
chrX	626405	626905	10.6	11.75	1.15	2.91E-09	3.13E-07	TTS (Rg0026703)	TTS (NR_122363)	1114	[Rg0026703] [Rf001076176]
chr3R	21066756	21067256	8.76	9.91	1.15	2.29E-08	1.80E-06	intron (Rg0000083, intron 1 of 4)	CpG	1124	[Rg0000083] [Rf00136797]
chr3L	11436057	11436557	10.31	11.47	1.15	3.67E-08	2.70E-06	promoter-TSS (Rg0037901)	promoter-TSS (NM_141818)	428	[Rg0037902] [Rf001080291]
chr3R	29148859	29149359	10.66	11.81	1.15	3.41E-07	1.70E-05	promoter-TSS (Rg0039642)	promoter-TSS (NM_143419)	748	[Rg0039642] [Rf001080674]
chr3R	863786	864286	7.88	9.02	1.15	4.70E-07	2.22E-05	intron (Rg00267431, intron 2 of 2)	CpGp12_TIR TIR CpGp	141415	[Rg00267431] [Rf001080148]
chr4	1305651	1306151	7.36	8.51	1.15	2.25E-06	8.19E-05	Intergenic	Intergenic	74019	[Rg0036363] [Rf001091630]
chr3R	18853439	18853939	10.11	11.28	1.16	2.17E-10	3.86E-08	promoter-TSS (Rg0034403)	promoter-TSS (NM_137540)	-646	[Rg0034403] [Rf001072328]
chr3R	31670624	31671124	8.9	10.06	1.16	3.10E-06	0.000189	exon (Rg0039863, exon 3 of 9)	exon (NM_170563, exon 3 of 10)	1410	[Rg0039863] [Rf001080930]
chr2L	1979491	1979541	9.46	10.63	1.16	0.00026	0.0026	exon (Rg0034933, exon 2 of 3)	exon (NM_137563, exon 2 of 3)	633	[Rg0034933] [Rf001081314]
chr2L	6945702	6946202	9.88	11.14	1.16	1.65E-05	0.000911	promoter-TSS (Rg0011871)	promoter-TSS (NM_00127242)	-663	[Rg0011871] [Rf001080930]
chr3R	18295667	18296167	8.59	9.76	1.17	0.00042	0.00522	intron (Rg0010877, intron 1 of 3)	intron (NM_143294, intron 1 of 3)	-163	[Rg0010877] [Rf001080930]
chr3L	1479055	1479555	9.57	10.75	1.18	8.83E-10	8.17E-08	promoter-TSS (Rg0020248)	promoter-TSS (NM_176273)	-364	[Rg0020248] [Rf001072713]
chrX	3448211	3448711	7.97	9.15	1.18	1.31E-08	1.13E-06	intron (Rg0029657, intron 1 of 6)	intron (NM_001272276, intron 1 of 6)	482	[Rg0029657] [Rf001080930]
chr3L	9695175	9695675	9.76	10.95	1.19	2.46E-11	5.16E-09	promoter-TSS (Rg0036030)	promoter-TSS (NM_168360)	16	[Rg0036030] [Rf001076416]
chr3L	6977484	6977984	8.5	9.69	1.19	0.000253	0.00357	exon (Rg0047205, exon 3 of 3)	non-coding (NR_001944, exon 3 of 3)	1413	[Rg0047205] [Rf001076899]
chr2R	16338012	16338512	9.79	10.99	1.2	2.37E-10	3.60E-08	promoter-TSS (Rg0010611)	promoter-TSS (NM_166168)	-39	[Rg0010611] [Rf001080148]
chr2L	15064476	15064976	10.38	11.58	1.2	9.80E-08	5.84E-06	intron (Rg0024181, intron 1 of 4)	intron (NM_165107, intron 1 of 4)	3071	[Rg0024181] [Rf001045834]
chr3L	5785731	5786231	7.51	8.71	1.2	4.15E-07	2.03E-05	TTS (Rg0025418)	TTS (NR_139389)	223	[Rg0025418] [Rf001076176]
chrX	2352784	2353284	8.75	9.95	1.2	6.10E-06	0.00214	intron (Rg0003159, intron 1 of 3)	intron (NM_001258559, intron 1 of 3)	1234	[Rg0003159] [Rf001074043]
chrY_CP007111v1_random	13407	13907	7.46	8.68	1.21	0.000356	0.00458	NA	TAR1 LINE Jockey	NA	NA
chrX	1156861	1156911	9.8	11.02	1.22	1.57E-10	2.47E-08	exon (Rg0000777, exon 2 of 4)	exon (NM_078560, exon 2 of 4)	1115	[Rg0000777] [Rf001073542]
chr3L	15564210	15564710</									

chr3L	22999735	23000235	626	8.5	2.25	2.68E-16	1.39E-13	intron # Bgn0262509, intron 1 of Z3	JNAREP1_DM RC H3K9me3	164	Bgn0262509 Bbu0304530
chr3L	1474669	1475169	881	11.14	2.33	2.74E-18	1.73E-15	TTS (Bgn0020248)	TTS (NM_176273)	338	Bgn0262467 Bbu0310161
chr3L	22997396	22997896	551	7.92	2.41	2.24E-11	4.83E-09	promoter-TSS # Bgn0262509	promoter-TSS #NM_001043156	725	Bgn0262509 Bbu0304530
chr3L	22988072	22988572	755	10.21	2.66	3.15E-35	6.95E-32	promoter-TSS # Bgn0262509	promoter-TSS #NM_001043156	49	Bgn0262509 Bbu0304530
chr3R	27961166	27961666	-0.18	10.05	10.23	2.83E-116	2.50E-112	promoter-TSS #Bgn0051253	promoter-TSS #NM_170364	405	Bgn0262408 Bbu0346202

## II. The concerted activity of epigenomic effectors is essential to establish transcriptional programs during oogenesis

### 1. Article Presentation

In our first study, a genetic screen allowed us to identify Lid and Sin3A as essential regulators of *dhd* expression. These factors have been found in a repressive complex (Moshkin et al., 2009), which made us wonder if other chromatin complexes were involved in *dhd* regulation. Broadening our analysis to other knockdowns led us to identify two additional factors, essential for *dhd* expression: Snr1, a subunit of the chromatin remodeler Swi/Snf and the chromatin factor Mod(mdg4) mainly known for its insulator role. We thus wondered how are all of these factors promoting the hyperactivation of *dhd*?

To tackle this question, in this second article, I investigated the impact of these different knockdowns on the epigenome, using the chromatin profiling method Cut&Run. I also used a dedicated data analysis strategy to identify potential regulatory elements associated to histone marks.

Of note, this revised version of the article has been accepted by PLOS Genetics.

**Three classes of epigenomic regulators converge to hyperactivate the essential maternal gene *deadhead* within a heterochromatin mini-domain.**

Daniela Torres-Campana<sup>1</sup> , Béatrice Horard<sup>1</sup> , Sandrine Denaud<sup>2</sup> , Gérard Benoit<sup>1</sup> , Benjamin Loppin<sup>1\*</sup> & Guillermo A. Orsi<sup>1,3\*</sup>.

<sup>1</sup>: Laboratoire de Biologie et Modélisation de la Cellule, CNRS UMR5239, École Normale Supérieure de Lyon, University of Lyon, France.

<sup>2</sup>: Institute of Human Genetics, UMR 9002, CNRS–University of Montpellier, 34396 Montpellier, France.

<sup>3</sup>: Current address: Institute for Advanced Biosciences, INSERM U1209, CNRS, Université Grenoble Alpes, France.

\*: correspondence: [benjamin.loppin@ens-lyon.fr](mailto:benjamin.loppin@ens-lyon.fr); [guillermo.orsi@inserm.fr](mailto:guillermo.orsi@inserm.fr)

## Abstract

The formation of a diploid zygote is a highly complex cellular process that is entirely controlled by maternal gene products stored in the egg cytoplasm. This highly specialized transcriptional program is tightly controlled at the chromatin level in the female germline. As an extreme case in point, the massive and specific ovarian expression of the essential thioredoxin Deadhead (DHD) is critically regulated in *Drosophila* by the histone demethylase Lid and its partner, the histone deacetylase complex Sin3A/Rpd3, via yet unknown mechanisms. Here, we identified Snr1 and Mod(mdg4) as essential for *dhd* expression and investigated how these epigenomic effectors act with Lid and Sin3A to hyperactivate *dhd*. Using Cut&Run chromatin profiling with a dedicated data analysis procedure, we found that *dhd* is intriguingly embedded in an H3K27me3/H3K9me3-enriched mini-domain flanked by DNA regulatory elements, including a *dhd* promoter-proximal element essential for its expression. Surprisingly, Lid, Sin3a, Snr1 and Mod(mdg4) impact H3K27me3 and this regulatory element in distinct manners. However, we show that these effectors activate *dhd* independently of H3K27me3/H3K9me3, and that *dhd* remains silent in the absence of these marks. Together, our study demonstrates an atypical and critical role for chromatin regulators Lid, Sin3A, Snr1 and Mod(mdg4) to trigger tissue-specific hyperactivation within a unique heterochromatin mini-domain.

## Author Summary

Multicellular development depends on a tight control of gene expression in each cell type. This relies on the coordinated activities of nuclear proteins that interact with DNA or its histone scaffold to promote or restrict gene transcription. For example, we previously showed that the histone modifying enzymes Lid and Sin3A/Rpd3 are required in *Drosophila* ovaries for the massive expression of *deadhead* (*dhd*), a gene encoding for a thioredoxin that is essential for fertility. In this paper, we have further identified two additional *dhd* regulators, Snr1 and Mod(mdg4) and dissected the mechanism behind hyperactivation of this gene. Using the epigenomic profiling method Cut&Run with a dedicated data analysis approach, we unexpectedly found that *dhd* is embedded in an unusual chromatin mini-domain featuring repressive histone modifications H3K27me3 and H3K9me3 and flanked by two regulatory elements. However, we further showed that Lid, Sin3A, Snr1 and Mod(mdg4) behave like obligatory activators of *dhd* independently of this mini-domain. Our study unveils how multiple broad-acting epigenomic effectors operate in non-canonical manners to ensure a critical and specialized gene activation event. These findings challenge our knowledge on these regulatory mechanisms and their roles in development and pathology.

## Introduction

Gene expression is tightly controlled in eukaryotic cells by the composition, organization and dynamics of nucleosomes, consisting of an octamer of histone proteins wrapped in ~146bp of DNA. The concerted activity of protein complexes including histone chaperones, readers and writers as well as nucleosome remodelers, defines the positioning, composition and post-translational modifications of nucleosomes [1–3]. The resulting chromatin landscape is further organized by insulator proteins that delimit tridimensional contacts along the genome, forming sub-nuclear domains and guiding contacts between promoters and their cognate regulatory elements [4]. This tightly regulated epigenomic environment profoundly influences RNA Polymerase access to DNA and transcriptional activity.

Tremendous efforts in the past decades aimed at dissecting the roles of these epigenomic effectors *in vivo*. A privileged method is ablation or dosage manipulation of each component to measure its impact on gene expression. While these approaches can yield precious functional insight, the ubiquitous expression and wide range of activities of these factors, as well as redundancies in their interactions, make it difficult to infer their precise function. Understanding their function therefore requires identifying biologically relevant situations where disrupting these effectors impacts transcription in a critical and specific manner. We previously described one of such cases, where perturbation of the histone H3K4 demethylase Lid/KDM5 or the histone deacetylase complex Sin3A/Rpd3 in *Drosophila* ovaries dramatically abrogated the expression of the maternal gene *deadhead* (*dhd*), which is essential for female fertility [5].

The *Drosophila* egg is loaded with maternal gene products synthesized by germline nurse cells that enable early embryonic development in the absence of zygotic

transcription [6]. An extreme example of this specialized transcriptome, *dhd* is among the most highly expressed genes in adult ovaries, while it is almost completely silent in any other tissue and developmental stage [5,7–9]. The DHD protein is a thioredoxin involved in regulating the general redox state in oocytes [10,11]. In addition, DHD plays a critical role at fertilization to reduce cysteine-cysteine disulfide bonds on the Protamine-like proteins that replace histones on chromatin during spermiogenesis [9,12]. In the absence of DHD, paternal chromosomes fail to decondense and are excluded from the first zygotic nucleus, leading to haploid gynogenetic development and embryonic lethality. The *dhd* locus, which produces a single, short (952bp), intronless transcript is packed within a 1369bp region that separates its flanking genes *Trx-T* and *CG4198*. Remarkably, these two genes are expressed exclusively in the male germline, thereby constituting an apparently unfavorable environment for *dhd* transcription in ovaries. In addition, we showed that a 4305bp transgene spanning only *Trx-T*, *dhd* and part of *CG4198* largely recapitulates the expression of *dhd* [5,9], indicating that regulatory elements sufficient for *dhd* activation are contained within this restricted region. Our previous study further found that Lid and Sin3A are essential activators of *dhd* in *Drosophila* ovaries, in striking contrast to their otherwise relatively modest impact on the rest of the transcriptome. Considering these unusual features, we postulated that the exquisite sensitivity of *dhd* to these broad-acting chromatin effectors revealed a singular mode of epigenomic regulation that enables its massive and specific ovarian expression [5].

Here, we exploited this singular model locus to understand how multiple classes of epigenomic effectors converge to achieve programmed transcriptional hyperactivation. We identified the Brahma chromatin remodeler component Snr1 [13] and the BTB/POZ-domain protein Mod(mdg4) [14] as factors that share with Lid and

Sin3A a critical and highly specific role in activating *dhd*. By exploiting the chromatin profiling method Cut&Run [15] and an adapted data analysis strategy, we found that *dhd* is unexpectedly embedded within a heterochromatin mini-domain flanked by two border regulatory elements. One of these is a *dhd*-proximal element, which encompasses a DNA Replication-related Element (DRE-box) motif [16] that is essential for *dhd* expression. Yet, exploiting knockdown and transgenic tools, we found that Lid, Sin3A, Snr1 and Mod(mdg4) activate *dhd* independently of the associated heterochromatin mini-domain. Furthermore, this mini-domain is not required to restrict *dhd* expression to ovaries. Together, our results put into perspective our understanding on these epigenomic regulators by revealing how they exert a biologically essential control of *dhd* via non-canonical mechanisms.

## Results

### **Mod(mdg4) and Snr1 are essential for *dhd* expression**

We previously performed a female germline RNA interference screen to identify chromatin factors required for paternal chromosome incorporation into the zygote at fertilization. As part of that screen, the histone H3K4 demethylase Lid, Sin3A and Rpd3, which participate in deacetylase complexes targeting various lysine residues in H3 and H4 [17,18], were identified as essential regulators of *dhd* expression. Because Lid and Sin3A can interact within a co-repressor complex [19,20], we asked whether other chromatin regulatory complexes might also be involved in *dhd* regulation. We therefore broadened our analysis to other knockdowns that caused maternal effect sterility associated with a *dhd*-like mutant phenotype, i.e. defective sperm nuclear decompaction

at fertilization. Among these, we focused on two additional UAS-controlled small hairpin RNA (shRNA) constructs from the TRiP collection [21], respectively targeting *mod(mdg4)* and *Snr1*. *Snr1* is an essential subunit of the Brahma chromatin remodeler that mediates protein-protein interactions within this complex as well as with external interacting partners [13,22]. The *mod(mdg4)* gene codes for up to 31 isoforms [23], all of which are targeted by the shRNA construct. Among these, the most well characterized, *Mod(mdg4)<sup>67.2</sup>* is a common component of boundary insulators in the *Drosophila* genome [24], but other non-insulating isoforms exhibiting activator functions have also been identified [4,25,26]. These two candidates belonged to two classes of epigenomic effectors distinct from *Lid* and *Sin3A*, and we thus decided to investigate their function during the oocyte to zygote transition.

When activated by the Maternal Triple Driver (MTD) Gal4 source, these shRNAs efficiently reduced the levels of *mod(mdg4)* and *Snr1* transcripts (FigS1-A). Previous studies reported defective oogenesis and diminished egg production in *mod(mdg4)* as well as *Snr1* mutant females [22,25]. Consistently, females with ovarian knockdown of *mod(mdg4)* or *Snr1* (hereby referred to as *mod(mdg4)* KD or *Snr1* KD females) were almost completely sterile (Table 1). Indeed, while KD females were able to lay more eggs than mutants, these almost systematically failed to hatch. Focusing on paternal chromatin organization at fertilization in these embryos, we found that both *mod(mdg4)* and *Snr1* ovarian KDs systematically led to failure of male pronucleus decondensation, which remained elongated (Fig1-A). Concomitantly, these eggs exhibited retention of the protamine fluorescent marker *Mst35Ba::GFP* (*ProtA::GFP*) [27] in paternal chromatin, as observed in *dhd* loss of function mutants [9,12].

**Table 1. Embryo hatching rates.**

The *w<sup>1118</sup>* strain is used as reference.

<i>Knockdowns</i>			
Female Genotype	Male Genotype	Number of eggs	Hatch. rate (%)
<i>Control</i>	<i>w<sup>1118</sup></i>	1561	98.27%
<i>Snr1</i> KD	<i>w<sup>1118</sup></i>	791	0.00%
<i>mod(mdg4)</i> KD	<i>w<sup>1118</sup></i>	1589	1.01%
<i>lid</i> KD (val22)	<i>w<sup>1118</sup></i>	1403	2.14%
<i>lid</i> KD (val21)	<i>w<sup>1118</sup></i>	1144	1.05%
<i>Sin3a</i> KD	<i>w<sup>1118</sup></i>	1221	0.25%
<i>E(z)</i> KD	<i>w<sup>1118</sup></i>	843	0.00%
<i>Rescue with WT or ΔDRE mutant transgene</i>			
<i>w<sup>1118</sup></i>	<i>w<sup>1118</sup></i>	344	97.67%
<i>dhd<sup>Δ5</sup></i>	<i>w<sup>1118</sup></i>	375	0.00%
<i>dhd<sup>Δ5</sup>::;pW8-dhd<sup>WT</sup></i>	<i>w<sup>1118</sup></i>	663	85.67%
<i>dhd<sup>Δ5</sup>::;pW8-dhd<sup>ΔDRE</sup></i>	<i>w<sup>1118</sup></i>	475	2.15%
<i>dhd<sup>Δ5</sup>::;pW8-dhd<sup>FD</sup></i>	<i>w<sup>1118</sup></i>	410	87.80%
<i>Knockdown rescue with the WT transgene</i>			
<i>dhd<sup>Δ5</sup>::; lid KD(val21), pW8-dhd<sup>WT</sup></i>	<i>w<sup>1118</sup></i>	175	1.92%
<i>dhd<sup>Δ5</sup>::; Sin3a KD, pW8-dhd<sup>WT</sup></i>	<i>w<sup>1118</sup></i>	271	0.37%
<i>dhd<sup>Δ5</sup>::; Snr1 KD, pW8-dhd<sup>WT</sup></i>	<i>w<sup>1118</sup></i>	247	0.00%
<i>dhd<sup>Δ5</sup>::; mod(mdg4) KD, pW8-dhd<sup>WT</sup></i>	<i>w<sup>1118</sup></i>	462	0.43%

The above results suggest that Mod(mdg4) and Snr1 could regulate *dhd* expression. RNA-sequencing on *mod(mdg4)* and *Snr1* KD ovaries indeed revealed that *dhd* is dramatically downregulated in both KDs, with a fold reduction of almost two orders of magnitude (Fig1-B,C, and FigS1-B,E). *dhd* was the first most strongly affected gene in *mod(mdg4)* KD ovaries in terms of fold-change in expression, and the 14<sup>th</sup> most affected gene in *Snr1* KD ovaries. Consistently, DHD protein levels assessed by Western Blot in KD ovaries were also dramatically reduced (Fig1-D). This was in contrast to a more modest impact of both KDs on the rest of the transcriptome and the limited overlap in their effects (Fig S1-B,C,D). In particular, genes in the vicinity of *dhd* were not significantly affected by the KDs (Fig1-C and FigS1-B). Therefore, despite the packed

genomic organization of the *dhd* locus, its expression strictly and singularly depends on multiple epigenomic effectors.

## **Cut&Run with dedicated analysis reveals both the distribution of histone modifications and their associated regulatory elements**

To more precisely characterize the chromatin landscape at the *dhd* locus, we next implemented the Cut&Run epigenomic profiling method [15]. In Cut&Run, histone modifications of interest are targeted *in situ* by a specific antibody following tissue permeabilization. Target-bound antibodies are subsequently coupled to a fusion between the bacterial Protein A and Micrococcal Nuclease (ProteinA-MNase) that cleaves exposed DNA in the vicinity of the antibody, releasing target nucleosomal particles into solution. Importantly, MNase is expected to also cleave exposed DNA in the immediate spatial vicinity of the nucleosome-bound antibody, causing the release of DNA particles bound by other proteins such as polymerases or DNA sequence-specific transcription factors (Fig2-A). In particular, DNA regulatory elements occupied by sequence-specific transcription factors are typically associated with MNase footprints distinctly shorter than nucleosomes [28–30]. Partially unwrapped dynamic nucleosomes typically associated with regulatory elements can also produce such distinctly short footprints [31]. Following paired-end sequencing, such released DNA fragments can be distinguished and separated by their size, yielding a map of nucleosomes (>146bp) and sub-nucleosomal particles, putatively corresponding to

regulatory elements (<120bp). A single Cut&Run experiment should thus identify DNA regulatory elements that are in physical proximity of target histone modifications.

With this in mind, we conducted H3K27me3 Cut&Run in *Drosophila* ovaries. Using only 12 pairs of ovaries per sample, we robustly revealed H3K27me3 domains. Remarkably, visualization of Cut&Run fragments shorter than 120bp (which excludes fully wrapped octameric nucleosomes) revealed that these were enriched at discrete peaks within H3K27me3 domains. Genome-wide analysis identified 679 peaks of fragments <120bp (hereon referred to as “short fragment peaks”) that were ~250bp-wide in average (Fig2-B,D). We hypothesized that short fragment peaks represented H3K27me3-associated regulatory elements occupied by transcription factors. Within H3K27me3 domains, we expected these to include Polycomb Response Elements (PREs) as well as insulators. For example, short fragment peaks corresponded to several well-described PREs and insulators in the Bithorax complex H3K27me3 domain [26,32,33] (Fig2-C), consistent with observations in larval tissue [34]. To ask whether this reflects a broader genome-wide trend, we compared short fragment peaks with PRE and insulator markers genome-wide. Although there is scarce genome-wide data available for *Drosophila* ovaries, H3K27me3 domains are generally present in most cell types. We thus exploited datasets from embryonic-derived S2 and Kc cell lines. Consistent with their occupancy by transcription factors, ATAC-seq peaks [35] -revealing hyper-accessible DNA- coincide with Polycomb regulatory elements in flies and mice [35,36]. Genome-wide, our small fragment peaks identified in ovaries were enriched for ATAC-seq signal, arguing that these indeed correspond to DNA regulatory elements (Fig2-D). Enrichment at these peaks of the Polycomb protein [37] and the insulator protein CP190 [38] further argues that these elements often correspond to functional PREs or insulators. Accordingly, at the borders of H3K27me3 domains, short fragment peaks

were more frequently associated with CP190, confirming previous reports that this factor is associated with H3K27me3 domain boundaries [24,39] (Fig2-D). Instead, Polycomb was rather enriched at peaks localized internally within these domains. Our Cut&Run analysis strategy can therefore be used to reveal not only the breadth of histone modification domains in ovaries but also their associated DNA regulatory elements.

### ***dhd* lies within an H3K27me3/H3K9me3 mini-domain flanked by DNA regulatory elements.**

To gain insight on *dhd* regulation, we next sought to analyze its associated chromatin configuration. We previously showed that the active transcription modification H3K4me3 is enriched at the *dhd* promoter and that this mark is lost in *lid* KD ovaries [5](FigS2-A). Using available ChIP-seq datasets from embryonic derived S2 cells, we further observed that that *dhd* lies within a ~5kbp mini-domain featuring two types of repressive histone modifications: H3K27me3 and H3K9me3 (FigS2-A) [40]. H3K27me3 is the hallmark of Polycomb-based repression [41,42], whereas H3K9me3 dictates Heterochromatin Protein 1 (HP1)-based repression [43,44]. Interestingly, this mini-domain was also found in ChIP-seq data from fly ovaries (FigS2-A) [45]. Potentially regulating this chromatin environment, Lid and Sin3A were described as participating in a co-repressor complex [20], but their global impact on repressive histone modifications is unclear. In turn, previous reports showed that depletion of insulator proteins Mod(mdg4), as well as CTCF, Su(Hw), CP190 or BEAF-32, did not affect the spread of Polycomb-associated domains but instead caused a general decrease in H3K27me3 levels [24]. In contrast, the Brahma/BAF complex is typically considered as

counteracting Polycomb repression based on work in mammals [46], but this interplay has not been analyzed in *Drosophila*.

Based on these observations, we sought to better characterize the distribution of H3K27me3 and H3K9me3 in ovaries at the *dhd* locus. Using our Cut&Run approach, we confirmed that *dhd* is included in a ~5450bp heterochromatic H3K27me3/H3K9me3 mini-domain that extends from the promoter region of *dhd* to the promoter of the next gene active in ovaries, *Sas10* (Fig3-A). While our whole-tissue Cut&Run approach cannot distinguish which cells harbor this domain, published H3K27me3 ChIP-seq profiles from either somatic or germline cells in ovaries indicate that this mark is present in both (Figure S2-A). We segmented the Cut&Run H3K27me3 signal in control ovaries and identified 278 discrete H3K27me3 domains, ranging from 3 to 240kb in width. The *dhd* H3K27me3 domain stood out when considering its enrichment in this mark relative to its length, compared to other domains (Fig3-B). Our analyses indicate that despite its reduced size, the *dhd* locus is capable of accumulating proportionately high amounts of this repressive modification. While we also identified other previously described H3K9me3 domains lodged in euchromatic regions (FigS3), the signal is, as expected, largely dominated by pericentric heterochromatin. We could thus not robustly call such euchromatic H3K9me3 domains, preventing us from conducting an analogous analysis for *dhd* on this mark.

Surprisingly, short fragment peak analysis revealed two putative DNA regulatory elements associated with both histone marks, precisely at the mini-domain borders, with no internal peaks present (Fig3-A). ATAC-seq data from S2 cell lines confirmed presence of only these two border elements (FigS2-B). In addition, in Kc cells, *dhd* border elements are occupied by CP190 and Mod(mdg4), both of which can be found at the boundaries of *Drosophila* H3K27me3 domains [24,47]. However, the insulating

isoform Mod(mdg4)<sup>67.2</sup> is not found at the *dhd* locus (FigS2-B), suggesting that a different isoform playing an activator function is responsible for *dhd* regulation. Finally, the *dhd*-proximal 5' border element featured a significant, although very modest enrichment for PRE markers Polycomb and Polyhomeotic (Fig-S2-B). This regulatory architecture was quite unusual, as we could not find any other H3K27me3 domain in the genome sharing this particular organization with two border elements and no internal elements. Together, these results revealed that *dhd* lies within a unique H3K27me3/H3K9me3 mini-domain featuring only border elements.

### **Sin3A, Snr1 and Mod(mdg4) control the regulatory architecture of the *dhd* mini-domain.**

We next aimed at evaluating the potential role for Lid, Sin3A, Mod(mdg4) and Snr1 in regulating this heterochromatin mini-domain. We used KD ovaries for these factors and included as a control a KD for the H3K27 methyltransferase Enhancer of zeste (*E(z)*), induced in germ cells by the MTD-Gal4 driver. While *E(z)* KD females were sterile as previously described [48,49] (Table1), they were able to lay eggs and displayed only a moderate effect on *dhd* expression (a 25% reduction compared to controls) (FigS4-A). Immunofluorescence staining on dissected control ovaries showed that H3K27me3 marks follicle cell nuclei, the karyosome (i.e the oocyte nucleus) and nurse cell nuclei, although nurse cell staining was relatively weaker (FigS3-B), consistent with previous reports [48]. As expected, H3K27me3 was undetectable in the karyosome and in nurse cells of *E(z)* KD ovaries, whereas follicle cells (which do not express MTD-driven shRNAs) still carried this mark at normal levels. While *lid*, *Sin3a* and *mod(mdg4)* KD ovaries displayed normal H3K27me3 staining, we observed a

moderate reduction in H3K27me3 levels in nurse cells in *Snr1* KD ovaries, even while H3K27me3 levels were not affected on the karyosome (FigS4-B).

We next carried out H3K27me3 Cut&Run on ovaries from all KDs. Within our 278 identified H3K27me3 domains (see above), we compared the average enrichment in H3K27me3 signal in control and KD ovaries (Fig3-C). In *E(z)* KD ovaries, Cut&Run experiments revealed only a moderate loss of H3K27me3 signal (35% average reduction at these domains compared to controls) (Fig3-C), contrasting with the strong global reduction in H3K27me3 immunofluorescence signal. This difference is likely to reflect the fact that the H3K27me3 signal from Cut&Run experiments originates from both germline and somatic cells. Accordingly, *E(z)* KD completely abrogated H3K27me3 signal at the *spen*, *Corto* or *ptc* loci, all of which are decorated with H3K27me3 in nurse cells but not in follicle cells (FigS4-C) [50]. In contrast, the *gl*, *dpp*, or *repo* loci, which show stronger H3K27me3 in follicle cells compared to nurse cells, were only slightly affected in *E(z)* KD ovaries (FigS4-C). Together, these results show that our Cut&Run strategy detects H3K27me3 signal from both germline and somatic cells and is able to detect quantitative differences in the averaged signal when nurse cells are strongly affected. Consistent with immunofluorescence experiments, *lid*, *Sin3a* and *mod(mdg4)* KDs had only a modest global impact on average H3K27me3 levels (5% reduction compared to controls), and no effect on the spread of H3K27me3 domains (Fig3-C). Also consistent with our immunofluorescence experiments, *Snr1* KD led to a more severe average reduction of H3K27me3 Cut&Run signal compared to controls (20%), although not as dramatic as *E(z)* KD.

In agreement with genome-wide observations, the levels of H3K27me3 in the *dhd* mini-domain were reduced in *E(z)* KD ovaries and unaffected in *Sin3a* or *mod(mdg4)* KD ovaries. More surprisingly, the domain was not measurably affected in

*Snr1* KD ovaries, despite the fact that H3K27me3 is globally impacted by this knockdown (Fig3-D and FigS5-A). Within the sensitivity limits of our approach, these results indicate that *Sin3a*, *Snr1* and *mod(mdg4)* KDs have little if any impact on H3K27me3 at the *dhd* locus. Conversely, in *lid* KD ovaries, in which global H3K27me3 levels were unaffected, we detected an increase in H3K27me3 levels at the *dhd* mini-domain (Fig3-C,D and FigS5-A). This raised the possibility that Lid could facilitate *dhd* expression by counteracting Polycomb-mediated repression.

Since the *dhd* mini-domain also featured H3K9me3, we next turned to Cut&Run followed by qPCR to evaluate its status in KD ovaries. H3K27me3 Cut&Run-qPCR measures the expected enrichments at H3K27me3 domains and detects variations in the signal coherent with Cut&Run-seq results (Fig3-E and FigS5-B). To validate the H3K9me3 Cut&Run-qPCR approach in ovaries, we exploited the *CG12239* gene as a positive control [45], and detected an expected enrichment in H3K9me3 signal at this locus (Fig3-E and FigS5-B). At the *dhd* locus, H3K9me3 was enriched as expected from ChIP-seq results. Importantly, knockdown of *lid*, *Sin3a*, *mod(mdg4)* or *Snr1* had no effect on this enrichment. (Fig3-E). The *dhd* heterochromatin mini-domain including H3K27me3 and H3K9me3 is thus independent of Sin3A, Snr1, whereas Lid counteracts H3K27me3.

We next evaluated the impact of different KDs on the *dhd* mini-domain short fragment peaks at border regions. We first analyzed the effect of our different knockdowns on the full set of 679 peaks previously defined (Fig2-B). Both *E(z)* and *Snr1* KD led to a strong (~63%) decrease in short fragment peak average counts genome-wide (Fig4-A). Since these KDs also affect global H3K27me3 levels, this reduction could result from a general absence of histone modification-targeted MNase on chromatin. Remarkably, *Sin3a* KD led to a similarly strong effect on short fragment peak counts that

could not be attributed to its global impact on H3K27me3. Instead, this data suggests that Sin3A is required to ensure proper occupancy and organization of transcription factors and/or nucleosomes at DNA regulatory elements associated with H3K27me3. In contrast, *lid* or *mod(mdg4)* KD did not globally affect short fragment peak counts, indicating that these factors do not play such a role (Fig4-A).

Consistent with their effects genome-wide, short fragment counts at the *dhd* mini-domain border elements were strongly diminished upon *E(z)* and *Sin3a* KDs (Fig4-B and FigS5-C). Intriguingly, *mod(mdg4)* KD led to a similar impact on these border elements (particularly the *dhd*-proximal one), even though it did not globally affect H3K27me3-associated elements genome-wide (Fig4-B and FigS5-C). This observation could indicate that the *dhd* border elements become less frequently occupied by transcription factors, that these factors become less frequently associated with H3K27me3, and/or that their nucleosomal organization is compromised. In all cases, this suggests that Mod(mdg4) is required to ensure chromatin organization of the border DNA regulatory elements at the *dhd* mini-domain. Remarkably, *Snr1* KD led to a similar effect on border elements without affecting H3K27me3 levels at the *dhd* mini-domain, suggesting that Snr1 is also required for the proper organization of the *dhd* border elements. In striking contrast, *lid* KD had no detectable effect on these regulatory elements (Fig4-B and FigS5-C). We concluded that Lid, although essential for *dhd* expression, was not required to ensure the proper organization of *dhd* border elements.

Altogether our results, summarized in Fig4-C, indicate that Lid, Sin3A, Snr1 and Mod(mdg4), impact H3K27me3 or its associated regulatory elements genome-wide and/or at the *dhd* mini-domain in four distinct manners.

## **The *dhd* promoter-proximal DNA regulatory element is required for *dhd* expression independently of its heterochromatin mini-domain.**

We next performed sequence analysis of the *dhd* mini-domain border elements, screening against the flyreg.v2 transcription factor DNA binding motif database [51,52]. At the 5' border element, which mapped to the *dhd* promoter region, we identified four perfect matches for the DNA replication-related element (DRE) motif, TATCGATA (Fig5-A). This motif is recognized by the insulator-associated factor BEAF-32 [53] and the core-promoter factor DREF [16]. These four DRE motifs overlap in the palindromic sequence TATCGATATCGATA, 37bp upstream of the *dhd* transcription start site. Consistently, BEAF-32 and DREF both occupy this element in Kc cells (FigS6) [38]. Previous studies showed that BEAF-32 null females are partially fertile (~40% hatching rate) [54], indicating that this factor is not essential for *dhd* expression. In turn, DREF is essential in a cell-autonomous manner and indeed *dref* mutations cause oogenesis defects [55]. Accordingly, we observed severe atrophy and failure to produce oocytes in *dref* KD ovaries. Because this precluded studying the role of DREF in *dhd* regulation, we instead sought to probe the importance of the DRE motifs themselves.

The *dhd*<sup>Δ5</sup> null allele is a 1.4 kb deletion affecting the entire promoter region including the promoter-proximal regulatory element, and part of the coding region of *dhd* [7,9] (Fig5-A). A *pW8-dhd*<sup>WT</sup> transgenic construct, bearing the entire *dhd* gene - including its promoter region-, restores *dhd* expression as well as fertility in *dhd*<sup>Δ5</sup> mutants [9] (Fig5-A,B, Table1). We now constructed a second rescue transgene based on the *pW8-dhd*<sup>WT</sup>, where the 14bp carrying the DRE motifs were deleted (*pW8-dhd*<sup>ΔDRE</sup>)

(Fig5-A). These constructs were inserted into the same genomic location as *pW8-dhd<sup>WT</sup>* (62E1) and combined with the *dhd<sup>l5</sup>* deficiency. In striking contrast to *pW8-dhd<sup>WT</sup>*, the *pW8-dhd<sup>ADRE</sup>* construct was unable to rescue *dhd* expression, or substantially improve fertility in *dhd<sup>l5</sup>* deficient flies (Fig5-B, Table1). The DRE motifs are thus essential to ensure *dhd* expression.

To test a role for this regulatory element and its DRE motifs in regulating the H3K27me3/H3K9me3 mini-domain, we performed Cut&Run-seq and Cut&Run-qPCR on homozygous *dhd<sup>l5</sup>* ovaries, as well as rescue *dhd<sup>l5</sup>::pW8-dhd<sup>WT</sup>* and non-rescued *dhd<sup>l5</sup>::pW8-dhd<sup>ADRE</sup>* ovaries. Strikingly, the 5.4kbp *dhd* H3K27me3 mini-domain was completely lost in *dhd<sup>l5</sup>* ovaries (Fig5-C,D and FigS7), despite the fact that 90% of this mini-domain were intact in the deficient chromosome. This indicates that the *dhd*-proximal border of this mini-domain is essential for establishment and/or maintenance of H3K27me3. Furthermore, H3K27me3 signal was absent within the mini-domain in *dhd<sup>l5</sup>::pW8-dhd<sup>WT</sup>* rescue ovaries (Fig5-C,D and FigS7), suggesting that the 5'-most 2.8kbp of the domain are also insufficient to establish and/or maintain H3K27me3. This result further confirms that *dhd* can be expressed at high levels in the absence of H3K27me3, consistent with results from *E(z)* KD ovaries (FigS4-A). Finally, the H3K27me3 mini-domain was also completely absent in *dhd<sup>l5</sup>::pW8-dhd<sup>ADRE</sup>* ovaries (Fig5-C), indicating that the DRE motifs are required for *dhd* expression independently of H3K27me3.

Based on these observations, we hypothesized that the complete mini-domain sequence, including both border regulatory elements, might be necessary for restoring heterochromatin marks. We thus constructed a transgene containing the full domain sequence of the *dhd* heterochromatin domain (*pW8-dhd<sup>FD</sup>*)(Fig5-A), inserted at the same genomic location as the *pW8-dhd<sup>WT</sup>* transgene. Interestingly, this transgene

restored *dhd* expression (Fig5-B) and rescued fertility (Table 1) but was unable to restore H3K27me3 (Fig5-D and FigS7). These results indicate that the border-to-border mini-domain is not autonomous and suggest that its genomic location impacts its chromatin configuration.

We next focused on the H3K9me3 mark. In contrast to H3K27me3, Cut&Run analysis in *dhd<sup>l5</sup>* mutants showed that H3K9me3 was lost at the *dhd*-proximal half of the domain, while this mark was maintained at the *dhd*-distal part (Fig5-C). Cut&Run-qPCR using primers across the *dhd* domain revealed that H3K9me3 was not restored at the *dhd*-proximal part of the H3K9me3 domain in *dhd<sup>l5</sup>::pW8-dhd<sup>WT</sup>* or *dhd<sup>l5</sup>::pW8-dhd<sup>FD</sup>* ovaries (Fig5-D and FigS7). Together, these results indicate that the border-to-border mini-domain is not autonomous to establish its own heterochromatin configuration, and that *dhd* expression can proceed at near normal levels independently of these marks.

## **Lid, Sin3A, Snr1 and Mod(mdg4) activate *dhd* independently of its heterochromatin mini-domain.**

The fact that the *pW8-dhd<sup>WT</sup>* transgene restored most of *dhd* expression without re-establishment of the heterochromatin mini-domain at this locus provided an opportunity to clarify the role of our set of *dhd* regulators. KD of *lid* is associated with increased H3K27me3 at the *dhd* mini-domain, suggesting that Lid may operate as an anti-repressor by counteracting heterochromatinization of the locus. However, we have previously found that *dhd* expression is not re-established in *lid* KD ovaries carrying a *pW8-dhd<sup>WT</sup>* rescue transgene [5]. Lid is thus required for *dhd* expression not only at its endogenous locus but also from the rescue transgene not decorated by H3K27me3

(Fig5). Therefore, Lid activates *dhd* independently of heterochromatin, suggesting that it does not operate strictly as an anti-repressor.

To discriminate between anti-repressive or activating roles of Sin3A, Mod(mdg4) and Snr1, we generated flies combining a *dhd*<sup>J5</sup> deficiency, the *pW8-dhd*<sup>WT</sup> transgene and an shRNA targeting *lid*, *Sin3a*, *Snr1* or *mod(mdg4)*, driven in germ cells by a *nos-Gal4* driver (Fig6-A). We confirmed by RT-qPCR that knockdowns were still efficient when using this driver (Fig-S8-A). Remarkably, all of these flies were almost completely sterile, and showed strong downregulation of *dhd* revealed by RT-qPCR (Fig6-B and Table1). Using Cut&Run-qPCR at the *dhd* locus, we further confirmed that these knockdowns had no effect on H3K27me3, which remained depleted in all conditions (Fig6-C and FigS8-B). Lid, Sin3A, Snr1 and Mod(mdg4) therefore stimulate *dhd* transcription in the absence of its heterochromatin mini-domain.

Our results indicate that the *dhd* heterochromatin mini-domain does not play a repressive role in ovaries, but do not exclude that it might maintain *dhd* silent in other tissues. RT-qPCR analysis on dissected ovaries, testes and male and female carcasses from transgenic lines expressing *dhd*<sup>J5</sup>;*pW8-dhd*<sup>WT</sup> revealed *dhd* expression uniquely from ovaries (Fig6-D). Because this transgene rescues *dhd* expression without restoring heterochromatin marks, these results suggest that the *dhd* heterochromatin mini-domain is not essential to repress ectopic *dhd* expression in adults. We note, however, that we cannot exclude that *dhd* was weakly and/or transiently expressed in certain cell types in these conditions, or that the rescue transgene could accumulate repressive marks in tissues other than ovaries.

## Discussion

### The ovarian hyperactivation of *dhd*

Here, we sought to understand how the genomic and epigenomic environments of *dhd* contributed to its remarkable regulation, its expression being both among the highest in *Drosophila*, and absolutely specific to adult ovaries [5,9]. Lid, Sin3A, Snr1 and Mod(mdg4) all shared a critical and rather specific role in ensuring *dhd* expression. Yet, these four broadly expressed proteins play multiple roles other than *dhd* regulation. For example, transcriptomic analyses following individual depletion of Lid, Sin3A or Snr1 in S2 cells, wing discs or pupae shows activation or repression of hundreds of targets [19,22,56]. ChIP-seq data further indicates that Mod(mdg4), Sin3A and Lid each target several thousand sites in the genome [24,26,57,58]. Consistently, our RNA-seq analyses did reveal that each of these knockdowns were associated to up- or down-regulation of 407 to 2020 genes in ovaries, with *dhd* being in every case among the most strongly dependent on these factors. We propose that *dhd* is a hypersensitive gene that reacts radically to epigenome imbalances.

The key question is therefore what is the formula for *dhd* ovarian hyperactivation. One reasonable hypothesis was that *dhd* could be highly regulated by distal enhancers. This would be notably consistent with the previously described role of Mod(mdg4) in organizing 3D contacts between regulatory elements and promoters [26]. It would also be consistent with recent findings that H3K27me3 micro-domains may reflect such contacts [59]. However, no interaction between *dhd* and any other locus can be found in Hi-C data, and our rescue transgene experiments show that a small, ectopic genomic segment almost fully recapitulates its expression, arguing that

the genomic and epigenomic environment at the endogenous *dhd* region may play only a minor role in its ovary-specific hyperactivation.

We indeed found a key regulatory element containing a tandem DRE motif, known to recruit the DREF core promoter factor. The minimal DRE motif (TATCGATA) is found in thousands of gene promoters [60], while multiple genes were individually shown to require this motif for proper activation. These include genes with ovarian expression, and, accordingly, DREF mutations cause oogenesis defects and female sterility [55]. In contrast, the particular tandem DRE motif in the *dhd* regulatory sequence is uncommon, being only found in 9 other gene promoters. Yet, among these 9 genes, only 4 displayed an expression bias in ovaries, and none were nearly as highly transcribed as *dhd*. Therefore, this motif does not seem to be autonomously sufficient for ovarian hyperexpression.

Another unusual feature of *dhd* is its surrounding heterochromatin mini-domain bearing both H3K27me3 and H3K9me3 marks, as well as H3K4me3. The co-occurrence of these active and repressive modifications at an ensemble of developmentally regulated genes in mammals led to the concept of bivalent promoters [61]. It is speculated that such promoters may be poised for rapid activation or repression upon differentiation. In *Drosophila*, bivalent chromatin is associated with genes that can be strongly activated in a tissue-specific manner [62,63]. Our experiments showed that *dhd* is expressed at ~60-70% of its normal levels in *E(z)* KD ovaries, as well as in rescue transgenes - conditions in which the H3K27me3/H3K9me3 mini-domain is impaired. We thus cannot exclude that these heterochromatin marks play a positive role in *dhd* activation to ensure its transcription at maximum capacity, perhaps via establishment of a bivalent configuration. We also note that our whole-tissue experiments leave the

possibility open that these histone modifications may decorate *dhd* in different cell types and/or at different times during gametogenesis.

Altogether, we uncovered multiple unusual genomic and epigenomic characteristics at the *dhd* locus, but failed to identify any single feature that was truly defining. The dramatic regulation of *dhd* may rely not on any individual trait but rather on a unique combination of such rare features. Further work will be needed to elucidate how these different components may together achieve ovarian hyperexpression.

## **A non-canonical chromatin domain**

The unique properties of *dhd* led us to uncover interesting features of its epigenomic regulators. First, *dhd* is embedded in an H3K27me3 mini-domain flanked by regulatory elements. A recent report suggested that H3K27me3 domain borders may be established independently of PREs or border elements, provided that an immediately neighboring active gene instead delimits H3K27me3 spreading [47]. The case of *dhd* is however peculiar in that the H3K27me3 domain border overlaps with this highly active gene, a scenario that was not found in other domains. The coincidence of H3K27me3 and H3K9me3 is also uncommon and, in fact, we could not find any other such dual domain in ovaries. Our result favors the view that this heterochromatin domain does not silence *dhd* expression. Nonetheless, H3K9me3 was always maintained at the *dhd*-distal portion of the domain. We therefore cannot exclude that this mark represses *dhd* neighbors.

An intriguing question is then how this heterochromatin mini-domain is formed. We found that a transgene containing the full mini-domain sequence is unable to restore H3K27me3 or H3K9me3, suggesting that genomic location of this domain is a

critical determinant of *dhd* heterochromatin. From this perspective, the border elements may act as weak PREs, as described in other contexts [64]. Interestingly, we also showed that H3K9me3 can be partially maintained at the distal part of the domain in *dhd<sup>Δ5</sup>* mutants while H3K27me3 is completely lost. This indicates that these marks are not necessarily inter-dependent at this locus, and H3K9me3 may benefit from additional mechanisms ensuring its deposition. While not much is known on highly localized euchromatic deposition of H3K9me3, Smolko and colleagues suggested that Setdb1-dependent accumulation of H3K9me3 at certain target genes is dependent on the RNA-binding protein Sxl [45]. At the *dhd* domain, different mechanisms could thus ensure H3K27me3 and H3K9me deposition, both of which would depend on the endogenous genomic location.

Along these lines, another recent study reported the existence of H3K27me3 micro-domains (typically 2-8 nucleosomes wide) that depend on 3D contacts with larger H3K27me3 domains, mediated, in particular, by BEAF-32 and CP190 [59]. The *dhd* mini-domain is wider and much more strongly enriched in H3K27me3 than typical micro-domains. Nonetheless, our data is consistent with a model whereby H3K27me3 could be deposited via such looping interactions. First, BEAF-32 and CP190 are indeed found at the border elements of the *dhd* mini-domain. Second, this mini-domain does not feature internal PREs and border elements are only weakly if at all bound by Polycomb proteins, arguing against an autonomous recruitment of E(z). Finally, a deletion of the BEAF-32/CP190-bearing regulatory element in the *dhd<sup>Δ5</sup>* mutant, or its displacement to an ectopic genomic location in rescue transgenes both abrogate H3K27me3 deposition. Consistent with such a model, data from Heurteau *et al.* show a modest reduction of H3K27me3 enrichment at the *dhd* mini-domain upon BEAF-32 depletion. Of note, BEAF-32 was also previously shown to facilitate H3K9me3

deposition at sites featuring multiple instances of the CGATA motif, analogous to those found at the *dhd* promoter [65]. Other studies found that ATCGAT motifs recognized by BEAF-32, also found at the *dhd* promoter, are more broadly enriched at the promoters of Lid-activated genes [66], which is the case of *dhd*. Thus, it is possible that a BEAF-32-mediated looping mechanism is responsible for H3K27me3 enrichment at the *dhd* mini-domain. However, our results also show that this mark is not strictly required to repress nor to activate *dhd* in adults, and that Lid, Sin3A, Snr1 and Mod(mdg4) activate *dhd* independently of it.

Scrutiny of *dhd* regulation further uncovered how its four regulators have convergent yet distinct roles. This was particularly intriguing for Lid and Sin3A, which can be found in a co-repressor complex [20], at odds with their positive impact on *dhd*. Indeed, their dual depletion in cultured cells causes the misregulation of hundreds of genes [19]. Interestingly, in that study, only 55 out of 849 affected genes were similarly impacted by individual and dual knockdowns, indicating that Lid and Sin3A functionally cooperate only at a minor subset of their common targets. This seems to be the case at the *dhd* locus, where individual KD of these factors caused an equally catastrophic collapse of transcriptional activity, suggesting a cooperative activity. Yet, Lid, but not Sin3A, acted as a negative regulator of H3K27me3 at the *dhd* locus, revealing at least partially independent functions. In contrast, Sin3A, but not Lid, controlled the stability of regulatory elements associated with this H3K27me3, not only at the *dhd* domain but also genome-wide.

Our results further show a critical role for Mod(mdg4) as a transcriptional activator. In cell lines, ChIP-seq experiments specifically mapping the insulating Mod(mdg4)<sup>67.2</sup> isoform or total Mod(mdg4) showed that additional isoforms are recruited to DNA [24]. Isoforms other than the 67.2 were found in particular at gene

promoters in ovaries and female heads [4]. Such is the case at the *dhd* promoter, where total Mod(mdg4) is found but not the 67.2 isoform (FigS2-B). Non-insulating roles of Mod(mdg4) were previously discussed in the context of the Polycomb-repressed Bithorax complex where the close binding of Mod(mdg4) to *Abd-B* transcription start sites suggested a role in transcription activation [26]. While we cannot rule out indirect effects, these observations argue that an activating isoform of Mod(mdg4) operates directly at the *dhd* promoter. In agreement, Mod(mdg4) appears to be essential to activate *dhd* within its H3K27me3 mini-domain, seemingly by stabilizing the *dhd* promoter regulatory element, although its function is equally essential in the absence of heterochromatin marks in the *dhd* transgenic rescue construct.

The Snr1-containing Brahma complex is required for activation of target genes in *Drosophila in vivo*, notably during immune responses [60] and tissue regeneration [56]. In ovaries, while Snr1 has a global impact on nuclear integrity and architecture, previous immunostaining experiments interestingly showed that this factor is only expressed during a restricted time in early oogenesis [22]. This underlines the fact that *dhd* may be dynamically regulated during oogenesis, with different regulatory components intervening at particular times. Considering that *Snr1* KD causes a disruption of the *dhd* promoter-proximal regulatory element associated with H3K27me3, this would suggest that its associated DNA-binding transcription factors also intervene during a restricted time in oogenesis. A precise dissection of the timing of *dhd* transcription, and determining whether these factors target *dhd* directly and simultaneously, would be essential to understand the cascade of events leading to its massive expression.

The case of *dhd* indeed illustrates the complexity of understanding the chromatin landscape at cell type-specific genes, when the starting material is a complex tissue. In

this context, the Cut&Run analysis implemented in our study allowed us to reveal the co-occupancy of H3K27me3 nucleosomes and associated transcription factors. While this approach cannot identify the cell of origin of each individual DNA molecule, it can be used to make important deductions on the combinatorial co-occupancy on DNA of different chromatin components. This approach joins other recent methods comparable in their principle, namely the DNA methyl-transferase single-molecule footprinting (dSMF) method [67] and the low-salt antibody-targeted tagmentation (CUTAC) approach [68]. Together with single-cell methodologies, these approaches hold the potential to begin uncovering complex epigenomic regulation processes, such as that of *dhd*, that were until recently inaccessible.

## **Acknowledgements**

We thank Dr. Kami Ahmad for sharing reagents and advice on Cut&Run. We are grateful to the TRiP projects and Bloomington Drosophila Stock Center for fly stocks. We acknowledge the contribution of SFR Biosciences (UAR3444/CNRS, US8/Inserm, ENS de Lyon, UCBL) facilities PLATIM and Arthro-tools. Sequencing was performed by the GenomEast platform, a member of the 'France Génomique' consortium. We would like to thank Raphaëlle Dubruille and Francesca Palladino for critical reading of the manuscript. We also warmly thank them, as well as Lucas Waltzer and all members of the Loppin lab for their input throughout this project. This work was supported by an Association pour la Recherche sur le Cancer (ARC) Foundation grant (PJA20191209671) to BL. DTC was supported by a PhD fellowship from the Ministère de l'Enseignement supérieur, de la Recherche et de l'Innovation and from the ARC (ARCD0C42020020001727).

## **Competing Interests Statement:**

The authors declare no competing interests.

## **Author Contributions**

**Conceptualization:** Daniela Torres-Campana, Benjamin Loppin, Guillermo A. Orsi.

**Funding acquisition:** Benjamin Loppin, Guillermo A. Orsi.

**Investigation:** Daniela Torres-Campana, Béatrice Horard, Sandrine Denaud, Benjamin Loppin, Guillermo A. Orsi.

**Data curation and formal analysis:** Daniela Torres-Campana, Gérard Benoit, Guillermo A. Orsi.

**Methodology:** Daniela Torres-Campana, Guillermo A. Orsi

**Supervision:** Béatrice Horard, Benjamin Loppin, Guillermo A. Orsi.

**Validation:** Daniela Torres-Campana, Guillermo A. Orsi.

**Writing – original draft:** Daniela Torres-Campana, Guillermo A. Orsi.

**Writing – review & editing:** Daniela Torres-Campana, Béatrice Horard, Gérard Benoit, Benjamin Loppin and Guillermo A. Orsi.

## **Materials & Methods**

### **Drosophila strains**

Flies were raised at 25°C on standard medium. The following stocks were obtained from the Bloomington *Drosophila* Stock Center (simplified genotypes are given):

*P{TRiP.HMS00849}attP2* (*mod(mdg4)* shRNA; #33907), *P{TRiP.HMS00363}attP2* (*Snr1* shRNA; #32372), *P{TRiP.GL00612}attP40* (*lid* shRNA; #36652), *P{TRiP.GLV21071}attP2* (*lid* shRNA; #35706), *P{TRiP.HMS00359}attP2* (*Sin3a* shRNA; #32368), *P{TRiP.HMS00066}attP2* (*E(z)* shRNA; #33659), *P{y[+t7.7]=CaryP}attP2* (Control line for TRiP RNAi lines; #B36303), *P{otu-GAL4::VP16.R}1*; *P{GAL4-nos.NGT}40*; *P{GAL4::VP16-nos.UTR}MVD1* (Maternal Triple Driver or “MTD-Gal4”; #31777), *P{GAL4::VP16-nos.UTR}MVD1* (“nos-Gal4”; #4937). Other stocks are: *w<sup>1118</sup>*, *Df(1)J5/FM7c* (Salz et al., 1994), *P[Mst35Ba-EGFP]* (Manier et al., 2010), *pW8-dhd<sup>WT</sup>* (Tirmarche et al., 2016). TRiP lines target all predicted isoforms of their respective target genes. “Control” in shRNA experiments refers to the offspring of the control line for TRiP lines crossed with the MTD-Gal4 line.

For the *pW8-dhd<sup>ΔDRE</sup>* mutant, two fragments were amplified by PCR from *w<sup>1118</sup>* genomic DNA using the primers ΔDRE-1-for/ ΔDRE-1-rev and ΔDRE-2-for/ ΔDRE-2-rev (Table S1). PCR products were assembled and cloned into the *pW8-dhd<sup>WT</sup>* vector (Tirmarche et al., 2016) previously digested by KpnI and BamHI using the NEBuilder HiFi DNA Assembly Cloning Kit (NEB, #E5520S). *dhd<sup>ΔDRE</sup>* transgene was integrated in the *PBac{attP-3B}VK00031* platform (62E1) using PhiC31-mediated transformation (Bischof et al., 2007) and flies were generated by The Best Gene (TheBestGene.com).

## Germline knock-down and fertility tests

To obtain *KD* females, virgin shRNA transgenic females were mass crossed with transgenic Gal4 males at 25°C and females of the desired genotype were recovered in the F1 progeny. All RNAi experiments were carried at 25°C. To measure fertility, virgin

females of different genotypes were mated to males in a 1:1 ratio and placed for 2 days at 25°C. They were then transferred to a new vial and allowed to lay eggs for 24 hours. Embryos were counted and then let to develop for at least 36 hours at 25°C. Unhatched embryos were counted to determine hatching rates.

## **Gene expression analysis by RT-QPCR**

Total RNA was extracted from ovaries of 3-day-old females using the NucleoSpin RNA isolation kit (Macherey-Nagel), following the instructions of the manufacturer. 1µg of total RNA was reverse transcribed using the SuperScript II Reverse Transcriptase kit (Invitrogen) with oligo (dT) primers. RT-qPCR reactions were performed in duplicates as described previously (Torres-Campana et al., 2020). Primer sets used are provided in Table S1. Statistical tests were performed using GraphPad Prism version 9.2.0 for Mac OS (GraphPad Software).

## **Immunofluorescence and imaging**

Early (0–30 min) embryos laid by females of the indicated genotypes were collected on agar plates. Embryos were dechorionated in bleach, fixed in a 1:1 heptane:methanol mixture and stored at -20°C. Embryos were washed three times (10 min each) with PBS 0.1%, Triton X-100 (PBS-T) and then incubated with primary antibodies in the same buffer on a wheel overnight at 4°C. They were then washed three times (20 min each) with PBS-T. Incubations with secondary antibodies were performed identically. Embryos were mounted in DAKO mounting medium containing DAPI.

Ovaries were dissected in PBS-T and fixed at room temperature in 4% formaldehyde in PBS for 25 minutes. Immunofluorescence was performed as for embryos. Ovaries were then mounted as described above.

Antibodies used are provided in Table S2. Images were acquired on an LSM 800 confocal microscope (Carl Zeiss). Images were processed with Zen imaging software (Carl Zeiss) and ImageJ software.

## Western blotting

Ovaries from 30 females were collected and homogenized in lysis buffer (20mM HEPES pH7.9, 100mM KCl, 0.1mM EDTA, 0.1mM EGTA, 5% Glycerol, 0.05% Igepal and protease inhibitors (Roche)). Protein extracts were cleared by centrifugation and purified with Pierce GST Spin Purification Kit (ThermoFisher Scientific, #16106). Western analysis was performed using standard procedures and used antibodies and concentrations are presented in Table S2.

## Ovarian RNA sequencing and analysis

Samples were processed as previously described (Torres-Campana et al., 2020).

Sequencing was completed on two biological replicates of the following genotypes:

*mod(mdg4)* KD (*MTD-Gal4>shRNA mod(mdg4)*), i.e

$P\{w[+mC] = otu-GAL4::VP16.R\}1, w[*]/y[1] sc[*] v[1]; P\{w[+mC] = GAL4-nos.NGT\}40/+;$

$P\{w[+mC] = GAL4::VP16-nos.UTR\}CG6325[MVD1]/P\{y[+t7.7] v[+t1.8] = TRiP.$

HMS00849} attP2

*Snr1* KD (*MTD-Gal4>shRNA Snr1*), i.e

$P\{w[+mC] = otu-GAL4::VP16.R\}1, w[*]/y[1] sc[*] v[1]; P\{w[+mC] = GAL4-nos.NGT\}40/+;$

$P\{w [+mC] = GAL4::VP16-nos.UTR\}CG6325[MVD1]/P\{y[+t7.7] v[+t1.8] = TRiP.$

$HMS00363\}attP2$

## Chromatin profiling by CUT&RUN

Cut&Run in *Drosophila* tissues was previously described [37]. Briefly, ovaries from 3-day-old flies were dissected in Wash+ Buffer (20 mM HEPES pH 7.5, 150 mM NaCl, 0.9 mM spermidine, 0.1% BSA with cOmplete protease inhibitor, Roche) and were bound to BioMag Plus Concanavalin-A-conjugated magnetic beads (ConA beads, Polysciences, Inc). Tissues were then permeabilized for 10min in dbE+ Buffer (20 mM HEPES pH 7.5, 150 mM NaCl, 0.9 mM spermidine, 2 mM EDTA, 0.1% BSA, 0.05% digitonin and protease inhibitors). Samples were then incubated with gentle rocking overnight at 4°C with primary antibody solution in dbE+ buffer (see Table S2 for antibody concentrations). Protein A fused to micrococcal nuclease (p-AMNase) was added in dbE+ buffer and samples were incubated with rotation at room temperature for 1 hour. Cleavage was done in WashCa+ buffer (20 mM HEPES pH 7.5, 150 mM NaCl, 0.9 mM spermidine, 0.1% BSA, 2 mM CaCl<sub>2</sub> with and protease inhibitors) at 0° for 30 minutes. Digestion was stopped with addition of 2XSTOP Buffer (200mM NaCl, 20mM EDTA, 4mM EGTA, 62.5µg/mL RNaseA). Samples were incubated at 37°C for 30 min to digest RNA and release DNA fragments. Cleaved DNA was then recovered with Ampure XP beads (Beckman Coulter) immediately after protease treatment. Antibodies used for CUT&RUN are listed in Table S2. Retrieved DNA was used either for qPCR or for library preparation followed by deep sequencing. Sequencing libraries for each sample were synthesized using Diagenode MicroPlex Library Preparation kit according to supplier recommendations (version 2.02.15) and were sequenced on Illumina HiSeq 4000

sequencer as Paired-End 100 base reads following Illumina's instructions (GenomEast platform, IGBM, Strasbourg, France). Image analysis and base calling were performed using RTA 2.7.7 and bcl2fastq 2.17.1.14. Adapter dimer reads were removed using DimerRemover.

## **Cut&Run-qPCR**

0,1 ng of retrieved DNA in Cut&Run were used as template in a real time quantitative PCR assay using SYBR Premix Ex Taq II (Tli RNaseH Plus) (Takara). All qPCR reactions were performed in duplicates using Bio-Rad CFX-96 Connect system with the following conditions: 95°C for 30s followed by 40 cycles of denaturation at 95°C for 5s and annealing and extension at 59°C for 30s. As a normalization control, we processed ovary samples from each studied genotype as for Cut&Run, except the antibody and pA-MNase incubation steps were omitted and instead we incubated tissue with 10U of Micrococcal Nuclease for 30min at 37°C (ThermoFisher Scientific, #88216). Fold change in histone mark enrichment was determined relative to this whole MNase control and relative to the *Sas10* gene, which was depleted in the histone marks tested in this study. Primer sets used are provided in Table S1.

## **Sequencing data processing**

Paired-end reads were mapped to the release 6 of the *D. melanogaster* genome using Bowtie2 (v. 2.4.2). To compare samples with identical readcount for genome coverage quantifications, we employed Downsample SAM/BAM (Galaxy Version 2.18.2.1). To obtain short fragment datasets for DNA regulatory element identification, peak calling and visualization, we selected fragments shorter than 120 bp from SAM files. These

were typically a small minority of all fragments, as our Cut&Run datasets were largely dominated by nucleosome-sized fragments (150-250bp). We therefore could separately analyze modification-bearing nucleosome coverage (for which the complete Cut&Run dataset, “All fragments”, was a good approximation) or putative regulatory element coverage (<120bp fragments). For genomic track visualization, we used bamCoverage from deepTools 2.0 (Galaxy Version 3.3.2.0.0) to calculate read coverage per 25bp bin for all fragments or 10bp bin for short fragments, with paired-end extension. Peak calling was done on sorted short fragments (<120 bp) with MACS2 (v. 2.1.1.20160309) with the following parameters: -nomodel, -p-value =0.0001, -keep-dup=all and the rest by default. To establish a high-confidence short fragment peak list we retained peaks that were present in biological replicates from the control genotype. Genome browser views screenshots were produced with the IGV software, for Cut&Run we used a 25bp bin for all fragments and a 10bp bin for short fragments (<120bp). For the midpoint-plot of fragment sizes around short fragment peaks, the length of each fragment was plotted as a function of the distance from the fragment midpoint to the summit of the peak identified by MACS2. For signal quantification at the *dhd* locus , normalized read counts were counted within the domain (Coordinates [5,312,054-5,317,465]) or within border element peaks (5' element: [5,312,120-5,312,211], 3' element: [5,317,300-5,317,447])

Heatmaps were generated with RStudio (RStudio Team (2016). RStudio: Integrated Development for R. RStudio, Inc., Boston, MA URL) and the packages ‘gplots’ (v.3.1.1) and ‘plyr’ (Wickham, 2011).

## **Data Availability:**

Original sequencing data from this publication have been deposited to the Gene Expression Omnibus with identifiers GSE174263 (RNA-seq) and GSE174250 (Cut&Run).

Additional sequencing data used in this study are available from GEO under the following accession numbers: GSE151981 (ATAC-seq), GSE37444 and GSE146993 (H3K27me3 ChIP-seq), GSE99027 (H3K9me3 ChIP-seq), GSE36393 (Mod(mdg4) ChIP-seq), GSE62904 (CP190, Beaf-32 and Dref ChIP-seq) and GSE24521 (Polycomb and Polyhomeotic ChIP-seq).

## Motif scanning

Motif scanning on the *pW8-dhd<sup>WT</sup>* transgene sequence was done with FIMO (v. 5.3.3) [69] using the flyreg v.2 motif database with default parameters.

## Figure Legends

### Figure 1. Mod(mdg4) and Snr1 are required for *dhd* expression.

A—Maternal Mod(mdg4) and Snr1 are required for protamine removal and sperm nuclear decompaction at fertilization. Top: Confocal images of pronuclear apposition in eggs from Control (*MTD>+*), *dhd<sup>l5</sup>*, *mod(mdg4)* KD or *Snr1* KD females mated with transgenic *ProtA::GFP* males. The sperm nucleus in *dhd<sup>l5</sup>*, *mod(mdg4)* KD and *Snr1* KD eggs retains ProtA::GFP (green) and has a needle-shape morphology. Bottom: zoom on the sperm nucleus. Scale bars: 5µm.

B— *dhd* is strongly downregulated in *mod(mdg4)* KD and *Snr1* KD ovaries. RNA-seq normalized reads per gene (in RPKM) are shown for *mod(mdg4)* KD vs Control (top) and *Snr1* KD vs Control (bottom). Genes downregulated (green) or upregulated (red) in KD ovaries are highlighted.

C— Genome Browser view of Control, *dhd<sup>l5</sup>*, *lid* KD, *Sin3a* KD, *mod(mdg4)* KD and *Snr1* KD ovarian RNA-seq signal at the *dhd* region showing dramatic downregulation in all KD conditions. Note that the Control track is represented at two different scales to fit

the high read count for *dhd* (top track) or the low read count for its neighboring genes (bottom track).

D— The DHD protein is undetectable in KD ovaries. Western blot analysis using an anti-DHD antibody on ovary extracts of the indicated genotypes. Alpha-tubulin is used as a loading control.

**Figure 2. A single Cut&Run experiment maps both histone modifications and their associated regulatory elements.**

A— Schematic overview of the Cut&Run procedure for dissected *Drosophila* ovaries. After tissue permeabilization and antibody targeting, ProteinA-MNase cleaves nearby exposed DNA allowing the solubilization and retrieval of both nucleosomal particles carrying the targeted histone modification and DNA particles occupied by transcription factors in the immediate vicinity.

B— Cut&Run reveals nucleosomes and transcription factor binding sites. Mid-point plot of ovarian H3K27me3 Cut&Run data centered at peaks identified by MACS2 from short fragments (<120bp) in the same experiment. This plot represents all paired-end sequenced fragments as their middle point coordinate in the X-axis, and their size in the Y-axis, revealing a class of clustered short fragments (50-130bp) flanked by nucleosome-sized fragments (>140bp).

C— H3K27me3 Cut&Run at the bithorax complex (BX-C) in *Drosophila* ovaries reveals its regulatory architecture. Genome browser track displaying all Cut&Run fragments and <120 bp fragments separately. Multiple well-described Polycomb Response Elements (PRE) and insulators within the Bithorax complex detected as short fragment peaks are indicated (arrows).

D— Cut&Run re-discovers regulatory elements associated with H3K27me3 genome-wide. Upper panels: short fragment peaks read density heatmaps of ovarian H3K27me3 Cut&Run (all fragments and <120bp fragments), ATAC-seq (from S2 cells, [35]), CP190 ChIP-seq (from Kc cells, [38]) and Polycomb ChIP-seq (Pc, from S2 cells, [37]) plotted at  $\pm 1$ kb around peak summit. Data is sorted by the ratio of H3K27me3 Cut&Run total reads at the 3' versus 5' flanks to reveal short fragment peaks at the borders or within H3K27me3 domains (dashed lines). Lower panels: average profiles corresponding to the top heatmaps, distinguishing 5' border peaks, 3' border peaks and peaks embedded within domains. Cut&Run short fragment peaks are enriched for ATAC-seq signal as well as CP190 (particularly at border peaks) and Polycomb (particularly at middle peaks).

**Figure 3. *dhd* is embedded in an H3K27me3/H3K9me3 mini-domain flanked by regulatory elements.**

A— The *dhd* region features an H3K27me3 and H3K9me3 mini-domain. Genome browser snapshots showing the distribution of all fragments and <120 bp fragments in the *dhd* region, revealing that *dhd* lies within a ~5450bp heterochromatin mini-domain

flanked by border regulatory elements associated with both H3K27me3 and H3K9me3. Arrows indicate direction of transcription.

B-The *dhd* mini-domain is highly enriched in H3K27me3 relative to its size. Scatter plot of our 278 ovarian H3K27me3 domains identified in Cut&Run, representing their average read counts normalized to domain size in the Y-axis versus domain size in the X-axis. C- Effect of the KDs on H3K27me3 enrichment genome-wide. Average normalized counts of H3K27me3 Cut&Run (all fragments) in H3K27me3 domains (plotted as meta-domains and including  $\pm 3$ kb from domain borders) in Control (*MTD>+*), *lid* KD, *Sin3a* KD, *mod(mdg4)* KD, *Snr1* KD and *E(z)* KD (arrows).

D- *lid* KD, but not *Sin3a*, *Snr1* or *mod(mdg4)*, impacts H3K27me3 enrichment at the *dhd* mini-domain. Left: genome browser plots of normalized H3K27me3 Cut&Run signal (all fragments) at the *dhd* genomic region in Control and KD ovaries. Right: Quantification of normalized read counts for the same samples. Data in this figure is for one representative replicate: other replicates are shown in FigS5-A.

E- Weak impact of KDs on heterochromatic marks at *dhd*. H3K27me3 and H3K9me3 Cut&Run-qPCR in Control and KD ovaries using the *Sas10* gene as negative control and *Ubx* and *CG12239* as positive controls for H3K27me3 and H3K9me3 respectively. Fold enrichment was calculated relative to *Sas10*. Error bars show technical variability from a representative replicate. Data in this figure is for one representative replicate: other replicates are shown in FigS5-B. P values indicate one-way ANOVA with Dunnett's multiple comparisons test to a control (\* P < 0.0001; n.s = not significant).

#### **Figure 4. Sin3A, Snr1 and Mod(mdg4) control the regulatory architecture of the *dhd* H3K27me3 mini-domain**

A- *Sin3a* and *Snr1* KD, but not *lid* or *mod(mdg4)*, impact H3K27me3-associated regulatory elements genome-wide. Left: H3K27me3 Cut&Run <120 bp fragments normalized counts in Control and KD ovaries, plotted at  $\pm 1$ kb around the summit of short fragment peaks. Right: Heatmaps displaying H3K27me3 Cut&Run short fragment peaks normalized read counts  $\pm 1$ kb around peak center in Control and KD ovaries.

B- Sin3A, Snr1 and Mod(mdg4), but not Lid, impact the organization of regulatory elements at the borders of the *dhd* H3K27me3 mini-domain. Left: genome browser plots of normalized Control H3K27me3 Cut&Run signal (all fragments, top) and of normalized signal from <120bp fragments retrieved in H3K27me3 Cut&Run in Control and KD ovaries. Right: Quantification of <120bp fragments normalized read counts for the same samples. 5' and 3' border elements are plotted separately. Data in this figure is for one representative replicate: other replicates are shown in FigS4-C.

C- Table recapitulating the effect of the different KDs on H3K27me3 and H3K27me3-associated regulatory elements (H3K27me3-RE) genome-wide and at the *dhd* locus. “ $\approx$ ” indicates modest or no change, “ $\nearrow$ ” indicates an increase and “ $\searrow$ ” a decrease in average read counts compared to Control. “?” indicates inability to conclude.

#### **Figure 5. The *dhd* promoter-proximal DRE motifs are required for its expression.**

A- Schematic representation of the genotypes studied in this figure. Upper panels: genomic browser views recapitulating the Control distribution of H3K27me3 Cut&Run signal (all fragments and <120bp fragments) as well as RNA-seq signal from Figures 1 and 2 at the *dhd* locus and showing lack of signal at the transgene insertion locus in the absence of any transgenic construct. Middle panel: schematic representation of the genomic composition of *w<sup>1118</sup>* (reference strain), mutant and rescue flies, indicating the status of the *dhd* locus and the composition of the rescue transgene. Dashed lines indicate the targeted region by primer couples (primers R and 1-5) used for RT- and Cut&Run-qPCR in panels B and D. Bottom panel: sequence of the *dhd* promoter at the endogenous location (left) and in the  $\Delta$ DRE mutant transgene where the 14bp containing the DRE motifs were deleted.

B- The DRE motifs at the *dhd* promoter are necessary for its expression. RT-qPCR quantification of *dhd* mRNA levels in ovaries from wild-type *w<sup>1118</sup>* flies, *dhd<sup>l5</sup>* mutants or *dhd<sup>l5</sup>* mutants carrying either a WT (*pW8-dhd<sup>WT</sup>*) or a mutant (*pW8-dhd <sup>$\Delta$ DRE</sup>*) or a full domain (*pW8-dhd<sup>FD</sup>*) transgene (measured using the R primers, normalized to *rp49* and relative to expression in *w<sup>1118</sup>*). Data from biological duplicates analyzed in technical duplicates are presented as mean  $\pm$  SEM. P values indicate one-way ANOVA with Tukey's multiple comparisons test (\* P < 0.0001; n.s = not significant).

C- The *dhd* heterochromatin domain is affected in *dhd*-containing transgenic constructs. Genome browser plots of normalized ovarian H3K27me3 and H3K9me3 Cut&Run signal at the *dhd* genomic region in the indicated genotypes. The H3K27me3 domain is abolished in all transgenic rescues. The H3K9me3 domain is partly affected in the *dhd<sup>l5</sup>* mutant, being lost the *dhd*-proximal end but maintained in the *dhd*-distal end. Dashed lines and numbers (1 to 5) indicate the targeted region by primer couples used for qPCR in panel D.

D- A transgene containing the full *dhd* domain does not restore heterochromatin marks. H3K27me3 and H3K9me3 Cut&Run-qPCR in Control, *dhd<sup>l5</sup>*, *dhd<sup>l5</sup>;;pW8-dhd<sup>WT</sup>* and *dhd<sup>l5</sup>;;pW8-dhd<sup>FD</sup>* ovaries. Fold enrichment was calculated relative to *Sas10*. Error bars show technical variability from a representative replicate. Data in this figure is for one representative replicate: other replicates are shown in FigS7.

**Figure 6. Lid, Sin3A, Mod(mdg4) and Snr1 are necessary for *dhd* expression in the absence of its heterochromatin domain.**

A-Schematic representation of the genomic composition of *w<sup>1118</sup>* (reference strain) and mutant flies carrying a rescue transgene and shRNA constructs controlled by the female germline specific nanos-Gal4 driver, respectively inserted at the platforms *attP 3B-62E1* and *attP 2- 68A4*.

B-The rescue transgene does not restore *dhd* expression in KD ovaries. RT-qPCR quantification of *dhd* mRNA levels in ovaries of the indicated genotypes (normalized to *rp49* and relative to expression in *w<sup>1118</sup>* ovaries). Data from biological duplicates analyzed in technical duplicates are presented as mean  $\pm$  SEM. P value indicates one-way ANOVA with Tukey's multiple comparisons test (\* P < 0.0001),

C-H3K27me3 is absent from the *dhd* rescue transgene. H3K27me3 Cut&Run-qPCR in the indicated genotypes. The *Sas10* gene was used as negative control and *Ubx* as positive control. Fold enrichment was calculated relative to *Sas10*. Error bars show technical variability from a representative replicate. Error bars show technical variability from a representative replicate. Data in this figure is for one representative replicate: other replicates are shown in FigS8.

D- *dhd* is not ectopically expressed in adult tissues in the absence of its heterochromatin domain. RT-qPCR quantification of *dhd* mRNA levels in dissected ovaries or corresponding female carcasses as well as testes or corresponding male carcasses, in all indicated genotypes (normalized to *rp49* and relative to expression in ovaries in *w<sup>1118</sup>*). Data from biological duplicates analyzed in technical duplicates are presented as mean  $\pm$  SEM. P value indicates one-way ANOVA with Tukey's multiple comparisons test (\* P < 0.0001).

## REFERENCES

1. Bannister AJ, Kouzarides T. Regulation of chromatin by histone modifications. *Cell Res.* 2011;21: 381–395. doi:10.1038/cr.2011.22
2. Hammond CM, Strømme CB, Huang H, Patel DJ, Groth A. Histone chaperone networks shaping chromatin function. *Nat Rev Mol Cell Biol.* 2017;18: 141–158. doi:10.1038/nrm.2016.159
3. Tyagi M, Imam N, Verma K, Patel AK. Chromatin remodelers: We are the drivers!! *Nucleus.* 2016;7: 388–404. doi:10.1080/19491034.2016.1211217
4. Melnikova LS, Georgiev PG, Golovnin AK. The Functions and Mechanisms of Action of Insulators in the Genomes of Higher Eukaryotes. *Acta Naturae.* 2020;12: 15–33. doi:10.32607/actanaturae.11144
5. Torres-Campana D, Kimura S, Orsi GA, Horard B, Benoit G, Loppin B. The Lid/KDM5 histone demethylase complex activates a critical effector of the oocyte-to-zygote transition. Bosco G, editor. *PLoS Genet.* 2020;16: e1008543. doi:10.1371/journal.pgen.1008543
6. Spradling A. The development of *Drosophila melanogaster*. 1993.
7. Salz HK, Flickinger TW, Mittendorf E, Pellicena-Palle A, Petschek JP, Albrecht EB. The *Drosophila* maternal effect locus deadhead encodes a thioredoxin homolog required for female meiosis and early embryonic development. *Genetics.* 1994;136: 1075–1086. doi:10.1093/genetics/136.3.1075

8. Svensson MJ, Chen JD, Pirrotta V, Larsson J. The ThioredoxinT and deadhead gene pair encode testis- and ovary-specific thioredoxins in *Drosophila melanogaster*. *Chromosoma*. 2003;112: 133–143. doi:10.1007/s00412-003-0253-5
9. Tirmarche S, Kimura S, Dubruille R, Horard B, Loppin B. Unlocking sperm chromatin at fertilization requires a dedicated egg thioredoxin in *Drosophila*. *Nat Commun*. 2016;7: 13539. doi:10.1038/ncomms13539
10. Petrova B, Liu K, Tian C, Kitaoka M, Freinkman E, Yang J, et al. Dynamic redox balance directs the oocyte-to-embryo transition via developmentally controlled reactive cysteine changes. *Proc Natl Acad Sci USA*. 2018;115: E7978–E7986. doi:10.1073/pnas.1807918115
11. Freier R, Aragón E, Bagiński B, Pluta R, Martin-Malpartida P, Ruiz L, et al. Structures of the germline-specific Deadhead and thioredoxin T proteins from *Drosophila melanogaster* reveal unique features among thioredoxins. *IUCrJ*. 2021;8: 281–294. doi:10.1107/S2052252521000221
12. Emelyanov AV, Fyodorov DV. Thioredoxin-dependent disulfide bond reduction is required for protamine eviction from sperm chromatin. *Genes Dev*. 2016;30: 2651–2656. doi:10.1101/gad.290916.116
13. Dingwall AK, Beek SJ, McCallum CM, Tamkun JW, Kalpana GV, Goff SP, et al. The *Drosophila* snr1 and brm proteins are related to yeast SWI/SNF proteins and are components of a large protein complex. *MBoC*. 1995;6: 777–791. doi:10.1091/mbc.6.7.777
14. Gerasimova TI, Gdula DA, Gerasimov DV, Simonova O, Corces VG. A *drosophila* protein that imparts directionality on a chromatin insulator is an enhancer of position-effect variegation. *Cell*. 1995;82: 587–597. doi:10.1016/0092-8674(95)90031-4
15. Skene PJ, Henikoff S. An efficient targeted nuclease strategy for high-resolution mapping of DNA binding sites. *eLife*. 2017;6: e21856. doi:10.7554/eLife.21856
16. Hirose F, Yamaguchi M, Handa H, Inomata Y, Matsukage A. Novel 8-base pair sequence (*Drosophila* DNA replication-related element) and specific binding factor involved in the expression of *Drosophila* genes for DNA polymerase alpha and proliferating cell nuclear antigen. *J Biol Chem*. 1993;268: 2092–2099.
17. Spain MM, Caruso JA, Swaminathan A, Pile LA. *Drosophila* SIN3 isoforms interact with distinct proteins and have unique biological functions. *J Biol Chem*. 2010;285: 27457–27467. doi:10.1074/jbc.M110.130245
18. Das TK, Sangodkar J, Negre N, Narla G, Cagan RL. Sin3a acts through a multi-gene module to regulate invasion in *Drosophila* and human tumors. *Oncogene*. 2013;32: 3184–3197. doi:10.1038/onc.2012.326
19. Gajan A, Barnes VL, Liu M, Saha N, Pile LA. The histone demethylase dKDM5/LID interacts with the SIN3 histone deacetylase complex and shares functional

- similarities with SIN3. *Epigenetics & Chromatin*. 2016;9: 4. doi:10.1186/s13072-016-0053-9
20. Moshkin YM, Kan TW, Goodfellow H, Bezstarosti K, Maeda RK, Pilyugin M, et al. Histone Chaperones ASF1 and NAP1 Differentially Modulate Removal of Active Histone Marks by LID-RPD3 Complexes during NOTCH Silencing. *Molecular Cell*. 2009;35: 782–793. doi:10.1016/j.molcel.2009.07.020
  21. Ni J-Q, Zhou R, Czech B, Liu L-P, Holderbaum L, Yang-Zhou D, et al. A genome-scale shRNA resource for transgenic RNAi in *Drosophila*. *Nat Methods*. 2011;8: 405–407. doi:10.1038/nmeth.1592
  22. Zraly CB, Marendra DR, Nanchal R, Cavalli G, Muchardt C, Dingwall AK. SNR1 is an essential subunit in a subset of *Drosophila* brm complexes, targeting specific functions during development. *Dev Biol*. 2003;253: 291–308. doi:10.1016/s0012-1606(02)00011-8
  23. Dorn R, Reuter G, Loewendorf A. Transgene analysis proves mRNA trans-splicing at the complex *mod(mdg4)* locus in *Drosophila*. *Proc Natl Acad Sci U S A*. 2001;98: 9724–9729. doi:10.1073/pnas.151268698
  24. Van Bortle K, Ramos E, Takenaka N, Yang J, Wahi JE, Corces VG. *Drosophila* CTCF tandemly aligns with other insulator proteins at the borders of H3K27me3 domains. *Genome Res*. 2012;22: 2176–2187. doi:10.1101/gr.136788.111
  25. Büchner K, Roth P, Schotta G, Krauss V, Saumweber H, Reuter G, et al. Genetic and Molecular Complexity of the Position Effect Variegation Modifier *mod(mdg4)* in *Drosophila*. *Genetics*. 2000;155: 141–157. doi:10.1093/genetics/155.1.141
  26. Savitsky M, Kim M, Kravchuk O, Schwartz YB. Distinct Roles of Chromatin Insulator Proteins in Control of the *Drosophila* Bithorax Complex. *Genetics*. 2016;202: 601–617. doi:10.1534/genetics.115.179309
  27. Manier MK, Belote JM, Berben KS, Novikov D, Stuart WT, Pitnick S. Resolving mechanisms of competitive fertilization success in *Drosophila melanogaster*. *Science*. 2010;328: 354–357. doi:10.1126/science.1187096
  28. Henikoff JG, Belsky JA, Krassovsky K, MacAlpine DM, Henikoff S. Epigenome characterization at single base-pair resolution. *Proceedings of the National Academy of Sciences*. 2011;108: 18318–18323. doi:10.1073/pnas.1110731108
  29. Kasinathan S, Orsi GA, Zentner GE, Ahmad K, Henikoff S. High-resolution mapping of transcription factor binding sites on native chromatin. *Nat Methods*. 2014;11: 203–209. doi:10.1038/nmeth.2766
  30. Orsi GA, Kasinathan S, Hughes KT, Saminadin-Peter S, Henikoff S, Ahmad K. High-resolution mapping defines the cooperative architecture of Polycomb response elements. *Genome Research*. 2014;24: 809–820. doi:10.1101/gr.163642.113

31. Ramachandran S, Ahmad K, Henikoff S. Transcription and Remodeling Produce Asymmetrically Unwrapped Nucleosomal Intermediates. *Molecular Cell*. 2017;68: 1038-1053.e4. doi:10.1016/j.molcel.2017.11.015
32. Cleard F, Wolle D, Taverner AM, Aoki T, Deshpande G, Andolfatto P, et al. Different Evolutionary Strategies To Conserve Chromatin Boundary Function in the Bithorax Complex. *Genetics*. 2017;205: 589–603. doi:10.1534/genetics.116.195586
33. Kyrchanova O, Mogila V, Wolle D, Deshpande G, Parshikov A, Cléard F, et al. Functional Dissection of the Blocking and Bypass Activities of the Fab-8 Boundary in the *Drosophila* Bithorax Complex. Sánchez-Herrero E, editor. *PLoS Genet*. 2016;12: e1006188. doi:10.1371/journal.pgen.1006188
34. Ahmad K, Spens AE. Separate Polycomb Response Elements control chromatin state and activation of the vestigial gene. Cavalli G, editor. *PLoS Genet*. 2019;15: e1007877. doi:10.1371/journal.pgen.1007877
35. Jain SU, Rashoff AQ, Krabbenhoft SD, Hoelper D, Do TJ, Gibson TJ, et al. H3 K27M and EZHIP Impede H3K27-Methylation Spreading by Inhibiting Allosterically Stimulated PRC2. *Mol Cell*. 2020;80: 726-735.e7. doi:10.1016/j.molcel.2020.09.028
36. Minoux M, Holwerda S, Vitobello A, Kitazawa T, Kohler H, Stadler MB, et al. Gene bivalency at Polycomb domains regulates cranial neural crest positional identity. *Science*. 2017;355: eaal2913. doi:10.1126/science.aal2913
37. Enderle D, Beisel C, Stadler MB, Gerstung M, Athri P, Paro R. Polycomb preferentially targets stalled promoters of coding and noncoding transcripts. *Genome Res*. 2011;21: 216–226. doi:10.1101/gr.114348.110
38. Li L, Lyu X, Hou C, Takenaka N, Nguyen HQ, Ong C-T, et al. Widespread Rearrangement of 3D Chromatin Organization Underlies Polycomb-Mediated Stress-Induced Silencing. *Molecular Cell*. 2015;58: 216–231. doi:10.1016/j.molcel.2015.02.023
39. Bartkuhn M, Straub T, Herold M, Herrmann M, Rathke C, Saumweber H, et al. Active promoters and insulators are marked by the centrosomal protein 190. *EMBO J*. 2009;28: 877–888. doi:10.1038/emboj.2009.34
40. Colmenares SU, Swenson JM, Langley SA, Kennedy C, Costes SV, Karpen GH. *Drosophila* Histone Demethylase KDM4A Has Enzymatic and Non-enzymatic Roles in Controlling Heterochromatin Integrity. *Developmental Cell*. 2017;42: 156-169.e5. doi:10.1016/j.devcel.2017.06.014
41. Kassis JA, Kennison JA, Tamkun JW. Polycomb and Trithorax Group Genes in *Drosophila*. *Genetics*. 2017;206: 1699–1725. doi:10.1534/genetics.115.185116
42. Schuettengruber B, Bourbon H-M, Di Croce L, Cavalli G. Genome Regulation by Polycomb and Trithorax: 70 Years and Counting. *Cell*. 2017;171: 34–57. doi:10.1016/j.cell.2017.08.002

43. Brower-Toland B, Riddle NC, Jiang H, Huisinga KL, Elgin SCR. Multiple SET methyltransferases are required to maintain normal heterochromatin domains in the genome of *Drosophila melanogaster*. *Genetics*. 2009;181: 1303–1319. doi:10.1534/genetics.108.100271
44. Ninova M, Fejes Tóth K, Aravin AA. The control of gene expression and cell identity by H3K9 trimethylation. *Development*. 2019;146: dev181180. doi:10.1242/dev.181180
45. Smolko AE, Shapiro-Kulnane L, Salz HK. The H3K9 methyltransferase SETDB1 maintains female identity in *Drosophila* germ cells. *Nat Commun*. 2018;9: 4155. doi:10.1038/s41467-018-06697-x
46. Kadoch C, Williams RT, Calarco JP, Miller EL, Weber CM, Braun SMG, et al. Dynamics of BAF–Polycomb complex opposition on heterochromatin in normal and oncogenic states. *Nat Genet*. 2017;49: 213–222. doi:10.1038/ng.3734
47. De S, Gehred ND, Fujioka M, Chan FW, Jaynes JB, Kassis JA. Defining the Boundaries of Polycomb Domains in *Drosophila*. *Genetics*. 2020;216: 689–700. doi:10.1534/genetics.120.303642
48. Iovino N, Ciabrelli F, Cavalli G. PRC2 controls *Drosophila* oocyte cell fate by repressing cell cycle genes. *Dev Cell*. 2013;26: 431–439. doi:10.1016/j.devcel.2013.06.021
49. Phillips MD, Shearn A. Mutations in polycombetic, a *Drosophila* polycomb-group gene, cause a wide range of maternal and zygotic phenotypes. *Genetics*. 1990;125: 91–101.
50. DeLuca SZ, Ghildiyal M, Pang L-Y, Spradling AC. Differentiating *Drosophila* female germ cells initiate Polycomb silencing by regulating PRC2-interacting proteins. *eLife*. 2020;9: e56922. doi:10.7554/eLife.56922
51. Bergman CM, Carlson JW, Celniker SE. *Drosophila* DNase I footprint database: a systematic genome annotation of transcription factor binding sites in the fruitfly, *Drosophila melanogaster*. *Bioinformatics*. 2005;21: 1747–1749. doi:10.1093/bioinformatics/bti173
52. Daniel Avery Pollard. *Drosophila* Sequence Specific Transcription Factor Binding Site Matrices. Available: <http://www.danielpollard.com/matrices.html>
53. Zhao K, Hart CM, Laemmli UK. Visualization of chromosomal domains with boundary element-associated factor BEAF-32. *Cell*. 1995;81: 879–889. doi:10.1016/0092-8674(95)90008-X
54. Roy S, Gilbert MK, Hart CM. Characterization of *BEAF* Mutations Isolated by Homologous Recombination in *Drosophila*. *Genetics*. 2007;176: 801–813. doi:10.1534/genetics.106.068056

55. Park J-S, Choi Y-J, Thao DTP, Kim Y-S, Yamaguchi M, Yoo M-A. DREF is involved in the steroidogenesis via regulation of shadow gene. *Am J Cancer Res.* 2012;2: 714–725.
56. Tian Y, Smith-Bolton RK. Regulation of growth and cell fate during tissue regeneration by the two SWI/SNF chromatin-remodeling complexes of *Drosophila*. Duronio R, editor. *Genetics.* 2021;217: 1–16. doi:10.1093/genetics/iyaa028
57. Liu X, Secombe J. The Histone Demethylase KDM5 Activates Gene Expression by Recognizing Chromatin Context through Its PHD Reader Motif. *Cell Reports.* 2015;13: 2219–2231. doi:10.1016/j.celrep.2015.11.007
58. Saha N, Liu M, Gajan A, Pile LA. Genome-wide studies reveal novel and distinct biological pathways regulated by SIN3 isoforms. *BMC Genomics.* 2016;17: 111. doi:10.1186/s12864-016-2428-5
59. Heurteau A, Perrois C, Depierre D, Fosseprez O, Humbert J, Schaak S, et al. Insulator-based loops mediate the spreading of H3K27me3 over distant microdomains repressing euchromatin genes. *Genome Biol.* 2020;21: 193. doi:10.1186/s13059-020-02106-z
60. Gurudatta B, Yang J, Van Bortle K, Donlin-Asp P, Corces V. Dynamic changes in the genomic localization of DNA replication-related element binding factor during the cell cycle. *Cell Cycle.* 2013;12: 1605–1615. doi:10.4161/cc.24742
61. Bernstein BE, Mikkelsen TS, Xie X, Kamal M, Huebert DJ, Cuff J, et al. A bivalent chromatin structure marks key developmental genes in embryonic stem cells. *Cell.* 2006;125: 315–326. doi:10.1016/j.cell.2006.02.041
62. Akmammedov A, Geigges M, Paro R. Bivalency in *Drosophila* embryos is associated with strong inducibility of Polycomb target genes. *Fly (Austin).* 2019;13: 42–50. doi:10.1080/19336934.2019.1619438
63. Schertel C, Albarca M, Rockel-Bauer C, Kelley NW, Bischof J, Hens K, et al. A large-scale, in vivo transcription factor screen defines bivalent chromatin as a key property of regulatory factors mediating *Drosophila* wing development. *Genome Res.* 2015;25: 514–523. doi:10.1101/gr.181305.114
64. De S, Mitra A, Cheng Y, Pfeifer K, Kassis JA. Formation of a Polycomb-Domain in the Absence of Strong Polycomb Response Elements. Bantignies F, editor. *PLoS Genet.* 2016;12: e1006200. doi:10.1371/journal.pgen.1006200
65. Emberly E, Blattes R, Schuettengruber B, Hennion M, Jiang N, Hart CM, et al. BEAF Regulates Cell-Cycle Genes through the Controlled Deposition of H3K9 Methylation Marks into Its Conserved Dual-Core Binding Sites. Misteli T, editor. *PLoS Biology.* 2008;6: e327. doi:10.1371/journal.pbio.0060327
66. Zamurrad S, Hatch HAM, Drelon C, Belalcazar HM, Secombe J. A *Drosophila* Model of Intellectual Disability Caused by Mutations in the Histone Demethylase KDM5. *Cell Rep.* 2018;22: 2359–2369. doi:10.1016/j.celrep.2018.02.018

67. Krebs AR, Imanci D, Hoerner L, Gaidatzis D, Burger L, Schübeler D. Genome-wide Single-Molecule Footprinting Reveals High RNA Polymerase II Turnover at Paused Promoters. *Molecular Cell*. 2017;67: 411-422.e4. doi:10.1016/j.molcel.2017.06.027
68. Henikoff S, Henikoff JG, Kaya-Okur HS, Ahmad K. Efficient chromatin accessibility mapping *in situ* by nucleosome-tethered tagmentation. *Genomics*; 2020 Apr. doi:10.1101/2020.04.15.043083
69. Grant CE, Bailey TL, Noble WS. FIMO: scanning for occurrences of a given motif. *Bioinformatics*. 2011;27: 1017–1018. doi:10.1093/bioinformatics/btr064

## Supporting Information Captions:

### Figure S1. *mod(mdg4)* KD and *Snr1* KD downregulate *dhd*

A-*mod(mdg4)* KD and *Snr1* KD are efficient in the female germline. Left: RT-qPCR quantification of *mod(mdg4)* (top) or *Snr1* (bottom) mRNA levels in Control and KD ovaries (normalized to *rp49* and relative to expression in Control ovaries). Data from biological duplicates analyzed in technical duplicates are presented as mean  $\pm$  SEM. **Right:** Quantification of *mod(mdg4)* (top) and *Snr1*(bottom) counts in RNA-seq data from Fig1B. Both duplicates are shown.

B-*lid*, *Sin3a*, *Snr1* and *mod(mdg4)* KDs downregulate *dhd* but do not significantly affect its neighboring genes. Quantification of counts in RNA-seq data for *dhd* and its neighboring genes in Control, *lid*, *Sin3a*, *Snr1* and *mod(mdg4)* KD show that low-expressing genes in the *dhd* region are not or only modestly impacted by the KDs. Both duplicates are shown.

C-Limited overlap in the effects of *mod(mdg4)* and *Snr1* KDs. Hierarchical clustering of sample distance heatmap of RNA-seq samples.

D-Principal component analysis for RNA-seq samples.

E- *lid*, *Sin3a*, *mod(mdg4)* and *Snr1* KD severely downregulate *dhd* expression. RT-qPCR quantification of *dhd* mRNA levels in ovaries of indicated genotypes (normalized to *rp49* and relative to expression in Control ovaries). Two different shRNA constructs (val21 and val22) against *lid* were tested. Data from biological duplicates analyzed in technical duplicates are presented as mean  $\pm$  SEM.

### Figure S2. Cut&Run is consistent with ChIP-seq data.

A—Histone modification profiles at the *dhd* region in cultured embryonic cells and ovaries. ChIP-seq data showing the active mark H3K4me3 (yellow) [5], and the repressive marks H3K9me3 (green) [40,45] and H3K27me3 (blue) (accession number GSE146993, [50]).

B—Short fragment peaks align with known regulatory elements. Genome browser views of the bithorax complex (BX-C) (left) and the *dhd* region (right). Display of H3K27me3 Cut&Run (from Control ovaries, all fragments and <120bp fragments), ATAC-seq (from S2 cells, [35]), CP190 ChIP-seq (from Kc cells, [38]), Mod(*mdg4*) (all isoforms) and Mod(*mdg4*)67.2 isoform ChIP-seq (from Kc cells, [24]) Polycomb (Pc) and Polyhomeotic (Ph) ChIP-seq (from S2 cells, [37]). Cut&Run short fragments largely overlap with peaks from the other tracks displayed.

**Figure S3. Cut&Run maps H3K9me3 in ovaries.**

A- Cut&Run shows the expected enrichment of H3K9me3 at pericentromeric heterochromatin. Genome browser views of H3K9me3 ChIP-seq [45] and Cut&Run signal in all chromosomes.

B- Cut&Run detects a previously identified H3K9me3 peak over a testis-specific TSS [45]. Genome browser view of *phf7* and neighboring genes. Blue arrow indicates testis-specific TSS and magenta arrow indicates ovary-specific TSS.

**Figure S4. Whole-ovary experiments yield signal from both somatic follicle cells and germline cells.**

A-*E(z)* KD does not severely affect *dhd* expression. RT-qPCR quantification of *dhd* mRNA levels in Control and *E(z)* KD ovaries (normalized to *rp49* and relative to expression in Control ovaries). Data from biological duplicates analyzed in technical duplicates are presented as mean ± SEM.

B- *E(z)* KD and *Snr1* KD affect H3K27me3 levels in nurse cells. Confocal images of representative egg chambers in Control, *E(z)* KD, *lid* KD, *Sin3a* KD, *mod(mdg4)* KD and *Snr1* KD. In control ovaries, H3K27me3 staining marks somatic follicle cell nuclei, the karyosome and germline nurse cell nuclei. In *E(z)* KD ovaries the karyosome and nurse cells loose staining of the histone mark but follicle cells are marked normally. No notable change is observed in *lid* KD, *Sin3a* KD or *mod(mdg4)* KD while in *Snr1* KD nurse cells staining is less intense. Scale bar 10µm.

C- Cut&Run in whole ovaries captures signal from both somatic and germline cells. Genome browser views of H3K27me3 Cut&Run signal in Control and *E(z)* KD ovaries and H3K27me3 ChIP-seq from FACS sorted nurse cells and somatic follicle cells [50]. Upper panels show representative loci enriched for the mark solely in nurse cells (germline) and absent in *E(z)* KD ovaries. Lower panels show H3K27me3 domains where the signal comes almost exclusively from follicle cells and is not significantly affected in the germline *E(z)* KD.

**Figure S5. Cut&Run is reproducible among replicates.**

A—H3K27me3 Cut&Run signal at the *dhd* locus from Control and KD ovaries. Left: Dotplot showing normalized read counts of H3K27me3 Cut&Run at the *dhd* domain from independent biological triplicates of the indicated genotypes (duplicates for *E(z)* KD).

B— Cut&Run qPCR yields reproducible data among replicates. Biological replicates from H3K27me3 and H3K9me3 Cut&Run-qPCR in Control and KD ovaries shown in Fig3-E. The *Sas10* gene was used as negative control and *Ubx* and *CG12239* as positive controls for H3K27me3 and H3K9me3 respectively. Fold enrichment was calculated relative to *Sas10*. Error bars show technical variability.

C— *Sin3a* KD, *Snr1* KD and *mod(mdg4)* KD affect the stability of the H3K27me3-associated regulatory elements at the *dhd* mini-domain. Dotplot showing normalized read counts of H3K27me3 Cut&Run <120bp fragments at *dhd* regulatory elements from independent biological triplicates of the indicated genotypes (duplicates for *E(z)* KD). 5' and 3' border elements are plotted separately.

**Figure S6. Dref and Beaf-32 are found at *dhd* regulatory elements.**

Genome browser views of ovarian H3K27me3 Cut&Run (all fragments and <120bp fragments) and Dref and Beaf-32 CHIP-seq (from Kc cells, [38]). <120 bp fragment peaks at the *dhd* domain borders align with DREF and Beaf-32 peaks.

**Figure S7. Cut&Run qPCR generates reproducible data from transgenes**

Biological replicates of H3K27me3 and H3K9me3 Cut&Run-qPCR in Control, *dhd<sup>Δ5</sup>*, *dhd<sup>Δ5</sup>::pW8-dhd<sup>WT</sup>* and *dhd<sup>Δ5</sup>::pW8-dhd<sup>FD</sup>* ovaries shown in Fig5-D. Fold enrichment was calculated relative to *Sas10*. Error bars show technical variability.

**Figure S8. In *lid* KD, *Sin3a* KD, *mod(mdg4)* KD and *Snr1* KD rescue flies, H3K27me3 is absent from the *dhd* rescue transgene**

A— *lid* KD, *Sin3a* KD, *mod(mdg4)* KD and *Snr1* KD are efficient in the female germline of rescue flies. From left to right: RT-qPCR quantification of *lid*, *Sin3a*, *mod(mdg4)* and *Snr1* mRNA levels in ovaries of the indicated genotypes (normalized to *rp49* and relative to expression in *w<sup>1118</sup>* ovaries). Data from biological duplicates analyzed in technical duplicates are presented as mean ± SEM.

B— The *dhd* rescue transgene does not restore H3K27me3 in KD flies. Biological replicates of H3K27me3 Cut&Run-qPCR in the indicated genotypes shown in Fig6-C. The *Sas10* gene was used as negative control and *Ubx* as positive control. Fold enrichment was calculated relative to *Sas10*. Error bars show technical variability.

**Table S1. List of primers used in this paper.**

**Table S2. List of antibodies used in this paper.**

Figure 1

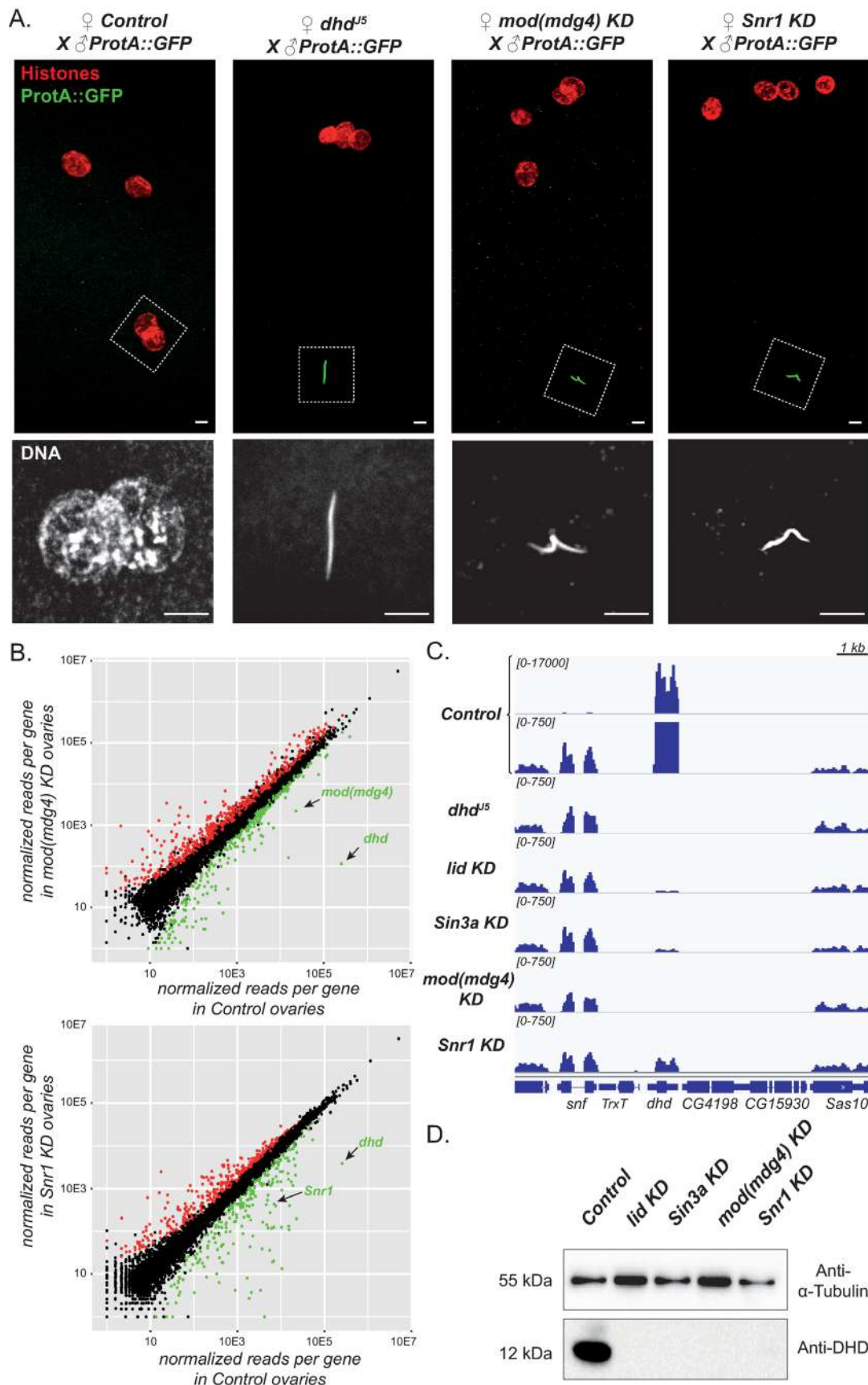


Figure 2

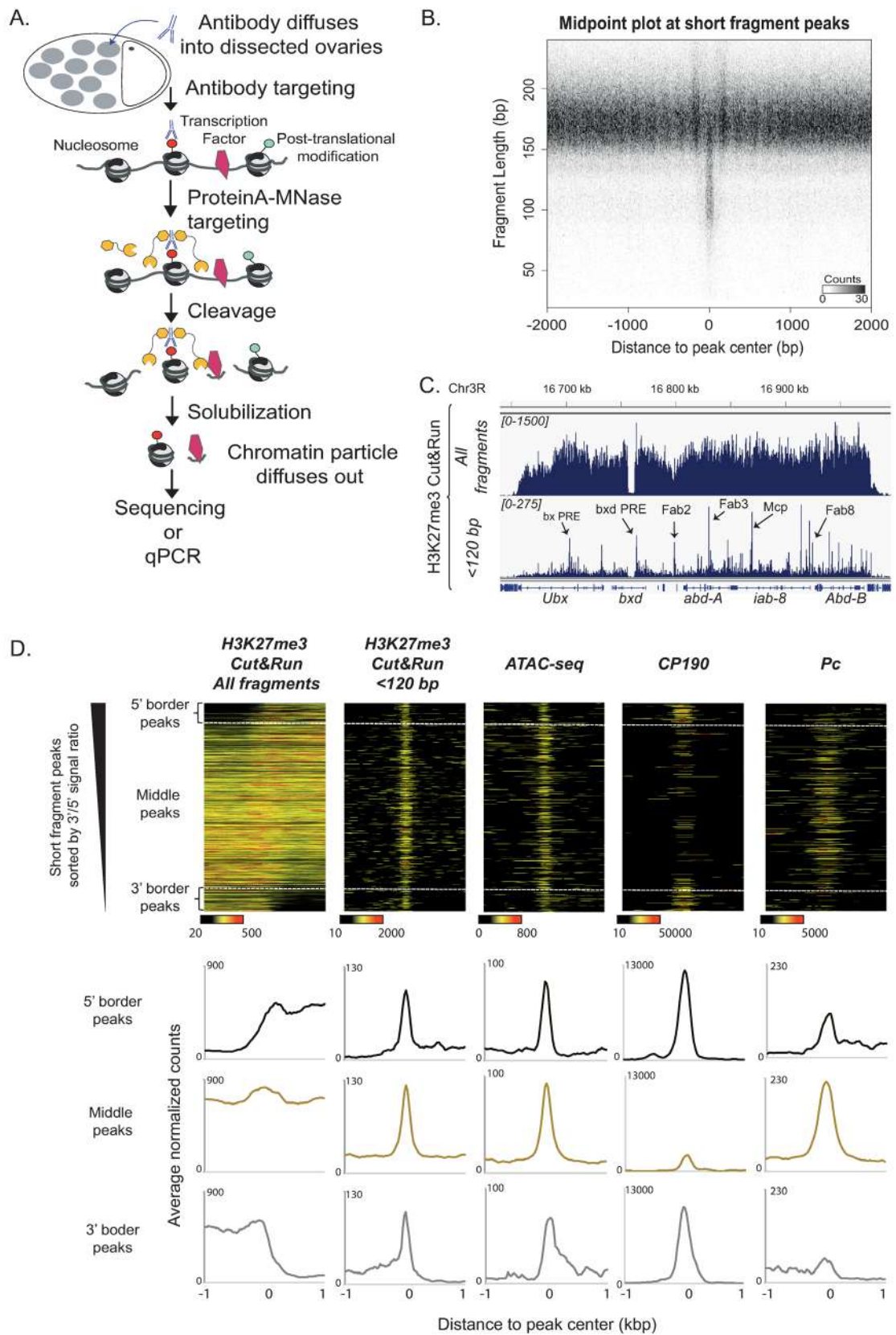


Figure 3

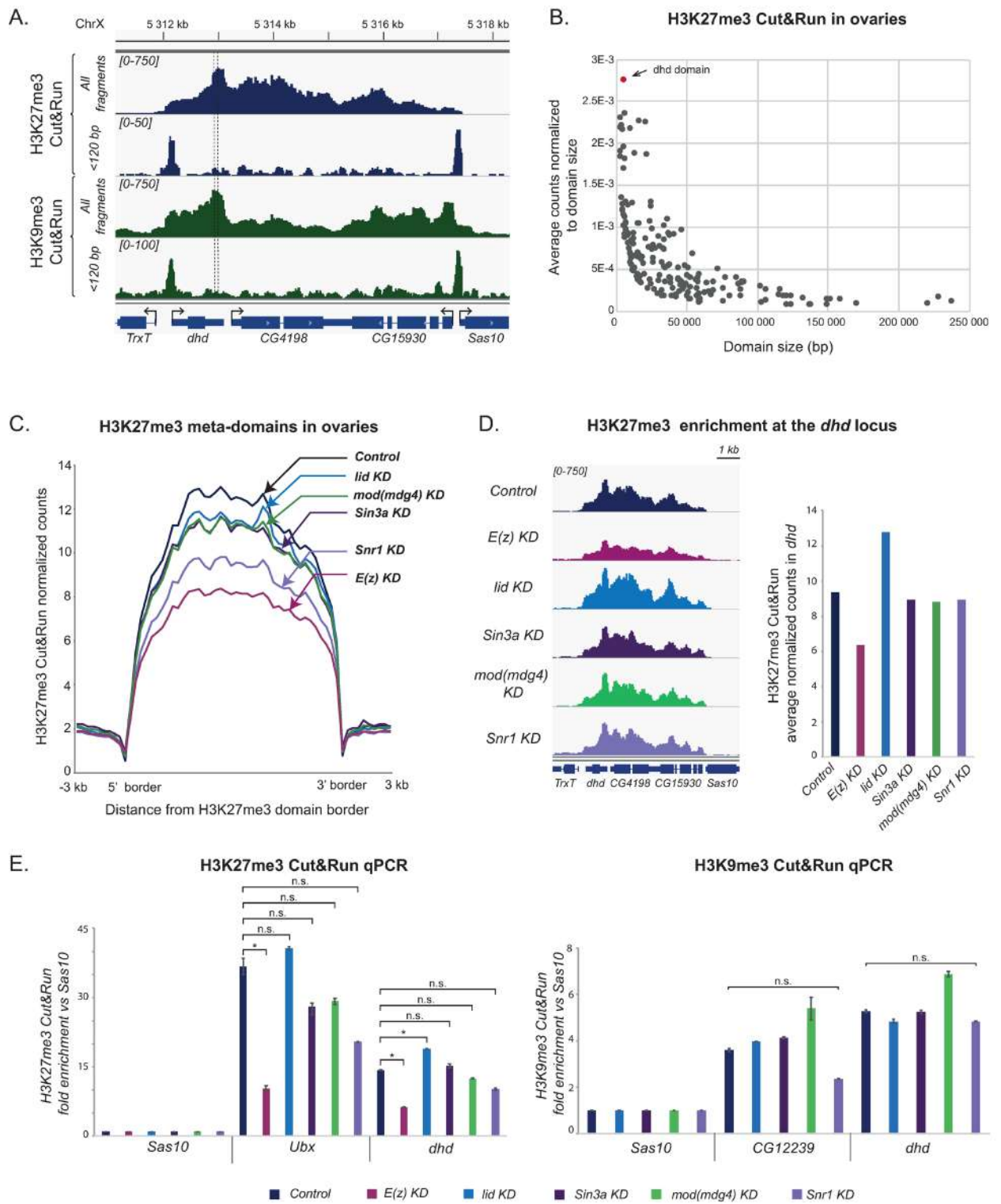


Figure 4

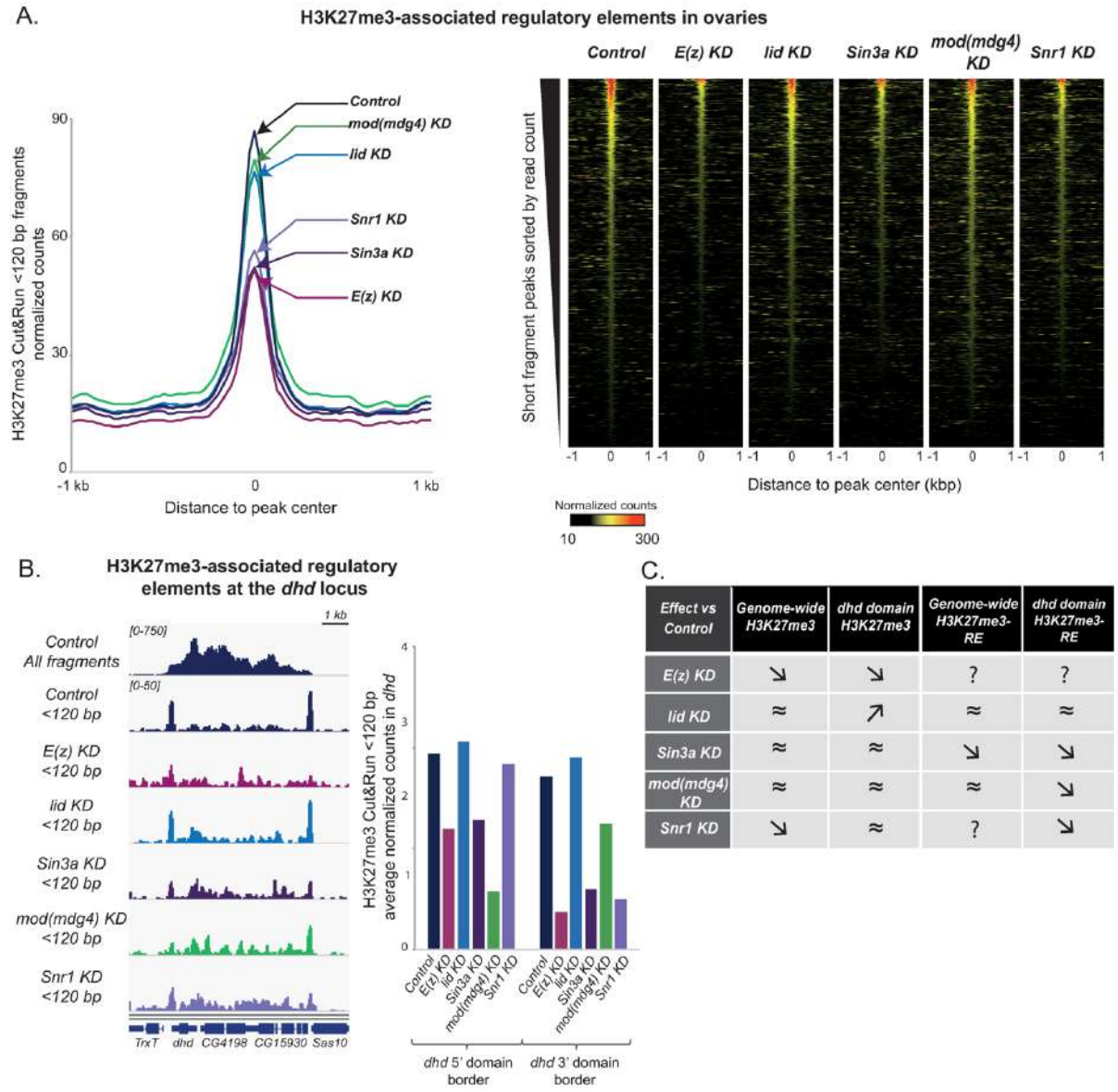


Figure 5

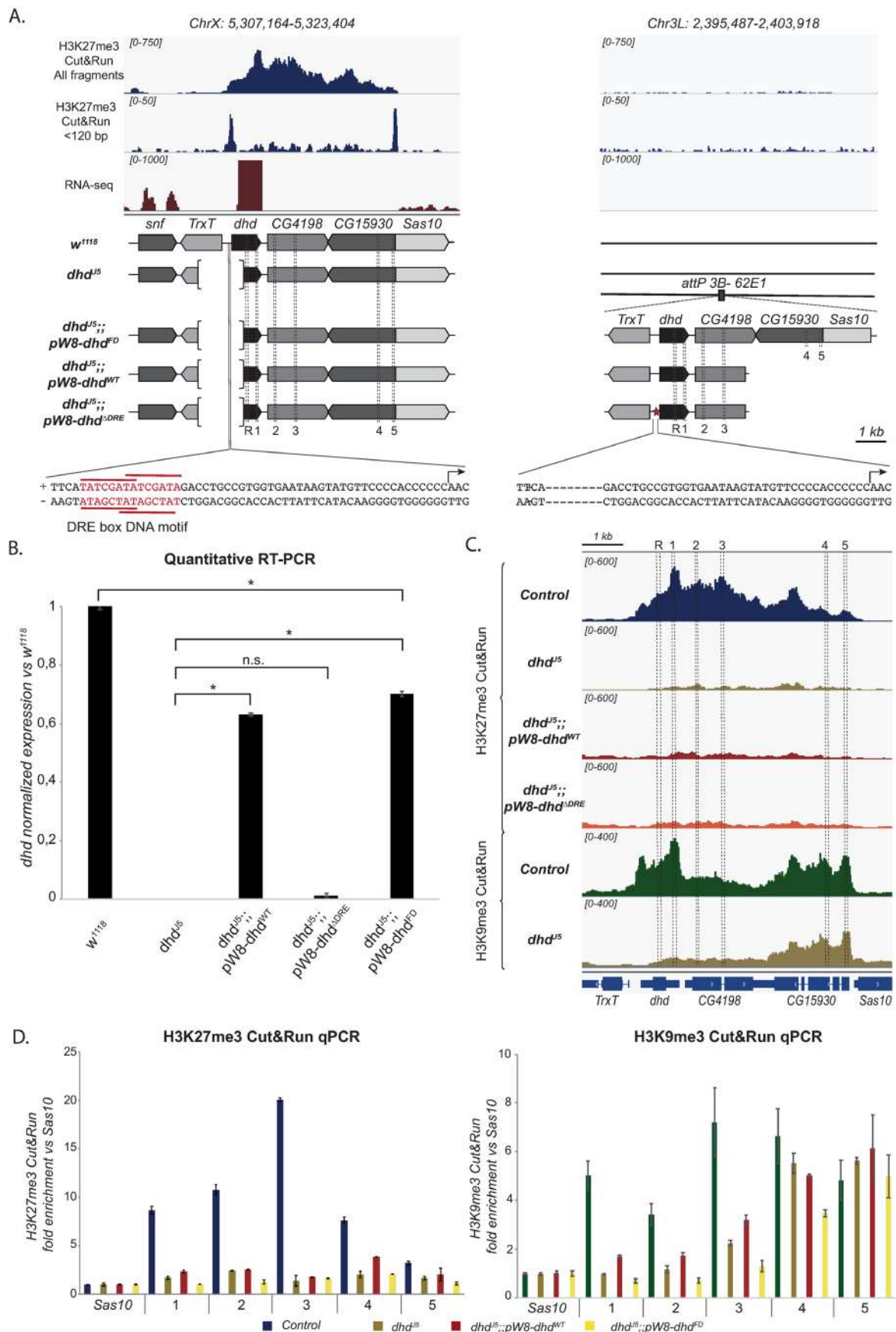


Figure 6

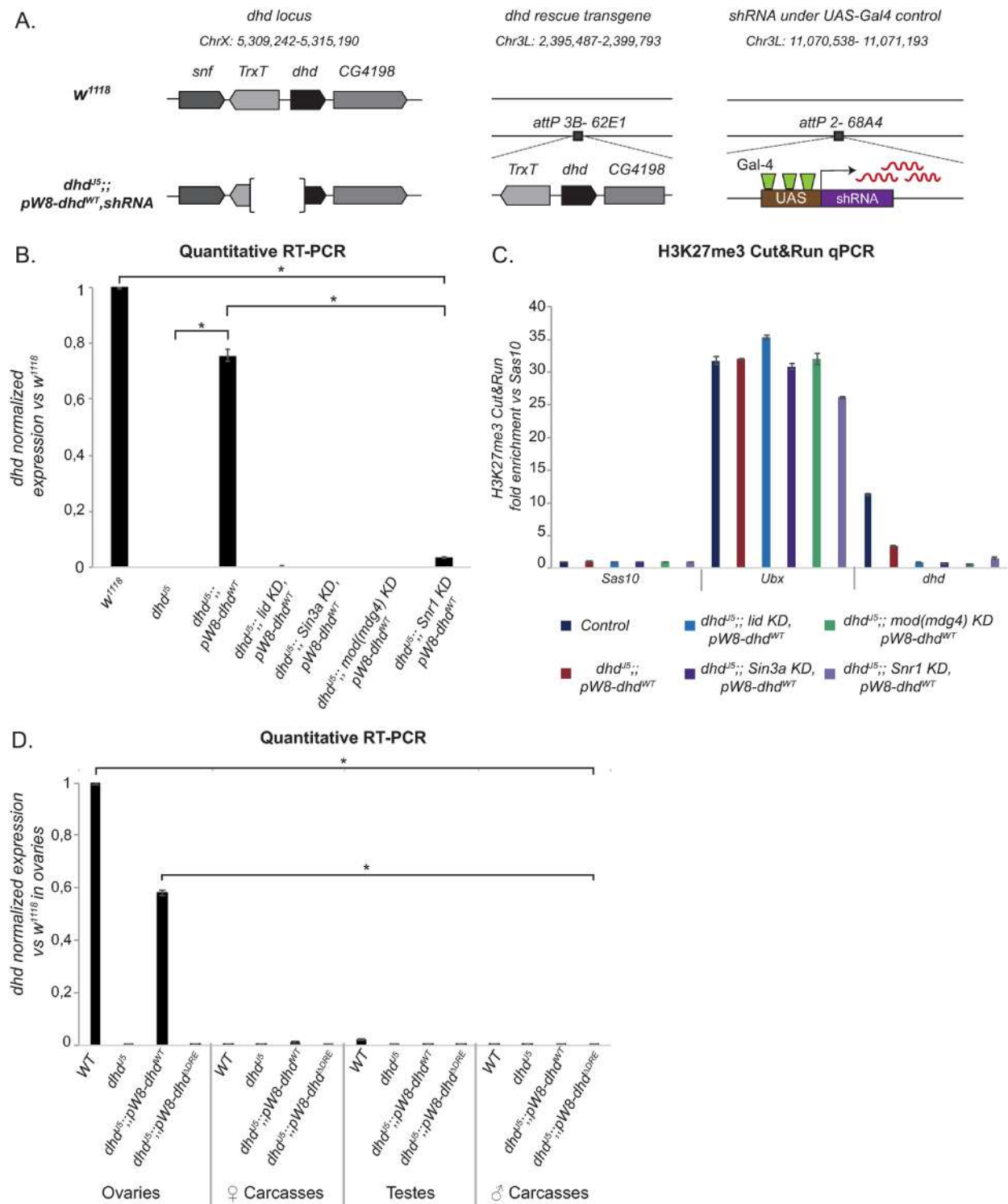


Figure S1

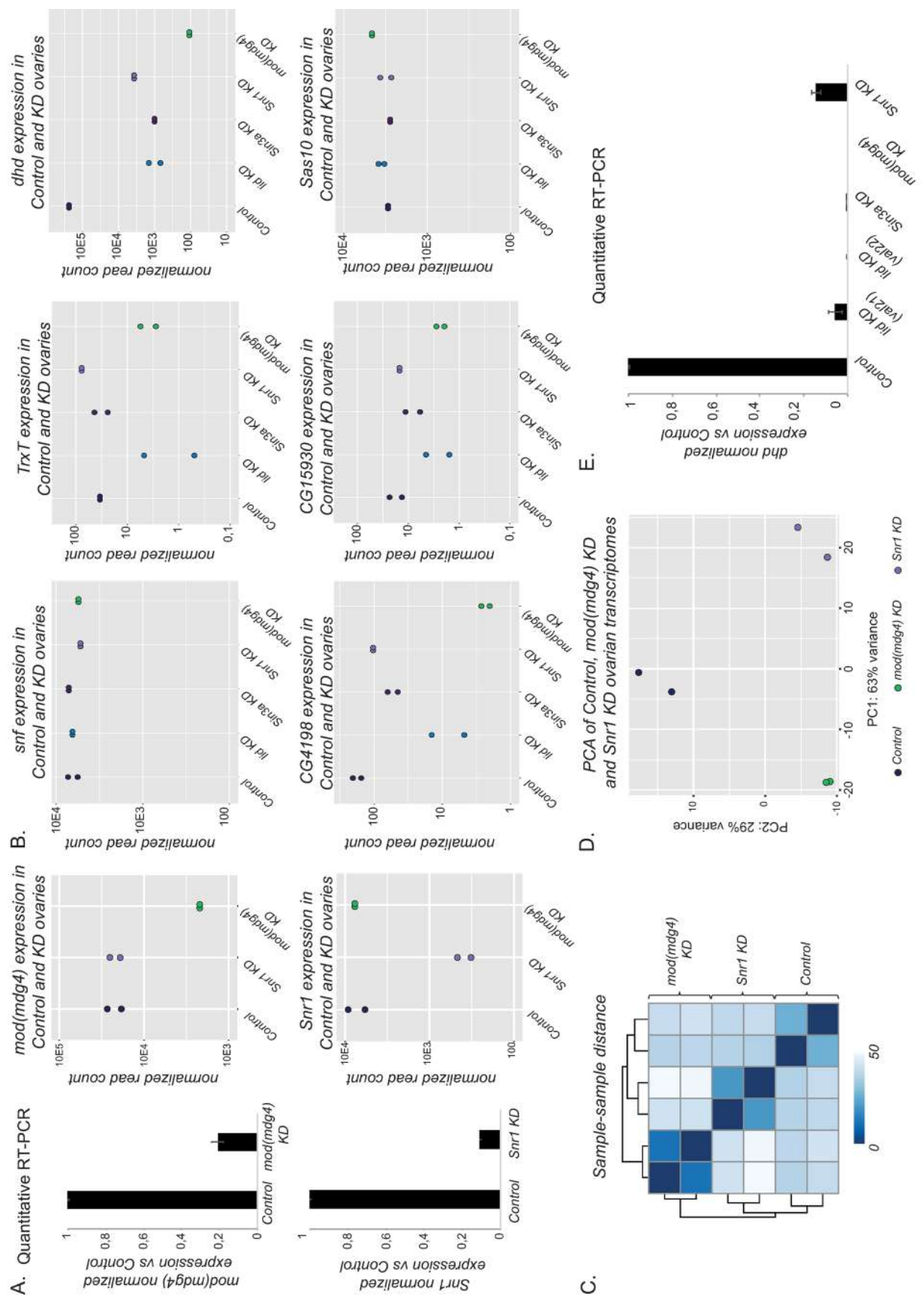
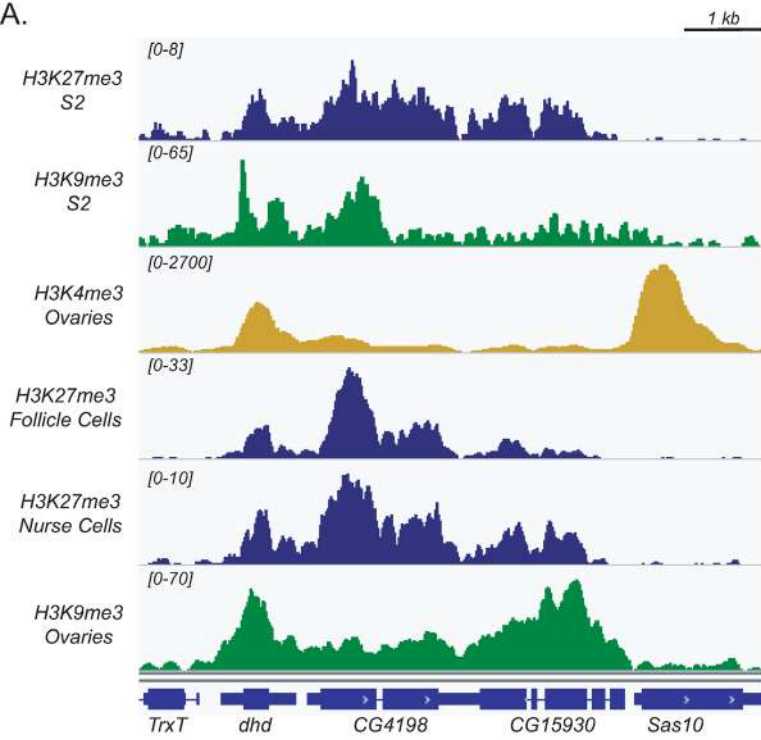


Figure S2

A.



B.

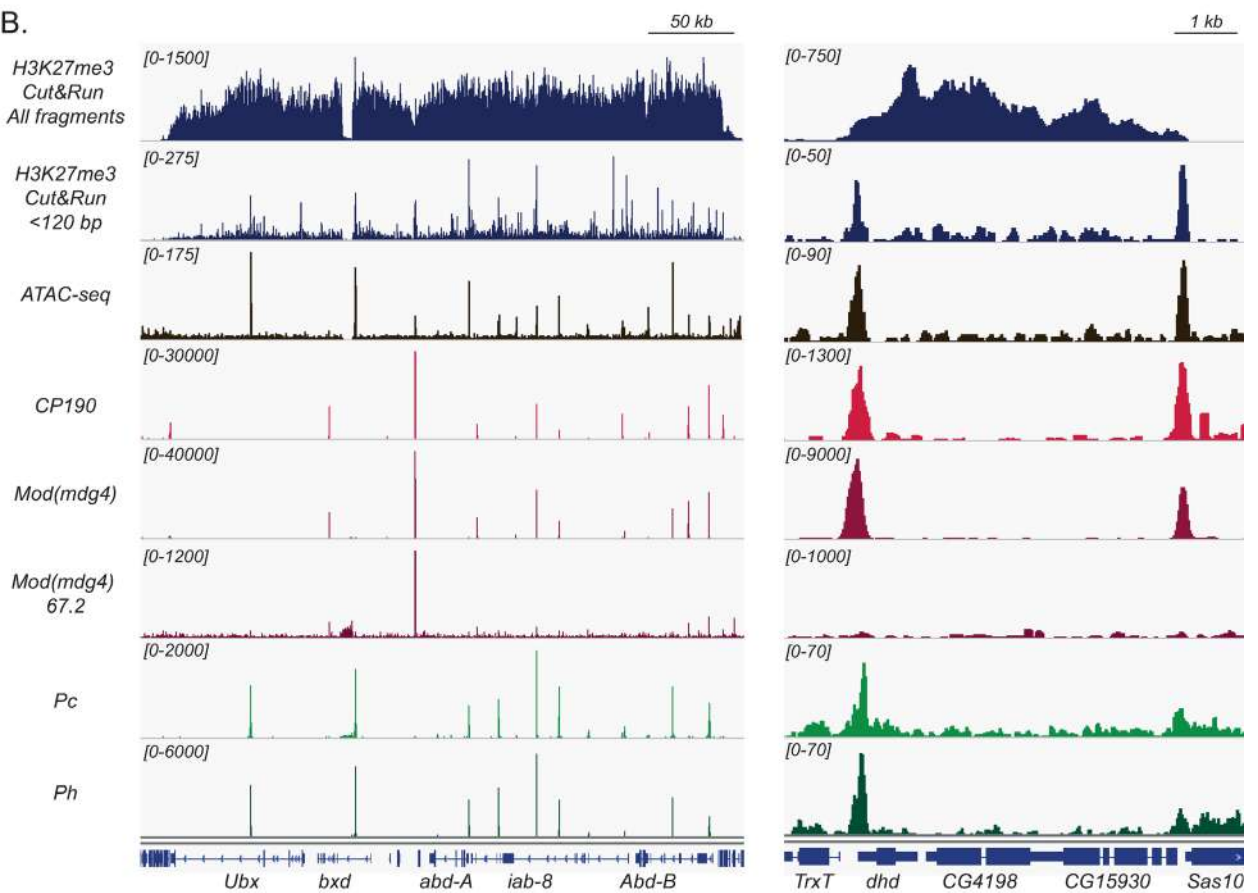


Figure S3

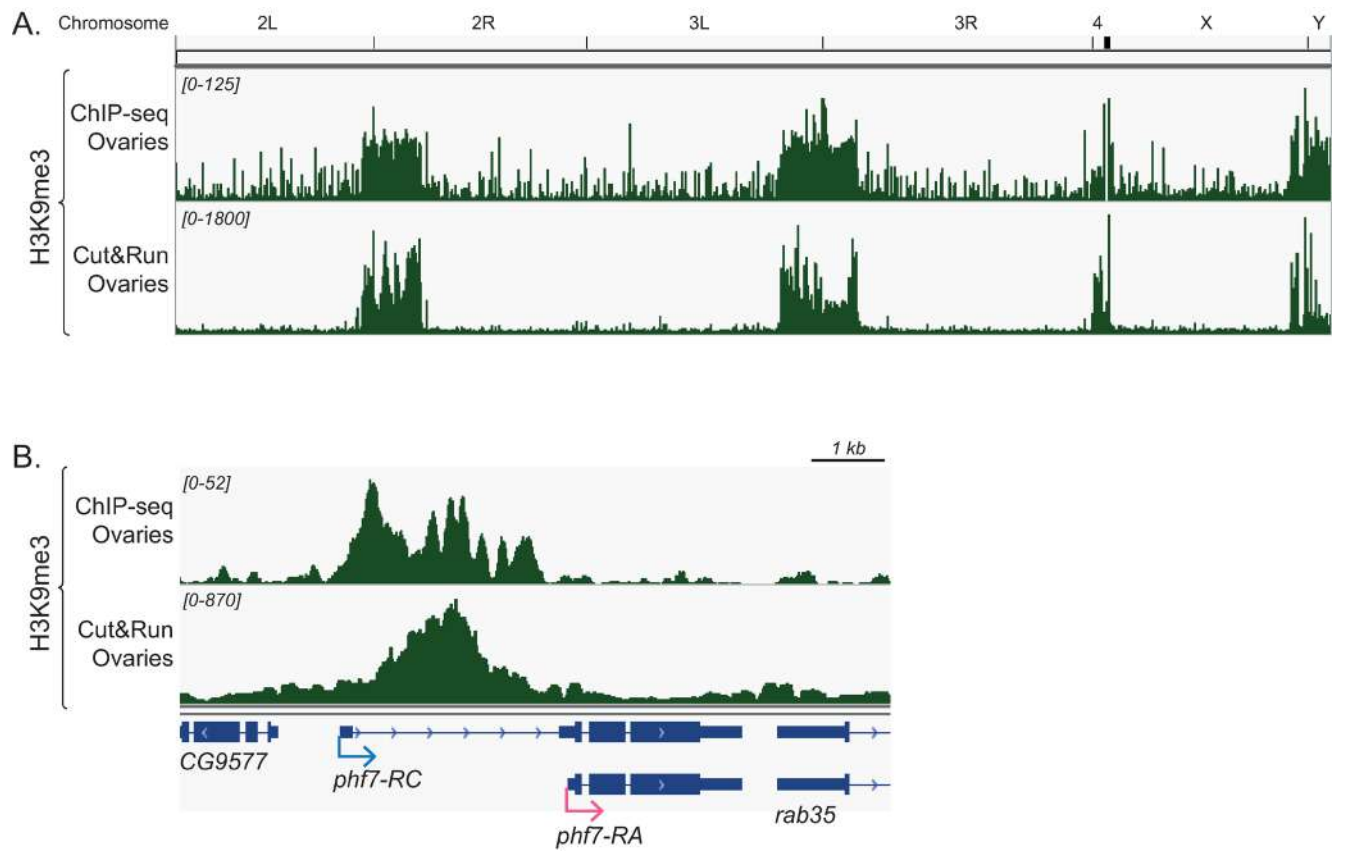


Figure S4

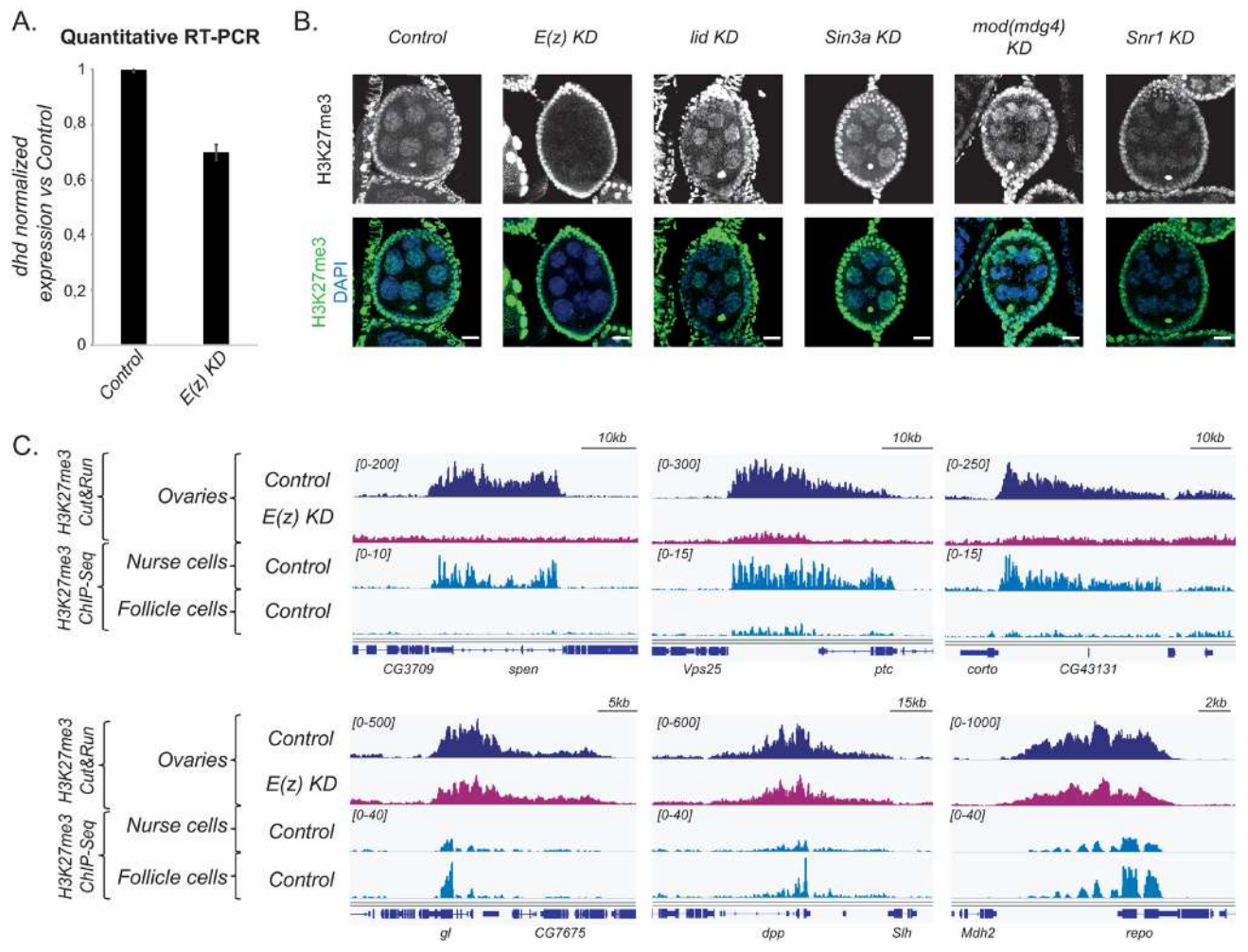


Figure S5

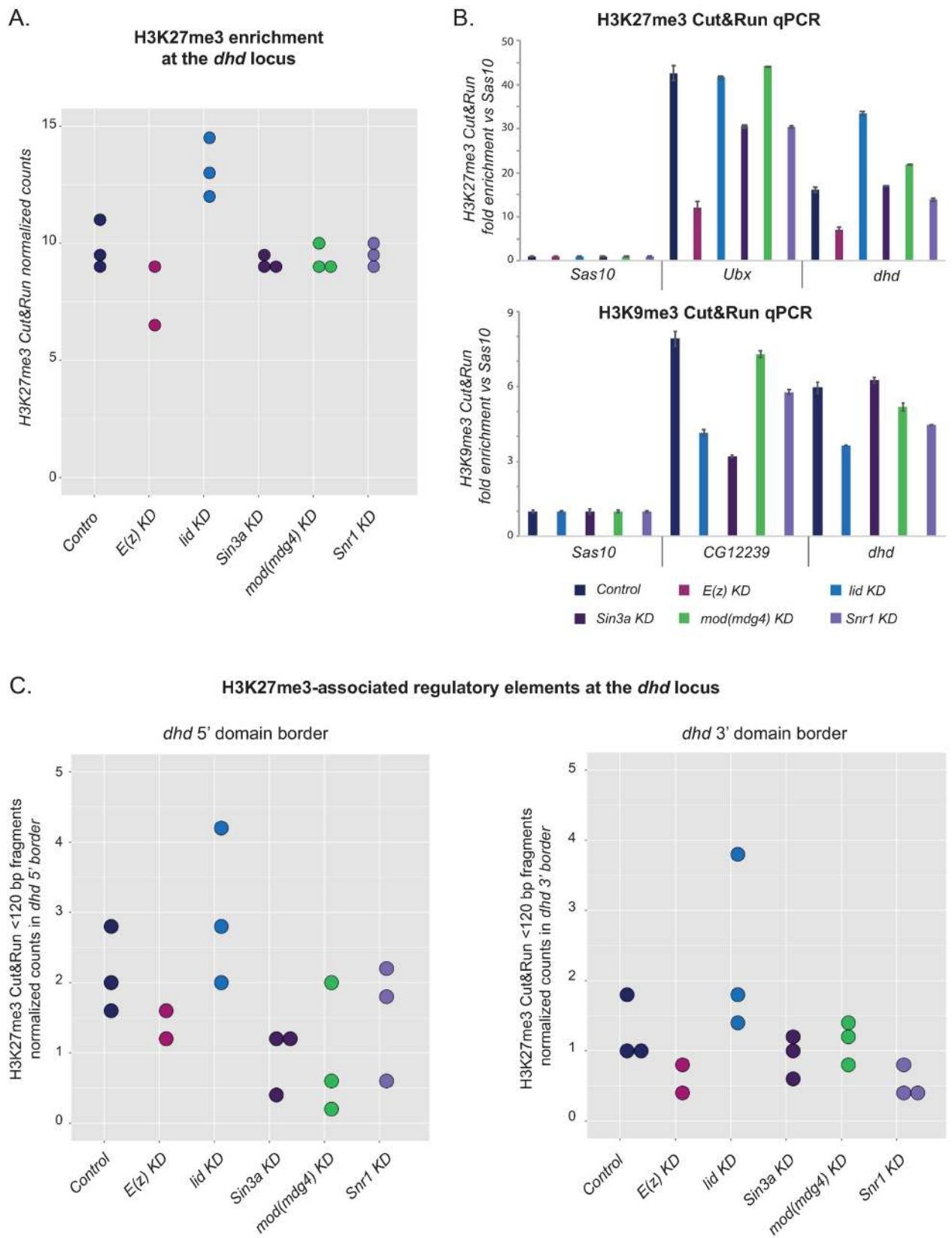


Figure S6

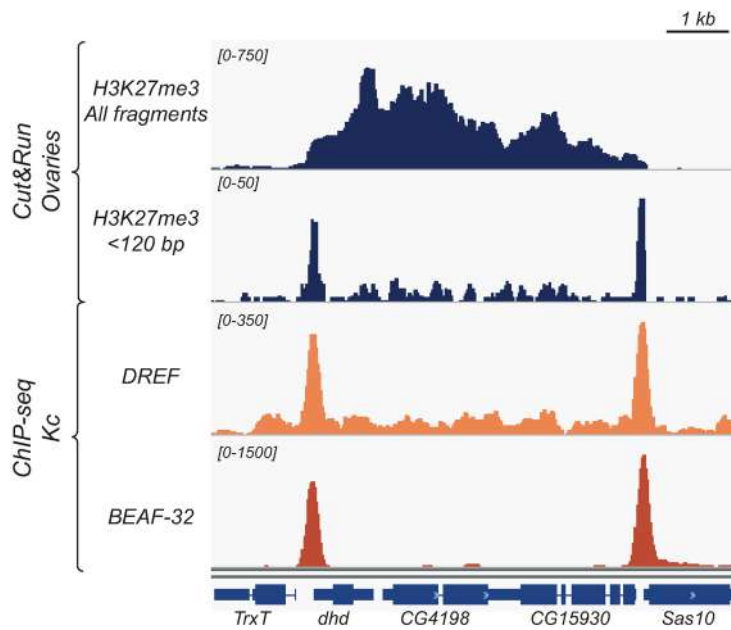


Figure S7

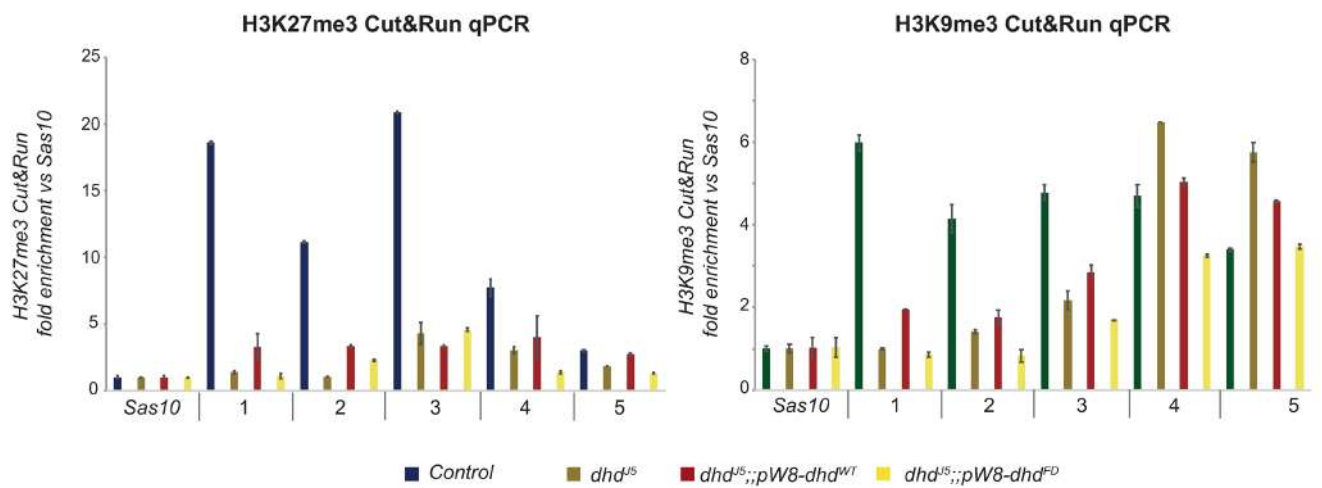
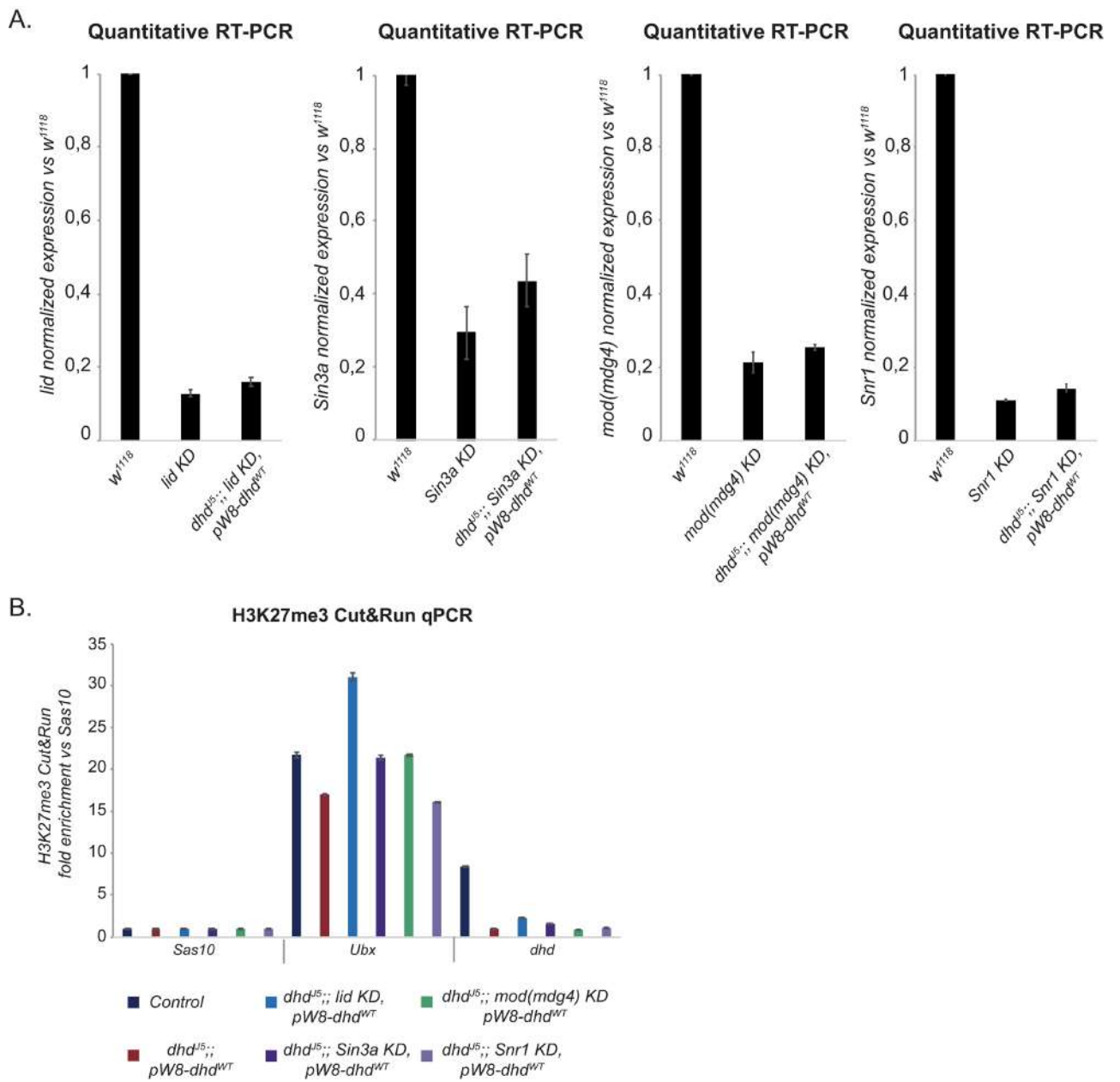


Figure S8



**Table S1. List of primers used in this paper.**

<b>Primer</b>	<b>Sequence (5' → 3')</b>	<b>Purpose</b>
dhd-for	TCTATGCGACATGGTGTGGT	RT-qPCR
dhd-rev	TCCACATCGATCTTGAGCAC	RT-qPCR
lid-for	ATTGGTTTCACGAGGATTGC	RT-qPCR
lid-rev	CATAGCCACTTGGGTCGATT	RT-qPCR
Sin3a-for	CGACAAATGGGTATCGTTCC	RT-qPCR
Sin3a-rev	GACCAGGTCCAGCTCGAAT	RT-qPCR
mod(mdg4)-for	CAACAGATCACCGTGCAAAC	RT-qPCR
mod(mdg4)-rev	GTTCAGATTTTCGTGGGCAAT	RT-qPCR
Snr1-for	TCAGCTCCCACATCTTAGCC	RT-qPCR
Snr1-rev	ACTGGCGTATCGGAAGTGTT	RT-qPCR
Rp49-for	AAGATCGTGAAGAAGCGCAC	RT-qPCR
Rp49-rev	GATACTGTCCCTTGAAGCGG	RT-qPCR
Ubx-for	AAAATTCCTCGGCCTGATTC	Cut&Run-qPCR
Ubx-rev	AAAAATGGGCGTAGCTCAGA	Cut&Run-qPCR
Sas10-for	AGGAGGAGCAGCAGGATGT	Cut&Run-qPCR
Sas10-rev	AGATCGCGGTCATCGTCTT	Cut&Run-qPCR
CG12239-for	AGATGAGGGACGAAGGATTG	Cut&Run-qPCR
CG12239-rev	TTCCTCGGTACGTTTCAGCTT	Cut&Run-qPCR
dhd-3UTR-for	GTTTAGCTTGTAAGCGCGAGA	Cut&Run-qPCR
dhd-3UTR-rev	ATATCATCTGGTCACTGCTGTTG	Cut&Run-qPCR
CG4198-1-for	GAGCAAGAAGAATGGCCAAC	Cut&Run-qPCR
CG4198-1-rev	CGATCGTTGAACTCCTGGAT	Cut&Run-qPCR
CG4198-2-for	GTGTCCATAGCGCAGCAG	Cut&Run-qPCR
CG4198-2-rev	AAGGTGAACATAACCCACAA	Cut&Run-qPCR
CG15930-1-for	ACCTGGACATCGGCTACATC	Cut&Run-qPCR
CG15930-1-rev	ACCATGTGCGAATTTTCGAT	Cut&Run-qPCR

CG15930-2-for	TTATTCCGCATTTTGGCACT	Cut&Run-qPCR
CG15930-2-for	GGAAGAAGCCGAGGATAACA	Cut&Run-qPCR
ΔDRE-1-for	GAGCAGCAGCCGAATTCGGTACCCCATATCCCTCCCATATCC	ΔDRE-transgene
ΔDRE-1-rev	CACGGCAGGTCTGAATATTATTATCGTAATTATGGCAAAATAATGGC	ΔDRE-transgene
ΔDRE-2-for	GATAATAATATTAGACCTGCCGTGGTGAATAAG	ΔDRE-transgene
ΔDRE-2-rev	CACAGGGATGCCACCCGGGATCCGCTAATGGAATCGCAATCGT	ΔDRE-transgene
FD-for	GATTGCGATTCCATTAGCGAATGCGGACGATATGCCAACGC	FD-transgene
FD-rev	GTCACAGGGATGCCACCCGGGATCCACAAAGAGAAAACTGTTGTA A	FD-transgene

**Table S2. List of antibodies used in this paper.**

<b>Antibody</b>	<b>Host animal</b>	<b>Dilution</b>	<b>Experiment</b>	<b>Company (Catalog#)</b>
Anti-Histones	mouse, monoclonal	1:1000	Immunofluorescence	Merck (#F152.C25.WJJ)
Anti-GFP	mouse, monoclonal	1:200	Immunofluorescence	Roche (#118144600001)
Anti-H3K27me3	rabbit, polyclonal	1:500	Immunofluorescence	Merck (#07-449)
Anti-H3K27me3	rabbit, monoclonal	1:100	Cut&Run	Cell Signalling Technology (#9733)
Anti-H3K9me3	rabbit, polyclonal	1:50	Cut&Run	Abcam (#8898)
Anti-DHD	rabbit, polyclonal	1:1000	Western Blot	<i>Tirmarche et al., 2016</i>
Anti- $\alpha$ -tubulin	mouse, monoclonal	1:500	Western Blot	Merck (#T9026)

### III. Additional Results and Discussion

The oocyte-to-zygote transition involves a series of complex nuclear and cellular events, including completion of meiosis, selective translation of maternal RNAs and formation of male and female pronuclei. These events are mainly controlled by maternal factors present in the oocyte at the moment of fertilization. For example, the maternal HIRA histone chaperone complex is essential for the assembly of paternal chromatin at fertilization (Bonney et al., 2007), hinting thus on the importance of chromatin factors involved in zygote formation. This opened the question of what other maternal chromatin factors are required for the integration of paternal chromosomes into the zygote. To answer this, we performed a female germline specific shRNA genetic screen. Remarkably, among the 8 genes causing paternal chromosome loss (among 380 targets tested), 3 belonged to the HIRA complex and the rest were found to abolish *dhd* expression on a rather specific manner. This result revealed a complex network of epigenomic effectors dedicated to the hyperactivation of this small gene. I thus investigated the molecular mechanisms underlying this regulation.

#### 1. Is there an “ovarian hyperactivation code”?

My work led me to discover a series of epigenomic effectors that play general roles in gene regulation but are critical for *dhd* expression in ovaries. I focused thus on the mechanisms mediated by: (i) the H3K4me3 demethylase Lid, (ii) the deacetylase complex scaffold Sin3A, (iii) the Snr1 subunit of the remodeler Swi/Snf complex and (iv) the chromatin factor Mod(mdg4). Available data in other cell contexts showed that depletion of Lid/dKDM5, Sin3A and Snr1 affects hundreds or even thousands of genes (Gajan et al., 2016; Liu and Secombe, 2015; Saha et al., 2016; Xie et al., 2017; Zamurrad et al., 2018). Genome-wide impact on transcription after for Mod(mdg4) depletion has not been studied. Nonetheless, this factor has also been involved in gene regulation (Gerasimova et al., 1995; Savitsky et al., 2016). Strikingly our RNA-seq data analysis showed that *dhd* is hypersensitive to the loss of any of these factors, suggesting that these ubiquitous regulators of gene expression have a specificity for *dhd* in ovaries.

A hypothesis we considered to explain *dhd* hyperactivation was the control of *dhd* by specific distal regulatory elements and/or its positioning in a genomic environment favorable to high transcription levels. There is more and more evidence that links the 3D folding of the genome to transcription. Indeed, the eukaryotic genome is constrained in the nucleus and it has been observed that it is partitioned in domains with similar transcriptional state (Szabo et al., 2019). An emerging hypothesis is that this can favor gene activation by creating compartments containing the necessary factors to favor transcription (Cho et al., 2018; Cramer, 2019; Sabari et al., 2018). Many factors are required for gene transcription, this could be thus a way to deliver quickly and in sufficient amount the necessary proteins at sites of high transcription activity. At a lower scale, eukaryotic genomes, including *Drosophila*'s are organized in self-interacting regions: TADs (Schwartz and Cavalli, 2017; Szabo et al., 2019). This means that DNA sequences within a TAD physically interact with each other more frequently than with sequences outside the TAD. It was reasonable therefore to consider that the 3D organization of the genome could favor *dhd* interaction with specific regulatory regions. However, using available Hi-C data in embryonic fly cells we did not identify any particular contacts at the *dhd* locus (Fig24). The expression of *dhd* is strictly restricted to ovaries, it is thus possible that specific contacts are only established in the germline at a precise developmental stage and are thus undetectable in other cells. Nevertheless, our *pW8-attB-dhd<sup>WT</sup>* transgene inserted in the chromosome III is capable of restoring *dhd* expression to high levels, arguing against *dhd* endogenous genomic environment as a key feature for its hyperactivation. This suggests that, at least in some specific cases, a gene can be massively expressed quite independently of its genomic context and putative 3D contacts.

Chromosome X: 5,153,253 - 5,261,457

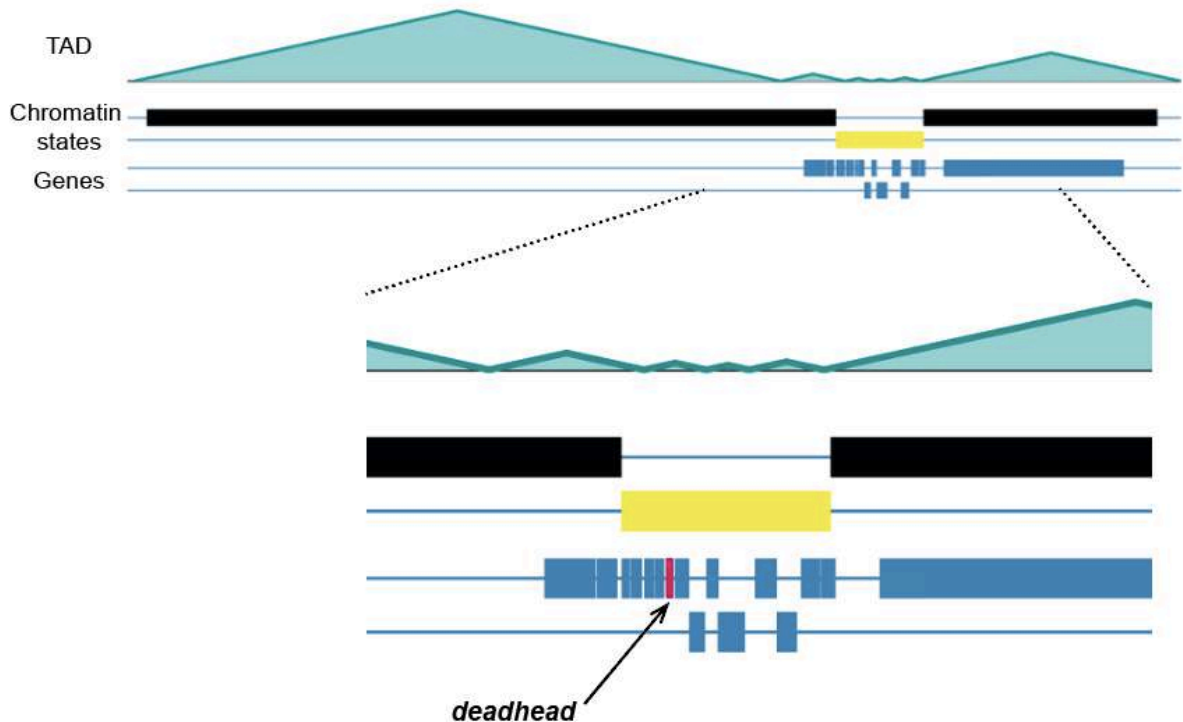


**Fig24: *dhd* does not show contacts with other loci in cultured cells.**

Representation of Hi-C datasets from *Drosophila* Kc embryonic cell using the ChoroGenome Navigator (Ramírez et al., 2018), showing TADs, chromatin state and genes at the indicated coordinates and a zoom on the *dhd* region. Yellow corresponds to active chromatin and black to inactive chromatin.

To explain *dhd* hyperactivation we can also look at the gene itself. Indeed, *dhd* gene architecture, short and intronless, could contribute to explain its hyperactivation. The process of eliminating introns is energy- and time-consuming. Therefore, *dhd* structure could provide an advantage in transcription and translation efficiency, resulting in its high expression. In humans, shorter gene length is associated with high expression, smaller proteins, and little intronic content. It was hypothesized that, due to the great levels of expression in smaller genes, there is a selective pressure to maximize protein synthesis efficiency (Urrutia, 2003). Also, the main fraction of intronless genes correspond to those coding for histones and G protein-coupled receptors and both of this gene families are abundantly expressed (Bryson-Richardson et al., 2004; Doenecke and Albig, 2005; Louhichi et al., 2011). Genes with longer transcripts are mostly associated with functions in the early development stages, while genes with smaller transcripts have important roles in more general functions (Lopes et al., 2021). A correlation between gene length and function has therefore been established. Shorter genes tend to be associated with housekeeping functions, however *dhd* is required only at a very

specific time and contrary to housekeeping genes, it does not need to be constitutively expressed. While *dhd* length could confer an advantage for high expression, the latter must be precisely regulated. Notably, the *dhd* transcribed region would correspond to ~4 nucleosomes. Nucleosomes represent a barrier for RNA Pol II progression, requiring thus a coordinated dance of nucleosomes sliding, evicting, assembling, among others. It is then possible that this low number of nucleosomes favors transcriptional efficiency.

Promoter-enhancer communication is a key point in transcriptional regulation. Both of these elements are bound by transcription factors recognizing specific DNA motifs. Motif scanning at the *dhd* promoter identified a tandem DRE motif. Remarkably, only 4 other gene promoters in the genome presented this motif with ovary-bias expression but none had high levels of expression, similar to *dhd*. DRE motifs are enriched at core promoters of highly expressed housekeeping genes (FitzGerald et al., 2006; Ohler et al., 2002). Additionally, DRE-binding factor Dref, preferentially binds to and activates housekeeping enhancers that are located closely to ubiquitously expressed genes with specificity to its core promoter, and suggests that the DRE motif is required and sufficient for housekeeping enhancer function (Zabidi et al., 2015). Although we were not able to identify any obvious candidate enhancer element in the vicinity of the *dhd* gene region we cannot exclude that this tandem DRE motif plays an important role in *dhd* hyperactivation by recruiting a still unknown enhancer. Nonetheless, this motif by its own, is not sufficient for ovarian hyperactivation.

As mentioned before, *dhd* is a short gene, it was then reasonable to consider that in order to optimize this retrained space, regulatory elements could be present within the coding sequence (CDS). During my PhD I used a rescue transgene, *pW8-attB-dhd<sup>WT</sup>*, capable of restoring *dhd* expression to ~70% of its endogenous level. I also had at my disposal a transgenic line with a construct identical to the *pW8-attB-dhd<sup>WT</sup>* transgene except that *dhd* CDS had been replaced by the similar in size CDS of the ubiquitous thioredoxin *Trx2* (Fig25-A) (Tirmarche, 2016). I thus sought to establish if the *pW8-attB-dhd>Trx2* transgene was able to induce similar *Trx2* levels to those found for *dhd* with the *pW8-attB-dhd<sup>WT</sup>* transgene. Along with a master student, we tackled this question by measuring by RT-qPCR in ovaries transcripts emerging either from the *pW8-attB-dhd<sup>WT</sup>* or the *pW8-attB-dhd>Trx2* transgene in a *dhd<sup>J5</sup>* null mutant context. For this, we used primers targeting *dhd* 3'UTR region allowing us to measure endogenous *dhd* expression in the control as well as transcripts originating from both transgenes. We used the same method as described in (Torres-Campana et al.,

2020). Our preliminary results indicated that as previously observed, the *dhd* transgene is able to restore high *dhd* expression. However, transcripts emerging from the *pW8-attB-dhd>Trx2* transgene were weakly expressed. Indeed, they represented ~10% of the endogenous *dhd* levels and ~15% of the *dhd* levels retrieved with the *pW8-attB-dhd<sup>WT</sup>* transgene (Fig25-B). Replacing the CDS of *dhd* by the CDS of *Trx2* does not suffice to induce high transcript levels of *Trx2*, comparable to those of *dhd*. These results suggest that *dhd* CDS is important to achieve high levels of transcription.

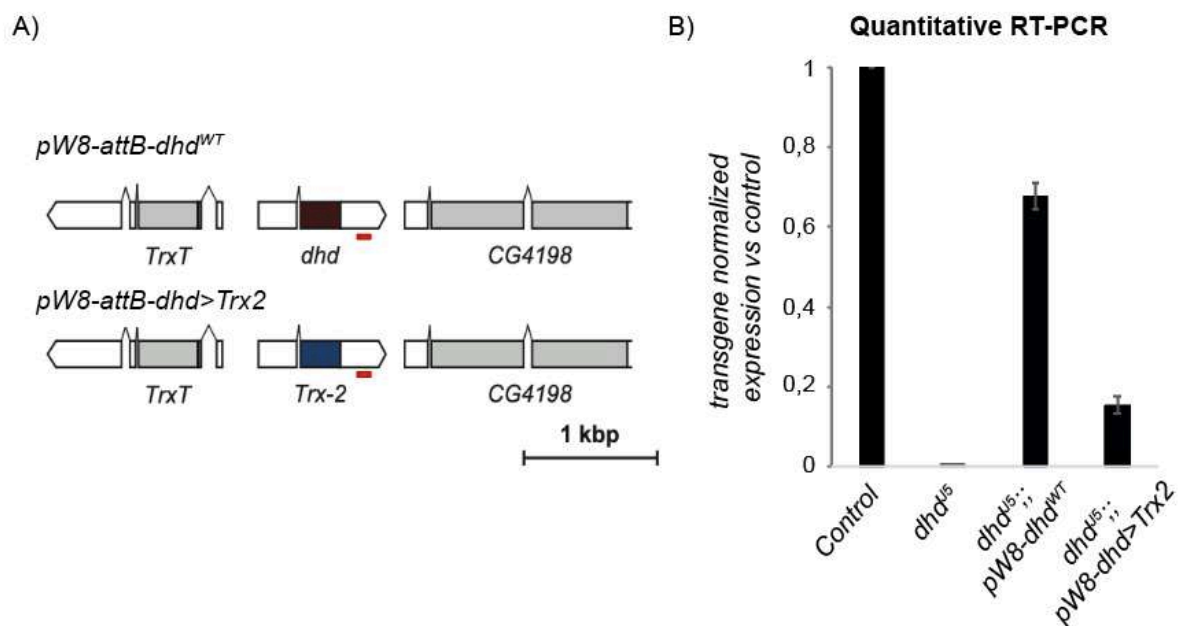


**Fig 25- Replacement of *dhd* coding sequence does not replicate its highly expressed levels**

(A) Schematic representation of the *pW8-attB-dhd<sup>WT</sup>* and *pW8-attB-dhd>Trx2* transgenes. The *pW8-attB-dhd<sup>WT</sup>* contains a genomic region of 4.3 kb containing the *dhd* gene. In the *pW8-attB-dhd>Trx2* transgene, the coding sequence of *dhd* (brown) was replaced by the one of *Trx2* (blue), to place it under the control of the *dhd* promoter. The red line indicates the region covered by the primers used in (B) (Tirmarche, 2016). (B) RT-qPCR quantification of *pW8-attB-dhd<sup>WT</sup>* and *pW8-attB-dhd>Trx2* mRNA levels in ovaries from control flies, *dhd<sup>J5</sup>* mutants or *dhd<sup>J5</sup>* mutants carrying one of the two transgenes (normalized to *Rp49* and relative to expression in control). Data from biological duplicates analyzed in technical duplicates are presented as mean  $\pm$  SEM.

How can a sequence be optimized for high transcription? Codon usage bias, the preference for certain synonymous codons, is a feature of eukaryotic and prokaryotic genomes that plays an important role in gene expression levels. It has been observed that this is, at least in part,

due to codon usage influence on translation rates (Duret and Mouchiroud, 1999; Weinberg et al., 2016; Yu et al., 2015; Zhao et al., 2017). Recent studies have also found a correlation between codon usage on mRNA levels due to changes in transcription in *Neurospora* (Zhou et al., 2016), suggesting that codon optimization could also play a role at the transcriptional level. It is thus reasonable, to hypothesize that *dhd* sequence contributes to its hyperactivation by this mechanism. It could thus be interesting to determine if *dhd* shows codon usage bias and if so, assess the impact on expression level when such codons are replaced by synonym codons. Also, the comparison of codon usage between *dhd* and other highly transcribed genes could shed light into the optimization of the CDS for transcriptional efficiency.

Finally, the peculiar genomic landscape of *dhd* is also worth considering in the recipe for hyperactivation. I found that *dhd* is embedded within a heterochromatic domain harboring both H3K27me3 and H3K9me3 while also being enriched for H3K4me3. The type of promoters carrying both active and repressive marks *i.e.*, bivalent promoters are associated to developmental genes in mammals (Bernstein et al., 2006; Lesch et al., 2013). When carrying both marks genes are repressed or weakly transcribed and upon cell differentiation, these bivalent regions undergo either full activation or stable silencing (Gaertner et al., 2012; Mikkelsen et al., 2007; Pan et al., 2007; Zhao et al., 2007). Recently, this kind of domains were identified in *Drosophila* embryos at a handful of *Hox* genes (Akmammedov et al., 2019). If these domains represent promoters poised for activation or repression has not been investigated yet. However, our *dhd* rescue transgene is expressed to high levels even in the absence of both heterochromatic marks indicating that this epigenetic configuration is not necessary for *dhd* massive expression. Importantly, our data comes from whole ovaries, that is a mix of germ cells and somatic cells at various stages of differentiation. Due to technical limitations in our study, we cannot exclude that these marks are not cell-type and oogenesis-stage-specific.

In conclusion, I uncovered a series of specific features at the *dhd* gene. However, none of them alone seems to define an “ovarian hyperactivation code”. It is more likely that the ensemble of the particular characteristics of *dhd* are necessary to achieve its massive expression.

## 2. An unusual heterochromatic domain

Both H3K9me3 and H3K27me3 are commonly found in large extended domains however we uncovered an H3K27me3/H3K9me3 mini-domain flanked by regulatory elements.

How can this be achieved? In *Drosophila*, insulators and active transcription have been found important for Polycomb/H3K27me3 domain boundaries (De et al., 2020; Fujioka et al., 2013). CP190 is a protein common to most insulators (Ahanger et al., 2013) and in embryonic fly cells it binds both borders of the *dhd* H3K27me3 domain. The study by De et al., reported different categories of Polycomb boundaries in fly larvae (De et al., 2020). 22% of the boundaries analyzed corresponded to an insulator and an active promoter next to the Polycomb domain, transcribing away from the domain. This is the case observed at the *Sas10*-proximal boundary of the mini-domain we identified. However, the scenario of a gene transcribing towards the H3K27me3 domain, as is the case at the *dhd*-proximal border, was not observed in this study. Although the case of *dhd* transcribing within the heterochromatic domain is peculiar, both borders of the domain show active transcription and insulator proteins. It is thus possible that the presence of these two elements helps define these boundaries.

One of the features of heterochromatic H3K9me3 domains it's their ability to spread. However, we and others observe in the female germline a highly localized deposition of H3K9me3 [Smolko et al., 2018]. To target H3K9me3 deposition, RNA-based mechanisms or DNA-binding proteins mechanisms have been described. In their study, Smolko and colleagues found that H3K9me3 deposition by the histone methyltransferase dSETDB1 depended on Sxl, an RNA binding protein. It is thus possible that an RNA-based mechanism is at play. Of the three *Drosophila* enzymes known to methylate H3K9, only dSETDB1 is required for germline development. It is thus possible that this methyltransferase achieves a localized deposition of H3K9me3 through specific features and interactions with determined partners such as Sxl. In some cases, H3K9me3 is permissive to – or even required for – transcription (Lu et al., 2000; Smolko et al., 2018; Wakimoto and Hearn, 1990). Active heterochromatic genes have H3K9me3 on their bodies but not their TSSs, it is tempting to speculate that H3K9me3 is repressive only at promoter regions, while being compatible with, or even promoting, transcription on gene bodies.

Both H3K27me3 and H3K9me3 are known as important to mediate gene repression. The role they play at the *dhd* locus is thus intriguing. First, as suggested by the *dhd* rescue transgene, these marks are not necessary to achieve high levels of expression. Next, we did

not detect an ectopic expression of *dhd* in adult tissues when these marks were absent, arguing thus against a repressive role outside of ovarian tissue. Nonetheless, we cannot exclude a repressive role at other developmental stages.

H3K27me3 and H3K9me3 are compatible with transcription (Ahmad and Spens, 2019; Lu et al., 2000; Smolko et al., 2018; Wakimoto and Hearn, 1990) we can thus wonder if they could actually play a role in promoting transcription of *dhd*. It is also possible that this mini-domain has a role in repressing the other two genes present within it, *CG4198*, which is testis-specific, and *CG15930*, which shows low expression in larval imaginal discs (<http://flybase.org>). Of note, these two hypotheses are not mutually exclusive. Further studies will be necessary to elucidate the role of this heterochromatic mini-domain and shed light on the roles played by these marks on transcription regulation.

### 3. Different roles for epigenomic regulators

Lid, Sin3A, Snr1 and Mod(mdg4) are essential for *dhd* expression. They regulate *dhd* without significantly impacting H3K27me3 enrichment in the *dhd* domain, except for Lid who slightly counteracts it. This suggests that depletion of epigenomic effectors can alter transcription without major changes in the surrounding epigenomic landscape. In agreement, a recent study reported that depletion of the H3K4me1/2 demethylase dLsd1 in the female germline results in both up and down-regulation of gene expression in similar proportions, with a subset of misregulated genes directly bound by dLsd1 (Lepesant et al., 2020). In this study, they assessed histone marks in fly embryonic cells at four dLsd1-bound genes, two up-regulated and two down-regulated. The mark targeted by dLsd1, H3K4me2, increased upon its depletion. Interestingly, none of the other marks tested, H3K4me3, H3K9me2 and H3K27me3 were significantly affected. However, contrary to the case of *dhd*, low-transcribed genes in ovaries were enriched for the H3K27me3 mark while active ones were not, highlighting the enigmatic role of H3K27me3 at the *dhd* locus.

Snr1 is part of the *Drosophila* Swi/Snf remodeler complex, known to oppose Polycomb repression (Kassis et al., 2017; Kingston and Tamkun, 2014; Schuettengruber et al., 2017). In mammalian cells it has been found that mSWI/SNF can actively remove PRC complexes from chromatin thereby counteracting its repression (Kadoch et al., 2017). Surprisingly, we found that upon *snr1* knockdown there is a genome-wide decrease on H3K27me3, suggesting thus that Snr1 could play a role favoring this mark. Interestingly, a

recent study described a role for the mSWI/SNF complex in promoting polycomb repression (Weber et al., 2021). Their model proposes that in the absence of mSWI/SNF, PRC complexes accumulate where mSWI/SNF normally evicts them, thereby causing their redistribution away from heavily occupied sites and causing derepression at these sites. This result illustrates a mechanism where control of one locus can be exerted by effectively maintaining a certain amount of soluble repressive complexes in the cell. It would thus be interesting to measure the composition of soluble regulatory complexes in our knockdown conditions. This could help identify a putative regulator of *dhd* that becomes altered upon our knockdown conditions.

Another level of complexity in the study of the molecular mechanisms promoted by a single factor, comes from the fact that the latter can have different isoforms with different effects. Therefore, the impact on transcription can vary. This is particularly relevant for Mod(mdg4) since ~ 30 isoforms have been identified to date with a common N-Terminal domain (Büchner et al., 2000). Little is known about the impact of Mod(mdg4) depletion on genome-wide transcription. Nonetheless, it has been found that it promotes *Hox* gene activation (Gerasimova et al., 1995; Savitsky et al., 2016). Isoforms other than the insulator isoform 67.2 were found at gene promoters (Melnikova et al., 2019), as is the case for *dhd*, indicating potential targets regulated by specific Mod(mdg4) isoforms. We can wonder if there is a functional significance in having a single gene encoding for such a large number of isoforms. Gabler and colleagues compared *mod(mdg4)* orthologous loci from *D. melanogaster* and *D. virilis* and found an evolutionary conservation of all Mod(mdg4) isoforms (Gabler et al., 2005). The large number of isoforms is thus functionally important in both *Drosophila* species. Additionally, they observed the conservation of the unique C-terminal regions pointing towards a functional differentiation between single isoforms. It would therefore be interesting to assess if, as in *D. melanogaster*, in other species, Mod(mdg4) isoforms can play distinct roles such as insulation and activation.

Emerging evidence, including my study, suggest that the influence of epigenomic effectors on transcriptional outcomes cannot just be categorized as activating or repressing. Most of these factors have pivotal roles depending on cellular context, interactors and targets.

#### 4. An approach to profile regulatory architecture of chromatin domains.

Due to heterogenous cell populations in complex tissues, the study of the chromatin landscape at cell-type specific genes is a major challenge. Great efforts have thus been deployed in the development of single-cell profiling technologies (Lee et al., 2020), opening the possibility to profile chromatin in isolated single cells. Clustering analysis can then be used to retrospectively assign identities to individual cells and give an insight into the epigenomic features of individual cell types. Yet, these approaches suffer from low per-cell throughput, leading to relatively low resolution, high false-negative rates and therefore complicating the interpretations.

Alternatively, the dual-enzyme single-molecule footprinting (dSMF) allows to measure protein-DNA contacts at the level of single molecules (Krebs et al., 2017). This method uses both GpC and CpG DNA methyltransferases to methylate exposed DNA *in vivo*, followed by bisulfite long-read sequencing. With this approach, the occupation of chromatin by nucleosomes, transcription factors and polymerases can be resolved on individual DNA molecules at the scale of several kilobases. While this approach cannot identify the cell of origin of each individual DNA molecule, it can be used to make deductions on the co-occupancy on DNA of different chromatin components. Analogously, the Cut&Run analysis I implemented revealed the co-occupancy on DNA of H3K27me3 nucleosomes and transcription factors at their associated insulators and PREs. This was possible because in Cut&Run, antibody-bound MNase does not restrict its activity to its sole protein target but can rather cleave DNA in spatial proximity of the affected nucleosome.

Similarly, a recent study described the CUTAC method (Henikoff et al., 2020). Authors showed that lowering salt concentrations during antibody tethering in Cut&Tag can reveal H3K4me3-associated DNA regulatory elements (*i.e.*, associated with active chromatin). A relative advantage to our strategy is that histone modifications and regulatory elements can be mapped simultaneously, under a single experimental condition. Yet, compared to CUTAC, our approach presents two likely caveats. First, DNA regulatory inference from Cut&Run is likely to be more difficult to apply to lower input samples, as small cleavage fragments are quite rare compared to nucleosome-sized fragments (1 in 10

approximately). Second, DNA regulatory elements which transcription factor footprint is at least as large as a nucleosome are likely to be missed.

Further exploration of how combination of these approaches may help circumvent the issues associated to each approach. For example, a recent study has combined high-resolution nuclease footprinting with single-molecule methylation profiling (MNase-seq, ORGANIC ChIP, CUT&RUN, and dSMF) to study transcription factor cooperativity at active enhancers on a genome-wide scale in *Drosophila* embryonic cells. This shows how the combination of different approaches can yield valuable insight on the chromatin regulatory landscape. These are thus promising methods, as they hold the potential to universally map the regulatory landscape around histone modifications, which are universal, opening the possibility to implement them in any tissue or species.

## General Conclusion

In almost every animal, the first stages of life depend almost exclusively on maternal products contained in the mature oocyte. Preparation of a competent egg represents an extreme cellular differentiation process where complex transcriptional programs must be tightly regulated. Emerging evidence has highlighted the importance of epigenetic mechanisms in the establishment of the molecular basis of the crucial and complex oocyte-to-zygote transition.

Indeed, the work I presented focused on the intricate regulatory network of epigenomic effectors to achieve hyperactivation of the oocyte-to-zygote effector: the maternal thioredoxin Deadhead. Interestingly, the *dhd* gene can achieve massive levels of transcription with a short regulatory sequence, surrounded by silenced genes, without apparent particular 3D contacts and embedded in a heterochromatic mini-domain. While in different cellular contexts, *dhd* regulators, Lid, Sin3A, Snr1 and Mod(mdg4) have broad effects on transcription, in ovaries, the *dhd* gene represents a hypersensitive target to the loss of any of these factors. The example of *dhd* is thus an illustration of how the activation of a single gene in the right place, at the right time and in the right amount, requires a unique recipe involving a series of factors, that at first glance might not be expected to cooperate.

This study also raises the question of the role of non-canonical heterochromatin domains. Although *dhd* was embedded in an H3K27me3/H3K9me3 mini-domain, these marks were not necessary for its expression in ovaries, nor for its repression in adult tissues. Further studies will be needed to understand the role of these marks, usually mediating transcriptional repression, at actively transcribed genes.

Altogether, my work identified a series of chromatin factors necessary for the establishment of specific transcriptional programs during oogenesis. Importantly, it showed how mechanisms underlying chromatin-based gene regulation are highly dependent on cellular context, interactors of effectors and targeted genes.

## References:

Adam M, Robert F, Laroche M, Gaudreau L. H2A.Z Is Required for Global Chromatin Integrity and for Recruitment of RNA Polymerase II under Specific Conditions. *Mol Cell Biol* 2001;21:6270–9. <https://doi.org/10.1128/MCB.21.18.6270-6279.2001>.

Agarwal N, Ansari A. Enhancement of Transcription by a Splicing-Competent Intron Is Dependent on Promoter Directionality. *PLoS Genet* 2016;12:e1006047. <https://doi.org/10.1371/journal.pgen.1006047>.

Ahanger SH, Shouche YS, Mishra RK. Functional sub-division of the *Drosophila* genome via chromatin looping: The emerging importance of CP190. *Nucleus* 2013;4:115–22. <https://doi.org/10.4161/nucl.23389>.

Ahmad K, Henikoff S. The Histone Variant H3.3 Marks Active Chromatin by Replication-Independent Nucleosome Assembly. *Molecular Cell* 2002;9:1191–200. [https://doi.org/10.1016/S1097-2765\(02\)00542-7](https://doi.org/10.1016/S1097-2765(02)00542-7).

Ahmad K, Spens AE. Separate Polycomb Response Elements control chromatin state and activation of the vestigial gene. *PLoS Genet* 2019;15:e1007877. <https://doi.org/10.1371/journal.pgen.1007877>.

Ahn SH, Kim M, Buratowski S. Phosphorylation of Serine 2 within the RNA Polymerase II C-Terminal Domain Couples Transcription and 3' End Processing. *Molecular Cell* 2004;13:67–76. [https://doi.org/10.1016/S1097-2765\(03\)00492-1](https://doi.org/10.1016/S1097-2765(03)00492-1).

Akkouche A, Mugat B, Barckmann B, Varela-Chavez C, Li B, Raffel R, et al. Piwi Is Required during *Drosophila* Embryogenesis to License Dual-Strand piRNA Clusters for Transposon Repression in Adult Ovaries. *Molecular Cell* 2017;66:411–419.e4. <https://doi.org/10.1016/j.molcel.2017.03.017>.

Akmammedov A, Geigges M, Paro R. Bivalency in *Drosophila* embryos is associated with strong inducibility of Polycomb target genes. *Fly (Austin)* 2019;13:42–50. <https://doi.org/10.1080/19336934.2019.1619438>.

Albert B, Léger-Silvestre I, Normand C, Ostermaier MK, Pérez-Fernández J, Panov KI, et al. RNA polymerase I-specific subunits promote polymerase clustering to enhance the rRNA gene transcription cycle. *Journal of Cell Biology* 2011;192:277–93. <https://doi.org/10.1083/jcb.201006040>.

Allshire RC, Madhani HD. Ten principles of heterochromatin formation and function. *Nat Rev Mol Cell Biol* 2018;19:229–44. <https://doi.org/10.1038/nrm.2017.119>.

Andersen PR, Tirian L, Vunjak M, Brennecke J. A heterochromatin-dependent transcription machinery drives piRNA expression. *Nature* 2017;549:54–9. <https://doi.org/10.1038/nature23482>.

Aravin AA, Naumova NM, Tulin AV, Vagin VV, Rozovsky YM, Gvozdev VA. Double-stranded RNA-mediated silencing of genomic tandem repeats and transposable elements in the *D. melanogaster* germline. *Current Biology* 2001;11:1017–27. [https://doi.org/10.1016/S0960-9822\(01\)00299-8](https://doi.org/10.1016/S0960-9822(01)00299-8).

Ardehali MB, Mei A, Zobeck KL, Caron M, Lis JT, Kusch T. *Drosophila* Set1 is the major histone H3 lysine 4 trimethyltransferase with role in transcription: dSet1 is the major H3K4 trimethyltransferase. *The EMBO Journal* 2011;30:2817–28. <https://doi.org/10.1038/emboj.2011.194>.

Arents G, Burlingame RW, Wang BC, Love WE, Moudrianakis EN. The nucleosomal core histone octamer at 3.1 Å resolution: a tripartite protein assembly and a left-handed superhelix. *Proceedings of the National Academy of Sciences* 1991;88:10148–52. <https://doi.org/10.1073/pnas.88.22.10148>.

Arimbasseri AG, Maraia RJ. RNA Polymerase III Advances: Structural and tRNA Functional Views. *Trends in Biochemical Sciences* 2016;41:546–59. <https://doi.org/10.1016/j.tibs.2016.03.003>.

Arnér ESJ, Holmgren A. Physiological functions of thioredoxin and thioredoxin reductase: Thioredoxin and thioredoxin reductase. *European Journal of Biochemistry* 2000;267:6102–9. <https://doi.org/10.1046/j.1432-1327.2000.01701.x>.

Arnold CD, Gerlach D, Stelzer C, Boryn LM, Rath M, Stark A. Genome-Wide Quantitative Enhancer Activity Maps Identified by STARR-seq. *Science* 2013;339:1074–7. <https://doi.org/10.1126/science.1232542>.

Avilés-Pagán EE, Kang ASW, Orr-Weaver TL. Identification of New Regulators of the Oocyte-to-Embryo Transition in *Drosophila*. *G3* 2020;10:2989–98. <https://doi.org/10.1534/g3.120.401415>.

Avilés-Pagán EE, Orr-Weaver TL. Activating embryonic development in *Drosophila*. *Seminars in Cell & Developmental Biology* 2018;84:100–10. <https://doi.org/10.1016/j.semcdb.2018.02.019>.

Ayyanathan K. Regulated recruitment of HP1 to a euchromatic gene induces mitotically heritable, epigenetic gene silencing: a mammalian cell culture model of gene variegation. *Genes & Development* 2003;17:1855–69. <https://doi.org/10.1101/gad.1102803>.

Banerji J, Rusconi S, Schaffner W. Expression of a  $\beta$ -globin gene is enhanced by remote SV40 DNA sequences. *Cell* 1981;27:299–308. [https://doi.org/10.1016/0092-8674\(81\)90413-X](https://doi.org/10.1016/0092-8674(81)90413-X).

Bannister AJ, Kouzarides T. Regulation of chromatin by histone modifications. *Cell Res* 2011;21:381–95. <https://doi.org/10.1038/cr.2011.22>.

Bastock R, St Johnston D. *Drosophila* oogenesis. *Curr Biol* 2008;18:R1082-1087. <https://doi.org/10.1016/j.cub.2008.09.011>.

Becker PB, Workman JL. Nucleosome Remodeling and Epigenetics. *Cold Spring Harbor Perspectives in Biology* 2013;5:a017905–a017905. <https://doi.org/10.1101/cshperspect.a017905>.

Bernstein BE, Kamal M, Lindblad-Toh K, Bekiranov S, Bailey DK, Huebert DJ, et al. Genomic Maps and Comparative Analysis of Histone Modifications in Human and Mouse. *Cell* 2005;120:169–81. <https://doi.org/10.1016/j.cell.2005.01.001>.

Bernstein BE, Mikkelsen TS, Xie X, Kamal M, Huebert DJ, Cuff J, et al. A bivalent chromatin structure marks key developmental genes in embryonic stem cells. *Cell* 2006;125:315–26. <https://doi.org/10.1016/j.cell.2006.02.041>.

Bernstein BE, Tong JK, Schreiber SL. Genomewide studies of histone deacetylase function in yeast. *Proceedings of the National Academy of Sciences* 2000;97:13708–13. <https://doi.org/10.1073/pnas.250477697>.

Beuchle D, Struhl G, Muller J. Polycomb group proteins and heritable silencing of *Drosophila* Hox genes. *Development* 2001;128:993–1004. <https://doi.org/10.1242/dev.128.6.993>.

Biswas S, Rao CM. Epigenetic tools (The Writers, The Readers and The Erasers) and their implications in cancer therapy. *European Journal of Pharmacology* 2018;837:8–24. <https://doi.org/10.1016/j.ejphar.2018.08.021>.

Blastyák A, Mishra RK, Karch F, Gyurkovics H. Efficient and Specific Targeting of Polycomb Group Proteins Requires Cooperative Interaction between Grainyhead and Pleiohomeotic. *Mol Cell Biol* 2006;26:1434–44. <https://doi.org/10.1128/MCB.26.4.1434-1444.2006>.

Boettiger AN, Bintu B, Moffitt JR, Wang S, Beliveau BJ, Fudenberg G, et al. Super-resolution imaging reveals distinct chromatin folding for different epigenetic states. *Nature* 2016;529:418–22. <https://doi.org/10.1038/nature16496>.

Bolzer A, Kreth G, Solovei I, Koehler D, Saracoglu K, Fauth C, et al. Three-Dimensional Maps of All Chromosomes in Human Male Fibroblast Nuclei and Prometaphase Rosettes. *PLoS Biol* 2005;3:e157. <https://doi.org/10.1371/journal.pbio.0030157>.

Bonev B, Mendelson Cohen N, Szabo Q, Fritsch L, Papadopoulos GL, Lubling Y, et al. Multiscale 3D Genome Rewiring during Mouse Neural Development. *Cell* 2017;171:557-572.e24. <https://doi.org/10.1016/j.cell.2017.09.043>.

Bonnefoy E, Orsi GA, Couble P, Loppin B. The Essential Role of *Drosophila* HIRA for De Novo Assembly of Paternal Chromatin at Fertilization. *PLoS Genet* 2007;3:e182. <https://doi.org/10.1371/journal.pgen.0030182>.

Bowman SK, Deaton AM, Domingues H, Wang PI, Sadreyev RI, Kingston RE, et al. H3K27 modifications define segmental regulatory domains in the *Drosophila* bithorax complex. *ELife* 2014;3:e02833. <https://doi.org/10.7554/eLife.02833>.

Brent MM, Anand R, Marmorstein R. Structural Basis for DNA Recognition by FoxO1 and Its Regulation by Posttranslational Modification. *Structure* 2008;16:1407–16. <https://doi.org/10.1016/j.str.2008.06.013>.

Brown JL, Kassis JA. Spps, a *Drosophila* Sp1/KLF family member, binds to PREs and is required for PRE activity late in development. *Development* 2010;137:2597–602. <https://doi.org/10.1242/dev.047761>.

Bryson-Richardson RJ, Logan DW, Currie PD, Jackson IJ. Large-scale analysis of gene structure in rhodopsin-like GPCRs: evidence for widespread loss of an ancient intron. *Gene* 2004;338:15–23. <https://doi.org/10.1016/j.gene.2004.05.001>.

Buchenau P, Hodgson J, Strutt H, Arndt-Jovin DJ. The Distribution of Polycomb-Group Proteins During Cell Division and Development in *Drosophila* Embryos: Impact on Models for Silencing. *Journal of Cell Biology* 1998;141:469–81. <https://doi.org/10.1083/jcb.141.2.469>.

Büchner K, Roth P, Schotta G, Krauss V, Saumweber H, Reuter G, et al. Genetic and Molecular Complexity of the Position Effect Variegation Modifier *mod(mdg4)* in *Drosophila*. *Genetics* 2000;155:141–57. <https://doi.org/10.1093/genetics/155.1.141>.

Bulut-Karslioglu A, Perrera V, Scaranaro M, de la Rosa-Velazquez IA, van de Nobelen S, Shukeir N, et al. A transcription factor-based mechanism for mouse heterochromatin formation. *Nat Struct Mol Biol* 2012;19:1023–30. <https://doi.org/10.1038/nsmb.2382>.

Buratowski S. Progression through the RNA Polymerase II CTD Cycle. *Molecular Cell* 2009;36:541–6. <https://doi.org/10.1016/j.molcel.2009.10.019>.

Burke TW, Kadonaga JT. *Drosophila* TFIID binds to a conserved downstream basal promoter element that is present in many TATA-box-deficient promoters. *Genes & Development* 1996;10:711–24. <https://doi.org/10.1101/gad.10.6.711>.

Burton A, Brochard V, Galan C, Ruiz-Morales ER, Rovira Q, Rodriguez-Terrones D, et al. Heterochromatin establishment during early mammalian development is regulated by pericentromeric RNA and characterized by non-repressive H3K9me3. *Nat Cell Biol* 2020;22:767–78. <https://doi.org/10.1038/s41556-020-0536-6>.

Cairns BR. The logic of chromatin architecture and remodelling at promoters. *Nature* 2009;461:193–8. <https://doi.org/10.1038/nature08450>.

Cammas F. Association of the transcriptional corepressor TIF1 with heterochromatin protein 1 (HP1): an essential role for progression through differentiation. *Genes & Development* 2004;18:2147–60. <https://doi.org/10.1101/gad.302904>.

Cano-Rodriguez D, Gjaltema RAF, Jilderda LJ, Jellema P, Dokter-Fokkens J, Ruiters MHJ, et al. Writing of H3K4Me3 overcomes epigenetic silencing in a sustained but context-dependent manner. *Nat Commun* 2016;7:12284. <https://doi.org/10.1038/ncomms12284>.

Cao R, Wang L, Wang H, Xia L, Erdjument-Bromage H, Tempst P, et al. Role of Histone H3 Lysine 27 Methylation in Polycomb-Group Silencing. *Science* 2002;298:1039–43. <https://doi.org/10.1126/science.1076997>.

Carey M, Li B, Workman JL. RSC Exploits Histone Acetylation to Abrogate the Nucleosomal Block to RNA Polymerase II Elongation. *Molecular Cell* 2006;24:481–7. <https://doi.org/10.1016/j.molcel.2006.09.012>.

Carrozza MJ, Li B, Florens L, Suganuma T, Swanson SK, Lee KK, et al. Histone H3 Methylation by Set2 Directs Deacetylation of Coding Regions by Rpd3S to Suppress Spurious Intragenic Transcription. *Cell* 2005;123:581–92. <https://doi.org/10.1016/j.cell.2005.10.023>.

Cattoni DI, Cardozo Gizzi AM, Georgieva M, Di Stefano M, Valeri A, Chamousset D, et al. Single-cell absolute contact probability detection reveals chromosomes are organized by multiple low-frequency yet specific interactions. *Nat Commun* 2017;8:1753. <https://doi.org/10.1038/s41467-017-01962-x>.

Cesarini E, Mozzetta C, Marullo F, Gregoretti F, Gargiulo A, Columbaro M, et al. Lamin A/C sustains PcG protein architecture, maintaining transcriptional repression at target genes. *Journal of Cell Biology* 2015;211:533–51. <https://doi.org/10.1083/jcb.201504035>.

- Chaubal A, Pile LA. Same agent, different messages: insight into transcriptional regulation by SIN3 isoforms. *Epigenetics & Chromatin* 2018;11:17. <https://doi.org/10.1186/s13072-018-0188-y>.
- Cho W-K, Spille J-H, Hecht M, Lee C, Li C, Grube V, et al. Mediator and RNA polymerase II clusters associate in transcription-dependent condensates. *Science* 2018;361:412–5. <https://doi.org/10.1126/science.aar4199>.
- Chubb JR, Trcek T, Shenoy SM, Singer RH. Transcriptional Pulsing of a Developmental Gene. *Current Biology* 2006;16:1018–25. <https://doi.org/10.1016/j.cub.2006.03.092>.
- Clapier CR, Cairns BR. The Biology of Chromatin Remodeling Complexes. *Annu Rev Biochem* 2009;78:273–304. <https://doi.org/10.1146/annurev.biochem.77.062706.153223>.
- Claycomb J, Orrweaver T. Developmental gene amplification: insights into DNA replication and gene expression. *Trends in Genetics* 2005;21:149–62. <https://doi.org/10.1016/j.tig.2005.01.009>.
- Cramer P. Organization and regulation of gene transcription. *Nature* 2019;573:45–54. <https://doi.org/10.1038/s41586-019-1517-4>.
- Cubeñas-Potts C, Rowley MJ, Lyu X, Li G, Lei EP, Corces VG. Different enhancer classes in *Drosophila* bind distinct architectural proteins and mediate unique chromatin interactions and 3D architecture. *Nucleic Acids Research* 2017;45:1714–30. <https://doi.org/10.1093/nar/gkw1114>.
- Curry E, Zeller C, Masrour N, Patten DK, Gallon J, Wilhelm-Benartzi CS, et al. Genes Predisposed to DNA Hypermethylation during Acquired Resistance to Chemotherapy Are Identified in Ovarian Tumors by Bivalent Chromatin Domains at Initial Diagnosis. *Cancer Res* 2018;78:1383–91. <https://doi.org/10.1158/0008-5472.CAN-17-1650>.
- Czermin B, Melfi R, McCabe D, Seitz V, Imhof A, Pirrotta V. *Drosophila* Enhancer of Zeste/ESC Complexes Have a Histone H3 Methyltransferase Activity that Marks Chromosomal Polycomb Sites. *Cell* 2002;111:185–96. [https://doi.org/10.1016/S0092-8674\(02\)00975-3](https://doi.org/10.1016/S0092-8674(02)00975-3).
- van Daal A, White EM, Gorovsky MA, Elgin CR. *Drosophila* has a single copy of the gene encoding a highly conserved histone H2A variant of the H2A. F/Z type. *Nucl Acids Res* 1988;16:7487–97. <https://doi.org/10.1093/nar/16.15.7487>.
- Das TK, Sangodkar J, Negre N, Narla G, Cagan RL. Sin3a acts through a multi-gene module to regulate invasion in *Drosophila* and human tumors. *Oncogene* 2013;32:3184–97. <https://doi.org/10.1038/onc.2012.326>.

- Davidson, E. *Gene Activity in Early Development*. Academic Press, Orlando, FL; 1986.
- De S, Gehred ND, Fujioka M, Chan FW, Jaynes JB, Kassis JA. Defining the Boundaries of Polycomb Domains in *Drosophila*. *Genetics* 2020;216:689–700. <https://doi.org/10.1534/genetics.120.303642>.
- Deal RB, Henikoff JG, Henikoff S. Genome-Wide Kinetics of Nucleosome Turnover Determined by Metabolic Labeling of Histones. *Science* 2010;328:1161–4. <https://doi.org/10.1126/science.1186777>.
- Deaton AM, Gómez-Rodríguez M, Mieczkowski J, Tolstorukov MY, Kundu S, Sadreyev RI, et al. Enhancer regions show high histone H3.3 turnover that changes during differentiation. *ELife* 2016;5:e15316. <https://doi.org/10.7554/eLife.15316>.
- Dej KJ, Spradling AC. Nurse cell chromosome reorganization 1999:11.
- Déjardin J, Rappailles A, Cuvier O, Grimaud C, Decoville M, Locker D, et al. Recruitment of *Drosophila* Polycomb group proteins to chromatin by DSP1. *Nature* 2005;434:533–8. <https://doi.org/10.1038/nature03386>.
- Delattre M, Spierer A, Tonka CH, Spierer P. The genomic silencing of position-effect variegation in *Drosophila melanogaster*: interaction between the heterochromatin-associated proteins Su(var)3-7 and HP1. *J Cell Sci* 2000;113 Pt 23:4253–61.
- DeLuca SZ, Ghildiyal M, Niu W, Pang L-Y, Spradling AC. Differentiating *Drosophila* female germ cells initiate Polycomb silencing by altering PRC2 sampling. *Developmental Biology*; 2020. <https://doi.org/10.1101/2020.02.03.932582>.
- Deng WM, Althausen C, Ruohola-Baker H. Notch-Delta signaling induces a transition from mitotic cell cycle to endocycle in *Drosophila* follicle cells. *Development* 2001;128:4737–46.
- de Wit E, Vos ESM, Holwerda SJB, Valdes-Quezada C, Verstegen MJAM, Teunissen H, et al. CTCF Binding Polarity Determines Chromatin Looping. *Molecular Cell* 2015;60:676–84. <https://doi.org/10.1016/j.molcel.2015.09.023>.
- Di Stefano L, Walker JA, Burgio G, Corona DFV, Mulligan P, Naar AM, et al. Functional antagonism between histone H3K4 demethylases in vivo. *Genes & Development* 2011;25:17–28. <https://doi.org/10.1101/gad.1983711>.
- Dingwall AK, Beek SJ, McCallum CM, Tamkun JW, Kalpana GV, Goff SP, et al. The *Drosophila* snr1 and brm proteins are related to yeast SWI/SNF proteins and are components of a large protein complex. *MBoC* 1995;6:777–91. <https://doi.org/10.1091/mbc.6.7.777>.
- Dixon JR, Selvaraj S, Yue F, Kim A, Li Y, Shen Y, et al. Topological domains in mammalian genomes identified by analysis of chromatin interactions. *Nature* 2012;485:376–80. <https://doi.org/10.1038/nature11082>.

Doenecke D, Albig W. Intronless Genes. In: John Wiley & Sons, Ltd, editor. Encyclopedia of Life Sciences, Chichester: John Wiley & Sons, Ltd; 2005, p. a0005022.  
<https://doi.org/10.1038/npg.els.0005022>.

Dorafshan E, Kahn TG, Schwartz YB. Hierarchical recruitment of Polycomb complexes revisited. *Nucleus* 2017;8:496–505. <https://doi.org/10.1080/19491034.2017.1363136>.

Dorn R, Krauss V, Reuter G, Saumweber H. The enhancer of position-effect variegation of *Drosophila*, E(var)3-93D, codes for a chromatin protein containing a conserved domain common to several transcriptional regulators. *PNAS* 1993;90:11376–80.  
<https://doi.org/10.1073/pnas.90.23.11376>.

Douillet D, Sze CC, Ryan C, Piunti A, Shah AP, Ugarenko M, et al. Uncoupling histone H3K4 trimethylation from developmental gene expression via an equilibrium of COMPASS, Polycomb and DNA methylation. *Nat Genet* 2020;52:615–25.  
<https://doi.org/10.1038/s41588-020-0618-1>.

Drelon C, Belalcazar HM, Secombe J. The Histone Demethylase KDM5 Is Essential for Larval Growth in *Drosophila*. *Genetics* 2018;genetics.301004.2018.  
<https://doi.org/10.1534/genetics.118.301004>.

Drouin S, Laramée L, Jacques P-É, Forest A, Bergeron M, Robert F. DSIF and RNA Polymerase II CTD Phosphorylation Coordinate the Recruitment of Rpd3S to Actively Transcribed Genes. *PLoS Genet* 2010;6:e1001173.  
<https://doi.org/10.1371/journal.pgen.1001173>.

Du Z, Zheng H, Huang B, Ma R, Wu J, Zhang Xianglin, et al. Allelic reprogramming of 3D chromatin architecture during early mammalian development. *Nature* 2017;547:232–5.  
<https://doi.org/10.1038/nature23263>.

Duret L, Mouchiroud D. Expression pattern and, surprisingly, gene length shape codon usage in *Caenorhabditis*, *Drosophila*, and *Arabidopsis*. *Proceedings of the National Academy of Sciences* 1999;96:4482–7. <https://doi.org/10.1073/pnas.96.8.4482>.

Dwyer K, Agarwal N, Pile L, Ansari A. Gene Architecture Facilitates Intron-Mediated Enhancement of Transcription. *Front Mol Biosci* 2021;8:669004.  
<https://doi.org/10.3389/fmolb.2021.669004>.

Ecco G, Cassano M, Kauzlaric A, Duc J, Coluccio A, Offner S, et al. Transposable Elements and Their KRAB-ZFP Controllers Regulate Gene Expression in Adult Tissues. *Developmental Cell* 2016;36:611–23. <https://doi.org/10.1016/j.devcel.2016.02.024>.

Egloff S, Dienstbier M, Murphy S. Updating the RNA polymerase CTD code: adding gene-specific layers. *Trends in Genetics* 2012;28:333–41. <https://doi.org/10.1016/j.tig.2012.03.007>.

Egloff S, O'Reilly D, Chapman RD, Taylor A, Tanzhaus K, Pitts L, et al. Serine-7 of the RNA Polymerase II CTD Is Specifically Required for snRNA Gene Expression. *Science* 2007;318:1777–9. <https://doi.org/10.1126/science.1145989>.

Eichhorn SW, Subtelny AO, Kronja I, Kwasniewski JC, Orr-Weaver TL, Bartel DP. mRNA poly(A)-tail changes specified by deadenylation broadly reshape translation in *Drosophila* oocytes and early embryos. *eLife* 2016;5:e16955. <https://doi.org/10.7554/eLife.16955>.

Emelyanov AV, Fyodorov DV. Thioredoxin-dependent disulfide bond reduction is required for protamine eviction from sperm chromatin. *Genes Dev* 2016;30:2651–6. <https://doi.org/10.1101/gad.290916.116>.

Erceg J, Pakozdi T, Marco-Ferrerres R, Ghavi-Helm Y, Girardot C, Bracken AP, et al. Dual functionality of *cis*-regulatory elements as developmental enhancers and Polycomb response elements. *Genes Dev* 2017;31:590–602. <https://doi.org/10.1101/gad.292870.116>.

Eskeland R, Eberharter A, Imhof A. HP1 Binding to Chromatin Methylated at H3K9 Is Enhanced by Auxiliary Factors. *Mol Cell Biol* 2007;27:453–65. <https://doi.org/10.1128/MCB.01576-06>.

Esnault C, Ghavi-Helm Y, Brun S, Soutourina J, Van Berkum N, Boschiero C, et al. Mediator-Dependent Recruitment of TFIIH Modules in Preinitiation Complex. *Molecular Cell* 2008;31:337–46. <https://doi.org/10.1016/j.molcel.2008.06.021>.

Eychenne T, Novikova E, Barrault M-B, Alibert O, Boschiero C, Peixeiro N, et al. Functional interplay between Mediator and TFIIB in preinitiation complex assembly in relation to promoter architecture. *Genes Dev* 2016;30:2119–32. <https://doi.org/10.1101/gad.285775.116>.

Ferreira H, Flaus A, Owen-Hughes T. Histone Modifications Influence the Action of Snf2 Family Remodelling Enzymes by Different Mechanisms. *Journal of Molecular Biology* 2007;374:563–79. <https://doi.org/10.1016/j.jmb.2007.09.059>.

Fischer T, Cui B, Dhakshnamoorthy J, Zhou M, Rubin C, Zofall M, et al. Diverse roles of HP1 proteins in heterochromatin assembly and functions in fission yeast. *Proceedings of the National Academy of Sciences* 2009;106:8998–9003. <https://doi.org/10.1073/pnas.0813063106>.

FitzGerald PC, Sturgill D, Shyakhtenko A, Oliver B, Vinson C. Comparative genomics of *Drosophila* and human core promoters. *Genome Biol* 2006;7:R53. <https://doi.org/10.1186/gb-2006-7-7-r53>.

Flavahan WA, Drier Y, Liao BB, Gillespie SM, Venteicher AS, Stemmer-Rachamimov AO, et al. Insulator dysfunction and oncogene activation in IDH mutant gliomas. *Nature* 2016;529:110–4. <https://doi.org/10.1038/nature16490>.

Franke M, Ibrahim DM, Andrey G, Schwarzer W, Heinrich V, Schöpflin R, et al. Formation of new chromatin domains determines pathogenicity of genomic duplications. *Nature* 2016;538:265–9. <https://doi.org/10.1038/nature19800>.

Freier R, Aragón E, Bagiński B, Pluta R, Martin-Malpartida P, Ruiz L, et al. Structures of the germline-specific Deadhead and thioredoxin T proteins from *Drosophila melanogaster* reveal unique features among thioredoxins. *IUCrJ* 2021;8:281–94. <https://doi.org/10.1107/S2052252521000221>.

Fudenberg G, Abdennur N, Imakaev M, Goloborodko A, Mirny LA. Emerging Evidence of Chromosome Folding by Loop Extrusion. *Cold Spring Harb Symp Quant Biol* 2017;82:45–55. <https://doi.org/10.1101/sqb.2017.82.034710>.

Fudenberg G, Imakaev M, Lu C, Goloborodko A, Abdennur N, Mirny LA. Formation of Chromosomal Domains by Loop Extrusion. *Cell Reports* 2016;15:2038–49. <https://doi.org/10.1016/j.celrep.2016.04.085>.

Fujioka M, Sun G, Jaynes JB. The *Drosophila* eve Insulator Homie Promotes eve Expression and Protects the Adjacent Gene from Repression by Polycomb Spreading. *PLoS Genet* 2013;9:e1003883. <https://doi.org/10.1371/journal.pgen.1003883>.

Fukaya T, Lim B, Levine M. Enhancer Control of Transcriptional Bursting. *Cell* 2016;166:358–68. <https://doi.org/10.1016/j.cell.2016.05.025>.

Furger A, O’Sullivan JM, Binnie A, Lee BA, Proudfoot NJ. Promoter proximal splice sites enhance transcription. *Genes Dev* 2002;16:2792–9. <https://doi.org/10.1101/gad.983602>.

Gabler M, Volkmar M, Weinlich S, Herbst A, Dobberthien P, Sklarss S, et al. Trans-splicing of the mod(mdg4) Complex Locus Is Conserved Between the Distantly Related Species *Drosophila melanogaster* and *D. virilis*. *Genetics* 2005;169:723–36. <https://doi.org/10.1534/genetics.103.020842>.

Gaertner B, Johnston J, Chen K, Wallaschek N, Paulson A, Garruss AS, et al. Poised RNA Polymerase II Changes over Developmental Time and Prepares Genes for Future Expression. *Cell Reports* 2012;2:1670–83. <https://doi.org/10.1016/j.celrep.2012.11.024>.

Gajan A, Barnes VL, Liu M, Saha N, Pile LA. The histone demethylase dKDM5/LID interacts with the SIN3 histone deacetylase complex and shares functional similarities with SIN3. *Epigenetics & Chromatin* 2016;9:4. <https://doi.org/10.1186/s13072-016-0053-9>.

- Ganapathi M, Srivastava P, Sutar S, Kumar K, Dasgupta D, Pal Singh G, et al. Comparative analysis of chromatin landscape in regulatory regions of human housekeeping and tissue specific genes. *BMC Bioinformatics* 2005;6:126. <https://doi.org/10.1186/1471-2105-6-126>.
- Garcia JF, Dumesic PA, Hartley PD, El-Samad H, Madhani HD. Combinatorial, site-specific requirement for heterochromatic silencing factors in the elimination of nucleosome-free regions. *Genes & Development* 2010;24:1758–71. <https://doi.org/10.1101/gad.1946410>.
- Gates LA, Foulds CE, O'Malley BW. Histone Marks in the 'Driver's Seat': Functional Roles in Steering the Transcription Cycle. *Trends in Biochemical Sciences* 2017;42:977–89. <https://doi.org/10.1016/j.tibs.2017.10.004>.
- Georgiev PG, Gerasimova TI. Novel genes influencing the expression of the yellow locus and *mdg4* (*gypsy*) in *Drosophila melanogaster*. *Molec Gen Genet* 1989;220:121–6. <https://doi.org/10.1007/BF00260865>.
- Gerasimova TI, Corces VG. Polycomb and Trithorax Group Proteins Mediate the Function of a Chromatin Insulator. *Cell* 1998;92:511–21. [https://doi.org/10.1016/S0092-8674\(00\)80944-7](https://doi.org/10.1016/S0092-8674(00)80944-7).
- Gerasimova TI, Gdula DA, Gerasimov DV, Simonova O, Corces VG. A drosophila protein that imparts directionality on a chromatin insulator is an enhancer of position-effect variegation. *Cell* 1995;82:587–97. [https://doi.org/10.1016/0092-8674\(95\)90031-4](https://doi.org/10.1016/0092-8674(95)90031-4).
- Ghosh SK, Jost D. How epigenome drives chromatin folding and dynamics, insights from efficient coarse-grained models of chromosomes. *PLoS Comput Biol* 2018;14:e1006159. <https://doi.org/10.1371/journal.pcbi.1006159>.
- Goldberg AD, Banaszynski LA, Noh K-M, Lewis PW, Elsaesser SJ, Stadler S, et al. Distinct Factors Control Histone Variant H3.3 Localization at Specific Genomic Regions. *Cell* 2010;140:678–91. <https://doi.org/10.1016/j.cell.2010.01.003>.
- Gorgoni B. The roles of cytoplasmic poly(A)-binding proteins in regulating gene expression: A developmental perspective. *Briefings in Functional Genomics and Proteomics* 2004;3:125–41. <https://doi.org/10.1093/bfgp/3.2.125>.
- Gu B, Lee M. Histone H3 lysine 4 methyltransferases and demethylases in self-renewal and differentiation of stem cells. *Cell Biosci* 2013;3:39. <https://doi.org/10.1186/2045-3701-3-39>.
- Guenther MG, Levine SS, Boyer LA, Jaenisch R, Young RA. A Chromatin Landmark and Transcription Initiation at Most Promoters in Human Cells. *Cell* 2007;130:77–88. <https://doi.org/10.1016/j.cell.2007.05.042>.
- Guillemette B, Bataille AR, Gévry N, Adam M, Blanchett

e M, Robert F, et al. Variant Histone H2A.Z Is Globally Localized to the Promoters of Inactive Yeast Genes and Regulates Nucleosome Positioning. *PLoS Biol* 2005;3:e384. <https://doi.org/10.1371/journal.pbio.0030384>.

Guo Y, Xu Q, Canzio D, Shou J, Li J, Gorkin DU, et al. CRISPR Inversion of CTCF Sites Alters Genome Topology and Enhancer/Promoter Function. *Cell* 2015;162:900–10. <https://doi.org/10.1016/j.cell.2015.07.038>.

Gurudatta BV, Corces VG. Chromatin insulators: lessons from the fly. *Briefings in Functional Genomics and Proteomics* 2009;8:276–82. <https://doi.org/10.1093/bfpg/elp032>.  
Haberle V, Stark A. Eukaryotic core promoters and the functional basis of transcription initiation. *Nat Rev Mol Cell Biol* 2018;19:621–37. <https://doi.org/10.1038/s41580-018-0028-8>.

Hall AW, Battenhouse AM, Shivram H, Morris AR, Cowperthwaite MC, Shpak M, et al. Bivalent Chromatin Domains in Glioblastoma Reveal a Subtype-Specific Signature of Glioma Stem Cells. *Cancer Res* 2018;78:2463–74. <https://doi.org/10.1158/0008-5472.CAN-17-1724>.

Hall IM. Establishment and Maintenance of a Heterochromatin Domain. *Science* 2002;297:2232–7. <https://doi.org/10.1126/science.1076466>.

Hammond CM. Histone chaperone networks shaping chromatin function 2017:18.  
Hammond MP, Laird CD. Chromosome structure and DNA replication in nurse and follicle cells of *Drosophila melanogaster*. *Chromosoma* 1985;91:267–78. <https://doi.org/10.1007/BF00328222>.

Harvey AJ, Bidwai AP, Miller LK. Doom, a product of the *Drosophila* *mod(mdg4)* gene, induces apoptosis and binds to baculovirus inhibitor-of-apoptosis proteins. *Mol Cell Biol* 1997;17:2835–43. <https://doi.org/10.1128/MCB.17.5.2835>.

Heintzman ND, Stuart RK, Hon G, Fu Y, Ching CW, Hawkins RD, et al. Distinct and predictive chromatin signatures of transcriptional promoters and enhancers in the human genome. *Nat Genet* 2007;39:311–8. <https://doi.org/10.1038/ng1966>.

Henikoff S, Henikoff JG, Kaya-Okur HS, Ahmad K. Efficient chromatin accessibility mapping *in situ* by nucleosome-tethered tagmentation. *Genomics*; 2020. <https://doi.org/10.1101/2020.04.15.043083>.

Henikoff S, Henikoff JG, Sakai A, Loeb GB, Ahmad K. Genome-wide profiling of salt fractions maps physical properties of chromatin. *Genome Research* 2008;19:460–9. <https://doi.org/10.1101/gr.087619.108>.

- Henry KW. Transcriptional activation via sequential histone H2B ubiquitylation and deubiquitylation, mediated by SAGA-associated Ubp8. *Genes & Development* 2003;17:2648–63. <https://doi.org/10.1101/gad.1144003>.
- Hödl M, Basler K. Transcription in the Absence of Histone H3.2 and H3K4 Methylation. *Current Biology* 2012;22:2253–7. <https://doi.org/10.1016/j.cub.2012.10.008>.
- Hoffmann NA, Jakobi AJ, Moreno-Morcillo M, Glatt S, Kosinski J, Hagen WJH, et al. Molecular structures of unbound and transcribing RNA polymerase III. *Nature* 2015;528:231–6. <https://doi.org/10.1038/nature16143>.
- Horard B, Loppin B. Fécondation: Le noyau spermatique déverrouillé par une thiorédoxine ultraspécialisée. *Med Sci (Paris)* 2017;33:585–7. <https://doi.org/10.1051/medsci/20173306009>.
- Horner VL, Wolfner MF. Transitioning from egg to embryo: Triggers and mechanisms of egg activation. *Dev Dyn* 2008;237:527–44. <https://doi.org/10.1002/dvdy.21454>.
- Hornung G, Bar-Ziv R, Rosin D, Tokuriki N, Tawfik DS, Oren M, et al. Noise-mean relationship in mutated promoters. *Genome Research* 2012;22:2409–17. <https://doi.org/10.1101/gr.139378.112>.
- Howe FS, Fischl H, Murray SC, Mellor J. Is H3K4me3 instructive for transcription activation? *BioEssays* 2017;39:e201600095. <https://doi.org/10.1002/bies.201600095>.
- Hsin J-P, Manley JL. The RNA polymerase II CTD coordinates transcription and RNA processing. *Genes & Development* 2012;26:2119–37. <https://doi.org/10.1101/gad.200303.112>.
- Hug CB, Grimaldi AG, Kruse K, Vaquerizas JM. Chromatin Architecture Emerges during Zygotic Genome Activation Independent of Transcription. *Cell* 2017;169:216-228.e19. <https://doi.org/10.1016/j.cell.2017.03.024>.
- Imbeault M, Helleboid P-Y, Trono D. KRAB zinc-finger proteins contribute to the evolution of gene regulatory networks. *Nature* 2017;543:550–4. <https://doi.org/10.1038/nature21683>.
- Iovino N, Ciabrelli F, Cavalli G. PRC2 controls *Drosophila* oocyte cell fate by repressing cell cycle genes. *Dev Cell* 2013;26:431–9. <https://doi.org/10.1016/j.devcel.2013.06.021>.
- Ito H, Sato K, Koganezawa M, Ote M, Matsumoto K, Hama C, et al. Fruitless Recruits Two Antagonistic Chromatin Factors to Establish Single-Neuron Sexual Dimorphism. *Cell* 2012;149:1327–38. <https://doi.org/10.1016/j.cell.2012.04.025>.

- Ivanov AV, Peng H, Yurchenko V, Yap KL, Negorev DG, Schultz DC, et al. PHD Domain-Mediated E3 Ligase Activity Directs Intramolecular Sumoylation of an Adjacent Bromodomain Required for Gene Silencing. *Molecular Cell* 2007;28:823–37. <https://doi.org/10.1016/j.molcel.2007.11.012>.
- J. Svensson M, Larsson J. Thioredoxin-2 affects lifespan and oxidative stress in *Drosophila*: Thioredoxins in *Drosophila*. *Hereditas* 2007;144:25–32. <https://doi.org/10.1111/j.2007.0018-0661.01990.x>.
- Jacobs SA, Taverna SD, Zhang Y, Briggs SD, Li J, Eissenberg JC, et al. Specificity of the HP1 chromo domain for the methylated N-terminus of histone H3. *EMBO J* 2001;20:5232–41. <https://doi.org/10.1093/emboj/20.18.5232>.
- Jiang C, Pugh BF. Nucleosome positioning and gene regulation: advances through genomics. *Nat Rev Genet* 2009;10:161–72. <https://doi.org/10.1038/nrg2522>.
- Jiang Z, Zhang B. On the role of transcription in positioning nucleosomes. *PLoS Comput Biol* 2021;17:e1008556. <https://doi.org/10.1371/journal.pcbi.1008556>.
- Jost D, Carrivain P, Cavalli G, Vaillant C. Modeling epigenome folding: formation and dynamics of topologically associated chromatin domains. *Nucleic Acids Research* 2014;42:9553–61. <https://doi.org/10.1093/nar/gku698>.
- Kadamb R, Mittal S, Bansal N, Batra H, Saluja D. Sin3: Insight into its transcription regulatory functions. *European Journal of Cell Biology* 2013;92:237–46. <https://doi.org/10.1016/j.ejcb.2013.09.001>.
- Kadoch C, Crabtree GR. Mammalian SWI/SNF chromatin remodeling complexes and cancer: Mechanistic insights gained from human genomics. *Sci Adv* 2015;1:e1500447. <https://doi.org/10.1126/sciadv.1500447>.
- Kadoch C, Williams RT, Calarco JP, Miller EL, Weber CM, Braun SMG, et al. Dynamics of BAF–Polycomb complex opposition on heterochromatin in normal and oncogenic states. *Nat Genet* 2017;49:213–22. <https://doi.org/10.1038/ng.3734>.
- Kahn TG, Dorafshan E, Schultheis D, Zare A, Stenberg P, Reim I, et al. Interdependence of PRC1 and PRC2 for recruitment to Polycomb Response Elements. *Nucleic Acids Res* 2016:gkw701. <https://doi.org/10.1093/nar/gkw701>.
- Kahn TG, Schwartz YB, Dellino GI, Pirrotta V. Polycomb Complexes and the Propagation of the Methylation Mark at the *Drosophila* Ubx Gene. *Journal of Biological Chemistry* 2006;281:29064–75. <https://doi.org/10.1074/jbc.M605430200>.

Kao C-F. Rad6 plays a role in transcriptional activation through ubiquitylation of histone H2B. *Genes & Development* 2004;18:184–95. <https://doi.org/10.1101/gad.1149604>.

Karimi MM, Goyal P, Maksakova IA, Bilenky M, Leung D, Tang JX, et al. DNA Methylation and SETDB1/H3K9me3 Regulate Predominantly Distinct Sets of Genes, Retroelements, and Chimeric Transcripts in mESCs. *Cell Stem Cell* 2011;8:676–87. <https://doi.org/10.1016/j.stem.2011.04.004>.

Kassis JA, Brown JL. Polycomb Group Response Elements in *Drosophila* and Vertebrates. *Advances in Genetics*, vol. 81, Elsevier; 2013, p. 83–118. <https://doi.org/10.1016/B978-0-12-407677-8.00003-8>.

Kassis JA, Kennison JA, Tamkun JW. Polycomb and Trithorax Group Genes in *Drosophila*. *Genetics* 2017;206:1699–725. <https://doi.org/10.1534/genetics.115.185116>.

Ke Y, Xu Y, Chen X, Feng S, Liu Z, Sun Y, et al. 3D Chromatin Structures of Mature Gametes and Structural Reprogramming during Mammalian Embryogenesis. *Cell* 2017;170:367–381.e20. <https://doi.org/10.1016/j.cell.2017.06.029>.

Keller C, Adaixo R, Stunnenberg R, Woolcock KJ, Hiller S, Bühler M. HP1Swi6 Mediates the Recognition and Destruction of Heterochromatic RNA Transcripts. *Molecular Cell* 2012;47:215–27. <https://doi.org/10.1016/j.molcel.2012.05.009>.

King, RC. Ovarian development in *Drosophila melanogaster*. New York. Academic.; 1970. Kingston RE, Tamkun JW. Transcriptional Regulation by Trithorax-Group Proteins. *Cold Spring Harbor Perspectives in Biology* 2014;6:a019349–a019349. <https://doi.org/10.1101/cshperspect.a019349>.

Klattenhoff C, Xi H, Li C, Lee S, Xu J, Khurana JS, et al. The *Drosophila* HP1 Homolog Rhino Is Required for Transposon Silencing and piRNA Production by Dual-Strand Clusters. *Cell* 2009;138:1137–49. <https://doi.org/10.1016/j.cell.2009.07.014>.

Klymenko T, Müller J. The histone methyltransferases Trithorax and Ash1 prevent transcriptional silencing by Polycomb group proteins. *EMBO Rep* 2004;5:373–7. <https://doi.org/10.1038/sj.embor.7400111>.

Kochetov AV, Ponomarenko MP, Frolov AS, Kisselev LL, Kolchanov NA. Prediction of eukaryotic mRNA translational properties. *Bioinformatics* 1999;15:704–12. <https://doi.org/10.1093/bioinformatics/15.7.704>.

Krebs AR, Imanci D, Hoerner L, Gaidatzis D, Burger L, Schübeler D. Genome-wide Single-Molecule Footprinting Reveals High RNA Polymerase II Turnover at Paused Promoters. *Molecular Cell* 2017;67:411–422.e4. <https://doi.org/10.1016/j.molcel.2017.06.027>.

Kronja I, Whitfield ZJ, Yuan B, Dzek K, Kirkpatrick J, Krijgsveld J, et al. Quantitative proteomics reveals the dynamics of protein changes during *Drosophila* oocyte maturation and the oocyte-to-embryo transition. *Proc Natl Acad Sci USA* 2014;111:16023–8. <https://doi.org/10.1073/pnas.1418657111>.

Kubik S, Bruzzone MJ, Jacquet P, Falcone J-L, Rougemont J, Shore D. Nucleosome Stability Distinguishes Two Different Promoter Types at All Protein-Coding Genes in Yeast. *Molecular Cell* 2015;60:422–34. <https://doi.org/10.1016/j.molcel.2015.10.002>.

Kusch T, Mei A, Nguyen C. Histone H3 lysine 4 trimethylation regulates cotranscriptional H2A variant exchange by Tip60 complexes to maximize gene expression. *Proc Natl Acad Sci USA* 2014;111:4850–5. <https://doi.org/10.1073/pnas.1320337111>.

Kutach AK, Kadonaga JT. The Downstream Promoter Element DPE Appears To Be as Widely Used as the TATA Box in *Drosophila* Core Promoters. *Mol Cell Biol* 2000;20:4754–64. <https://doi.org/10.1128/MCB.20.13.4754-4764.2000>.

Kuzmichev A. Histone methyltransferase activity associated with a human multiprotein complex containing the Enhancer of Zeste protein. *Genes & Development* 2002;16:2893–905. <https://doi.org/10.1101/gad.1035902>.

Kyrchanova O, Georgiev P. Chromatin insulators and long-distance interactions in *Drosophila*. *FEBS Letters* 2014;588:8–14. <https://doi.org/10.1016/j.febslet.2013.10.039>.

Larson AG, Elnatan D, Keenen MM, Trnka MJ, Johnston JB, Burlingame AL, et al. Liquid droplet formation by HP1 $\alpha$  suggests a role for phase separation in heterochromatin. *Nature* 2017;547:236–40. <https://doi.org/10.1038/nature22822>.

Lauberth SM, Nakayama T, Wu X, Ferris AL, Tang Z, Hughes SH, et al. H3K4me3 Interactions with TAF3 Regulate Preinitiation Complex Assembly and Selective Gene Activation. *Cell* 2013;152:1021–36. <https://doi.org/10.1016/j.cell.2013.01.052>.

Lavarone E, Barbieri CM, Pasini D. Dissecting the role of H3K27 acetylation and methylation in PRC2 mediated control of cellular identity. *Nat Commun* 2019;10:1679. <https://doi.org/10.1038/s41467-019-09624-w>.

Lee C-K, Shibata Y, Rao B, Strahl BD, Lieb JD. Evidence for nucleosome depletion at active regulatory regions genome-wide. *Nat Genet* 2004;36:900–5. <https://doi.org/10.1038/ng1400>.

Lee J, Hyeon DY, Hwang D. Single-cell multiomics: technologies and data analysis methods. *Exp Mol Med* 2020;52:1428–42. <https://doi.org/10.1038/s12276-020-0420-2>.

- Lepesant JMJ, Iampietro C, Galeota E, Augé B, Aguirrenbengoa M, Mercé C, et al. A dual role of dLsd1 in oogenesis: regulating developmental genes and repressing transposons. *Nucleic Acids Research* 2020;48:1206–24. <https://doi.org/10.1093/nar/gkz1142>.
- Lesch BJ, Dokshin GA, Young RA, McCarrey JR, Page DC. A set of genes critical to development is epigenetically poised in mouse germ cells from fetal stages through completion of meiosis. *Proceedings of the National Academy of Sciences* 2013;110:16061–6. <https://doi.org/10.1073/pnas.1315204110>.
- Lhoumaud P, Hennion M, Gamot A, Cuddapah S, Queille S, Liang J, et al. Insulators recruit histone methyltransferase dMes4 to regulate chromatin of flanking genes. *The EMBO Journal* 2014;33:1599–613. <https://doi.org/10.15252/embj.201385965>.
- Li B, Gogol M, Carey M, Lee D, Seidel C, Workman JL. Combined Action of PHD and Chromo Domains Directs the Rpd3S HDAC to Transcribed Chromatin. *Science* 2007;316:1050–4. <https://doi.org/10.1126/science.1139004>.
- Li H, Liefke R, Jiang J, Kurland JV, Tian W, Deng P, et al. Polycomb-like proteins link the PRC2 complex to CpG islands. *Nature* 2017;549:287–91. <https://doi.org/10.1038/nature23881>.
- Li L, Greer C, Eisenman RN, Secombe J. Essential Functions of the Histone Demethylase Lid. *PLoS Genetics* 2010;6:e1001221. <https://doi.org/10.1371/journal.pgen.1001221>.
- Lianoglou S, Garg V, Yang JL, Leslie CS, Mayr C. Ubiquitously transcribed genes use alternative polyadenylation to achieve tissue-specific expression. *Genes & Development* 2013;27:2380–96. <https://doi.org/10.1101/gad.229328.113>.
- Lieberman-Aiden E, van Berkum NL, Williams L, Imapkaev M, Ragozcy T, Telling A, et al. Comprehensive Mapping of Long-Range Interactions Reveals Folding Principles of the Human Genome. *Science* 2009;326:289–93. <https://doi.org/10.1126/science.1181369>.
- Lim J, Lee M, Son A, Chang H, Kim VN. mTAIL-seq reveals dynamic poly(A) tail regulation in oocyte-to-embryo development. *Genes Dev* 2016;30:1671–82. <https://doi.org/10.1101/gad.284802.116>.
- Liu X, Greer C, Secombe J. KDM5 Interacts with Foxo to Modulate Cellular Levels of Oxidative Stress. *PLoS Genetics* 2014;10:e1004676. <https://doi.org/10.1371/journal.pgen.1004676>.
- Liu X, Secombe J. The Histone Demethylase KDM5 Activates Gene Expression by Recognizing Chromatin Context through Its PHD Reader Motif. *Cell Reports* 2015;13:2219–31. <https://doi.org/10.1016/j.celrep.2015.11.007>.

Lloret-Llinares M, Pérez-Lluch S, Rossell D, Morán T, Ponsa-Cobas J, Auer H, et al. dKDM5/LID regulates H3K4me3 dynamics at the transcription-start site (TSS) of actively transcribed developmental genes. *Nucleic Acids Res* 2012;40:9493–505. <https://doi.org/10.1093/nar/gks773>.

Lobanenkov VV, Nicolas RH, Adler VV, Paterson H, Klenova EM, Polotskaja AV, et al. A novel sequence-specific DNA binding protein which interacts with three regularly spaced direct repeats of the CCCTC-motif in the 5'-flanking sequence of the chicken c-myc gene. *Oncogene* 1990;5:1743–53.

Lopes I, Altab G, Raina P, de Magalhães JP. Gene Size Matters: An Analysis of Gene Length in the Human Genome. *Front Genet* 2021;12:559998. <https://doi.org/10.3389/fgene.2021.559998>.

Loppin B, Dubruille R, Horard B. The intimate genetics of *Drosophila* fertilization. *Open Biol* 2015;5:150076. <https://doi.org/10.1098/rsob.150076>.

Loubiere V, Delest A, Thomas A, Bonev B, Schuettengruber B, Sati S, et al. Coordinate redeployment of PRC1 proteins suppresses tumor formation during *Drosophila* development. *Nat Genet* 2016;48:1436–42. <https://doi.org/10.1038/ng.3671>.

Louhichi A, Fourati A, Rebaï A. IGD: A resource for intronless genes in the human genome. *Gene* 2011;488:35–40. <https://doi.org/10.1016/j.gene.2011.08.013>.

Lu BY, Emtage PC, Duyf BJ, Hilliker AJ, Eissenberg JC. Heterochromatin protein 1 is required for the normal expression of two heterochromatin genes in *Drosophila*. *Genetics* 2000;155:699–708.

Lucas T, Ferraro T, Roelens B, De Las Heras Chanes J, Walczak AM, Coppey M, et al. Live Imaging of Bicoid-Dependent Transcription in *Drosophila* Embryos. *Current Biology* 2013;23:2135–9. <https://doi.org/10.1016/j.cub.2013.08.053>.

Luger K, Mäder AW, Richmond RK, Sargent DF, Richmond TJ. Crystal structure of the nucleosome core particle at 2.8 Å resolution. *Nature* 1997;389:251–60. <https://doi.org/10.1038/38444>.

Lupiáñez DG, Kraft K, Heinrich V, Krawitz P, Brancati F, Klopocki E, et al. Disruptions of Topological Chromatin Domains Cause Pathogenic Rewiring of Gene-Enhancer Interactions. *Cell* 2015;161:1012–25. <https://doi.org/10.1016/j.cell.2015.04.004>.

Luzhin AV, Flyamer IM, Khrameeva EE, Ulianov SV, Razin SV, Gavrilov AA. Quantitative differences in TAD border strength underly the TAD hierarchy in *Drosophila* chromosomes. *J Cell Biochem* 2019;120:4494–503. <https://doi.org/10.1002/jcb.27737>.

Lynch MD, Smith AJH, De Gobbi M, Flenley M, Hughes JR, Vernimmen D, et al. An interspecies analysis reveals a key role for unmethylated CpG dinucleotides in vertebrate Polycomb complex recruitment: An interspecies analysis of chromatin bivalency. *The EMBO Journal* 2012;31:317–29. <https://doi.org/10.1038/emboj.2011.399>.

Mahowald AP, Tiefert M. Fine structural changes in the *Drosophila* oocyte nucleus during a short period of RNA synthesis: An autoradiographic and ultrastructural study of RNA synthesis in the oocyte nucleus of *Drosophila*. *W Roux' Archiv f Entwicklungsmechanik* 1970;165:8–25. <https://doi.org/10.1007/BF00576994>.

Malone CD, Brennecke J, Dus M, Stark A, McCombie WR, Sachidanandam R, et al. Specialized piRNA Pathways Act in Germline and Somatic Tissues of the *Drosophila* Ovary. *Cell* 2009;137:522–35. <https://doi.org/10.1016/j.cell.2009.03.040>.

Mangus DA, Evans MC, Jacobson A. Poly(A)-binding proteins: multifunctional scaffolds for the post-transcriptional control of gene expression. *Genome Biol* 2003;4:223. <https://doi.org/10.1186/gb-2003-4-7-223>.

Margaritis T, Oreal V, Brabers N, Maestroni L, Vitaliano-Prunier A, Benschop JJ, et al. Two Distinct Repressive Mechanisms for Histone 3 Lysine 4 Methylation through Promoting 3'-End Antisense Transcription. *PLoS Genet* 2012;8:e1002952. <https://doi.org/10.1371/journal.pgen.1002952>.

Martire S, Banaszynski LA. The roles of histone variants in fine-tuning chromatin organization and function. *Nat Rev Mol Cell Biol* 2020;21:522–41. <https://doi.org/10.1038/s41580-020-0262-8>.

Marullo F, Cesarini E, Antonelli L, Gregoret F, Oliva G, Lanzaolo C. Nucleoplasmic Lamin A/C and Polycomb group of proteins: An evolutionarily conserved interplay. *Nucleus* 2016;7:103–11. <https://doi.org/10.1080/19491034.2016.1157675>.

Matharu N, Ahituv N. Minor Loops in Major Folds: Enhancer–Promoter Looping, Chromatin Restructuring, and Their Association with Transcriptional Regulation and Disease. *PLoS Genet* 2015;11:e1005640. <https://doi.org/10.1371/journal.pgen.1005640>.

Matsui T, Leung D, Miyashita H, Maksakova IA, Miyachi H, Kimura H, et al. Proviral silencing in embryonic stem cells requires the histone methyltransferase ESET. *Nature* 2010;464:927–31. <https://doi.org/10.1038/nature08858>.

Matsui T, Segall J, Weil PA, Roeder RG. Multiple factors required for accurate initiation of transcription by purified RNA polymerase II. *J Biol Chem* 1980;255:11992–6.

- Mavrich TN, Jiang C, Ioshikhes IP, Li X, Venters BJ, Zanton SJ, et al. Nucleosome organization in the *Drosophila* genome. *Nature* 2008;453:358–62. <https://doi.org/10.1038/nature06929>.
- Mayer A, Heidemann M, Lidschreiber M, Schrieck A, Sun M, Hintermair C, et al. CTD Tyrosine Phosphorylation Impairs Termination Factor Recruitment to RNA Polymerase II. *Science* 2012;336:1723–5. <https://doi.org/10.1126/science.1219651>.
- Mayer A, Lidschreiber M, Siebert M, Leike K, Söding J, Cramer P. Uniform transitions of the general RNA polymerase II transcription complex. *Nat Struct Mol Biol* 2010;17:1272–8. <https://doi.org/10.1038/nsmb.1903>.
- McClelland S, Shrivastava R, Medh JD. Regulation of Translational Efficiency by Disparate 5' -UTRs of PPAR  $\gamma$  Splice Variants. *PPAR Research* 2009;2009:1–8. <https://doi.org/10.1155/2009/193413>.
- McCracken S., Fong N, Rosonina E, Yankulov K, Brothers G, Siderovski D, et al. 5'-Capping enzymes are targeted to pre-mRNA by binding to the phosphorylated carboxy-terminal domain of RNA polymerase II. *Genes & Development* 1997;11:3306–18. <https://doi.org/10.1101/gad.11.24.3306>.
- McCracken Susan, Fong N, Yankulov K, Ballantyne S, Pan G, Greenblatt J, et al. The C-terminal domain of RNA polymerase II couples mRNA processing to transcription. *Nature* 1997;385:357–61. <https://doi.org/10.1038/385357a0>.
- McDonel P, Costello I, Hendrich B. Keeping things quiet: Roles of NuRD and Sin3 co-repressor complexes during mammalian development. *The International Journal of Biochemistry & Cell Biology* 2009;41:108–16. <https://doi.org/10.1016/j.biocel.2008.07.022>.
- McLaughlin JM, Bratu DP. *Drosophila melanogaster* Oogenesis: An Overview. In: Bratu DP, McNeil GP, editors. *Drosophila Oogenesis*, vol. 1328, New York, NY: Springer New York; 2015, p. 1–20. [https://doi.org/10.1007/978-1-4939-2851-4\\_1](https://doi.org/10.1007/978-1-4939-2851-4_1).
- Melnikova L, Elizar'ev P, Erokhin M, Molodina V, Chetverina D, Kostyuchenko M, et al. The same domain of Su(Hw) is required for enhancer blocking and direct promoter repression. *Sci Rep* 2019;9:5314. <https://doi.org/10.1038/s41598-019-41761-6>.
- Melnikova L, Juge F, Gruzdeva N, Mazur A, Cavalli G, Georgiev P. Interaction between the GAGA factor and Mod(mdg4) proteins promotes insulator bypass in *Drosophila*. *Proceedings of the National Academy of Sciences* 2004;101:14806–11. <https://doi.org/10.1073/pnas.0403959101>.
- Melnikova L, Kostyuchenko M, Molodina V, Parshikov A, Georgiev P, Golovnin A. Multiple interactions are involved in a highly specific association of the Mod(mdg4)-67.2

isoform with the Su(Hw) sites in *Drosophila*. *Open Biol* 2017;7:170150.  
<https://doi.org/10.1098/rsob.170150>.

Melnikova LS, Georgiev PG, Golovnin AK. The Functions and Mechanisms of Action of Insulators in the Genomes of Higher Eukaryotes. *Acta Naturae* 2020;12:15–33.  
<https://doi.org/10.32607/actanaturae.11144>.

Mendenhall EM, Koche RP, Truong T, Zhou VW, Issac B, Chi AS, et al. GC-Rich Sequence Elements Recruit PRC2 in Mammalian ES Cells. *PLoS Genet* 2010;6:e1001244.  
<https://doi.org/10.1371/journal.pgen.1001244>.

Messmer S, Franke A, Paro R. Analysis of the functional role of the Polycomb chromo domain in *Drosophila melanogaster*. *Genes & Development* 1992;6:1241–54.  
<https://doi.org/10.1101/gad.6.7.1241>.

Mikkelsen TS, Ku M, Jaffe DB, Issac B, Lieberman E, Giannoukos G, et al. Genome-wide maps of chromatin state in pluripotent and lineage-committed cells. *Nature* 2007;448:553–60.  
<https://doi.org/10.1038/nature06008>.

Miller D, Brinkworth M, Iles D. Paternal DNA packaging in spermatozoa: more than the sum of its parts? DNA, histones, protamines and epigenetics. *REPRODUCTION* 2010;139:287–301. <https://doi.org/10.1530/REP-09-0281>.

Minsky N, Shema E, Field Y, Schuster M, Segal E, Oren M. Monoubiquitinated H2B is associated with the transcribed region of highly expressed genes in human cells. *Nat Cell Biol* 2008;10:483–8. <https://doi.org/10.1038/ncb1712>.

Mito Y, Henikoff JG, Henikoff S. Histone Replacement Marks the Boundaries of cis-Regulatory Domains. *Science* 2007;315:1408–11. <https://doi.org/10.1126/science.1134004>.  
Mohan M, Herz H-M, Smith ER, Zhang Y, Jackson J, Washburn MP, et al. The COMPASS Family of H3K4 Methylases in *Drosophila*. *Mol Cell Biol* 2011;31:4310–8.  
<https://doi.org/10.1128/MCB.06092-11>.

Mohrmann L, Langenberg K, Krijgsveld J, Kal AJ, Heck AJR, Verrijzer CP. Differential Targeting of Two Distinct SWI/SNF-Related *Drosophila* Chromatin-Remodeling Complexes. *MCB* 2004;24:3077–88. <https://doi.org/10.1128/MCB.24.8.3077-3088.2004>.

Moshkin YM, Kan TW, Goodfellow H, Bezstarosti K, Maeda RK, Pilyugin M, et al. Histone Chaperones ASF1 and NAP1 Differentially Modulate Removal of Active Histone Marks by LID-RPD3 Complexes during NOTCH Silencing. *Molecular Cell* 2009;35:782–93.  
<https://doi.org/10.1016/j.molcel.2009.07.020>.

- Müller J, Hart CM, Francis NJ, Vargas ML, Sengupta A, Wild B, et al. Histone Methyltransferase Activity of a *Drosophila* Polycomb Group Repressor Complex. *Cell* 2002;111:197–208. [https://doi.org/10.1016/S0092-8674\(02\)00976-5](https://doi.org/10.1016/S0092-8674(02)00976-5).
- Nagano T, Lubling Y, Stevens TJ, Schoenfelder S, Yaffe E, Dean W, et al. Single-cell Hi-C reveals cell-to-cell variability in chromosome structure. *Nature* 2013;502:59–64. <https://doi.org/10.1038/nature12593>.
- Navarro-Costa P, McCarthy A, Prudêncio P, Greer C, Guilgur LG, Becker JD, et al. Early programming of the oocyte epigenome temporally controls late prophase I transcription and chromatin remodelling. *Nat Commun* 2016;7:12331. <https://doi.org/10.1038/ncomms12331>.
- Nègre N, Brown CD, Shah PK, Kheradpour P, Morrison CA, Henikoff JG, et al. A Comprehensive Map of Insulator Elements for the *Drosophila* Genome. *PLoS Genet* 2010;6:e1000814. <https://doi.org/10.1371/journal.pgen.1000814>.
- Neri F, Rapelli S, Krepelova A, Incarnato D, Parlato C, Basile G, et al. Intragenic DNA methylation prevents spurious transcription initiation. *Nature* 2017;543:72–7. <https://doi.org/10.1038/nature21373>.
- Nilsen TW, Graveley BR. Expansion of the eukaryotic proteome by alternative splicing. *Nature* 2010;463:457–63. <https://doi.org/10.1038/nature08909>.
- Nojima T, Gomes T, Grosso ARF, Kimura H, Dye MJ, Dhir S, et al. Mammalian NET-Seq Reveals Genome-wide Nascent Transcription Coupled to RNA Processing. *Cell* 2015;161:526–40. <https://doi.org/10.1016/j.cell.2015.03.027>.
- Nora EP, Goloborodko A, Valton A-L, Gibcus JH, Uebersohn A, Abdennur N, et al. Targeted Degradation of CTCF Decouples Local Insulation of Chromosome Domains from Genomic Compartmentalization. *Cell* 2017;169:930-944.e22. <https://doi.org/10.1016/j.cell.2017.05.004>.
- Nordman J, Orr-Weaver TL. Regulation of DNA replication during development. *Development* 2012;139:455–64. <https://doi.org/10.1242/dev.061838>.
- Nott A. A quantitative analysis of intron effects on mammalian gene expression. *RNA* 2003;9:607–17. <https://doi.org/10.1261/rna.5250403>.
- van Oevelen C, Wang J, Asp P, Yan Q, Kaelin WG, Kluger Y, et al. A Role for Mammalian Sin3 in Permanent Gene Silencing. *Molecular Cell* 2008;32:359–70. <https://doi.org/10.1016/j.molcel.2008.10.015>.
- Ogienko AA, Fedorova SA, Baricheva EM. Basic aspects of ovarian development in *Drosophila melanogaster*. *Russ J Genet* 2007;43:1120–34. <https://doi.org/10.1134/S1022795407100055>.

Ohler U, Liao G, Niemann H, Rubin GM. Computational analysis of core promoters in the *Drosophila* genome 2002;12.

Orphanides G, Lagrange T, Reinberg D. The general transcription factors of RNA polymerase II. *Genes & Development* 1996;10:2657–83. <https://doi.org/10.1101/gad.10.21.2657>.

Orsi GA, Kasinathan S, Hughes KT, Saminadin-Peter S, Henikoff S, Ahmad K. High-resolution mapping defines the cooperative architecture of Polycomb response elements. *Genome Research* 2014;24:809–20. <https://doi.org/10.1101/gr.163642.113>.

Ozata DM, Gainetdinov I, Zoch A, O'Carroll D, Zamore PD. PIWI-interacting RNAs: small RNAs with big functions. *Nat Rev Genet* 2019;20:89–108. <https://doi.org/10.1038/s41576-018-0073-3>.

Özdemir, Gambetta. The Role of Insulation in Patterning Gene Expression. *Genes* 2019;10:767. <https://doi.org/10.3390/genes10100767>.

Pai C-Y, Lei EP, Ghosh D, Corces VG. The Centrosomal Protein CP190 Is a Component of the gypsy Chromatin Insulator. *Molecular Cell* 2004;16:737–48. <https://doi.org/10.1016/j.molcel.2004.11.004>.

Pan G, Tian S, Nie J, Yang C, Ruotti V, Wei H, et al. Whole-Genome Analysis of Histone H3 Lysine 4 and Lysine 27 Methylation in Human Embryonic Stem Cells. *Cell Stem Cell* 2007;1:299–312. <https://doi.org/10.1016/j.stem.2007.08.003>.

Parisi M, Nuttall R, Edwards P, Minor J, Naiman D, Lü J, et al. A survey of ovary-, testis-, and soma-biased gene expression in *Drosophila melanogaster* adults. *Genome Biology* 2004;18.

Pascucci T, Perrino J, Mahowald AP, Waring GL. Eggshell Assembly in *Drosophila*: Processing and Localization of Vitelline Membrane and Chorion Proteins. *Developmental Biology* 1996;177:590–8. <https://doi.org/10.1006/dbio.1996.0188>.

Pavri R, Zhu B, Li G, Trojer P, Mandal S, Shilatifard A, et al. Histone H2B Monoubiquitination Functions Cooperatively with FACT to Regulate Elongation by RNA Polymerase II. *Cell* 2006;125:703–17. <https://doi.org/10.1016/j.cell.2006.04.029>.

Pengelly AR, Copur O, Jackle H, Herzig A, Muller J. A Histone Mutant Reproduces the Phenotype Caused by Loss of Histone-Modifying Factor Polycomb. *Science* 2013;339:698–9. <https://doi.org/10.1126/science.1231382>.

Pengelly AR, Kalb R, Finkl K, Müller J. Transcriptional repression by PRC1 in the absence of H2A monoubiquitylation. *Genes Dev* 2015;29:1487–92. <https://doi.org/10.1101/gad.265439.115>.

Perino M, van Mierlo G, Karemaker ID, van Genesen S, Vermeulen M, Marks H, et al. MTF2 recruits Polycomb Repressive Complex 2 by helical-shape-selective DNA binding. *Nat Genet* 2018;50:1002–10. <https://doi.org/10.1038/s41588-018-0134-8>.

Petrova B, Liu K, Tian C, Kitaoka M, Freinkman E, Yang J, et al. Dynamic redox balance directs the oocyte-to-embryo transition via developmentally controlled reactive cysteine changes. *Proc Natl Acad Sci USA* 2018;115:E7978–86. <https://doi.org/10.1073/pnas.1807918115>.

Pherson M, Misulovin Z, Gause M, Mihindikulasuriya K, Swain A, Dorsett D. Polycomb repressive complex 1 modifies transcription of active genes. *Sci Adv* 2017;3:e1700944. <https://doi.org/10.1126/sciadv.1700944>.

Phillips-Cremins JE, Sauria MEG, Sanyal A, Gerasimova TI, Lajoie BR, Bell JSK, et al. Architectural Protein Subclasses Shape 3D Organization of Genomes during Lineage Commitment. *Cell* 2013;153:1281–95. <https://doi.org/10.1016/j.cell.2013.04.053>.

Plath K. Role of Histone H3 Lysine 27 Methylation in X Inactivation. *Science* 2003;300:131–5. <https://doi.org/10.1126/science.1084274>.

Prudêncio P, Guilgur LG, Sobral J, Becker JD, Martinho RG, Navarro-Costa P. The Trithorax group protein dMLL3/4 instructs the assembly of the zygotic genome at fertilization. *EMBO Rep* 2018;19. <https://doi.org/10.15252/embr.201845728>.

Raab JR, Chiu J, Zhu J, Katzman S, Kurukuti S, Wade PA, et al. Human tRNA genes function as chromatin insulators: Human tRNA genes function as chromatin insulators. *The EMBO Journal* 2012;31:330–50. <https://doi.org/10.1038/emboj.2011.406>.

Rach EA, Winter DR, Benjamin AM, Corcoran DL, Ni T, Zhu J, et al. Transcription Initiation Patterns Indicate Divergent Strategies for Gene Regulation at the Chromatin Level. *PLoS Genet* 2011;7:e1001274. <https://doi.org/10.1371/journal.pgen.1001274>.

Racko D, Benedetti F, Goundaroulis D, Stasiak A. Chromatin Loop Extrusion and Chromatin Unknotting. *Polymers* 2018;10:1126. <https://doi.org/10.3390/polym10101126>.

Raj A, Peskin CS, Tranchina D, Vargas DY, Tyagi S. Stochastic mRNA Synthesis in Mammalian Cells. *PLoS Biol* 2006;4:e309. <https://doi.org/10.1371/journal.pbio.0040309>.

- Ramakrishnan S, Pokhrel S, Palani S, Pflueger C, Parnell TJ, Cairns BR, et al. Counteracting H3K4 methylation modulators Set1 and Jhd2 co-regulate chromatin dynamics and gene transcription. *Nat Commun* 2016;7:11949. <https://doi.org/10.1038/ncomms11949>.
- Ramírez F, Bhardwaj V, Arrigoni L, Lam KC, Grüning BA, Villaveces J, et al. High-resolution TADs reveal DNA sequences underlying genome organization in flies. *Nat Commun* 2018;9:189. <https://doi.org/10.1038/s41467-017-02525-w>.
- Rangan P, Malone CD, Navarro C, Newbold SP, Hayes PS, Sachidanandam R, et al. piRNA Production Requires Heterochromatin Formation in *Drosophila*. *Current Biology* 2011;21:1373–9. <https://doi.org/10.1016/j.cub.2011.06.057>.
- Rao SSP, Huang S-C, Glenn St Hilaire B, Engreitz JM, Perez EM, Kieffer-Kwon K-R, et al. Cohesin Loss Eliminates All Loop Domains. *Cell* 2017;171:305-320.e24. <https://doi.org/10.1016/j.cell.2017.09.026>.
- Rao SSP, Huntley MH, Durand NC, Stamenova EK, Bochkov ID, Robinson JT, et al. A 3D Map of the Human Genome at Kilobase Resolution Reveals Principles of Chromatin Looping. *Cell* 2014;159:1665–80. <https://doi.org/10.1016/j.cell.2014.11.021>.
- Ray P, De S, Mitra A, Bezstarosti K, Demmers JAA, Pfeifer K, et al. Combgap contributes to recruitment of Polycomb group proteins in *Drosophila*. *Proc Natl Acad Sci USA* 2016;113:3826–31. <https://doi.org/10.1073/pnas.1520926113>.
- Reddington JP, Perricone SM, Nestor CE, Reichmann J, Youngson NA, Suzuki M, et al. Redistribution of H3K27me3 upon DNA hypomethylation results in de-repression of Polycomb target genes. *Genome Biol* 2013;14:R25. <https://doi.org/10.1186/gb-2013-14-3-r25>.
- Rennie S, Dalby M, van Duin L, Andersson R. Transcriptional decomposition reveals active chromatin architectures and cell specific regulatory interactions. *Nat Commun* 2018;9:487. <https://doi.org/10.1038/s41467-017-02798-1>.
- Ringrose L, Paro R. Epigenetic Regulation of Cellular Memory by the Polycomb and Trithorax Group Proteins. *Annu Rev Genet* 2004;38:413–43. <https://doi.org/10.1146/annurev.genet.38.072902.091907>.
- Rodriguez J, Munoz M, Vives L, Frangou CG, Groudine M, Peinado MA. Bivalent domains enforce transcriptional memory of DNA methylated genes in cancer cells. *Proceedings of the National Academy of Sciences* 2008;105:19809–14. <https://doi.org/10.1073/pnas.0810133105>.
- Roelens B, Clémot M, Leroux-Coyau M, Klapholz B, Dostatni N. Maintenance of Heterochromatin by the Large Subunit of the CAF-1 Replication-Coupled Histone Chaperone

Requires Its Interaction with HP1a Through a Conserved Motif. *Genetics* 2017;205:125–37. <https://doi.org/10.1534/genetics.116.190785>.

Royzman I, Orr-Weaver TL. S phase and differential DNA replication during *Drosophila* oogenesis: Endo cell cycle in *Drosophila* oogenesis. *Genes to Cells* 1998;3:767–76. <https://doi.org/10.1046/j.1365-2443.1998.00232.x>.

Sabari BR, Dall’Agnese A, Boija A, Klein IA, Coffey EL, Shrinivas K, et al. Coactivator condensation at super-enhancers links phase separation and gene control. *Science* 2018;361:eaar3958. <https://doi.org/10.1126/science.aar3958>.

Saha N, Liu M, Gajan A, Pile LA. Genome-wide studies reveal novel and distinct biological pathways regulated by SIN3 isoforms. *BMC Genomics* 2016;17:111. <https://doi.org/10.1186/s12864-016-2428-5>.

Sahu SC, Swanson KA, Kang RS, Huang K, Brubaker K, Ratcliff K, et al. Conserved Themes in Target Recognition by the PAH1 and PAH2 Domains of the Sin3 Transcriptional Corepressor. *Journal of Molecular Biology* 2008;375:1444–56. <https://doi.org/10.1016/j.jmb.2007.11.079>.

Sakai A, Schwartz BE, Goldstein S, Ahmad K. Transcriptional and Developmental Functions of the H3.3 Histone Variant in *Drosophila*. *Current Biology* 2009;19:1816–20. <https://doi.org/10.1016/j.cub.2009.09.021>.

Salz HK, Flickinger TW, Mittendorf E, Pellicena-Palle A, Petschek JP, Albrecht EB. The *Drosophila* maternal effect locus deadhead encodes a thioredoxin homolog required for female meiosis and early embryonic development. *Genetics* 1994;136:1075–86. <https://doi.org/10.1093/genetics/136.3.1075>.

Santaguida S, Musacchio A. The life and miracles of kinetochores. *EMBO J* 2009;28:2511–31. <https://doi.org/10.1038/emboj.2009.173>.

Sanz AB, García R, Rodríguez-Peña JM, Nombela C, Arroyo J. Cooperation between SAGA and SWI/SNF complexes is required for efficient transcriptional responses regulated by the yeast MAPK Slt2. *Nucleic Acids Res* 2016:gkw324. <https://doi.org/10.1093/nar/gkw324>.

Savitsky M, Kim M, Kravchuk O, Schwartz YB. Distinct Roles of Chromatin Insulator Proteins in Control of the *Drosophila* Bithorax Complex. *Genetics* 2016;202:601–17. <https://doi.org/10.1534/genetics.115.179309>.

Schmitges FW, Prusty AB, Faty M, Stützer A, Lingaraju GM, Aiwazian J, et al. Histone Methylation by PRC2 Is Inhibited by Active Chromatin Marks. *Molecular Cell* 2011;42:330–41. <https://doi.org/10.1016/j.molcel.2011.03.025>.

Schuettengruber B, Bourbon H-M, Di Croce L, Cavalli G. Genome Regulation by Polycomb and Trithorax: 70 Years and Counting. *Cell* 2017;171:34–57. <https://doi.org/10.1016/j.cell.2017.08.002>.

Schuettengruber B, Ganapathi M, Leblanc B, Portoso M, Jaschek R, Tolhuis B, et al. Functional Anatomy of Polycomb and Trithorax Chromatin Landscapes in *Drosophila* Embryos. *PLoS Biol* 2009;7:e1000013. <https://doi.org/10.1371/journal.pbio.1000013>.

Schultz DC. SETDB1: a novel KAP-1-associated histone H3, lysine 9-specific methyltransferase that contributes to HP1-mediated silencing of euchromatic genes by KRAB zinc-finger proteins. *Genes & Development* 2002;16:919–32. <https://doi.org/10.1101/gad.973302>.

Schwabish MA, Struhl K. The Swi/Snf Complex Is Important for Histone Eviction during Transcriptional Activation and RNA Polymerase II Elongation In Vivo. *Mol Cell Biol* 2007;27:6987–95. <https://doi.org/10.1128/MCB.00717-07>.

Schwabish MA, Struhl K. Evidence for Eviction and Rapid Deposition of Histones upon Transcriptional Elongation by RNA Polymerase II. *Mol Cell Biol* 2004;24:10111–7. <https://doi.org/10.1128/MCB.24.23.10111-10117.2004>.

Schwartz YB, Cavalli G. Three-Dimensional Genome Organization and Function in *Drosophila*. *Genetics* 2017;205:5–24. <https://doi.org/10.1534/genetics.115.185132>.

Schwartz YB, Kahn TG, Nix DA, Li X-Y, Bourgon R, Biggin M, et al. Genome-wide analysis of Polycomb targets in *Drosophila melanogaster*. *Nat Genet* 2006;38:700–5. <https://doi.org/10.1038/ng1817>.

Schwartz YB, Kahn TG, Stenberg P, Ohno K, Bourgon R, Pirrotta V. Alternative Epigenetic Chromatin States of Polycomb Target Genes. *PLoS Genet* 2010;6:e1000805. <https://doi.org/10.1371/journal.pgen.1000805>.

Schwartz YB, Linder-Basso D, Kharchenko PV, Tolstorukov MY, Kim M, Li H-B, et al. Nature and function of insulator protein binding sites in the *Drosophila* genome. *Genome Res* 2012;22:2188–98. <https://doi.org/10.1101/gr.138156.112>.

Scott KC, Merrett SL, Willard HF. A Heterochromatin Barrier Partitions the Fission Yeast Centromere into Discrete Chromatin Domains. *Current Biology* 2006;16:119–29. <https://doi.org/10.1016/j.cub.2005.11.065>.

Secombe J, Li L, Carlos L, Eisenman RN. The Trithorax group protein Lid is a trimethyl histone H3K4 demethylase required for dMyc-induced cell growth. *Genes & Development* 2007;21:537–51. <https://doi.org/10.1101/gad.1523007>.

Segal E, Widom J. What controls nucleosome positions? *Trends in Genetics* 2009;25:335–43. <https://doi.org/10.1016/j.tig.2009.06.002>.

Sentenac A. Eukaryotic RNA Polymerase. *Critical Reviews in Biochemistry* 1985;18:31–90. <https://doi.org/10.3109/10409238509082539>.

Sexton T, Yaffe E, Kenigsberg E, Bantignies F, Leblanc B, Hoichman M, et al. Three-Dimensional Folding and Functional Organization Principles of the *Drosophila* Genome. *Cell* 2012;148:458–72. <https://doi.org/10.1016/j.cell.2012.01.010>.

Shaul O. How introns enhance gene expression. *The International Journal of Biochemistry & Cell Biology* 2017;91:145–55. <https://doi.org/10.1016/j.biocel.2017.06.016>.

Shlyueva D, Stampfel G, Stark A. Transcriptional enhancers: from properties to genome-wide predictions. *Nat Rev Genet* 2014;15:272–86. <https://doi.org/10.1038/nrg3682>.

Silverstein RA, Ekwall K. Sin3: a flexible regulator of global gene expression and genome stability. *Curr Genet* 2005;47:1–17. <https://doi.org/10.1007/s00294-004-0541-5>.

Simon JA, Kingston RE. Occupying chromatin: Polycomb mechanisms for getting to genomic targets, stopping transcriptional traffic, and staying put. *Mol Cell* 2013;49:808–24. <https://doi.org/10.1016/j.molcel.2013.02.013>.

Smolko AE, Shapiro-Kulnane L, Salz HK. The H3K9 methyltransferase SETDB1 maintains female identity in *Drosophila* germ cells. *Nat Commun* 2018;9:4155. <https://doi.org/10.1038/s41467-018-06697-x>.

Spellman PT, Rubin GM. Evidence for large domains of similarly expressed genes in the *Drosophila* genome. *J Biol* 2002;1:5. <https://doi.org/10.1186/1475-4924-1-5>.

Spradling A. *The development of Drosophila melanogaster*. 1993.

Stevens TJ, Lando D, Basu S, Atkinson LP, Cao Y, Lee SF, et al. 3D structures of individual mammalian genomes studied by single-cell Hi-C. *Nature* 2017;544:59–64. <https://doi.org/10.1038/nature21429>.

Stitzel ML, Seydoux G. Regulation of the Oocyte-to-Zygote Transition. *Science* 2007;316:407–8. <https://doi.org/10.1126/science.1138236>.

Strahl BD, Ohba R, Cook RG, Allis CD. Methylation of histone H3 at lysine 4 is highly conserved and correlates with transcriptionally active nuclei in *Tetrahymena*. *Proceedings of the National Academy of Sciences* 1999;96:14967–72. <https://doi.org/10.1073/pnas.96.26.14967>.

Strom AR, Emelyanov AV, Mir M, Fyodorov DV, Darzacq X, Karpen GH. Phase separation drives heterochromatin domain formation. *Nature* 2017;547:241–5. <https://doi.org/10.1038/nature22989>.

Svensson MJ, Chen JD, Pirrotta V, Larsson J. The ThioredoxinT and deadhead gene pair encode testis- and ovary-specific thioredoxins in *Drosophila melanogaster*. *Chromosoma* 2003;112:133–43. <https://doi.org/10.1007/s00412-003-0253-5>.

Svensson MJ, Stenberg P, Larsson J. Organization and regulation of sex-specific thioredoxin encoding genes in the genus *Drosophila*. *Dev Genes Evol* 2007;217:639–50. <https://doi.org/10.1007/s00427-007-0175-y>.

Szabo Q, Bantignies F, Cavalli G. Principles of genome folding into topologically associating domains. *Sci Adv* 2019;5:eaaw1668. <https://doi.org/10.1126/sciadv.aaw1668>.

Szenker E, Lacoste N, Almouzni G. A Developmental Requirement for HIRA-Dependent H3.3 Deposition Revealed at Gastrulation in *Xenopus*. *Cell Reports* 2012;1:730–40. <https://doi.org/10.1016/j.celrep.2012.05.006>.

Tadros W, Goldman AL, Babak T, Menzies F, Vardy L, Orr-Weaver T, et al. SMAUG Is a Major Regulator of Maternal mRNA Destabilization in *Drosophila* and Its Translation Is Activated by the PAN GU Kinase. *Developmental Cell* 2007;12:143–55. <https://doi.org/10.1016/j.devcel.2006.10.005>.

Talbert PB, Henikoff S. Histone variants on the move: substrates for chromatin dynamics. *Nat Rev Mol Cell Biol* 2017;18:115–26. <https://doi.org/10.1038/nrm.2016.148>.

Tie F, Banerjee R, Fu C, Stratton CA, Fang M, Harte PJ. Polycomb inhibits histone acetylation by CBP by binding directly to its catalytic domain. *Proc Natl Acad Sci USA* 2016;113:E744–53. <https://doi.org/10.1073/pnas.1515465113>.

Tie F, Banerjee R, Stratton CA, Prasad-Sinha J, Stepanik V, Zlobin A, et al. CBP-mediated acetylation of histone H3 lysine 27 antagonizes *Drosophila* Polycomb silencing. *Development* 2009;136:3131–41. <https://doi.org/10.1242/dev.037127>.

Tirmarche S. Fonctions des thiorédoxines sexuelles et contrôle de l'état rédox des protamines chez la drosophile 2016:157.

Tirmarche S, Kimura S, Dubruille R, Horard B, Loppin B. Unlocking sperm chromatin at fertilization requires a dedicated egg thioredoxin in *Drosophila*. *Nat Commun* 2016;7:13539. <https://doi.org/10.1038/ncomms13539>.

Torné J, Ray-Gallet D, Boyarchuk E, Garnier M, Le Baccon P, Coulon A, et al. Two HIRA-dependent pathways mediate H3.3 de novo deposition and recycling during transcription. *Nat Struct Mol Biol* 2020;27:1057–68. <https://doi.org/10.1038/s41594-020-0492-7>.

Torres-Campana D, Kimura S, Orsi GA, Horard B, Benoit G, Loppin B. The Lid/KDM5 histone demethylase complex activates a critical effector of the oocyte-to-zygote transition. *PLoS Genet* 2020;16:e1008543. <https://doi.org/10.1371/journal.pgen.1008543>.

Ulianov SV, Khrameeva EE, Gavrilov AA, Flyamer IM, Kos P, Mikhaleva EA, et al. Active chromatin and transcription play a key role in chromosome partitioning into topologically associating domains. *Genome Res* 2016;26:70–84. <https://doi.org/10.1101/gr.196006.115>.

Urrutia AO. The Signature of Selection Mediated by Expression on Human Genes. *Genome Research* 2003;13:2260–4. <https://doi.org/10.1101/gr.641103>.

Van Bortle K, Nichols MH, Li L, Ong C-T, Takenaka N, Qin ZS, et al. Insulator function and topological domain border strength scale with architectural protein occupancy. *Genome Biol* 2014;15:R82. <https://doi.org/10.1186/gb-2014-15-5-r82>.

Van Bortle K, Ramos E, Takenaka N, Yang J, Wahi JE, Corces VG. *Drosophila* CTCF tandemly aligns with other insulator proteins at the borders of H3K27me3 domains. *Genome Res* 2012;22:2176–87. <https://doi.org/10.1101/gr.136788.111>.

Verdel A. RNAi-Mediated Targeting of Heterochromatin by the RITS Complex. *Science* 2004;303:672–6. <https://doi.org/10.1126/science.1093686>.

Vo ngoc L, Wang Y-L, Kassavetis GA, Kadonaga JT. The punctilious RNA polymerase II core promoter. *Genes Dev* 2017;31:1289–301. <https://doi.org/10.1101/gad.303149.117>.

Voigt P, LeRoy G, Drury WJ, Zee BM, Son J, Beck DB, et al. Asymmetrically Modified Nucleosomes. *Cell* 2012;151:181–93. <https://doi.org/10.1016/j.cell.2012.09.002>.

Voigt P, Tee W-W, Reinberg D. A double take on bivalent promoters. *Genes & Development* 2013;27:1318–38. <https://doi.org/10.1101/gad.219626.113>.

Volpe TA. Regulation of Heterochromatic Silencing and Histone H3 Lysine-9 Methylation by RNAi. *Science* 2002;297:1833–7. <https://doi.org/10.1126/science.1074973>.

Wakimoto BT, Hearn MG. The effects of chromosome rearrangements on the expression of heterochromatic genes in chromosome 2L of *Drosophila melanogaster*. *Genetics* 1990;125:141–54.

Wang C, Lin H. Roles of piRNAs in transposon and pseudogene regulation of germline mRNAs and lncRNAs. *Genome Biol* 2021;22:27. <https://doi.org/10.1186/s13059-020-02221-x>.

Wang H, Wang L, Erdjument-Bromage H, Vidal M, Tempst P, Jones RS, et al. Role of histone H2A ubiquitination in Polycomb silencing. *Nature* 2004;431:873–8. <https://doi.org/10.1038/nature02985>.

Wang Q, Sun Q, Czajkowsky DM, Shao Z. Sub-kb Hi-C in *D. melanogaster* reveals conserved characteristics of TADs between insect and mammalian cells. *Nat Commun* 2018;9:188. <https://doi.org/10.1038/s41467-017-02526-9>.

Weber CM, Hafner A, Kirkland JG, Braun SMG, Stanton BZ, Boettiger AN, et al. mSWI/SNF promotes Polycomb repression both directly and through genome-wide redistribution. *Nat Struct Mol Biol* 2021;28:501–11. <https://doi.org/10.1038/s41594-021-00604-7>.

Weinberg DE, Shah P, Eichhorn SW, Hussmann JA, Plotkin JB, Bartel DP. Improved Ribosome-Footprint and mRNA Measurements Provide Insights into Dynamics and Regulation of Yeast Translation. *Cell Reports* 2016;14:1787–99. <https://doi.org/10.1016/j.celrep.2016.01.043>.

Weiner A, Chen HV, Liu CL, Rahat A, Klien A, Soares L, et al. Systematic Dissection of Roles for Chromatin Regulators in a Yeast Stress Response. *PLoS Biol* 2012;10:e1001369. <https://doi.org/10.1371/journal.pbio.1001369>.

Williams K, Christensen J, Pedersen MT, Johansen JV, Cloos PAC, Rappsilber J, et al. TET1 and hydroxymethylcytosine in transcription and DNA methylation fidelity. *Nature* 2011;473:343–8. <https://doi.org/10.1038/nature10066>.

Wolf G, Yang P, Füchtbauer AC, Füchtbauer E-M, Silva AM, Park C, et al. The KRAB zinc finger protein ZFP809 is required to initiate epigenetic silencing of endogenous retroviruses. *Genes Dev* 2015;29:538–54. <https://doi.org/10.1101/gad.252767.114>.

Wutz G, Várnai C, Nagasaka K, Cisneros DA, Stocsits RR, Tang W, et al. Topologically associating domains and chromatin loops depend on cohesin and are regulated by CTCF, WAPL, and PDS5 proteins. *EMBO J* 2017;36:3573–99. <https://doi.org/10.15252/embj.201798004>.

Xi Y, Yao J, Chen R, Li W, He X. Nucleosome fragility reveals novel functional states of chromatin and poises genes for activation. *Genome Research* 2011;21:718–24. <https://doi.org/10.1101/gr.117101.110>.

Xie G, Chen H, Jia D, Shu Z, Palmer WH, Huang Y-C, et al. The SWI/SNF Complex Protein Snr1 Is a Tumor Suppressor in *Drosophila* Imaginal Tissues. *Cancer Res* 2017;77:862–73. <https://doi.org/10.1158/0008-5472.CAN-16-0963>.

Yamada T, Fischle W, Sugiyama T, Allis CD, Grewal SIS. The Nucleation and Maintenance of Heterochromatin by a Histone Deacetylase in Fission Yeast. *Molecular Cell* 2005;20:173–85. <https://doi.org/10.1016/j.molcel.2005.10.002>.

Yu C-H, Dang Y, Zhou Z, Wu C, Zhao F, Sachs MS, et al. Codon Usage Influences the Local Rate of Translation Elongation to Regulate Co-translational Protein Folding. *Molecular Cell* 2015;59:744–54. <https://doi.org/10.1016/j.molcel.2015.07.018>.

Zabidi MA, Arnold CD, Schernhuber K, Pagani M, Rath M, Frank O, et al. Enhancer–core-promoter specificity separates developmental and housekeeping gene regulation. *Nature* 2015;518:556–9. <https://doi.org/10.1038/nature13994>.

Zamurrad S, Hatch HAM, Drelon C, Belalcazar HM, Secombe J. A *Drosophila* Model of Intellectual Disability Caused by Mutations in the Histone Demethylase KDM5. *Cell Rep* 2018;22:2359–69. <https://doi.org/10.1016/j.celrep.2018.02.018>.

Zhang H, Roberts DN, Cairns BR. Genome-Wide Dynamics of Htz1, a Histone H2A Variant that Poises Repressed/Basal Promoters for Activation through Histone Loss. *Cell* 2005;123:219–31. <https://doi.org/10.1016/j.cell.2005.08.036>.

Zhang K, Mosch K, Fischle W, Grewal SIS. Roles of the Clr4 methyltransferase complex in nucleation, spreading and maintenance of heterochromatin. *Nat Struct Mol Biol* 2008;15:381–8. <https://doi.org/10.1038/nsmb.1406>.

Zhao F, Yu C, Liu Y. Codon usage regulates protein structure and function by affecting translation elongation speed in *Drosophila* cells. *Nucleic Acids Research* 2017;45:8484–92. <https://doi.org/10.1093/nar/gkx501>.

Zhao XD, Han X, Chew JL, Liu J, Chiu KP, Choo A, et al. Whole-Genome Mapping of Histone H3 Lys4 and 27 Trimethylations Reveals Distinct Genomic Compartments in Human Embryonic Stem Cells. *Cell Stem Cell* 2007;1:286–98. <https://doi.org/10.1016/j.stem.2007.08.004>.

Zhaunova L, Ohkura H, Breuer M. Kdm5/Lid Regulates Chromosome Architecture in Meiotic Prophase I Independently of Its Histone Demethylase Activity. *PLoS Genet* 2016;12:e1006241. <https://doi.org/10.1371/journal.pgen.1006241>.

Zhou Z, Dang Y, Zhou M, Li L, Yu C, Fu J, et al. Codon usage is an important determinant of gene expression levels largely through its effects on transcription. *Proc Natl Acad Sci USA* 2016;113:E6117–25. <https://doi.org/10.1073/pnas.1606724113>.

Zraly CB, Dingwall AK. The chromatin remodeling and mRNA splicing functions of the Brahma (SWI/SNF) complex are mediated by the SNR1/SNF5 regulatory subunit. *Nucleic Acids Research* 2012;40:5975–87. <https://doi.org/10.1093/nar/gks288>.

Zraly CB, Marena DR, Nanchal R, Cavalli G, Muchardt C, Dingwall AK. SNR1 is an essential subunit in a subset of *Drosophila* brm complexes, targeting specific functions during development. *Dev Biol* 2003;253:291–308. [https://doi.org/10.1016/s0012-1606\(02\)00011-8](https://doi.org/10.1016/s0012-1606(02)00011-8).

Zraly CB, Middleton FA, Dingwall AK. Hormone-response genes are direct in vivo regulatory targets of Brahma (SWI/SNF) complex function. *J Biol Chem* 2006;281:35305–15. <https://doi.org/10.1074/jbc.M607806200>.